A Single-Atom Upgrade to Polydicyclopentadiene

by

Benjamin Godwin
B.Sc., University of Calgary, 2020

A Dissertation Submitted in Partial Fulfillment
Of the Requirements for the Degree of

DOCTOR OF PHILOSOPHY

In the Department of Chemistry

Supervisory Committee

A Single-Atom Upgrade to Polydicyclopentadiene

by

Benjamin Godwin
B.Sc., University of Calgary, 2020

Supervisory Committee

Dr. Jeremy Wulff, Supervisor
Department of Chemistry

Dr. David Leitch, Departmental Member
Department of Chemistry

Dr. Christopher Dennison, Outside Member
Department of Mechanical Engineering

Abstract

Polydicyclopentadiene (PDCPD) is an engineering plastic produced through the ring-opening metathesis polymerization (ROMP) of dicyclopentadiene (DCPD), a petrochemical waste product. Owing to its high glass transition temperature, high storage modulus, high tensile strength, and general robustness to chemical or physical attack, PDCPD has enjoyed commercial use for making body panels for automobiles and heavy machinery. However, PDCPD is a simple polyolefin composed of only hydrogen and carbon atoms; it is thus low surface energy and not chemically tunable. The low surface energy also makes the application of paints and adhesives challenging.

Herein I describe a ketone-functionalized derivative of dicyclopentadiene (oxaDCPD). When polymerized oxaPDCPD displays a unique non-canonical hydrogen bond between the ketone and an adjacent vinyl hydrogen within the polymer. Partly as a result of this interaction, the thermoset polymer has an increased glass transition temperature, storage modulus, Young's modulus, compression strength, and surface functionality compared to the native material. I also describe the copolymerization of dicyclopentadiene with the novel oxa-dicyclopentadiene monomer to produce copolymers. These copolymers display remarkably tunable (and improved) mechanical and thermal properties. Additionally, the copolymers have improved surface functionality and display resistance to oxidative embrittlement.

Many thermosets—including PDCPD and oxaPDCPD—are produced in a process called reaction injection molding (RIM) wherein neat monomer is directly transformed to solid polymer using a catalyst. In these polymerizations the crosslinks between the polymer chains form alongside the polymer, rapidly forming a solid. It is therefore challenging to study these kinds of processes. I have developed a method suitable for laboratory-scale studies of these reactions. This

method is high-throughput and low cost. Remarkably, not only can various initiators be compared but the mechanical and thermal properties of the final material can be generally predicted.

Finally, despite PDCPD's industrial niche remaining in the body panel market for decades there is a large volume of high-impact research dedicated to it. As part of a Natural Sciences and Engineering Research Council of Canada (NSERC) Lab to Market (L2M) Grant I conducted stakeholder interviews to determine industry pain points and determine a path towards commercialization of new PDCPD technologies.

Table of Contents

List of Figures

List of Tables

List of Abbreviations

°C	Degrees Celsius
^{13}C NMR	Carbon 13 nuclear magnetic resonance spectroscopy
^{13}C SSNMR	Carbon 13 solid state nuclear magnetic resonance spectroscopy
^{1}H NMR	Proton nuclear magnetic resonance spectroscopy
ACPs	Atom-centered potentials
app	Apparent
ATIR	Attenuated total reflectance infrared spectroscopy
BHG	Bertrand-Hoveyda-Grubbs based initiator
br	Broad
CAAC	Cyclic alkyl amino carbene
CP	Cyclopentadiene
CRN	Composite research network
Cy	Cyclohexane
D	Doublet
DCM	Dichloromethane
DCPD	Dicyclopentadiene
dd	Doublet of doublets
ddd	Doublet of doublets of doublets
dddd	Doublet of doublets of doublets of doublets
DFT	Density functional theory
DMSO	Dimethyl sulfoxide
DMTA	Dynamic mechanical thermal analysis
DNA	Deoxyribonucleic acid
dq	Doublet of quartets
DSC	Differential scanning calorimetry
dt	Doublet of triplets
dtd	Doublet of triplet of doublets
E	Young's modulus
E'	Storage modulus
E'_m	Minimum storage modulus
E''	Loss modulus
ENB	Ethylidene norbornene
EPA	Environmental Protection Agency
EVE	Ethyl vinyl ether
*f*DCPD	1st generation ester functionalized dicyclopentadiene
*f*PDCPD	1st generation ester functionalized polydicyclopentadiene
FTIR	Fourier transform infrared spectroscopy
GC1	Grubbs 1st generation catalyst
GC2	Grubbs 2nd generation catalyst

GC3	Grubbs 3rd generation catalyst
GPC	Gel permeation chromatography
HRMS	High resolution mass spectrometry
IDEaS	Innovation for Defence Excellence and Security grant
ILSS	Interlaminar shear strength
L2M	Lab to market grant
LLDPE	Linear low-density polyethylene
LMR	Liquid molding resin
m	Multiplet
m.p.	Melting point
M_c	Molecular weight between crosslinks
MD	Molecular dynamics
M_n	Number average molecular weight
M_w	Weight average molecular weight
NHC	N-heterocyclic carbene
NMR	Nuclear magnetic resonance
NSERC	Natural Sciences and Engineering Council of Canada
OAc	Acetoxy functional group
OBz	Benzoyl functional group
OMe	Methoxy functional group
OOc	Oxtoxy functional group
OPr	Propoxy functional group
oxaDCPD	2nd generation ketone functionalized dicyclopentadiene
$oxaDCPD_{rd}$	2nd generation ketone functionalized dicyclopentadiene reduced
oxaPDCPD	2nd generation ketone functionalized polydicyclopentadiene
oxaRD	2nd generation ketone functionalized dicyclopentadiene reduced
p	Pentet
PDCPD	Polydicyclopentadiene
PEX	Crosslinked polyetheylene
ppb	Parts per billion
ppm	parts per million
q	Quartet
qd	Quartet of doublets
QM	Quantum mechanics
quint	Quintet
RIM	Reaction injection molding
ROMP	Ring-opening metathesis polymerization
s	Singlet
SBR	Styrene-butadiene rubber
sept	Septet
sext	Sextet

SMC	Sheet molding compound
SMT	Smoke time
SMT_{90}	Smoke time at 90°C
SRu	Sulfur chelating ruthenium catalyst
t	Triplet
TBP	Tri-n-butyl phosphite
td	Triplet of doublets
T_g	Glass transition temperature
TGA	Thermogravimetric analysis
THF	Tetrahydrofuran
T_{pk}	Peak temperature of thermogram
TPP	Tetraphenyl porphyrin
UBCO	University of British Columbia Okanagen campus
UV	Ultra-violet
VH	Vickers hardness
X-ray	Unknown ray
θ	Angle in degrees
σ_l	Surface tension
σ_l^D	Surface tension dispersive
σ_l^P	Surface tension polar

Acknowledgements

I would like to begin by thanking my committee members, Dr. David Leitch and Dr. Chris Dennison for their time, support and efforts in the creation of this dissertation.

I would also like to thank my supervisor, Dr. Jeremy Wulff. This dissertation would not have been possible without you. Thank you for your endless enthusiasm in my projects and ideas, I can't say enough how much your excitement for science inspired me throughout my PhD journey. Thank you for the thousands of hours of editing and support, impromptu meetings to troubleshoot many problems and to celebrate little wins. Thank you for trusting me to lead in my projects and take the onus with collaborators. I am so very thankful for the mentorship and leadership opportunities I have had in your research group.

I have also had the privilege to work side by side with many amazing people throughout my PhD. I would like to thank Dr. Stefania Musolino, Jon Sader and Dr. Rashid Nazir for countless hours of company, many more questions answered, and tireless support through my entire PhD. I would also like to thank the present and past Wulff Group and Xlynx members who have made the office and lab space a supportive, welcoming environment, and much joy to my life over the last four years: Dr. Tong Li, Dr. Liting Bi, Dr. Derek Blevins, Dr. Pothana Gandhi Nellepalli, Austin Burman, Lily Pestereva, Lorenzo Michelini, Dr. Sun Kly, Nora Struchtrup, Adam Sylvain-Stewart, Dr. Miranda Baran, Cole Brawner, Madisen MacFarlane, Spencer Petras, Huyen Tran, Julia Levy, Tanya Slaney, Zoe McGhan, Luca Swainson, and Lucas Luciano.

I have also had the privilege of incredible collaborations throughout my PhD, I would like to thank Professor Abbas Milani, Dr. Tina Olfatbakhsh, Dr. Mahshid Mahbod, Olivia Margoto, Professor Gino DiLabio, Dr. Monir Anvari, Ryan Mandau, Professor Marc Mauduit, Dylan

Bouetard, Jakub Talcik, Dr. Antonio Del Vecchio, Fanny Morvan, and Thierry Roisnel. This dissertation would not have happened without your contributions.

I would also like to give special thanks to Kody Matthews, Chris Secord and Sean Adams for making my project come to life; it would not have been possible without your support.

Thank you to Dr. Michelle Mills for many conversations, support, advice, and laughter over many hours of teaching. In addition, thank you to Dr. Peter Marrs, and Dr. Kelli Fawks. I would also like to thank Chris Barr for many conversations and teaching me about NMR. I would also like to thank Alex Wlasenko for his support and training on many experiments.

A special thank you to my friends and colleagues in the department of which there are too many to name for your support, and camaraderie over the years.

Thank you to my mentors at the University of Calgary, Dr. Simon Trudel, Dr. Greg Welch, Dr. Max Anikovskiy, Dr. Viola Birss, Dr. Josh Koenig, Dr. Katelynn Daley, Dr. Martin Schoen, Dr. Nick Randell, and Dr. Oliver Calderon, I would not be the scientist I am today without the guidance I have received from each of you.

I would also like to thank my close friends Becca Smith, Mike Hudson, Tanner Owca, Bryce Molder, Faelen Prentice, Stef Melon, and Brandon MacMullin for many thousands of kilometers, and hundreds of thousands of vertical meters walked, run, biked, skied, and trudged across the country. This kept me sane, and I can't thank each of you enough. To my best friend and partner, Rachel, thank you for your unconditional love and support, and for always being an island of calm.

Finally, to my parents and family, thank you for your patience and believing in me. I couldn't have done it without your love and support.

Chapter 1: Introduction

1.1. Thermosetting Materials

Polymers are large macromolecules composed of long, entangled chains made of repeating covalently bonded subunits called monomers.[1,2] Polymers can be natural—like our DNA—or synthetic, such as styrene-butadiene rubber (SBR) or polyethylene (Figure 1.1).[1–5]

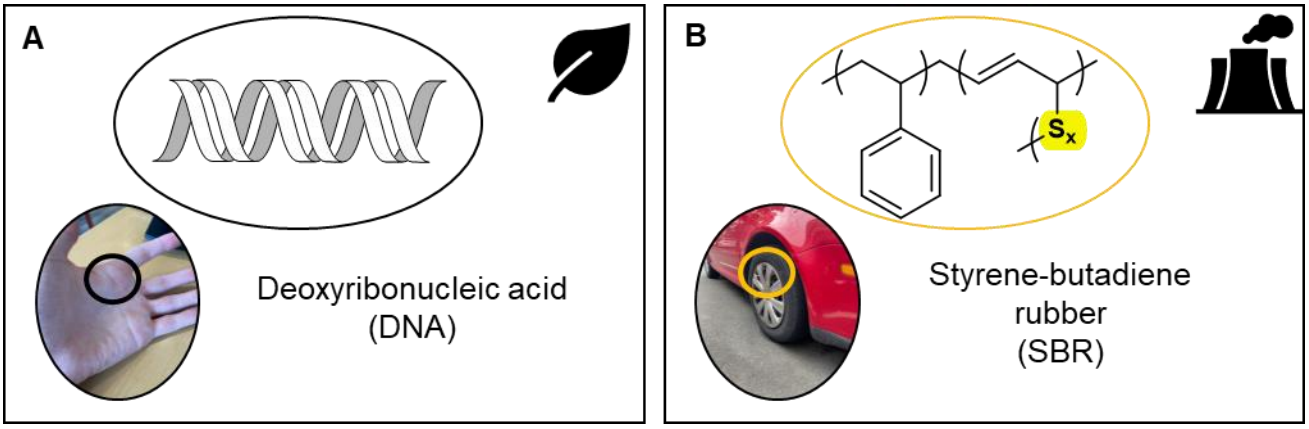

Figure 1.1. A: Deoxyribonucleic acid (DNA) is an example of a natural polymer found in living things. B: Styrene-butadiene rubber is an example of a synthetic polymer found in car tires. The ratio of styrene:butadiene controls performance attributes such as durability, rolling resistance and wet/cold weather grip.

The length of the polymer chains heavily dictates the resulting polymer properties, as long chains lead to more entanglements, allowing the material to resist stress.[1,2] These entanglements contribute heavily to the mechanical and thermal properties of the material. The diversity of polymer building blocks, along with synthetic control over chain length, allow polymers to have diverse properties. Low-cost monomers, which are generally byproducts of the petrochemical industry, have led to the ubiquitous incorporation of polymeric materials in society.[1,2,5–8] In comparison to other materials, such as metals, polymers can be processed at relatively low temperatures—150–300°C vs >700°C for metals—this results in a relatively low energy cost for

their manufacturing.[1,2] The ease of manufacturing has been a substantial contributing factor in their adoption.

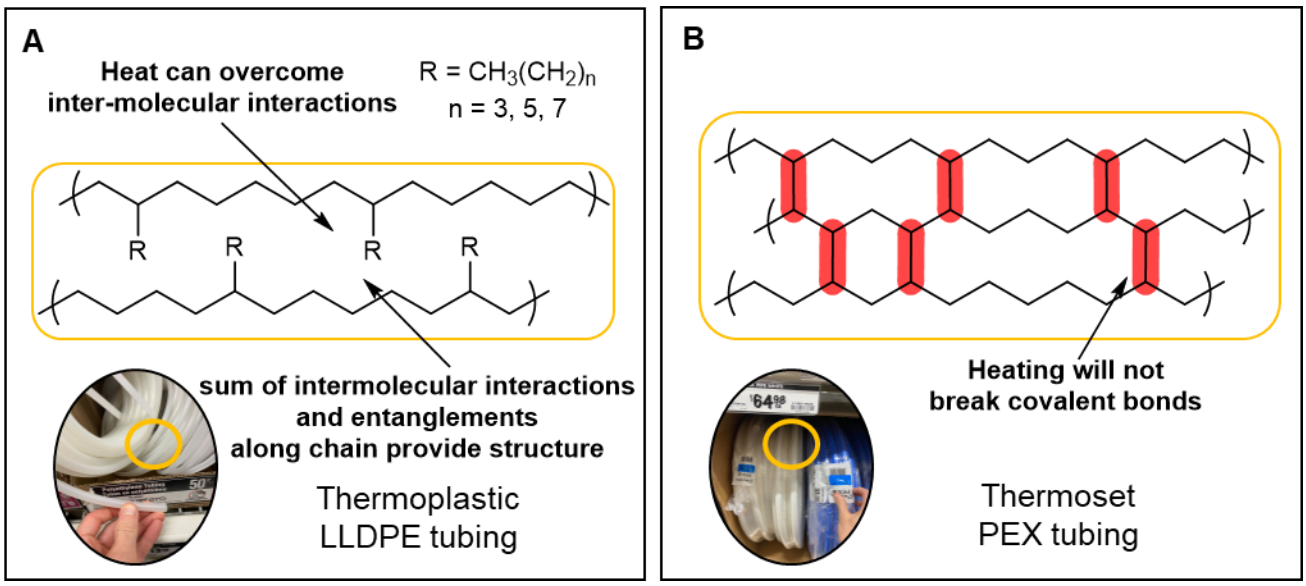

Figure 1.2. A: Linear low-density polyethylene (LLDPE) is a thermoplastic used here to make tubing. LLDPE tubing is suitable for low-temperature applications such as a water purifier or a fish tank. B: Crosslinked polyethylene (PEX) is a thermoset variation of high-density polyetheylene used here to make tubing. PEX tubing is suitable for applications with high-temperatures such as in heated floors or for a household hotwater tank.

Broadly, polymer materials can be categorized as either thermosets or thermoplastics (Figure 1.2).[1,2,8,9] Thermoplastic materials rely solely on chain entanglements and intermolecular interactions between the chains to resist stresses.[1,8,9] Thermosets have—in addition to chain entanglements and intermolecular interactions—covalent bonds between chains called crosslinks, leading to enhanced thermal and mechanical properties.[1,2,10,11] Most of the polymer materials used today are thermoplastic materials. As thermoplastics do not have crosslinks between polymer chains, these types of materials can be melted at high enough temperatures, which allows for them to be reprocessed into new shapes and recycled (Figure 1.2).[1,2,5,12] Sadly, less than 10–20% of all

plastic sent for recycling is recycled.[5,7,8] Often the recycled plastic has reduced mechanical properties due to chain fragmentation that occurs during the recycling process, this significantly limits the utility of the recycled material.[5,8,13] In addition, the reduced thermal and mechanical properties of thermoplastic materials limit the scope of applications they are applicable for.[8,9]

Thermosets generally have much higher resistance to temperature, as the crosslinks resist chain flow when the polymer would otherwise melt.[1,2,9,14] In the same vein, the glass transition temperature—the temperature at which the material transitions from a hard glass-like state to a rubbery one—is also generally higher for thermosets than thermoplastics.[9,15] Thermosets often have substantially higher impact resistance, as well as improved resistance to chemical corrosion, electrical discharge, and biological degradation.[9,15] They have increased mechanical properties including toughness, stiffness, and tensile strength, among others.[8,11,15] Importantly, resistance to creep—the slow deformation of a material under load—is also reduced as compared to thermoplastics. These benefits do come at the cost of recycling as the matrix of interconnected chains prevent the material from melting and being reformed. However, owing to their increased durability the service life can be much longer.[8,14]

The crosslinked matrix of thermosets makes them insoluble, this makes it hard to perform precise structural characterization on thermosets with traditional solution state techniques.[16] This excludes common polymer characterization techniques such as gel permeation chromatography and solution state proton nuclear magnetic resonance spectroscopy (^{1}H NMR). However, most other standard techniques for characterization of polymers are applicable. Infrared spectroscopy can be used to probe the surface chemistry and reveal information about the functional groups present on the surface.[1,11] Solid state carbon 13 nuclear magnetic resonance spectroscopy (^{13}C SSNMR) can be used to assess for changes to the backbone of the material.[1,16] While most polymers are not fully

crystalline, X-ray diffraction can be used to measure the repeating periodicity of the material and to characterize regions of the semicrystalline materials.[1,17] By far one of the most used polymer characterization tools for thermosets is differential scanning calorimetry (DSC). DSC is used to measure the glass transition temperature of the material.[1,2,11,14,18] DSC may also be used to determine the melting point of crystalline regions in the polymer, and by extension the crystallinity of the material.[1,19] The glass transition temperature of polymer materials is especially informative as it is directly correlated to the strength of the interactions between polymer chains, such as crosslink density, and can thus predict the mechanical properties.[1,2,10,20] Thermogravimetric analysis (TGA) may also be used to thermally characterize polymers. TGA can determine the maximum service temperature of a material by identifying the thermal stability of the material.[1,2] The char yield, or the mass remaining in the TGA pan after analysis may also be used to determine the effectiveness of additives like flame retardants.[1,2,21–23] Finally, the mechanical properties of polymers may be directly measured through a plethora of tests. Tensile testing allows for the determination of the Young's modulus, yield strength, ultimate tensile strength, ductility, and toughness.[2] Dynamic mechanical thermal analysis (DMTA) can give insight into the viscoelastic properties of polymeric materials, such as the storage modulus (E'), loss modulus (E"), and loss factor.[1,2,24] In addition, DMTA can also be used to determine the glass transition temperature (often with greater precision than DSC) as well as the response of the material at different frequencies of strain.[1,2,20,25,26] Most mechanical tests require the ability to produce many, large, regular dimensioned samples that are disposable, which can greatly limit the accessibility of such tests in the academic laboratory.

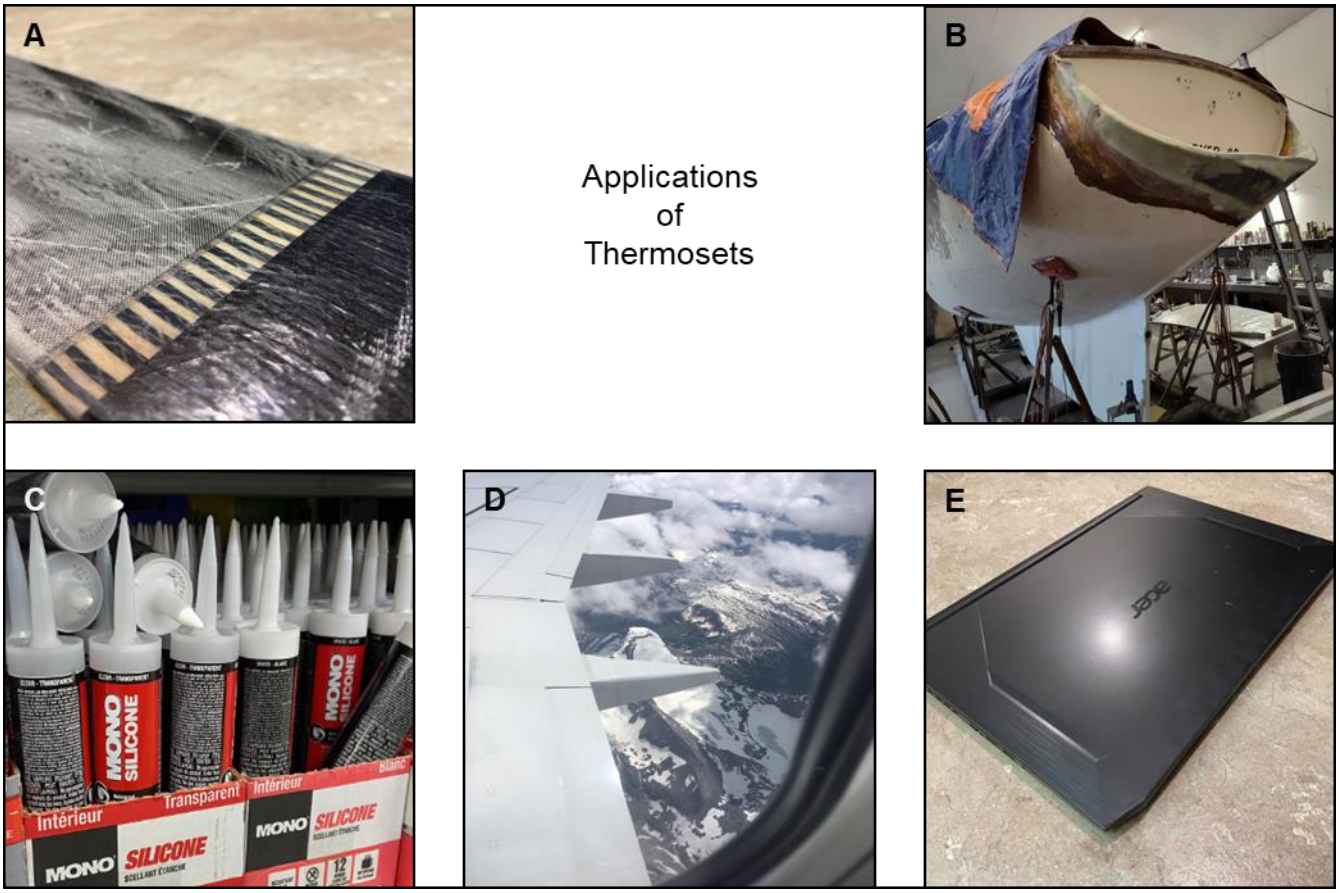

Figure 1.3. Examples of thermosets A: Epoxy carbon-fiber-wood layup in a ski. B: Polyester resin on a sailboat. C: Household silicon caulk. D: Airplane wings are now being made from composites utilizing thermosetting resins instead of aluminum. E: Acrylonitrile-butadiene-styrene is used on consumer electronics and household electrical boxes.

Due to their enhanced mechanical and thermal properties, thermosets are an indispensable component of modern infrastructure.[6,27,28] Thermosets are often found in the aerospace industry due to their high strength:weight ratio and good mechanical performance under constant loads and heat (Figure 1.3D).[29–31] This is often further enhanced by utilizing composite materials, wherein the thermoset is used as a matrix to surround reinforcing materials, often glass fibers or carbon fibers which greatly enhances the materials' properties through load sharing between matrix and fiber (Figure 1.3A).[29–32] Thermosets are also utilized in the marine, and automotive sectors where

they are useful for their impact and corrosion resistance (Figure 1.3B).[33,34] Another application is on medical devices like implants, where biological, or general degradation could be extremely harmful to the patient.[35,36] Thermosets are also found in many other industries like construction and semiconductor/electronics (Figure 1.3C and E).[37,38]

Thermosets may be shaped into useful parts in a variety of ways. However, they must be shaped before the crosslinks are developed and in general, may only be shaped once.[14,28] Many thermosets are first manufactured as telechelic polymers, then cured (crosslinked) in place (like caulk Figure1.3C) or in a mold.[39] To this end, many techniques have been developed. Compression molding is a widely employed example of this technique that cures already formed polymer chains (Figure 1.4). In compression molding, the polymer to be molded is placed in a heated open-face mold. A top section of mold is then used to apply pressure to the material, forcing it to fill the mold cavity, heat and pressure are applied until the polymer is cured. A classic example of this is vulcanization which is the curing of tire rubbers like SBR. This is applied on huge scale worldwide, for the production of tires and other rubber goods like seals and hoses.[40,41] In vulcanization, rubber (poly(butadiene) poly(isoprene), or SBR is pressed into shape and heated in the presence polymeric sulfur, an accelerant (mercaptans) and activator (metal salt, commonly zinc).[4,39] This crosslinks the rubber chains together resulting in a product with significantly enhanced wear resistance.[42,43] Another common use of compression molding is for sheet molding compound (SMC). SMC consists of rolls of thermosetting resin impregnated with reinforcing fibers.[44,45]

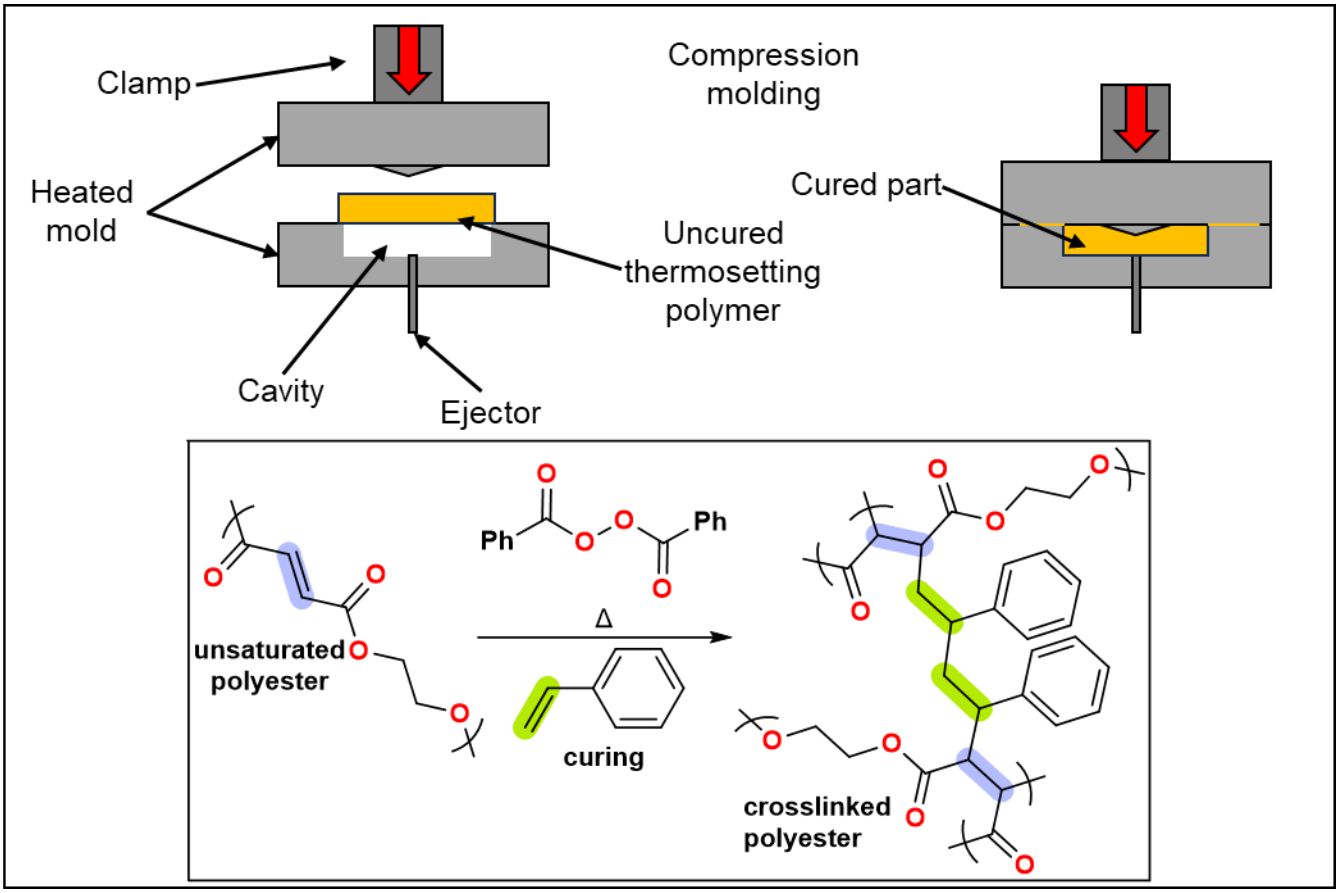

Figure 1.4. Block diagram of compression molding system. Inset: Radical crosslinking of a polyester derived from the condensation of fumaric acid and glycol utilizing an organic peroxide (benzoyl peroxide) and styrene.

The most common combination is unsaturated polyester resin and glass fibers (Figure 1.4).[45] Epoxies and other ester resins are also common, as is carbon fiber.[46,47] The roll of material is unrolled into a mold, the desired part is stamped, and the polyester resin is cured through compression molding. Other examples of this include household two-part epoxy resins, wherein epoxy-containing telechelic polymers are crosslinked by a hardener. The hardener is often an oligoamine but in principle can contain any nucleophilic functional group, like a thiol or alcohol.[1] The number of reactive end groups, as well as the type of end group can be used to control the

speed of the curing reaction and the subsequent mechan ical and thermal properties of the final material.[1]

Thermosets may also be made directly from the monomer. Reaction injection molding (RIM) is an example of this technique (Figure 1.5). In traditional injection molding used for thermoplastics, the polymers are heated above their melting temperature then forced into a mold under intense pressure to achieve the desired shape. While thermoplastic polymers are malleable when molten, they are still very viscous. As such injection molding machines are large and the machines and molds are often very expensive owing to having to deliver and withstand high clamping forces, often in the tons. RIM has two key differences. The low viscosity of many types of thermoset precursors (resins) means that significantly reduced pressures can be used. Secondly, the monomeric resins must react to form the polymer and simultaneously, cure and form crosslinks as shown in Figure 1.5. One advantage is reduced pressures meaning that molds can be made from far more economical materials such as aluminum or even wood for small batches and/or testing.[6] But most of the advantages are based on the resin that is used. RIM is commonly used for polyurethane, but is also used for polyesters and polydicyclopentadiene (PDCPD).[6,48]

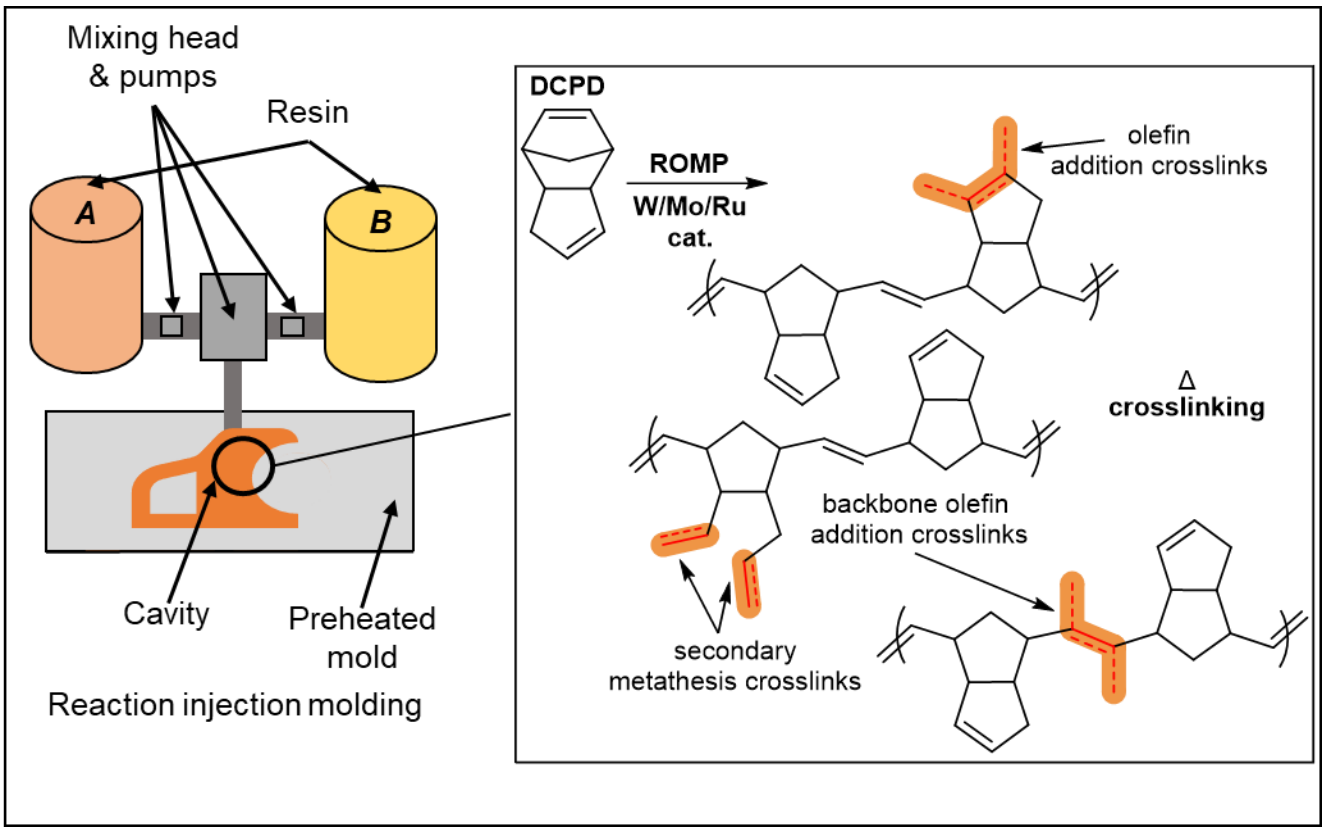

Figure 1.5. Block diagram of a reaction injection molding system. Inset: Ring-opening metathesis polymerization (ROMP) of polydicyclopentadiene and associated crosslinks formed during the exothermic reaction.

1.2. An Introduction to Polydicyclopentadiene

Polydicyclopentadiene (PDCPD) is a thermosetting engineering plastic made from the petrochemical waste product dicyclopentadiene (DCPD). DCPD is produced as a byproduct during the steam cracking of heavy hydrocarbons, like naphtha, to produce ethylene. PDCPD is more commonly known by the various trade names form the companies that produce it, such as Metton®, Telene® or Pentam®.[6] It was invented in the 1970s at the B.F. Goodrich Company, wherein DCPD was copolymerized with cyclopentene using tungsten to produce a linear polymer.[49] This was quickly improved upon in the early 80's by the Hercules Company which filed several patents for PDCPD. These patents focused heavily on the reaction injection moldable

thermoset as opposed to the linear polymer.[50–53] This resulted in a brief patent war between the two companies, with the Hercules company ultimately being victorious. Both systems rely upon a similar two-part catalyst system: a tungsten precatalyst, which is inactive to metathesis and thus ROMP, and an activator that transforms the inactive tungsten catalyst into a center for metathesis. Typically, the tungsten precatalyst is either a mixture of tungsten hexachloride WCl_6 and tungsten oxytetrachloride ($WOCl_4$), or simply WCl_6 mixed with an alcohol, preferably phenol.[50] For the activator many different alkyl tin or aluminum species will work, but the preferred activator is diethylaluminum chloride (Et_2AlCl).[6,49,50] All of these compounds readily dissolve in the DCPD monomer and are inactive towards it until combined. This enables reaction injection molding of the material, wherein the resin can be easily sold as two separate mixtures of DCPD "A" and "B". These are shipped in airtight drums under a blanket of nitrogen. In a mixing head the two components are forced together and injected into the mold wherein the catalyst rapidly activates resulting in the simultaneous polymerization and curing (crosslinking) of the material (Figure 1.6). The commercial catalyst system is highly intolerant of moisture necessitating the tanks, tools, and molds to be kept under a blanket of nitrogen gas. It also precludes the use of polar additives, which will similarly deactivate the catalyst system. In part this sensitivity has also prevented the development of PDCPD composites, as the microscopic moisture content of the glass fibers can also kill the catalyst. This system was commercialized as Metton® liquid molding resin (LMR).[54] B.F. Goodrich Company developed a very similar molybdenum based system, which has since been well developed by RimTec and commercialized as Telene® or Pentam®.[6] Telene®, Pentam® and Metton® are still produced today and used to make body panels for transport trucks, tractors and industrial equipment. The Telene® brand has now expanded to include catalysts based on

ruthenium and tungsten, as well as the original molybdenum-based systems. VIPO has also produced a new type of PDCPD called NexTene®.

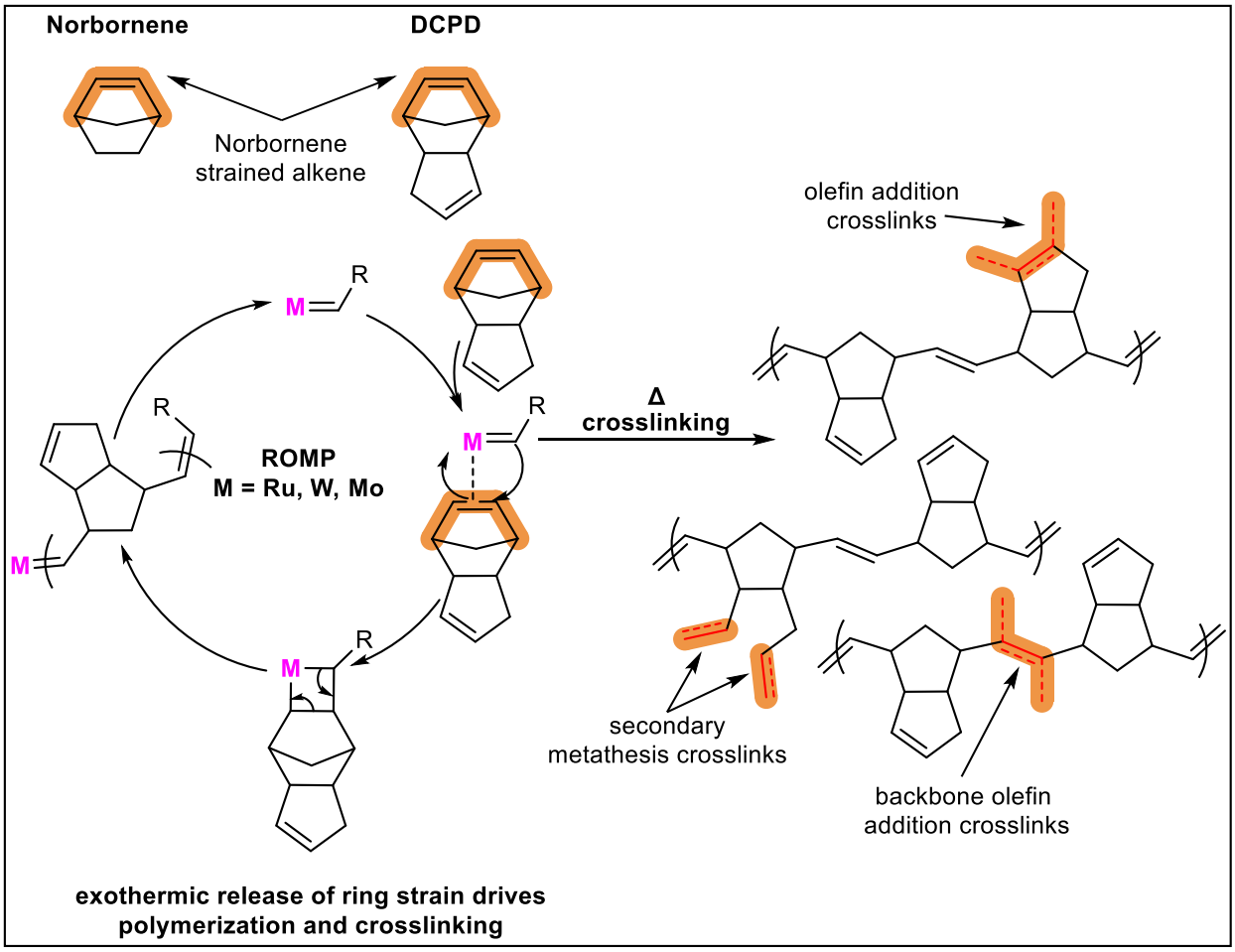

Figure 1.6. Mechanism of ring-opening metathesis polymerization of polydicyclopentadiene and associated crosslinking pathways driven by the heat released. Inset: Norbornene, and the norbornene type alkene on DCPD.

Regardless of the catalyst system used to produced PDCPD, the material has a high glass transition temperature (T_g, ~160°C), high storage modulus (E', ~1 GPa), high impact strength, low density (1.03 g/cm^3) and good chemical resistance.[6,32,55,56] PDCPD is light, tough, and retains those properties even when exposed to harsh chemicals or high or low temperatures.[6,56] Manufacturing of PDCPD parts industrially is done exclusively through reaction injection molding (RIM).[6,55] As

the DCPD resin(s) is low viscosity, the RIM process can be low pressure, and molds may be made easily from aluminum or even wood for very small batches and/or testing.[6] In comparison to traditional injection molding, this dramatically reduces tooling and operation startup costs for manufactures.[6] Additionally, because the resin flows so easily, the RIM process can accommodate complex parts with variable thicknesses and geometries, and these parts may be very large. As the reaction is highly exothermic, only a small amount of heat is necessary to initiate the reaction, substantially reducing the energy cost associated with manufacturing large parts. RIM is both high throughput and low cost.[6]

However, despite its valuable mechanical and thermal properties, as well as waste diversion and low energy manufacturing, PDCPD is not without its faults. As the crosslinking and polymerization reaction are competitive during RIM, unreacted monomer may remain trapped within finished material, resulting in a persistent and unpleasant odor which is perceptible at 3–5 ppb.[6,57] As the polymer consists only of carbon and hydrogen atoms, it lacks any sort of polar chemical functionality. This makes PDCPD not chemically tunable and results in a low surface energy upon initial preparation. This low surface energy is a principal concern in industry, as without a separate surface oxidation step, paints and adhesives may not adhere to the surface. This can bottleneck the otherwise rapid RIM process.[6] The low polarity of the matrix also results in poor compatibility with commercial fiber reinforcements with typical (polar) sizing for epoxy and polyester based resin systems.[6,32] Additionally, as with other thermosets, the covalent crosslink matrix in the material prevents melting and reformation in traditional recycling processes.[14,32]

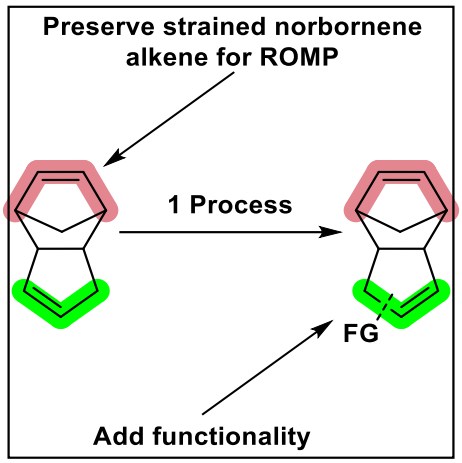

Figure 1.7. Strategy for functionalized DCPD. The norbornene ring must be preserved to drive ROMP and crosslinking during RIM.

By adding a functional group to dicyclopentadiene, most of these issues can be resolved. At first this may appear straightforward, as DCPD contains two alkene functional groups (Figure 1.7). However, addition of functionality is not trivial, as one of these alkenes is a norbornene alkene and it must not be synthetically edited, as its significant ring strain is what drives the exothermic polymerization reaction.[6,26,55,57] This ring strain also makes the norbornene alkene the likely target of any attempts to functionalize the monomer. The preservation of this strained alkene is thus a key design principle in any functional DCPD monomer.[18,26,57,58] To this end, the desired regioselectivity for functionalization of the unstrained cyclopentene alkene has been achieved in the literature previous to this dissertation through two methods.

1.3. Synthetic Strategies for Functionalizing DCPD Monomers

Including the work in this dissertation, there are now three synthetic strategies for making functionalized DCPD monomers in the literature that can deliver a functional group to the unstrained alkene. The previously disclosed methods are described herein.

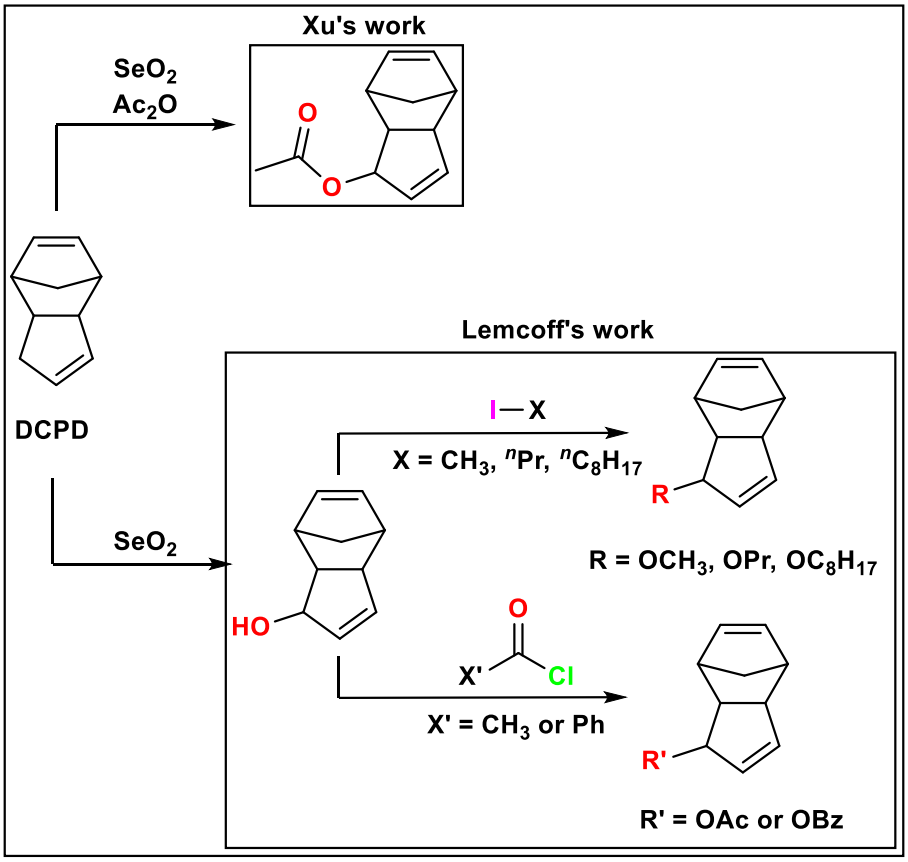

Figure 1.8. Synthetic routes to functionalized PDCPD by the Xu and Lemcoff groups.

The first strategy developed exploited the facile allylic oxidation of DCPD and was used by the Xu and Lemcoff groups to synthesize the first functionalized PDCPD (Figure 1.8).[26,57–61] Owing to the increase in vapor pressure due to the inclusion of the oxygen heteroatom, the monomers synthesized by Xu and Lemcoff do not possess the acrid odor of DCPD. In the approach utilized by the Xu group, DCPD is oxidized using selenium dioxide in the presence of acetic acid which results in the formation of acetoxy-DCPD monomer. This monomer was polymerized using the

Grubbs first-generation catalyst in solution to make a linear acetoxy- PDCPD.[58] The thermal properties of this material were investigated using differential scanning calorimetry and thermal gravimetric analysis.[58] This revealed a glass transition temperature of 136–159°C for the linear material, substantially higher than the ~53°C reported for unfunctionalized linear PDCPD.[58,62] This is a high T_g for a linear polymer—similar to that of the crosslinked materials studied by Lemcoff—and suggests that this linear material undergoes crosslinking during the T_g measurement.[18,58] Thermal crosslinking is reported to happen with other linear functionalized PDCPDs.[11,16] The linear acetoxy-PDCPD was also shown to have poor thermal stability compared to that of the native material with a two-step decomposition observed upon heating above ~220°C (~400°C for the native material) (Figure 1.9).[58,63] Presumably, the presence of the allylic functional group leads to heterolytic cleavage and a resonance stabilized cation leading to the first thermal decomposition.

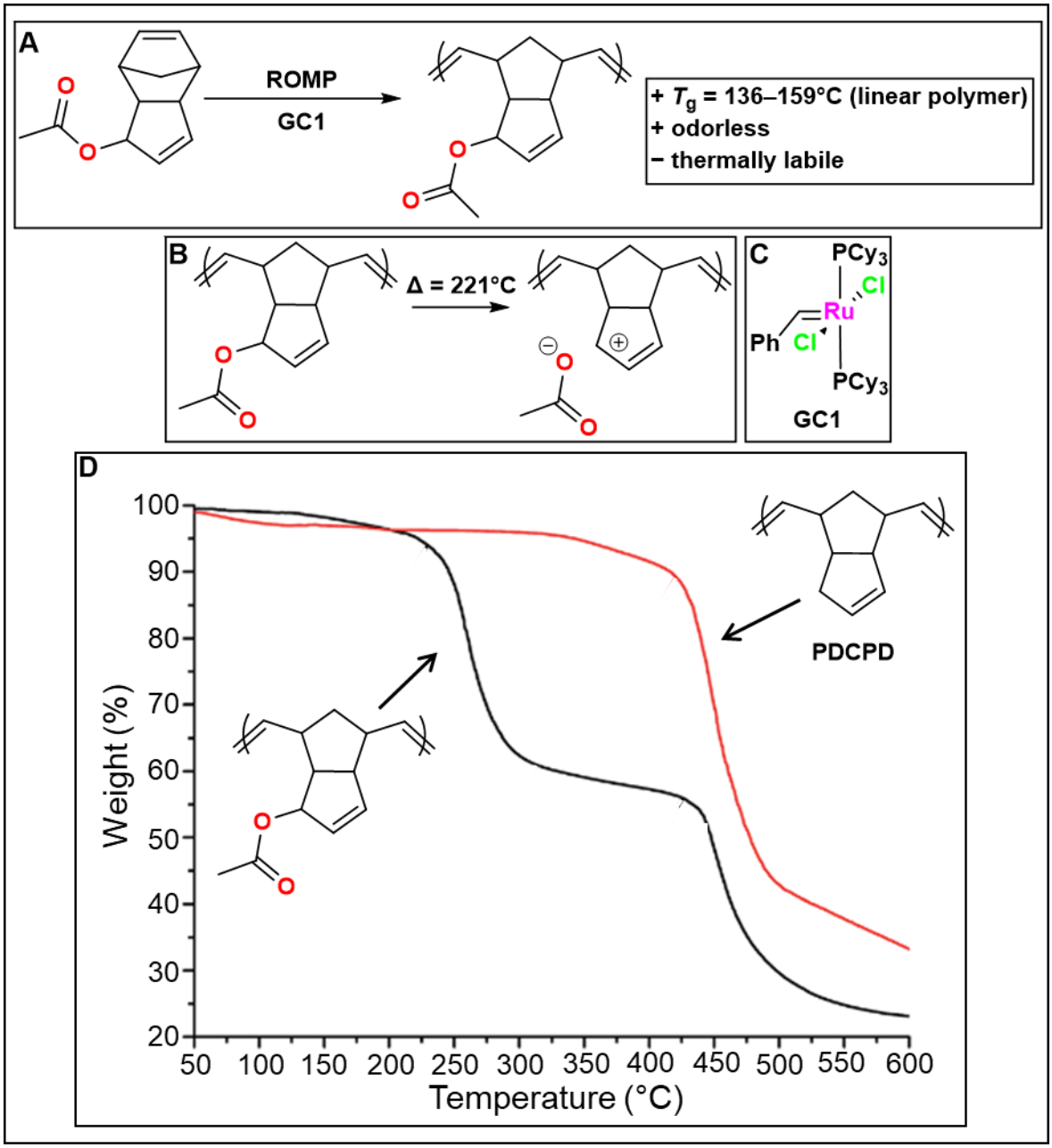

Figure 1.9. A: ROMP of Acetoxy-PDCPD using Grubbs 1st Generation catalyst to yield linear polymer. B: Heterolytic cleavage of acetoxy-PDCPD. C: Grubbs 1st Generation Catalyst D: Thermogravimetric analysis of Acetoxy-PDCPD showing two-stage decomposition. Adapted with permission from the literature.[58]

While there are several other academic works that focus on the production of linear polydicyclopentadiene—including the first PDCPD patent—the general PDCPD industry is overwhelmingly only interested in the reaction injection molded thermoset.[6,32,49] The Lemcoff group has expanded on the original synthesis of the acetoxy-DCPD, synthesizing additional derivatives. In addition, they produced crosslinked macroscale-samples through lab-scale reaction injection molding.[57] These derivatives are synthesized utilizing the same basic selenium oxide mediated oxidation utilized by Xu, and structural diversity was achieved by varying the electrophile (Figure 1.8). These derivatives include alcohol (OH), acetoxy (OAc), benzoyl (OBz), methoxy (OMe), propoxy (OPr), and octoxy (OOc) functionalized DCPD.[57]

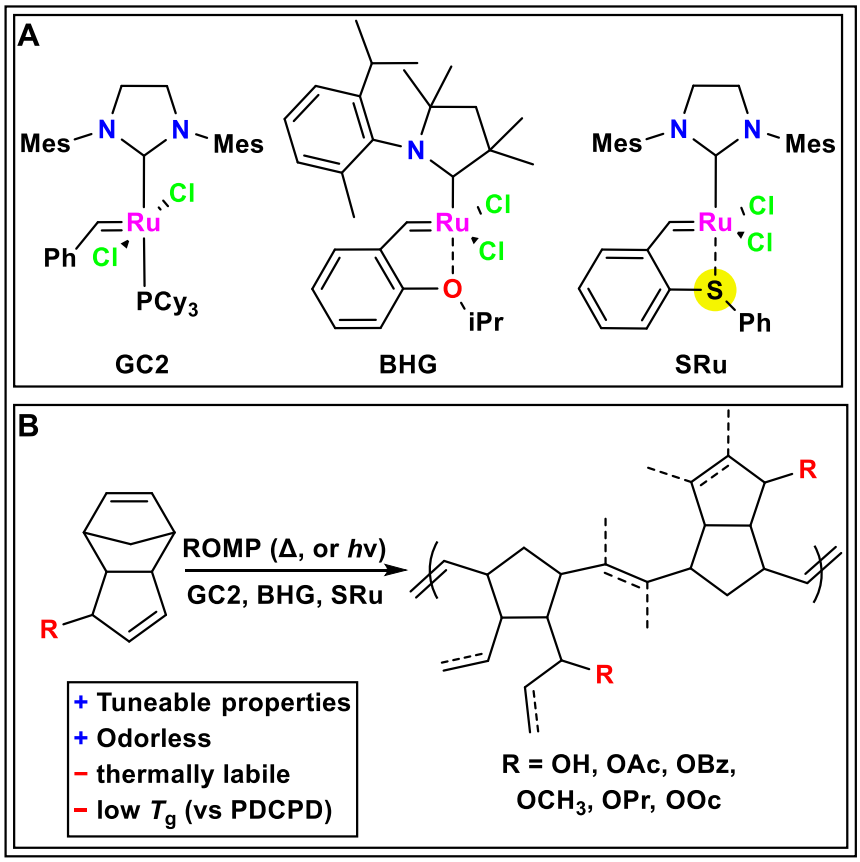

Figure 1.10. A: Catalysts used by the Lemcoff group to produce crosslinked functionalized PDCPD. B: Functionalized crosslinked PDCPD.

These functionalized DCPD monomers all undergo neat polymerization in the presence of the Grubbs second generation catalyst and the reactions yielded solid glassy macromolecules as the products. The single exception was the OBz-DCPD which required the use of a sulfur-chelated ruthenium catalyst due to its high melting point of 70°C (Figure 1.10). This necessitated a more latent catalyst to control reactivity during the molding process resulting in a rubbery solid. All products possessed decomposition temperatures slightly higher than Xu's acetoxy-PDCPD at ~250°C but share in the same two-step decomposition process characteristic of the allylic functional group. In contrast to Xu's work, the Lemcoff group reported substantially lower glass transition temperatures for their functionalized PDCPDs, with the highest reported temperature for the OH-PDCPD being ~110°C. This is interesting as the crosslinked materials should have significantly higher glass transition temperatures owing to the immobilization of the polymer chains in the material due to the covalent bonds.[1,2,16] It is possible that this discrepancy is due to differences in the measurement protocol or spontaneous thermal crosslinking of Xu's linear material during heating in the DSC measurement.[18] It is also possible that the inclusion of the low boiling solvent dichloromethane (DCM) in Lemcoff's process caused the formation of bubbles as the solvent boiled during the molding process.[64] These bubbles could adversely affect the mechanical and thermal properties of the material. Further efforts to derivatize these functional monomers were conducted in a follow-up, study wherein three ruthenium-based initiators were utilized to create reaction injection molded products.[26] The Grubbs 2nd generation initiator (GC2), a cyclic alkyl amino carbene containing Bertrand-Hoveyda-Grubbs based initiator (BHG) and a sulfur chelated benzylidene-based ruthenium catalyst (SRu) were used to polymerize the alcohol (OH), acetoxy (OAc) and propoxy (OPr) functionalized DCPD (Figure 1.10). Both GC2 and BHG were shown to be able to completely cure these functionalized monomers in under an hour at 90°C,

but the latent SRu required up to 5 hours.[26] It was also possible to polymerize these monomers using SRu and ultraviolet light, though this required 24 hours of irradiation. This study showed that the color of the resulting material was correlated with initiator loading, with a lower loading corresponding to a darker color. The authors also showed that the presence of the functionalizing substituents significantly hinders the ROMP reactions.

Investigation of the thermal properties of these materials using dynamic mechanical thermal analysis (DMTA) revealed that by varying the initiator loading and type of initiator the properties of the functionalized PDCPD could be tuned. A maximum glass transition temperature of 140°C was observed for the OH-PDCPD, while OPr-PDCPDs displayed the lowest glass transition temperatures. Polymers made with photo-activation displayed the lowest glass transition temperatures of all materials tested. The authors showed that the size of the substituent installed in the allylic position played a significant role in determining the glass transition temperature.[26] In the allylic position, large substituents substantially increase the degrees of freedom experienced by the polymer chain and subsequently reduce the glass transition temperature. It was found that by combining OH-DCPD and OPr-DCPD and polymerizing, the resulting glass transition temperature was higher for the copolymers as compared to the neat polymers of either monomer.[26]

The materials reported by Xu and Lemcoff demonstrate the feasibility of functionalized monomers as a strategy to solve the problems associated with PDCPD. The functionalization of the DCPD monomer by targeting the cyclopentene alkene preserves the strained norbornene alkene for ROMP, and the addition of the polar functional group increases the glass transition temperature. Additionally, the reduced vapor pressure eliminates the odor of the monomer. However, this strategy significantly impairs the thermal stability of functionalized PDCPD. It also

relies upon a synthesis that utilizes stoichiometric quantities of toxic material, which makes it challenging to scale to industrial quantities, even as a comonomer.[65–67]

The second strategy for functionalizing PDCPD through the polymerization of a functional monomer was developed by Drs. Jun Chen, Tyler Cuthbert and Tong Li in the Wulff research group.[16,18,24,68,69] They reported an ester-functionalized DCPD monomer (*f*DCPD). *f*DCPD was discovered during work with *bis*-carboxylated DCPD, known as Thiele's ester.[70–72] The Thiele's ester is not polymerizable because one of the carboxyl groups is attached to the norbornene alkene which prevents its metathesis.

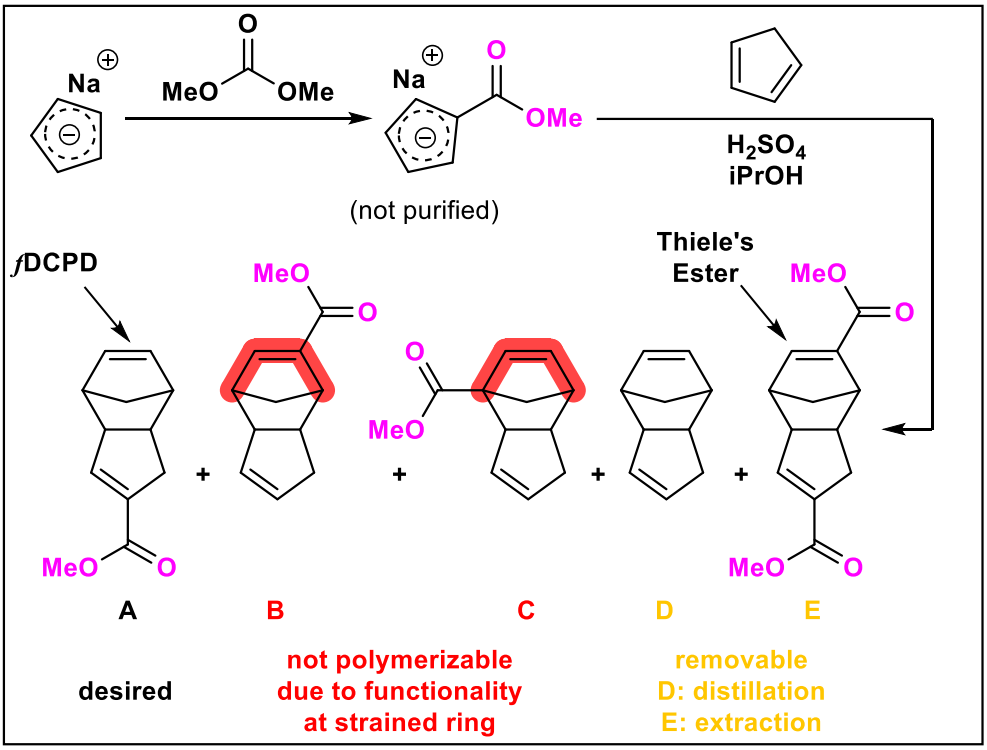

Figure 1.11. Synthesis of *f*DCPD through the Diels-Alder reaction of carboxylated cyclopentadiene (CP) and CP. Adapted with permission from the literature.[24]

To synthesize *f*DCPD, DCPD is first cracked producing cyclopentadiene, sodium hydride is then used to synthesize the sodium cyclopentadiene. The anion is subsequently reacted with the

electrophile dimethyl carbonate and quenched, yielding carboxylated cyclopentadiene. This carboxylated cyclopentadiene then undergoes a Diels-Alder reaction with cyclopentadiene producing *f*DCPD as mixture of isomers.[18,24] *f*DCPD and unreactive regioisomers could easily be isolated through column chromatography on a multi-gram scale (Figure 1.11). *f*DCPD could then be selectively polymerized with the GC2 initiator in the presence of the regioisomer. The resulting linear polymer could then be precipitated away from the regioisomers.[18]

Further work enabled *f*DCPD to be isolated as the sole product of a refined purification strategy. First, the homodimerization products (Theile's ester and DCPD) could be removed by aqueous extraction with hexanes and gentle distillation, respectively. The difference in reactivity between *f*DCPD and the remaining regioisomer allowed for the conjugate addition of a diamine to the regioisomer, enabling its removal through another aqueous extraction (Figure 1.12). Any remaining impurities could be removed with column chromatography. This synthetic route was refined such that over 100 g could be produced in a single batch.[24]

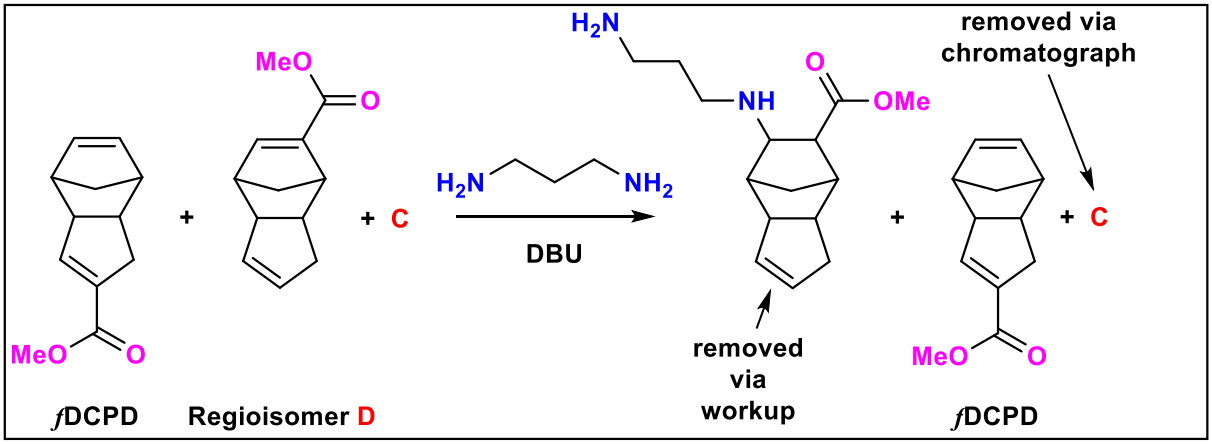

Figure 1.12. Removal of undesired regioisomers by conjugate addition of diamine followed by aqueous workup. Adapted with permission from the literature.[24]

Owing to the inclusion of the ester functional group, this monomer has a pleasant fruity odor instead of the unpleasant acrid odor associated with DCPD. When polymerized as a linear polymer

and subsequently thermally cured, *f*PDCPD had the highest glass transition temperature reported for a PDCPD—172°C—but has since been eclipsed by the next generation of functionalized PDCPD, polydicyclopentadienone (oxaPDCPD, Chapter 2).[18]

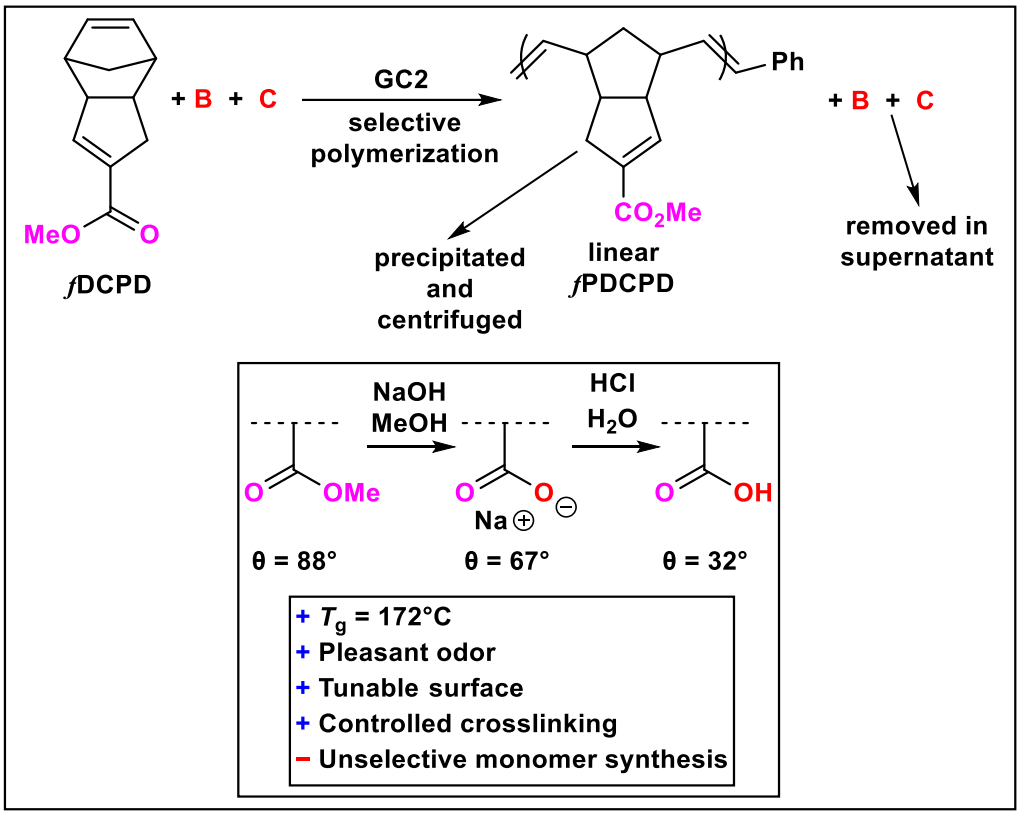

Figure 1.13. Synthesis and purification of linear *f*PDCPD. Inset: Control over the surface energy of the polymer exerted via the installed methyl ester functional group. Adapted with permission from the literature.[18,24]

In addition, the linear polymer could be spin-cast onto a surface and then thermally cured. Then the surface of *f*PDCPD could be tuned through the saponification and/or the hydrolysis of the ester functional group, enabling dramatic changes in surface energy (Figure 1.13).[18] Importantly, the installation of the ester functional group with a sp^2-sp^3 C-C bond removes thermal liability, and *f*PDCPD matches the thermal stability of PDCPD. The controllable thermal crosslinking of the linear *f*PDCPD enabled the precise determination of the structure of the polymer and the associated

mechanism of crosslinking.[16] This was accomplished using FTIR, Raman and solid-state ^{13}C NMR studies using deuterated versions of the linear *f*PDCPD.[16] This work showed that head-to-tail olefin addition reactions around the installed ester were the principal crosslinking mechanism.[16] Backbone olefin addition crosslinks and associated oxidative crosslinking were also shown to be a factors.[16,73]

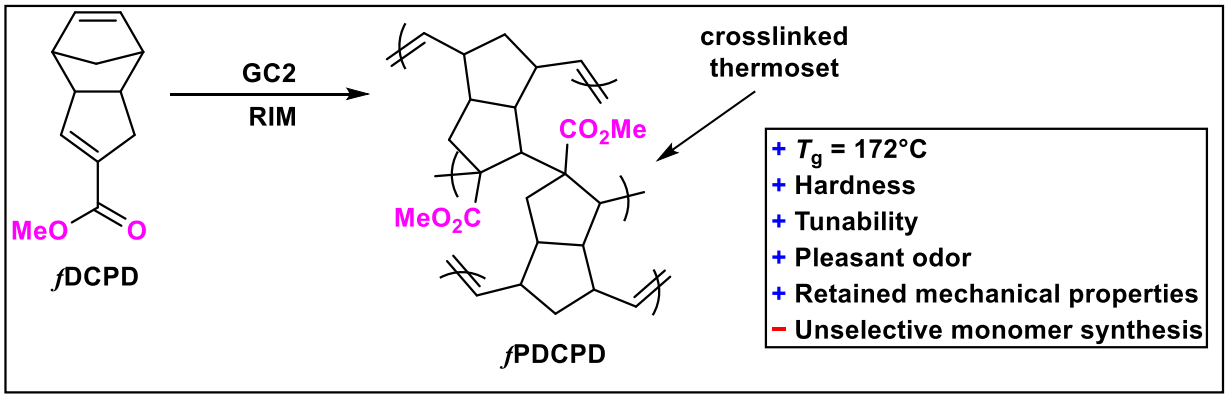

Figure 1.14. Synthesis of crosslinked *f*PDCPD via reaction injection molding.

*f*DCPD was also amenable to reaction injection molding. The reaction injection molding derivative of *f*PDCPD displayed an identical glass transition temperature to the cured linear polymer (Figure 1.14).[24] Dynamic mechanical thermal analysis showed a comparable storage modulus and hardness to regular PDCPD.[24] Vickers microhardness measurements showed *f*PDCPD had a superior hardness to PDCPD.[24] *f*PDCPD has mechanically similar properties to PDCPD but is thermally superior, has an inoffensive odor and offers tunability. More importantly, it has been shown that copolymers produced from mixtures of *f*DCPD and DCPD maintain good mechanical properties and thermal stability while retaining the ability to have a modified surface.[69] The surface of *f*PDCPD—in addition to the aforementioned surface energy tuning through saponification and/or hydrolysis—can be further functionalized with dyes or drugs to create a truly functional polymer.[1,68] Utilizing the controllable crosslinking through the ester, it was shown that

*f*PDCPD could be covalently attached to a glass surface. The surface-bound polymer could then be saponified and could support a variety of moieties for making smart surfaces (Figure 1.15). The surface was shown to be capable of housing the antibiotic chloramphenicol, which imbued the surface with antimicrobial properties towards *E. coli* bacteria (Figure 1.15A).[68] Alternatively, the attachment of cyclic arginine-glycine-aspartate (RGD) peptide, supported the growth of HeLa cells better then commercially available plasma treated tissue culture plates (Figure 1.15B).[68]

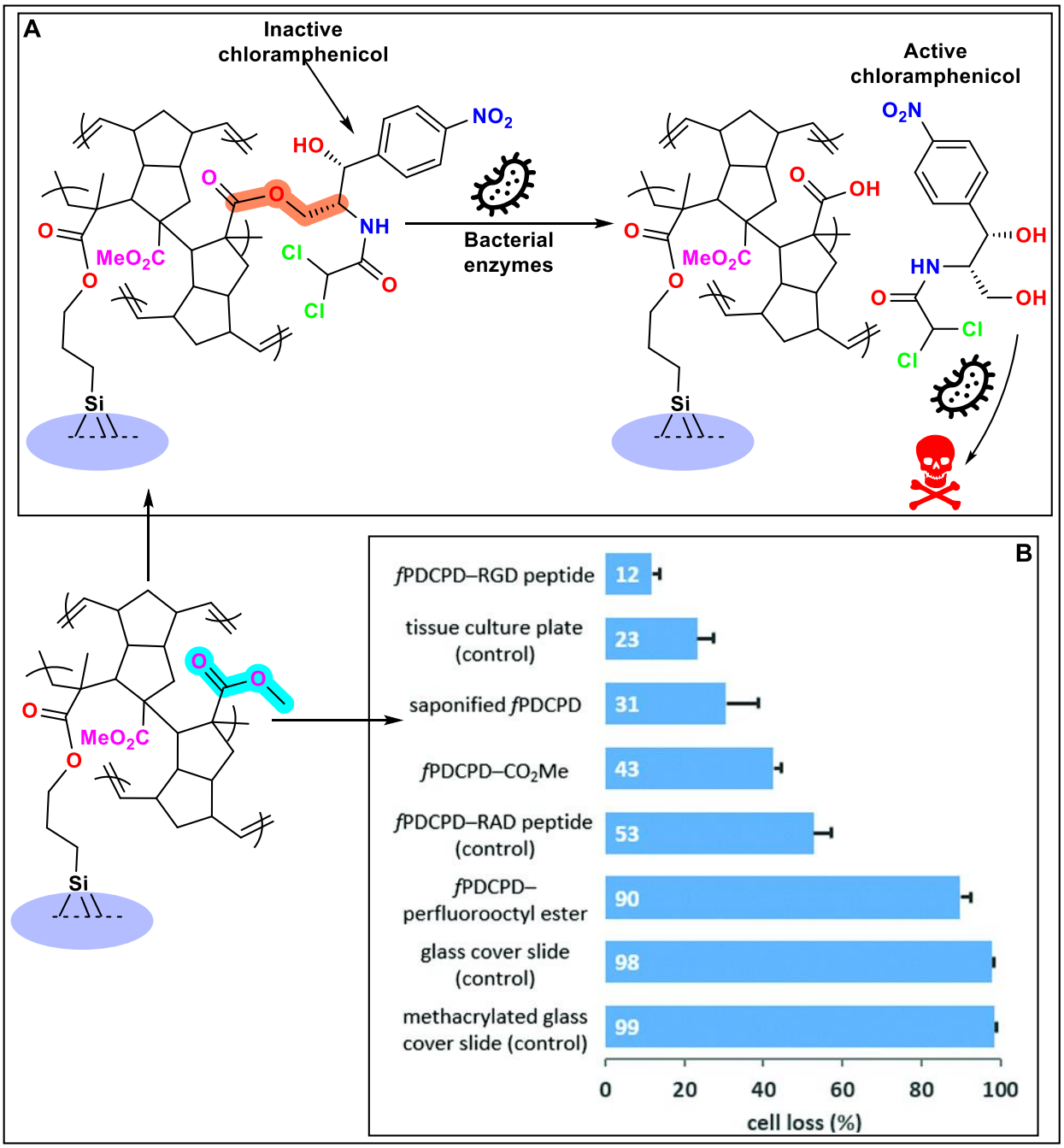

Figure 1.15. A: Smart surface enabled by crosslinked *f*PDCPD loaded with drug. Drug release and activation initiated by endogenous bacterial enzyme. B: Cell surface adhesion controlled by adaptation of crosslinked *f*PDCPD. Adapted with permission from the literature.[68]

This work demonstrates that with judicious selection of the functional group, its linkage, and position it is possible to incorporate functionality into PDCPD through the monomer without introducing thermal liabilities. Li *et al.* have also shown that this functionality can be exploited to produce a functional polymer, significantly improving the potential impact of PDCPD beyond that of just an engineering plastic. Further, they were able to show that these benefits could be conferred without disrupting the mechanical and thermal properties of the material. Additionally, copolymers would retain these functional properties while using significantly less of the potentially expensive *f*DCPD monomer.

Both strategies highlight the potential of functionalized DCPD monomers to produce upgraded, functional PDCPD. However, both have significant limitations that could be improved upon. Production is a key issue, as these methods struggle with atom economy. Xu and Lemcoff's approach require stoichiometric reagents while the route pioneered by Chen *et al.* produces many coproducts. This not only reduces atom economy—though, since the Diels-Alder reaction is reversible, in theory this method could be made to be highly atom economical—it adds significant complexity through purification, which would hinder industry adoption.

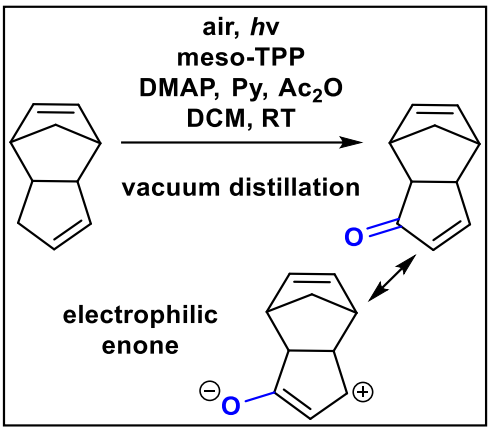

Figure 1.16. Synthesis of oxaDCPD monomer, an enone functionalized DCPD.

Recognizing that the Diels-Alder approach will always require some substantial purification, we pivoted to directly functionalizing DCPD. The allylic position of the cyclopentene can also be oxidized photochemically, producing an enone (Figure 1.16). This enone has been known for some time and used in other syntheses, but it had never been polymerized prior to the work described in this dissertation.[74,75] The installation of the enone adjusts the overall electronics of the molecule, making the unstrained alkene electrophilic (Figure 1.16). The enone-functionalized DCPD (oxaDCPD) can be synthesized directly through a photooxidation using air (oxygen) as the oxidant and a low loading (0.002 mol%) of a commercial photosensitizer. This avoids the use of stoichiometric selenium as an oxidant.[75–82] The study of this remarkable molecule is the subject of the third method for functionalizing PDCPD through the use of functional monomers and is the subject of this dissertation.

1.4. Dissertation Summary

In **Chapter 2**, I first developed a large scale photoreactor in tandem with the University of Victoria glass blower Sean Adams and machinists Chris Secord and Kody Matthews. This enables the synthesis of oxaDCPD to be scaled from 3 to 300 g! I also establish that oxaDCPD can be easily purified using vacuum distillation, an industrially relevant purification method. I then created a lab scale reaction injection molding protocol, which allowed me to directly produce macroscale samples for tensile testing (dogbones), dynamic mechanical thermal analysis (rectangles) and compression testing (cylinders). In collaboration with the Milani research group at the University of British Columbia Okanagan (UBCO), we were able to do complete mechanical and thermal characterization of oxaPDCPD using those samples. We show that oxaPDCPD has superior mechanical and thermal properties when compared to regular PDCPD. Computational chemistry performed by our collaborators in the DiLabio research group at UBCO show that the source of these remarkable improvements in properties is, in part, due to the presence of a non-canonical hydrogen bond between the enone and the beta-hydrogen of an adjacent enone. In addition to the reaction injection molded polymer, I show that oxaPDCPD can be made in a linear fashion as well.

In **Chapter 3**, I showed that the benefits of oxaPDCPD can be realized through the synthesis of copolymers. I synthesized five different copolymers consisting of varying amounts of oxaDCPD and DCPD monomers through reaction injection molding. In addition, I made another five copolymers that incorporated ethylidene norbornene, a common additive to PDCPD formulations in academia. In this study, I reaction injected molded rectangular plaques of material and the samples required for mechanical and thermal testing were cut by the University of Victoria Science machine shop. Using these I explored the mechanical and thermal properties of the copolymers through tensile testing, dynamic mechanical thermal analysis and differential scanning

calorimetry. Using these techniques, I demonstrate that copolymerization could be useful for tuning the mechanical properties of PDCPD-based materials as well as improving the surface energy, and thus adhesion to paints and bonding agents.

In **Chapter 4**, I developed a low-cost, high-throughput technique for the laboratory, in order to benchmark catalysts to produce PDCPD and oxaPDCPD. I tested ten different initiators, three of which are commercially available. The seven other initiators where prepared by our collaborators in the Mauduit Group at the University of Rennes. Using the technique I screened forty different initiator/resin combinations in total and show a general structure–function relationships between the ruthenium initiators and the peak temperature of the reaction injection molding process. Furthermore, I was able to demonstrate that this technique can be used to predict the thermal and mechanical properties of materials simply by observing the peak temperature of the reaction.

Finally, in **Chapter 5**, I investigated the commercial viability of oxaPDCPD during a Natural Sciences and Engineering Research Council of Canada (NSERC) Lab-to-Market (L2M) program at Toronto Metropolitan University. I conducted primary market research in the form of 15 stakeholder interviews to collect qualitative data on the perception of the PDCPD industry to new innovations. I investigated what industry perceives to be the issues associated with PDCPD and identified targetable markets and pain points of the industry that can be addressed by both oxaDCPD and future academic work.

1.5. References

(1) Odian, G. *Principles of Polymerization*, Fourth Edition.; John Wiley & Sons, Inc.: College of Staten Island, 2004.

(2) Callister, W., Jr.; Rethwisch, D. *Materials Science and Engineering an Introduction*, 9th ed.; John Wiley & Sons, Inc.

(3) Schwab, S. T.; Baur, M.; Nelson, T. F.; Mecking, S. Synthesis and Deconstruction of Polyethylene-Type Materials. *Chem. Rev.* **2024**, *124* (5), 2327–2351. https://doi.org/10.1021/acs.chemrev.3c00587.

(4) Karger-Kocsis, J.; Mészáros, L.; Bárány, T. Ground Tyre Rubber (GTR) in Thermoplastics, Thermosets, and Rubbers. *J. Mater. Sci.* **2013**, *48* (1), 1–38. https://doi.org/10.1007/s10853-012-6564-2.

(5) Häußler, M.; Eck, M.; Rothauer, D.; Mecking, S. Closed-Loop Recycling of Polyethylene-like Materials. *Nature* **2021**, *590* (7846), 423–427. https://doi.org/10.1038/s41586-020-03149-9.

(6) Vervacke, D. *An Introduction to PDCPD: Poly-Di-Cyclo-Penta-Diene*; Product Rescue, 2008.

(7) Hayes, G.; Laurel, M.; MacKinnon, D.; Zhao, T.; Houck, H. A.; Becer, C. R. Polymers without Petrochemicals: Sustainable Routes to Conventional Monomers. *Chem. Rev.* **2023**, *123* (5), 2609–2734. https://doi.org/10.1021/acs.chemrev.2c00354.

(8) Bi, L.; Godwin, B.; Baran, M. J.; Nazir, R.; Wulff, J. E. A Cleavable Crosslinking Strategy for Commodity Polymer Functionalization and Generation of Reprocessable Thermosets. *Angew. Chem. Int. Ed.* **2023**, *62* (30), e202304708. https://doi.org/10.1002/anie.202304708.

(9) Lepage, M. L.; Simhadri, C.; Liu, C.; Takaffoli, M.; Bi, L.; Crawford, B.; Milani, A. S.; Wulff, J. E. A Broadly Applicable Cross-Linker for Aliphatic Polymers Containing C–H Bonds. *Science* **2019**, *366* (6467), 875–878. https://doi.org/10.1126/science.aay6230.

(10) Long, T. R.; Elder, R. M.; Bain, E. D.; Masser, K. A.; Sirk, T. W.; Yu, J. H.; Knorr, D. B.; Lenhart, J. L. Influence of Molecular Weight between Crosslinks on the Mechanical Properties of Polymers Formed via Ring-Opening Metathesis. *Soft Matter.* **2018**, *14* (17), 3344–3360. https://doi.org/10.1039/C7SM02407J.

(11) Godwin, B.; Anvari, M. H.; Olfatbakhsh, T.; Mahbod, M.; Milani, A. S.; DiLabio, G. A.; Wulff, J. E. A Single-Atom Upgrade to Polydicyclopentadiene. *Macromolecules* **2023**, *56* (4), 1592–1600. https://doi.org/10.1021/acs.macromol.2c02260.

(12) Vollmer, I.; Jenks, M. J. F.; Roelands, M. C. P.; White, R. J.; van Harmelen, T.; de Wild, P.; van der Laan, G. P.; Meirer, F.; Keurentjes, J. T. F.; Weckhuysen, B. M. Beyond Mechanical Recycling: Giving New Life to Plastic Waste. *Angew. Chem. Int. Ed.* **2020**, *59* (36), 15402–15423. https://doi.org/10.1002/anie.201915651.

(13) Clarke, R. W.; Sandmeier, T.; Franklin, K. A.; Reich, D.; Zhang, X.; Vengallur, N.; Patra, T. K.; Tannenbaum, R. J.; Adhikari, S.; Kumar, S. K.; Rovis, T.; Chen, E. Y.-X. Dynamic Crosslinking Compatibilizes Immiscible Mixed Plastics. *Nature* **2023**, *616* (7958), 731–739. https://doi.org/10.1038/s41586-023-05858-3.

(14) Shieh, P.; Zhang, W.; Husted, K. E. L.; Kristufek, S. L.; Xiong, B.; Lundberg, D. J.; Lem, J.; Veysset, D.; Sun, Y.; Nelson, K. A.; Plata, D. L.; Johnson, J. A. Cleavable Comonomers Enable Degradable, Recyclable Thermoset Plastics. *Nature* **2020**, *583* (7817), 542–547. https://doi.org/10.1038/s41586-020-2495-2.

(15) Lin, W.; Shao, Z.; Dong, J.; Chung, T. C. M. Cross-Linked Polypropylene Prepared by PP Copolymers Containing Flexible Styrene Groups. *Macromolecules* **2009**, *42* (11), 3750–3754. https://doi.org/10.1021/ma9002775.

(16) Cuthbert, T. J.; Li, T.; Speed, A. W. H.; Wulff, J. E. Structure of the Thermally Induced Cross-Link in C -Linked Methyl Ester-Functionalized Polydicyclopentadiene (f PDCPD). *Macromolecules* **2018**, *51* (5), 2038–2047. https://doi.org/10.1021/acs.macromol.7b02750.

(17) Liu, C.; Morimoto, N.; Jiang, L.; Kawahara, S.; Noritomi, T.; Yokoyama, H.; Mayumi, K.; Ito, K. Tough Hydrogels with Rapid Self-Reinforcement. *Science* **2021**, *372* (6546), 1078–1081. https://doi.org/10.1126/science.aaz6694.

(18) Chen, J.; Burns, F. P.; Moffitt, M. G.; Wulff, J. E. Thermally Crosslinked Functionalized Polydicyclopentadiene with a High Tg and Tunable Surface Energy. *ACS Omega* **2016**, *1* (4), 532–540. https://doi.org/10.1021/acsomega.6b00193.

(19) Kong, Y.; Hay, J. N. The Measurement of the Crystallinity of Polymers by DSC. *Polym.* **2002**, *43* (14), 3873–3878. https://doi.org/10.1016/S0032-3861(02)00235-5.

(20) Lepage, M. L.; Takaffoli, M.; Simhadri, C.; Mandau, R.; Gashti, M. P.; Nazir, R.; Mohseni, M.; Li, W.; Liu, C.; Bi, L.; Falck, G.; Berrang, P.; Golovin, K.; Milani, A. S.; DiLabio, G. A.; Wulff, J. E. Influence of Topical Cross-Linking on Mechanical and Ballistic Performance of a Woven Ultra-High-Molecular-Weight Polyethylene Fabric Used in Soft Body Armor. *ACS Appl. Polym. Mater.* **2021**, *3* (11), 6008–6018. https://doi.org/10.1021/acsapm.1c01301.

(21) Gooneie, A.; Simonetti, P.; Rupper, P.; Nazir, R.; Jovic, M.; Gaan, S.; Heuberger, M. P.; Hufenus, R. Stabilizing Effects of Novel Phosphorus Flame Retardant on PET for High-

Temperature Applications. *Mater. Lett.* **2020**, *276*, 128225. https://doi.org/10.1016/j.matlet.2020.128225.

(22) Nazir, R.; Parida, D.; Borgstädt, J.; Lehner, S.; Jovic, M.; Rentsch, D.; Bülbül, E.; Huch, A.; Altenried, S.; Ren, Q.; Rupper, P.; Annaheim, S.; Gaan, S. In-Situ Phosphine Oxide Physical Networks: A Facile Strategy to Achieve Durable Flame Retardant and Antimicrobial Treatments of Cellulose. *Chem. Eng. J.* **2021**, *417*, 128028. https://doi.org/10.1016/j.cej.2020.128028.

(23) Nazir, R.; Gooneie, A.; Lehner, S.; Jovic, M.; Rupper, P.; Ott, N.; Hufenus, R.; Gaan, S. Alkyl Sulfone Bridged Phosphorus Flame-Retardants for Polypropylene. *Mater. Des.* **2021**, *200*, 109459. https://doi.org/10.1016/j.matdes.2021.109459.

(24) Cuthbert, T. J.; Li, T.; Wulff, J. E. Production and Dynamic Mechanical Analysis of Macro-Scale Functionalized Polydicyclopentadiene Objects Facilitated by Rational Synthesis and Reaction Injection Molding. *ACS Appl. Polym. Mater.* **2019**, *1* (9), 2460–2471. https://doi.org/10.1021/acsapm.9b00571.

(25) Long, T. R.; Elder, R. M.; Bain, E. D.; Masser, K. A.; Sirk, T. W.; Yu, J. H.; Knorr, D. B.; Lenhart, J. L. Influence of Molecular Weight between Crosslinks on the Mechanical Properties of Polymers Formed via Ring-Opening Metathesis. *Soft Matter.* **2018**, *14* (17), 3344–3360. https://doi.org/10.1039/C7SM02407J.

(26) S. Phatake, R.; Masarwa, A.; Gabriel Lemcoff, N.; Reany, O. Tuning Thermal Properties of Cross-Linked DCPD Polymers by Functionalization, Initiator Type and Curing Methods. *Polym. Chem.* **2020**, *11* (10), 1742–1751. https://doi.org/10.1039/C9PY01178A.

(27) Ma, S.; Webster, D. C. Degradable Thermosets Based on Labile Bonds or Linkages: A Review. *Prog. Polym. Sci.* **2018**, *76*, 65–110. https://doi.org/10.1016/j.progpolymsci.2017.07.008.

(28) Husted, K. E. L.; Brown, C. M.; Shieh, P.; Kevlishvili, I.; Kristufek, S. L.; Zafar, H.; Accardo, J. V.; Cooper, J. C.; Klausen, R. S.; Kulik, H. J.; Moore, J. S.; Sottos, N. R.; Kalow, J. A.; Johnson, J. A. Remolding and Deconstruction of Industrial Thermosets via Carboxylic Acid-Catalyzed Bifunctional Silyl Ether Exchange. *J. Am. Chem. Soc.* **2023**, *145* (3), 1916–1923. https://doi.org/10.1021/jacs.2c11858.

(29) Nazir, R.; Bi, L.; Musolino, S. F.; Margoto, O. H.; Çelebi, K.; Mobuchon, C.; Takaffoli, M.; Milani, A. S.; Falck, G.; Wulff, J. E. Polyamine–Diazirine Conjugates for Use as Primers in UHMWPE–Epoxy Composite Materials. *ACS Appl. Polym. Mater.* **2022**, *4* (3), 1728–1742. https://doi.org/10.1021/acsapm.1c01577.

(30) Khan, F.; Hossain, N.; Mim, J. J.; Rahman, S. M.; Iqbal, Md. J.; Billah, M.; Chowdhury, M. A. Advances of Composite Materials in Automobile Applications – A Review. *J. Eng. Res.* **2024**. https://doi.org/10.1016/j.jer.2024.02.017.

(31) Wazalwar, R.; Sahu, M.; Raichur, A. M. Mechanical Properties of Aerospace Epoxy Composites Reinforced with 2D Nano-Fillers: Current Status and Road to Industrialization. *Nanoscale Adv.* **2021**, *3* (10), 2741–2776. https://doi.org/10.1039/D1NA00050K.

(32) Vallons, K. A. M.; Drozdzak, R.; Charret, M.; Lomov, S. V.; Verpoest, I. Assessment of the Mechanical Behaviour of Glass Fibre Composites with a Tough Polydicyclopentadiene (PDCPD) Matrix. *Composites, Part A.* **2015**, *78*, 191–200. https://doi.org/10.1016/j.compositesa.2015.08.016.

(33) Li, Z.-J.; Wang, F.-S.; Lai, Y.-C.; Shi, Z.-E.; Yu, Y.-H. Flexible Epoxy Graphene Thermoset with Excellent Weather and Corrosion Resistance. *Prog. Org. Coat.* **2021**, *151*, 106052. https://doi.org/10.1016/j.porgcoat.2020.106052.

(34) Long, T. R.; Knorr, D. B.; Masser, K. A.; Elder, R. M.; Sirk, T. W.; Hindenlang, M. D.; Yu, J. H.; Richardson, A. D.; Boyd, S. E.; Spurgeon, W. A.; Lenhart, J. L. Ballistic Response of Polydicyclopentadiene vs. Epoxy Resins and Effects of Crosslinking. In *Dynamic Behavior of Materials, Volume 1*; Casem, D., Lamberson, L., Kimberley, J., Eds.; Conference Proceedings of the Society for Experimental Mechanics Series; Springer International Publishing: Cham, 2017; pp 285–290. https://doi.org/10.1007/978-3-319-41132-3_37.

(35) Hodrick, J. T.; Severson, E. P.; McAlister, D. S.; Dahl, B.; Hofmann, A. A. Highly Crosslinked Polyethylene Is Safe for Use in Total Knee Arthroplasty. *Clin. Orthop. Relat. Res.* **2008**, *466* (11), 2806–2812. https://doi.org/10.1007/s11999-008-0472-4.

(36) Geerdink, C. H.; Grimm, B.; Ramakrishnan, R.; Rondhuis, J.; Verburg, A. J.; Tonino, A. J. Crosslinked Polyethylene Compared to Conventional Polyethylene in Total Hip Replacement: Pre-Clinical Evaluation, in-Vitro Testing and Prospective Clinical Follow-up Study. *Acta Orthopaedica* **2006**, *77* (5), 719–725. https://doi.org/10.1080/17453670610012890.

(37) Zhang, H.; Heng, Z.; Zhou, J.; Shen, L.; Chen, Y.; Zou, H.; Liang, M. Robust Organic Semiconductor Thermoset Composite Films Based on Crystallization-Driven Self-Assembled Nanofibers of Poly(3-Hexylthiophene) Block Copolymers. *Chem. Eng. J.* **2022**, *430*, 132695. https://doi.org/10.1016/j.cej.2021.132695.

(38) Vespa, M.; R. MacFarlane, L.; M. Hudson, Z.; Manners, I. Crystallization-Driven Self-Assembly of Poly(3-Hexylthiophene)- b -Poly(2,5-Bis(2-Ethylhexyloxy) p -Phenylene), a π-

Conjugated Diblock Copolymer with a Rigid Rod Corona-Forming Block. *Polym. Chem.* **2024**, *15* (18), 1839–1850. https://doi.org/10.1039/D4PY00154K.

(39) Sebrei, L. B.; Boord, C. E. 1-Mercaptobenzothiazole and Its Derivatives as Accelerators of Rubber Vulcanization. *Ind. Eng. Chem.* **1923**, *15* (10), 1009–1014. https://doi.org/10.1021/ie50166a009.

(40) *Global natural & synthetic rubber consumption 1990-H1 2023*. Statista. https://www.statista.com/statistics/275399/world-consumption-of-natural-and-synthetic-caoutchouc/ (accessed 2024-07-21).

(41) Bi, L. Efficient Upcycling of Low-Functionality Polymers Using Trifluoromethyl Aryl Diazirine Chemistry, University of Victoria, Victoria, 2023.

(42) Bueche, F. Mechanical Properties of Natural and Synthetic Rubbers. *J. Polym. Sci.* **1957**, *25* (110), 305–324. https://doi.org/10.1002/pol.1957.1202511005.

(43) Yazıcı, N.; Kodal, M.; Özkoç, G. Lab-Scale Twin-Screw Micro-Compounders as a New Rubber-Mixing Tool: 'A Comparison on EPDM/Carbon Black and EPDM/Silica Composites.' *Polymers* **2021**, *13* (24), 4391. https://doi.org/10.3390/polym13244391.

(44) Trauth, A.; Pinter, P.; Weidenmann, K. A. Investigation of Quasi-Static and Dynamic Material Properties of a Structural Sheet Molding Compound Combined with Acoustic Emission Damage Analysis. *J. Compos. Sci.* **2017**, *1* (2), 18. https://doi.org/10.3390/jcs1020018.

(45) Boylan, S.; Castro, J. M. Effect of Reinforcement Type and Length on Physical Properties, Surface Quality, and Cycle Time for Sheet Molding Compound (SMC) Compression Molded Parts. *J. Appl. Polym. Sci.* **2003**, *90* (9), 2557–2571. https://doi.org/10.1002/app.12726.

(46) Cabrera-Ríos, M.; Castro, J. M. An Economical Way of Using Carbon Fibers in Sheet Molding Compound Compression Molding for Automotive Applications. *Polym. Compo.* **2006**, *27* (6), 718–722. https://doi.org/10.1002/pc.20257.

(47) Wulfsberg, J.; Herrmann, A.; Ziegmann, G.; Lonsdorfer, G.; Stöß, N.; Fette, M. Combination of Carbon Fibre Sheet Moulding Compound and Prepreg Compression Moulding in Aerospace Industry. *Procedia Eng.* **2014**, *81*, 1601–1607. https://doi.org/10.1016/j.proeng.2014.10.197.

(48) Koo, M. S.; Chung, K.; Youn, J. R. Reaction Injection Molding of Polyurethane Foam for Improved Thermal Insulation. *Polym. Eng. Sci.* **2001**, *41* (7), 1177–1186. https://doi.org/10.1002/pen.10819.

(49) Minchak, R. J. Cyclopentene-Dicyclopentadiene Copolymers and Method of Making Same. US4002815A, January 11, 1977.

(50) Klosiewicz, D. W. Method for Making a Dicyclopentadiene Thermoset Polymer. US4400340A, August 23, 1983.

(51) Matlack, A. S. Metathesis Polymerization of Thermally Oligomerized Dicyclopentadiene. US4703098A, October 27, 1987

(52) Espy, H. H.; Matlack, A. S. Conversion of Solid Dicyclopentadiene to a Liquid Monomer for Use in Reaction Injection Molding. EP0271007A2, June 15, 1988.

(53) Klosiewicz, D. W.; Tom, G. M. A Dicyclopentadiene Thermoset Polymer and a Catalyst and a Method for Making It. EP0084888B1, June 16, 1987.

(54) Khasat, N. P.; Leach, D. Polydicyclopentadiene Having Improved Stability and Toughened with Polymeric Particles. US5480940A, January 2, 1996.

(55) Kovačič, S.; Slugovc, C. Ring-Opening Metathesis Polymerisation Derived Poly(Dicyclopentadiene) Based Materials. *Mater. Chem. Front.* **2020**, *4* (8), 2235–2255. https://doi.org/10.1039/D0QM00296H.

(56) Le Gac, P. Y.; Choqueuse, D.; Paris, M.; Recher, G.; Zimmer, C.; Melot, D. Durability of Polydicyclopentadiene under High Temperature, High Pressure and Seawater (Offshore Oil Production Conditions). *Polym. Degrad. Stab.* **2013**, *98* (3), 809–817. https://doi.org/10.1016/j.polymdegradstab.2012.12.023.

(57) Saha, S.; Ginzburg, Y.; Rozenberg, I.; Iliashevsky, O.; Ben-Asuly, A.; Lemcoff, N. G. Cross-Linked ROMP Polymers Based on Odourless Dicyclopentadiene Derivatives. *Polym. Chem.* **2016**, *7* (18), 3071–3075. https://doi.org/10.1039/C6PY00378H.

(58) Gong, L.; Liu, K.; Ou, E.; Xu, F.; Lu, Y.; Wang, Z.; Gao, T.; Yang, Z.; Xu, W. ROMP of Acetoxy-Substituted Dicyclopentadiene to a Linear Polymer with a High Tg. *RSC Adv.* **2015**, *5* (33), 26185–26188. https://doi.org/10.1039/C5RA01855B.

(59) Rosenblum, M. Preparation and Thermal Rearrangement of Several Dicyclopentadiene Derivatives. *J. Am. Chem. Soc.* **1957**, *79* (12), 3179–3181. https://doi.org/10.1021/ja01569a050.

(60) Woodward, R. B.; Katz, T. J. The Mechanism of the Diels-Alder Reaction. *Tetrahedron* **1959**, *5* (1), 70–89. https://doi.org/10.1016/0040-4020(59)80072-7.

(61) Mironov, V. A.; Fadeeva, T. M.; Stepanyants, A. U.; Akhrem, A. A. Thermal Isomerization of 1-Methylcyclopentadiene. *Russ. Chem. Bull.* **1967**, *16* (2), 418–420. https://doi.org/10.1007/BF00912463.

(62) Abadie, M. J.; Dimonie, M.; Couve, C.; Dragutan, V. New Catalysts for Linear Polydicyclopentadiene Synthesis. *Eur. Polym. J.* **2000**, *36* (6), 1213–1219. https://doi.org/10.1016/S0014-3057(99)00185-8.

(63) Constable, G. S.; Lesser, A. J.; Coughlin, E. B. Morphological and Mechanical Evaluation of Hybrid Organic−Inorganic Thermoset Copolymers of Dicyclopentadiene and Mono- or Tris(Norbornenyl)-Substituted Polyhedral Oligomeric Silsesquioxanes. *Macromolecules* **2004**, *37* (4), 1276–1282. https://doi.org/10.1021/ma034989w.

(64) Suslick, B. A.; Stawiasz, K. J.; Paul, J. E.; Sottos, N. R.; Moore, J. S. Survey of Catalysts for Frontal Ring-Opening Metathesis Polymerization. *Macromolecules* **2021**, *54* (11), 5117–5123. https://doi.org/10.1021/acs.macromol.1c00566.

(65) Niimi, A. J.; Laham, Q. N. Relative Toxicity of Organic and Inorganic Compounds of Selenium to Newly Hatched Zebrafish (Brachydanio Rerio). *Can. J. Zool.* **1976**, *54* (4), 501–509. https://doi.org/10.1139/z76-056.

(66) Hadrup, N.; Ravn-Haren, G. Acute Human Toxicity and Mortality after Selenium Ingestion: A Review. *J. Trace Elem. Med. and Bio.* **2020**, *58*, 126435. https://doi.org/10.1016/j.jtemb.2019.126435.

(67) Köppel, C.; Baudisch, H.; Beyer, K. H.; Klöppel, I.; Schneider, Prof. V. Fatal Poisoning with Selenium Dioxide. *J. Toxicol. Clin. Toxicol.* **1986**, *24* (1), 21–35. https://doi.org/10.3109/15563658608990443.

(68) Li, T.; Shumka, H.; J. Cuthbert, T.; Liu, C.; E. Wulff, J. Harnessing the Surface Chemistry of Methyl Ester Functionalized Polydicyclopentadiene and Exploring Surface Bioactivity. *Mater. Adv.* **2020**, *1* (6), 1753–1762. https://doi.org/10.1039/D0MA00480D.

(69) Li, T.; Wulff, J. E. Copolymers of Functionalized and Nonfunctionalized Polydicyclopentadiene. *ACS Appl. Polym. Mater.* **2021**, *3* (1), 110–115. https://doi.org/10.1021/acsapm.0c01196.

(70) Chen, J. Applications of Thiele's Ester Derivatives from Biological to Material. **2018**.

(71) Chen, J.; Wulff, J. E. Revisiting the Mechanistic Origins of Thiele's Ester Dimerization: Probing the Reliability of Predictive Models for Cycloadditions. *Org. and Biomol. Chem.* **2016**, *14* (43), 10170–10174. https://doi.org/10.1039/c6ob02218a.

(72) Chen, J.; Kilpatrick, B.; Oliver, A. G.; Wulff, J. E. Expansion of Thieles Acid Chemistry in Pursuit of a Suite of Conformationally Constrained Scaffolds. *J. Org. Chem.* **2015**, *80* (18), 8979–8989. https://doi.org/10.1021/acs.joc.5b01332.

(73) David, A.; Huang, J.; Richaud, E.; Yves Le Gac, P. Impact of Thermal Oxidation on Mechanical Behavior of Polydicylopentadiene: Case of Non-Diffusion Limited Oxidation. *Polym Degrad. Stab.* **2020**, *179*, 109294. https://doi.org/10.1016/j.polymdegradstab.2020.109294.

(74) Shao, C.; Yu, H.-J.; Wu, N.-Y.; Feng, C.-G.; Lin, G.-Q. C1-Symmetric Dicyclopentadienes as New Chiral Diene Ligands for Asymmetric Rhodium-Catalyzed Arylation of N-Tosylarylimines. *Org. Lett.* **2010**, *12* (17), 3820–3823. https://doi.org/10.1021/ol101531r.

(75) Li, J.; Stoltz, B. M.; Grubbs, R. H. Enantioselective Synthesis of 15-Deoxy-Δ12,14-Prostaglandin J2. *Org. Lett.* **2019**, *21* (24), 10139–10142. https://doi.org/10.1021/acs.orglett.9b04198.

(76) Silvestrini, M.; Ciappa, A.; Fabris, F.; Borsato, G.; De Lucchi, O. Detection of Singlet Oxygen Generated by Commercial Fine Art Organic Pigments by Means of a Novel, Robust Chemical Probe. *Dyes Pigm.* **2012**, *92* (3), 1351–1354. https://doi.org/10.1016/j.dyepig.2011.09.018.

(77) Kuga, T.; Sasano, Y.; Iwabuchi, Y. IBX as a Catalyst for Dehydration of Hydroperoxides: Green Entry to α,β-Unsaturated Ketones via Oxygenative Allylic Transposition. *Chem. Commun.* **2018**, *54* (7), 798–801. https://doi.org/10.1039/C7CC08957K.

(78) Álvarez, C.; Peláez, R.; Medarde, M. New Dicyclopentadiene-Based Scaffolds. *Tetrahedron* **2007**, *63* (10), 2132–2141. https://doi.org/10.1016/j.tet.2007.01.001.

(79) Mihelich, E. D.; Eickhoff, D. J. One-Pot Conversion of Olefins to a,β-Unsaturated Carbonyl Compounds. An Easy Synthesis of 2-Cyclopentenone and Related Compounds. *J. Org. Chem.* **1983**, *48* (22), 4135–4137. https://doi.org/10.1021/jo00170a060.

(80) Benaglia, M.; Danelli, T.; Fabris, F.; Sperandio, D.; Pozzi, G. Poly(Ethylene Glycol)-Supported Tetrahydroxyphenyl Porphyrin: A Convenient, Recyclable Catalyst for Photooxidation Reactions. *Org. Lett.* **2002**, *4* (24), 4229–4232. https://doi.org/10.1021/ol0267230.

(81) Pozzi, G.; Mercs, L.; Holczknecht, O.; Martimbianco, F.; Fabris, F. Straightforward Synthesis of a Fluorous Tetraarylporphyrin: An Efficient and Recyclable Sensitizer for Photooxygenation Reactions. *Adv. Synth. Catal.* **2006**, *348* (12–13), 1611–1620. https://doi.org/10.1002/adsc.200606092.

(82) Borsato, G.; De Lucchi, O.; Fabris, F.; Lucchini, V.; Frascella, P.; Zambon, A. Synthesis and Evaluation of New Chiral Diols Based on the Dicyclopentadiene Skeleton. *Tetrahedron Lett.* **2003**, *44* (17), 3517–3520. https://doi.org/10.1016/S0040-4039(03)00664-6.

Chapter 2: A Single-Atom Upgrade to Polydicyclopentadiene

Benjamin Godwin[a], Monir H. Anvari, Tina Olfatbakhsh , Mahshid Mahbod, Abbas S. Milani, Gino A. DiLabio, and Jeremy E. Wulff

2.0. Contributions

Synthetic work, sample preparation, dynamic mechanical thermal analysis, contact angle measurements, swelling measurements, IR spectroscopy, differential scanning calorimetry, and ^{1}H and ^{13}C solution NMR was performed by Benjamin Godwin. Computational work was performed by Monir H. Anvari and Prof. Gino Dilabio at the University of British Columbia, Okanagen Campus. Mechanical testing was performed by Tina Olfatbakhsh and Mahshid Mahbod under the supervision of Prof. Abbas S. Milani at the University of British Columbia, Okanagen Campus. Ballistics measurements were conducted by Ryan Mandau at the University of British Columbia, Okanagen Campus Survive and Thrive Applied Research laboratory. The photoreactor was built by Sean Adams, Kody Matthews and Chris Secord at the University of Victoria. Solid state ^{13}C NMR spectroscopy was performed by Eric Ye at the Simon Fraser University.

2.1. Abstract:

Chemical crosslinks within polymers increase mechanical strength and rigidity. Such crosslinks can either be irreversible (e.g. those derived from carbon–carbon bonds) or reversible (e.g. those that depend on X–H···O hydrogen bonds). Here we describe a ketone-functionalized derivative of polydicyclopentadiene that establishes an unprecedented network of vinyl C–H···O hydrogen bonds within the polymer. The resulting thermoset displays a significantly increased glass transition temperature relative to the unfunctionalized polymer, together with enhancements to storage modulus, Young's modulus, and compression strength.

2.2. Introduction:

Polydicyclopentadiene (PDCPD; $\mathbf{1_{p,c}}$) is a tough, highly crosslinked thermoset polymer that is used industrially to make body panels for heavy-duty trucks and construction vehicles.[1,2] Much of PDCPD's utility can be traced to its high storage modulus (*ca.* 1 GPa), excellent thermal stability (up to *ca.* 380 °C) and good tensile strength (*ca.* 40 MPa), together with a high glass transition temperature (*ca.* 160 °C)[3] that is correlated with a good performance at both high and low operating temperatures. Nonetheless, PDCPD has certain disadvantages that have restricted its broader application in society. These include a low surface energy when freshly prepared—making it difficult to apply paints or coatings without a surface-oxidation step—together with a lack of chemical tunability, and a lack of recyclability without the incorporation of specifically designed cleavable units within the polymer chain.[4,5] Moreover, the final polymer material is often plagued by a persistent, unpleasant odor (owing to residual dicyclopentadiene monomer)[2,6] and the low intrinsic polarity makes it a challenge to manufacture fiber-reinforced composites using PDCPD as a matrix.[7,8]

In principle, many of these disadvantages could be solved by adding a functional group to the dicyclopentadiene monomer ($\mathbf{1_m}$; DCPD). Doing so would reduce or eliminate odor (thanks to a

reduced vapor pressure), and would increase surface energy while potentially installing functional group ‘handles’ that could be leveraged for chemical recycling strategies. In addition, the presence of surface functional groups could allow one to conveniently attach sensors, dyes, or bioactive elements.[9] However, because the DCPD monomer is itself a Diels–Alder homodimer of cyclopentadiene, it is challenging to add functionality in such a way that the strained norbornene double bond—which is required for polymerization—is unaffected.

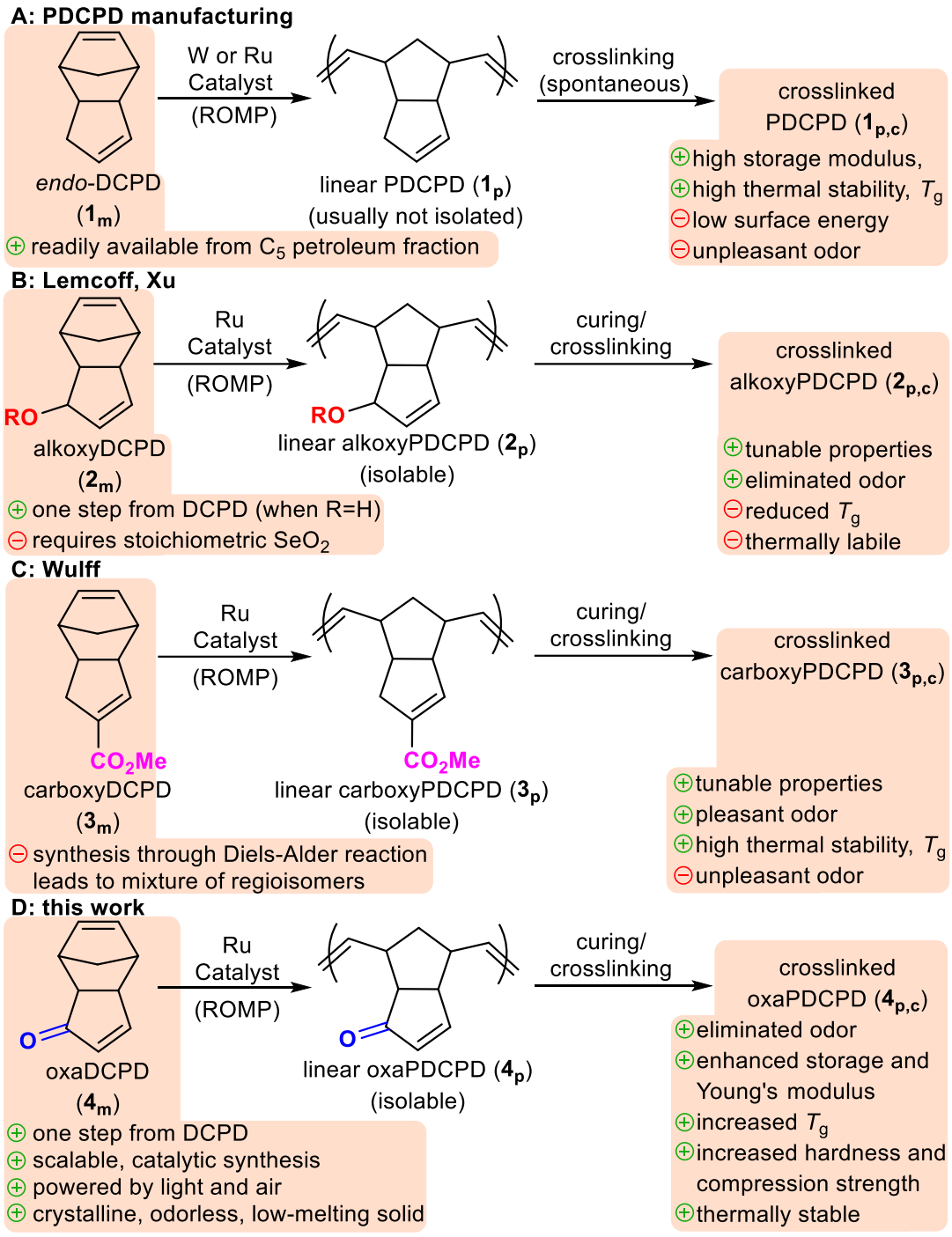

Figure 2.1. Polydicyclopentadiene manufacturing, previous approaches to functionalized forms of PDCPD, and the current work describing an upgraded form of functionalized PDCPD. See Figure A46 in Appendix A for structures of likely crosslink motifs present within the various cured products.

To date, two general strategies have emerged to permit functionalization of the DCPD monomer, in such a way that polymerization is still maintained, and a functionalized polymer product is produced. In the first of these strategies, the Xu[10] and Lemcoff[6,11] groups separately reported the allylic oxidation of dicyclopentadiene[12–14] using stoichiometric quantities of toxic selenium dioxide.[15,16] The resulting allylic alcohol (**2$_m$**, Figure 2.1) could be further functionalized by esterification or etherification, after which polymerization afforded the desired functionalized material (**2$_p$** and **2$_{p,c}$**). Unfortunately the presence of allylic alcohol or allylic ester/ether groups within the final product allows for facile heterolytic bond cleavage at elevated temperatures, which leads polymers **2$_{p,c}$** to exhibit step-function decomposition above *ca.* 220 °C.[6] Additionally, polymers manufactured from **2$_m$** generally exhibit glass transition temperatures of <100 °C.[6,11]

Our lab took a different approach, adding a functional group (a *C*-linked methyl ester) through a strong sp^2–sp^2 linkage at the less-strained alkene of the monomer (**3$_m$**, Figure 2.1).[17–20] This yielded a polymer product (**3$_p$** and **3$_{p,c}$**) with superior properties, in which the T_g, storage modulus, and thermal stability were all broadly equivalent to those of the parent PDCPD, but where the surface energy could be readily tuned (or even patterned) through surface saponification,[17–19] and where dyes or drug molecules could be attached through esterification or amidation protocols.[9] Unfortunately, while **3$_{p,c}$** (which could be readily manufactured through reaction-injection molding, akin to PDCPD itself) had many desirable features, the requisite ester-containing *monomer* was somewhat challenging to synthesize on >100-gram scale, since its production through the partially selective Diels-Alder reaction of cyclopentadiene and carboxylated cyclopentadiene necessarily led to a mixture of regioisomers, only one of which was a substrate for metathesis polymerization.

Seeking to combine the positive attributes of **2** (easy monomer synthesis) and **3** (desirable polymer properties), while eliminating the disadvantages noted above (e.g. the use of toxic oxidants or the need to purify away regioisomers at the monomer stage), we were attracted to the possibility of polymerizing dicyclopentadien-1-one (oxaDCPD; $\mathbf{4_m}$). Ketone $\mathbf{4_m}$ has long been known (in both *endo* and *exo* diastereomeric forms) as an intermediate in complex-molecule synthesis,[21–30] but its polymerization by ring-opening metathesis polymerization (ROMP) methods has not previously been described.[31–33] Compellingly, the 1-step oxidation[34] of DCPD ($\mathbf{1_m}$) to $\mathbf{4_m}$ has been reported previously under photocatalytic conditions, and is known to afford only a single regioisomer of the target compound, in good yield.[38–43] If this reaction could be adapted toward large-scale production, it could provide an attractive monomer synthesis that is both economically and environmentally sustainable. Moreover, if polymerization of $\mathbf{4_m}$ were to proceed similarly to the previously known functionalized monomers $\mathbf{2_m}$ and $\mathbf{3_m}$, this could afford a novel functionalized polydicyclopentadiene ($\mathbf{4_p}$ and/or $\mathbf{4_{p,c}}$) that has a somewhat increased surface energy relative to the parent PDCPD (due to the polar ketone group), while also encoding a useful synthetic handle for further derivatization and avoiding the labile allylic alcohol (or allylic ester) functionality that limited the high-temperature performance and T_g in polymer $\mathbf{2_p}$).

Here we describe an optimized method for producing monomer $\mathbf{4_m}$, its successful polymerization to afford functionalized linear ($\mathbf{4_p}$) and crosslinked ($\mathbf{4_{p,c}}$) polymer materials, and a detailed assessment of the mechanical properties of macro-scale objects made using reaction-injection molding. Remarkably, we find that not only does $\mathbf{4_{p,c}}$ meet the standard for thermal stability set by the parent DCPD ($\mathbf{1_{p,c}}$), it significantly exceeds DCPD's benchmarks in T_g, storage modulus, Young's modulus, tensile strength, and compression strength. Computational modeling (using both molecular mechanics and DFT methods), together with control experiments carried out on a

partially hydrogenated version of **4p**, reveals that the enhancement of material properties is due to both dipolar effects (owing to the introduction of the ketone) and to the presence of an unexpected vinyl C–H···O hydrogen bond. While several examples of these types of noncanonical hydrogen bonds are known in small-molecule systems due to the pioneering work of June Sutor,[35–37] we believe this to be the first observation of a vinyl C–H···O hydrogen bond serving as a reversible inter-chain crosslink within a polymeric material.

2.3. Results and Discussion

Monomer **4m** (oxaDCPD) was synthesized in one step from dicyclopentadiene (**1m**), using 0.01 mol% of a commercially available photocatalyst (*meso*-tetraphenylporphyrin), and employing air as the stoichiometric oxidant (Figure 2.2). Other groups have described the photocatalytic production of **4m** from DCPD but have always used oxygen gas as the oxidant;[34,38–43] optimization of the reaction toward the use of air in place of O_2 was done with the goal of improving scalability and operator safety. While the synthesis of **4m** proceeded smoothly and in near-quantitative conversion on 10-gram scale using optimized conditions (resulting in a 73% isolated yield), the reaction rate decreased substantially on larger scale due to the inability of light to penetrate into the dark-colored reaction mixture. Fortunately, this limitation could be partially resolved by using a simple custom-built photochemical reactor (refer to the methods (section 2.5) for details) that placed a 500W halogen light source inside a 5L reaction flask. Using this improved reactor design, >165g (50% isolated yield) of *endo*-**4m** can be produced in a single batch from 300g of *endo*-DCPD (following 27 days irradiation), and >1kg has been synthesized to date. The reaction also proceeds efficiently to produce *exo*-**4m** from the corresponding *exo*-DCPD. Conveniently, both the *endo*- and *exo*-forms of monomer **4m** can be purified by vacuum distillation; *endo*-**4m** is obtained as white crystalline solid (m.p. = 54–59 °C), while *exo*-**4m** is a liquid at room temperature. Neither diastereomeric form has any appreciable odor.

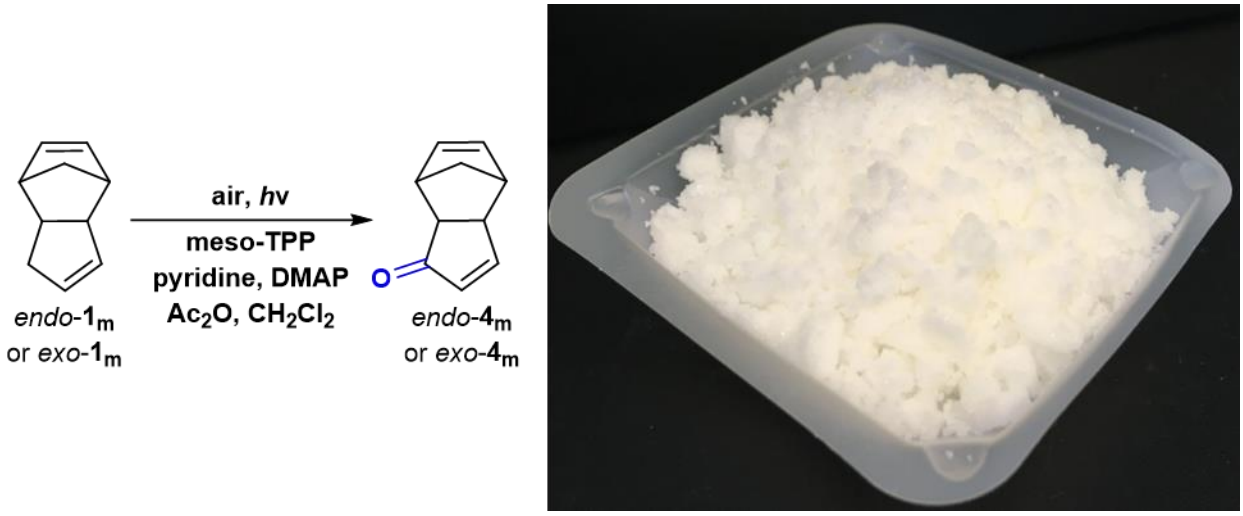

Figure 2.2. Synthesis of the oxaDCPD monomer. The inset photo shows a batch of *endo*-$\mathbf{4_m}$, which is isolated by distillation as a white solid with no significant odor. *exo*-$\mathbf{4_m}$ is isolated as a liquid.

Treatment of a THF solution of *endo*- or *exo*-$\mathbf{4_m}$ with the second- or third-generation Grubbs catalyst (at concentrations down to 0.5 mol%) afforded a linear polymer ($\mathbf{4_p}$) that was soluble in halogenated solvents (Figure 2.3), facilitating characterization by solution-state NMR. Spectral data were largely as expected, except for a surprising degree of splitting observed in the signal associated with the β-hydrogen of the enone motif. (See below for further discussion of this feature).

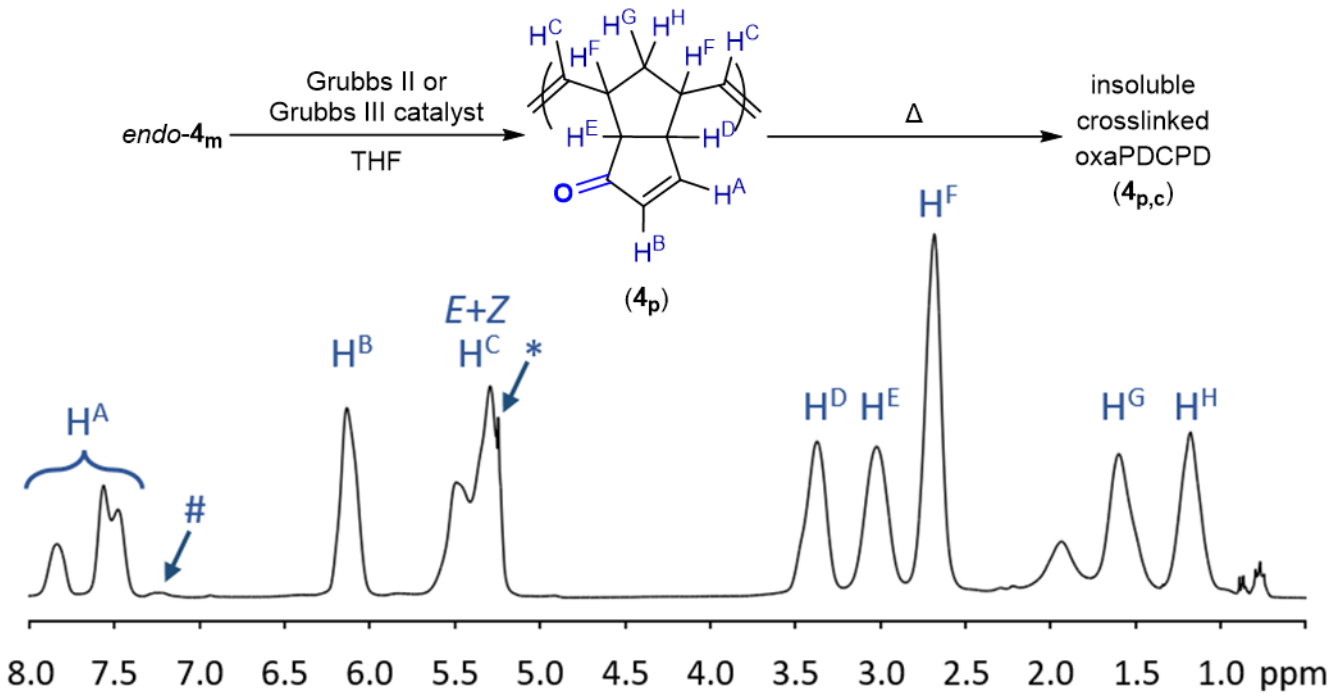

Figure 2.3. Polymerization of *endo*-$\mathbf{4_m}$ to generate a soluble linear polymer. The * symbol indicates residual protonated solvent present in the CD_2Cl_2. The # symbol indicates a small peak at *ca.* 7.2 ppm that is assigned to the phenyl group transferred from the Grubbs catalyst to the growing polymer chain. For discussion of splitting associated with the H^A proton, see below.

The linear polymer could be thermally cured to initiate crosslinking, resulting in the formation of an insoluble thermoset material ($\mathbf{4_{p,c}}$). Following the crosslinking process by IR spectroscopy revealed changes in the carbonyl stretch (Figure A21), which were consistent with (but do not conclusively prove) a principal crosslinking mechanism in which the pendent enone motif undergoes self-initiated radical polymerization—akin to the crosslinking mechanism established for ester-containing polymer $\mathbf{3_p}$.[18] However, the absence of additional peaks in the solid-state ^{13}C NMR spectrum of thermally cured $\mathbf{4_p}$ (in *contrast* to what was observed in earlier work with $\mathbf{3_p}$) indicated that the density of covalent crosslinks within the material was substantially lower than

what had previously been observed upon treating $\mathbf{3_p}$ under identical conditions. Indeed, while some covalent crosslinks are certainly formed upon thermal curing (refer to Figure A46 for crosslink structures), the density of these crosslinks must be less than the detection limit of the solid-state NMR experiment (*ca.* 10%). Neither IR nor NMR spectroscopy suggested any evidence of metathesis crosslinks, which was consistent with expectation.

While the initial production of a soluble linear polymer is convenient from a characterization perspective, industrial production of PDCPD is almost exclusively performed by reaction injection molding (RIM) methods. We therefore investigated the direct conversion of $\mathbf{4_m}$ to $\mathbf{4_{p,c}}$ in laboratory-scale[19] RIM assemblies (Figure 2.4). To this end, molten *endo*-$\mathbf{4_m}$ was combined with the Grubbs 2nd generation catalyst (0.05 mol%) and a thermally labile metathesis inhibitor (BuO_3P; 0.1 mol%). After sonication to obtain a homogenous resin, the mixture was injected into an aluminum mold preheated to *ca.* 45 °C. The assembled mold was then transferred to a 110 °C oven for 40 minutes to initiate polymerization and simultaneous thermal crosslinking, resulting in the production of regular-dimensioned macro-scale crosslinked oxaPDCPD objects suitable for mechanical testing. Control samples of PDCPD were prepared using *endo*-dicyclopentadiene monomer ($\mathbf{1_m}$) containing 5% ethylidene norbornene (ENB) to facilitate injection of the DCPD resin into the mold. A copolymer was also prepared, from a 1:1 mixture (by weight) mixture of *endo*-$\mathbf{4_m}$:$\mathbf{1_m}$.

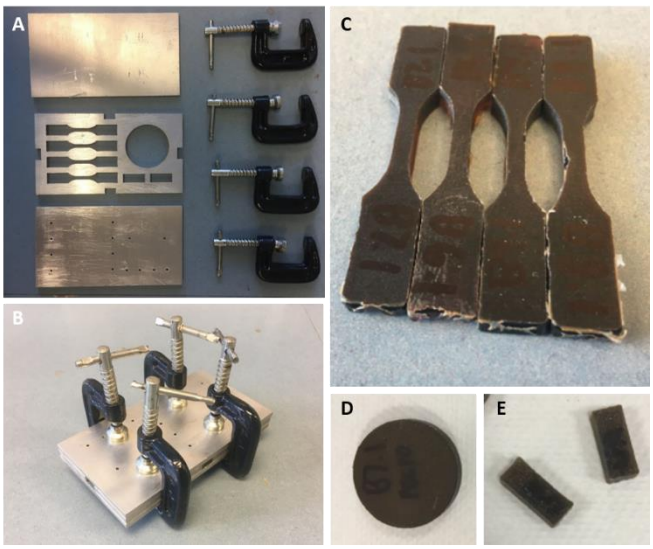

Figure 2.4. Reaction injection molding of oxaPDCPD. A: laboratory-scale RIM apparatus consisting of shaped aluminum blocks that can be clamped together to form a mold. B: assembled mold, with sprue holes for injection of resin. C: 'dogbone' shaped oxaPDCPD bars for tensile testing. D: oxaPDCPD disk for impact testing. E: oxaPDCPD bars for DMTA analysis.

As anticipated, consistently lower water contact angles (Θ_{C,H_2O}) were measured at the surfaces of the oxaPDCPD samples, as well as of the poly(**1**$_m$-*co*-**4**$_m$) copolymer, relative to the parent PDCPD material (Table 2.1). However, the difference in surface polarity was modest, and no statistically significant differences in overall surface energy were found when two-solvent contact angle studies were performed. In part this is likely due to the known surface oxidation of polydicyclopentadiene materials, which presumably raises the surface energy of all samples tested here, but possibly not at an equivalent rate. Additionally, packing effects may result in the localized concentration of ketone functional groups within **4**$_{p,c}$ being different at the surface than within the bulk.[20]

Table 2.1. Mechanical properties for oxaPDCD vs. PDCPD[a].

property	PDCPD[b]	oxaPDCPD[c]	poly(**1m**-*co*-**4m**)[d]
θ_{C,H_2O}	108.2 ± 1.7°	94.1 ± 2.6°	94.1 ± 1.7°
tensile strength	39.8 ± 1.8 MPa	53.5 ± 2.3 MPa	49.1 ± 7.9 MPa
strain at break	7.2 ± 1.7%	4.6 ± 1.2%	1.9 ± 0.2%
Young's modulus	1.22 ± 0.02 GPa	1.47 ± 0.14 GPa	3.62 ± 0.27 GPa
storage modulus	1005 ± 81 MPa	1601 ± 152 MPa	1247 ± 33 MPa
compression strength	56 ± 7 MPa	70 ± 3 MPa	64 ± 7 MPa
T_g (DMTA)	175.5 ± 4.7 °C	208.9 ± 8.7 °C	180.0 ± 11.2 °C

[a]All samples were prepared by reaction injection molding. Water contact angles are reported as the average measurement ± standard error across 3 independently prepared samples, assessing left and right contact angles for at least 15 total droplets. All other values are reported as average ± standard deviation. [b]Generated from 0.95:0.05 $\mathbf{1_m}$:ENB. [c]Generated from *endo*-$\mathbf{4_m}$. [d]Generated from 0.50:0.50 *endo*-$\mathbf{4_m}$:$\mathbf{1_m}$.

To probe deeper into the polarity differences of the bulk materials, therefore, we conducted swelling experiments upon PCPD and oxaPDCPD samples, using both a polar and nonpolar solvent (methanol and toluene, respectively). As illustrated in Figure 2.5, we observed a dramatic difference between the two polymer materials. PDCPD samples swelled rapidly in toluene, but did not absorb any amount of methanol. By contrast, oxaPDCPD samples took up relatively small amounts of toluene, but exhibited significant swelling in methanol. These data provide conclusive evidence for increased polarity within the polymer matrix, resulting from incorporation of the ketone functional group.

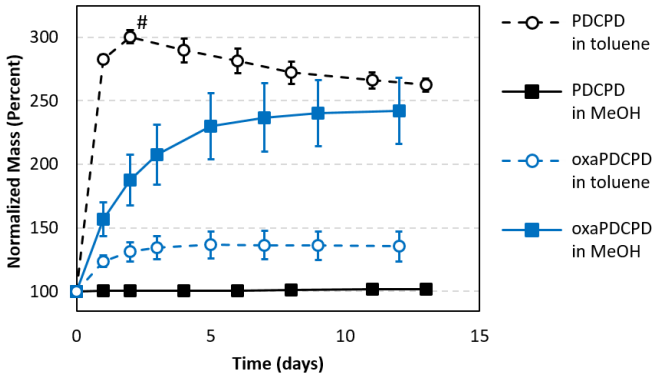

Figure 2.5. Swelling of PDCPD (black) and oxaPDCPD (blue) in polar and non-polar solvents. #: The PDCPD samples softened so much that they began to shed material after 2 days in toluene. No material loss was observed for the other samples. Error bars indicate standard deviation across 3 replicates.

Turning our attention toward mechanical assessment of the two materials, we were surprised to find that reaction injection molded oxaPDCPD displayed a significantly increased tensile strength, Young's modulus, storage modulus, and glass transition temperature (T_g) compared with the PDCPD controls (Table 2.1). In fact, the measured T_g for oxaPDCPD (209 °C) is the highest reported for any freshly prepared polydicyclopentadiene. The increase in storage modulus (measured by dynamic mechanical thermal analysis; DMTA) was equally notable—whereas the earlier ester-functionalized polydicyclopentadiene, $\mathbf{3}_{p,c}$, had a storage modulus that was identical (within experimental error) to that of the parent polydicyclopentadiene ($\mathbf{1}_{p,c}$), polymer $\mathbf{4}_{p,c}$ exhibited a storage modulus that was over 50% higher. This was accompanied by a >30% increase in tensile strength and a 25% increase in compression strength.

The remarkable increase in T_g and stiffness, together with the increase in both tensile and compressive strengths, was accompanied by a decrease in the ductility, as assessed by the degree of elongation at break. This suggested that oxaPDPCD might be more brittle than PDCPD, a hypothesis that was confirmed by drop-tower tests that resulted in sample fracture for oxaPDCPD

samples but plastic deformation for equivalently prepared PDCPD samples (Figure A47). Samples prepared from the copolymer—despite displaying a very short elongation at break in tensile testing (Table 2.1)—generally exhibited superior performance in drop-tower damage assessments, and were better able to dissipate energy throughout the polymer matrix (Figure A48). Interestingly, the copolymer also displayed a significantly higher Young's modulus (3.62 GPa) than either homopolymer (1.22 GPa and 1.47 GPa for PDCPD and oxaPDCPD, respectively), despite possessing a storage modulus, tensile strength, and compression strength that fall midway between the values for each homopolymer. The different performance of the copolymer (relative to the two homopolymers) in different experiments likely originates from the fact that monomer $\mathbf{4_m}$ polymerizes more slowly than $\mathbf{1_m}$ (see Chapter 4), resulting in the production of poly($\mathbf{1_m}$-*co*-$\mathbf{4_m}$) as a gradient copolymer. This may distribute ketone groups unevenly throughout the polymer matrix, making it especially likely to perform differently in response to mechanical measurements conducted at different strain rates. Building upon the hypothesis that the copolymer would perform best in high strain rate experiments, we conducted preliminary live-fire ballistics testing on plaques generated from either PDCPD or the poly($\mathbf{1_m}$-*co*-$\mathbf{4_m}$) copolymer. These revealed significantly better performance for the copolymer, in the ability to stop the penetration of fragment simulating projectiles (FSPs) through the plaque (Figure A51).

Taken together, the increased strength and stiffness, increased brittleness (for the homopolymer) and increased glass transition temperature are all consistent with an increase to the effective crosslinking density within $\mathbf{4_{p,c}}$, compared with the parent PDCPD. However, the solid-state NMR experiments discussed above indicate a modest density of covalent crosslinks within oxaPDCPD.

To resolve the apparent conflict between the observation that cured oxaPDPCD functioned like a densely crosslinked material despite evidently a possessing a lower chemical crosslink density

than previously studied forms of functionalized polydicyclopentadiene,[18] we initially conducted a series of molecular dynamics (MD) simulations using PDCPD and oxaPDCPD oligomers (each of which was 20 residues in length for linear polymers, and 40 or 80 residues after crosslinking). We found that the MD calculations appropriately recapitulated in silico key experimental observations. Specifically, the T_g and Young's modulus were both found to increase in moving from PDCPD to oxaPDCPD, in both the linear and crosslinked polymer models. Analysis of the MD data suggested that the enhancements of T_g and Young's modulus arise from increases in dipolar, electrostatic, and van der Waals interactions in oxaPDCPD compared to PDCPD. To provide further insight into the relationship between electronic structure and mechanical properties, we turned to quantum mechanical simulations.

Four oligomers consisting of 6 residues of oxaPDCPD were modeled using CAM-B3LYP/6-31G(d) augmented by atom-centered potentials (ACPs) designed to mitigate the effects of basis set incompleteness.[44–47] These include two molecules in which the dicyclopentadieneone residues were connected in head-to-tail fashion down the polymer chain, and two molecules in which the residues were connected head-to-head. For each of these possible regiochemical outcomes, one oligomer was modeled using all-trans backbone alkenes, while one was modeled using all-cis backbone alkenes. Across the series of four molecules, the head-to-tail all-trans oligomer was the most energetically stable structure, while the head-to-head all-trans isomer was predicted to be 1.6 kcal/mol higher in energy. The two all-cis structures were predicted to be more than 11 kcal/mol above the lowest energy oligomer. Most significantly, in the two head-to-tail oligomers, we found close contacts between two ketones from two separate dicyclopentadiene residues and two ß-hydrogen atoms associated with the enone motifs of two other dicyclopentadiene residues. One such close contact was found in the head-to-head trans oligomer. The vinyl C–H···O contacts

determined from the QM calculations are well within the range expected for this type of hydrogen bond.[48] Figure 2.6 highlights these interactions in the lowest energy oligomer.

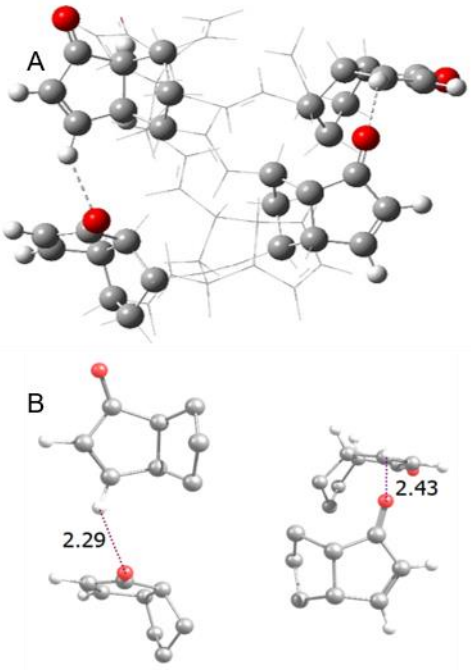

Figure 2.6. Lowest energy head-to-tail all-trans oxaPDCPD structure obtained from DFT simulations (panel A). Panel B shows the same structure as that in panel A, with all but the hydrogen-bonded monomers removed from the image. The distances (in Å) between the ß-hydrogen of the vinyl group and the ketone oxygen are shown. Key: C = gray, H = white, O = red. Hydrogen bonding interactions are shown with dashed lines.

To determine the energetics associated with the interaction, the monomer moieties associated with the C–H···O separation of *ca.* 2.40 Å were extracted from the modeled oligomer, and their ethylene groups were replaced with hydrogen atoms. The energy of the system was computed using M06-2X/def2-TZVPP,[49,50] and then was calculated again with the fragments separated by 20 Å. The resulting energy difference of 2.3 kcal/mol (Figure 2.7) is well within the range expected for vinyl C–H···O hydrogen bonds,[48] and indicates a strongly stabilizing interaction.

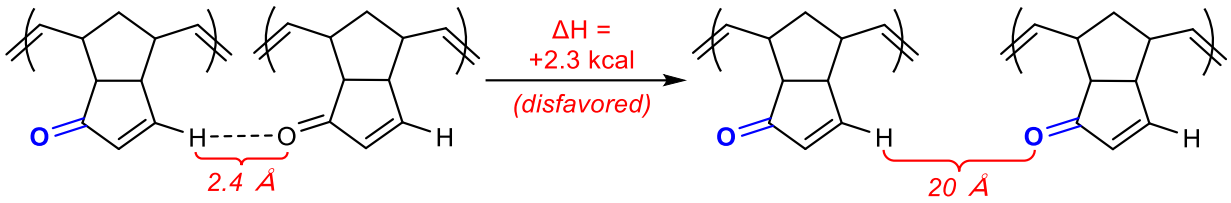

Figure 2.7. Quantitative determination of vinyl C–H···O=C hydrogen-bonding enthalpy by QM simulation (M06-2X /def2-TZVPP).

The vinyl C–H···O interactions resulted in a significant deshielding effect for the enone ß-hydrogen, as determined by the calculated ^{1}H NMR spectrum (B3LYP/def2QZVPP//CAM-B3LYP/6-31G(d)-ACP)[49,51,52] depicted in Figure 2.8 for the all-trans head-to-tail linked oxaPDCPD hexamer. Compellingly, a qualitatively similar pattern of splitting in the signal corresponding to the enone ß-hydrogen was observed in the experimental ^{1}H NMR spectrum of linear oxaPDCPD, in both polar (DMSO-d_6) and non-polar (CD_2Cl_2 and $CDCl_3$) solvents (Figure 2.8). The excellent agreement between calculated and experimental NMR spectra shown in Figure 2.8 provides strong evidence for the validity of the vinyl C–H···O=C hydrogen-bonding interaction within oxaPDCPD.

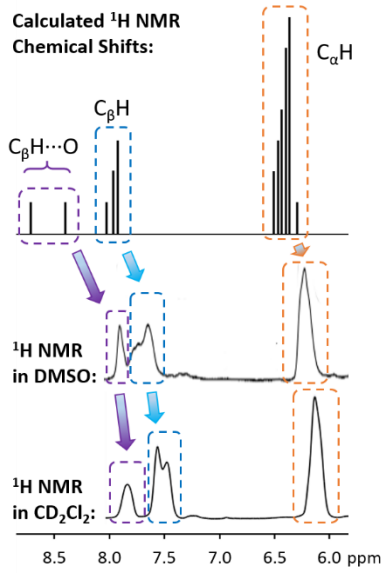

Figure 2.8. Comparison of calculated and experimental 1H NMR spectra for oxaPDCPD, indicating the presence of vinyl C–H···O=C hydrogen bonds within the material.

The presence of polar functional groups is known to affect mechanical properties and increase glass transition temperatures for many types of polymer materials.[53] In order to separately consider the polar effects resulting from installation of the ketone with any effects that are specific to the vinyl C–H hydrogen bond, we prepared a control polymer in which the ketone was maintained but the conjugated alkene was removed. As shown in Figure 2.9, the control polymer (oxaPDCPD$_{RD}$; **5p**) was efficiently synthesized through regioselective zinc-promoted reduction of the enone monomer (**4$_m$**)[54] followed by polymerization with the Grubbs 2nd or 3rd generation catalyst.

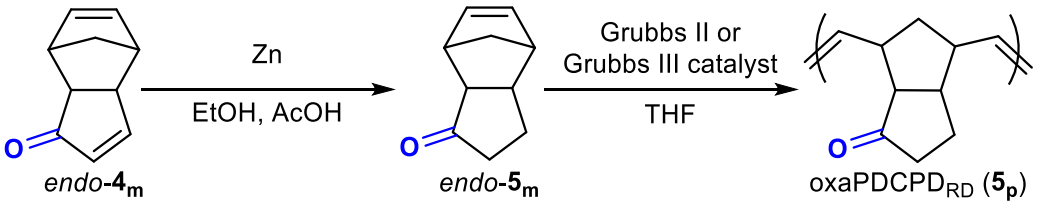

Figure 2.9. Synthesis of a reduced polymer control.

Interestingly, we found that while *endo*-**5$_m$** could be polymerized with the Grubbs 3rd generation catalyst to give linear polymer (**5$_p$**) with number average molecular weight values (M_n) that agreed relatively well with predicted molecular weights (calculated from the loading of the initiator), in all cases *endo*-**4$_m$** polymerized to give linear **4$_p$** that had approximately double this molecular weight (Table 2.2). While this could potentially be due to partial catalyst inactivation by enone **4$_m$**, the apparent doubling of M_n for a given initiator loading suggests the possibility that the enone-containing polymer may be undergoing a selective post-polymerization ligation event, in which the terminal enone residues can facilitate a specific dimerization reaction (see Figure A52 for one possible mechanism that would support the observed doubling of molecular weight). The Novak group has previously noted molecular weight doublings in a related polymer system, and has likewise proposed that chain-end dimerization may occur once reactive monomer is depleted from the system.[32] As expected based upon literature precedent,[55] polymerizations with the Grubbs 2nd generation catalyst were less-well controlled due to slow initiation, resulting in higher molecular weights, higher polydispersity, and poorer correlation of M_n with the substrate/initiator ratio.

Table 2.2. GPC data for formation of linear polymers from **4m** or **5m**[a].

monomer	[initiator]	predicted M_n (kDa)	experimental M_n(kDa)	M_w/M_n
5m	2.33 mol%	6.4	7.6	1.23
5m	1.13 mol%	13.2	17.8	1.33
5m	0.60 mol%	24.6	32.7	1.52
4m	2.33 mol%	6.3	14.6	1.82
4m	1.17 mol%	12.6	38.7	1.66
4m	0.58 mol%	25.1	65.0	1.84

[a]All samples were polymerized using 3rd generation Grubbs catalyst. M_n and M_w values were measured using a GPC instrument calibrated with polystyrene standards. For polymerization data collected using 2nd generation Grubbs catalyst, refer to Table A1.

We next prepared a series of reaction-injection molded polymer samples from monomers **4m**, **5m**, and **1m** (with or without ENB, as required for formulation of the sample), and calculated the approximate molecular weight between crosslinks (M_c), using the storage modulus of the rubbery region of the DMTA curve and the theory of rubber elasticity.[56] As shown in Table 2.3, we found a low effective M_c in the oxaPDCPD samples (1270 g/mol; equivalent to *ca.* 8.7 monomer units), compared with the M_c in the parent PDCPD material (1914 g/mol; equivalent to *ca.* 14.5 monomer units). This observation indicates that although the density of *covalent* crosslinks in oxaPDCPD is lower than that in PDCPD (established earlier by NMR), the *effective* crosslink density is higher—consistent with the mechanical results discussed above. By comparison, the M_c in oxaPDCPD$_{RD}$ is much longer (3187 g/mol; equivalent to a spacing of *ca.* 21.5 monomer units). This confirms that the ketone itself is insufficient to provide a high effective crosslink density. These data suggest

that above the glass transition temperature, the vinyl C–H···O=C hydrogen bond plays at least some role in dictating the physicochemical properties of the material.[57] As expected, high-temperature aging of oxaPDCDP introduced additional covalent crosslinks into the material, further reducing the M_c.

Table 2.3. Calculated distance between crosslinks for reaction-injected polymers prepared from **4m**, **5m**, or **1**[a].

polymer	M_c (Da)
PDCPD[b]	1914 ± 159
oxaPDCPD[c]	1270 ± 111
poly(**1m**-*co*-**4m**)[d]	1302 ± 47
oxaPDCPD$_{RD}$[e]	3187 ± 823
poly(**4m**-*co*-ENB)[f]	1975 ± 122
aged oxaPDCPD[g]	110

[a]All samples were prepared by reaction injection molding. Unless otherwise indicated, data are reported as the average measurement ± standard error across 3 independently prepared samples. [b]Generated from 0.95:0.05 **1m**:ENB. [c]Generated from *endo*-**4m**. [d]Generated from 0.50:0.50 *endo*-**4m**:**1m**. [e]Generated from 0.80:0.20 **5m**:ENB. [f]Generated from 0.80:0.20 **4m**:ENB. [g]Measurement of a single sample of oxaPDCPD after ageing 104 days at 120 °C.

Mechanical measurements made below the T_g told a different story. Despite being prepared with 20% ENB, the storage modulus for oxaPDCPD$_{RD}$ was 1277 ± 20 MPa (within experimental error of the 1197 ± 80 MPa for oxaPDCPD prepared using the equivalent amount of ENB), while the glass transition temperature (measured by DMTA) was 178 ± 14 °C (within experimental error of the 173 ± 2 °C for oxaPDCPD prepared using the equivalent amount of ENB). These data indicate

that below the T_g it is polar effects from the ketone (e.g. dipole–dipole interactions and induced dipole interactions), rather than the vinyl C–H···O=C hydrogen bond, which contribute the greatest amount to certain properties of the material.

2.4. Conclusions

Dicyclopentadien-1-one is readily accessible from dicyclopentadiene, in a single-step photocatalytic transformation that can be carried out using sparged air as the stoichiometric oxidant. The product, a white crystalline solid that can be easily isolated on large scale by distillation, functions as a useful monomer in ring-opening metathesis polymerizations. These reactions can either be carried out in solvent (in which case a soluble linear polymer can be readily isolated) or else in a reaction-injection molding setup. The latter protocol affords regular-dimensioned thermoset objects that display a significantly enhanced T_g, storage modulus, tensile strength, and compression strength, relative to the properties of the parent dicyclopentadiene material. While some degree of ductility is sacrificed in the ketone-containing homopolymer, copolymerization with unfunctionalized dicyclopentadiene affords a material with good damage resistance properties, especially in high strain rate measurements; further assessment of poly(**1**$_m$-*co*-**4**$_m$) materials are underway.

From a structural perspective, several lines of experimental and computational evidence indicate that the thermoset material produced from dicyclopentadien-1-one encodes three separate types of inter-chain interactions: (1) covalent crosslinks that most likely arise from olefin-addition polymerizations across the embedded enone motif (as previously observed for an analagous α,ß-unsaturated ester-containing polymer, which forms these types of crosslinks in greater density[18]); (2) an unexpected network of vinyl C–H···O=C hydrogen bonds; and (3) dipole–dipole interactions resulting from the ketone groups. Control experiments with a selectively hydrogenated polymer that retains the ketone but that cannot participate in vinyl C–H···O=C hydrogen bonding

suggest that dipole–dipole forces are particularly important in establishing the high T_g and high storage modulus found within crosslinked poly(dicyclopentadien-1-one).

2.5. Methods

All commercial materials were used as received. THF was dried in a sodium-benzophenone still under a nitrogen atmosphere. Grubbs 3rd generation catalyst was synthesized from Grubbs 2nd generation catalyst >98% by NMR from Chem-Impex using pyridine according to the literature.[58]

Spectroscopy

^{1}H and ^{13}C NMR spectra were obtained using a Bruker AVANCE 300 (300.27 MHz for ^{1}H, 75.51 MHz for ^{13}C) or a Bruker AVANCE NEO 500 (500.27 MHz for ^{1}H, 125.81 MHz for ^{13}C). Variable temperature ^{1}H NMR was done on a Bruker AVANCE 360 (360.28 MHz for ^{1}H). Solid state cross-polarization and magic angle spinning ^{13}C NMR was done at Simon Fraser University using a Bruker AVANCE III 400 (100.62 MHz for ^{13}C). Data were processed using MestReNova. Singlet = s, d = doublet, t = triplet, br = broad, app = apparent. In ^{13}C NMR of polymers shift ranges are given where identical carbons are in different environments. IR spectra were recorded using a Perkin-Elmer Spectrum Two FT-IR spectrometer with ATIR attachment. Samples were measured as solids or by drop casting from deuterated chloroform or dichloromethane.

Thermal analysis

Differential scanning calorimetry samples were run on a TA instruments DSC25 using TZero aluminum DSC pans with hermetic lid. A pin hole was added for solid samples using the tip of a 21 ½ gauge needle. An empty TZero aluminum DSC pan with TZero aluminum hermetic lid and pin hole was used as a reference. Samples were measured from -50°C to 250°C for two complete heating and cooling cycles at 10°C per minute. Thermogravimetric analysis was done at Simon Fraser University on a Shimadzu TGA-50 or on a TA instruments SDT Q600. Samples were run at 2 or 5°C a minute to 700°C under a nitrogen atmosphere.

Mechanical testing

Dynamic mechanical thermal analysis was done on an Anton Paar Modular Compact Rheometer 302 fitted with an Anton Paar SRF-12 geometry and CTD 600 oven. Samples were measured through 25-250°C using a logarithmic strain of 0.01-0.1% at 1 Hz and a normal force of 0.1 N. Regular dimensioned 20 x 8 x 4.75 mm (Length x Height) bar type samples were obtained via reaction injection molding. Glass transition temperatures were obtained from the peak of the loss factor and storage modulus from the first point taken in a run. The distance between crosslinks was calculated using equation 1.[56] T is the temperature of the minimum storage modulus, E'_m is the minimum storage modulus, ρ is the measured density, R is the universal gas constant, and M_c is the molecular weight between crosslinks.

$$\text{Equation 1: } M_c = \frac{3\rho RT}{E'_m}$$

Tensile and compression tests were performed at University of British Columbia, Composite Research Network (CRN) lab using Dual Column Load Frame Instron machine model 5969. Regular dimensioned ASTM Type V dog bone samples produced via reaction injection molding were used for the tensile test. The ends of the samples were fixed between the grips and subjected to a loading rate of 5 mm/min. Regular dimensioned 5 x 4.75 mm (Diameter x Height) cylinder type samples were used for compression testing and were obtained via reaction injection molding. The cylindrical sample was put between the load cells and a loading rate of 5 mm/min was applied to the sample by the upper load cell. Force-displacement curves were obtained in both tests and converted to stress-strain curves. The stress is defined as the force on the cross-section area of the sample while strain represents the displacement to the initial length of the specimen.

Gel permeation chromatography

Gel permeation chromatography was run on a Malvern Viscotek TDAmax fitted with a Malvern viscotek TDA refractive index detector. GPC grade THF with 0.1 wt% tetrabutylammonium bromide was used as an eluent at a flow rate of 1 mL/min. A polystyrene standard curve was used to calibrate the runs. Samples were dissolved in HPLC grade THF to 1 mg/mL and filtered with 0.45 μm PTFE prior to analysis.

Melting points

Melting points were taken on either an SRS digimelt or a Gallenkamp melting point apparatus.

Contact angle measurements

Contact angle measurements were obtained on a Holomarc Contact Angle Meter. 2 μL droplets were placed on a treated substrate using a mechanical dispenser. Images were taken using CMOS sensor. Substrates were polished with 220 grit sandpaper, washed with water and ethanol, then dried at 110°C overnight. Water was used as the polar liquid and diiodo methane was used as the purely dispersive liquid. Surface energies were calculated using the Fowkes Model and equations 2 and 3.[59–61] σ_l is the surface tension of diiodomethane or water. σ_l^P and σ_l^D are the polar and dispersive components the surface tension respectively of either diiodomethane or water. σ_s^P and σ_s^D are the polar and dispersive components respectively of the surface energy of the solid. σ_s is the surface energy of the solid. θ is the measured contact angle. σ_s^D is calculated using the contact angle θ obtained using diiodomethane and equation 2. σ_s^D is then used along with the contact angle θ obtained using water and equation 2 to obtain σ_s^P. The sum of the dispersive and polar components of the surface energy is the total surface energy.

$$\text{Equation 2: } 0.5\sigma_l(1 + cos\theta) = \sqrt{\sigma_l^D \sigma_s^D} + \sqrt{\sigma_l^P \sigma_s^P}$$

$$\text{Equation 3: } \sigma_s = \sigma_S^D + \sigma_S^P$$

Table S2.1. Table of contact angle parameters.

Symbol	Diiodomethane	Value (mN/m)
σ_l^P	surface tension polar	0
σ_l^D	surface tension dispersive	50.8
σ_l	surface tension	50.8
Symbol	**Water**	**Value (mN/m)**
σ_l^P	surface tension polar	51.0
σ_l^D	surface tension dispersive	21.8
σ_l	surface tension	72.8
θ	contact angle	measured

Swelling Experiments

Swelling experiments were performed using regular dimensioned 4.75 x 10 mm (height x diameter) disk samples. Samples were subjected to high vacuum at 0.15 mm Hg for 6 hours prior to weighing, weighed then submerged in 10 mL of either methanol or toluene in a sealed vial. After the desired interval, samples were removed from the solvent, gently dabbed dry and weighed. Samples were then placed back into the solvent.

Large Scale Photoreactor

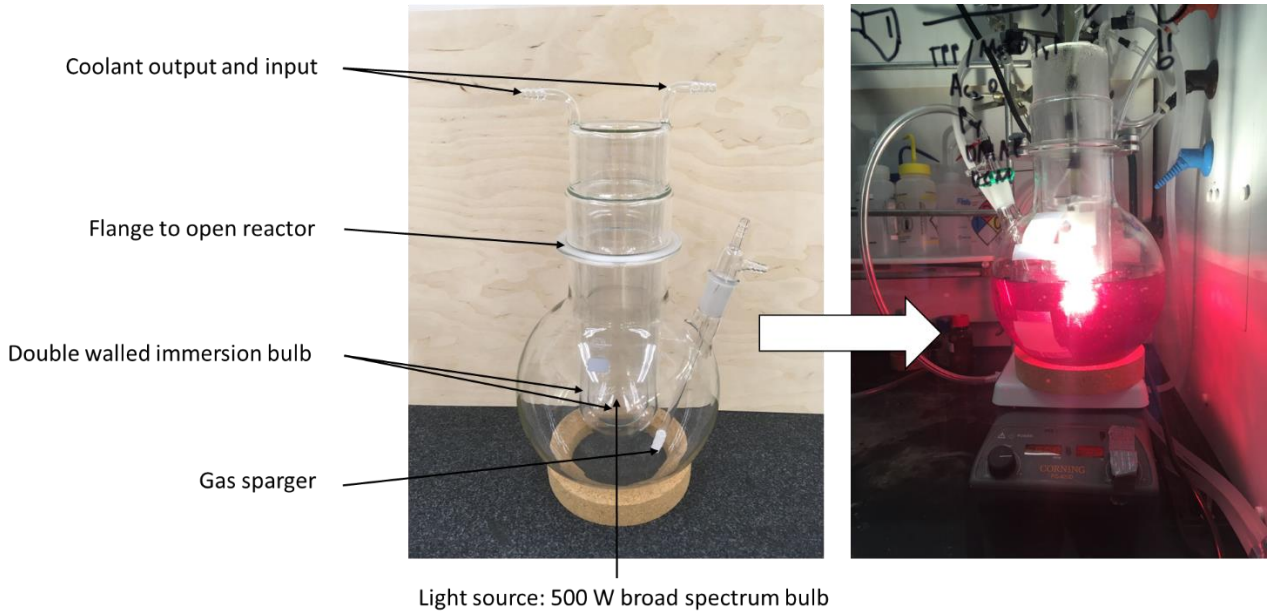

This 5-liter photoreactor was built at the University of Victoria glass shop by scientific glassblower Sean Adams. The reactor flask is fitted with a double walled immersion well. This houses a 500-watt broad spectrum sunlite P28s BASE 120 V light bulb centered in the reactants using an aluminum jig heatsink, made by the Science Machine Shop at the University of Victoria. Water from a chiller is pumped through the immersion well removing heat generated by the light source. Additional air cooling was also utilized by blowing a stream of air into the well with the light bulb. This setup offers substantially better photon penetration through the reactants as compared to external lights. Additionally, this reactor significantly reduces solvent consumption through evaporation and maintained the reaction at a constant temperature.

Classical Molecular Mechanics Simulations

For PDCPD simulations, the bulk material was represented by 375 linear 20-mer chains in the all-trans configuration. Crosslinked structures were prepared by covalently bonding one central site of a 20-mer with the end site of a second molecule, resulting in a molecular structure with 40 segments. The constituent components of each system are schematically shown in Table A7.

CHARMM force field parameters were used and simulations were performed using LAMMPS [LAMMPS - a flexible simulation tool for particle-based materials modeling at the atomic, *meso*, and continuum scales.[62,63] Equilibrations were carried out by subjecting the structures to up to 10 ns NPT run, using the Nosé-Hoover barostat and thermostat. Integration of equations of motion was done by Velocity Verlet algorithm using timestep of 0.5 fs, and van der Waals and electrostatic non-bonded interactions were explicitly accounted within a cut-off distance of 12 Å. Lennard-Jones parameters between pairs of unlike atoms were evaluated by the arithmetic mixing rule:

$$\sigma_{i,j} = \frac{\sigma_{i,i} + \sigma_{j,j}}{2}$$
$$\varepsilon_{i,j} = \sqrt{\varepsilon_{i,i}\varepsilon_{j,j}}$$

Beyond the cut-off distance, long-range electrostatic interactions were calculated using the particle-particle particle-mesh. Analysis of raw data was performed by MATLAB [MATLAB and Statistics Toolbox Release 2016a, The MathWorks, Inc., Natick, Massachusetts, United States] and, OVITO software was used for visualization of the calculated trajectories.[64]

i) Glass Transition Temperature

To evaluate glass transition temperature (T_g), changes in density with temperature were determined by equilibrating the periodic system for 8-to-15-million-time steps over the temperature range of 250 to 600 K. The T_g values were determined by identifying the change in slope in the density-temperature plots. The increase in *T*g of the crosslinked structures as compared

to their linear counterparts is an indication of the increased rigidity in the branched molecules. The spatial constraints caused by cross linking hinder mobility of the molecules, resulting in transforming to the glassy state at higher temperatures.

ii) Young's Modulus

Response of the system to external forces was quantified by Young's modulus (E), calculated as the initial slope of stress-strain curves.

The applied strain rate would determine the dynamic elongation of the simulation box along a pre-defined direction. The stress along a particular direction (the x-axis in this work), was calculate as the sum of x component of the forces exerted on every particle present in the system.

The stress response is dependent on the applied strain rate. For all calculations herein, the rate of 8 10^9 s^{-1} was used, as this value yielded the closest Young's Modulus to experimental values presented in the literature for crosslinked PDCPD (*viz*. 1.7 GPa).[65]

iii) Molecular Interactions

Analysis of the dipolar, electrostatic, and van der Waals interactions in the oxa-modified PDCPD structures provide insight into the origin of the changes in T_g and Young's modulus, see Table A9. Hydrogen-bonding interactions were estimated by evaluating the average strength of interactions between ring ethylene hydrogen atoms and the ketone oxygen atoms, see Table A11.

Quantum Mechanical Calculations

All structures subjected to QM simulations underwent conformer searching to determine their lowest energy structures. The molecules contain several rotatable bonds and, in some cases, the possibility of intramolecular hydrogen bonding. This requires a careful examination of the conformational space of each structure. For this task, the genetic algorithm module implemented in Open Babel was employed.[66] The approach generates a collection of low-energy conformers

optimized and ranked by MMFF944 force field energies.[66] The energies of the most stable conformers for each structure emerging from the genetic search (up to 30 conformers in most cases) were then determined using a single-point quantum mechanical calculation at the CAM-B3LYP-D3(BJ) /6-31G(d)-BSIP2 level of theory. CAM-B3LYP was chosen because the functional displays low delocalization error, a deficiency in DFT that often leads to poorly predicted properties (including barrier heights); D3(BJ) is a semiempirical correction for dispersion employed because dispersion physics is absent from most density functionals; 6-31G(d) is a Gaussian basis set employing two functions per occupied orbital and was chosen to maximize the throughput of the calculations; and, BSIP2 are basis set incompleteness potentials developed to mitigate the errors arising from the use of incomplete basis sets (such as that employed in the present work).[44,47,67,68] All QM calculations utilized the Gaussian 16 program package.[69]

QM simulations were performed on hexamers of oxaDCPD. To understand the energetics associated with different primary polymerization outcomes, calculations were performed on four types of structures: all *cis* head-to-tail, all *cis* head-to-head, all *trans* head-to-tail, and all *trans* head-to-head. These structure types are illustrated in Figure A45. In all cases, *endo* monomers were used. QM simulations of the nuclear magnetic resonance (NMR) using the gauge-invariant atomic orbital approach and B3LYP/def2QZVPP.[70,51,52]

Energetics of structure arising from different primary polymerization outcomes

In Table A12 are collected the relative energies associated with the four types of structures arising from different primary polymerization outcomes – see text for additional information.

The ordering of *trans* vs. *cis* structures can be rationalized on the basis of steric arguments, that is, the *cis* species are expected to contain more repulsive contacts than *trans* species. The lower energies of the head-to-tail species compared to their head-to-head analogs can be understood on

the basis of favourable electrostatic interactions between the ketone oxygen and the hydrogen on the beta ethylene carbon in the cyclopentene ring moieties. In 1, there are two such close contacts with C=O···H-C= separations of 2.40 and 2.57 Å. (A third interaction involving a terminal ethylene group and a C=O group (2.70 Å separation) is also present.) 2 has a single close contact (2.52 Å) of a similar kind, 3 has two close contacts similar to 1, and 4 appears to have no close contacts involving C=O···H-C= moieties.

Only a small amount of energy, 13.1 kcal/mol, separates structures 1 to 4, and this translates into 2.2 kcal/mol per monomer. This suggests that it is energetically feasible that the structures obtained from primary polymerization of oxaDCPD will be highly heterogeneous. It is reasonable to assume, based on the relative energies, that "*trans*, head-to-tail" and "*trans*, head-to-head" will be the most common structural motifs, with relatively fewer occurrences of the "all *cis*" structures being present in a given polymer molecule.

To explore the nature of the C=O···H-C= interactions further, the monomer moieties associated with the C=O···H-C= separation of 2.40 Å were extracted from 1 and their ethylene groups replaced with H atoms. The energies of the structure was computed using M06-2X/def2TZVPP and again with the fragments separated by 20 Å.[50] The resulting energy difference of 2.3 kcal/mol suggests that these types of C=O···H-C= interactions are stabilizing. An analysis of the electrostatics support the suggestion, with the partial charges of +0.07 and -0.39 electrons on the H and O atoms, respectively. Some component of the interactions may also involve favourable orbital overlaps.

Synthesis of Monomers

Large Scale Synthesis of Dicyclopentadienone (oxaDCPD, 4_m)

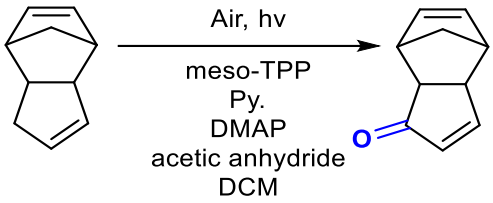

meso-Tetraphenylporphyrin (*meso*-TPP; 171 mg; 0.28 mmol; 0.012 mol%) and DMAP (5.5812 g; 45.68 mmol) were dissolved in DCM (2.2 L). Acetic anhydride (230 mL; 2.43 mol), pyridine (94 mL; 1.16 mol) and dicyclopentadiene (DCPD; 300.36 g; 2.27 mol) were subsequently added. The mixture was irradiated in a 5 L photoreactor using a Boryli BTL P28S 500W halogen bulb contained in a cold finger. The mixture was sparged with air and reacted for 27 days. The reaction mixture was washed with 2 M HCl and then with saturated sodium bicarbonate. The aqueous extracts were back extracted with DCM. All DCM fractions were combined and concentrated *in vacuo* yielding a black oil. The crude reaction mixture was adhered to a silica gel plug and washed with hexanes then eluted with 3:1 hexane to ethyl acetate. The resulting concentrate was then purified via vacuum distillation (70°C at 0.15 mmHg) in a 90°C water bath yielding 167.54 g (50% yield) of oxaDCPD as a white crystalline solid. Identical protocols were used for *endo*- and *exo*-4_m. *endo*-1-dicyclopentadienone (*endo*-4_m): Yield: up to 51% on 300 g scale; up to 72.6% on 10 g scale. Physical State: White, large crystals, melting point: 53.9-59.3°C. ^{1}H NMR (300.27 MHz, Chloroform-*d*) δ 7.38 (dd, *J* = 5.8, 2.6 Hz, 1H), 5.98 – 5.92 (m, 2H), 5.78 (dd, *J* = 5.4, 2.9 Hz, 1H) 3.45 – 3.39 (m, 1H), 3.22 (br s, 1H), 2.97 (app s, 1H), 2.80 (app t, *J* = 5.1 Hz, 1H), 1.76 (dd, *J* = 8.4, 1.0 Hz, 1H), 1.63 (d, *J* = 8.5 Hz, 1H). ^{13}C NMR (125.81 MHz, Chloroform-*d*) δ 209.12, 163.79, 135.93, 131.76, 131.52, 51.84, 49.29, 47.36, 44.17, 43.28. *exo*-1-dicyclopentadienone (*exo*-4_m) Physical State: Colorless oil. ^{1}H NMR (300.27 MHz, Chloroform-*d*) δ 7.56 (dd, *J* = 5.7,

2.6 Hz, 1H), 6.31 – 6.25 (m, 2H), 6.21 (dd, *J* = 5.7, 3.0 Hz, 1H) 2.93 (app s, 1H), 2.89 – 2.84 (m, 1H), 2.72 (app s, 1H), 2.27 (dt, *J* = 5.0, 1.4 Hz, 1H), 1.41 (dt, *J* = 9.4, 1.5 Hz, 1H), 1.32 – 1.27 (m, 1H).

Synthesis of Dicyclopentaenone (oxaRD, 5_m)

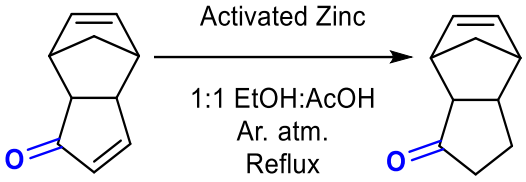

Zinc dust (21.0197 g; 0.3215 mol) was activated in ethanol (50 mL) with a crystal of iodine under an argon atmosphere with vigorous stirring for 1 hour. *Endo*-oxaDCPD (6.7025 g; 0.046 mol) and acetic acid (50 mL) were then added, and the mixture was refluxed under argon for 24 hours. The mixture was cooled and filtered through a celite plug and the solvent was removed *in vacuo* obtaining a red oil. The oil was dissolved in DCM and washed with a saturated sodium bicarbonate solution. The organic extracts were purified by flash-column chromatography, using 9:1 hexanes : ethyl acetate then concentrated *in vacuo* to obtain 3.57 g (52% yield) of white solid. Yield: 52%. Physical State: White crystals, melting point: 95-96°C. ^{1}H NMR (300.27 MHz, Chloroform-*d*) δ 6.22 (dd, *J* = 5.8, 2.8 Hz, 1H), 6.11 (dd, *J* = 5.7, 2.9 Hz, 1H), 3.22 – 3.17 (m, 1H) 3.00 (app s, 1H), 2.99 – 2.92 (m, 1H), 2.85 (ddd, *J* = 9.1, 4.6, 1.2 Hz, 1H), 2.19 – 1.92 (m, 3H), 1.60 – 1.48 (m, 2H), 1.42 (app d, *J* = 8.3, 1H). ^{13}C NMR (75.51 MHz, Chloroform-*d*) δ 222.50, 136.29, 134.88, 54.45, 52.39, 47.60, 47.15, 41.34, 40.69, 22.79.

Synthesis of Linear Polymers

Synthesis of Linear polymer (oxaPDCPD, 4_p) (GC3)

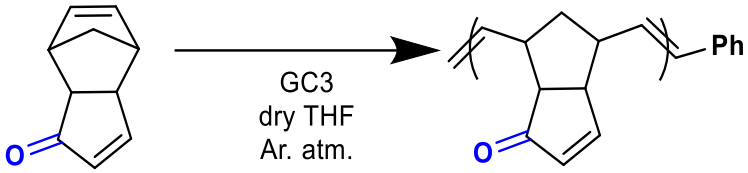

Dry THF (5 mL) was added to Grubbs 3rd generation catalyst (11.5 mg; 0.016 mmol), under an argon atmosphere in flame dried glass. A standard solution of oxaDCPD was prepared by adding dry THF (20 mL) to oxaDCPD (400 mg; 2.74 mmol) under an argon atmosphere. 5 mL of this solution was then injected into the catalyst solution. After 60 minutes ethyl vinyl ether (1 mL, 10.5 mmol) was injected, and the solution was stirred for 10 minutes. The resulting polymer was precipitated in methanol (45 mL) and isolated via centrifugation at 3270 x g for 30 minutes. poly-*endo*-dicyclopentadienone (*endo*-4_p): Yield: 90% Physical State: light brown, solid. ^{1}H NMR (300.27 MHz, Methylene Chloride-d_2) δ 8.01 – 7.47 (m, 1H), 6.22 (br s, 1H), 5.71 – 5.33 (m, 2H), 3.46 (br s, 1H), 3.11 (br s, 1H), 2.76 (br s, 2H), 1.68 (br s, 1H), 1.28 (br s, 1H). ^{13}C NMR (75.51 MHz, Methylene Chloride-d_2) δ 210.39 – 209.37, 166.12 – 164.44, 137.71 – 136.61, 132.35 – 129.25, 53.70 – 52.77, 45.61 – 44.52, 41.24 – 39.80, 38.85 – 35.25.

Synthesis of Linear polymer (oxaPDCPD) (GC2)

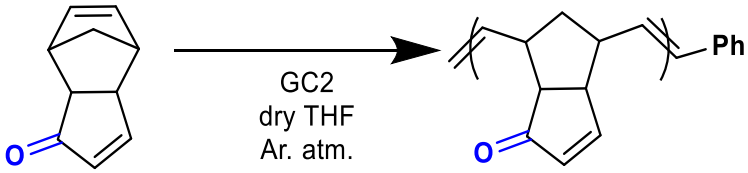

Dry THF (5 mL) was added to Grubbs 2nd generation catalyst (11.5 mg; 0.014 mmol), under an argon atmosphere in flame dried glass. A standard solution of oxaDCPD was prepared by adding dry THF (20 mL) to oxaDCPD (400 mg; 2.74 mmol) under an argon atmosphere. 5 mL of this solution was then injected into the catalyst solution. After 60 minutes ethyl vinyl ether (1 mL, 10.5

mmol) was injected, and the solution was stirred for 10 minutes. The resulting polymer was precipitated in methanol (45 mL) and isolated via centrifugation at 3270 x g for 30 minutes. poly-*endo*-dicyclopentadienone (*endo*-4_p): ^{1}H NMR (500.27 MHz, Methylene Chloride-d_2) δ 8.00 – 7.48 (m, 1H), 6.30 – 6.10 (m, 1H), 5.72 – 5.33 (m, 2H), 3.60 – 3.36 (m, 1H), 3.12 (br s, 1H), 2.76 (br s, 2H), 1.69 (br s, 1H), 1.28 (br s, 1H). Solid State ^{13}C NMR (100.62 MHz) δ 208.99, 165.26, 137.04, 131.67, 53.12, 44.37, 40.54. poly-*exo*-dicyclopentadienone (*exo*-4_p): Physical State: light brown, solid. ^{1}H NMR (300.27 MHz, Methylene Chloride-d2) δ 8.02 – 7.42 (m, 1H), 5.89 (br s, 1H), 5.74 – 5.33 (m, 2H), 3.13 (br s, 1H), 2.97 – 1.89 (m, 4H), 1.58 (br s, 2H).

Synthesis of Linear polymer (oxaPDCPD$_{RD}$ 5$_p$)

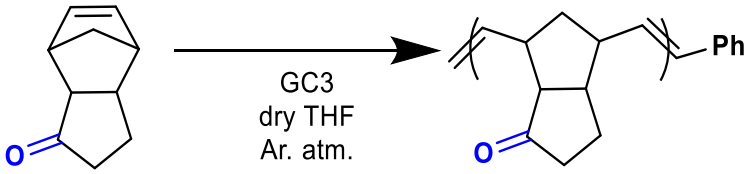

Dry THF (5 mL) was added to Grubbs 3nd generation catalyst (11.6 mg; 0.016 mmol), under an argon atmosphere in flame dried glass. A standard solution of oxaRD was prepared by adding dry THF (20 mL) to oxaRD (400 mg; 2.70 mmol) under an argon atmosphere. 5 mL of this solution was then injected into the catalyst solution. After 60 minutes ethyl vinyl ether (1 mL, 10.5 mmol) was injected, and the solution was stirred for 10 minutes. The resulting polymer was precipitated in methanol (45 mL) and isolated via centrifugation at 3270 x g for 30 minutes. poly-*endo*-dicyclopentaenone (*endo*-5_p): Yield: 71%. Physical State: light brown, solid. ^{1}H NMR (300.27 MHz, Chloroform-*d*) δ 5.62 – 5.18 (m, 2H), 3.27 – 2.59 (m, 4H), 2.25 – 1.62 (m, 5 H), 1.39 (br s, 1H). ^{13}C NMR (125.81 MHz, Methylene Chloride-d_2) δ 221.14 – 219.81, 132.76 – 129.49, 56.73 – 55.60, 47.50 – 45.26, 42.25 – 40.13, 39.64 – 37.28, 23.33 – 22.80.

Reaction Injection Molding

Reaction injection molding of dicyclopentadiene (5:95 ENB:DCPD)

DCPD (95.15 g; 0.72 mol) was melted at 30°C and ethylidene norbornene (ENB; 5.05 g; 0.042 mol) was added to obtain a liquid 95% DCPD, 5% ENB solution. Tri-n-butyl phosphite inhibitor (3.1 mg; 0.012 mmol; 2 eq vs GC2) was mixed into a 7.0060 g aliquot of this solution. Grubbs 2nd generation catalyst (GC2; 4.8 mg; 0.0058 mmol; ~0.01 mol%) was then added. The mixture was sonicated to obtain a homogenous resin. The resin was injected with a plastic syringe into an aluminum mold. Alternatively, a light vacuum was applied to the aluminum mold and resin was pulled through the mold. The mold was transferred to a 110°C oven and allowed to cure for 40 minutes.

Reaction injection molding of dicyclopentadienone (oxaDCPD)

Endo-oxaDCPD (2.0002 g; 13.68 mmol) was melted at 60°C and combined with tri-n-butyl phosphite inhibitor (3.2 mg; 0.013 mmol; 2 eq vs GC2). Grubbs 2nd generation catalyst (GC2; 5.4 mg; 0.0064 mmol; ~0.05 mol%) was then added. The mixture was sonicated in a warm bath to obtain a homogenous resin. The resin was then injected with a plastic syringe into a preheated aluminum mold. Alternatively, a light vacuum was applied to the aluminum mold and resin was pulled through the mold. The mold was transferred to a 110°C oven and allowed to cure for 40 minutes.

Reaction injection molding of dicyclopentadienone and dicyclopentadiene copolymers (1:1 PDCPD:oxaDCPD)

A 1:1 ratio of oxaDCPD (1.0269 g; 7.02 mmol) and DCPD (1.0021 g; 7.58 mmol) by weight were melted together at 60°C. Tri-n-butyl phosphite inhibitor (6.1 mg; 0.024 mmol; 2 eq vs GC2) was mixed into the liquid *endo*-oxaDCPD/DCPD. Grubbs 2nd generation catalyst (GC2; 6.2 mg; 0.0073 mmol; ~0.05 mol%) was then added. The mixture was sonicated in a warm bath to obtain a homogenous resin. The resin was then injected with a plastic syringe into a preheated aluminum mold. Alternatively, a light vacuum was applied to the aluminum mold and resin was pulled through the mold. The mold was transferred to a 110°C oven and allowed to cure for 40 minutes.

Reaction injection molding of dicyclopentadienone with ENB (2:8 ENB:oxaDCPD)

An 80:20 ratio of oxaDCPD (2.0017 g; 13.69 mmol) and ethylidene norbornene (0.5157 g; 4.29 mmol) by weight were melted together at 60°C. Tri-n-butyl phosphite inhibitor (5.2 mg; 0.021 mmol; 2 eq vs GC2) was mixed into the liquid *endo*-oxaDCPD/ENB. Grubbs 2nd generation catalyst (GC2; 7.9 mg; 0.0093 mmol; ~0.05 mol%) was then added. The mixture was sonicated to obtain a homogenous resin. The resin was then injected with a plastic syringe into an aluminum mold. Alternatively, a light vacuum was applied to the aluminum mold and resin was pulled through the mold. The mold was transferred to a 110°C oven and allowed to cure for 40 minutes.

Reaction injection molding of dicyclopentaenone with ENB (2:8 ENB:oxaRD)

An 80:20 ratio of oxaRD (1.5840 g; 10.69 mmol) and ethylidene norbornene (0.4053 g; 3.37 mmol) by weight were melted together at 90°C. Tri-n-butyl phosphite inhibitor (3.5 mg; 0.014 mmol; 2 eq vs GC2) was mixed into the liquid *endo*-oxaRD/ENB. Grubbs 2nd generation catalyst (6.4 mg; 0.0075 mmol; ~0.05 mol%) was then added. The mixture was sonicated to obtain a homogenous resin. The resin was then injected with a plastic syringe into an aluminum mold.

Alternatively, a light vacuum was applied to the aluminum mold and resin was pulled through the mold. The mold was transferred to a 110°C oven and allowed to cure for 40 minutes.

2.6. References

(1) Kovačič, S.; Slugovc, C. Ring-Opening Metathesis Polymerisation Derived Poly(Dicyclopentadiene) Based Materials. *Mater. Chem. Front.* **2020**, *4* (8), 2235–2255. https://doi.org/10.1039/D0QM00296H.

(2) Vervacke, D. *An Introduction to PDCPD*; Product Rescue: Waarschoot, Belgium, 2008.

(3) Beuguel, Q.; Kirillov, E.; Carpentier, J.-F.; Guillaume, S. M. Upgrading Toughness and the Glass Transition Temperature of Polydicyclopentadiene upon Addition of Styrene–Ethylene–Butylene–Styrene Thermoplastic Elastomer. *ACS Appl. Polym. Mater.* **2022**, *4* (4), 2251–2255. https://doi.org/10.1021/acsapm.1c01803.

(4) Shieh, P.; Zhang, W.; Husted, K. E. L.; Kristufek, S. L.; Xiong, B.; Lundberg, D. J.; Lem, J.; Veysset, D.; Sun, Y.; Nelson, K. A.; Plata, D. L.; Johnson, J. A. Cleavable Comonomers Enable Degradable, Recyclable Thermoset Plastics. *Nature* **2020**, *583* (7817), 542–547. https://doi.org/10.1038/s41586-020-2495-2.

(5) Husted, K. E. L.; Shieh, P.; Lundberg, D. J.; Kristufek, S. L.; Johnson, J. A. Molecularly Designed Additives for Chemically Deconstructable Thermosets without Compromised Thermomechanical Properties. *ACS Macro Lett.* **2021**, *10* (7), 805–810. https://doi.org/10.1021/acsmacrolett.1c00255.

(6) Saha, S.; Ginzburg, Y.; Rozenberg, I.; Iliashevsky, O.; Ben-Asuly, A.; Lemcoff, G. N. Cross-Linked ROMP Polymers Based on Odourless Dicyclopentadiene Derivatives. *Polym. Chem.* **2016**, *7* (18), 3071–3075. https://doi.org/10.1039/C6PY00378H.

(7) Kwon, D.-J.; Shin, P.-S.; Kim, J.-H.; Park, H.-S.; Beak, Y.-M.; DeVries, K. L.; Park, J.-M. Reinforcing Effects of Glass Fiber/p-DCPD with Fiber Concentrations, Types, Lengths and

Surface Treatment. *Compos. Part B Eng.* **2017**, *123*, 74–80. https://doi.org/10.1016/j.compositesb.2017.05.020.

(8) Hayne, D. J.; Singleton, M. A.; Patterson, B. A.; Wickramasingha, Y. A.; Sietins, J. M.; Knorr, D. B.; Stojcevski, F.; Henderson, L. C. Assessing the Properties of Poly(Dicyclopentadiene) Reinforced with Discontinuous Carbon Fibers. *Compos. Part A Appl. Sci. Manuf.* **2022**, *155*, 106839. https://doi.org/10.1016/j.compositesa.2022.106839.

(9) Li, T.; Shumka, H.; J. Cuthbert, T.; Liu, C.; E. Wulff, J. Harnessing the Surface Chemistry of Methyl Ester Functionalized Polydicyclopentadiene and Exploring Surface Bioactivity. *Mater. Adv.* **2020**, *1* (6), 1753–1762. https://doi.org/10.1039/D0MA00480D.

(10) Gong, L.; Liu, K.; Ou, E.; Xu, F.; Lu, Y.; Wang, Z.; Gao, T.; Yang, Z.; Xu, W. ROMP of Acetoxy-Substituted Dicyclopentadiene to a Linear Polymer with a High Tg. *RSC Adv.* **2015**, *5* (33), 26185–26188. https://doi.org/10.1039/C5RA01855B.

(11) Phatake, R. S.; Masarwa, A.; Lemcoff, N. G.; Reany, O. Tuning Thermal Properties of Cross-Linked DCPD Polymers by Functionalization, Initiator Type and Curing Methods. *Polym. Chem.* **2020**, *11* (10), 1742–1751. https://doi.org/10.1039/C9PY01178A.

(12) Rosenblum, M. Preparation and Thermal Rearrangement of Several Dicyclopentadiene Derivatives. *J. Am. Chem. Soc.* **1957**, *79* (12), 3179–3181. https://doi.org/10.1021/ja01569a050.

(13) Woodward, R. B.; Katz, T. J. The Mechanism of the Diels-Alder Reaction. *Tetrahedron* **1959**, *5* (1), 70–89. https://doi.org/10.1016/0040-4020(59)80072-7.

(14) Mironov, V. A.; Fadeeva, T. M.; Stepanyants, A. U.; Akhrem, A. A. Thermal Isomerization of 1-Methylcyclopentadiene. *Russ. Chem. Bull.* **1967**, *16* (2), 418–420. https://doi.org/10.1007/BF00912463.

(15) Niimi, A. J.; LaHam, Q. N. Relative Toxicity of Organic and Inorganic Compounds of Selenium to Newly Hatched Zebrafish (*Brachydanio Rerio*). *Can. J. Zool.* **1976**, *54* (4), 501–509. https://doi.org/10.1139/z76-056.

(16) Hadrup, N.; Ravn-Haren, G. Acute Human Toxicity and Mortality after Selenium Ingestion: A Review. *J. Trace Elem. Med. Biol.* **2020**, *58*, 126435.

(17) Chen, J.; Burns, F. P.; Moffitt, M. G.; Wulff, J. E. Thermally Crosslinked Functionalized Polydicyclopentadiene with a High Tg and Tunable Surface Energy. *ACS Omega* **2016**, *1* (4), 532–540. https://doi.org/10.1021/acsomega.6b00193.

(18) Cuthbert, T. J.; Li, T.; Speed, A. W. H.; Wulff, J. E. Structure of the Thermally Induced Cross-Link in *C*-Linked Methyl Ester-Functionalized Polydicyclopentadiene (*f*PDCPD). *Macromolecules* **2018**, *51* (5), 2038–2047. https://doi.org/10.1021/acs.macromol.7b02750.

(19) Cuthbert, T. J.; Li, T.; Wulff, J. E. Production and Dynamic Mechanical Analysis of Macro-Scale Functionalized Polydicyclopentadiene Objects Facilitated by Rational Synthesis and Reaction Injection Molding. *ACS Appl. Polym. Mater.* **2019**, *1* (9), 2460–2471. https://doi.org/10.1021/acsapm.9b00571.

(20) Li, T.; Wulff, J. E. Copolymers of Functionalized and Nonfunctionalized Polydicyclopentadiene. *ACS Appl. Polym. Mater.* **2021**, *3* (1), 110–115. https://doi.org/10.1021/acsapm.0c01196.

(21) Takano, S.; Inomata, K.; Ogasawara, K. Enantioconvergent Route to A-Cuparenone From Dicyclopentadiene. *J. Chem. Soc., Chem. Commun.* **1989**, 271–272.

(22) Zhu, J.; Yang, J.-Y.; Klunder, A. J. H.; Liu, Z.-Y.; Zwanenburg, B. A Stereo- and Enantioselective Approach to Clavulones from Tricyclodecadienone Using Flash Vacuum Thermolysis. *Tetrahedron* **1995**, *51* (20), 5847–5870. https://doi.org/10.1016/0040-4020(95)00237-3.

(23) Paquette, L. A.; Hamme, A. T.; Kuo, L. H.; Doyon, J.; Kreuzholz, R. Probe of the Stereochemically Determining Step in Squarate Ester Cascades. Proof That Helical Equilibration within the Octatetraene Intermediate Is Responsible and Definition of Steric Control Elements. *J. Am. Chem. Soc.* **1997**, *119* (6), 1242–1253. https://doi.org/10.1021/ja9632163.

(24) Nakada, Y.; Sugahara, T.; Ogasawara, K. An Enantioconvergent Route to (−)-Kainic Acid. *Tetrahedron Lett.* **1997**, *38* (5), 857–860. https://doi.org/10.1016/S0040-4039(96)02467-7.

(25) Tanaka, K.; Nakashima, H.; Taniguchi, T.; Ogasawara, K. A Concise Route to (+)-Estrone. *Org. Lett.* **2000**, *2* (13), 1915–1917. https://doi.org/10.1021/ol005988g.

(26) Sugahara, T.; Fukuda, H.; Iwabuchi, Y. Total Synthesis and Absolute Stereochemistry of Pentenocin B, a Novel Interleukin-1β Converting Enzyme Inhibitor. *J. Org. Chem.* **2004**, *69* (5), 1744–1747. https://doi.org/10.1021/jo035430x.

(27) Mander, L. N.; Thomson, R. J. Total Synthesis of Sordaricin. *J. Org. Chem.* **2005**, *70* (5), 1654–1670. https://doi.org/10.1021/jo048199b.

(28) Blakemore, D. C.; Bryans, J. S.; Carnell, P.; Chessum, N. E. A.; Field, M. J.; Kinsella, N.; Kinsora, J. K.; Osborne, S. A.; Williams, S. C. Synthesis and in Vivo Evaluation of 3-Substituted

Gababutins. *Bioorg. Med. Chem. Lett.* **2010**, *20* (1), 362–365. https://doi.org/10.1016/j.bmcl.2009.10.089.

(29) Dobler, D.; Reiser, O. Synthesis of 6-Substituted 2-Pyrones Starting from Renewable Resources: Total Synthesis of Sibirinone, (*E*)-6-(Pent-1-en-1-yl)-2*H*-pyran-2-one, and (*E*)-6-(Hept-1-en-1-yl)-2*H*-pyran-2-one. *J. Org. Chem.* **2016**, *81* (21), 10357–10365. https://doi.org/10.1021/acs.joc.6b01339.

(30) Kotha, S.; Keesari, R. R. A Modular Approach to Angularly Fused Polyquinanes via Ring-Rearrangement Metathesis: Synthetic Access to Cameroonanol Analogues and the Basic Core of Subergorgic Acid and Crinipellin. *J. Org. Chem.* **2021**, *86*, 17129–17155.

(31) While the polymerization of $\mathbf{4_m}$ has not, to the best of our knowledge, been reported previously, the polymerization of certain structurally related monomers derived by Pauson–Khand coupling of norbornene, CO, and alkynes has been described by Novak and co-workers; see refs. 32–33.

(32) Yamanaka, T.; Novak, B. M. Ring-Opening Metathesis Polymerization (ROMP) of Substituted Norbornenes Derived by the Pauson-Khand (PK) Reaction. *Polym. Prepr. (Am. Chem. Soc., Div. Polym. Chem.)* **1998**, *39*, 194–195.

(33) Sakai, T.; Novak, B. M. A Study of the Vinyl Addition Polymerization of Polar Substituted Norbornenes with Late Transition Metal Catalysts. *Polym. Prepr. (Am. Chem. Soc., Div. Polym. Chem.)* **2001**, *42*, 419–420.

(34) Mihelich, E. D.; Eickhoff, D. J. One-Pot Conversion of Olefins to a,β-Unsaturated Carbonyl Compounds. An Easy Synthesis of 2-Cyclopentenone and Related Compounds. *J. Org. Chem.* **1983**, *48* (22), 4135–4137. https://doi.org/10.1021/jo00170a060.

(35) Sutor, D. J. The C–H···O Hydrogen Bond in Crystals. *Nature* **1962**, *195*, 68–69. https://doi.org/10.1038/195068a0.

(36) Sutor, D. J. Evidence for the Existence of C–H···O Hydrogen Bonds in Crystals. *J. Chem. Soc.* **1963**, 1105–1110. https://doi.org/10.1039/JR9630001105.

(37) Schwalbe, C. H. June Sutor and the C–H···O Hydrogen Bonding Controversy. *Crystallogr. Rev.* **2012**, *18* (3), 191–206. https://doi.org/10.1080/0889311X.2012.674945.

(38) Benaglia, M.; Danelli, T.; Fabris, F.; Sperandio, D.; Pozzi, G. Poly(Ethylene Glycol)-Supported Tetrahydroxyphenyl Porphyrin: A Convenient, Recyclable Catalyst for Photooxidation Reactions. *Org. Lett.* **2002**, *4* (24), 4229–4232. https://doi.org/10.1021/ol0267230.

(39) Borsato, G.; De Lucchi, O.; Fabris, F.; Lucchini, V.; Frascella, P.; Zambon, A. Synthesis and Evaluation of New Chiral Diols Based on the Dicyclopentadiene Skeleton. *Tetrahedron Lett.* **2003**, *44* (17), 3517–3520. https://doi.org/10.1016/S0040-4039(03)00664-6.

(40) Pozzi, G.; Mercs, L.; Holczknecht, O.; Martimbianco, F.; Fabris, F. Straightforward Synthesis of a Fluorous Tetraarylporphyrin: An Efficient and Recyclable Sensitizer for Photooxygenation Reactions. *Adv. Synth. Catal.* **2006**, *348* (12–13), 1611–1620. https://doi.org/10.1002/adsc.200606092.

(41) Álvarez, C.; Peláez, R.; Medarde, M. New Dicyclopentadiene-Based Scaffolds. *Tetrahedron* **2007**, *63* (10), 2132–2141. https://doi.org/10.1016/j.tet.2007.01.001.

(42) Silvestrini, M.; Ciappa, A.; Fabris, F.; Borsato, G.; De Lucchi, O. Detection of Singlet Oxygen Generated by Commercial Fine Art Organic Pigments by Means of a Novel, Robust Chemical Probe. *Dyes Pigm.* **2012**, *92* (3), 1351–1354. https://doi.org/10.1016/j.dyepig.2011.09.018.

(43) Li, J.; Stoltz, B. M.; Grubbs, R. H. Enantioselective Synthesis of 15-Deoxy-$\Delta^{12,14}$-Prostaglandin J_2. *Org. Lett.* **2019**, *21* (24), 10139–10142. https://doi.org/10.1021/acs.orglett.9b04198.

(44) Yanai, T.; Tew, D. P.; Handy, N. C. A New Hybrid Exchange–Correlation Functional Using the Coulomb-Attenuating Method (CAM-B3LYP). *Chem. Phys. Lett.* **2004**, *393* (1), 51–57. https://doi.org/10.1016/j.cplett.2004.06.011.

(45) Hariharan, P. C.; Pople, J. A. The Influence of Polarization Functions on Molecular Orbital Hydrogenation Energies. *Theoret. Chim. Acta* **1973**, *28* (3), 213–222. https://doi.org/10.1007/BF00533485.

(46) Hehre, W. J.; Ditchfield, R.; Pople, J. A. Self-Consistent Molecular Orbital Methods. XII. Further Extensions of Gaussian-Type Basis Sets for Use in Molecular Orbital Studies of Organic Molecules. *J. Chem. Phys.* **1972**, *56* (5), 2257–2261. https://doi.org/10.1063/1.1677527.

(47) Otero-de-la-Roza, A.; DiLabio, G. A. Improved Basis-Set Incompleteness Potentials for Accurate Density-Functional Theory Calculations in Large Systems. *J. Chem. Theory Comput.* **2020**, *16* (7), 4176–4191. https://doi.org/10.1021/acs.jctc.0c00102.

(48) Steiner, T. C–H···O Hydrogen Bonding in Crystals. *Crystallogr. Rev.* **2003**, *9* (2–3), 177–228. https://doi.org/10.1080/08893110310001621772.

(49) Weigend, F.; Ahlrichs, R. Balanced Basis Sets of Split Valence, Triple Zeta Valence and Quadruple Zeta Valence Quality for H to Rn: Design and Assessment of Accuracy. *Phys. Chem. Chem. Phys.* **2005**, *7* (18), 3297–3305. https://doi.org/10.1039/b508541a.

(50) Zhao, Y.; Truhlar, D. G. The M06 Suite of Density Functionals for Main Group Thermochemistry, Thermochemical Kinetics, Noncovalent Interactions, Excited States, and Transition Elements: Two New Functionals and Systematic Testing of Four M06-Class Functionals and 12 Other Functionals. *Theor. Chem. Acc.* **2008**, *120* (1), 215–241. https://doi.org/10.1007/s00214-007-0310-x.

(51) Becke, A. D. Density-functional Thermochemistry. III. The Role of Exact Exchange. *J. Chem. Phys.* **1993**, *98*, 5648–5652. https://doi.org/10.1063/1.464913.

(52) Lee, C.; Yang, W.; Parr, R. G. Development of the Colle-Salvetti Correlation-Energy Formula into a Functional of the Electron Density. *Phys. Rev. B* **1988**, *37* (2), 785–789. https://doi.org/10.1103/PhysRevB.37.785.

(53) Li, Y.-L.; Jia, X.-M.; Zhang, X.-Z.; Lu, Z.-Y.; Qian, H.-J. Effect of the Polar Group Content on the Glass Transition Temperature of ROMP Copolymer. *Soft Matter.* **2023**, *19* (1), 128–136.

(54) Shao, C.; Yu, H.-J.; Wu, N.-Y.; Feng, C.-G.; Lin, G.-Q. C1-Symmetric Dicyclopentadienes as New Chiral Diene Ligands for Asymmetric Rhodium-Catalyzed Arylation of *N*-Tosylarylimines. *Org. Lett.* **2010**, *12* (17), 3820–3823. https://doi.org/10.1021/ol101531r.

(55) Choi, T.-L.; Grubbs, R. H. Controlled Living Ring-Opening-Metathesis Polymerization by a Fast-Initiating Ruthenium Catalyst. *Angew. Chem. Int. Ed.* **2003**, *42* (15), 1743–1746. https://doi.org/10.1002/anie.200250632.

(56) Long, T. R.; Elder, R. M.; Bain, E. D.; Masser, K. A.; Sirk, T. W.; Yu, J. H.; Knorr, D. B.; Lenhart, J. L. Influence of Molecular Weight between Crosslinks on the Mechanical Properties of Polymers Formed *via* Ring-Opening Metathesis. *Soft Matter.* **2018**, *14* (17), 3344–3360. https://doi.org/10.1039/C7SM02407J.

(57) One complicating factor in this analysis is that the three different materials discussed above necessarily all contained different amounts of ENB co-monomer, a known chain-extender (see ref. 56). However, control experiments in which ENB was added to monomer **4m** prior to polymerization confirm that the ENB concentration plays a less significant role in changing the M_c than does the monomer functionality. For example, adding 20% ENB to **4m** prior to polymerization results in an equivalent M_c to that of PDCPD prepared with only 5% ENB.

(58) Love, J. A.; Morgan, J. P.; Trnka, T. M.; Grubbs, R. H. A Practical and Highly Active Ruthenium-Based Catalyst That Effects the Cross Metathesis of Acrylonitrile. *Angew. Chem. Int. Ed.* **2002**, *41* (21), 4035–4037. https://doi.org/10.1002/1521-3773(20021104)41:21<4035::AID-ANIE4035>3.0.CO;2-I.

(59) Jańczuk, B.; Białopiotrowicz, T. Surface Free-Energy Components of Liquids and Low Energy Solids and Contact Angles. *J. Colloid Interface Sci.* **1989**, *127* (1), 189–204. https://doi.org/10.1016/0021-9797(89)90019-2.

(60) Fowkes, F. M. Attractive Forces at Interfaces. *Ind. Eng. Chem.* **1964**, *56* (12), 40–52. https://doi.org/10.1021/ie50660a008.

(61) Jie-Rong, C.; Wakida, T. Studies on the Surface Free Energy and Surface Structure of PTFE Film Treated with Low Temperature Plasma. *J. Appl. Polym. Sci.* **1997**, *63* (13), 1733–1739. https://doi.org/10.1002/(SICI)1097-4628(19970328)63:13<1733::AID-APP4>3.0.CO;2-H.

(62) MacKerell, A. D.; Bashford, D.; Bellott, M.; Dunbrack, R. L.; Evanseck, J. D.; Field, M. J.; Fischer, S.; Gao, J.; Guo, H.; Ha, S.; Joseph-McCarthy, D.; Kuchnir, L.; Kuczera, K.; Lau, F. T. K.; Mattos, C.; Michnick, S.; Ngo, T.; Nguyen, D. T.; Prodhom, B.; Reiher, W. E.; Roux, B.; Schlenkrich, M.; Smith, J. C.; Stote, R.; Straub, J.; Watanabe, M.; Wiórkiewicz-Kuczera, J.; Yin, D.; Karplus, M. All-Atom Empirical Potential for Molecular Modeling and Dynamics Studies of Proteins. *J. Phys. Chem. B* **1998**, *102* (18), 3586–3616. https://doi.org/10.1021/jp973084f.

(63) Thompson, A. P.; Aktulga, H. M.; Berger, R.; Bolintineanu, D. S.; Brown, W. M.; Crozier, P. S.; in 't Veld, P. J.; Kohlmeyer, A.; Moore, S. G.; Nguyen, T. D.; Shan, R.; Stevens, M. J.; Tranchida, J.; Trott, C.; Plimpton, S. J. LAMMPS - a Flexible Simulation Tool for Particle-Based Materials Modeling at the Atomic, Meso, and Continuum Scales. *Comput. Phys. Commun.* **2022**, *271* (108171). https://doi.org/10.1016/j.cpc.2021.108171.

(64) Stukowski, A. Visualization and Analysis of Atomistic Simulation Data with OVITO–the Open Visualization Tool. *Modelling Simul. Mater. Sci. Eng.* **2009**, *18* (1), 015012. https://doi.org/10.1088/0965-0393/18/1/015012.

(65) Knorr, D.; Masser, K.; Elder, R.; Sirk, T.; Hindenlang, M.; Yu, J.; Richardson, A.; Boyd, S.; Spurgeon, W.; Lenhart, J. Overcoming the Structural versus Energy Dissipation Trade-off in Highly Crosslinked Polymer Networks: Ultrahigh Strain Rate Response in Polydicyclopentadiene. *Compos. Sci. Technol.* **2015**, 114, 17–25 https://doi.org/10.1016/j.compscitech.2015.03.021

(66) O'Boyle, N. M.; Banck, M.; James, C. A.; Morley, C.; Vandermeersch, T.; Hutchison, G. R. Open Babel: An Open Chemical Toolbox. *J. Cheminfo.* **2011**, *3* (1), 33. https://doi.org/10.1186/1758-2946-3-33.

(67) Halgren, T. A. Merck Molecular Force Field. I. Basis, Form, Scope, Parameterization, and Performance of MMFF94. *J. Comput. Chem.* **1996**, *17* (5-6), 490–519. https://doi.org/10.1002/(sici)1096-987x(199604)17:5/6<490::aid-jcc1>3.0.co;2-p.

(68) Grimme, S.; Antony, J.; Ehrlich, S.; Krieg, H. A Consistent and Accurate Ab Initio Parametrization of Density Functional Dispersion Correction (DFT-D) for the 94 Elements H-Pu. *J. Chem. Phys.* **2010**, *132* (15), 154104. https://doi.org/10.1063/1.3382344.

(69) Frisch, M. J.; Trucks, G. W.; Schlegel, H. B.; Scuseria, G. E.; Robb, M. A.; Cheeseman, J. R.; Scalmani, G.; Barone, V.; Petersson, G. A.; Nakatsuji, H.; Li, X.; Caricato, M.; Marenich, A. V.; Bloino, J.; Janesko, B. G.; Gomperts, R.; Mennucci, B.; Hratchian, H. P.; Ortiz, J. V.; Izmaylov, A. F.; Sonnenberg, J. L.; Williams-Young, D.; Ding, F.; Lipparini, F.; Egidi, F.; Goings, J.; Peng, B.; Petrone, A.; Henderson, T.; Ranasinghe, D.; Zakrzewski, V. G.; Gao, J.; Rega, N.; Zheng, G.; Liang, W.; Hada, M.; Ehara, M.; Toyota, K.; Fukuda, R.; Hasegawa, J.; Ishida, M.; Nakajima, T.; Honda, Y.; Kitao, O.; Nakai, H.; Vreven, T.; Throssell, K.; Montgomery Jr., J. A.; Peralta, J. E.; Ogliaro, F., Bearpark, M. J.; Heyd, J. J.; Brothers, E. N.; Kudin, K. N.; Staroverov, V. N.; Keith, T. A.; Kobayashi, R.; Normand, J.; Raghavachari, K.; Rendell, A. P.; Burant, J. C.; Iyengar, S. S.; Tomasi, J.; Cossi, M.; Millam, J. M.; Klene, M.; Adamo, C.; Cammi, R.; Ochterski, J. W.; Martin, R. L.; Morokuma, K.; Farkas, O.; Foresman, J. B.; Fox, D. J. Gaussian 16 (Revision C.01), Gaussian Inc., Wallingford, CT, 2016.

(70) Cheeseman, J. R.; Trucks, G. W.; Keith, T. A.; Frisch, M. J. A Comparison of Models for Calculating Nuclear Magnetic Resonance Shielding Tensors. *J. Chem. Phys.* **1996**, *104* (14), 5497–5509. https://doi.org/10.1063/1.471789.

Chapter 3: Toughened Polydicyclopentadiene Copolymers by Dicyclopentadienone Monomer Incorporation

Benjamin Godwin, Adam Sylvain-Stewart, and Jeremy E. Wulff**

3.0. Contributions

Synthetic work, sample preparation, tensile testing, differential scanning calorimetry, thermogravimetric analysis and ^{1}H and ^{13}C solution NMR was performed by Benjamin Godwin. Dynamic mechanical thermal analysis, swelling, and IR spectroscopy was performed by Adam Sylvain-Stewart and Benjamin Godwin. The photoreactor was built by Sean Adams, Kody Matthews and Chris Secord at the University of Victoria. Chris Secord and Kody Matthews cut samples.

3.1. Abstract

Engineering plastics are a class of polymer materials with enhanced mechanical and thermal properties. Polydicyclopentadiene (PDCPD) is an emerging example of this class of material derived from petrochemical waste. Herein, we describe the copolymerization of dicyclopentadiene with novel oxa-dicyclopentadiene monomer to produce mechanically and thermally superior PDCPD based materials. We also improve surface functionality and resistance to oxidative embrittlement, two major barriers to further adoption of this material.

3.2. Introduction

Polydicyclopentadiene (PDCPD) is a thermosetting polymer derived from the ring opening metathesis polymerization (ROMP) of dicyclopentadiene (DCPD).[1,2] PDCPD has significant commercial value owing to its excellent mechanical and thermal properties. It is particularly favored for its impact resistance at both high and low temperatures.[3,4] It also benefits from a reduced carbon footprint, since DCPD is readily available as waste from the C5 faction of petroleum distillates (where it results from the spontaneous dimerization of cyclopentadiene, following distillation) and as the byproduct of steam cracking of heavy distillates to make ethylene.[1] Additionally, due to the energy contained in the strained norbornene ring of the monomer, the polymerization—and therefore the manufacturing—of PDCPD parts uses substantially less energy than other types of plastics such as polyethylene which requires a high temperature melt before injection molding in expensive high-pressure molds.[2,5,6]

Manufacturing of PDCPD is done through reaction injection molding (RIM).[2] In RIM a resin (mixture of catalyst, monomer(s), inhibitors, additives) is injected into a mold and heated to a moderate temperature.[2] This initial heating prompts the extremely exothermic ROMP reaction with temperatures often exceeding 200°C spontaneously.[2,5,6] This process requires low pressure molds and little energy input compared to that of typical injection molding, which dramatically

reduces tooling and energy costs associated with production.[2] The utility of RIM is a major advantage of PDCPD. RIM is high throughput (a typical cycle takes less than 5 minutes), and very large parts (up to 100 kg) can be made very quickly.[2] Complex geometries are easily incorporated owing to the low viscosity of the resin.[2] Recent advances by the Moore group have also shown that the energy required for PDCPD molding can be lowered even further using frontal polymerization, wherein only a small amount of initial heat is required to start the polymerization reaction.[5–8] The exotherm of the ROMP reaction maintains the heat required for continued polymerization and curing of the final product.[5–8]

While PDCPD has many good qualities, it has poor end-of-life utility owing to the crosslinked matrix that is required for its desirable mechanical and thermal properties.[1,2,9,10] Crosslinked thermosets do not melt, and therefore it is not possible to recycle the material using typical methods.[11] In addition to its lack of end-of-life utility, PDCPD has several other disadvantages that restrict its wider adoption. As the crosslinking and polymerization reactions occur simultaneously, monomer can be trapped in the polymer matrix leading to an unpleasant acrid odor (perceptible at 3–5 ppb).[2,12] Additionally, due to the lack of hetero-atom inclusion, PDCPD is not chemically tunable and has a low surface energy when it is freshly prepared.[2] The low surface energy precludes the use of paints and adhesives without a surface oxidation step. Waiting for the polymer to oxidize bottlenecks the otherwise rapid RIM process.[2] The low polarity of the matrix also results in low interfacial adhesion with commercially available fiber reinforcements with typical (polar) sizing geared towards epoxy and polyester resin systems.[2,13]

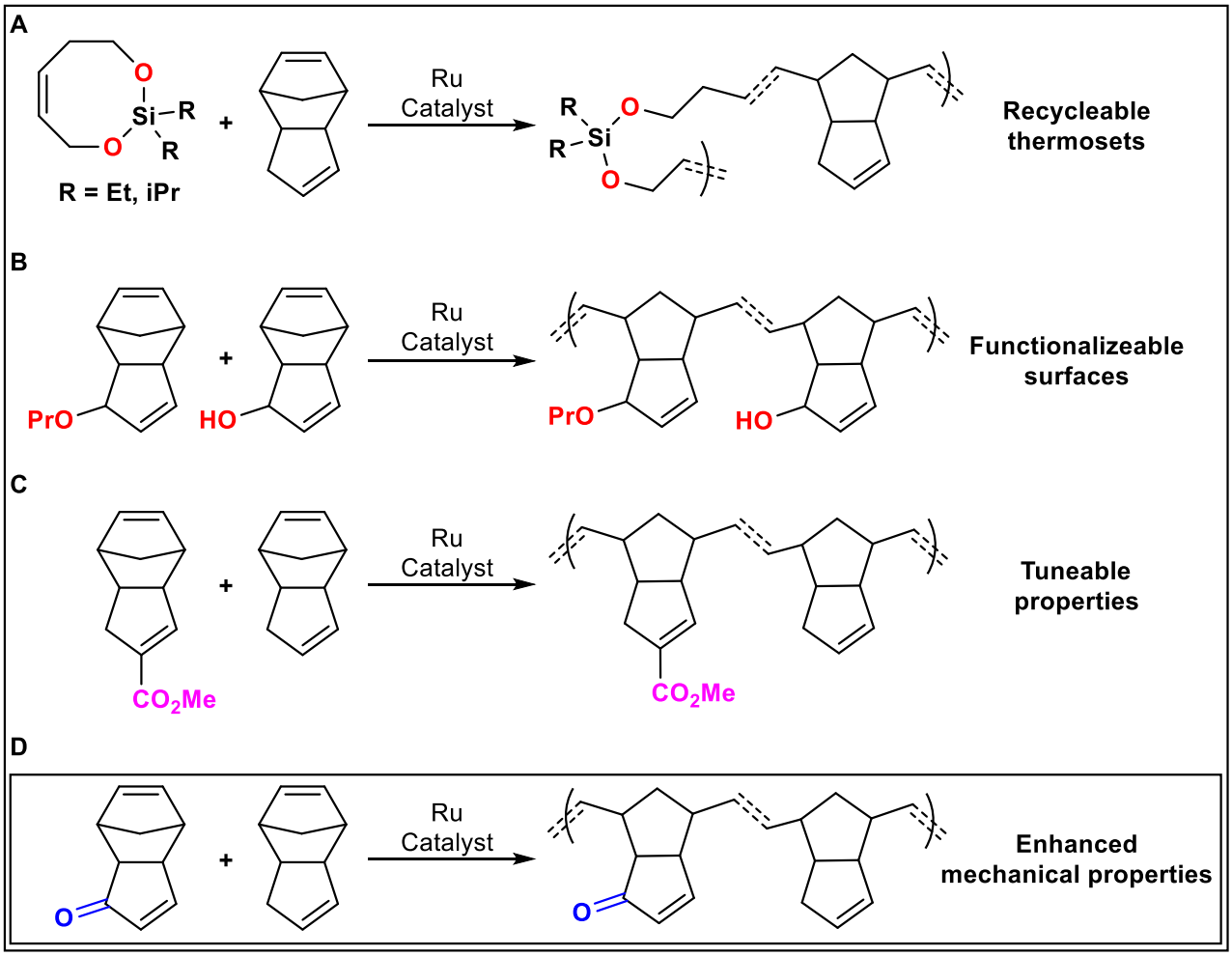

Figure 3.1. Recent copolymerization strategies for PDCPD. A: Degradable thermosets via copolymerization with cleavable silyl ethers. B: Copolymerization of functional DCPD based monomers leading to tunable PDCPD materials. C: Copolymerization of *f*DCPD and DCPD resulting in materials with adaptable and functional surfaces. D: This work, copolymerization of oxaDCPD and DCPD producing materials with enhanced mechanical properties.

In previous work, we and others have shown that many of these disadvantages can be solved by incorporating various functional groups.[12,14–17] Incorporation of functional groups reduces the vapor pressure or imparts pleasant odors to the monomer.[12,17,18] The polarity of these included functional groups lead to increased water contact angles and thus greater surface energy upon fresh

preparation.[12,14,17,18] Additionally, these functional monomers lead to enhanced or tunable mechanical properties.[16–18] The challenge and practicality of the installation of such functional groups ranges greatly, but in general leads to a monomer that is significantly more laborious and thus expensive to produce. Copolymerization has arisen as a suitable strategy to combat these and the other aforementioned issues.

The Johnson and Moore groups have shown that the inclusion of small amounts of silyl ether species into DCPD resins leads to thermosets that can be degraded into reuseable oligomers (Figure 3.1A).[9,10] The Xu and the Lemcoff groups each reported the selenium dioxide oxidation of DCPD. This preparation is simple to carry out but requires the use of stoichiometric selenium dioxide which has been shown to be toxic. More importantly, the atom economy of this method is poor and not practical for industrial purposes.[12,15] Nevertheless, the allylic alcohol product can derivatized through esterification or etherification, leading to a diverse range of monomers which all undergo polymerization in the presence of the Grubbs 1st and 2nd generation initiators.[12,15,16] However the resulting polymers and copolymers all suffer from the thermal liability of allylic functional groups. This leads to facile two-step decomposition above 200 °C observed via TGA. Furthermore, these polymers also display glass transition temperatures of <100 °C, which is not practical for current applications of PDCPD.

Our group has now pioneered two different approaches to functionalizing DCPD.[17,18] The first-generation, ester-functionalized DCPD (*f*DCPD) utilized a vinyl ester formed through the Diels–Alder reaction of cyclopentadiene and carboxylated cyclopentadiene.[18,19] This monomer produced a glassy polymer through reaction injection molding that had similar mechanical and thermal properties to native PDCPD but with the benefit of a fruity ester odor, tunable surface energy, and facile functionalization.[14,18,20] However, significant (1 mol%) quantities of initiator

and substantial reaction time were required for polymerization. The production of the *f*DCPD monomer through the Diels–Alder reaction is also not atom economical.

Inspired by the ease of the Xu and Lemcoff approach, we were able to synthesize a much improved second-generation *f*DCPD (oxaDCPD).[17] OxaDCPD is readily synthesized on large (>200 g per batch) scale in the laboratory, and is purified using industrially relevant methods (distillation). We have also shown that oxaDCPD yields a glassy polymer through reaction injection molding, using modest (0.05 mol%) initiator loadings, and that this glassy polymer exceeds the benchmark mechanical and thermal properties set by the parent PDCPD.[17] Regarding the cost of production, however, oxaDCPD needs to be generated in a separate step, which necessarily increases its cost (and that of the corresponding homopolymer) relative to that of unfunctionalized DCPD (which is a petrochemical waste material). To benefit from the remarkable properties of oxaDCPD at a practical cost, we synthesized a series of oxaDCPD-co-DCPD copolymers. We aimed to find the minimal required amount of oxaDCPD needed to engender an improvement in thermal and/or mechanical properties.

Here we show the synthesis of eight different oxaDCPD-containing materials and corresponding controls, ranging from pure DCPD, to 40% oxaDCPD content. We also explore the effects of adding ethylidene norbornene (ENB), a commonly employed comonomer in academic research of PDCPD.[5,6,21] We assessed each material's tensile strength, toughness, Young's modulus, storage modulus, glass transition temperature and thermal stability through the use of macro-scale regular dimensioned samples accessed through reaction injection molding.

3.3. Results and Discussion

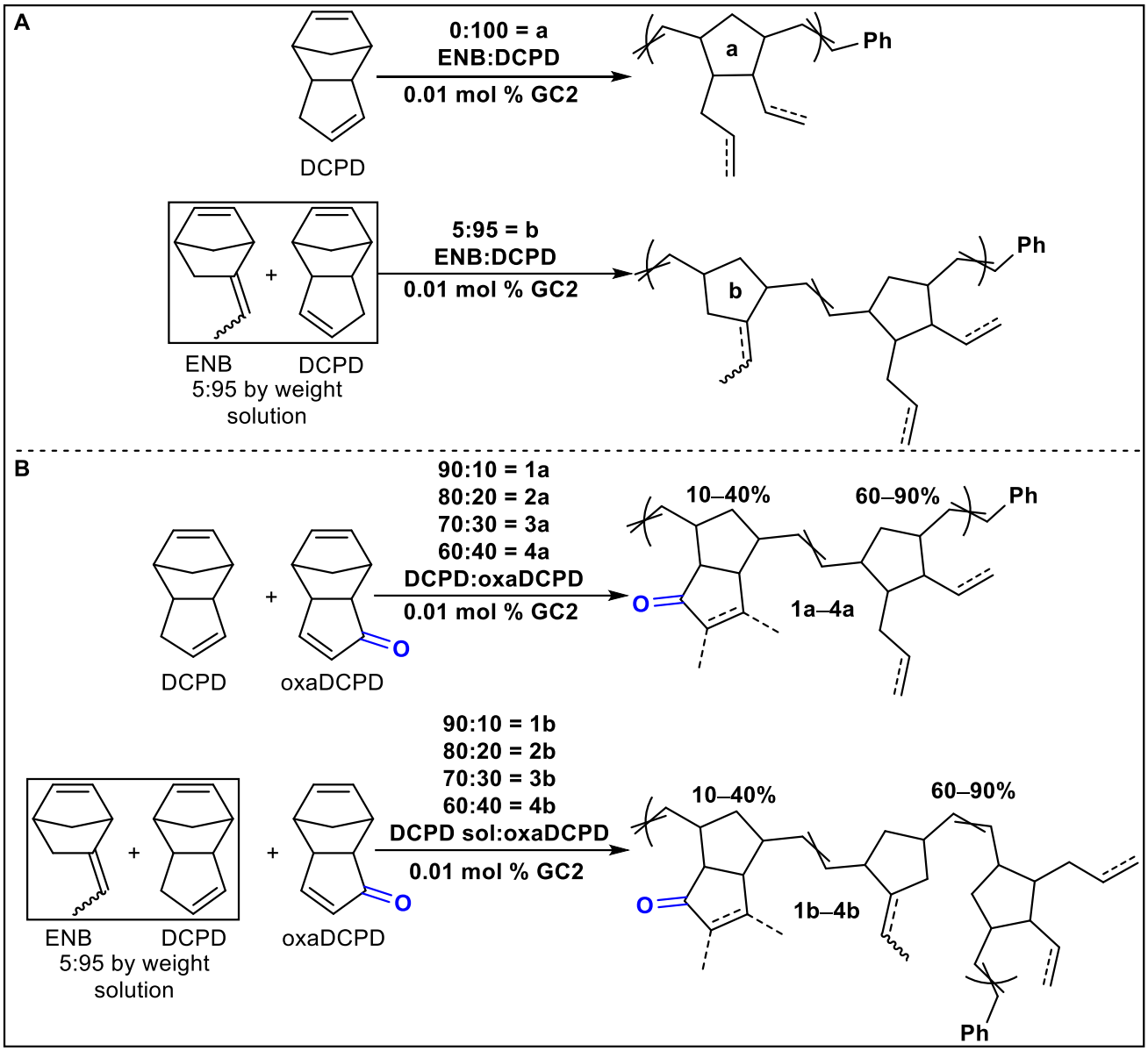

Figure 3.2. A: Synthesis of polydicyclopentadiene controls using Grubbs second generation initiator. B: Synthesis of oxaDCPD-*co*-DCPD copolymers.

Copolymers were produced via reaction injection molding, which is industrially relevant for PDCPD based materials.[1,2,22] We produced two different types of PDCPD-*co*-oxaDCPD copolymers and their respective PDCPD controls: in **type a** copolymers pure DCPD was used as

the comonomer, in **type b** copolymers a 95:5 solution of DCPD:ENB was used (Figure 3.2). This solution is commonly employed in the existing academic literature as a surrogate to DCPD. The addition of ENB depresses the melting point of DCPD (32.5 °C) below room temperature, making it easier to solubilize catalysts and inhibitors, and to enable simple laboratory reaction injection molding by preventing solidification of the resin during injection into a mold. Reaction injection molding of PDCPD control samples was initiated by adding Grubbs second-generation catalyst (GC2, 0.01 mol%) to a molten combination of monomers as shown in Figure 3.2A. Similarly, copolymers of DCPD, ENB, and oxaDCPD were made by combining various amounts of the different monomers by weight in the amounts shown in Figure 3.2B. Additional details are available in section 3.5.

In previous work we directly formed appropriately shaped samples for mechanical testing through RIM. However, due to the limitations of lab-scale reaction injection molding, this often leaves voids or other imperfections which leave many samples unusable. To remedy this, we produced rectangular, regular-dimensioned plaques that were then cut by the University of Victoria Science Machine Shop into the desired samples. The advantage to this is two-fold. It avoids wasting novel material on defective samples, and all samples are produced identically without any inconsistencies in surface- or edge-smoothness.

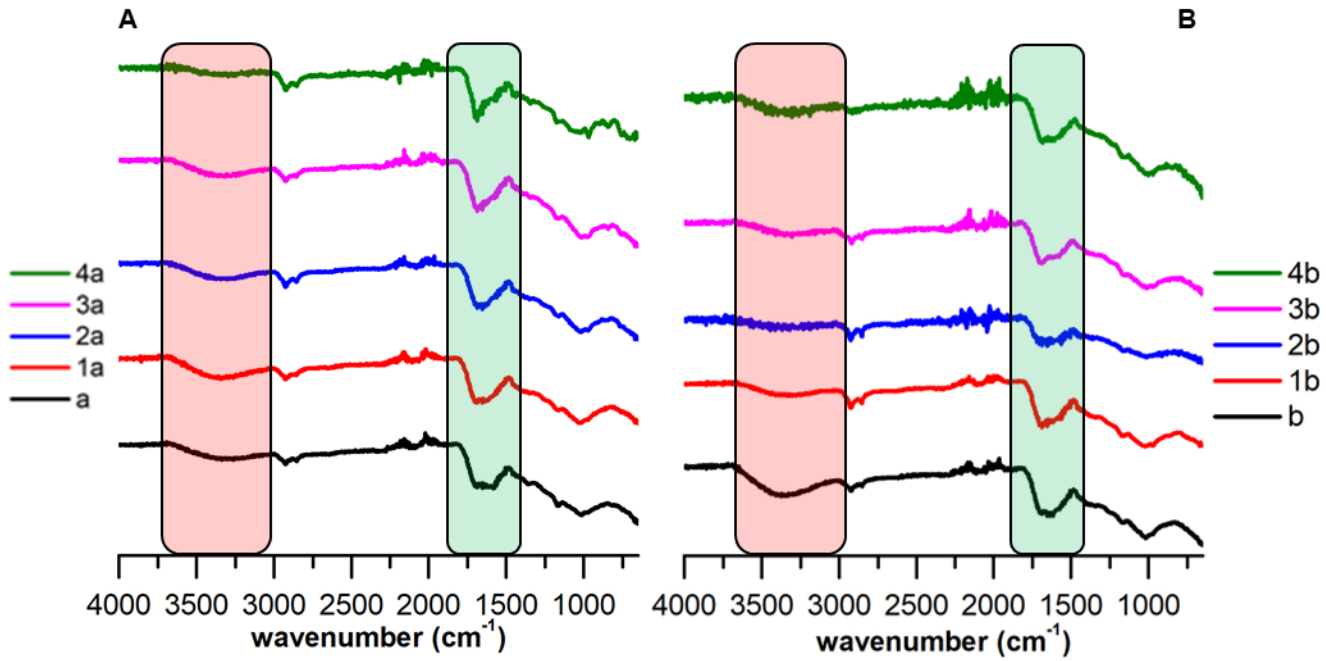

Figure 3.3. A: ATIR spectra of **a type** polymers after heating during DMTA. B: ATIR spectra of **b type** polymers after heating during DMTA.

Infrared spectroscopy of the freshly exposed surface of the reaction injection molded materials showed an increasing intensity of carbonyl stretch at *ca.* 1707 cm^{-1} in copolymers with increasing oxaDCPD content (Figures B4 and B7). There did not appear to be a difference in the presence of surface functionality between the **a** or **b** stream of copolymers. As expected, the freshly exposed surface of both PDCPD controls did not show any signals in the 3000–3300 cm^{-1} or ~1700 cm^{-1} regions, corresponding to hydroxyl or carbonyl functional groups. By contrast, samples exposed to air for greater than 24 hours after manufacturing showed both hydroxyl and carbonyl surface functionality (Figure B3 and B6). After heating during dynamic mechanical thermal analysis (DMTA, see the methods (section 3.5) for a detailed description of the heat treatment), PDCPD homopolymer samples showed higher intensities of hydroxyl surface functionality than did unheated PDCPD samples (Figure 3.3A and B). Interestingly, however, copolymers with

higher oxaDCPD content were able to resist the formation of surface hydroxyl groups, resulting in lower intensities of hydroxyl functionality.

The lack of surface functionality for freshly prepared PDCPD surfaces and over-oxidation upon exposure to air (resulting in autoxidation) are both major problems industrially.[2] Parts must be left to oxidize before painting or bonding can be done as lack of surface energy prevents these adhesives from sticking.[2] On the other hand, too much surface oxidation leads to oxidative embrittlement and reduces impact resistance, one of PDCPD's most prized characteristics.[23] The resistance of the copolymers to thermally induced oxidative embrittlement, while simultaneously presenting a controllably functionalized surface could be very advantageous to industry, offering decreased production times and tougher materials.

Both classes of copolymers and control PDCPD polymers swell dramatically (~200% of initial mass) in toluene, and all materials started to experience mass loss after 2 days of solvent exposure. The incorporation of polar oxaDCPD monomer into the copolymers did not seem to significantly increase the uptake of methanol as compared to neat samples of oxaDCPD prepared in previous work.[17]

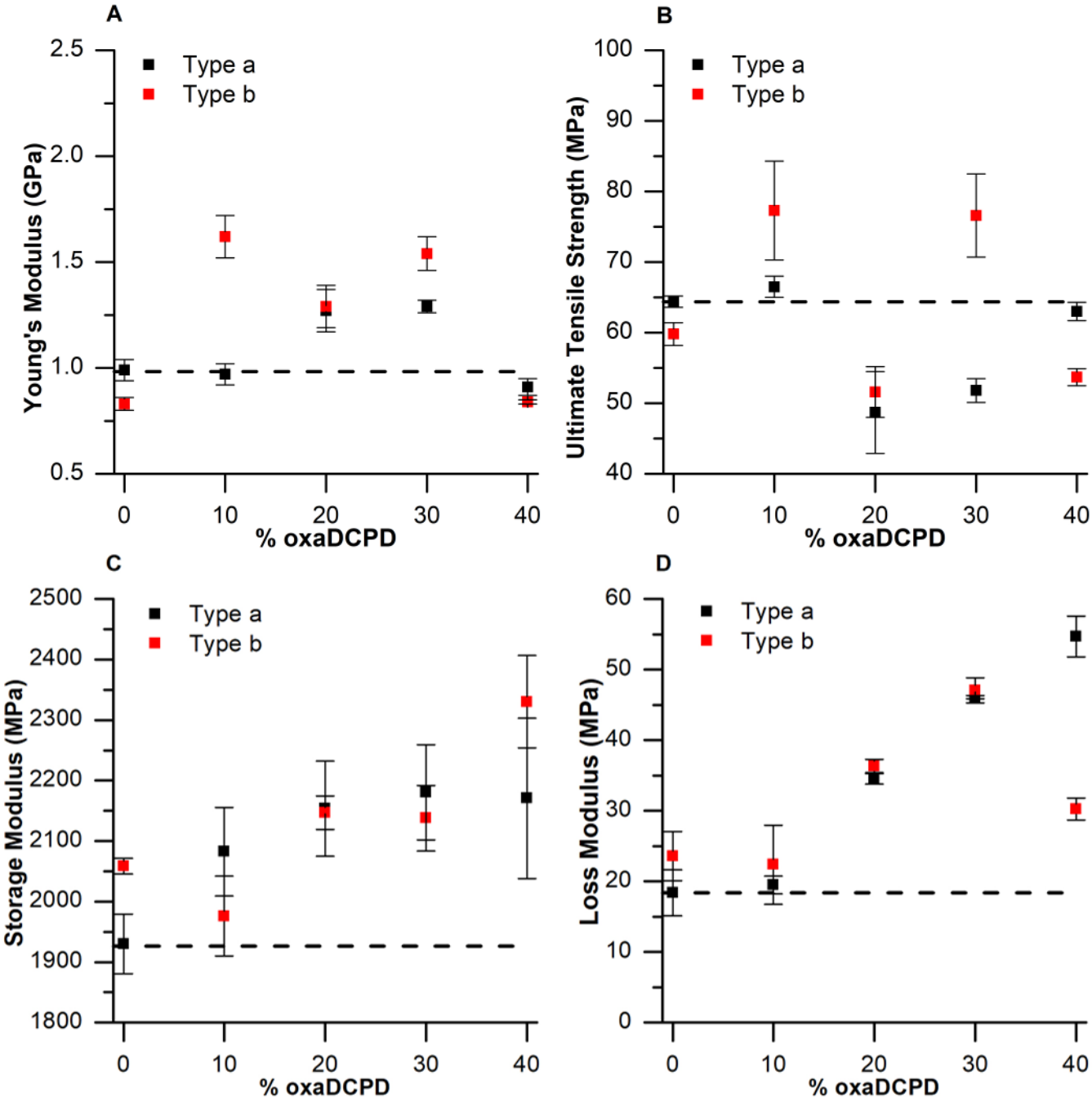

Figure 3.4. Mechanical properties of copolymers and corresponding PDCPD controls. A: Young's modulus. B: Ultimate tensile strength. C: Storage modulus. D: Loss modulus.

Data for panels A and B were obtained using ASTM d638 type V dogbone samples. Data for panels C and D were obtained using 25 x 10 x 3 mm bar samples. Error bars represent standard deviation of at least n = 3 replicates.

We interrogated the mechanical properties of the materials using dynamic mechanical thermal analysis (DMTA), and tensile testing. Young's modulus, ultimate tensile strength and toughness were assessed through tensile testing. The results are summarized in Figure 3.4A and 3.4B and Table B2. The increase in Young's modulus was consistently higher in **type b** samples and was highest overall for **1b**. The ultimate tensile strength of **type b** copolymers fluctuated greatly with increasing volume fraction of oxaDCPD. Similarly, **type a** copolymers also fluctuated with oxaDCPD content, with **1a** having the highest ultimate tensile strength of **type a** polymers. Modulus of toughness was calculated from the area under the curve of the tensile stress-strain curve (Figure 3.5). All **type b** samples except for **4b** had increased modulus of toughness than the native **b** polymer. Copolymers **1b** and **3b** showed the greatest increases in modulus of toughness. Samples **1a**, and **4a** had similar modulus of toughness as the type **a** homopolymer, whilst **2a** and **3a** exhibited lower toughness.

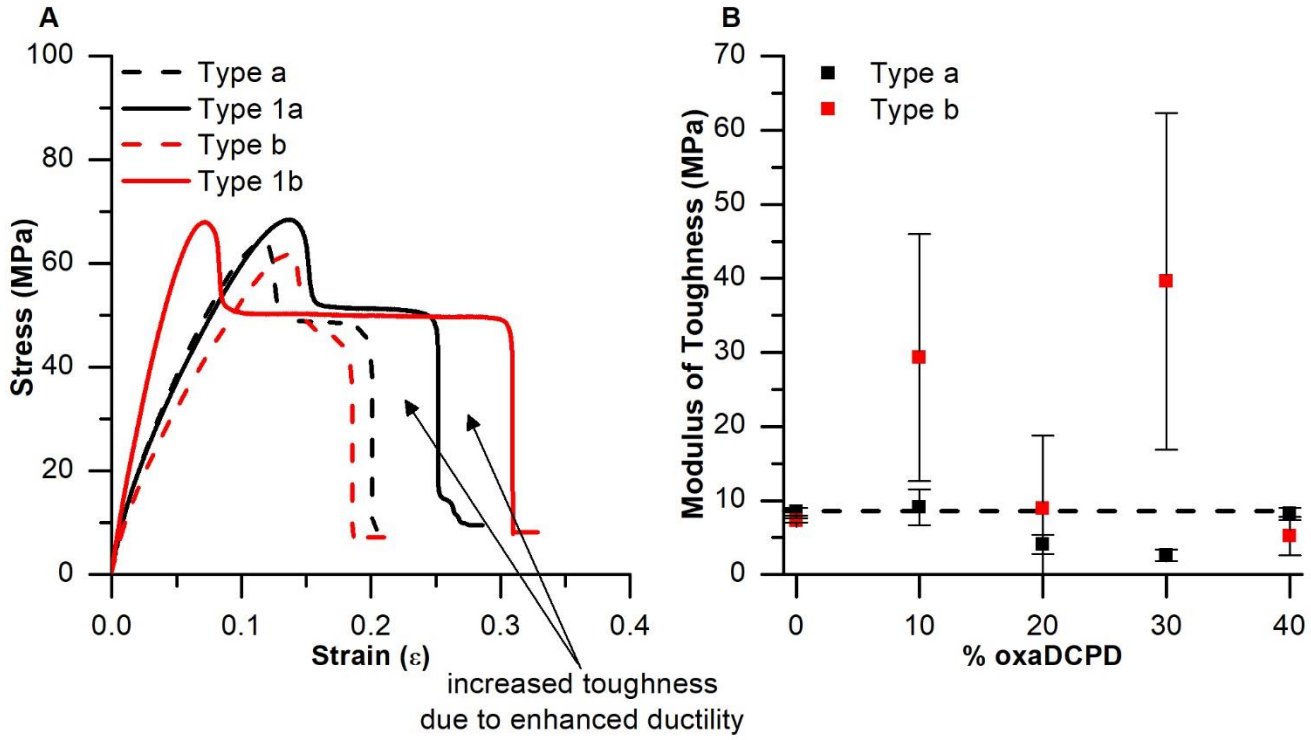

Figure 3.5. A: Tensile plots demonstrating the increased toughness of copolymers. B: Modulus of toughness of copolymers and corresponding PDCPD controls.

Data were obtained through tensile testing, using ASTM d638 type V dogbone samples. Error bars represent standard deviation of n = 3 for all samples.

The nonmonotonic differences between each copolymer and the variability in toughness may arise from the fact that the oxaDCPD monomer polymerizes more slowly than the native DCPD monomer (see Chapter 4). The reduction in reactivity is likely caused by temporary inhibition of the metathesis catalyst through the formation of a known oxygen chelate species.[24,25] This in turn may lead to the generation of a gradient copolymer wherein the concentration of ketones throughout the polymer is not uniform. Therefore, regions of the material may have higher concentrations of crosslinking density through the non-canonical hydrogen bonding interaction between the ketone and beta-hydrogen (Figure 3.6).[17,26–28] The size and morphology of these zones

likely also fluctuates with the volume fraction of oxaDCPD added through concentration dependent aggregation, crystallization and packing effects.

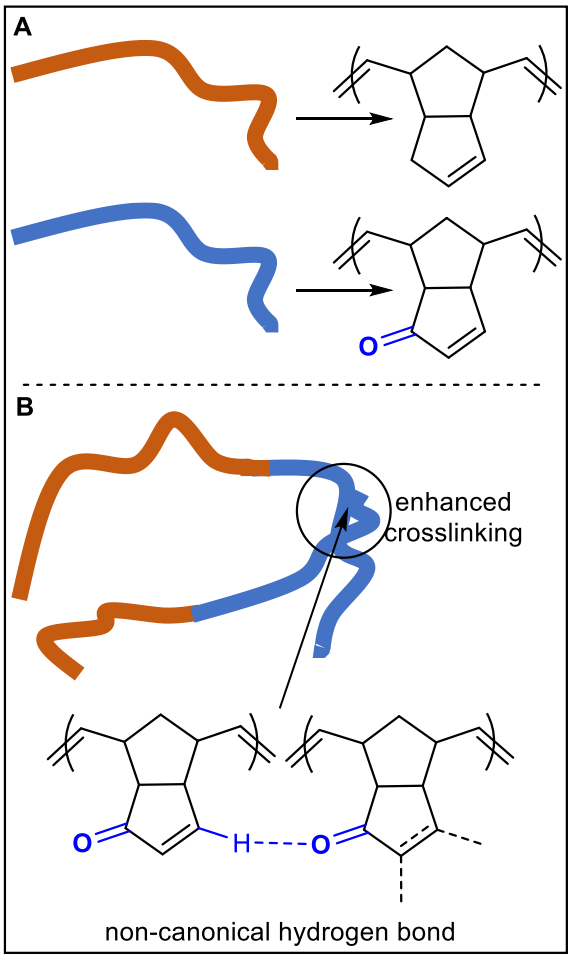

Figure 3.6. A: Cartoon depictions of PDCPD and oxaPDCPD. B: non-canonical hydrogen bonding in regions containing high concentrations of oxaDCPD.

The storage modulus and loss modulus were obtained via DMTA. The results are summarized in Figure 3.4C and 3.4D and Table B2. The storage modulus increased with the addition oxaDCPD content for both **type a** and **type b** copolymers. The exception being **1b** which saw a decrease in storage modulus. The loss modulus also followed a similar trend, increasing in a linear fashion from oxaDCPD fractions of 10% onward, except for **4b** which saw a sharp drop

in loss modulus. Interestingly, **1a** and **1b** did not show substantive increases in loss modulus like all other measured mechanical parameters. Instead, **1a** and **1b** had similar values of loss modulus compared to the native polymers **a** and **b** respectively. The maintenance and increase of the storage modulus in both classes of copolymers is of great significance, since PDCPD is an engineering plastic.[2,4] The ability to increase and tune both the stiffness and dampness of the material could be valuable when designing automative parts. By adding small amounts of oxaDCPD we can access a material that is stronger, stiffer, damper, and tougher than regular PDCPD. This could offer significant advantages, allowing automotive parts to be thinner and lighter—improving fuel economy while maintaining the required strength.

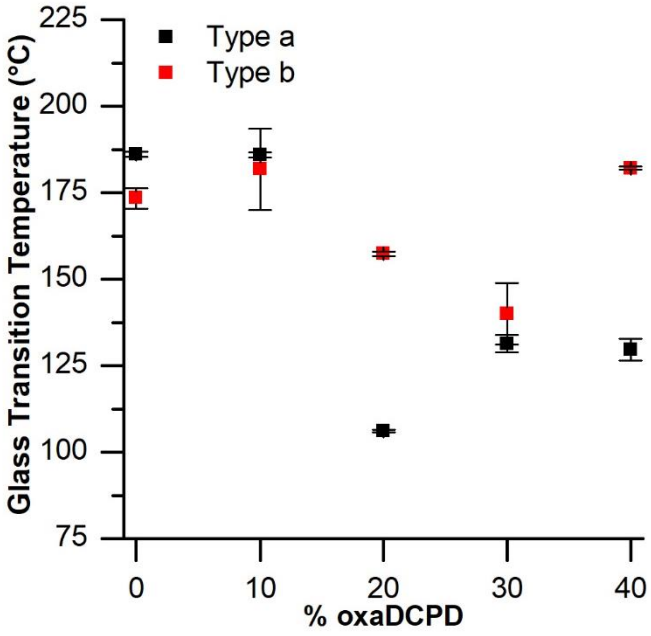

Figure 3.7. Glass transition temperatures of copolymers and corresponding PDCPD controls derived from the peak of the loss factor from DMTA experiments.

Error bars represent standard deviation of n = 3 for all samples.

We investigated the thermal properties of the new materials via DMTA, differential scanning calorimetry (DSC), and thermogravimetric analysis (TGA). The glass transition temperatures (T_g) were derived from the peak of the loss factor obtained through DMTA and further supported by DSC. The results are summarized in Figure 3.7, Table B1, and Figures B9–11, and B32 see the methods (section 3.5) for detailed experimental parameters. The T_g of copolymer **1a** was the highest of the copolymers, and was comparable to polymer **a**: 186.0°C vs 186.1°C. The T_g of **2a** was the lowest of all copolymers studied at 106.1 ± 0.4 °C. The **type b** samples were similar with an increase in T_g for sample **1b** and then a substantial depression of the T_g for sample **2b** and **3b**. In contrast to **4a** which had a depressed T_g of 129.7°C, sample **4b** had the highest T_g of **type b** samples at 182.1°C. This is possibly due to ENB acting as a chain extender reducing the crosslinking density in the **b type** homopolymer.[17,29] This results in a lowered T_g value as compared to the **a type** homopolymer. Once oxaDCPD is added, however, this increased chain flexibility enables ketone residues to form a greater number of crosslinks through non-canonical hydrogen bonding as compared to samples without ENB, leading to the observed increased T_g. Thermogravimetric analysis of samples **a**, **b**, **1a**, **1b**, **2b**, **3a**, **3b**, and **4b**, showed <10% mass loss up to 400 °C, indicated no thermal liabilities are introduced during the copolymerization process. Sample **4b** showed a small mass reduction at 300°C, probably due to loss of low molecular weight oligomers, but did not degrade beyond 15% mass loss before 400°C.

3.4. Conclusion

We manufactured eight novel PDPCD based copolymers using reaction injection molding, utilizing the easily accessible and scalable functional DCPD monomer oxaDCPD. We have shown that the addition of a small amount of this material to DCPD-based resins has a remarkable effect on the mechanical, chemical, and thermal properties on the resulting materials. We show that the tensile strength, Young's modulus, storage modulus, loss modulus, toughness, and glass transition

temperature can all be improved and/or tuned by utilizing oxaDCPD as a comonomer. We also show that resistance to surface autoxidation can be limited by the incorporation of oxaDCPD into the material. Additionally, the surface of freshly prepared material is already functionalized with polar ketone groups, enabling the potential for faster workflow and production. All of these properties are core to PDCPD's use as an engineering plastic on heavy machinery, and as a structural material.[2,4,13] The ability to improve these properties enables less material to be used to fulfill existing uses and may lead to further applications in niche markets like the aerospace industry that demand significantly more from materials.[2,4,13]

3.5. Methods

Materials

All commercial materials were used as received. Dicyclopentadiene (DCPD), 5-ethylidene-2-norbornene (ENB), and 4-dimethylaminopyridine were obtained from Millipore Sigma. Dichloromethane, pyridine, and acetic anhydride were obtained from Fisher Scientific. *Meso*-tetraphenylporphyrin was obtained for AK scientific. Tri-*n*-butyl-phosphite (TBP) was obtained from Alfa Aesar. Grubbs second generation catalyst (GC2) was obtained from Chem-Impex.

Spectroscopy

^{1}H and ^{13}C NMR spectra were obtained using a Bruker AVANCE 300 (300.27 MHz for ^{1}H, 75.51 MHz for ^{13}C) or a Bruker AVANCE NEO 500 (500.27 MHz for ^{1}H, 125.81 MHz for ^{13}C). Data were processed using MestReNova. Singlet = s, d = doublet, t = triplet, br = broad, app = apparent. IR spectra were recorded using an Agilent Cary 630 FTIR spectrometer with diamond ATIR attachment. Samples were measured as solids and pressed into the crystal using the supplied press.

Thermal analysis

Differential scanning calorimetry samples were run on a TA instruments DSC25 using TZero aluminum DSC pans with hermetic lid. A pin hole was added for solid samples using the tip of a 21 ½ gauge needle. An empty TZero aluminum DSC pan with TZero aluminum hermetic lid and pin hole was used as a reference. Samples were measured from 40°C to 250°C then cooled to −30 °C at 20 °C/min to erase thermal history then ramped at 10 °C/min from −30 °C to 250 °C. The T_g was obtained from the second trace. Thermogravimetric analysis was done on a TA instruments SDT Q600. Samples were heated at 20 °C per minute to a maximum temperature of 600°C, under a nitrogen atmosphere.

Mechanical testing

Dynamic mechanical thermal analysis was done on an Anton Paar Modular Compact Rheometer 302 fitted with an Anton Paar SRF-12 geometry and CTD 600 oven. Samples were measured through 25-T_g + 40 °C or 250 °C using a logarithmic strain of 0.01–0.1% at 1 Hz and a normal force of −0.1 N. Regular dimensioned 25 x 10 x 3 mm (Length x width x height) bar type samples were machined by the University of Victoria Science Machine Shop from reaction injection molded rectangular plaques. Glass transition temperatures were obtained from the peak of the loss factor and storage modulus at 25 °C or the closest next point. Tensile testing was performed using an Admet MtestQuattro machine. ASTM Type V dog bone samples were machined by the University of Victoria Science Machine Shop from reaction injection molded rectangular plaques. The ends of the samples were fixed between the grips and subjected to a loading rate of 10 mm/min. Force-displacement curves were obtained and converted to stress-strain curves. Stress is defined as the force on the cross-section area of the sample while strain represents the displacement to the initial length of the specimen. Strain was obtained as recorded from the instrument. Young's

modulus was obtained from the slope of the linear region of the stress–strain curve. Modulus of toughness was determined as the area under the stress–strain curve. Ultimate tensile strength was determined from the maximum of the stress–strain curve.

Melting points

Melting points were taken on an SRS digimelt and a Gallenkamp melting point apparatus.

Swelling Experiments

Swelling experiments were performed by subjecting polymer chunks to high vacuum at 0.15 mmHg for 2 hours prior to weighing. Samples were weighed then submerged in 10 mL of either methanol or toluene in a sealed vial. After the desired interval, samples were removed from the solvent, dabbed dry and weighed. Samples were then placed back into the solvent.

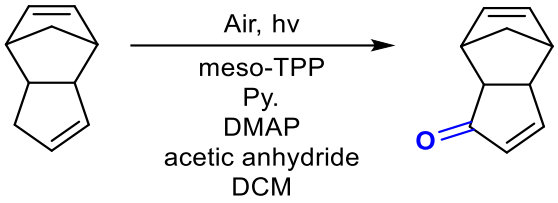

This compound was prepared as described in the literature.[17]

MP: 54–59 °C. ^{1}H NMR (300.27 MHz, Chloroform-*d*) δ 7.38 (dd, *J* = 5.8, 2.6 Hz, 1H), 5.98 – 5.92 (m, 2H), 5.78 (dd, *J* = 5.4, 2.9 Hz, 1H) 3.45 – 3.39 (m, 1H), 3.22 (br s, 1H), 2.97 (app s, 1H), 2.80 (app t, *J* = 5.1, 1H), 1.76 (dd, *J* = 8.4, 1.0 Hz, 1H), 1.63 (d, *J* = 8.5 Hz, 1H). ^{13}C NMR (125.81 MHz, Chloroform-*d*) δ 209.12, 163.79, 135.93, 131.76, 131.52, 51.84, 49.29, 47.36, 44.17, 43.28.

General reaction injection molding protocol

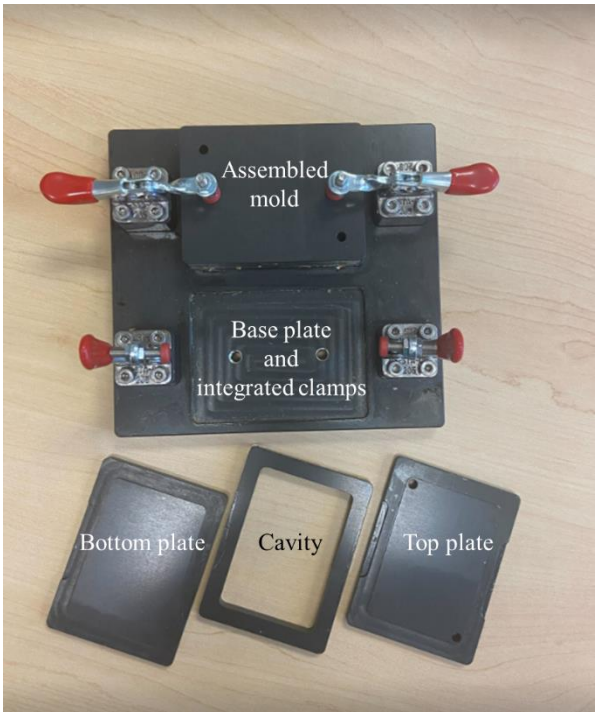

Monomer(s) were melted together at ~60°C and Tri-n-butyl-phosphite inhibitor was mixed into the liquid monomers. Grubbs 2nd generation catalyst was then added, and the mixture was sonicated to obtain a homogenous resin. The resin was poured into an aluminum 3 piece mold

through a plastic syringe until resin flowed back out through both sprue holes. The mold was tapped, tilted, and rotated from side to side and end to end to ensure the removal of all air bubbles. The mold was transferred to a 110°C oven and allowed to cure for 40 minutes.

a-Type reaction injection molding protocol

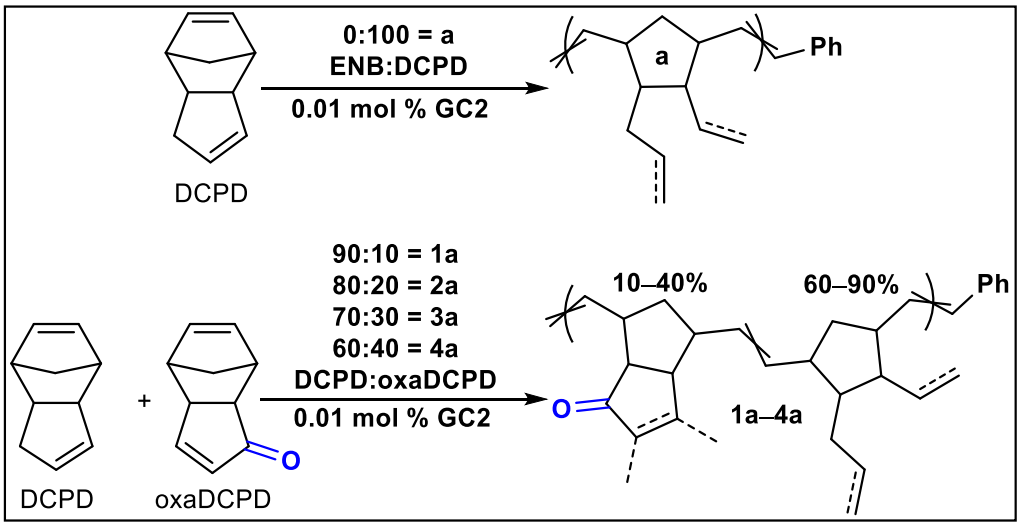

OxaDCPD (14.4091 g; 0.098 mol) and dicyclopentadiene (DCPD; 21.6284 g; 0.20 mol) were melted together until liquid. Tri-n-butyl-phosphite (15.6 mg; 0.062 mmol) was mixed in as an inhibitor. Grubbs 2nd generation catalyst (GC2; 22.0 mg; 0.026 mmol; ~0.01 mol%) was then added. The mixture was sonicated to obtain ~36 g of homogenous resin, 40% oxaDCPD by weight. This procedure was repeated for all weight fractions of 0, 10, 20, and 30 weight % of oxaDCPD. The resin was then injected through the barrel of a plastic syringe into a preheated (50 °C) aluminum mold until resin emerged from the opposite sprue hole. The mold was then tilted and tapped to ensure the removal of all air bubbles. The mold was transferred to a 110°C oven and allowed to cure for 40 minutes.

b-Type reaction injection molding protocol

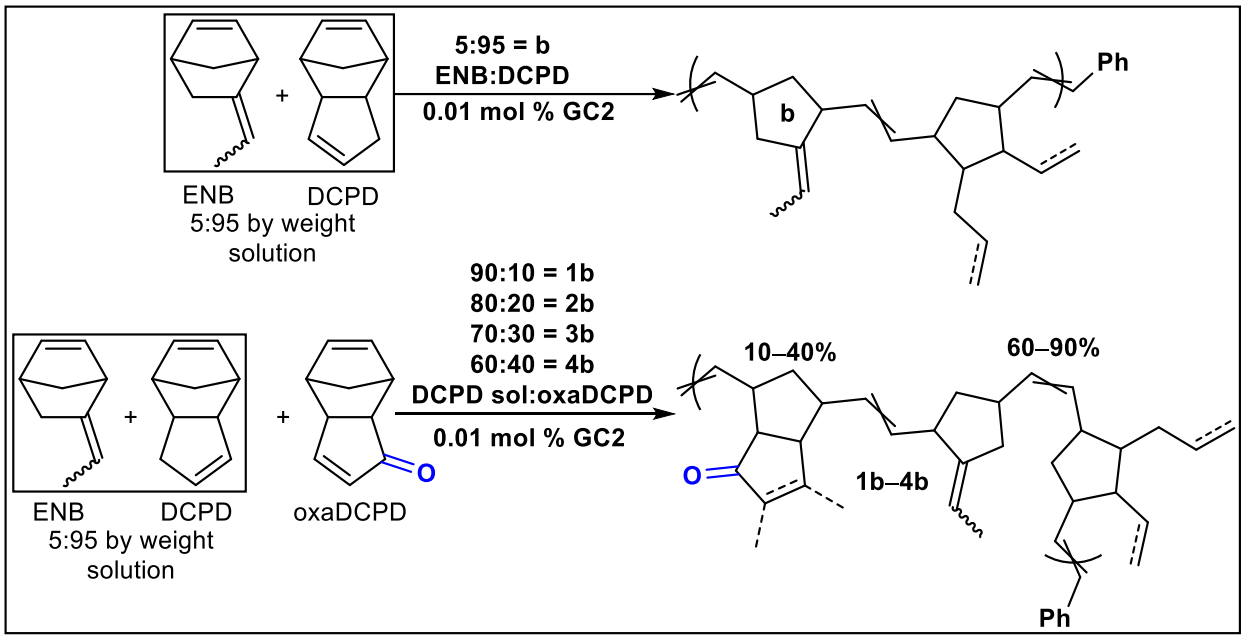

DCPD (151.44 g; 1.14 mol) was melted and ethylidene norbornene (ENB; 7.97 g; 0.066 mol) was added to obtain a liquid 95% DCPD, 5% ENB solution by weight. OxaDCPD (14.4159 g; 0.098 mol) was melted and added to a 21.6176 g aliquot of this solution. Tri-n-butyl-phosphite (17.5 mg; 0.069 mmol) was mixed in as an inhibitor. Grubbs 2nd generation catalyst (GC2; 21.5 mg; 0.025 mmol; ~0.01 mol%) was then added. The mixture was sonicated to obtain 36 g of homogenous 40% oxaDCPD by weight resin. This procedure was repeated for all weight fractions of 0, 10, 20, and 30 weight % of oxaDCPD. The resin was then injected through the barrel of a plastic syringe into an aluminum mold until resin emerged from the opposite sprue hole. The mold was then tilted and tapped to ensure the removal of all air bubbles. The mold was transferred to a 110°C oven and allowed to cure for 40 minutes.

3.6. References

(1) Kovačič, S.; Slugovc, C. Ring-Opening Metathesis Polymerisation Derived Poly(Dicyclopentadiene) Based Materials. *Mater. Chem. Front.* **2020**, *4* (8), 2235–2255. https://doi.org/10.1039/D0QM00296H.

(2) Vervacke, D. *An Introduction to PDCPD: Poly-Di-Cyclo-Penta-Diene*; Product Rescue, 2008.

(3) Beuguel, Q.; Kirillov, E.; Carpentier, J.-F.; Guillaume, S. M. Upgrading Toughness and the Glass Transition Temperature of Polydicyclopentadiene upon Addition of Styrene–Ethylene–Butylene–Styrene Thermoplastic Elastomer. *ACS Appl. Polym. Mater.* **2022**, *4* (4), 2251–2255. https://doi.org/10.1021/acsapm.1c01803.

(4) Le Gac, P. Y.; Choqueuse, D.; Paris, M.; Recher, G.; Zimmer, C.; Melot, D. Durability of Polydicyclopentadiene under High Temperature, High Pressure and Seawater (Offshore Oil Production Conditions). *Polym. Degrad. Stab.* **2013**, *98* (3), 809–817. https://doi.org/10.1016/j.polymdegradstab.2012.12.023.

(5) Robertson, I. D.; Yourdkhani, M.; Centellas, P. J.; Aw, J. E.; Ivanoff, D. G.; Goli, E.; Lloyd, E. M.; Dean, L. M.; Sottos, N. R.; Geubelle, P. H.; Moore, J. S.; White, S. R. Rapid Energy-Efficient Manufacturing of Polymers and Composites via Frontal Polymerization. *Nature* **2018**, *557* (7704), 223–227. https://doi.org/10.1038/s41586-018-0054-x.

(6) Suslick, B. A.; Stawiasz, K. J.; Paul, J. E.; Sottos, N. R.; Moore, J. S. Survey of Catalysts for Frontal Ring-Opening Metathesis Polymerization. *Macromolecules* **2021**, *54* (11), 5117–5123. https://doi.org/10.1021/acs.macromol.1c00566.

(7) Alzate-Sanchez, D. M.; Yu, C. H.; Lessard, J. J.; Paul, J. E.; Sottos, N. R.; Moore, J. S. Rapid Controlled Synthesis of Large Polymers by Frontal Ring-Opening Metathesis Polymerization. *Macromolecules* **2023**, *56* (4), 1527–1533. https://doi.org/10.1021/acs.macromol.2c01892.

(8) Robertson, I. D.; Pruitt, E. L.; Moore, J. S. Frontal Ring-Opening Metathesis Polymerization of Exo-Dicyclopentadiene for Low Catalyst Loadings. *ACS Macro Lett.* **2016**, *5* (5), 593–596. https://doi.org/10.1021/acsmacrolett.6b00227.

(9) Lloyd, E. M.; Cooper, J. C.; Shieh, P.; Ivanoff, D. G.; Parikh, N. A.; Mejia, E. B.; Husted, K. E. L.; Costa, L. C.; Sottos, N. R.; Johnson, J. A.; Moore, J. S. Efficient Manufacture, Deconstruction, and Upcycling of High-Performance Thermosets and Composites. *ACS Appl. Eng. Mater.* **2023**, *1* (1), 477–485. https://doi.org/10.1021/acsaenm.2c00115.

(10) Husted, K. E. L.; Brown, C. M.; Shieh, P.; Kevlishvili, I.; Kristufek, S. L.; Zafar, H.; Accardo, J. V.; Cooper, J. C.; Klausen, R. S.; Kulik, H. J.; Moore, J. S.; Sottos, N. R.; Kalow, J. A.; Johnson, J. A. Remolding and Deconstruction of Industrial Thermosets via Carboxylic Acid-Catalyzed Bifunctional Silyl Ether Exchange. *J. Am. Chem. Soc.* **2023**, *145* (3), 1916–1923. https://doi.org/10.1021/jacs.2c11858.

(11) Post, W.; Susa, A.; Blaauw, R.; Molenveld, K.; Knoop, R. J. I. A Review on the Potential and Limitations of Recyclable Thermosets for Structural Applications. *Polym. Rev.* **2020**, *60* (2), 359–388. https://doi.org/10.1080/15583724.2019.1673406.

(12) Saha, S.; Ginzburg, Y.; Rozenberg, I.; Iliashevsky, O.; Ben-Asuly, A.; Lemcoff, N. G. Cross-Linked ROMP Polymers Based on Odourless Dicyclopentadiene Derivatives. *Polym. Chem.* **2016**, *7* (18), 3071–3075. https://doi.org/10.1039/C6PY00378H.

(13) Vallons, K. A. M.; Drozdzak, R.; Charret, M.; Lomov, S. V.; Verpoest, I. Assessment of the Mechanical Behaviour of Glass Fibre Composites with a Tough Polydicyclopentadiene (PDCPD) Matrix. *Composites, Part A.* **2015**, *78*, 191–200. https://doi.org/10.1016/j.compositesa.2015.08.016.

(14) Li, T.; Wulff, J. E. Copolymers of Functionalized and Nonfunctionalized Polydicyclopentadiene. *ACS Appl. Polym. Mater.* **2021**, *3* (1), 110–115. https://doi.org/10.1021/acsapm.0c01196.

(15) Gong, L.; Liu, K.; Ou, E.; Xu, F.; Lu, Y.; Wang, Z.; Gao, T.; Yang, Z.; Xu, W. ROMP of Acetoxy-Substituted Dicyclopentadiene to a Linear Polymer with a High Tg. *RSC Adv.* **2015**, *5* (33), 26185–26188. https://doi.org/10.1039/C5RA01855B.

(16) S. Phatake, R.; Masarwa, A.; Gabriel Lemcoff, N.; Reany, O. Tuning Thermal Properties of Cross-Linked DCPD Polymers by Functionalization, Initiator Type and Curing Methods. *Polym. Chem.* **2020**, *11* (10), 1742–1751. https://doi.org/10.1039/C9PY01178A.

(17) Godwin, B.; Anvari, M. H.; Olfatbakhsh, T.; Mahbod, M.; Milani, A. S.; DiLabio, G. A.; Wulff, J. E. A Single-Atom Upgrade to Polydicyclopentadiene. *Macromolecules* **2023**, *56* (4), 1592–1600. https://doi.org/10.1021/acs.macromol.2c02260.

(18) Chen, J.; Burns, F. P.; Moffitt, M. G.; Wulff, J. E. Thermally Crosslinked Functionalized Polydicyclopentadiene with a High Tg and Tunable Surface Energy. *ACS Omega* **2016**, *1* (4), 532–540. https://doi.org/10.1021/acsomega.6b00193.

(19) Cuthbert, T. J.; Li, T.; Speed, A. W. H.; Wulff, J. E. Structure of the Thermally Induced Cross-Link in C -Linked Methyl Ester-Functionalized Polydicyclopentadiene (f PDCPD). *Macromolecules* **2018**, *51* (5), 2038–2047. https://doi.org/10.1021/acs.macromol.7b02750.

(20) Li, T.; Shumka, H.; J. Cuthbert, T.; Liu, C.; E. Wulff, J. Harnessing the Surface Chemistry of Methyl Ester Functionalized Polydicyclopentadiene and Exploring Surface Bioactivity. *Mater. Adv.* **2020**, *1* (6), 1753–1762. https://doi.org/10.1039/D0MA00480D.

(21) Shieh, P.; Zhang, W.; Husted, K. E. L.; Kristufek, S. L.; Xiong, B.; Lundberg, D. J.; Lem, J.; Veysset, D.; Sun, Y.; Nelson, K. A.; Plata, D. L.; Johnson, J. A. Cleavable Comonomers Enable Degradable, Recyclable Thermoset Plastics. *Nature* **2020**, *583* (7817), 542–547. https://doi.org/10.1038/s41586-020-2495-2.

(22) Yao, Z.; Zhou, L.; Dai, B.; Cao, K. Ring-Opening Metathesis Copolymerization of Dicyclopentadiene and Cyclopentene through Reaction Injection Molding Process. *J. Appl. Polym. Sci.* **2012**, *125* (4), 2489–2493. https://doi.org/10.1002/app.36359.

(23) David, A.; Huang, J.; Richaud, E.; Yves Le Gac, P. Impact of Thermal Oxidation on Mechanical Behavior of Polydicylopentadiene: Case of Non-Diffusion Limited Oxidation. *Polym. Degrad. Stab.* **2020**, *179*, 109294. https://doi.org/10.1016/j.polymdegradstab.2020.109294.

(24) Czelusniak, I.; Heywood, J. D.; Kenwright, A. M.; Khosravi, E. Investigation of Factors Affecting Ruthenium Complexation in ROMP Reactions of Oxygen-Containing Norbornene Derivatives Using Grubbs First Generation Initiator. *J. Mol. Catal. A: Chem.* **2008**, *280* (1), 29–34. https://doi.org/10.1016/j.molcata.2007.10.011.

(25) Hyatt, M. G.; Walsh, D. J.; Lord, R. L.; Andino Martinez, J. G.; Guironnet, D. Mechanistic and Kinetic Studies of the Ring Opening Metathesis Polymerization of Norbornenyl Monomers by a Grubbs Third Generation Catalyst. *J. Am. Chem. Soc.* **2019**, *141* (44), 17918–17925. https://doi.org/10.1021/jacs.9b09752.

(26) Sutor, D. J. Evidence for the Existence of C–H···O Hydrogen Bonds in Crystals. *J. Chem. Soc.* **1963**, No. 0, 1105–1110. https://doi.org/10.1039/JR9630001105.

(27) Sutor, D. J. The C–H… O Hydrogen Bond in Crystals. *Nature* **1962**, *195* (4836), 68–69. https://doi.org/10.1038/195068a0.

(28) Schwalbe, C. H. June Sutor and the C–H ··· O Hydrogen Bonding Controversy. *Crystallogr. Rev.* **2012**, *18* (3), 191–206. https://doi.org/10.1080/0889311X.2012.674945.

(29) Long, T. R.; Elder, R. M.; Bain, E. D.; Masser, K. A.; Sirk, T. W.; Yu, J. H.; Knorr, D. B.; Lenhart, J. L. Influence of Molecular Weight between Crosslinks on the Mechanical Properties of Polymers Formed via Ring-Opening Metathesis. *Soft Matter.* **2018**, *14* (17), 3344–3360. https://doi.org/10.1039/C7SM02407J.

Chapter 4: A Straightforward and Rapid Method to Assess ROMP Performance in Neat Thermosetting Resins

Benjamin Godwin[1], Dylan Bouetard[2], Jakub Talcik[2], Antonio Del Vecchio[2], Fanny Morvan[2], Thierry Roisnel[2], Marc Mauduit[2] and Jeremy Wulff*[1]*

4.0. Contributions

Crystal structures were obtained by Thierry Roisnel at the University of Rennes. Initiator **4** and CAAC precursors were synthesized and characterized by Fanny Morvan at the University of Rennes under the supervision of Prof. Marc Mauduit. Initiators **6**–**10** and CAAC precursors were synthesized and characterized by Dylan Bouetard at the University of Rennes under the supervision of Prof. Marc Mauduit. Monomer synthesis, sample preparation, IR spectroscopy, thermogravimetric analysis, differential scanning calorimetry, thermograms, and characterization of reaction products were performed by Benjamin Godwin. Hardness testing was performed by Ryan Mandau at the University of British Columbia, Okanagen Campus Survive and Thrive Applied Research laboratory. The photoreactor was built by Sean Adams, Kody Matthews and Chris Secord at the University of Victoria. Sample cutting was performed by Benjamin Godwin with assistance from Chris Secord.

4.1. Abstract

Polydicyclopentadiene (PDCPD) is a thermosetting material used to produce body panels for industrial equipment and vehicles. PDCPD and other important thermosets are produced by direct transformation of neat monomer (dicyclopentadiene) to solid polymer using a catalyst in a process called reaction injection molding. As the polymerization and crosslinking are competitive the polymerization process is therefore inherently challenging to study. In this work we develop a laboratory-scale method that is high-throughput and low cost, and which enables the comparison of initiators for ring opening metathesis polymerization. Additionally, the method enables the prediction of both the mechanical and thermal properties of the final material.

4.2. Introduction

Polydicyclopentadiene (PDCPD) is an advanced engineering plastic that is commonly used in the automotive and construction industries.[1,2] Large and complex PDCPD parts are produced using a process called reaction injection molding (RIM). In RIM, a one- or two-part resin consisting of dicyclopentadiene (DCPD) monomer, various fillers (such as carbon black), additives (fire suppressants), and catalyst (or cocatalysts) are injected into a low-pressure mold, commonly made from aluminum, which is maintained at a moderate temperature (typically 70–100°C).[1] Upon contact with the warm mold a highly exothermic ring opening metathesis polymerization (ROMP) reaction occurs, forming the polymer and crosslinking it simultaneously in seconds (Figure 4.1).[3–7] This exotherm commonly reaches temperature of 200°C or more. The entire RIM cycle including injection, polymerization, and demolding typically takes around five minutes.[1]

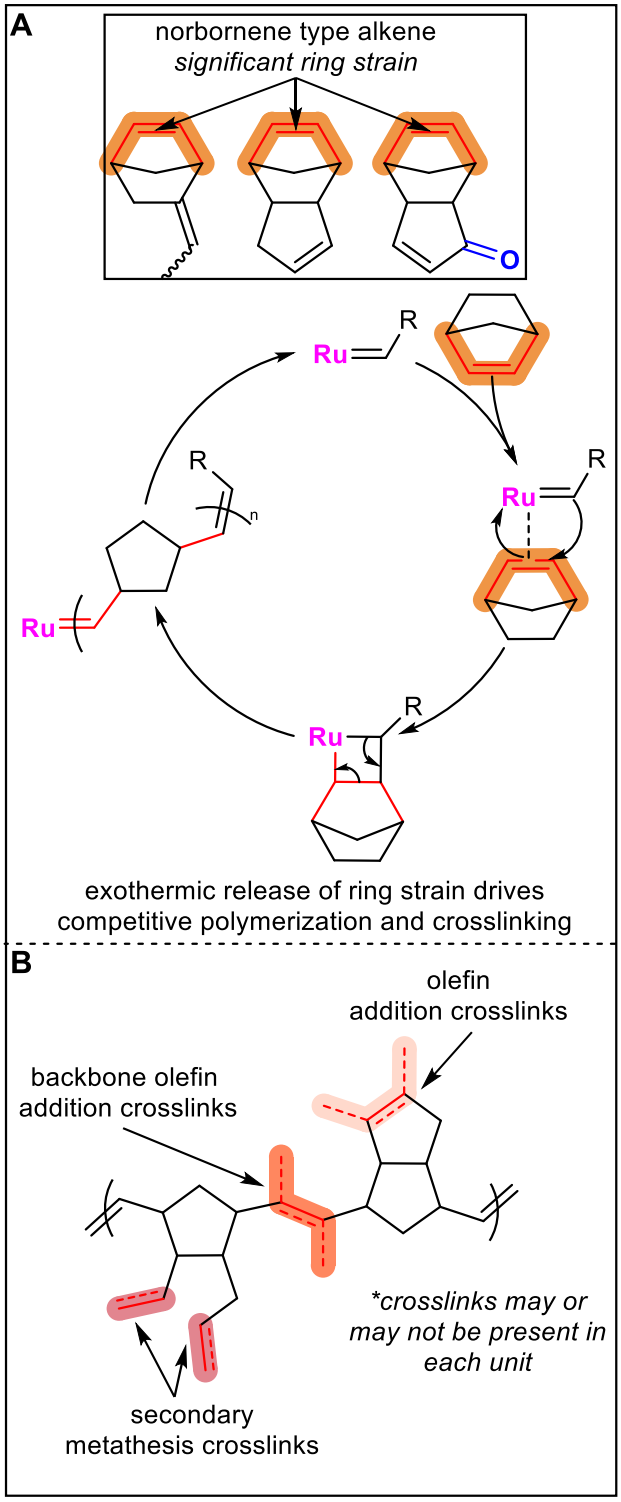

Figure 4.1. A: Ring strain contained in the norbornene fragment of various monomers generates heat during ROMP, which drives RIM. B: Various crosslinking motifs of PDCPD driven by the

exothermic polymerization. Note that the crosslinks are drawn on a single fragment for illustrative purposes only. The typical crosslinking density of PDCPD is ~10%.

Using RIM, large parts (up to 100 kg) with varying thicknesses or geometries can be made easily and quickly. RIM is also environmentally advantageous, since its quick cycle times and low input temperatures significantly reduce energy consumption compared to other thermosets that require high-temperature curing.[1] The mechanical and thermal properties of these parts and therefore the utility is heavily dictated by the catalyst system used.[8] Indeed, the only major difference between most commercial PDCPD is the catalyst system used, with tungsten and molybdenum systems both in wide use.[4–6] Ruthenium-based systems are also becoming more common, thanks to significant research and development in the academic world.[2,8–10]

Despite PDCPD's widespread use in the automotive and construction sectors, the material has struggled to breakout into new markets.[1] This is due to several key disadvantages mainly tied to its lack of surface functionality.[11–14] PDCPD like most thermosets is not recyclable, though since the DCPD monomer is a waste from the petrochemical industry, the polymer can be considered an upcycled product even in its virgin form. The monomer is very odorous, and since polymerization and crosslinking occur simultaneously any unreacted monomer ends up trapped in the polymer matrix, giving the final product an unpleasant and persistent odor.[1,14] PDCPD has no chemical tunability and further, a very low surface energy. This low surface energy leads to a substantial bottleneck in the manufacturing process, as manufacturers must wait for parts to autoxidize prior to painting and bonding.[1] To address this, we and others have synthesized several functionalized DCPD derivatives.[13–19] Our second-generation monomer, oxaDCPD, has proven amenable to scale-up in the laboratory and the resulting polymer (oxaPDCPD) possesses excellent thermal and mechanical properties that surpass those of regular PDCPD.[19] In addition, oxaPDCPD has an

immediately functionalized surface owing to the incorporation of a ketone functional group.[19] However, this derivative and our previous generation ester-functionalized DCPD both show reduced reactivity with the Grubbs second-generation initiator (GC2, **1**).[16,19] We therefore desired to seek out a more productive catalyst.

This is not, however, straightforward. The desired product, a glassy macromolecule, is completely insoluble in all solvents and is particularly prized for its resistance to chemical attack—making characterization methods suitable for soluble materials impractical.[8,15,20,21] Soluble linear and/or nearly linear polymerizations of DCPD with a variety of catalysts are known to proceed in solution and are characterizable using conventional methods such as ^{1}H NMR spectroscopy and gel permeation chromatography (GPC). However, these solution state reactions are significantly slower, taking the better part of an hour, and are conducted at low temperatures and low concentrations as compared to RIM reactions.[11,19,22–24] These in solution reactions give products whose mechanical and thermal properties do not reflect the those of the material made through the neat reaction. Conventional methods for studying and comparing catalysts such as ^{1}H NMR based kinetics therefore do not reflect those occurring during commercial reaction injection molding and must be considered fraught with assumptions.[21]

This is recognized by industry, and commercially catalyst systems for RIM of PDCPD are tested using thermograms, wherein a some resin is dispensed from the injector, and its reactivity is tracked as a function of time, temperature, and sometimes viscosity.[1] We were interested if this technique could be easily adapted to be rapid and lab-scale. Here we show a simple and rapid method for benchmarking ROMP catalysts and predicting their material properties in DCPD-based resin systems in the laboratory. We also show that the peak temperature obtained during the

thermogram can be correlated to the glass transition temperature and mechanical properties of the resulting material.

4.3. Results and Discussion

We tested three commercially available ruthenium initiators (Figure 4.2A, **1–3**): the second and third generation Grubbs catalysts (**1** and **2**) which are based on *N*-heterocyclic carbene (NHC) ligands with *N*-mesityl substituents, and the first generation Hoveyda catalyst (**3**) which contains a tricyclohexylphosphine ligand. We also tested seven prepared ruthenium initiators (Figure 4.2A, **4–10**). Initiator **5** is a 3:7 ratio of bis-unsaturated unsymmetrical (u2)-NHC Ru-indenylidene and tricyclohexylphosphine/(u2)-NHC Ru-indenylidene while initiator **4, 6–10** contain cyclic alkyl amino carbenes (CAAC) ligands with various substituents.[25–29] All initiators were then tested with four unique monomer resins (Figure 4.2B, **a–d**), successfully manufacturing a total of thirty-one novel materials of a possible forty-four.

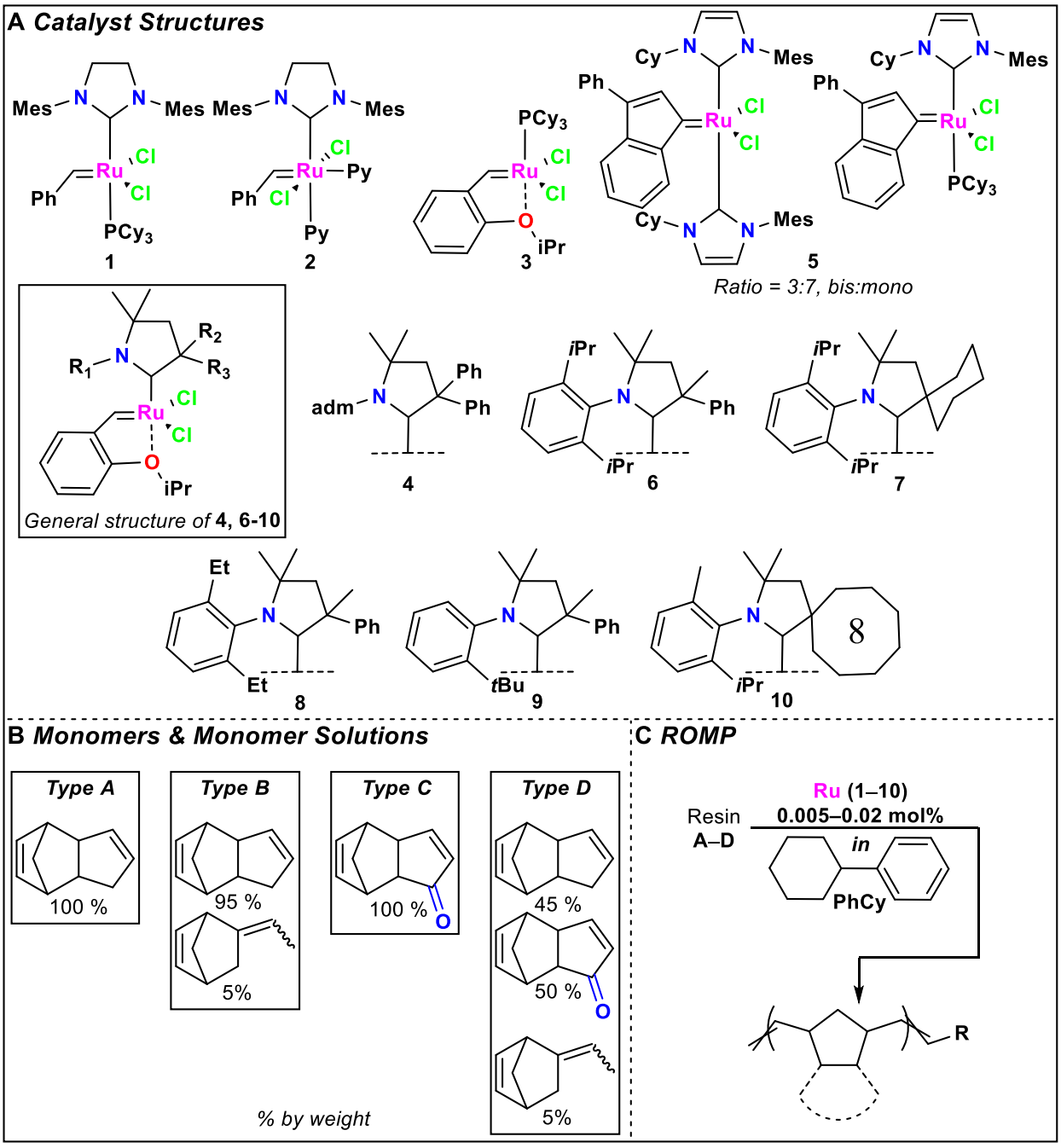

Figure 4.2. A: Structurally diverse chemical structures of ruthenium initiators utilized in this study. B: Monomers used to make up resins **a**–**d**. C: General ROMP reaction.

We compared initiators by simulating RIM with common laboratory equipment (Figure 4.3). We opted to use an oil bath heated to 90°C combined with a glass vial to act as a preheated mold.

The vial containing the liquified monomers was rapidly inserted into the oil bath once the catalyst was injected and well mixed to simulate the rapid injection of a live resin into a mold. The subsequent reaction was monitored using a thermocouple inserted in the vial and coupled to a low-cost datalogger. Rapid mixing of the catalyst into the resin mixture was facilitated by utilizing phenyl cyclohexane to dissolve the catalyst beforehand. This allowed for quick and repeatable dosing, and it has been previously shown to be an acceptable additive for the neat polymerization of DCPD with a wide range of ruthenium-based catalysts.[8]

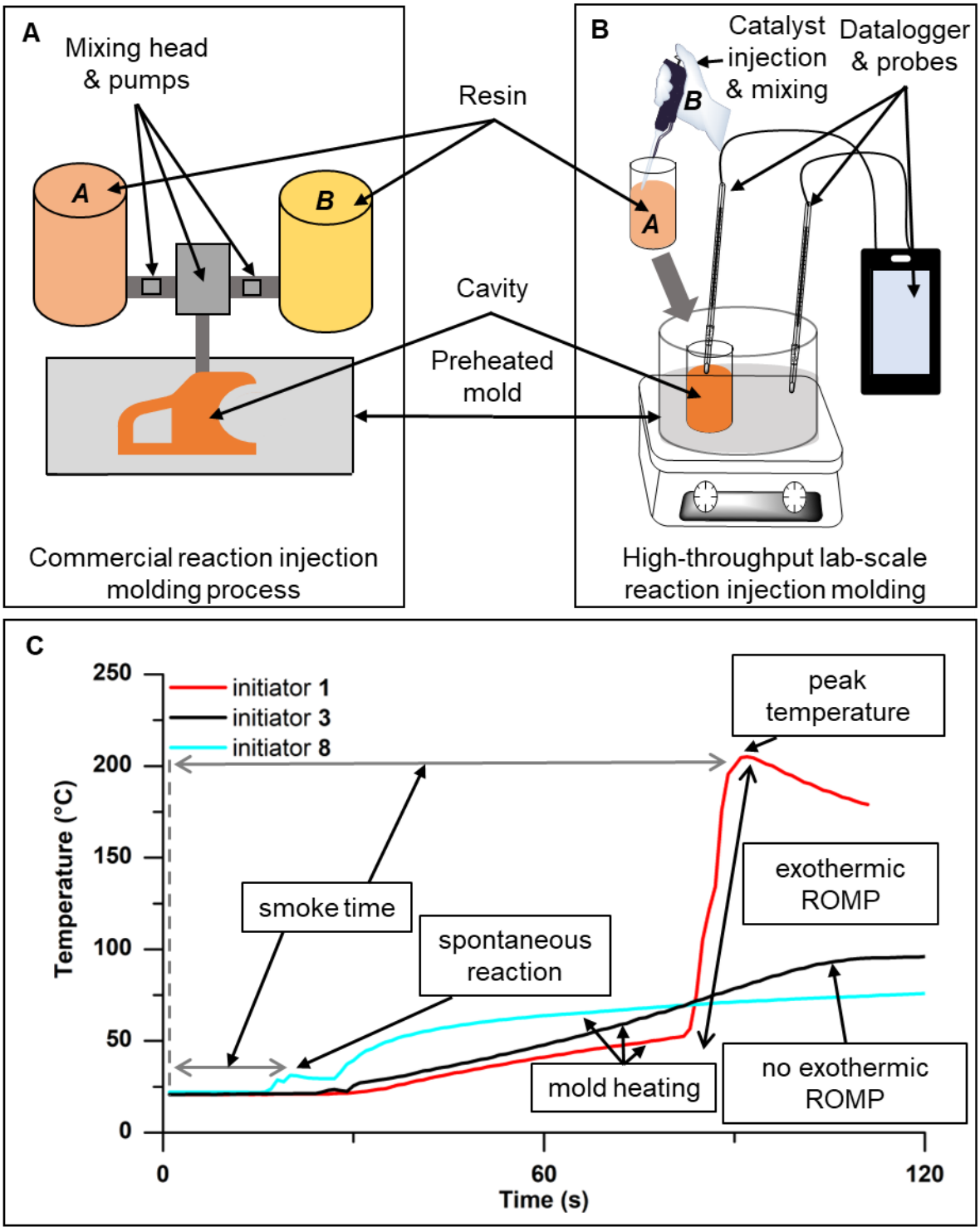

Figure 4.3. A: Block diagram of a reaction injection molding system. B: Simulated reaction injection molding setup for high-throughput laboratory testing. C: Representative thermograms obtained from datalogger. Thermograms obtained with resin **b** and 0.005 mol% initiator.

In contrast to previous work done on neat thermosetting systems — including prior research from our own group — we elected not to use inhibitors in our resin compositions.[8,19,21]

We began by testing initiators **1**–**10** at loadings of 0.005 mol% in resins **a** and **b**. These experiments showed large variations in peak temperature (T_{pk}) as shown in Figure 4.4. The highest T_{pk} of all initiators tested was observed for initiator **5** in resin **b**. Initiator **1** generated consistent, high T_{pk} values for all resin systems used. Interestingly in resin **a** initiator **5** was outperformed by initiators **1**, **6** and **7** which had all produced higher T_{pk} values. We noted that for the CAAC based initiators (**4**, **6–10**) as the steric bulk of the substituents on the CAAC ligand decreased, the reactivity of the initiators generally increased. Notably, initiators **8** and **9** both reacted nearly instantaneously with resins **a** and **b** (see Figure C29, C30), producing depressed T_{pk} values as the catalyst solution did not have time to fully mix with the monomer resin. As the initiator reacted with less resin than was available due to the speed of initiation, these T_{pk} values reflect a lower reaction scale than was intended and are thus suppressed. Similarly, initiator **2** (Grubbs 3rd generation catalyst), widely known for fast-initiating catalysis, also reacted nearly instantly, but owing to the decreased viscosity of resin **b**, was able to fully mix in this resin.[30] In contrast, initiator **4**, which only produced a polymeric gel with resins **a** and **b**, with its rigid and bulky adamantane substitutes never exceeded the bath temperature.

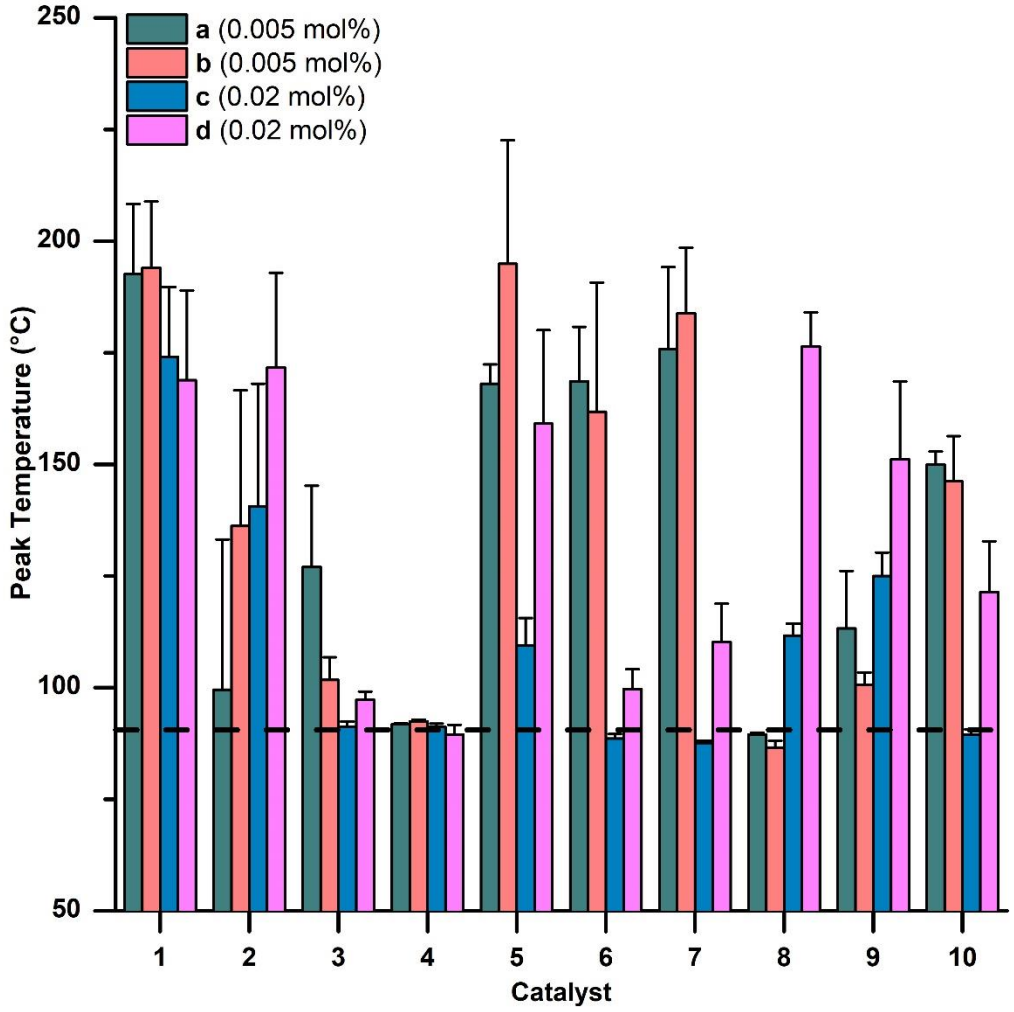

Figure 4.4. Peak temperatures achieved during simulated RIM by various initiators in different resin types at 90°C. Reactions that failed to produce exotherms above 90°C (black line) did not exceed the bath temperature. See Figure C22–C32 for complete thermograms of each catalyst and resin combination, and of **c** at 0.005 mol% and controls. Error bars represent standard deviation of n = 3 replicates.

Resin c was also tested at 0.005 mol% loading initially. However, the peak temperature was consistently that of the bath temperature and no glassy products were observed for any of the initiators used (see Figure 4.3C, (black trace) and Figures C16, C21, C23 and C24). We therefore opted to increase the catalyst loading to 0.02 mol% which resulted in the observation of satisfactory

exotherms (see Figure 4.4 and Figures C27 and C31). We also prepared a mixed resin (**d**) consisting of 5% ethylidene norbornene (ENB), 45% DCPD, and 50% oxaDCPD by weight which also produced satisfactory exotherms at 0.02 mol% loading (see Figure 4.4 and Figures C28 and C32). It is important to note that the most active initiator is not necessarily the best for RIM. If the reaction occurs too quickly the resin will not completely fill the mold, and the part will be defective. To this end, the particularly reactive initiators **2** and **8**—which are not suitable for RIM with resins **a** and **b**—synergize well with the inhibitory effect of oxaDCPD-containing resins **c** and **d**, leading to significantly higher T_{pk} values. Unsurprisingly, initiators that showed latent activity with resins **a** and **b** did not work at all with resins **c** and **d**. This is presumably due to chelation and inhibition of the catalyst by the carbonyl (Figure 4.5A).[31]

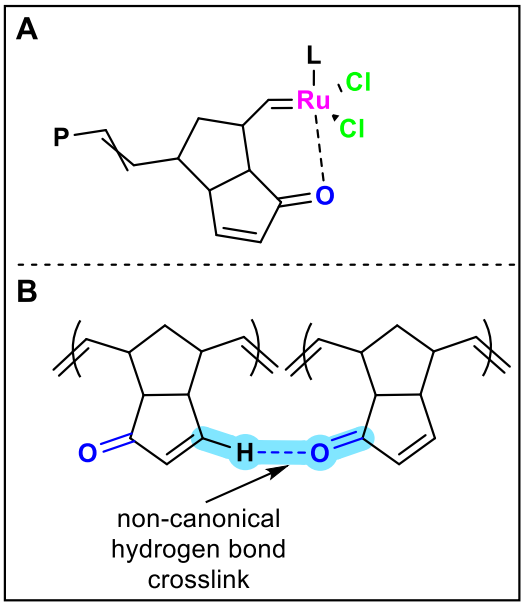

Figure 4.5. A: Proposed chelation and inhibition caused by inclusion of oxygen in DCPD monomers. B: Non-canonical hydrogen bonding between a lone pair on the carbonyl and the beta hydrogen of an adjacent enone. Both inter- and intra-chain interactions are believed to occur.

The carbene fragment type of the initiator did not seem to affect T_{pk}. Benzylidene, benzylidene chelates and indenylidene carbene based initiators were all shown to be capable of producing high T_{pk} values; however, the worst-performing initiators were based on benzylidene chelates.

Smoke time (SMT) is a parameter used in industry to verify reactivity and useability of resins.[1] It is defined as the time between the completion of resin injection and the appearance of smoke (generated by the heat of the exotherm) at a specified temperature.[1] This differs from the commonly measured pot-life—which is similar to the ETA-1000 (time taken to reach a viscosity of 1000 mPa.s) value measured in industry—which measures the amount of time required to critical chain entanglement wherein the resin will not flow.[1,8,10,20,21,32] On the other hand, SMT_{90} measures the time required to complete the exothermic reaction.[1] We approximated the smoke time of the various resin and catalysts combinations at 90°C (SMT_{90}) as the time from the start of the thermogram to the peak of the exotherm (Figure 4.3C). The observed smoke times are shown in Figure 4.6.

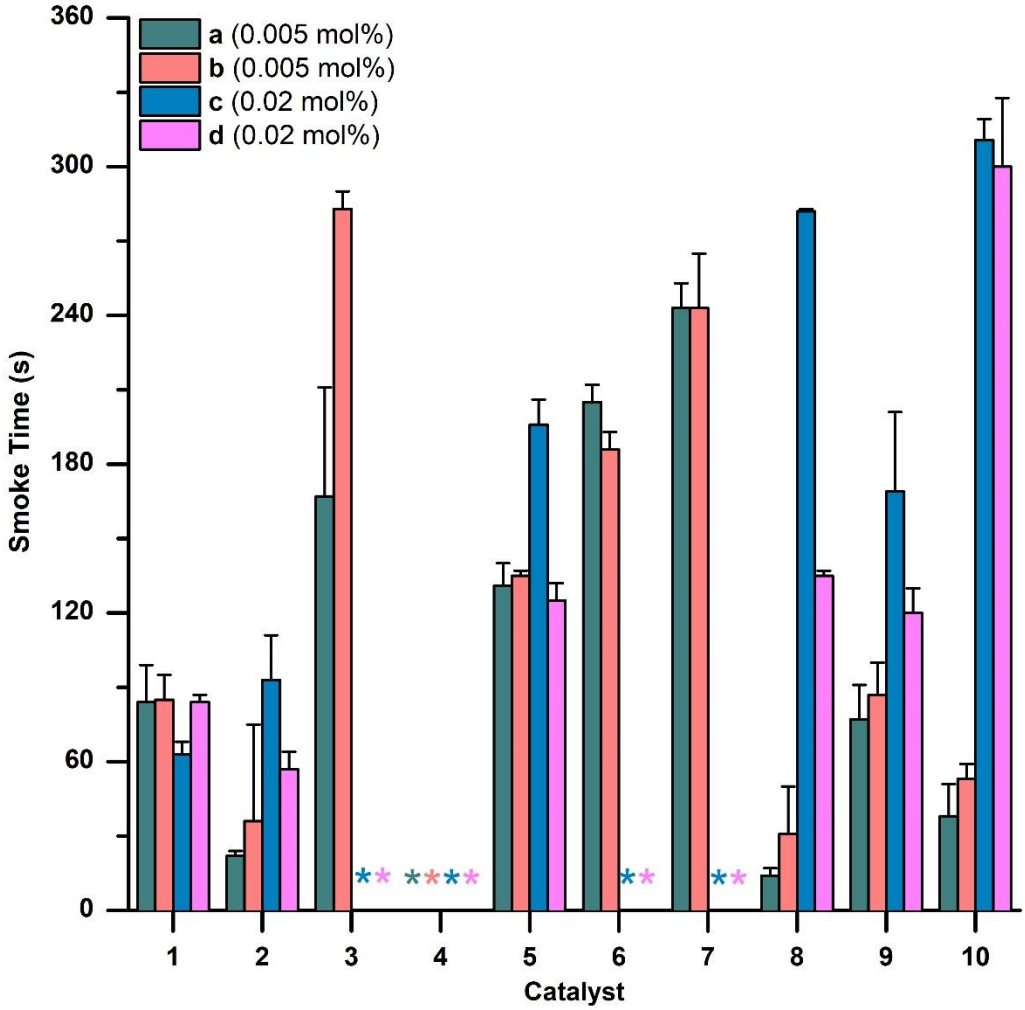

Figure 4.6. Smoke times at 90°C achieved during simulated RIM by various initiators in different resin types. Reactions that failed to produce distinct, exotherms are shown as *. Smoke times at 90°C (SMT_{90}) were approximated as the time from the start of the thermogram to peak of the exotherm. See Figure C22–C32 for complete thermograms of each catalyst and resin combination, and of **c** at 0.005 mol% and controls. Error bars represent standard deviation of n = 3 replicates.

In general, the presence of a benzylidene chelate type carbene resulted in a longer SMT_{90}. However, the shortest observed SMT_{90} was observed with initiator **8** in resins **a** and **b** followed by the fast initiating **2**. There was no well-defined correlation between T_{pk} and SMT_{90}. For example, initiators **6** and **7** both produced similar T_{pk} values to initiators **1** and **5** in resin **a** and **b** but the

former had much longer SMT_{90} values. Interestingly, with resins **c** and **d** SMT_{90} increased disproportionally for initiators with benzylidene chelate based carbenes as compared to those with indenylidene or non-chelating benzylidene. This is likely due to the replacement of a ligand (phosphine or pyridine) capable of reversibly interacting with the catalyst by the chelating oxygen on the benzylidene fragment, thus making the active catalyst more prone to chelation by the carbonyl containing substrate in resins **c** and **b**. As in previous reports, the indenylidene based initiator (**5**) required longer heating, and thus had a longer SMT_{90} then the comparable benzylidene based initiator (**1**).[8]

To investigate the quality of our materials, we performed differential scanning calorimetry to assess the glass transition temperature (T_g). A sharp exotherm is consistent with a high T_{pk} value. This steep exotherm is correlated with a consistent temperature of catalysis and with competitive crosslinking and polymerization, which ensures complete curing of the polymer matrix.[8] As shown in Figure 4.7, we observe strong a monotonic relationship between the T_{pk} and the T_g of the material produced. This is true regardless of the reaction time, as even in the case of initiators **3** and **4** where the reactions were allowed to run for a full 5 minutes—as opposed to initiators that quickly produced sharp exotherms such as **1** and **5** where the total reaction time was *ca.* 2 minutes—the T_g values are markedly lower. See the SI for full experimental parameters and reaction cutoffs. Initiator **1** produced the highest T_g values for resin **a** while also recording the highest T_{pk}. In resin **b**, initiator **5** produced the highest exotherm by a small margin and the resulting T_g is also the highest. In catalytic systems utilizing resin **d**, initiators **1**, **2**, **5** and **8** all produced similar T_{pk} values, however the T_g values are scattered.

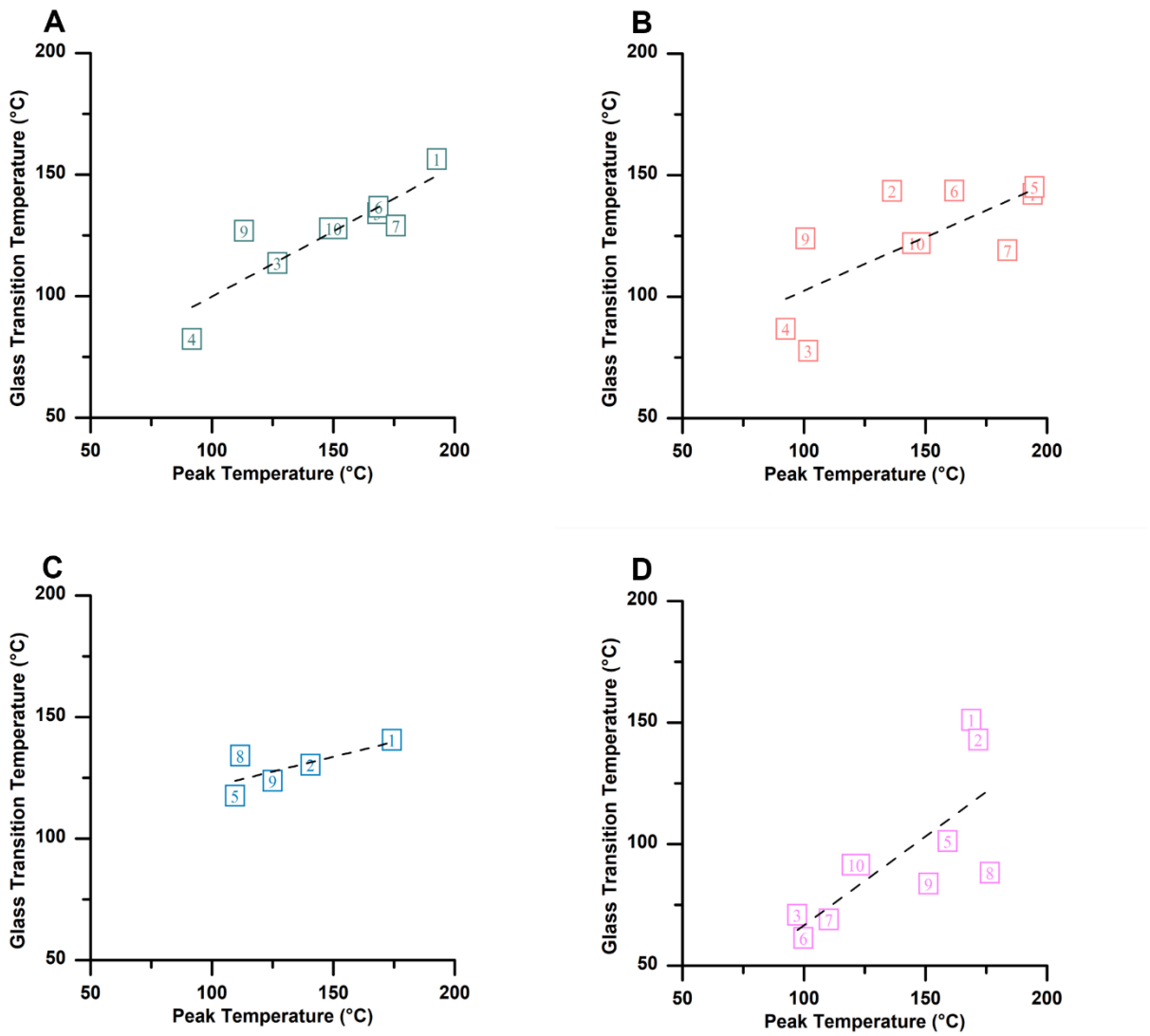

Figure 4.7. A: T_{pk} vs T_g of resin **a**, with a Spearman's rank correlation coefficient (ρ) = 0.90. B: T_{pk} vs T_g of resin **b**, ρ = 0.68. C: T_{pk} vs T_g of resin **c**, ρ = 0.95. D: T_{pk} vs T_g of resin **d**, ρ = 0.87. T_g values shown for n =1 of initiator/resin combinations that produced material suitable for analysis.

It is likely that the catalyst also plays a role in determining the specific properties of the material, perhaps by dictating polymer microstructure. Materials made using resin **c** and to some extent resin **d** displayed higher T_g values relative to T_{pk} than resin **a** and **b**. This is likely due to the presence of inter- and intra-molecular non-canonical hydrogen bonding interactions between β-hydrogen and

carbonyl of an adjacent residue (Figure 4.5B), as well as other polar interactions such as dipole-dipole and dipole-induced dipole interactions.[19,33–35] The presence of these extra pseudo-crosslinks and strong molecular forces give **c** and **b** resin based materials makes up for a lower covalent crosslink density caused by lower T_{pk} values.

The mechanical properties of a material are directly related to its T_g. To show this we assessed the mechanical properties of our materials using Vickers Hardness (VH) testing. Hardness testing is an advantageous mechanical test for small scale laboratory measurements as it can be performed quickly using a very small amount of material. Additionally, no special sample geometry is required, and the test is non-destructive.[36] Further, as hardness is a measure of a materials resistance to plastic deformation as is tensile strength, the tensile strength may be estimated (Table C7).[36–38] Some reactions that produced samples that were suitable for analysis by DSC—such as those produced by initiators **3** and **9** in resins **a** and **b—** produced materials that were too rubbery to test using Vickers Hardness and are thus excluded from this analysis. Material **5c** was too rubbery for the VH test and materials **3d**, **6d**, and **7d** were likewise too soft to provide quality data. Figure 4.8 shows the results of the VH testing displayed in MPa (see Table C5 for HV1 values). A strong monotonic relationship was observed between T_{pk} and the hardness of the material made from resins **a**, **c**, and **d**. For resin **b** the relationship was weaker, but there was still a positive correlation between T_{pk} and hardness. Materials made from resin **c** had generally lower hardness values, while resins **a**, **b**, and **d** were quite similar. It is likely that the hardness measurements were adversely affected by the inclusion of phenyl cyclohexane as a solubilizing agent for the catalyst.

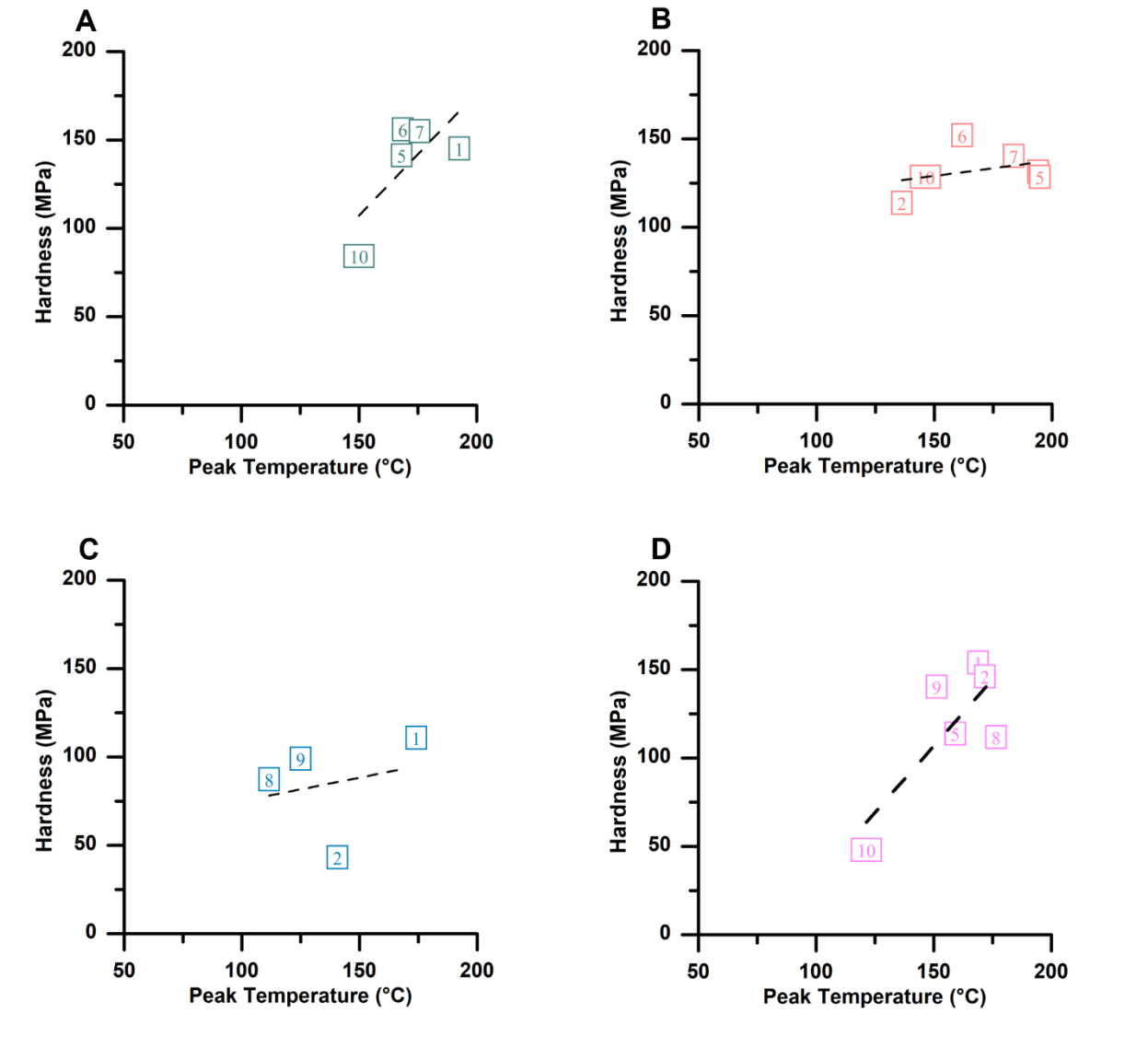

Figure 4.8. Vickers Hardness (VH) in MPa A: T_{pk} vs VH of resin **a**, ρ = 0.6. B: T_{pk} vs VH of resin **b**, ρ = 0.2. C: T_{pk} vs VH of resin **c**, ρ = 0.9. D: T_{pk} vs VH of resin **d**, ρ = 0.77. VH values shown for n = 3 of initiator/resin combinations that produced material suitable for analysis.

4.4. Conclusion

We have developed a simple and rapid method for screening ROMP initiators in neat thermosetting resins. Using this method, we screened forty-four different resin and initiator combinations. Remarkably, the glass transition temperatures and by extension mechanical properties are generally predicted by the peak temperature reached during the model RIM reaction.

This work will allow researchers to quickly and cheaply screen metathesis catalysts and resins to develop robust thermosetting materials.

4.5. Methods

Materials

Unless indicated otherwise, all reactions were performed under inert atmosphere using Schlenk line techniques. Reactions at elevated temperature were maintained by thermostatically controlled oil-bath. Tetrahydrofuran, toluene, dichloromethane, and diethyl ether were purified using MBraun MB-SPS-5 Solvent Purification System for the synthesis of initiators. Other solvents used for the synthesis of initiators were distilled over Sodium/Benzophenone or Calcium hydride. Silica gel chromatography was performed with Sigma-Aldrich's silica gel high-purity grade, pore size 60 Å, 230-400 mesh particle size, 40-63 μm particle size. Reactions were monitored by thin-layer chromatography carried out on silica gel plates (60F254) using UV light as visualizing agent and by staining with $KMnO_4$. Initiator **1** was obtained from Chem-Impex. Initiator **3** was obtained from Catapower.

Spectroscopy

^{1}H, and ^{13}C NMR spectra were aquired using a 300, 400, and 500 MHz Bruker instruments ^{1}H (300.27 MHz), ^{13}C (75.51 MHz) or ^{1}H (400 MHz), ^{13}C (101 MHz), or ^{1}H (500.27 MHz), ^{13}C (125.81 MHz). ^{19}F, ^{31}P, and ^{11}B NMR spectra were acquired on a 400 MHz Bruker instrument, ^{19}F (376 MHz), ^{31}P (162 MHz), ^{11}B (128 MHz). Data were processed using MestReNova. Chemicals shifts were reported relative to residual solvent peaks ($CDCl_3$ = 7.26 ppm for ^{1}H and 77.2 ppm for ^{13}C; CD_2Cl_2 = 5.32 ppm for ^{1}H and 53.84 ppm for ^{13}C); ^{19}F chemical shifts are reported with $CFCl_3$ (δ = 0.0 ppm) as the internal standard; ^{31}P chemical shifts are reported with H_3PO_4 (δ = 0.0 ppm) as the internal standard; ^{11}B chemical shifts are reported with $BF_3.Et_2O$ (δ = 0.0 ppm) as the internal standard. Coupling constants are reported in Hertz (Hz). Abbreviations are used as follows: s =

singlet, d = doublet, t = triplet, q = quartet, p = pentuplet, quint = quintet, sext = sextet, sept = septet, h = heptet, m = multiplet, dd = doublet of doublets, ddd = doublet of doublets of doublets, dddd = doublet of doublets of doublets of doublets dt = doublet of triplets, dq = doublet of quartets, td = triplet of doublet, dtd = doublet of triplet of doublets, pd = pentuplet of doublets, qd = quartet of doublets, br = broad, app = apparent. Mass spectrometric analyses were performed at Centre Régional de Mesures Physiques de l'Ouest. IR spectra were recorded using an Agilent Cary 630 FTIR spectrometer with diamond ATIR attachment. Samples were measured as solids and pressed into the crystal using the supplied press.

Melting point

Melting points were taken on an SRS digimelt melting point apparatus.

Thermal Characterization

Differential scanning calorimetry samples were run on a TA instruments DSC25 using TZero aluminum DSC pans with hermetic lid. A pin-hole was added for solid samples using the tip of a 21 ½ gauge needle. An empty TZero aluminum DSC pan with TZero aluminum hermetic lid and pin hole was used as a reference. Samples were measured from 40°C to 250°C then cooled to −50 °C at 20 °C/min to erase thermal history then ramped at 10 °C/min from −30 °C to 250 °C. The T_g was obtained from the second trace. Thermogravimetric analysis was done on a TA instruments SDT Q600. Samples were heated at 20 °C per minute to a maximum temperature of 600°C, under a nitrogen atmosphere.

Mechanical testing

Vickers microhardness testing was performed using a Buehler Wilson VH 3100 instrument with a Vickers diamond-shaped indenter using a dwell time of 10 seconds and a 1 kg load.

Thermograms

Thermograms were recorded using a 373 K/J Thermometer Data Logger PB01-0043 and utilized the provided EnviromentalTester PC interface software and disposable k-type thermocouples. Data were subsequently processed using Excel.

Crystallography

Data were collected on a D8 Venture (Bruker-AXS) diffractometer equipped with a CMOS-PHOTON 70 detector using Mo-K_α radiation (0.71073 Å) at T = 150 K.

Crystal structure was solved by dual-space algorithm using SHELXT program[39], and then refined with full-matrix least-squares methods based on F^2 (SHELXL program[40]). All non-Hydrogen atoms were refined with anisotropic atomic displacement parameters. H atoms were finally included in their calculated positions and treated as riding on their parent atom with constrained thermal parameters. A final refinement on F^2 with 7260 unique intensities and 393 parameters converged at $\omega R(F^2) = 0.2075$ (RF = 0.0723) for 6064 observed reflections with $I > 2\sigma(I)$.

The CIF files of 4 have been deposited with CCDC numbers: 237148.

Resin Formulations Catalyst Stock Solution, and Thermogram Sample Preparation

Resin compositions are described in Table S4.2. Type-a resin used dicyclopentadiene (DCPD) as received from Millipore Sigma. Type-b resin was prepared by melting 95.0674 g (0.7191 mol) DCPD and adding 5.0040 g (0.0416 mol) ethylidene norbornene (ENB). Type-c resin used neat oxaDCPD as synthesized under “synthesis of monomer”.[19] Type-d resin was prepared by melting

48.6321 g (0.3678 mol) DCPD and 54.0232 g (0.3695 mol) oxaDCPD together, and then adding 5.4070 g (0.0449 mol) ENB. Samples for thermograms were prepared by adding 3 g of resin a, b, c or d (Table S4.2) to a 1-dram glass snap cap vial.

Catalyst stock solutions were prepared such that the amount of catalyst delivered in 70 µL of stock solution was 0.005 mol% (resin-a, b) or 0.02 mol% (resin-c, d) relative to 3 g of the respective monomer. Catalyst (masses described in Table S4.3) was added to a 1-dram glass vial and sonicated to dissolution in the corresponding amount of phenyl cyclohexane (PhCy) (volume described in Table S4.3). Stock solutions were used immediately upon preparation.

Thermograms

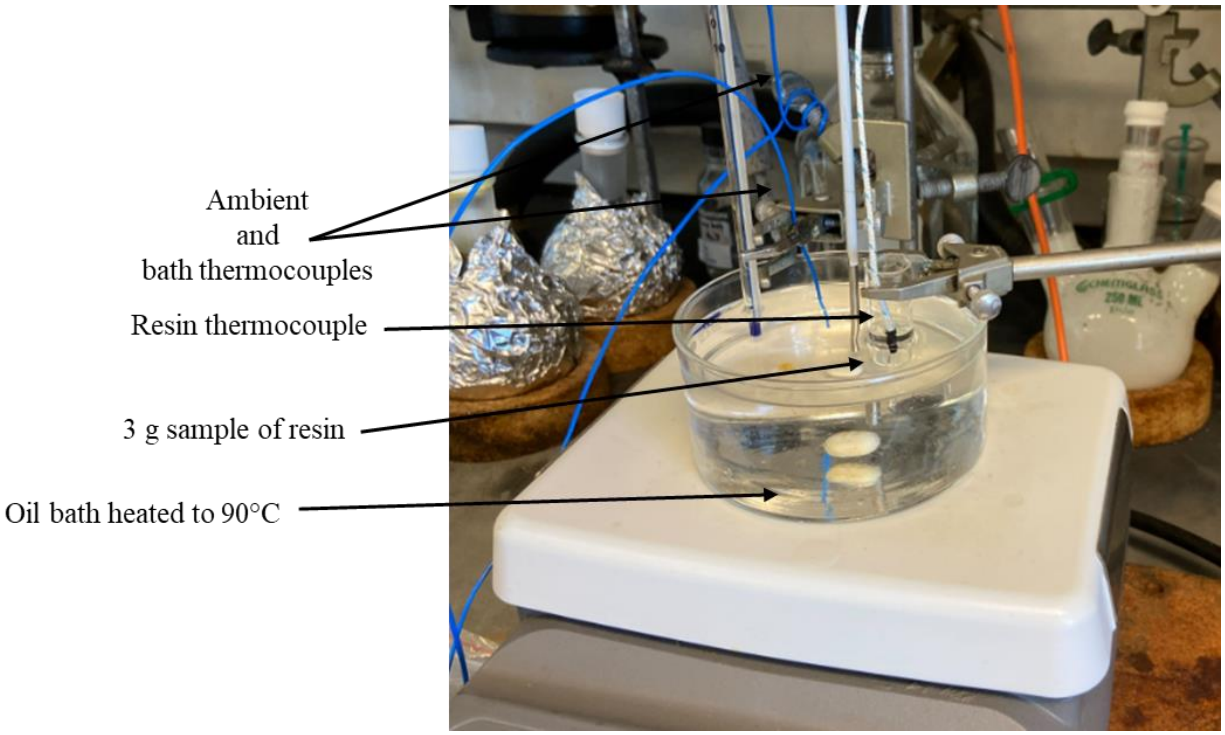

An oil bath was preheated to 90 °C for catalysts **1**–**10**. To ensure rapid mixing of the catalysts, the resins were melted into a liquid prior to initiating the measurement. Type-a resins were heated to 40 °C to melt the monomer. Type-b resins required no initial heating. Type-c resins were heated to 70 °C to melt the monomer. Type-d resins were heated to 30 °C to melt the monomer mixture.

A k-type thermocouple was then inserted into a 1-dram vial containing 3 g of melted resin. An Eppendorf pipette was then used to inject 70 µL of resin, and the tip was used to vigorously stir the vial for 3 seconds. The vial, now containing the active resin and thermocouple, was then rapidly lowered into the hot oil bath. The reaction temperature was monitored and logged using the 373 K/J thermometer data logger and EnviromentalTester PC interface. The vial was removed from the bath after it had cooled 20 °C from its peak temperature or after 5 minutes, whichever occurred first. The vial and contents were allowed to cool by standing, after which the outside of the vial was wiped to remove residual oil, and the sample was cataloged for analysis.

Table S4.1. Catalyst numbers, names, and corresponding molar mass.

Catalyst number	Catalyst name	Molar mass
1	Grubbs Catalyst 2nd Generation	848.98
2	Grubbs Catalyst 3rd Generation	727.76
3	Hoveyda-Grubbs Catalyst 1st Generation	600.61
4	FMO-316	703.75
5	Ratio Mono/BisIMesC6 7/3	907.744
6	DYB-749	667.72
7	DYB-751	645.71
8	DYB-753	639.67
9	DYB-755	639.67
10	DYB-761	645.71

Table S4.2. Resin formulations used for catalyst testing.

Resin type	DCPD (% mass)	ENB (% mass)	oxaDCPD (% mass)
a	100	0	0
b	95	5	0
c	0	0	100
d	45	5	0

Table S4.3. Sample of masses of catalysts used for each resin. Amount of phenyl cyclohexane (PhCy) used to make the stock solution is given in µL in brackets.

Catalyst	Mass of Catalyst (mg) (Volume of PhCy (µL)) for type-a [0.005 mol%]	Mass of Catalyst (mg) (Volume of PhCy (µL)) for type-b [0.005 mol%]	Mass of Catalyst (mg) (Volume of PhCy (µL)) for type-c [0.005 mol%]	Mass of Catalyst (mg) (Volume of PhCy (µL)) for type-c [0.02 mol%]	Mass of Catalyst (mg) (Volume of PhCy (µL)) for type-d [0.02 mol%]
1	9.7 (700)	9.7 (700)	4.4 (350)	17.6 (350)	18.2 (350)
2	4.2 (350)	4.1 (350)	3.7 (350)	15.3 (350)	15.9 (350)
3	3.3 (350)	6.9 (700)	3.6 (350)	12.3 (350)	12.8 (350)
4	4.1 (350)	4.0 (350)	3.6 (350)	14.1 (350)	15.0 (350)
5	5.3 (350)	5.2 (350)	4.7 (350)	18.6 (350)	20.0 (350)
6	3.9 (350)	3.8 (350)	3.5 (350)	13.4 (350)	14.9 (350)
7	3.8 (350)	3.7 (350)	3.4 (350)	13.4 (350)	14.0 (350)
8	3.5 (350)	3.6 (350)	3.1 (350)	13.2 (350)	14.0 (350)
9	3.6 (350)	3.6 (350)	3.2 (350)	13.4 (350)	13.5 (350)
10	3.8 (350)	3.7 (350)	3.3 (350)	13.2 (350)	13.8 (350)

Synthesis of Monomer

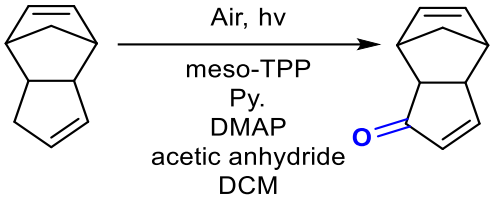

OxaDCPD was prepared as described in the literature.[19] For catalyst testing, 89.37 g (0.61 mol) oxaDCPD was dissolved in 190 mL of pentane. After 24 hours at −20°C, 70.18 g (0.48 mol) oxaDCPD was isolated via vacuum filtration as a white crystalline solid (79% recrystallized yield). MP: 54–59 °C. ^{1}H NMR (300.27 MHz, Chloroform-*d*) δ 7.38 (dd, *J* = 5.8, 2.6 Hz, 1H), 5.98 – 5.92 (m, 2H), 5.78 (dd, *J* = 5.4, 2.9 Hz, 1H) 3.45 – 3.39 (m, 1H), 3.22 (br s, 1H), 2.97 (app s, 1H), 2.80 (app t, *J* = 5.1, 1H), 1.76 (dd, *J* = 8.4, 1.0 Hz, 1H), 1.63 (d, *J* = 8.5 Hz, 1H). ^{13}C NMR (125.81 MHz, Chloroform-*d*) δ 209.12, 163.79, 135.93, 131.76, 131.52, 51.84, 49.29, 47.36, 44.17, 43.28.

Synthesis of CAAC Precursors

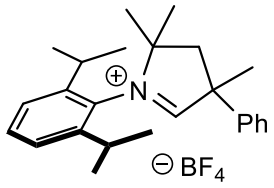

CAAC-a

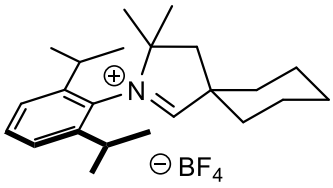

CAAC-b

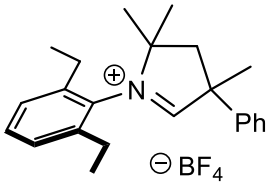

CAAC-c

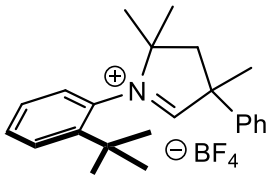

CAAC-d

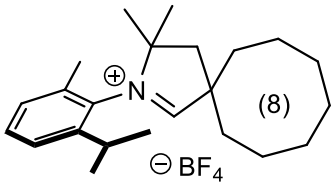

CAAC-e

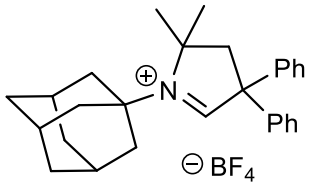

CAAC-f

CAAC-a,[41] **b**,[41] **c**,[42] and **d**,[29] are known compounds. **CAAC-e** and **f** were synthesized according to literature procedures.[43,44] Prior to use, CAAC salts were dried under high vacuum at 90°C overnight and stored in a glove box.

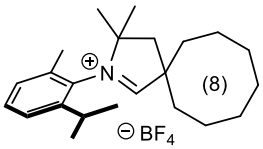

Chemical Formula: $C_{23}H_{36}BF_4N$
Molecular Weight: 413,35

CAAC-e was synthesized from the cyclooctanecarbaldehyde and 2-isopropyl-6-methylaniline according to the literature procedure (method B) and obtained as a white powder with an overall yield of 7%.[43]

^{1}H NMR (400 MHz, $CDCl_3$): δ (ppm) = 9.00 (s, 1H), 7.41 (t, J = 7.7 Hz, 1H), 7.30 (dd, J = 8.0, 1.5 Hz, 1H), 7.21 (dd, J = 7.7, 1.4 Hz, 1H), 2.62 (hept, J = 6.7 Hz, 1H), 2.45 – 2.42 (m, 1H), 2.37 – 2.33 (m, 1H), 2.28 (s, 3H), 2.23 – 2.12 (m, 1H), 1.87 (qd, J = 9.5, 5.9 Hz, 4H), 1.75 – 1.57 (m, 6H), 1.62 – 151 (m, 9H), 1.33 (d, J = 6.7 Hz, 3H), 1.09 (d, J = 6.8 Hz, 3H). ^{13}C NMR (101 MHz, $CDCl_3$): δ (ppm) = 191.3, 144.6, 133.9, 131.4, 130.8, 130.2, 125.0, 83.5, 55.5, 46.9, 34.0, 32.7, 29.7, 29.2, 28.2, 27.7, 27.6, 26.0, 24.3, 22.4, 22.3, 22.0, 19.5. ^{19}F NMR (376 MHz, $CDCl_3$): δ (ppm) = -151.8, -151.9. ^{11}B NMR (128 MHz, $CDCl_3$): δ (ppm) = -1.07. HRMS (ESI) for $C_{23}H_{36}N$ ($M^{+\cdot}$): calc.: 326.28423, found: 326.2840 (1 ppm).

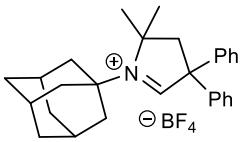

Chemical Formula: $C_{28}H_{34}BF_4N$
Molecular Weight: 471,39

CAAC-f was synthesized from the 2,2-diphenylacetaldehyde and the 1-adamantylamine according to the literature procedure and obtained as a white powder with an overall yield of 41%.[44]

^{1}H NMR (400 MHz, CD_2Cl_2): δ (ppm) = δ 9.48 (s, 1H), 7.45 – 7.40 (m, 4H), 7.36 – 7.32 (m, 2H), 7.29 – 7.25 (m, 4H), 3.08 (s, 2H), 2.33 (s, 9H), 1.77 (m, 6H), 1.71 (s, 6H).

^{13}C NMR (101 MHz, CD_2Cl_2): δ (ppm) = 181.2, 140.7, 130.2, 128.9, 127.2, 83.1, 72.0, 60.5, 52.4, 43.2, 35.1, 30.5, 29.4. ^{19}F NMR (376 MHz, CD_2Cl_2): δ (ppm) = -151.3, -151.4. ^{11}B NMR (128 MHz, CD_2Cl_2): δ (ppm) = -1.00. HRMS (ESI) for C_{28} H_{34} N ($M^{+\cdot}$): calc.: 384.26858, found: 384.2684 (0 ppm).

General Procedure for the Synthesis of CAAC-Ruthenium Complexes

Complexes 2,[30] **5**,[25] **6**, **7**, **8**[45] and **9**[29] were synthesized according to the literature conditions.

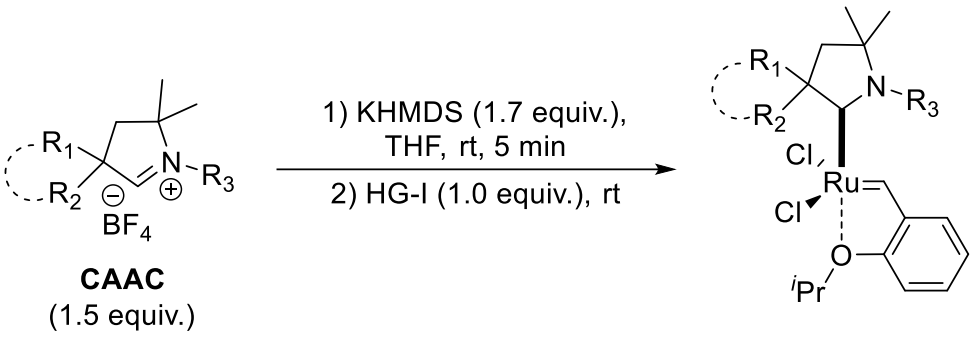

In a glovebox, CAAC salt (1.5 equiv.) and KHMDS (1.6 or 1.7 equiv.) were dissolved in dry/degassed solvent (0.067 or 0.1 M). The mixture was stirred at room temperature for 5 minutes. After this time, Hoveyda-Grubbs I complex (1.0 equiv.) was added and the resulting solution was stirred at rt the indicated time in the glovebox. THF was removed under reduced pressure and the crude product was purified by column chromatography (eluent toluene). The obtained solid was dissolved in a minimum amount of dichloromethane and precipitated in pentane.

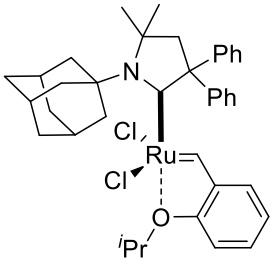

Chemical Formula: $C_{41}H_{48}Cl_2NORu$
Molecular Weight: 703,75

The general procedure for ruthenium complex synthesis was followed using **CAAC-f** (177 mg, 0.375 mmol, 1.5 equiv.), potassium bis(trimethylsilyl)amide, (80 mg, 0.40 mmol, 1.6 equiv.), Hoveyda-Grubbs I complex (150 mg, 0.25 mmol, 1 equiv.) and toluene (2.5 mL). The reaction was stirred 16 hours at room temperature. The desired ruthenium-complex **4** (98 mg, 0.14 mmol, 56% yield) was obtained as a green solid.

^{1}H NMR (400 MHz, $CDCl_3$): δ (ppm) = 17.97 (d, J = 0.8 Hz, 1H), 7.74 – 7.66 (m, 4H), 7.50 (ddd, J = 8.4, 7.2, 1.8 Hz, 1H), 7.29 – 7.26 (m, 3H), 7.25– 7.19 (m, 3H), 6.93 (d, J = 8.5 Hz, 1H), 6.84

– 6.70 (m, 2H), 5.07 (p, J = 6.1 Hz, 1H), 3.11 (s, 6H), 2.77 (s, 2H), 2.45 (s, 3H), 2.04 (d, J = 12.3 Hz, 3H), 1.79 (d, J = 12.3 Hz, 3H), 1.69 (d, J = 6.2 Hz, 6H), 1.45 (s, 6H). ^{13}C NMR (101 MHz, $CDCl_3$): δ (ppm) = 314.9 - 314.6 (1C), 268.2, 153.8, 146.3, 143.9, 132.3, 130.1, 127.8, 126.7, 124.4, 121.9, 113.4, 74.6, 74.2, 72.2, 66.1, 60.7, 43.7, 35.7, 31.9, 31.0, 22.6. HRMS (ESI) for $C_{38}H_{45}NO^{35}Cl_2{}^{102}Ru$ ($M^{+\cdot}$): calc.: 703.19162, found: 703.1918 (0 ppm). X-ray diffraction: Crystals of the complex were grown by slow diffusion of *n*-hexane into dichloromethane.

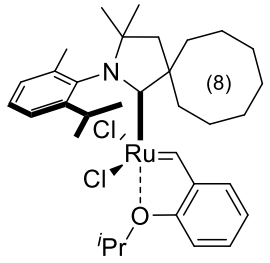

Chemical Formula: $C_{33}H_{47}Cl_2NORu$
Molecular Weight: 645,71

The general procedure for ruthenium complex synthesis was followed using **CAAC-e** (186 mg, 0.45 mmol, 1.5 equiv.), potassium bis(trimethylsilyl)amide, (102 mg, 0.51 mmol, 1.7 equiv.), Hoveyda-Grubbs I complex (180 mg, 0.30 mmol, 1.0 equiv.) and THF (4.5 mL). The reaction was stirred 18 hours at room temperature. The desired ruthenium-complex (123 mg, 0.19 mmol, 63% yield) **10** was obtained as a green solid.

^{1}H NMR (400 MHz, CD_2Cl_2): δ (ppm) = 16.45 (s, 1H), 7.62 – 7.44 (m, 3H), 7.29 (dd, J = 7.4, 1.7 Hz, 1H), 6.99 (d, J = 8.4 Hz, 1H), 6.90 (t, J = 7.4 Hz, 1H), 6.83 (dd, J = 7.6, 1.8 Hz, 1H), 5.18 – 5.04 (m, 1H), 3.16 (tdd, J = 15.0, 9.6, 2.1 Hz, 2H), 2.97 – 2.86 (m, 1H), 2.45 – 2.35 (m, 1H), 2.33 – 2.25 (m, 1H), 2.25 – 2.17 (m, 5H), 2.15 – 2.04 (m, 2H), 2.00 – 1.75 (m, 6H), 1.74 – 1.62 (m, 8H), 1.36 (s, 3H), 1.30 – 1.28 (m, 6H), 0.67 (d, J = 6.3 Hz, 3H). ^{13}C NMR (101 MHz, CD_2Cl_2): δ (ppm) = 302.0 - 301.9 (1C), 268.0, 152.6, 148.7, 144.4, 139.3, 138.3, 131.4, 130.0, 129.4, 126.1, 124.4, 122.3, 113.7, 77.9, 74.9, 66.5, 46.7, 33.5, 32.6, 30.1, 29.2, 29.0, 28.8, 28.7, 27.0, 26.8, 26.5, 25.5, 24.3, 22.6, 22.4, 21.7. HRMS (ESI) for $C_{33}H_{47}NO^{35}Cl_2{}^{102}Ru$ ($M^{+\cdot}$): calc.: 645.20727, found: 645.2077 (1 ppm).

4.6. References

(1) Vervacke, D. *An Introduction to PDCPD: Poly-Di-Cyclo-Penta-Diene*; Product Rescue, 2008.

(2) Kovačič, S.; Slugovc, C. Ring-Opening Metathesis Polymerisation Derived Poly(Dicyclopentadiene) Based Materials. *Mater. Chem. Front.* **2020**, *4* (8), 2235–2255. https://doi.org/10.1039/D0QM00296H.

(3) Minchak, R. J. Cyclopentene-Dicyclopentadiene Copolymers and Method of Making Same. US4002815A, January 11, 1977.

(4) Klosiewicz, D. W. Method for Making a Dicyclopentadiene Thermoset Polymer. US4400340A, August 23, 1983.

(5) Klosiewicz, D. W.; Tom, G. M. A Dicyclopentadiene Thermoset Polymer and a Catalyst and a Method for Making It. EP0084888B1, June 16, 1987.

(6) Matlack, A. S. Metathesis Polymerization of Thermally Oligomerized Dicyclopentadiene. US4703098A, October 27, 1987.

(7) Espy, H. H.; Matlack, A. S. Conversion of Solid Dicyclopentadiene to a Liquid Monomer for Use in Reaction Injection Molding. EP0271007A2, June 15, 1988.

(8) Suslick, B. A.; Stawiasz, K. J.; Paul, J. E.; Sottos, N. R.; Moore, J. S. Survey of Catalysts for Frontal Ring-Opening Metathesis Polymerization. *Macromolecules* **2021**, *54* (11), 5117–5123. https://doi.org/10.1021/acs.macromol.1c00566.

(9) Bielawski, C. W.; Grubbs, R. H. Highly Efficient Ring-Opening Metathesis Polymerization (ROMP) Using New Ruthenium Catalysts Containing N-Heterocyclic Carbene

Ligands. *Angew. Chem. Int. Ed.* **2000**, *39* (16), 2903–2906. https://doi.org/10.1002/1521-3773(20000818)39:16<2903::AID-ANIE2903>3.0.CO;2-Q.

(10) Eivgi, O.; Vaisman, A.; Lemcoff, N. G. Latent, Yet Highly Active Photoswitchable Olefin Metathesis Precatalysts Bearing Cyclic Alkyl Amino Carbene (CAAC)/Phosphite Ligands. *ACS Catal.* **2021**, *11* (2), 703–709. https://doi.org/10.1021/acscatal.0c04909.

(11) Chen, J.; Burns, F. P.; Moffitt, M. G.; Wulff, J. E. Thermally Crosslinked Functionalized Polydicyclopentadiene with a High Tg and Tunable Surface Energy. *ACS Omega* **2016**, *1* (4), 532–540. https://doi.org/10.1021/acsomega.6b00193.

(12) Gong, L.; Liu, K.; Ou, E.; Xu, F.; Lu, Y.; Wang, Z.; Gao, T.; Yang, Z.; Xu, W. ROMP of Acetoxy-Substituted Dicyclopentadiene to a Linear Polymer with a High Tg. *RSC Adv.* **2015**, *5* (33), 26185–26188. https://doi.org/10.1039/C5RA01855B.

(13) S. Phatake, R.; Masarwa, A.; Gabriel Lemcoff, N.; Reany, O. Tuning Thermal Properties of Cross-Linked DCPD Polymers by Functionalization, Initiator Type and Curing Methods. *Polym Chem.* **2020**, *11* (10), 1742–1751. https://doi.org/10.1039/C9PY01178A.

(14) Saha, S.; Ginzburg, Y.; Rozenberg, I.; Iliashevsky, O.; Ben-Asuly, A.; Lemcoff, N. G. Cross-Linked ROMP Polymers Based on Odourless Dicyclopentadiene Derivatives. *Polym. Chem.* **2016**, *7* (18), 3071–3075. https://doi.org/10.1039/C6PY00378H.

(15) Cuthbert, T. J.; Li, T.; Speed, A. W. H.; Wulff, J. E. Structure of the Thermally Induced Cross-Link in C -Linked Methyl Ester-Functionalized Polydicyclopentadiene (fPDCPD). *Macromolecules* **2018**, *51* (5), 2038–2047. https://doi.org/10.1021/acs.macromol.7b02750.

(16) Cuthbert, T. J.; Li, T.; Wulff, J. E. Production and Dynamic Mechanical Analysis of Macro-Scale Functionalized Polydicyclopentadiene Objects Facilitated by Rational Synthesis and Reaction Injection Molding. *ACS Appl. Polym. Mat.* **2019**, *1* (9), 2460–2471. https://doi.org/10.1021/acsapm.9b00571.

(17) Li, T.; Wulff, J. E. Copolymers of Functionalized and Nonfunctionalized Polydicyclopentadiene. *ACS Appl. Polym. Mater.* **2021**, *3* (1), 110–115. https://doi.org/10.1021/acsapm.0c01196.

(18) Li, T.; Shumka, H.; J. Cuthbert, T.; Liu, C.; E. Wulff, J. Harnessing the Surface Chemistry of Methyl Ester Functionalized Polydicyclopentadiene and Exploring Surface Bioactivity. *Mater. Adv.* **2020**, *1* (6), 1753–1762. https://doi.org/10.1039/D0MA00480D.

(19) Godwin, B.; Anvari, M. H.; Olfatbakhsh, T.; Mahbod, M.; Milani, A. S.; DiLabio, G. A.; Wulff, J. E. A Single-Atom Upgrade to Polydicyclopentadiene. *Macromolecules* **2023**, *56* (4), 1592–1600. https://doi.org/10.1021/acs.macromol.2c02260.

(20) McFadden, T. P.; Cope, R. B.; Muhlestein, R.; Layton, D. J.; Lessard, J. J.; Moore, J. S.; Sigman, M. S. Using Data Science Tools to Reveal and Understand Subtle Relationships of Inhibitor Structure in Frontal Ring-Opening Metathesis Polymerization. *J. Am. Chem. Soc.* **2024**. https://doi.org/10.1021/jacs.4c04622.

(21) Lessard, J. J.; Mejia, E. B.; Kim, A. J.; Zhang, Z.; Berkey, M. G.; Medina-Barreto, Z. S.; Ewoldt, R. H.; Sottos, N. R.; Moore, J. S. Unraveling Reactivity Differences: Room-Temperature Ring-Opening Metathesis Polymerization (ROMP) versus Frontal ROMP. *J. Am. Chem. Soc.* **2024**, *146* (11), 7216–7221. https://doi.org/10.1021/jacs.4c01578.

(22) Goetz, A. E.; Boydston, A. J. Metal-Free Preparation of Linear and Cross-Linked Polydicyclopentadiene. *J. Am. Chem. Soc.* **2015**, *137* (24), 7572–7575. https://doi.org/10.1021/jacs.5b03665.

(23) Yang, X.; Murphy, L. M.; Haque, F. M.; Grayson, S. M.; Boydston, A. J. A Highly Efficient Metal-Free Protocol for the Synthesis of Linear Polydicyclopentadiene. *Polym. Chem.* **2021**, *12* (19), 2860–2867. https://doi.org/10.1039/D1PY00191D.

(24) Steese, N. D.; Barvaliya, D.; Poole, X. D.; McLemore, D. E.; DiCesare, J. C.; Schanz, H.-J. Synthesis and Thermal Properties of Linear Polydicyclopentadiene via Ring-Opening Metathesis Polymerization with a Third Generation Grubbs-Type Ruthenium-Alkylidene Complex. *J. Polym. Sci. Part A: Polym. Chem.* **2018**, *56* (4), 359–364. https://doi.org/10.1002/pola.28909.

(25) Rouen, M.; Borré, E.; Falivene, L.; Toupet, L.; Berthod, M.; Cavallo, L.; Olivier-Bourbigou, H.; Mauduit, M. Cycloalkyl-Based Unsymmetrical Unsaturated (U 2)-NHC Ligands: Flexibility and Dissymmetry in Ruthenium-Catalysed Olefin Metathesis. *Dalton Trans.* **2014**, *43* (19), 7044–7049. https://doi.org/10.1039/C4DT00142G.

(26) Jazzar, R.; Soleilhavoup, M.; Bertrand, G. Cyclic (Alkyl)- and (Aryl)-(Amino)Carbene Coinage Metal Complexes and Their Applications. *Chem. Rev.* **2020**, *120* (9), 4141–4168. https://doi.org/10.1021/acs.chemrev.0c00043.

(27) Melaimi, M.; Jazzar, R.; Soleilhavoup, M.; Bertrand, G. Cyclic (Alkyl)(Amino)Carbenes (CAACs): Recent Developments. *Angew. Chem. Int. Ed.* **2017**, *56* (34), 10046–10068. https://doi.org/10.1002/anie.201702148.

(28) Morvan, J.; Mauduit, M.; Bertrand, G.; Jazzar, R. Cyclic (Alkyl)(Amino)Carbenes (CAACs) in Ruthenium Olefin Metathesis. *ACS Catal.* **2021**, *11* (3), 1714–1748. https://doi.org/10.1021/acscatal.0c05508.

(29) Sytniczuk, A.; Kajetanowicz, A.; Grela, K. "Inverted" Cyclic(Alkyl)(Amino)Carbene Ligands Allow Olefin Metathesis with Ethylene at Parts-per-Billion Catalyst Loading. *Chem Catal.* **2023**, *3* (9), 100713. https://doi.org/10.1016/j.checat.2023.100713.

(30) Love, J. A.; Morgan, J. P.; Trnka, T. M.; Grubbs, R. H. A Practical and Highly Active Ruthenium-Based Catalyst That Effects the Cross Metathesis of Acrylonitrile. *Angew. Chem. Int. Ed.* **2002**, *41* (21), 4035–4037. https://doi.org/10.1002/1521-3773(20021104)41:21<4035::AID-ANIE4035>3.0.CO;2-I.

(31) Czelusniak, I.; Heywood, J. D.; Kenwright, A. M.; Khosravi, E. Investigation of Factors Affecting Ruthenium Complexation in ROMP Reactions of Oxygen-Containing Norbornene Derivatives Using Grubbs First Generation Initiator. *J. Mol. Catal. A: Chem.* **2008**, *280* (1), 29–34. https://doi.org/10.1016/j.molcata.2007.10.011.

(32) Robertson, I. D.; Yourdkhani, M.; Centellas, P. J.; Aw, J. E.; Ivanoff, D. G.; Goli, E.; Lloyd, E. M.; Dean, L. M.; Sottos, N. R.; Geubelle, P. H.; Moore, J. S.; White, S. R. Rapid Energy-Efficient Manufacturing of Polymers and Composites via Frontal Polymerization. *Nature* **2018**, *557* (7704), 223–227. https://doi.org/10.1038/s41586-018-0054-x.

(33) Sutor, D. J. Evidence for the Existence of C–H···O Hydrogen Bonds in Crystals. *J. Chem. Soc.* **1963**, No. 0, 1105–1110. https://doi.org/10.1039/JR9630001105.

(34) Sutor, D. J. The C–H… O Hydrogen Bond in Crystals. *Nature* **1962**, *195* (4836), 68–69. https://doi.org/10.1038/195068a0.

(35) Schwalbe, C. H. June Sutor and the C–H ⋯ O Hydrogen Bonding Controversy. *Crystallography Reviews* **2012**, *18* (3), 191–206. https://doi.org/10.1080/0889311X.2012.674945.

(36) Callister, W., Jr.; Rethwisch, D. *Materials Science and Engineering an Introduction*, 9th ed.; John Wiley & Sons, Inc.

(37) Zhang, P.; Li, S. X.; Zhang, Z. F. General Relationship between Strength and Hardness. *Mater. Sci. Eng. A* **2011**, *529*, 62–73. https://doi.org/10.1016/j.msea.2011.08.061.

(38) Wu, H.; Dave, F.; Mokhtari, M.; Ali, M. M.; Sherlock, R.; McIlhagger, A.; Tormey, D.; McFadden, S. On the Application of Vickers Micro Hardness Testing to Isotactic Polypropylene. *Polym.* **2022**, *14* (9), 1804. https://doi.org/10.3390/polym14091804.

(39) Sheldrick, G. M. *SHELXT* – Integrated Space-Group and Crystal-Structure Determination. *Acta Crystallogr., Sect: A Found. Adv* **2015**, *71* (1), 3–8. https://doi.org/10.1107/S2053273314026370.

(40) Sheldrick, G. M. Crystal Structure Refinement with *SHELXL*. *Acta Crystallogr., sect: C Struct. Chem.* **2015**, *71* (1), 3–8. https://doi.org/10.1107/S2053229614024218.

(41) Morvan, J.; Vermersch, F.; Zhang, Z.; Falivene, L.; Vives, T.; Dorcet, V.; Roisnel, T.; Crévisy, C.; Cavallo, L.; Vanthuyne, N.; Bertrand, G.; Jazzar, R.; Mauduit, M. Optically Pure C1-Symmetric Cyclic(Alkyl)(Amino)Carbene Ruthenium Complexes for Asymmetric Olefin Metathesis. *J. Am. Chem. Soc.* **2020**, *142* (47), 19895–19901. https://doi.org/10.1021/jacs.0c10705.

(42) Morvan, J.; Vermersch, F.; Zhang, Z.; Vives, T.; Roisnel, T.; Crévisy, C.; Falivene, L.; Cavallo, L.; Vanthuyne, N.; Bertrand, G.; Jazzar, R.; Mauduit, M. Ambivalent Role of Rotamers in Cyclic(Alkyl)(Amino)Carbene Ruthenium Complexes for Enantioselective Ring-Opening Cross-Metathesis. *Organometallics* **2023**, *42* (6), 495–504. https://doi.org/10.1021/acs.organomet.3c00054.

(43) Vermersch, F.; Oliveira, L.; Hunter, J.; Soleilhavoup, M.; Jazzar, R.; Bertrand, G. Cyclic (Alkyl)(Amino)Carbenes: Synthesis of Iminium Precursors and Structural Properties. *J. Org. Chem.* **2022**, *87* (5), 3511–3518. https://doi.org/10.1021/acs.joc.1c03075.

(44) Madron du Vigné, A.; Cramer, N. Chiral Cyclic Alkyl Amino Carbene (CAAC) Transition-Metal Complexes: Synthesis, Structural Analysis, and Evaluation in Asymmetric Catalysis. *Organometallics* **2022**, *41* (19), 2731–2741. https://doi.org/10.1021/acs.organomet.2c00351.

(45) Marx, V. M.; Sullivan, A. H.; Melaimi, M.; Virgil, S. C.; Keitz, B. K.; Weinberger, D. S.; Bertrand, G.; Grubbs, R. H. Cyclic Alkyl Amino Carbene (CAAC) Ruthenium Complexes as Remarkably Active Catalysts for Ethenolysis. *Angew. Chem. Int. Ed.* **2015**, *54* (6), 1919–1923. https://doi.org/10.1002/anie.201410797.

Chapter 5: Do Research Outcomes in Materials Science have Real World Benefits?

Benjamin Godwin, Kate Withers Hess, Wesley Kosiba, and Jeremy Wulff

This market research study was conducted at the University of Toronto Metropolitan University as part of a Natural Sciences and Engineering Research Council of Canada Lab to Market grant.

5.0. Contributions

Stakeholder interviews, script drafts and data analysis were done by Benjamin Godwin.

5.1. Abstract

Polydicyclopentadiene (PDCPD) is an industrially relevant engineering plastic made through ring-opening metathesis polymerization. Despite being a niche material largely relegated to the production of body panels, there has been a spate of high-impact research into polydicyclopentadiene (PDCPD). In this study, we investigate the unmet needs of the PDCPD industry and the most likely path to commercialization for new PDCPD technologies.

5.2. Introduction

Polydicyclopentadiene (PDCPD) is a lightweight thermoset material with excellent mechanical and thermal properties produced through reaction injection molding (RIM). PDCPD is used industrially to make body panels for the auto sector primarily for heavy duty vehicles such as construction or agricultural equipment.[1] However, the broader application of PDCPD across industry, particularly in aerospace where other thermosets are widely used, has largely been limited. There has been substantial research investment into PDCPD (Figure 5.1). PDCPD has been investigated for its ballistic performance by both the Canadian—by us, as part of an Innovation for Defence and Excellence and Security (IDEaS) program—and American militaries.[2–6] Significant efforts have been made to upgrade its mechanical and thermal properties through a variety of different strategies, such as copolymerization.[7–11] Functionalized PDCPD materials have also been developed to improve the mechanical and thermal properties, or allow PDCPD to be a functional material with tunable properties and active surface control.[8,12–16] Research has shown that frontal ring opening polymerization reactions can be used to produce large PDCPD parts from a point heat source, significantly reducing the energy required for manufacturing.[17–20]

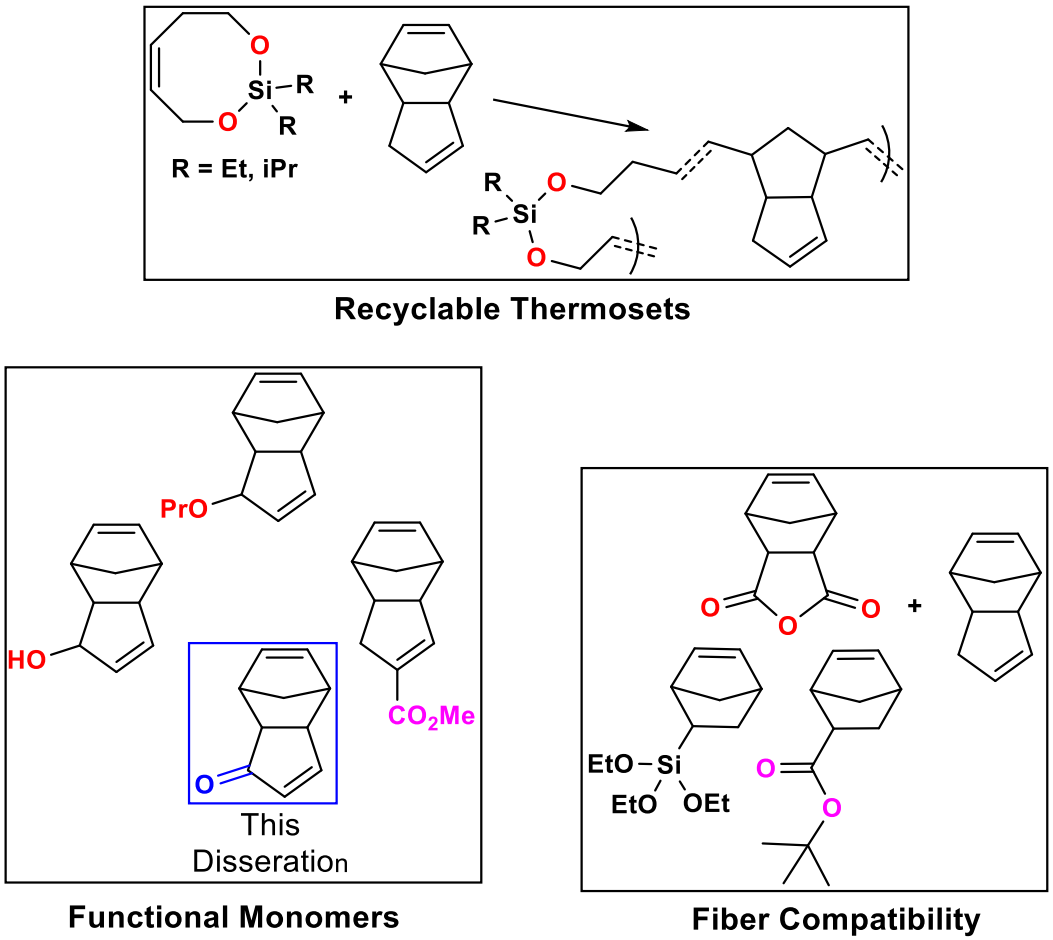

Figure 5.1. Select areas of academic research into PDCPD.

PDCPD can be made into a recyclable thermoset, through the incorporation of dynamic boronic ester bonds, or through the installation of cleavable silyl ether.[21–24] There is ongoing work to show that with simple chemical modifications glass and carbon fibers can be used to make impressive composite materials.[25] Despite this work there has been little deviation from the status quo in the PDCPD industry, with body panels for the auto industry continuing to dominate the market.[1] We were interested in determining the commercial viability of our functionalized PDCPD, polydicyclopentadienone (oxaPDCPD), and in determining firsthand what problems the PDCPD industry is facing.[13] Additionally, we were interested in what markets are most likely to be the early adopters of new PDCPD technology. We participated in a Natural Sciences and

Engineering Research Council of Canada (NSERC) Lab to Market (L2M) grant at the Toronto Metropolitan University and conducted primary market research to assess this.

5.3. Results and Discussion

We initially hypothesized that the use of PDCPD was largely limited due to some inherent key disadvantages. PDCPD lacks chemically modifiable groups (functional groups) on its surface, which limits the tunability of its properties.[12,13,15,16] Additionally, with ongoing advances in technology towards functional materials, we thought that making smart, structural materials through functional PDCPD polymers would be desirable.[26,27] The lack of functional groups also results in a low surface energy which makes the application of paints and adhesives challenging without first preparing or aging the surface.[9,12,13] We hypothesized that this would reduce manufacturing times and be a key pain point that industry would want addressed.[1] Additionally, the manufacturing of composite materials, which are heavily utilized in the aerospace industry, is challenging since most fiber reinforcements are designed to work with polar, functional group-decorated polymers such as epoxies and polyesters.[28–33] We anticipated that fiber reinforcement would be desirable to industry. In the same vein, we thought that general improvements to both mechanical strength and thermal properties would also be desired. PDCPD has a characteristic unpleasant odor that results from unreacted monomer (dicyclopentadiene (DCPD)), which prevents its use indoors, as this odor is perceptible at the ppb level.[1,16] We thought that by eliminating the odor, PDCPD could be expanded to interior applications instead of just exterior body panels. Additionally, since thermosets in general are not recyclable and there is a trend towards sustainable and circular economies in polymer and material science, we anticipated that reducing the environmental impact of PDCPD would be desirable.[34–36]

Primary market research was conducted in the form of fifteen stakeholder interviews as part of the NSERC L2M grant at Toronto Metropolitan University. Stakeholder interviews were conducted using scripts (see Appendix D) to ensure consistency. The interviews were approximately 40 minutes long and notes were taken during each interview. Stakeholders were contacted through email, phone, LinkedIn and in person. The data were then analyzed for keywords and patterns. Market research insights were derived by filtering for the keywords. We interviewed a diverse group of individuals from all aspects of the PDCPD industry, as well as individuals adjacent to the PDCPD industry who may participate in the future (Figure 5.2).

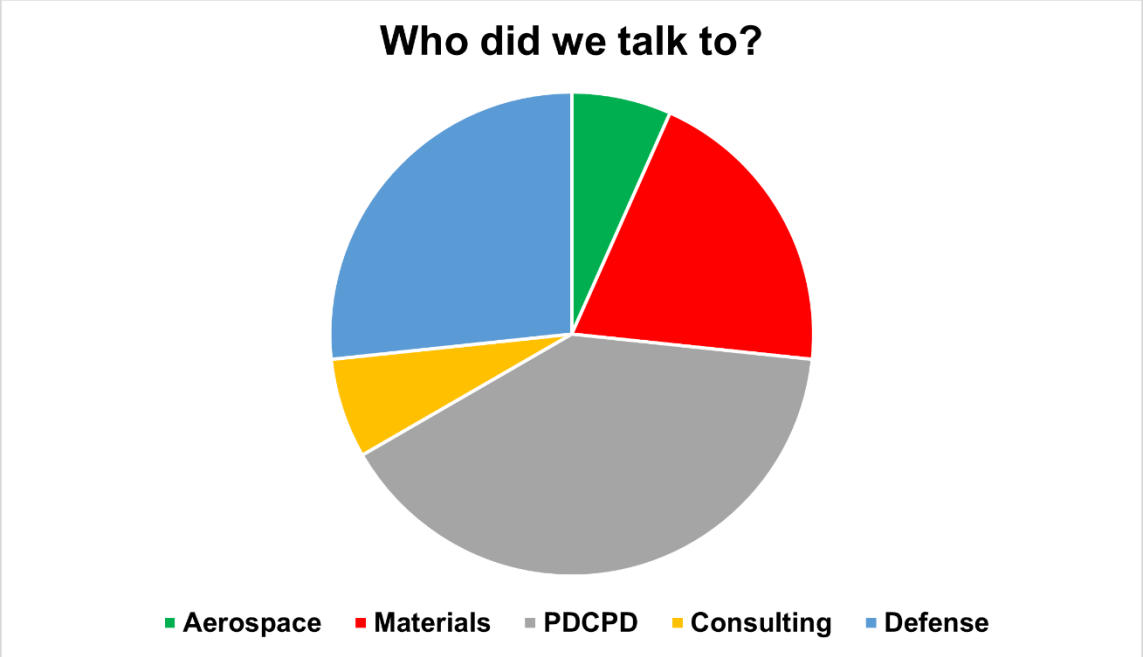

Figure 5.2. Breakdown of participants from broadly defined customer and industry segments.

In our initial interviews, we found that the ability to successfully incorporate fiber reinforcements into PDCPD or any material was the most important new development (Figure 5.3). It was of special importance that the materials be compatible with existing fiber reinforcements, as opposed to fibers that were made compatible with the matrix. This was

reinforced by conversations with the fiber industry; we were informed that there was not the manufacturing bandwidth to make specialty fibers for niche materials. Multiple participants stated that PDCPD composites, while costly, could do very well in high-performance materials markets such as defence. We also found that in some marine markets, materials without fiber reinforcement were automatically rejected due to durability concerns. Interestingly, most stakeholders did not identify improved mechanical or thermal properties of the material as a desired improvement (Figure 5.3). Though we did learn that the increase in mechanical strength of unreinforced material would need to be approximately double the current value to be relevant, and if that were achievable, it would be desired.

The odor of PDCPD was not a serious concern for most stakeholders. According to our respondents, improvements in the polymerization process eliminate nearly all the odorous monomer, and any odor that remains can be dealt with in a post-curing process. However, we did learn that some stakeholders had lost customers owing to the reputation of the material for odor.

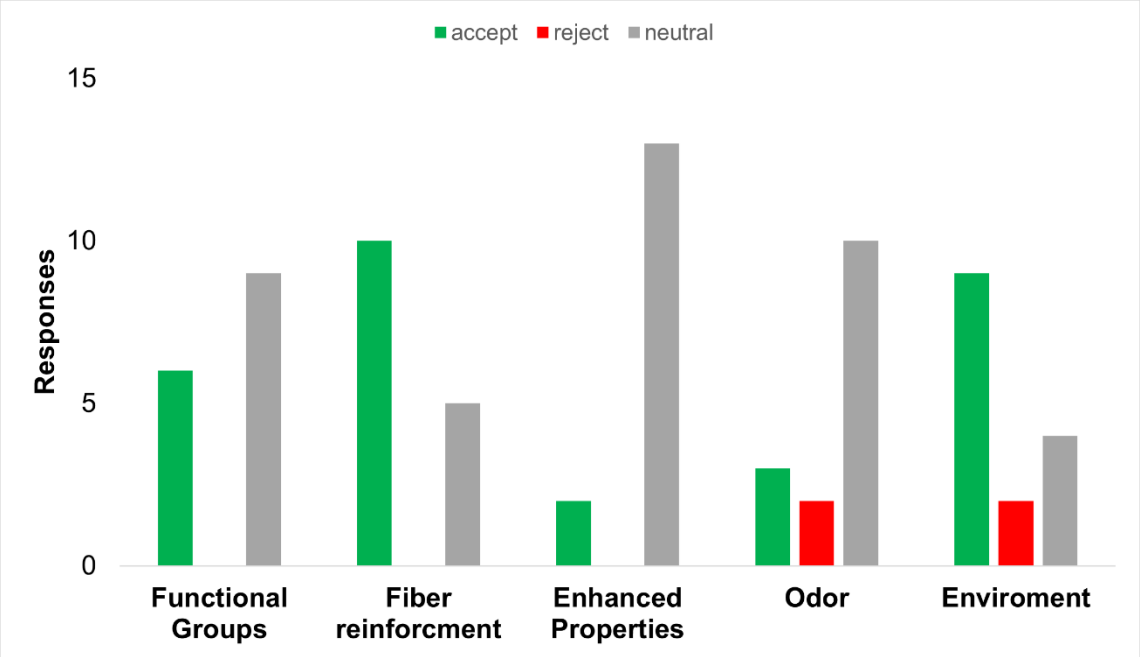

Figure 5.3. Responses to our hypothesis. Positive responses are shown in green, negative responses are shown in red. Interviews that did not specifically comment on a hypothesis are shown in grey.

Stakeholders were interested in functionalized PDCPD. Stakeholders were focused on finding methods to perform in-mold painting of the material, reduce workflow and protect the surface (Figure 5.3). The desire to protect the surface was driven by two things, to stop the surface from being contaminated during aging and/or prep for painting, and to protect the surface from extensive oxidation. This oxidation can lead to a deterioration in material properties.[37] Some stakeholders were also interested in precisely controlling the crosslinking reaction of the polymer.

Stakeholders were concerned about the environmental impact of PDCPD (Figure 5.3). The inability to recycle the current material was cited as a major disadvantage. Participants expressed concern about the toxicity of the monomer, especially in the European market. They also stated that customers were starting to inquire more about the lifecycle of the material. The sentiment of the participants was that there was not enough regulatory pressure to force the adoption of new

changes yet. This suggests that a recyclable version of the thermoset may be able to make inroads into the industry in the future.

It was frequently suggested by stakeholders that the defence and aerospace industries would be interested in a high performance PDCPD (Figure 5.4). We therefore set out to do a second round of interviews targeting the aerospace and defence industries, hoping that the demanding applications of these industries would provide a possible path for commercialization.

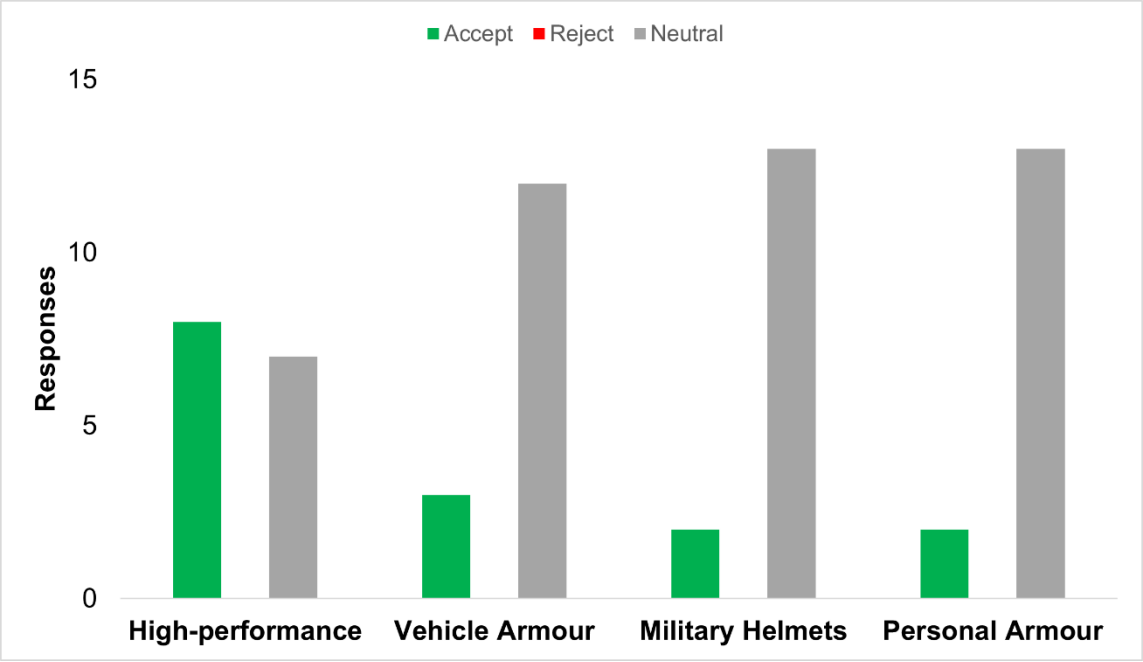

Figure 5.4. Stakeholder responses to questions regarding the application of PDCPD to high-performance applications. Positive responses are shown in green, negative responses are shown in red. Interviews that did not specifically comment on a hypothesis are shown in grey.

We learned that there is an imminent need for modular armour that can be applied to vehicles. Currently, ceramics are most often used due to their ability to stop projectiles. However, ceramic armour has several limitations. It is very fragile and can be written off if mishandled or dropped. Ceramic plates do not perform well against explosive threats, and this requires that the armour be encapsulated. It was suggested to us that PDCPD may be a suitable matrix for this task owing to

its high toughness. Another concern that was associated with current modular armour systems is the reduction in mobility and speed of a vehicle due to the weight of current systems. Stakeholders also expressed a need for more lighter systems to make it easier for technicians to handle the armour, as well as increase the ease of transporting the armour to the operation zone.

Stakeholders involved in the personal armour space stated that there is room for innovation in personal armour. Specifically, they mentioned combining the advantages of currently available systems. For instance, ceramic armour is very light and able to withstand multiple strikes, while steel plates are low-cost. Innovation in helmets was also discussed. Stakeholders suggested that PDCPD fiber-reinforced helmets could outperform current offerings. However, they also cautioned that helmets come with additional regulatory complexity—not only do they need to protect against ballistic threats, but also from other brain injuries, which can easily arise from other non-penetration-related factors, such as blasts, blunt impacts and rotational injuries—making this a less attractive entry point to the market.[38,39] After speaking with stakeholders in the aerospace industry, it quickly became clear that there would significant and expensive regulatory hurdles that would prevent the early adoption of new materials from academia.

5.4. Conclusions

Through our primary market research, we found that fiber reinforcement is the most desired trait in the PDCPD industry. We also found that increases in mechanical or thermal properties would need to be rather large to be considered worthwhile adopting in the mainstream industry. Interestingly, our hypothesis that the odor of the material was a significant problem proved to be incorrect. Manufacturers of parts were, in general, open to improvements but those improvements needed to fit into existing workflows. The most likely stakeholders to adopt new materials are those that face significant risks and require high-performance, as they are the most interested in incremental gains.

5.5. Methods

Primary market research was conducted in the form of stakeholder interviews. Stakeholder interviews were conducted using scripts. The interviews were approximately 40 minutes long and notes were taken during the interview. Stakeholders were contacted through email, phone, LinkedIn and in person. The data was then analyzed for key words and patterns. Market research insights were made by filtering for the key words.

5.6. References

(1) Vervacke, D. *An Introduction to PDCPD: Poly-Di-Cyclo-Penta-Diene*; Product Rescue, 2008.

(2) Defence, N. *Armour Up! Modular Lightweight Armour for Land Vehicles*. https://www.canada.ca/en/department-national-defence/programs/defence-ideas/element/competitive-projects/challenges/armour-up-modular-lightweight-armour-land-vehicles.html (accessed 2024-07-26).

(3) *Next-gen auto parts - University of Victoria*. UVic.ca. https://www.uvic.ca/news/topics/2021+knowledge-next-gen-auto-parts+news (accessed 2024-07-26).

(4) Long, T. R.; Elder, R. M.; Bain, E. D.; Masser, K. A.; Sirk, T. W.; Yu, J. H.; Knorr, D. B.; Lenhart, J. L. Influence of Molecular Weight between Crosslinks on the Mechanical Properties of Polymers Formed via Ring-Opening Metathesis. *Soft Matter.* **2018**, *14* (17), 3344–3360. https://doi.org/10.1039/C7SM02407J.

(5) Knorr, D. B.; Masser, K. A.; Elder, R. M.; Sirk, T. W.; Hindenlang, M. D.; Yu, J. H.; Richardson, A. D.; Boyd, S. E.; Spurgeon, W. A.; Lenhart, J. L. Overcoming the Structural versus Energy Dissipation Trade-off in Highly Crosslinked Polymer Networks: Ultrahigh Strain Rate Response in Polydicyclopentadiene. *Compos. Sci. Technol.* **2015**, *114*, 17–25. https://doi.org/10.1016/j.compscitech.2015.03.021.

(6) Masser, K. A.; Long, T. R.; Yu, J. H.; Knorr Jr., D. B.; Hindenlang, M. D.; Taylor, T.; Harris, D.; Lenhart, J. L. The Temperature-Dependent Ballistic Performance and the Ductile-to-

Brittle Transition in Polymer Networks. *J. Polym., Sci Part B: Polym. Phys.* **2019**, *57* (9), 511–523. https://doi.org/10.1002/polb.24807.

(7) Beuguel, Q.; Kirillov, E.; Carpentier, J.-F.; Guillaume, S. M. Upgrading Toughness and the Glass Transition Temperature of Polydicyclopentadiene upon Addition of Styrene–Ethylene–Butylene–Styrene Thermoplastic Elastomer. *ACS Appl. Polym. Mater.* **2022**, *4* (4), 2251–2255. https://doi.org/10.1021/acsapm.1c01803.

(8) S. Phatake, R.; Masarwa, A.; Gabriel Lemcoff, N.; Reany, O. Tuning Thermal Properties of Cross-Linked DCPD Polymers by Functionalization, Initiator Type and Curing Methods. *Polym. Chem.* **2020**, *11* (10), 1742–1751. https://doi.org/10.1039/C9PY01178A.

(9) Li, T.; Wulff, J. E. Copolymers of Functionalized and Nonfunctionalized Polydicyclopentadiene. *ACS Appl. Polym. Mater.* **2021**, *3* (1), 110–115. https://doi.org/10.1021/acsapm.0c01196.

(10) Yao, Z.; Zhou, L.; Dai, B.; Cao, K. Ring-Opening Metathesis Copolymerization of Dicyclopentadiene and Cyclopentene through Reaction Injection Molding Process. *J. Appl. Polym. Sci.* **2012**, *125* (4), 2489–2493. https://doi.org/10.1002/app.36359.

(11) Zhan, Q.; Yang, P. Upgrading of Thermosets and Composites via Sequential Frontal Ring-Opening Metathesis Polymerization and Radical Reactions. *J. Mater. Sci.* **2024**, *59* (18), 7779–7792. https://doi.org/10.1007/s10853-024-09674-6.

(12) Chen, J.; Burns, F. P.; Moffitt, M. G.; Wulff, J. E. Thermally Crosslinked Functionalized Polydicyclopentadiene with a High Tg and Tunable Surface Energy. *ACS Omega* **2016**, *1* (4), 532–540. https://doi.org/10.1021/acsomega.6b00193.

(13) Godwin, B.; Anvari, M. H.; Olfatbakhsh, T.; Mahbod, M.; Milani, A. S.; DiLabio, G. A.; Wulff, J. E. A Single-Atom Upgrade to Polydicyclopentadiene. *Macromolecules* **2023**, *56* (4), 1592–1600. https://doi.org/10.1021/acs.macromol.2c02260.

(14) Li, T.; Shumka, H.; J. Cuthbert, T.; Liu, C.; E. Wulff, J. Harnessing the Surface Chemistry of Methyl Ester Functionalized Polydicyclopentadiene and Exploring Surface Bioactivity. *Mater. Adv.* **2020**, *1* (6), 1753–1762. https://doi.org/10.1039/D0MA00480D.

(15) Gong, L.; Liu, K.; Ou, E.; Xu, F.; Lu, Y.; Wang, Z.; Gao, T.; Yang, Z.; Xu, W. ROMP of Acetoxy-Substituted Dicyclopentadiene to a Linear Polymer with a High Tg. *RSC Adv.* **2015**, *5* (33), 26185–26188. https://doi.org/10.1039/C5RA01855B.

(16) Saha, S.; Ginzburg, Y.; Rozenberg, I.; Iliashevsky, O.; Ben-Asuly, A.; Lemcoff, N. G. Cross-Linked ROMP Polymers Based on Odourless Dicyclopentadiene Derivatives. *Polym. Chem.* **2016**, *7* (18), 3071–3075. https://doi.org/10.1039/C6PY00378H.

(17) Robertson, I. D.; Yourdkhani, M.; Centellas, P. J.; Aw, J. E.; Ivanoff, D. G.; Goli, E.; Lloyd, E. M.; Dean, L. M.; Sottos, N. R.; Geubelle, P. H.; Moore, J. S.; White, S. R. Rapid Energy-Efficient Manufacturing of Polymers and Composites via Frontal Polymerization. *Nature* **2018**, *557* (7704), 223–227. https://doi.org/10.1038/s41586-018-0054-x.

(18) Suslick, B. A.; Stawiasz, K. J.; Paul, J. E.; Sottos, N. R.; Moore, J. S. Survey of Catalysts for Frontal Ring-Opening Metathesis Polymerization. *Macromolecules* **2021**, *54* (11), 5117–5123. https://doi.org/10.1021/acs.macromol.1c00566.

(19) Lessard, J. J.; Mejia, E. B.; Kim, A. J.; Zhang, Z.; Berkey, M. G.; Medina-Barreto, Z. S.; Ewoldt, R. H.; Sottos, N. R.; Moore, J. S. Unraveling Reactivity Differences: Room-Temperature

Ring-Opening Metathesis Polymerization (ROMP) versus Frontal ROMP. *J. Am. Chem. Soc.* **2024**, *146* (11), 7216–7221. https://doi.org/10.1021/jacs.4c01578.

(20) McFadden, T. P.; Cope, R. B.; Muhlestein, R.; Layton, D. J.; Lessard, J. J.; Moore, J. S.; Sigman, M. S. Using Data Science Tools to Reveal and Understand Subtle Relationships of Inhibitor Structure in Frontal Ring-Opening Metathesis Polymerization. *J. Am. Chem. Soc.* **2024**. https://doi.org/10.1021/jacs.4c04622.

(21) Hu, J.; Gao, Y.; Teng, J.; Li, L.; Zhang, T.; Zheng, S. Recycling of Polydicyclopentadiene Enabled with N-Coordinated Boronic Bonds. *Macromol. Rapid Commun.* **2024.** 2400169. https://doi.org/10.1002/marc.202400169.

(22) Shieh, P.; Zhang, W.; Husted, K. E. L.; Kristufek, S. L.; Xiong, B.; Lundberg, D. J.; Lem, J.; Veysset, D.; Sun, Y.; Nelson, K. A.; Plata, D. L.; Johnson, J. A. Cleavable Comonomers Enable Degradable, Recyclable Thermoset Plastics. *Nature* **2020**, *583* (7817), 542–547. https://doi.org/10.1038/s41586-020-2495-2.

(23) Husted, K. E. L.; Brown, C. M.; Shieh, P.; Kevlishvili, I.; Kristufek, S. L.; Zafar, H.; Accardo, J. V.; Cooper, J. C.; Klausen, R. S.; Kulik, H. J.; Moore, J. S.; Sottos, N. R.; Kalow, J. A.; Johnson, J. A. Remolding and Deconstruction of Industrial Thermosets via Carboxylic Acid-Catalyzed Bifunctional Silyl Ether Exchange. *J. Am. Chem. Soc.* **2023**, *145* (3), 1916–1923. https://doi.org/10.1021/jacs.2c11858.

(24) Lloyd, E. M.; Cooper, J. C.; Shieh, P.; Ivanoff, D. G.; Parikh, N. A.; Mejia, E. B.; Husted, K. E. L.; Costa, L. C.; Sottos, N. R.; Johnson, J. A.; Moore, J. S. Efficient Manufacture, Deconstruction, and Upcycling of High-Performance Thermosets and Composites. *ACS Appl. Eng. Mater.* **2023**, *1* (1), 477–485. https://doi.org/10.1021/acsaenm.2c00115.

(25) Wang, X.; Zhang, Z.; Gao, F.; He, X. Improved Interfacial Adhesion of Carbon Fiber-Reinforced Polydicyclopentadiene Layered Composite Material by Modification of Norbornene Derivatives. *Polym. Eng. Sci.* **2024**, *64* (7), 3289–3302. https://doi.org/10.1002/pen.26769.

(26) Li, J.; Bi, L.; Musolino, S. F.; Wulff, J. E.; Sask, K. N. Functionalization of Polydimethylsiloxane with Diazirine-Based Linkers for Covalent Protein Immobilization. *ACS Appl. Mater. Interfaces* **2024**, *16* (1), 1–16. https://doi.org/10.1021/acsami.3c08013.

(27) Shatila, F.; Tieman, G. M. O.; Musolino, S. F.; Wulff, J. E.; Buckley, H. L. Antimicrobial Photodynamic Inactivation of Planktonic and Biofilm Cells by Covalently Immobilized Porphyrin on Polyethylene Terephthalate Surface. *Int. Biodeterior. Biodegrad.* **2023**, *178*, 105567. https://doi.org/10.1016/j.ibiod.2023.105567.

(28) Odian, G. *Principles of Polymerization*, Fourth Edition.; John Wiley & Sons, Inc.: College of Staten Island, 2004.

(29) Callister, W., Jr.; Rethwisch, D. *Materials Science and Engineering an Introduction*, 9th ed.; John Wiley & Sons, Inc.

(30) Brøndsted, P.; Lilholt, H.; Lystrup, A. COMPOSITE MATERIALS FOR WIND POWER TURBINE BLADES. *Annu. Rev. Mater. Res.* **2005**, *35* (1), 505–538. https://doi.org/10.1146/annurev.matsci.35.100303.110641.

(31) Karbhari, V. M.; Seible, F. Fiber Reinforced Composites – Advanced Materials for the Renewal of Civil Infrastructure. *Appl. Compos. Mater.* **2000**, *7* (2), 95–124. https://doi.org/10.1023/A:1008915706226.

(32) Vallons, K. A. M.; Drozdzak, R.; Charret, M.; Lomov, S. V.; Verpoest, I. Assessment of the Mechanical Behaviour of Glass Fibre Composites with a Tough Polydicyclopentadiene (PDCPD) Matrix. *Composites, Part A.* **2015**, *78*, 191–200. https://doi.org/10.1016/j.compositesa.2015.08.016.

(33) Hayne, D. J.; Singleton, M. A.; Patterson, B. A.; Athulya Wickramasingha, Y.; Sietins, J. M.; Knorr, D. B.; Stojcevski, F.; Henderson, L. C. Assessing the Properties of Poly(Dicyclopentadiene) Reinforced with Discontinuous Carbon Fibers. *Composites, Part A.* **2022**, *155*, 106839. https://doi.org/10.1016/j.compositesa.2022.106839.

(34) Kiel, G. R.; Lundberg, D. J.; Prince, E.; Husted, K. E. L.; Johnson, A. M.; Lensch, V.; Li, S.; Shieh, P.; Johnson, J. A. Cleavable Comonomers for Chemically Recyclable Polystyrene: A General Approach to Vinyl Polymer Circularity. *J. Am. Chem. Soc.* **2022**, *144* (28), 12979–12988. https://doi.org/10.1021/jacs.2c05374.

(35) Vora, N.; Christensen, P. R.; Demarteau, J.; Baral, N. R.; Keasling, J. D.; Helms, B. A.; Scown, C. D. Leveling the Cost and Carbon Footprint of Circular Polymers That Are Chemically Recycled to Monomer. *Sci. Adv.* **2021**, *7* (15), eabf0187. https://doi.org/10.1126/sciadv.abf0187.

(36) Bi, L.; Godwin, B.; Baran, M. J.; Nazir, R.; Wulff, J. E. A Cleavable Crosslinking Strategy for Commodity Polymer Functionalization and Generation of Reprocessable Thermosets. *Angew. Chem. Int. Ed.* **2023**, *62* (30), e202304708. https://doi.org/10.1002/anie.202304708.

(37) David, A.; Huang, J.; Richaud, E.; Yves Le Gac, P. Impact of Thermal Oxidation on Mechanical Behavior of Polydicylopentadiene: Case of Non-Diffusion Limited Oxidation. *Polym. Degrad. Stab.* **2020**, *179*, 109294. https://doi.org/10.1016/j.polymdegradstab.2020.109294.

(38) Carr, D. J.; Lewis, E.; Horsfall, I. A Systematic Review of Military Head Injuries. *BMJ Mil. Health* **2017**, *163* (1), 13–19. https://doi.org/10.1136/jramc-2015-000600.

(39) Crouch, I. G. Body Armour – New Materials, New Systems. *Def. Technol.* **2019**, *15* (3), 241–253. https://doi.org/10.1016/j.dt.2019.02.002.

Chapter 6: Summary and Future Work

6.1. Summary

In **Chapter 2**, we showed that it was possible to produce an upgraded DCPD monomer in a single step by targeting the unstrained alkene using a photooxidation. We were also able to demonstrate the scalability of this method, synthesizing and purifying oxaDCPD on a 2 mol scale. Using a newly developed lab-scale reaction injection molding protocol, regular dimensioned macroscale samples were produced for characterization. In partnership with the Milani Research Group at the University of British Columbia Okanagan (UBCO), we performed a complete mechanical and thermal characterization of oxaPDCPD using those samples. We discovered that oxaPDCPD has enhanced mechanical and thermal properties as compared to regular PDCPD. An additional partnership at UBCO with the computational DiLabio Research Group was able to show that these enhancements were due, in part, to a non-canonical hydrogen bond between the enone and the beta-hydrogen of an adjacent enone. We also produced and characterized a linear oxaPDCPD.

Work in **Chapter 3** demonstrated that copolymerization is a suitable strategy for the economic incorporation of oxaDCPD into PDCPD workflows. This was done utilizing ten different copolymers consisting of varying amounts of oxaDCPD, DCPD, and ethylidene norbornene (ENB) monomers, made via reaction injection molding. We improved the method for manufacturing regular dimensioned macroscale samples by reaction injection molding a rectangular plaque of material and then cutting the required samples. This reduces defects and waste. With these samples, we demonstrated that copolymerization is useful for tuning the mechanical properties of PDCPD-based materials as well as improving the surface energy, and thus adhesion to paints and bonding agents.

Chapter 4 saw the development of a high-throughput technique for screening ring-opening metathesis polymerization (ROMP) catalysts using a low-cost datalogger. A partnership with the Mauduit Research Group at the University of Rennes provided seven prepared catalysts for screening. Including commercial catalysts, we screened a total of forty different initiator and resin combinations. We discovered general structure–function relationships between the ruthenium initiators and the peak temperature achieved during the reaction. We also demonstrated that the thermal and mechanical properties of materials could be predicted by the peak temperature.

Finally, in **Chapter 5**, we determined through 15 stakeholder interviews, that fiber reinforcement was the most desired improvement to PDCPD in industry. Surprisingly, industry was not very concerned about odor or improvements to thermal properties.

6.2. Future Work

6.2.1. Composite materials

As shown in Chapter 5, industry is predominantly interested in the development of fiber-reinforced materials. Composite materials are an important class of materials owing to their low weight and excellent mechanical properties. The incompatibility of non-polar PDCPD with common polar fiber sizing (coating) excludes PDCPD from this large and expanding market due to poor fiber adhesion.[1,2] Matrix adhesion to the fibers could be dramatically improved by the addition of the more polar oxaDCPD.

To explore PDCPD-based composites utilizing oxaDCPD, I suggest investigating a variety of different glass fibers, natural fibers, and carbon fibers to determine which fiber type is most suited for DCPD resin. Several different amounts of oxaDCPD should be selected to test the fibers with, such as 0, 1, 2, 3, 5, 50 and 100% oxaDCPD. Once it is determined that oxaDCPD can compatibilize the fibers, optimization should focus on the minimum amount of oxaDCPD required to achieve optimal matrix adhesion.

The interlaminar shear strength (ILSS)—the strength of the bond between the fiber and the matrix of the composite—has major implications for the overall performance of the material.[5] A stronger bond between fiber and matrix allows for load sharing, greatly increasing the durability and mechanical strength.[5] Thus, evaluating the ILSS is a good place to start for evaluating the composite materials. I propose two different strategies for evaluating the produced composites' ILSS. The first is 3-point bending, as the sample can be easily made and tested in high throughput. However, 3-point bending samples may not fail in a way that allows for the analysis of the ILSS (Figure 6.1A). Instead, the samples may fail in a flexural failure, or more likely, a combination of shear and flexural.[6,7] This has the potential to make analysis challenging. Alternatively, the single fiber pullout test can be used to isolate the adhesion of the matrix to the fiber (Figure 6.1B).[8] The samples required for this test are more challenging to produce and fragile as single fibers are easy to break. Once broken, samples' microstructure can be examined via scanning electron microscopy to better understand the debonding mechanisms.

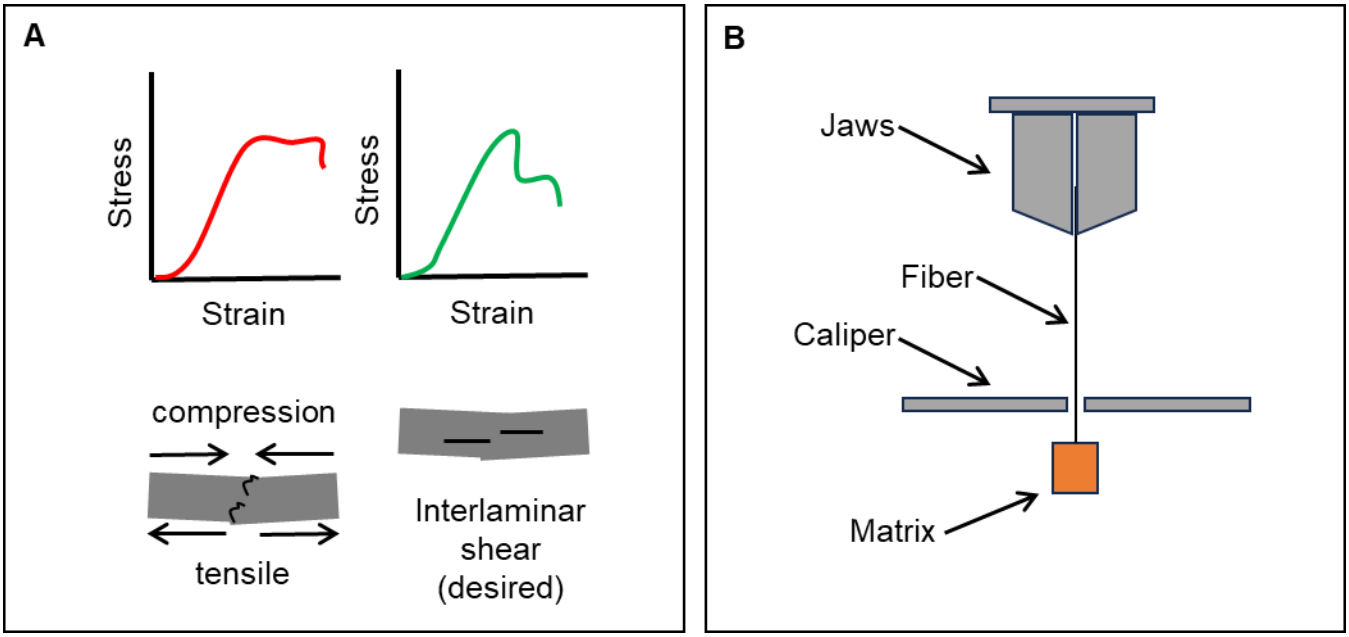

Figure 6.1. A: Different failure modes of the short beam shear test. B: Cartoon of the single fiber (or microfiber bundle) test setup.

This work would enable the production of low cost PDCPD composites with readily available commercial fibers. Additionally, production of low-cost PDCPD-based composites that match the stiffness of epoxy composites while vastly outperforming them at higher temperatures could have huge implications in high-value markets such as the aerospace and defence industries.

6.2.2. Flow Chemistry

We have shown that batch production of oxaDCPD is amenable to large-scale for the laboratory; however, it is unlikely that batch processes will work efficiently on the scale required for industry. Batch processes are especially limited for photochemical reactions because photon penetration drops drastically with volume (Figure 6.2A and B).[9–11] Similarly, gas mixing for the photooxygenation also becomes an issue in large volumes.[9–14] Flow chemistry is an attractive alternative as it allows excellent light penetration, gas mixing, optimal heat management, and scale-up (Figure 6.2C).[9–11]

Hermens *et al*. published a design for an easily assembled modular photochemical coaxial flow reactor called the OctoColor (Figure 6.2C).[11] Using this design as a base, it should be possible to implement flow chemistry to produce oxaDCPD in the laboratory. The complexity of the coaxial flow reactor could be reduced by utilizing segmented or slug flow. In these flow modes, "plugs" of liquid and gas are alternated in the tubing (Figure 6.2A).[9,10,12,14]

Dichloromethane (DCM) is used as the solvent in this reaction as it stabilizes the lifetime of the singlet oxygen.[15,16] However, the use of DCM as the reaction solvent should also be evaluated. Recent research has pointed overwhelmingly to the harm that DCM can cause to both the environment and to human health.[17–20] The use of DCM will also be heavily regulated going forward due to the ban on its use by the United States Environmental Protection Agency.[20] This will likely make any new process using DCM unattractive to industrial adoption. Recent work has pointed to the use of a mixture of methanol and DCM as an optimized solvent strategy for this chemistry and should make a suitable starting point.[21] The use of deuterated solvents has also been shown to enhance singlet oxygen lifetimes.[15] The successful implementation of flow chemistry and elimination of DCM from the synthesis would be a substantial step forward towards commercial viability for oxaDCPD.

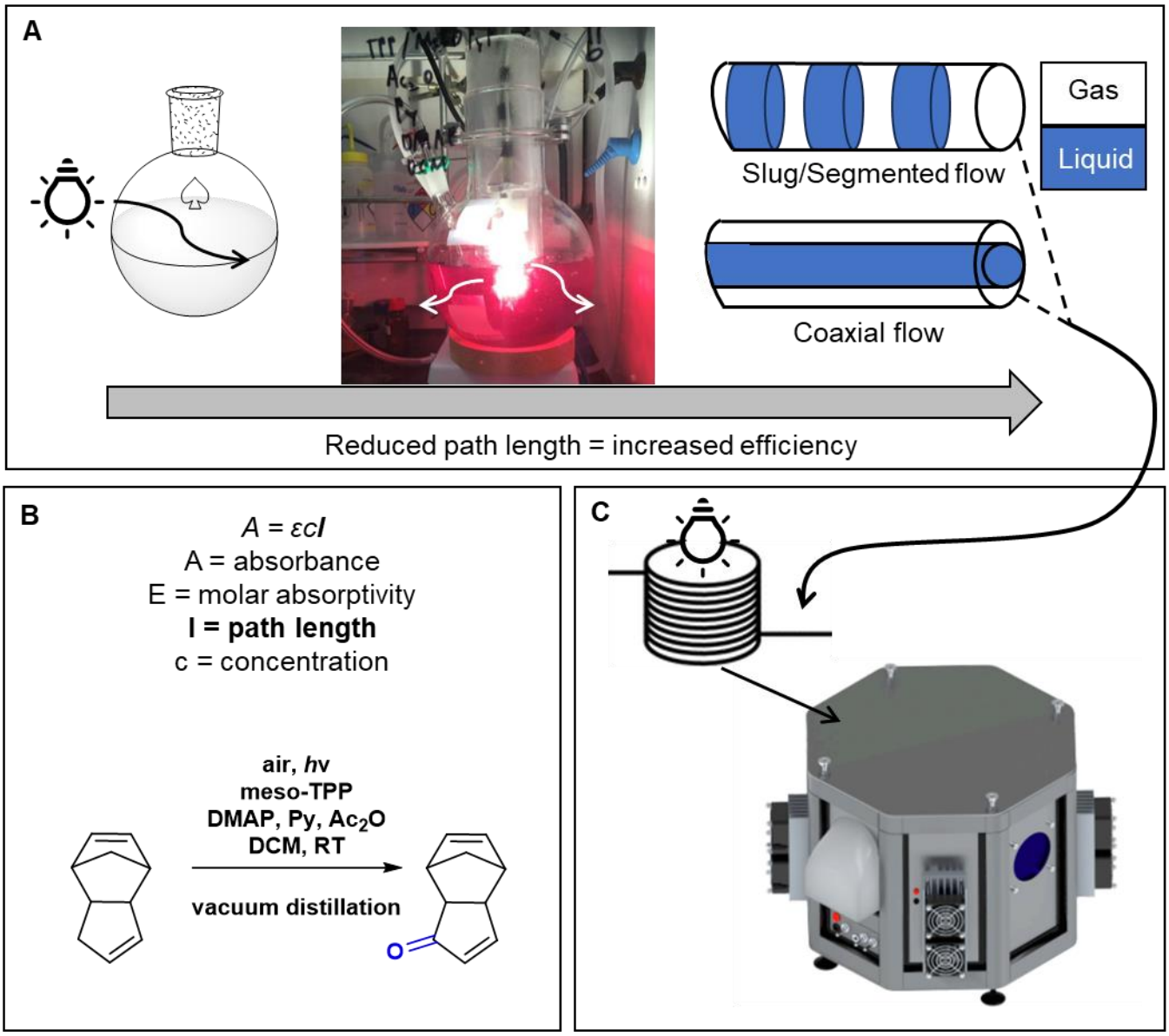

Figure 6.2. A: Examples of different photochemistry setups and a comparison between coaxial flow and slug/segmented flow. B: Beers Law, which describes the relationship between path length and absorbance. C: The OctoColor photoreactor. Adapted with permission from the literature.[11]

6.3. Conclusion

In conclusion, the work described in this dissertation demonstrates a selective, single-step method for functionalizing DCPD, and thus providing tractable access to functionalized PDCPD. This method preserves the design rules—the glass transition temperature is maintained or

improved, and the material is thermally stable—established in the first-generation functionalized PDCPD strategy (*f*DCPD). In addition, this work highlights the large impacts small modifications to molecular structures can have on material properties. I have also established a method for benchmarking catalysts and predicting the properties of the resulting polymers. Finally, we have laid out a roadmap of industrially relevant problems for future chemists interested in PDCPD to tackle.

6.4. References

(1) Vervacke, D. *An Introduction to PDCPD: Poly-Di-Cyclo-Penta-Diene*; Product Rescue, 2008.

(2) Vallons, K. A. M.; Drozdzak, R.; Charret, M.; Lomov, S. V.; Verpoest, I. Assessment of the Mechanical Behaviour of Glass Fibre Composites with a Tough Polydicyclopentadiene (PDCPD) Matrix. *Composites, Part A.* **2015**, *78*, 191–200. https://doi.org/10.1016/j.compositesa.2015.08.016.

(3) Dobler, D.; Reiser, O. Synthesis of 6-Substituted 2-Pyrones Starting from Renewable Resources: Total Synthesis of Sibirinone, (E)-6-(Pent-1-En-1-Yl)-2H-Pyran-2-One, and (E)-6-(Hept-1-En-1-Yl)-2H-Pyran-2-One. *J. Org. Chem.* **2016**, *81* (21), 10357–10365. https://doi.org/10.1021/acs.joc.6b01339.

(4) Wang, X.; Zhang, Z.; Gao, F.; He, X. Improved Interfacial Adhesion of Carbon Fiber-Reinforced Polydicyclopentadiene Layered Composite Material by Modification of Norbornene Derivatives. *Polym. Eng. Sci.* **2024**, *64* (7), 3289–3302. https://doi.org/10.1002/pen.26769.

(5) Callister, W., Jr.; Rethwisch, D. *Materials Science and Engineering an Introduction*, 9th ed.; John Wiley & Sons, Inc.

(6) Rai, S.; Rawat, P. Three-Point Bending, Interlaminar Shear, and Impact Strength in Bioinspired Helicoidal Basalt Fiber/Epoxy Composites: A Comparative Experimental Analysis. *Polym. Compos.* **2024**, *45* (10), 9407–9420. https://doi.org/10.1002/pc.28417.

(7) Fan, Z.; Santare, M. H.; Advani, S. G. Interlaminar Shear Strength of Glass Fiber Reinforced Epoxy Composites Enhanced with Multi-Walled Carbon Nanotubes. *Composites, Part A.* **2008**, *39* (3), 540–554. https://doi.org/10.1016/j.compositesa.2007.11.013.

(8) Wölfel, E.; Brünig, H.; Curosu, I.; Mechtcherine, V.; Scheffler, C. Dynamic Single-Fiber Pull-Out of Polypropylene Fibers Produced with Different Mechanical and Surface Properties for Concrete Reinforcement. *Materials* **2021**, *14* (4), 722. https://doi.org/10.3390/ma14040722.

(9) Sambiagio, C.; Noël, T. Flow Photochemistry: Shine Some Light on Those Tubes! *Trends Chem.* **2020**, *2* (2), 92–106. https://doi.org/10.1016/j.trechm.2019.09.003.

(10) Hone, C. A.; Kappe, C. O. The Use of Molecular Oxygen for Liquid Phase Aerobic Oxidations in Continuous Flow. *Top. Curr. Chem. (Z)* **2019**, *377* (1), 2. https://doi.org/10.1007/s41061-018-0226-z.

(11) Hermens, J. G. H.; Lepage, M. L.; Kloekhorst, A.; Keller, E.; Bloem, R.; Meijer, M.; Feringa, B. L. Development of a Modular Photoreactor for the Upscaling of Continuous Flow Photochemistry. *React. Chem. Eng.* **2022**. https://doi.org/10.1039/D2RE00310D.

(12) Greene, J. F.; Hoover, J. M.; Mannel, D. S.; Root, T. W.; Stahl, S. S. Continuous-Flow Aerobic Oxidation of Primary Alcohols with a Copper(I)/TEMPO Catalyst. *Org. Process Res. Dev.* **2013**, *17* (10), 1247–1251. https://doi.org/10.1021/op400207f.

(13) Steves, J. E.; Preger, Y.; Martinelli, J. R.; Welch, C. J.; Root, T. W.; Hawkins, J. M.; Stahl, S. S. Process Development of CuI/ABNO/NMI-Catalyzed Aerobic Alcohol Oxidation. *Org. Process Res. Dev.* **2015**, *19* (11), 1548–1553. https://doi.org/10.1021/acs.oprd.5b00179.

(14) Ye, X.; Johnson, M. D.; Diao, T.; Yates, M. H.; Stahl, S. S. Development of Safe and Scalable Continuous-Flow Methods for Palladium-Catalyzed Aerobic Oxidation Reactions. *Green Chem.* **2010**, *12* (7), 1180–1186. https://doi.org/10.1039/C0GC00106F.

(15) Bayer, P.; Pérez-Ruiz, R.; Jacobi von Wangelin, A. Stereoselective Photooxidations by the Schenck Ene Reaction. *ChemPhotoChem* **2018**, *2* (7), 559–570. https://doi.org/10.1002/cptc.201800058.

(16) Bregnhøj, M.; Westberg, M.; Jensen, F.; Ogilby, P. R. Solvent-Dependent Singlet Oxygen Lifetimes: Temperature Effects Implicate Tunneling and Charge-Transfer Interactions. *Phys. Chem. Chem. Phys.* **2016**, *18* (33), 22946–22961. https://doi.org/10.1039/C6CP01635A.

(17) Cooper, G. S.; Scott, C. S.; Bale, A. S. Insights from Epidemiology into Dichloromethane and Cancer Risk. *Int. J. Environ. Res. Public Health* **2011**, *8* (8), 3380–3398. https://doi.org/10.3390/ijerph8083380.

(18) Vidal, S. Safety First: A Recent Case of a Dichloromethane Injection Injury. *ACS Cent. Sci.* **2020**, *6* (2), 83–86. https://doi.org/10.1021/acscentsci.0c00100.

(19) Goulding, L. The Gist of the List. *ACS Chem. Health Saf.* **2024**, *31* (4), 272–273. https://doi.org/10.1021/acs.chas.4c00053.

(20) US EPA, O. *Biden-Harris Administration Finalizes Ban on Most Uses of Methylene Chloride, Protecting Workers and Communities from Fatal Exposure*. https://www.epa.gov/newsreleases/biden-harris-administration-finalizes-ban-most-uses-methylene-chloride-protecting (accessed 2024-07-23).

(21) Hasumi, M.; Tsutsumi, T.; Shikama, D.; Hayakawa, I. Efficient Oxidation with Singlet Oxygen from 5,10,15,20-Tetraphenylporphyrin under Blue LED Irradiation and Air Atmosphere: Simplified Preparation of Key Building Blocks for Natural Product Synthesis. *Synthesis 0*. https://doi.org/10.1055/a-2361-0069.

Appendix A: Supplemental Spectra, Plots, Figures and Tables for Chapter 2

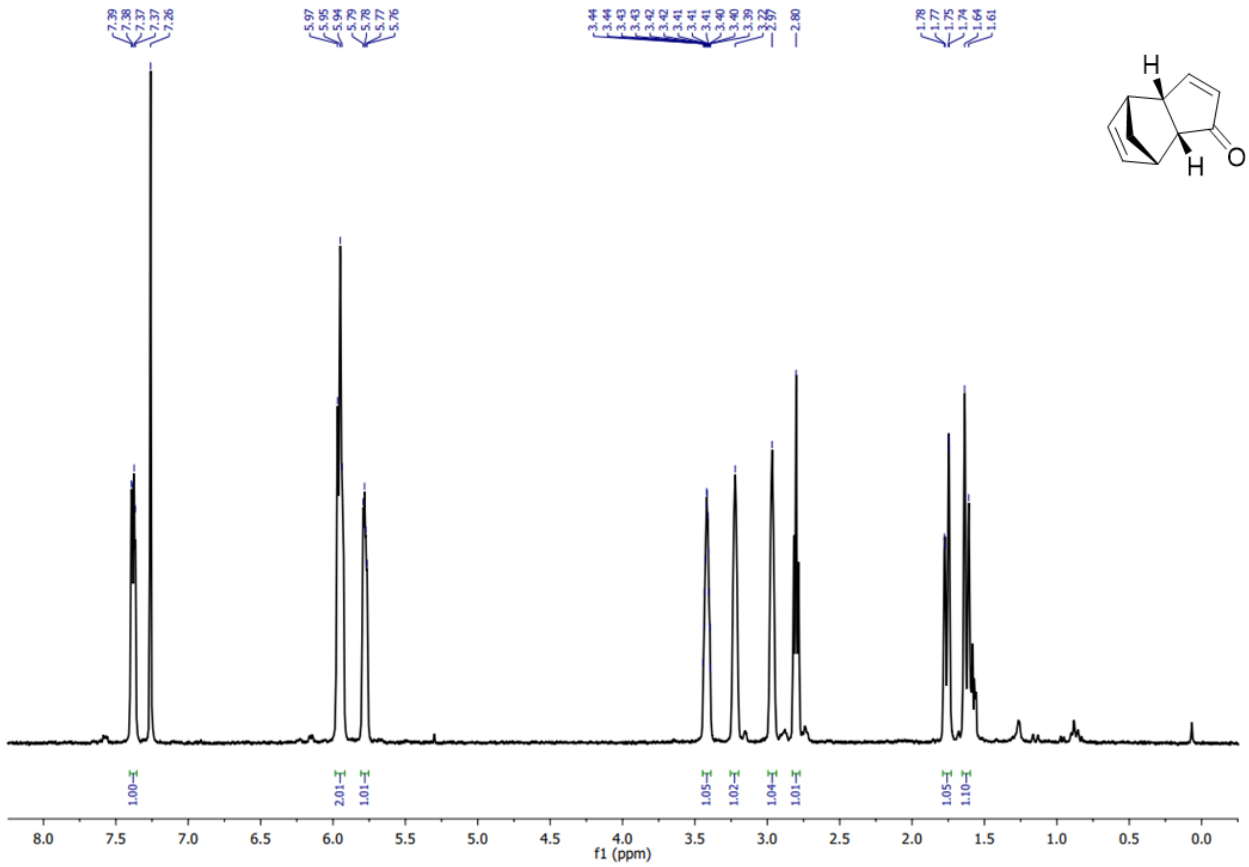

Figure A1. ^{1}H NMR spectrum of *endo*-dicyclopentadienone (oxaDCPD) at 300.27 MHz in $CDCl_3$. Contains traces of *exo*-dicyclopentadienone.

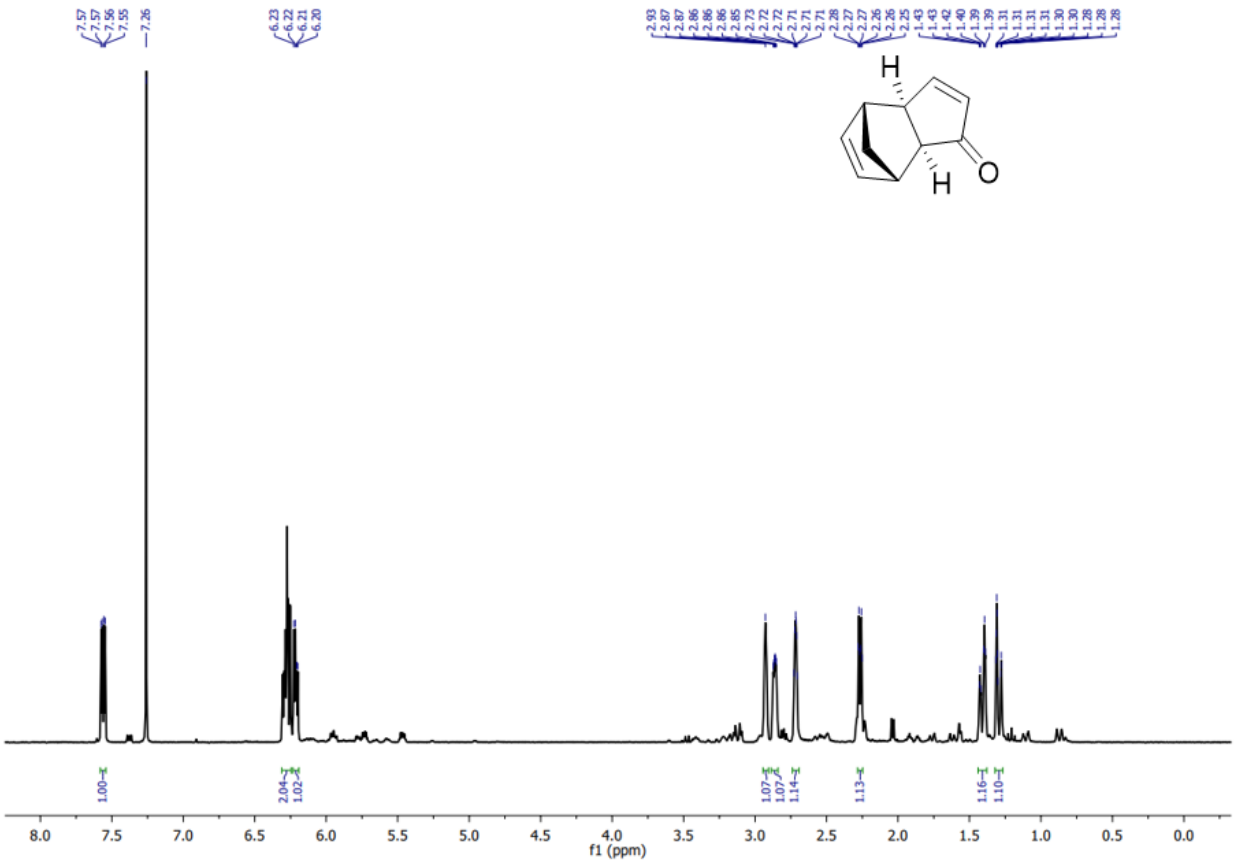

Figure A2. ^{1}H NMR spectrum of e*xo*-dicyclopentadienone at 300.27 MHz in $CDCl_3$. Contains traces of *endo*-dicyclopentadienone as well as other minor impurities resulting from the *exo*-DCPD synthesis.

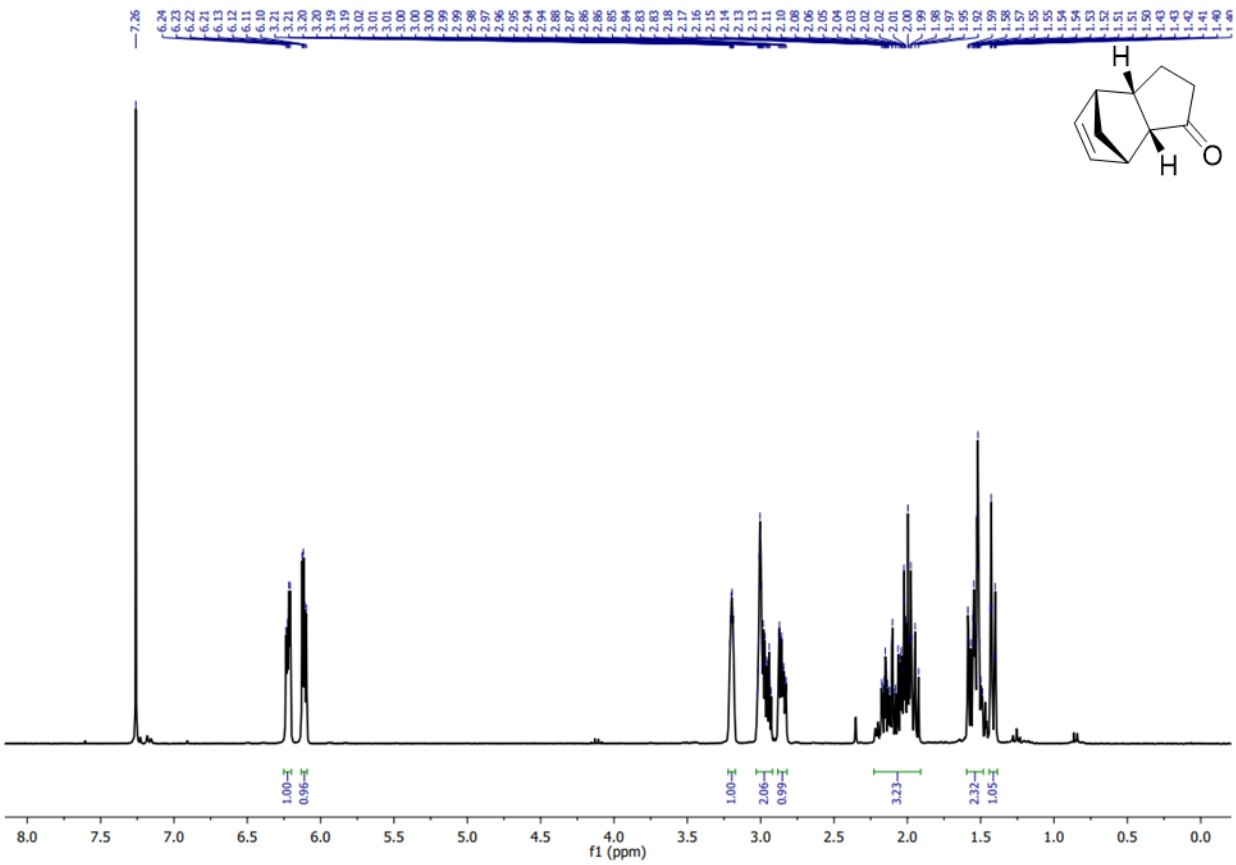

Figure A3. ^{1}H NMR spectrum of *endo*-dicyclopentaenone (oxaRD) at 300.27 MHz in $CDCl_3$.

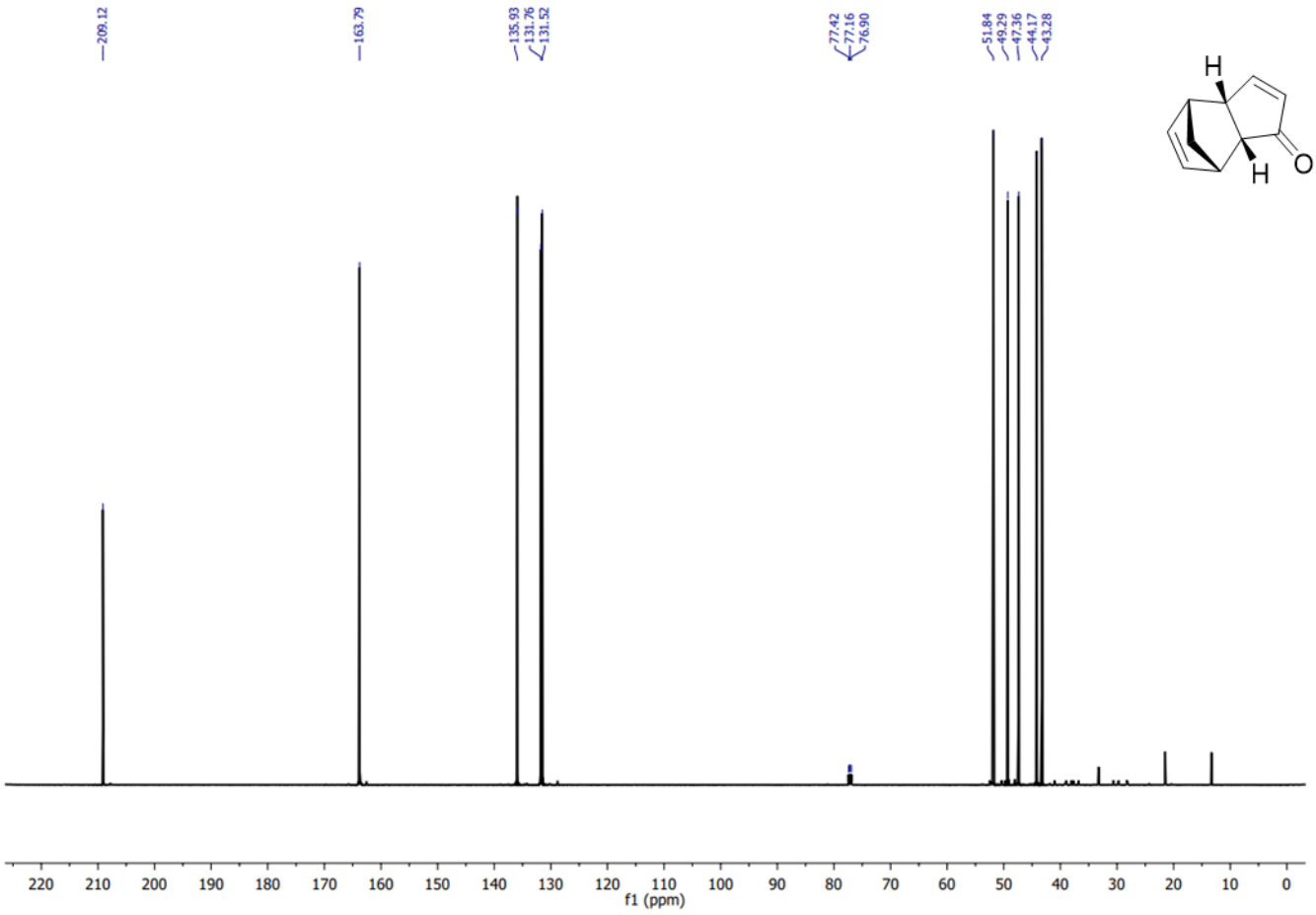

Figure A4. ^{13}C NMR spectrum of *endo*-dicyclopentadienone (oxaDCPD) at 125.81 MHz in $CDCl_3$.

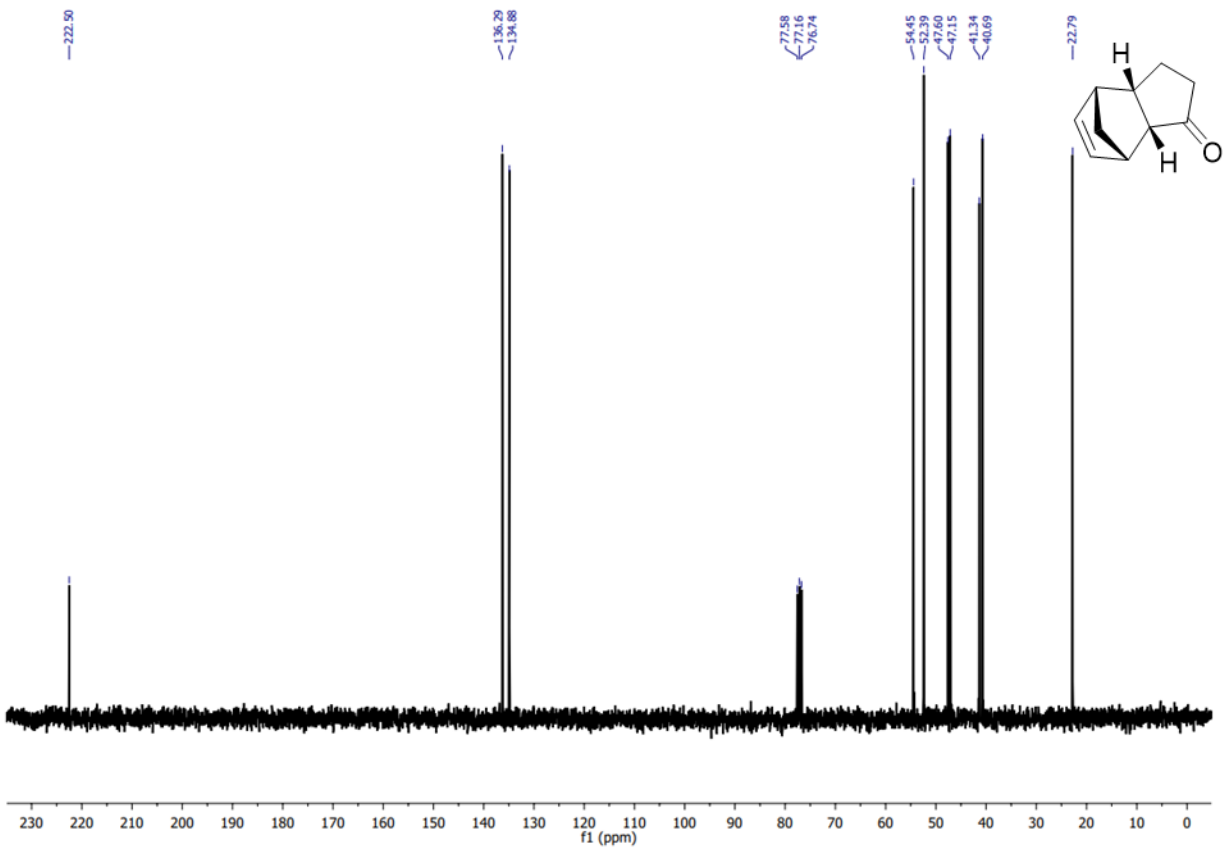

Figure A5. ^{13}C NMR spectrum of *endo*-dicyclopentaenone (oxaRD) at 75.51 MHz in $CDCl_3$.

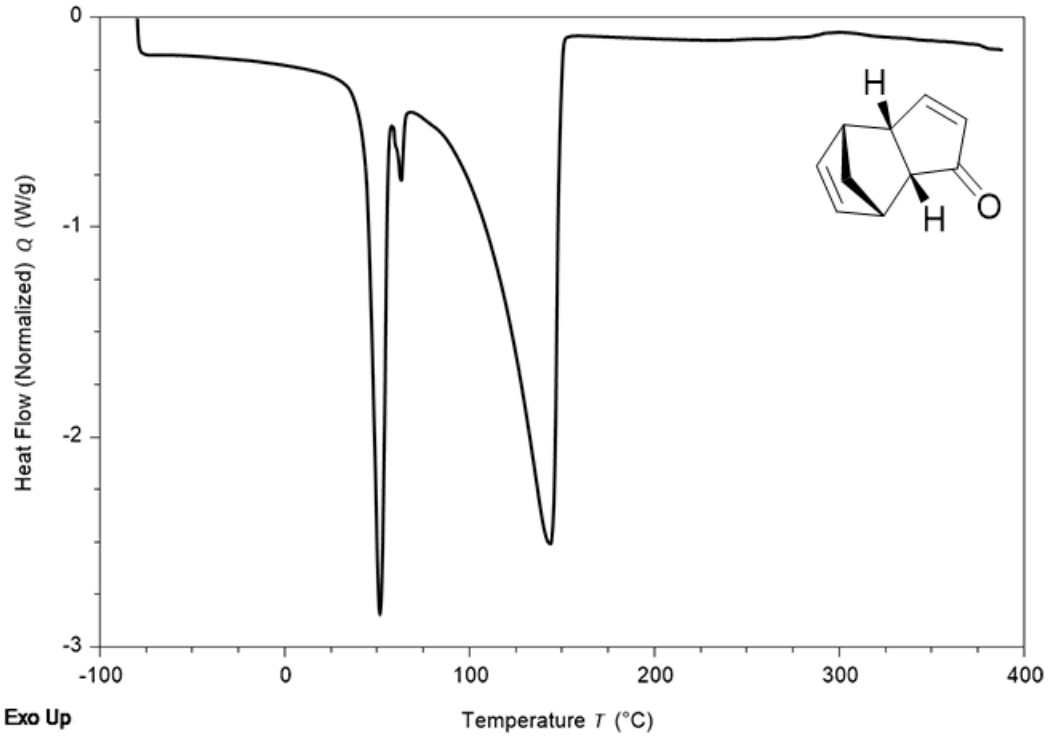

Figure A6. DSC data for *endo*-dicyclopentadienone. The large endotherm at *ca.* 145 °C suggests the occurrence of a *retro*-Diels–Alder reaction. The melting transition is visible at *ca.* 50 °C.

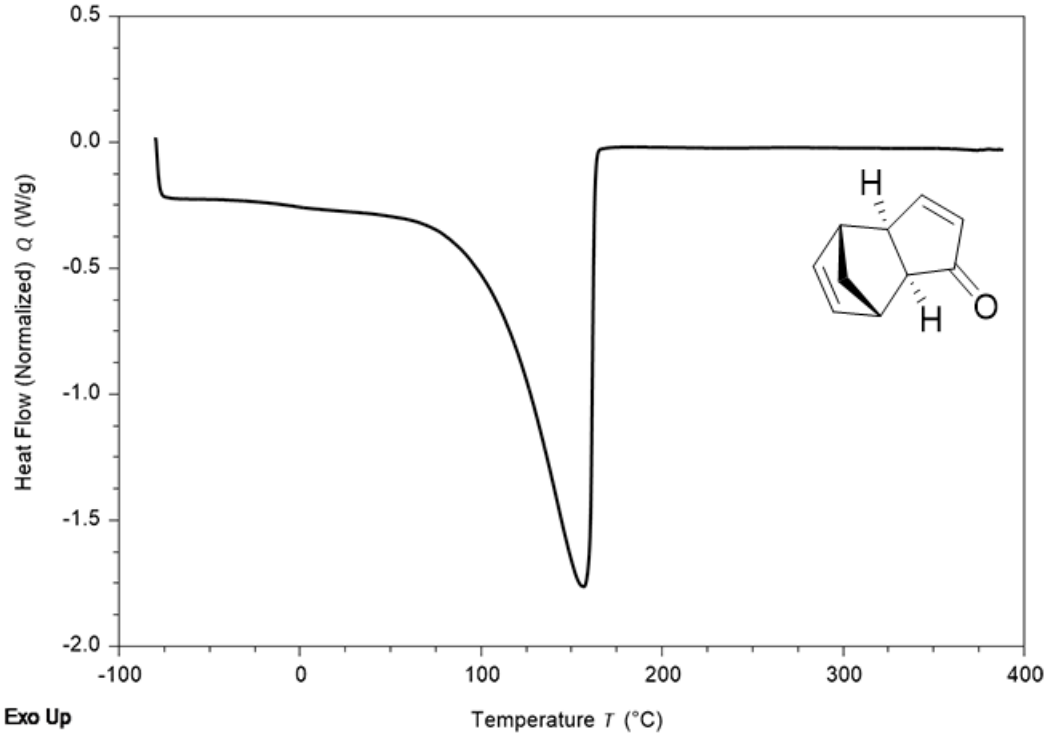

Figure A7. DSC data for *exo*-dicyclopentadienone. The large endotherm at *ca.* 155 °C suggests the occurrence of a *retro*-Diels–Alder reaction.

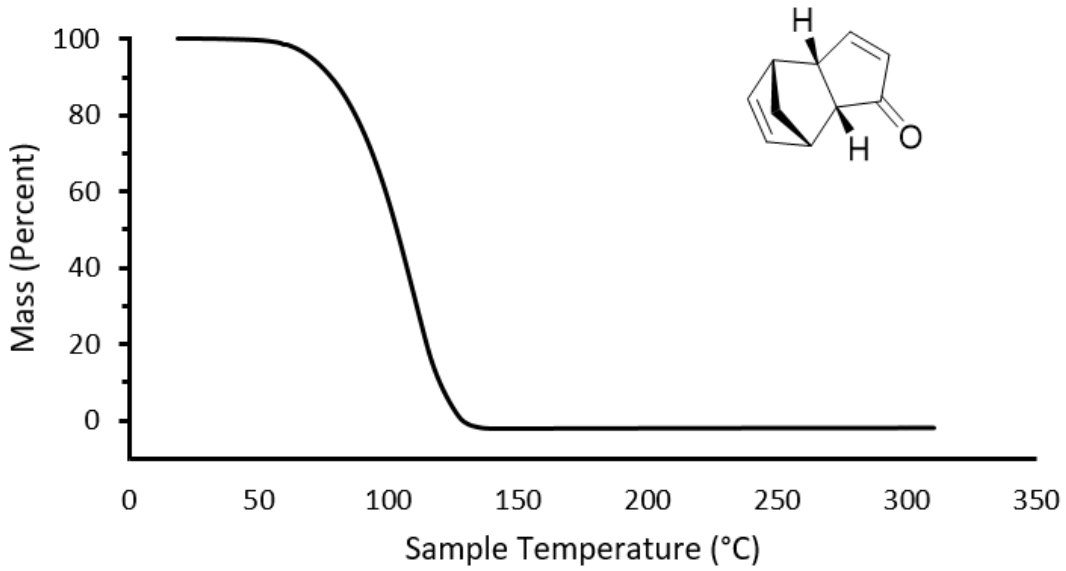

Figure A8. TGA data for *endo*-dicyclopentadienone. The loss of material by *ca.* 135 °C likely indicates a *retro*-Diels–Alder reaction that affords volatile sub-monomers.

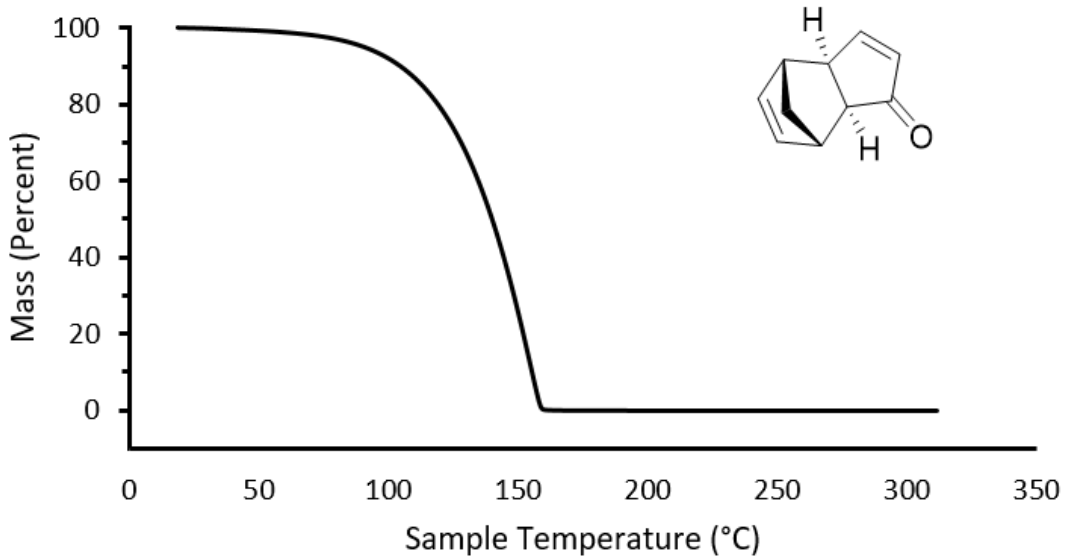

Figure A9. TGA data for *exo*-dicyclopentadienone. The loss of material by *ca.* 155 °C likely indicates a *retro*-Diels–Alder reaction that affords volatile sub-monomers.

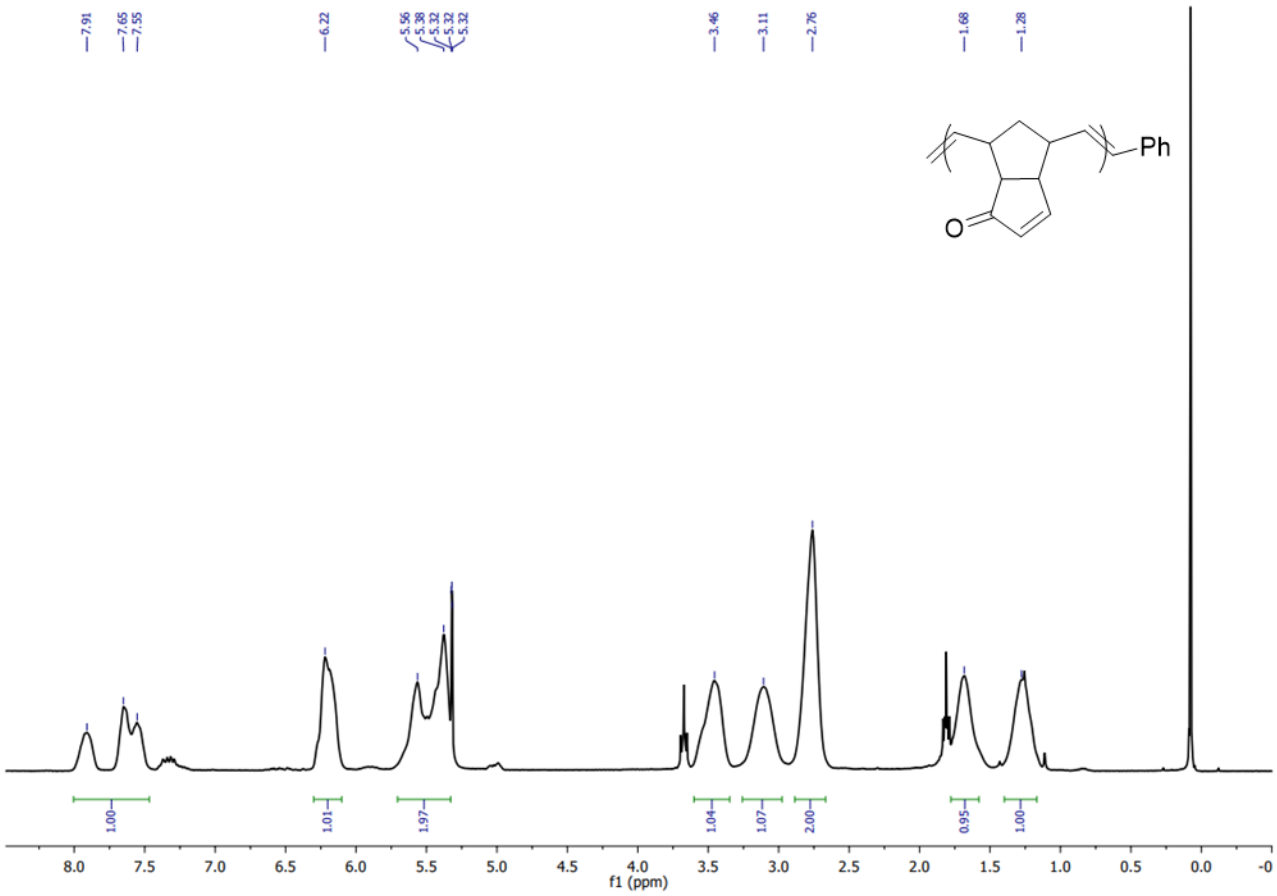

Figure A10. ^{1}H NMR spectrum of poly-*endo*-dicyclopentadienone (oxaPDCPD) at 300.27 MHz in CD_2Cl_2. Contains traces of THF (tetrahydrofuran) remaining from the synthesis. Synthesized with GC3.

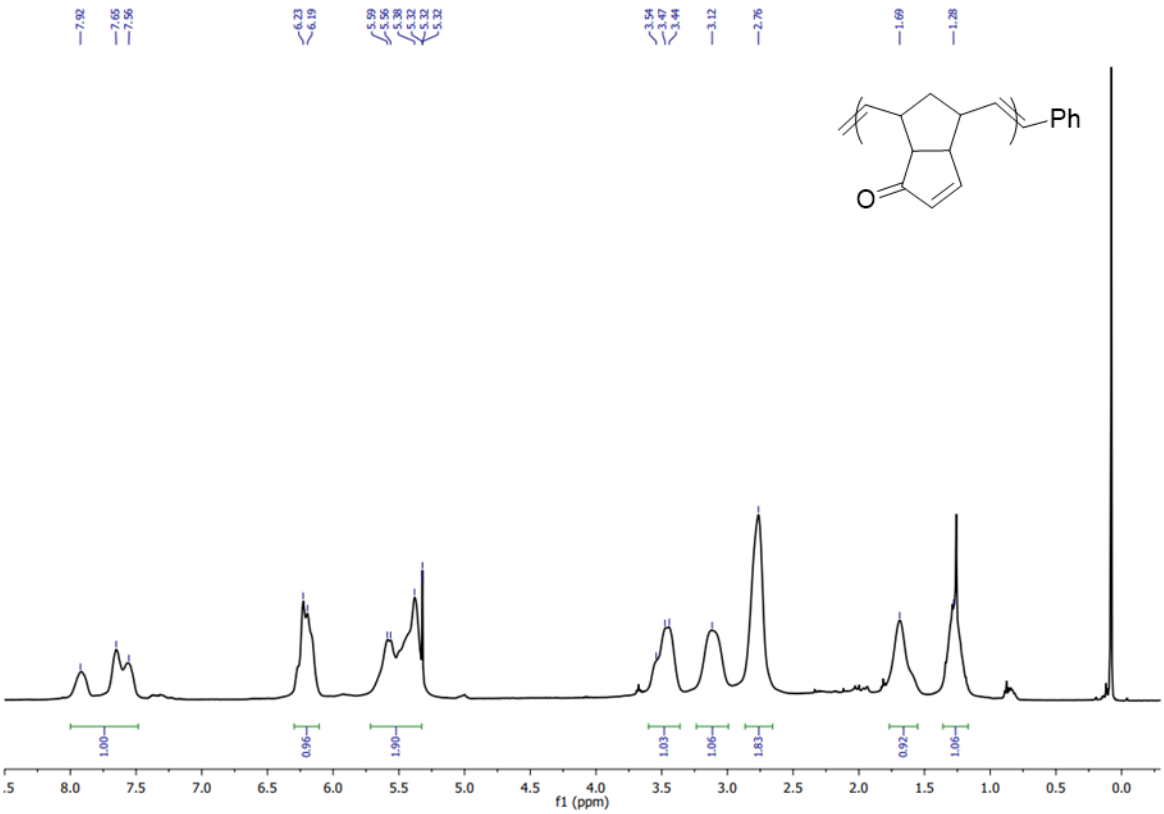

Figure A11. ^{1}H NMR spectrum of poly-*endo*-dicyclopentadienone (oxaPDCPD) at 500.27 MHz in CD_2Cl_2. Contains traces of THF remaining from the synthesis. Synthesized with GC2.

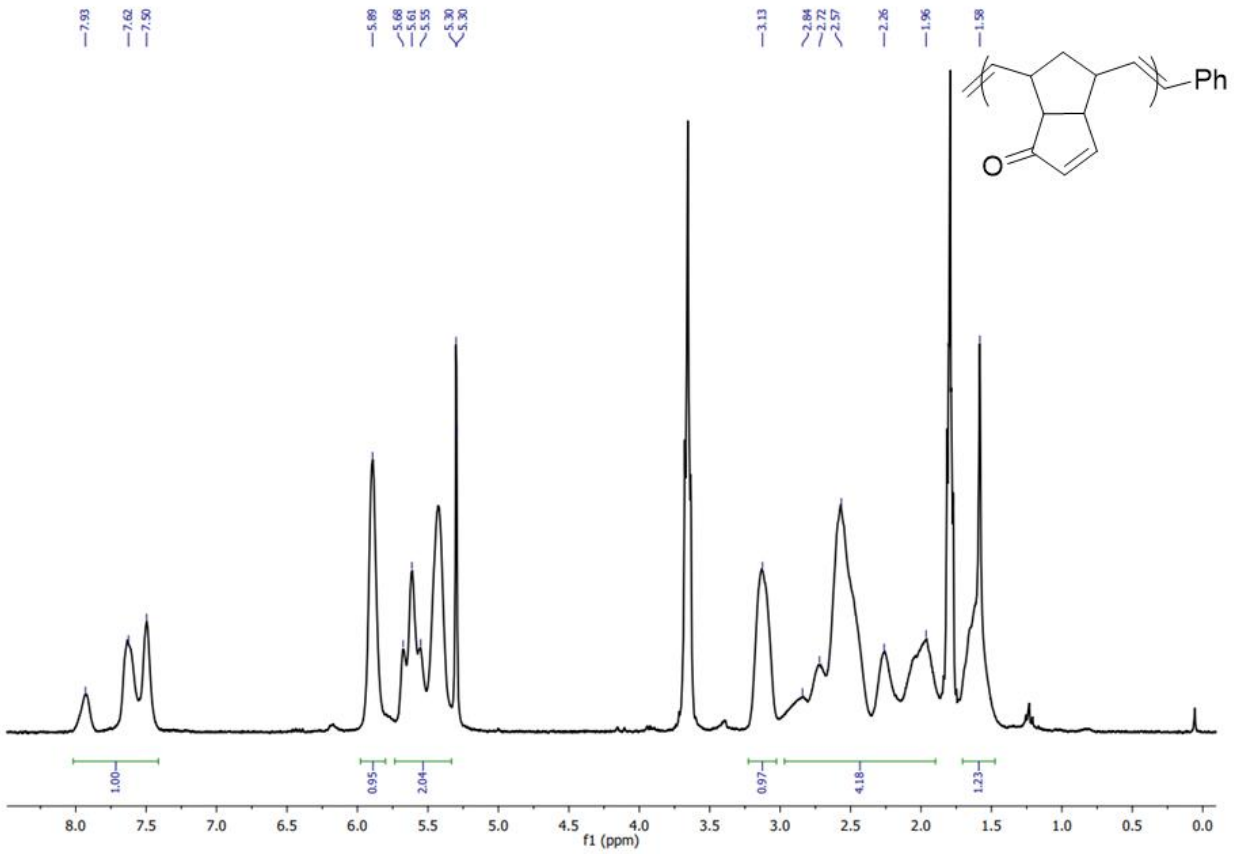

Figure A12. ^{1}H NMR spectrum of poly-*exo*-dicyclopentadienone (*exo*-oxaPDCPD) at 300.27 MHz in CD_2Cl_2. Contains THF remaining from the synthesis. Synthesized with GC2.

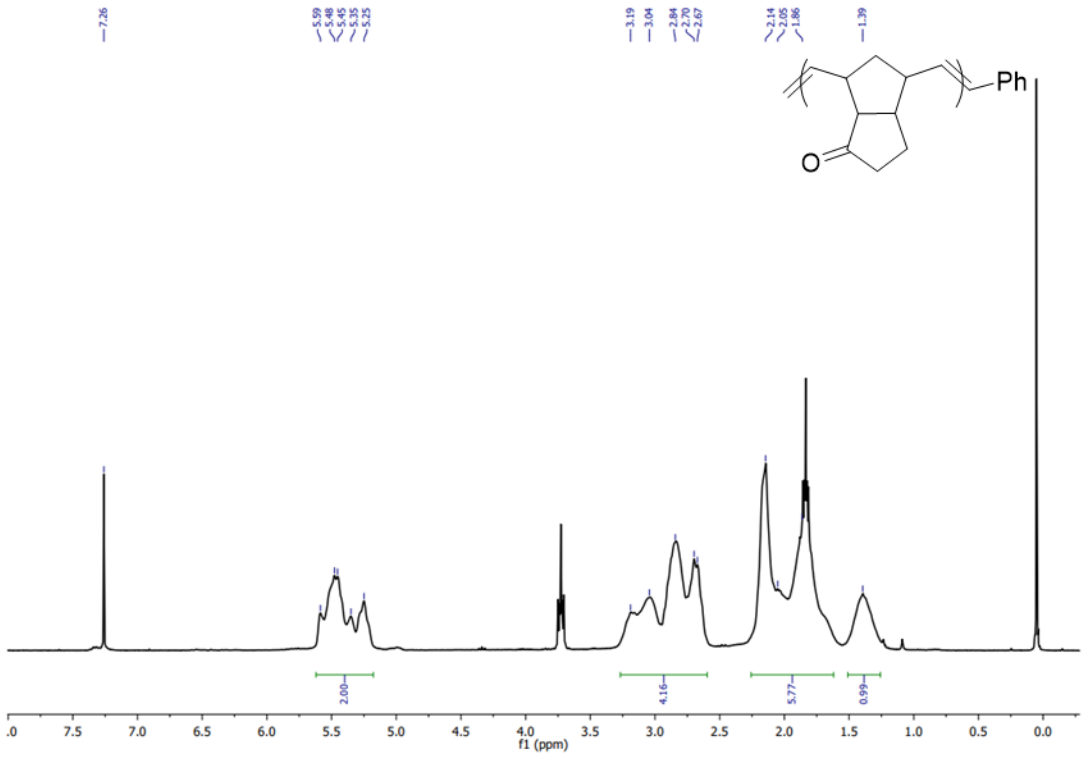

Figure A13. ^{1}H NMR spectrum of poly-*endo*-dicyclopentaenone (oxaPDCPD$_{RD}$) at 300.27 MHz in $CDCl_3$. Contains traces of THF remaining from the synthesis.

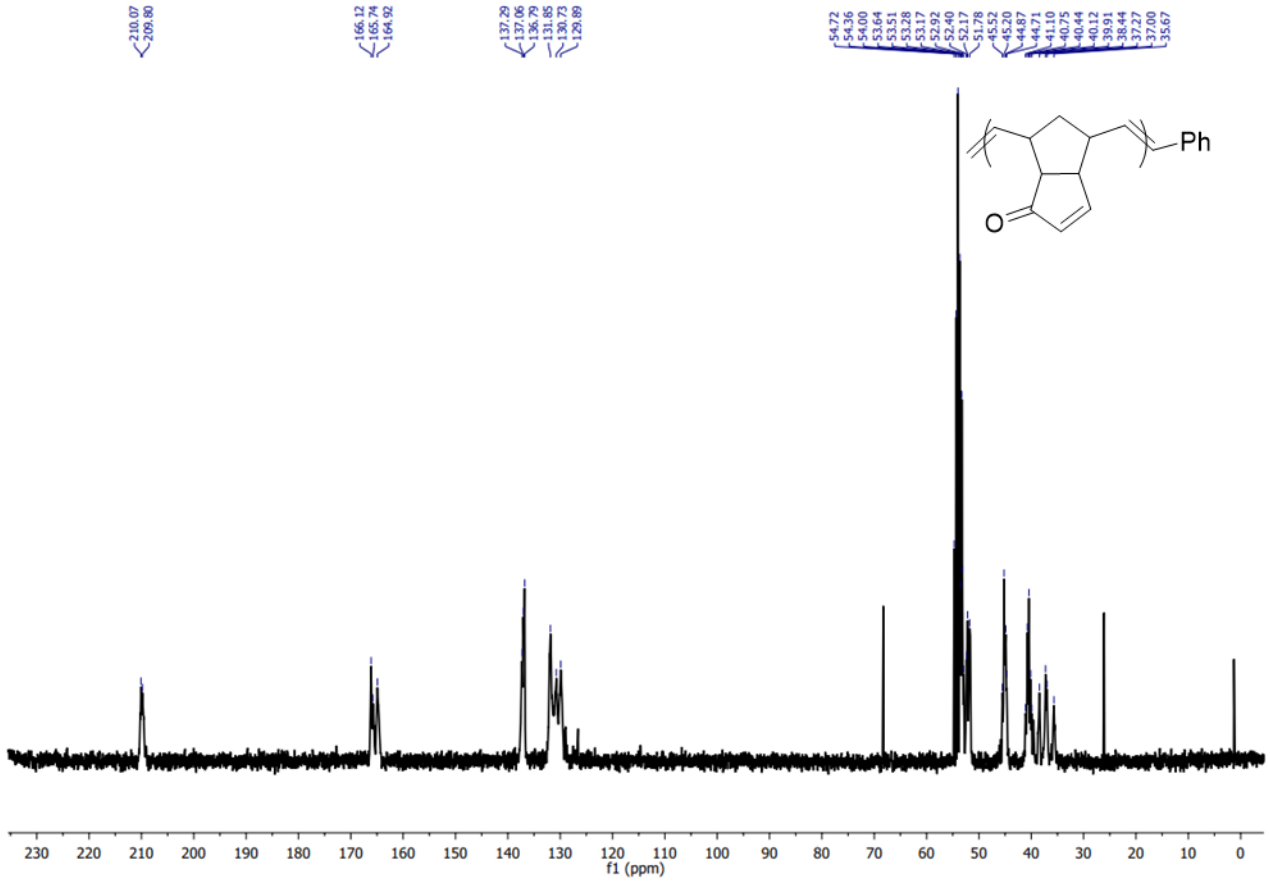

Figure A14. ^{13}C NMR spectrum of poly-*endo*-dicyclopentadienone at 75.51 MHz in CD_2Cl_2. Contains traces of THF remaining from the synthesis. Synthesized with GC3.

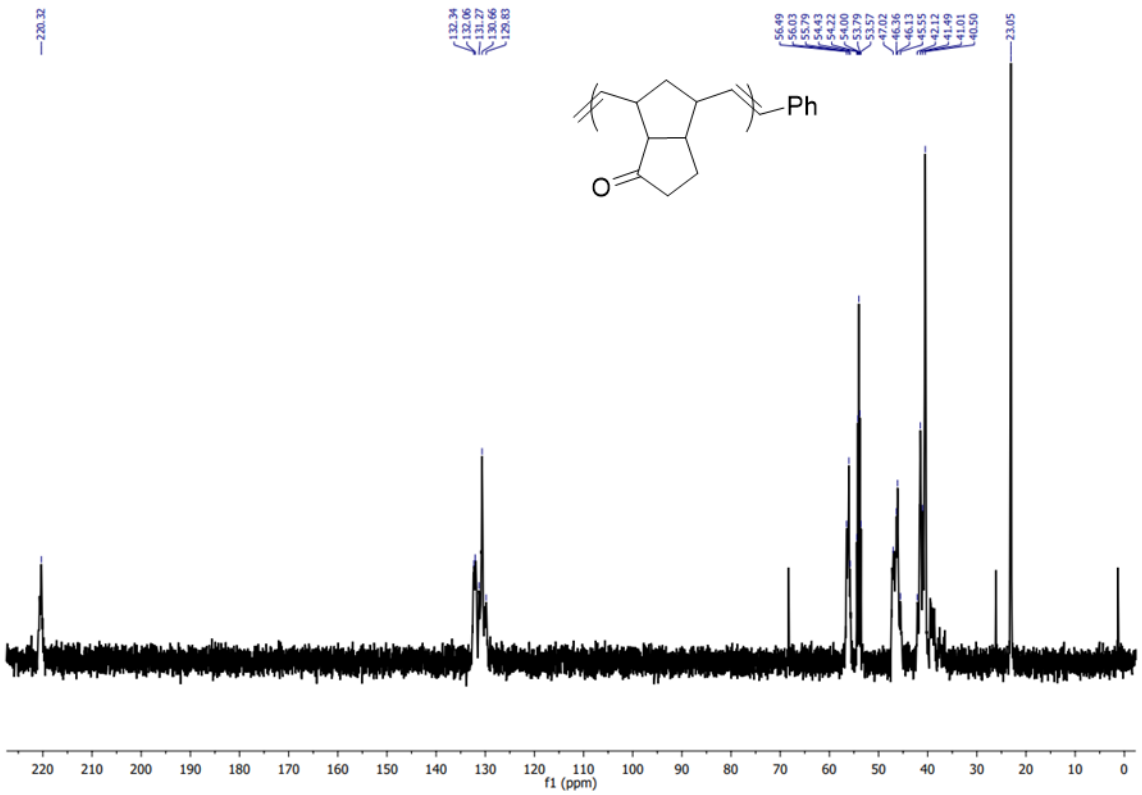

Figure A15. ^{13}C NMR spectrum of poly-*endo*-dicyclopentaenone (oxaPDCPD$_{RD}$) at 125.81 MHz in CD_2Cl_2. Contains traces of THF remaining from the synthesis.

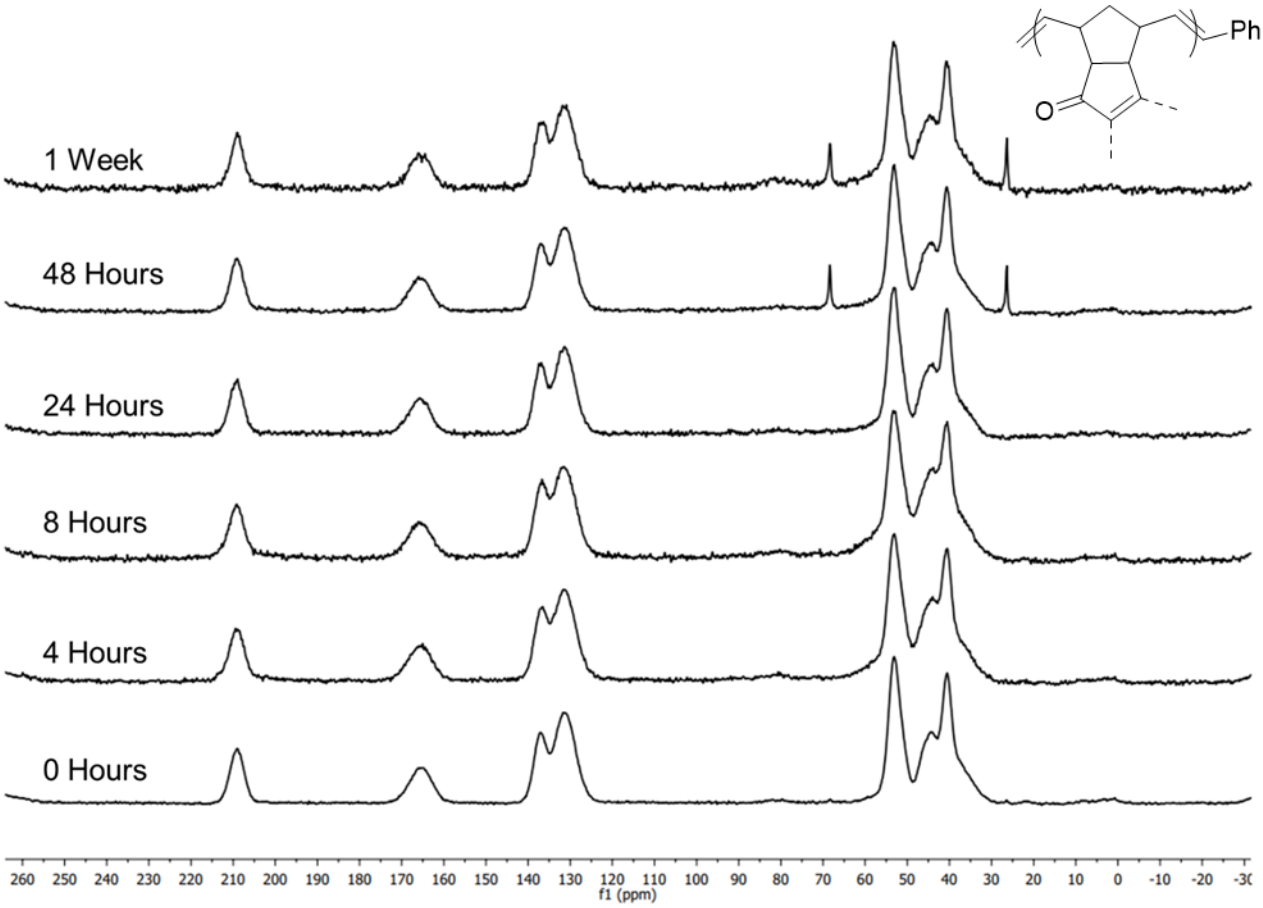

Figure A16. Solid State cross-polarization and magic angle spinning ^{13}C NMR spectrum of poly-*endo*-dicyclopentadienone (oxaPDCPD) at 100.62 MHz. Progressively crosslinked (bottom to top) in a 110°C oven. Synthesized with GC2.

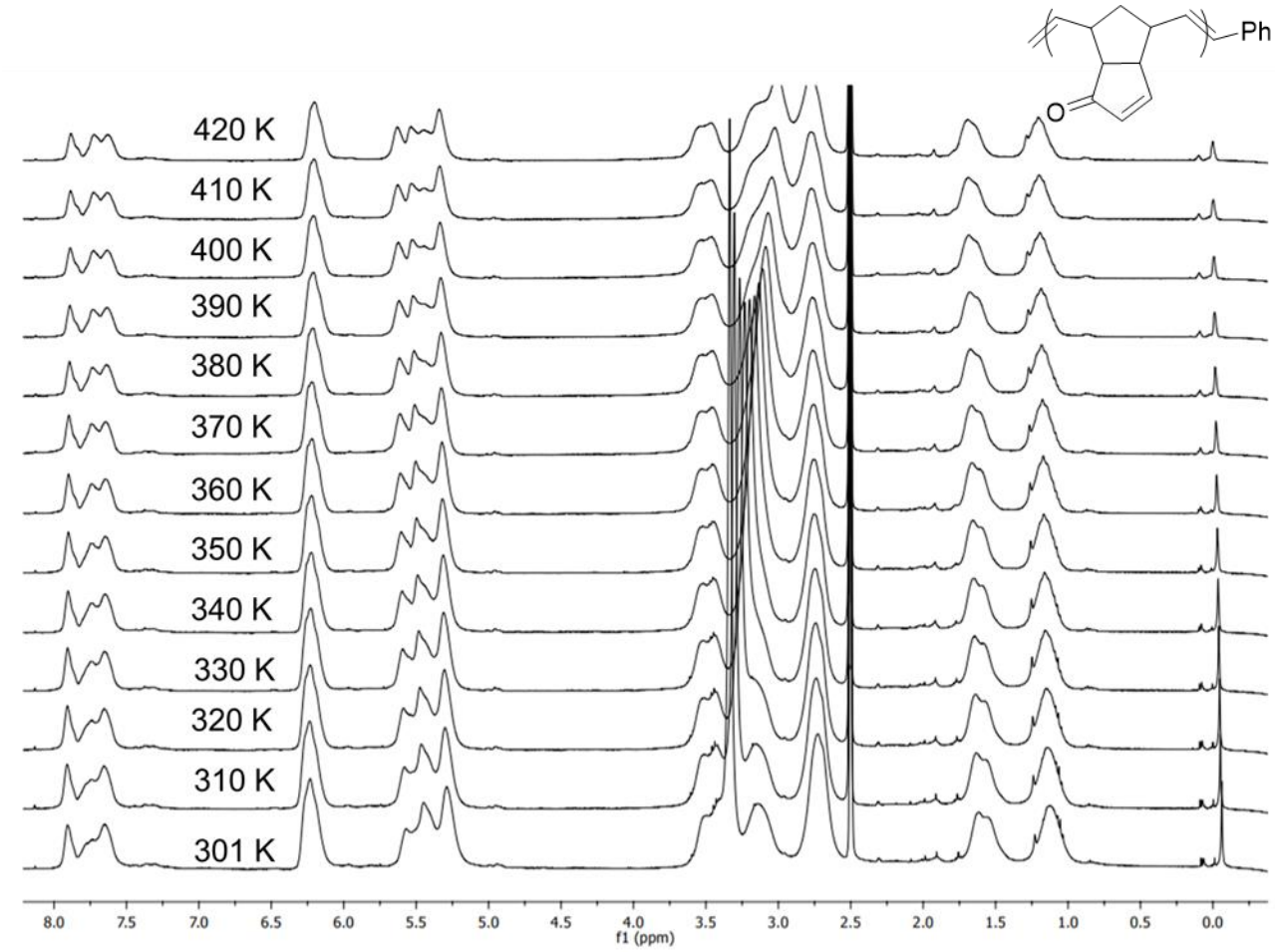

Figure A17. Variable temperature ^{1}H NMR spectrum of of poly-*endo*-dicyclopentadienone (oxaPDCPD) at 360.28 MHz in C_2D_6OS (deuterated dimethyl sulfoxide). Synthesized with GC2.

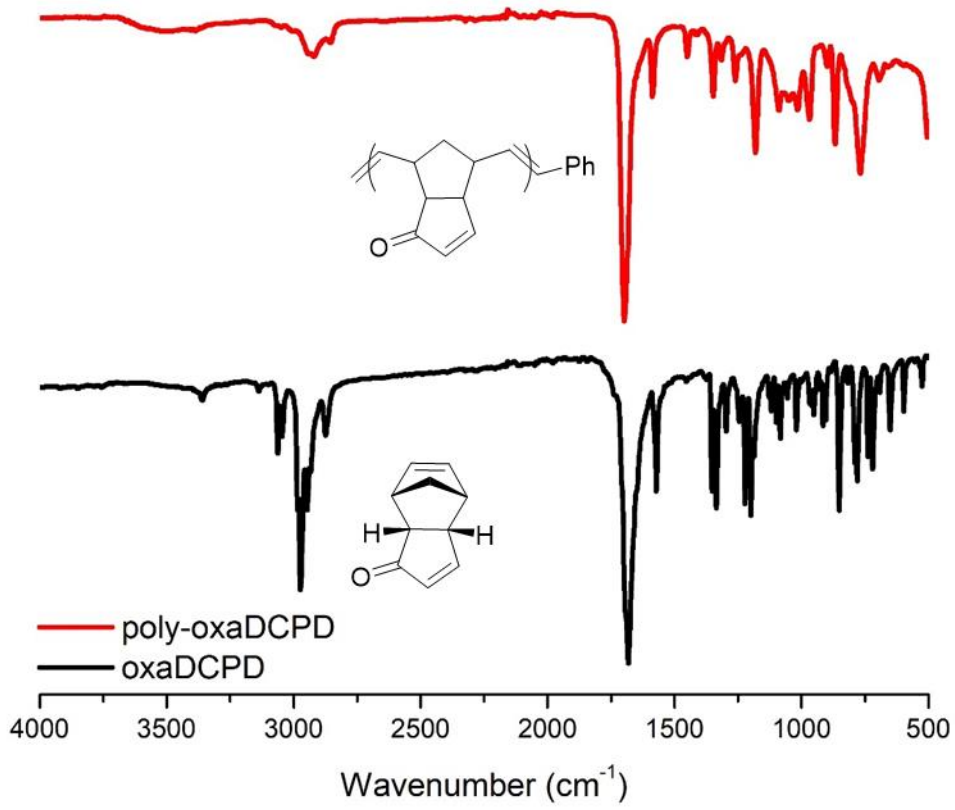

Figure A18. AT IR spectrum of *endo*-dicyclopentadienone (oxaDCPD) and poly-*endo*-dicyclopentadienone (oxaPDCPD), synthesized with GC2.

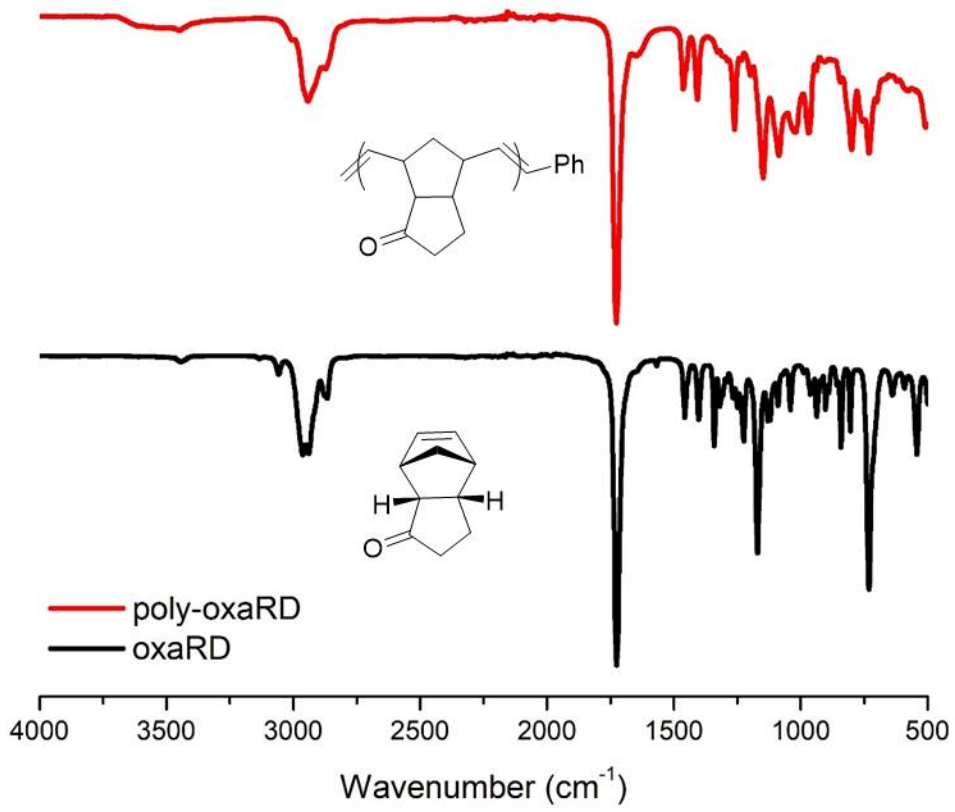

Figure A19. AT IR spectrum of *endo*-dicyclopentaenone (oxaRD) and poly-*endo*-dicyclopentaenone (oxaPDCPD$_{RD}$).

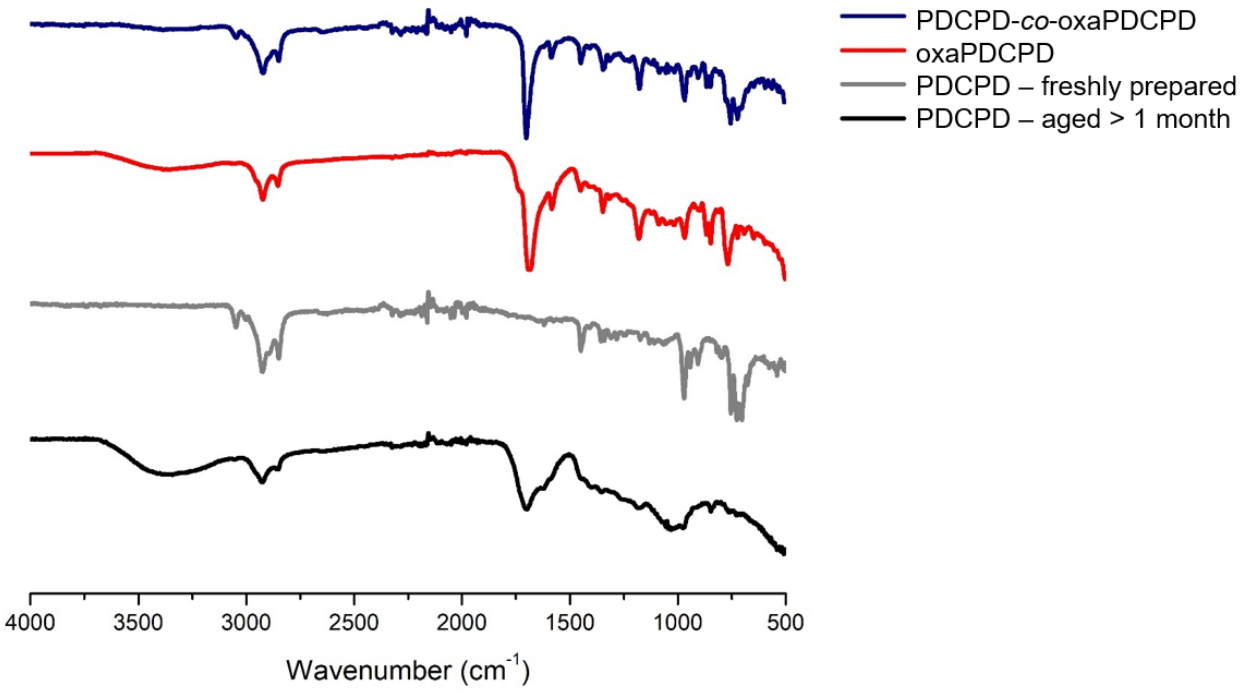

Figure A20. AT IR spectrum of reaction injection molded poly-*endo*-dicyclopentadiene, freshly prepared poly-*endo*-dicyclopentadiene, aged poly-*endo*-dicyclopentadienone and poly-*endo*-dicyclopentadiene-*co*-dicyclopentadienone. The aged PDCPD sample has clearly undergone surface oxidation, resulting in the appearance of O–H and C=O stretches in the IR spectrum.

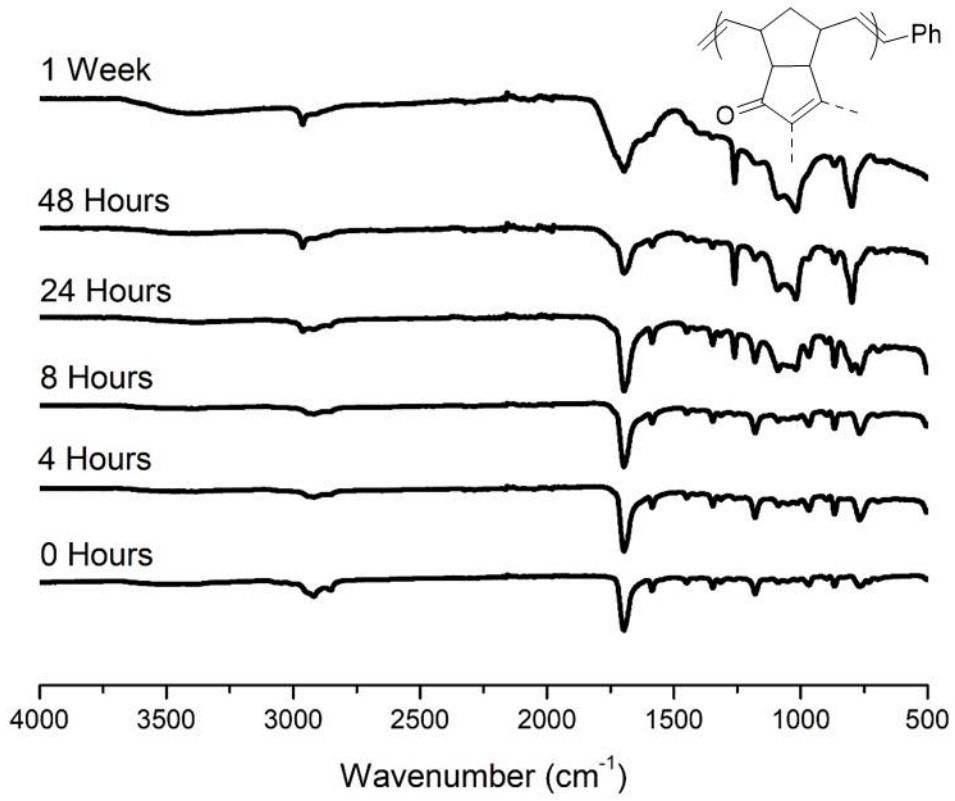

Figure A21. AT IR spectrum of poly-*endo*-dicyclopentadienone (oxaPDCPD) progressively crosslinked in a 110°C oven under argon. Synthesized with GC2.

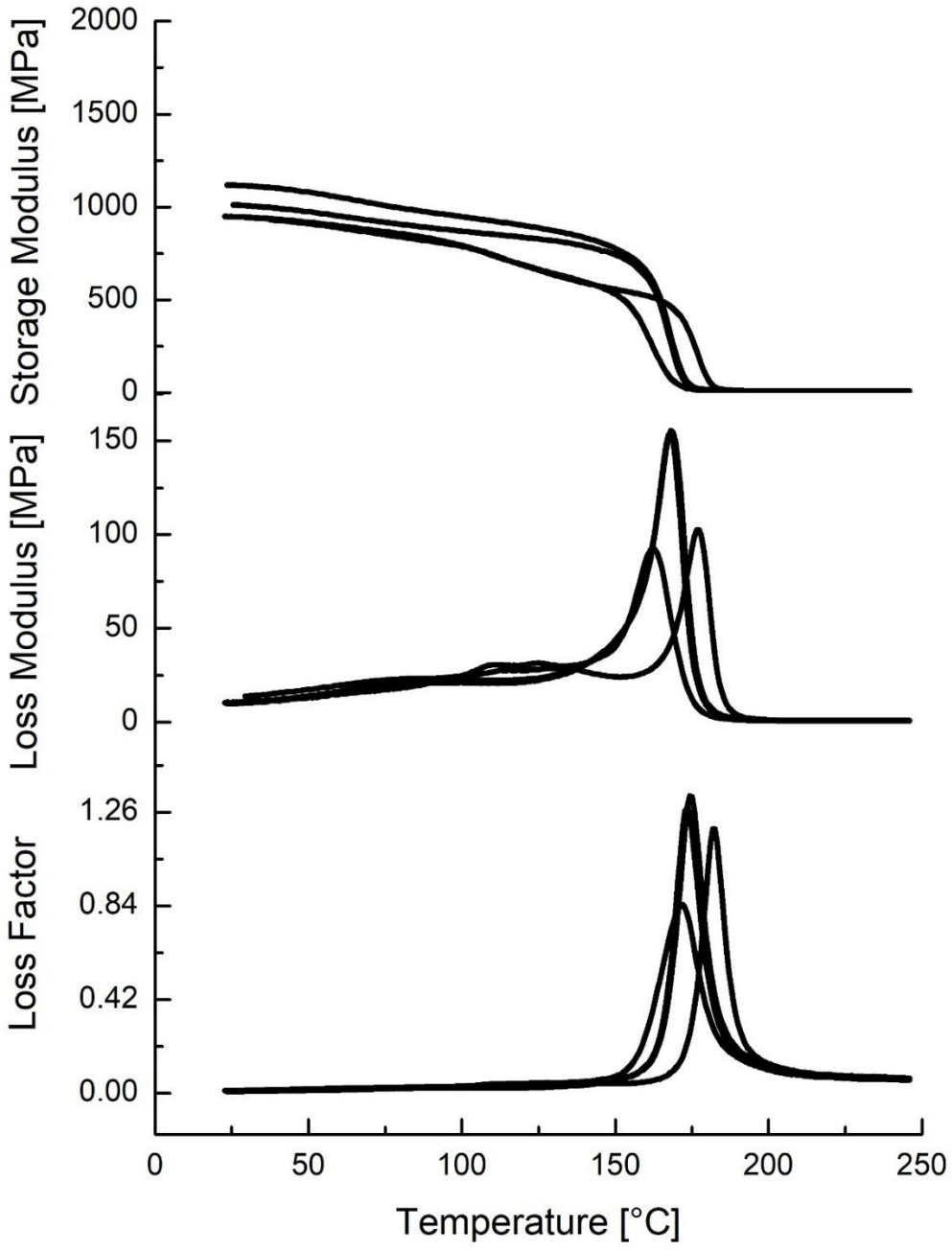

Figure A22. Four DMTA traces of reaction injection molded poly-*endo*-dicyclopentadiene (rim-PDCPD).

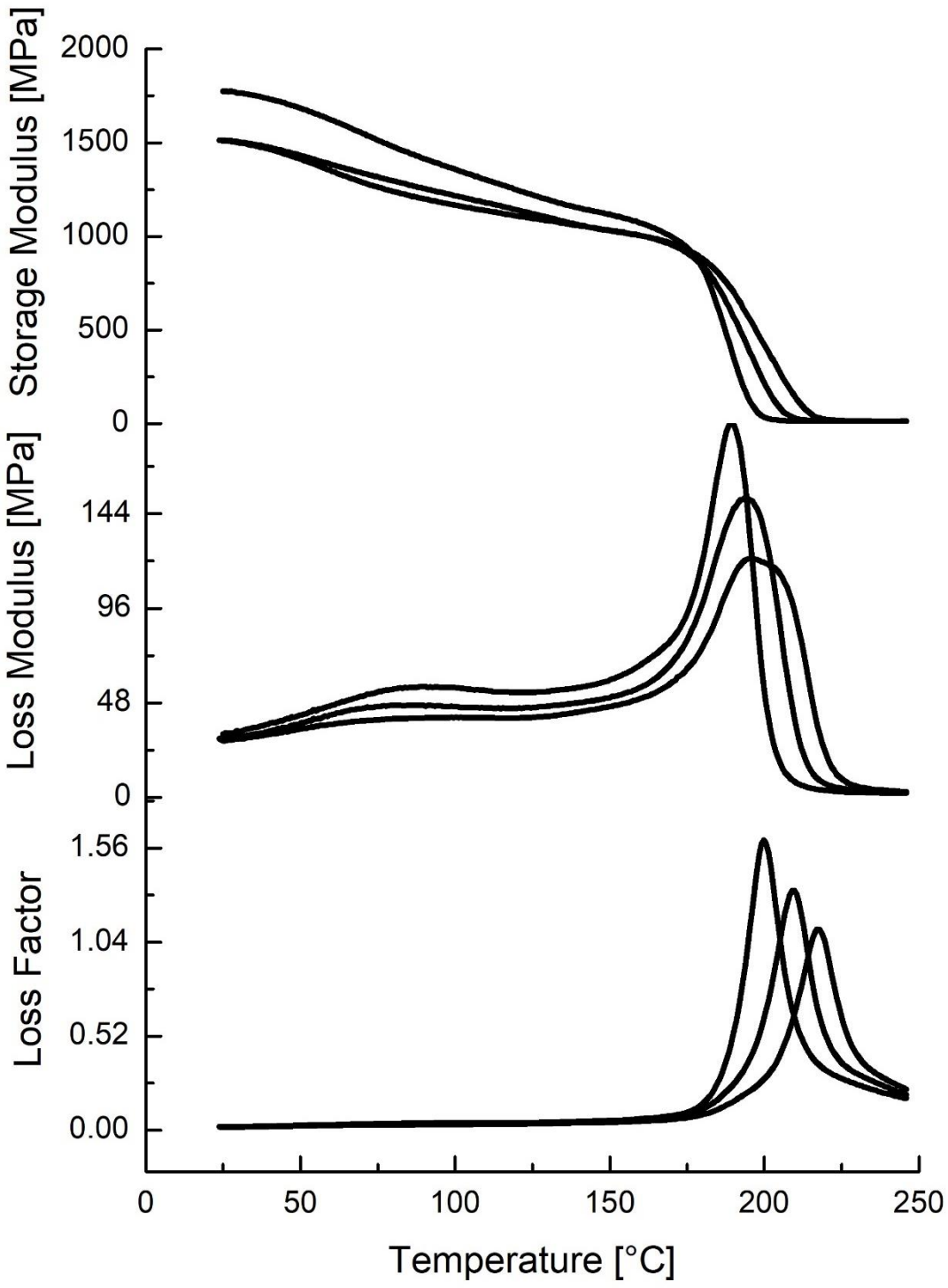

Figure A23. Three DMTA traces of reaction injection molded poly-*endo*-dicyclopentadienone (rim-oxaPDCPD).

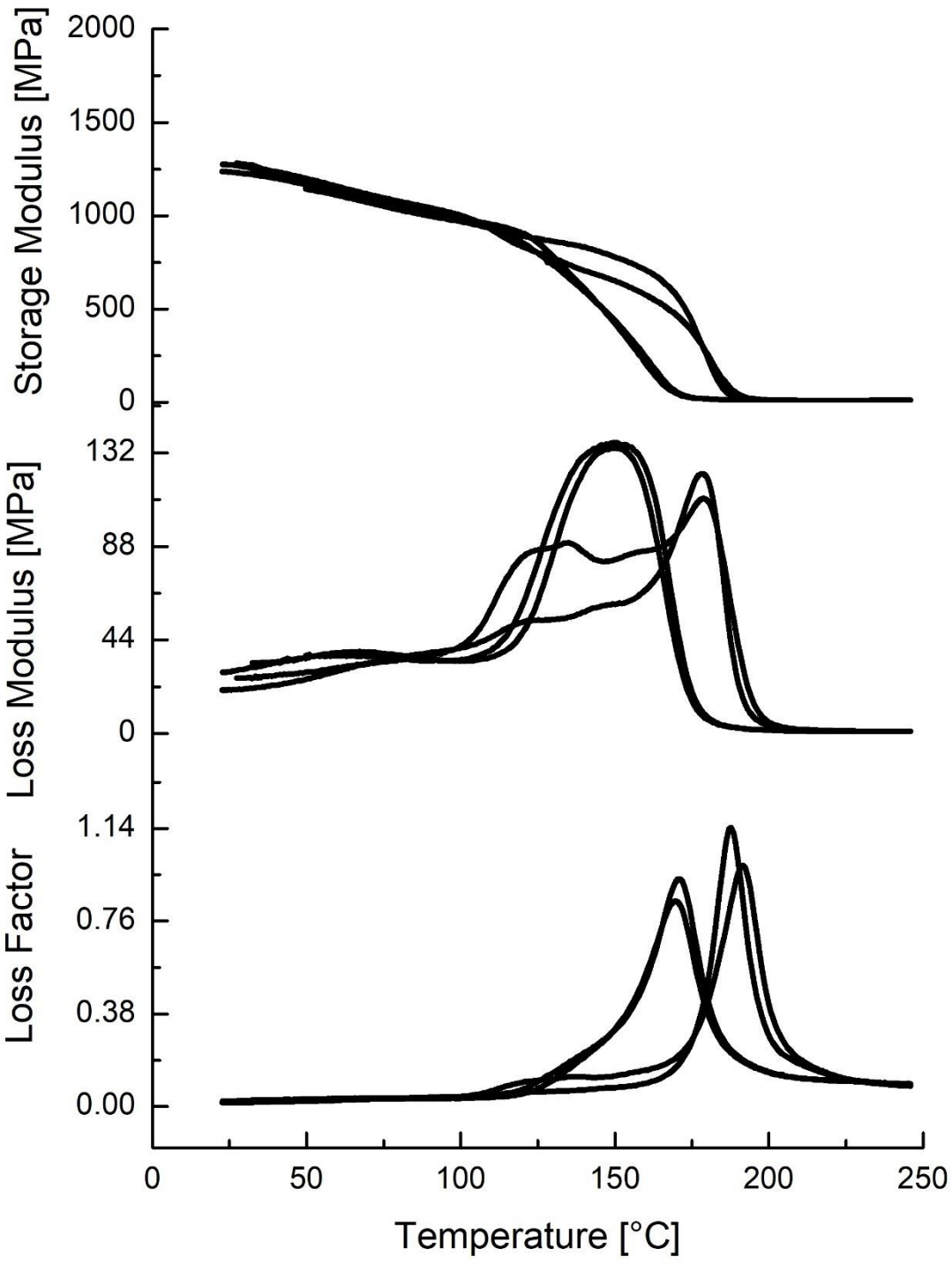

Figure A24. Four DMTA traces of reaction injection molded poly-*endo*-dicyclopentadiene-*co*-dicyclopentadienone (rim-PDCPD-*co*-oxaPDCPD).

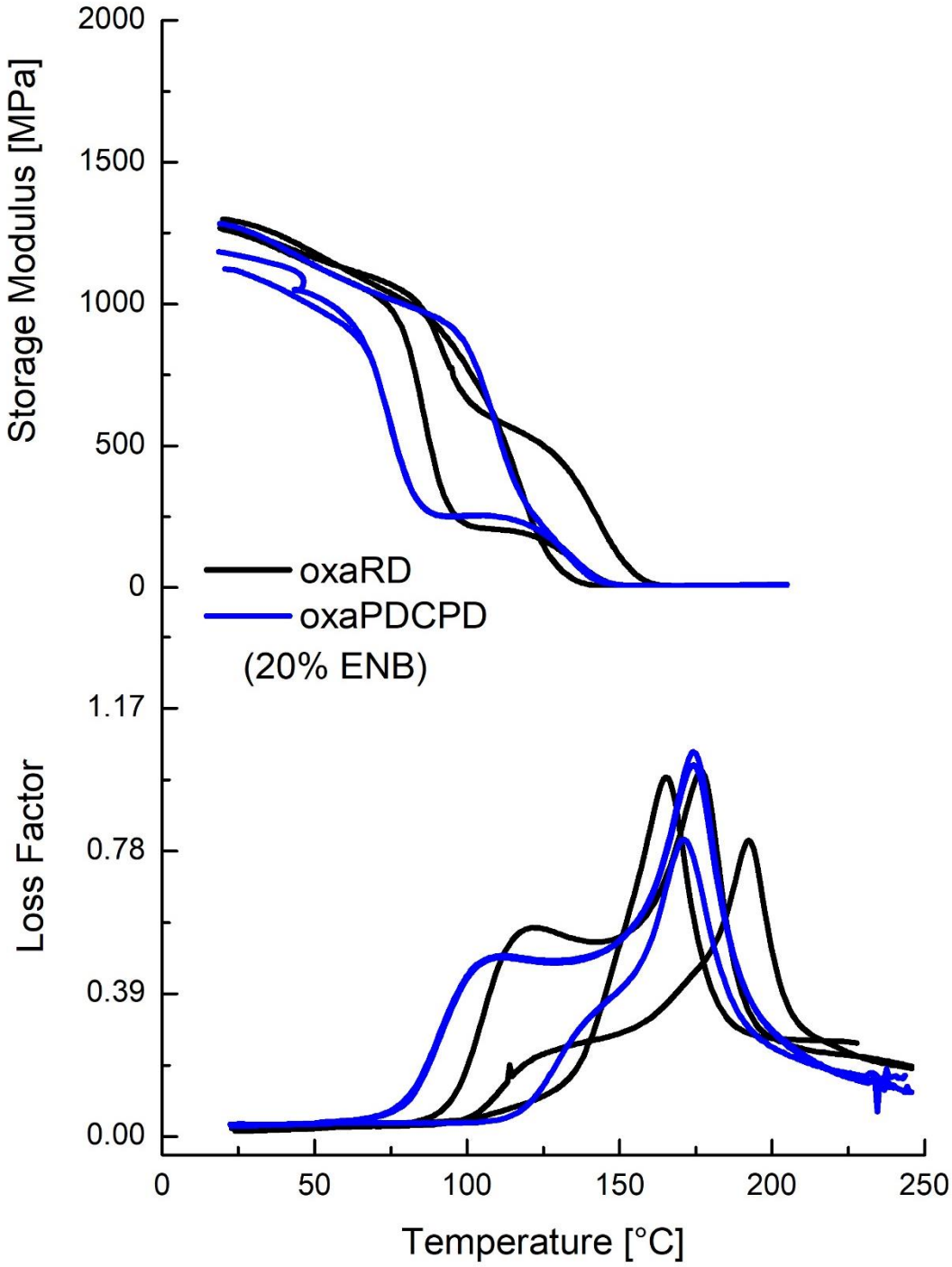

Figure A25. DMTA traces for reaction injection molded poly-*endo*-dicyclopentadienone rim-oxaPDCPD /w 20% ENB) and poly-*endo*-dicyclopentaenone (rim-oxaPDCPD$_{RD}$ /w 20% ENB). There are three traces for each polymer.

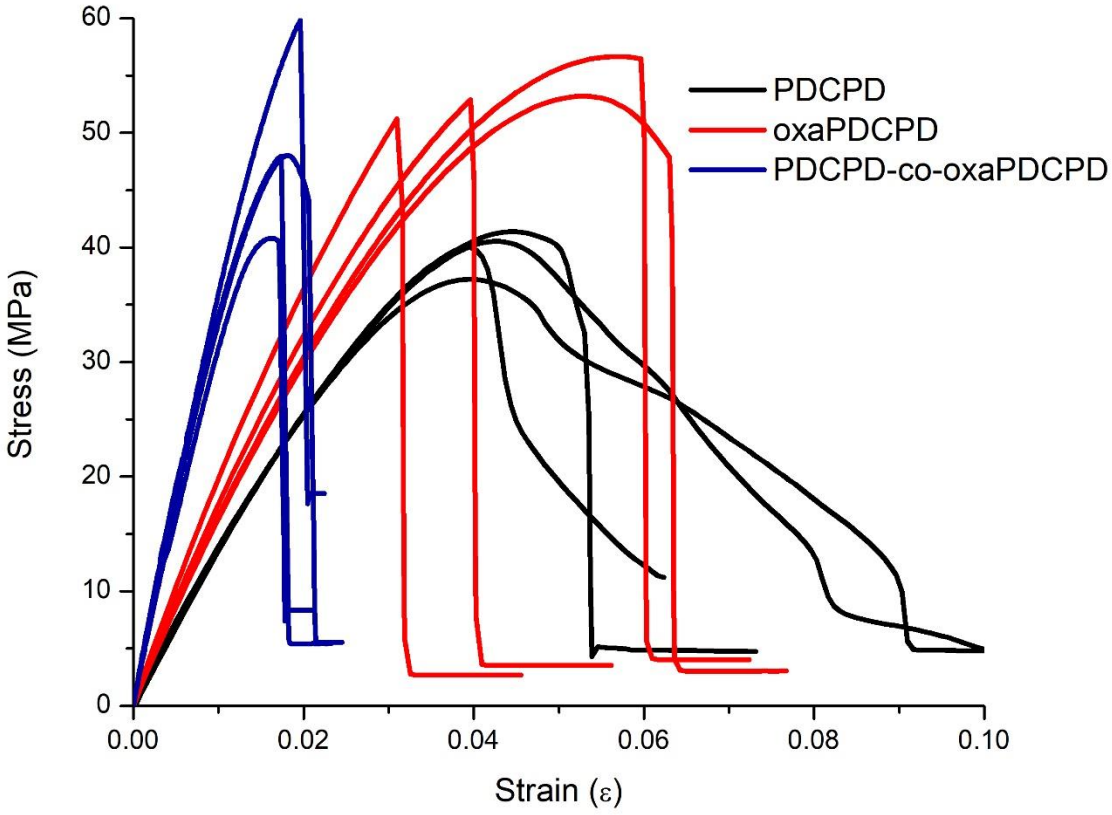

Figure A26. Stress-strain curves of ultimate tensile strength for reaction injection molded poly-*endo*-dicyclopentadiene, poly-*endo*-dicyclopentadienone and poly-*endo*-dicyclopentadiene-*co*-dicyclopentadienone, (rim-PDCPD, rim-oxaPDCPD, and rim-PDCPD-*co*-oxaPDCPD).

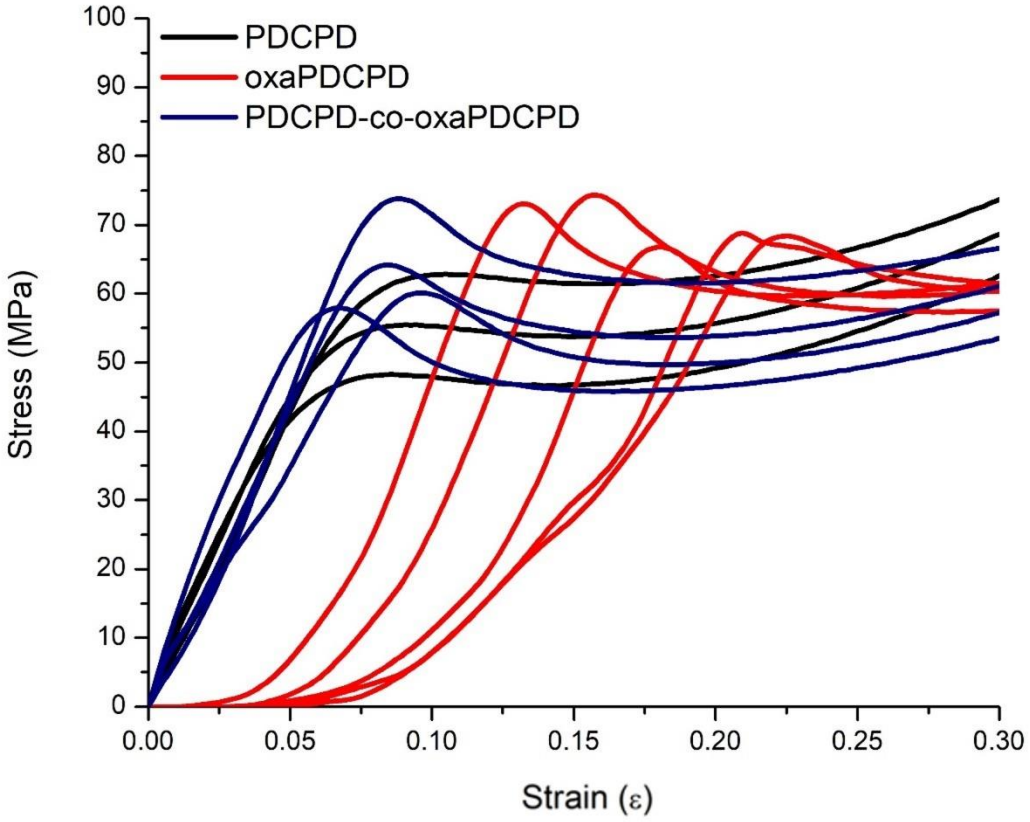

Figure A27. Stress-strain curves of low strain rate compression strength for reaction injection molded poly-*endo*-dicyclopentadiene, poly-*endo*-dicyclopentadienone and poly-*endo*-dicyclopentadiene-*co*-dicyclopentadienone, (rim-PDCPD, rim-oxaPDCPD, and rim-PDCPD-*co*-oxaPDCPD).

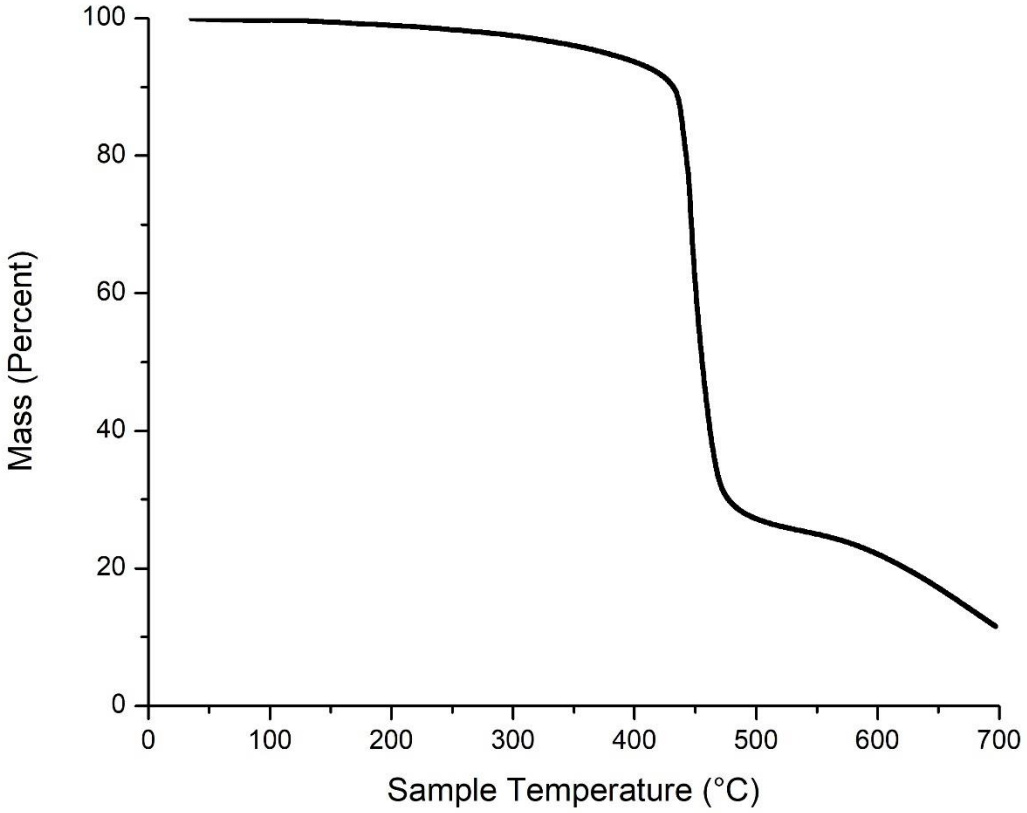

Figure A28. Representative TGA trace of reaction injection molded poly-*endo*-dicyclopentadiene (rim-PDCPD).

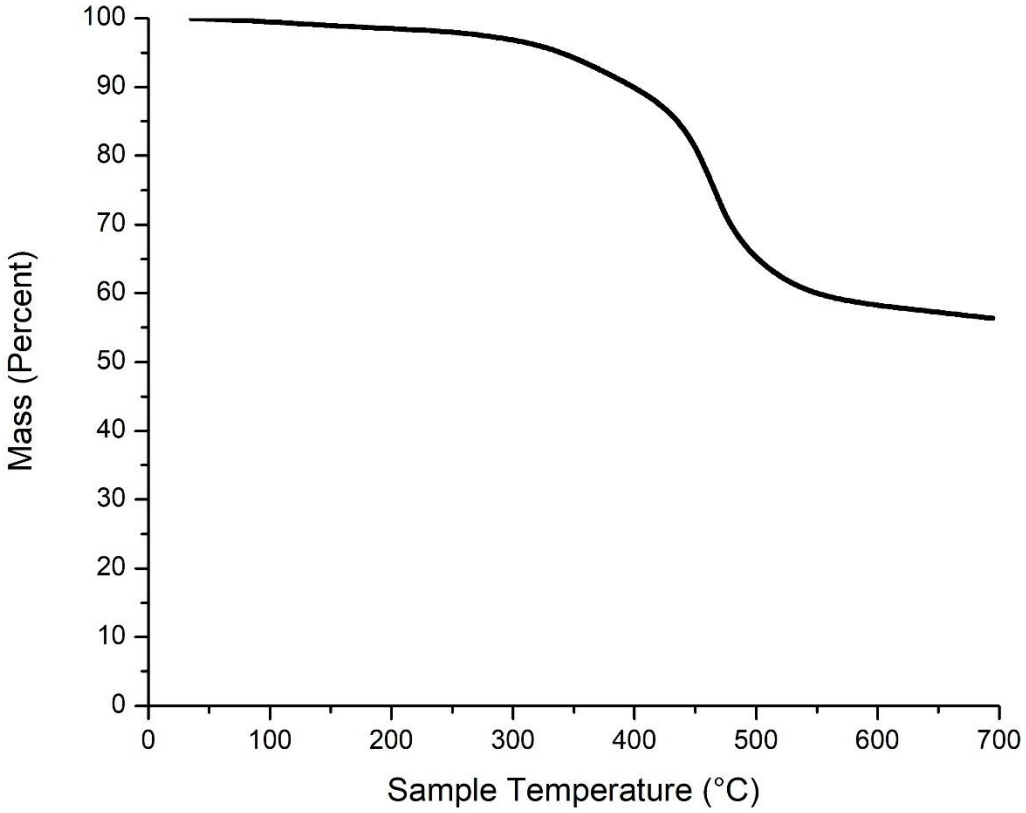

Figure A29. Representative TGA trace of reaction injection molded poly-*endo*-dicyclopentadienone (rim-oxaPDCPD).

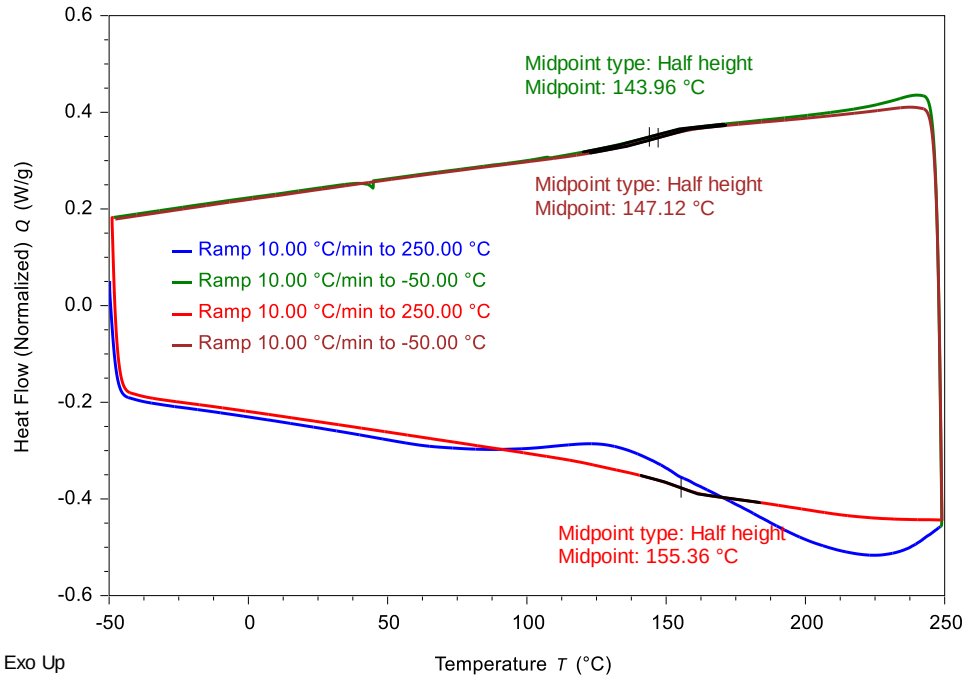

Figure A30. Representative DSC traces of reaction injection molded poly-*endo*-dicyclopentadiene (rim-PDCPD).

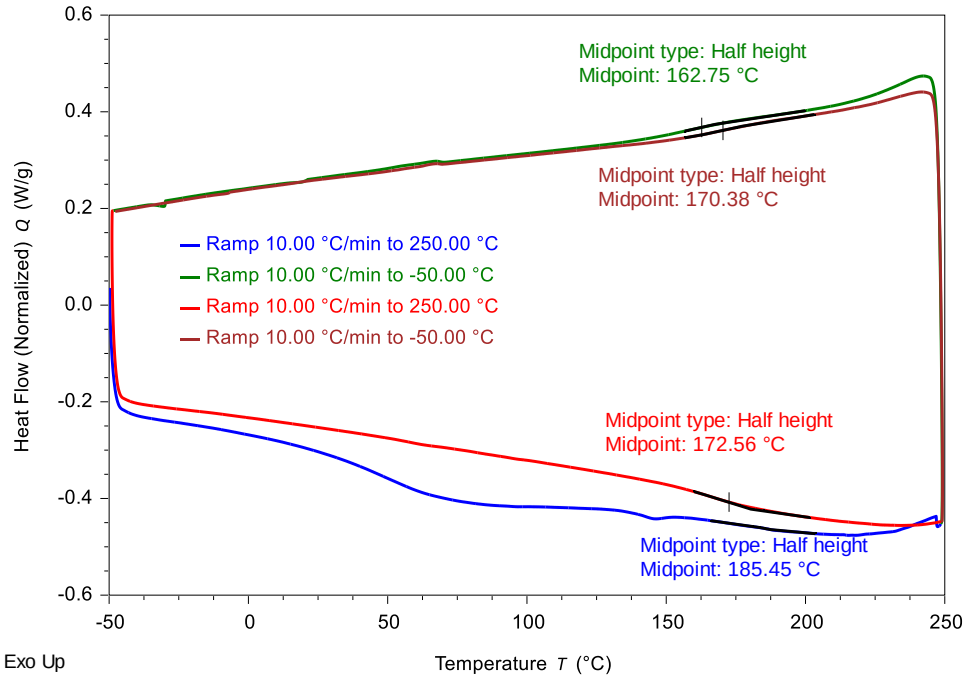

Figure A31. Representative DSC traces of reaction injection molded poly-*endo*-dicyclopentadienone (rim-oxaPDCPD).

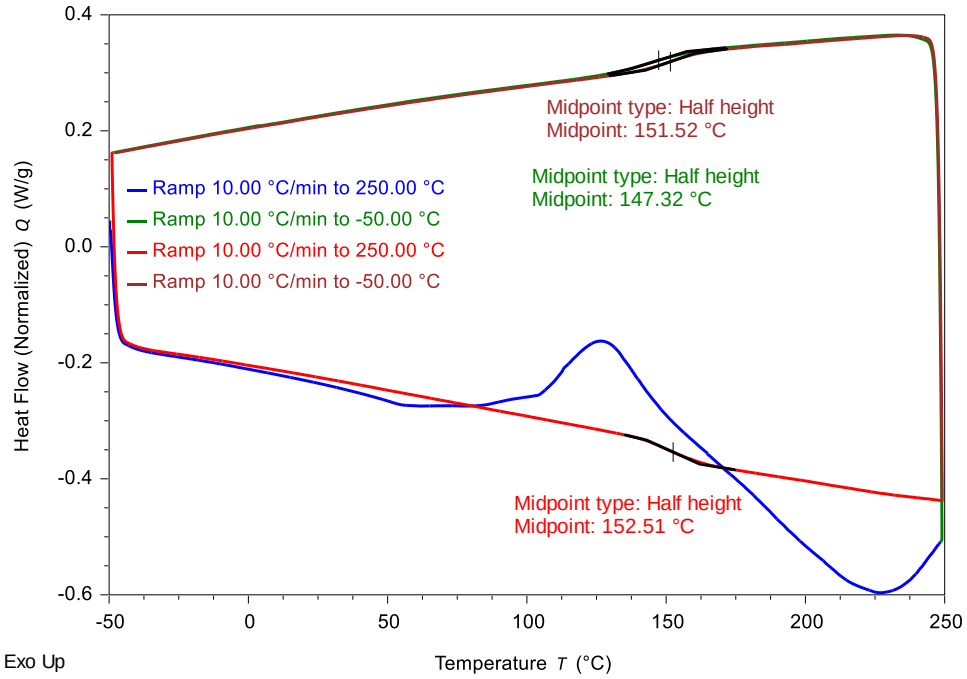

Figure A32. Representative DSC traces of reaction injection molded poly-*endo*-dicyclopentadiene-*co*-dicyclopentadienone (rim-PDCPD-*co*-oxaPDCPD).

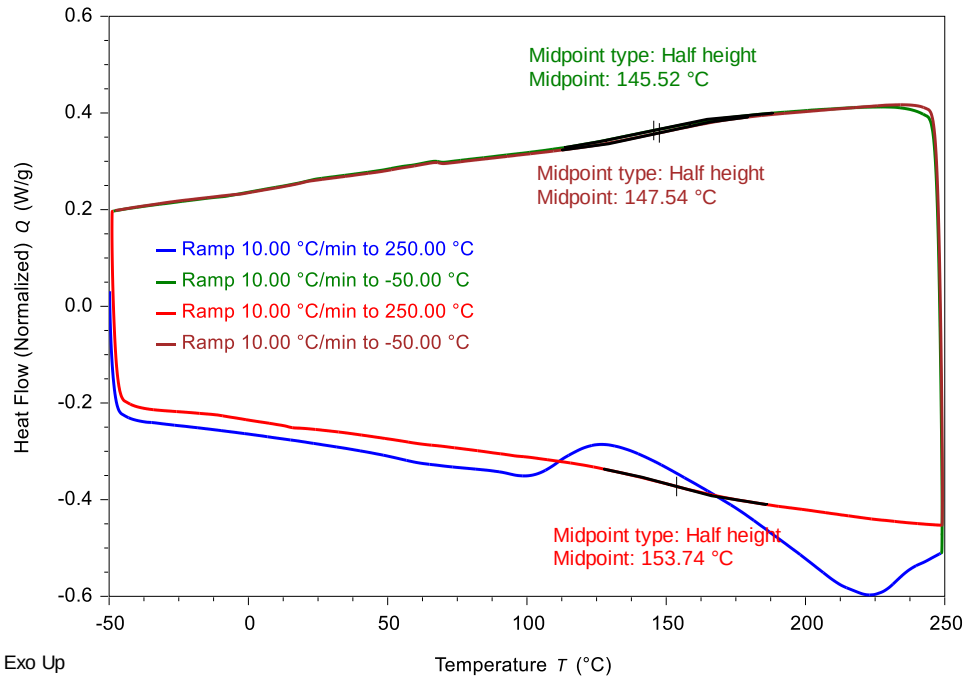

Figure A33. Representative DSC traces of reaction injection molded poly-*endo*-dicyclopentaenone (rimoxaPDCPD$_{RD}$ /w 20% ENB).

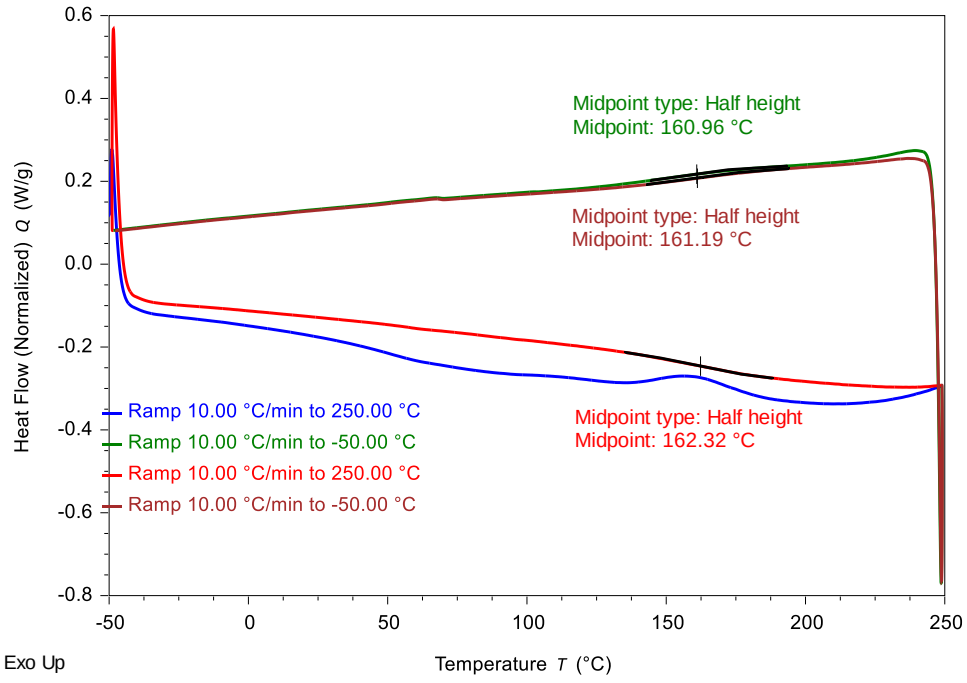

Figure A34. Representative DSC traces of reaction injection molded poly-*endo*-dicyclopentadienone (rim-oxaPDCPD /w 20% ENB).

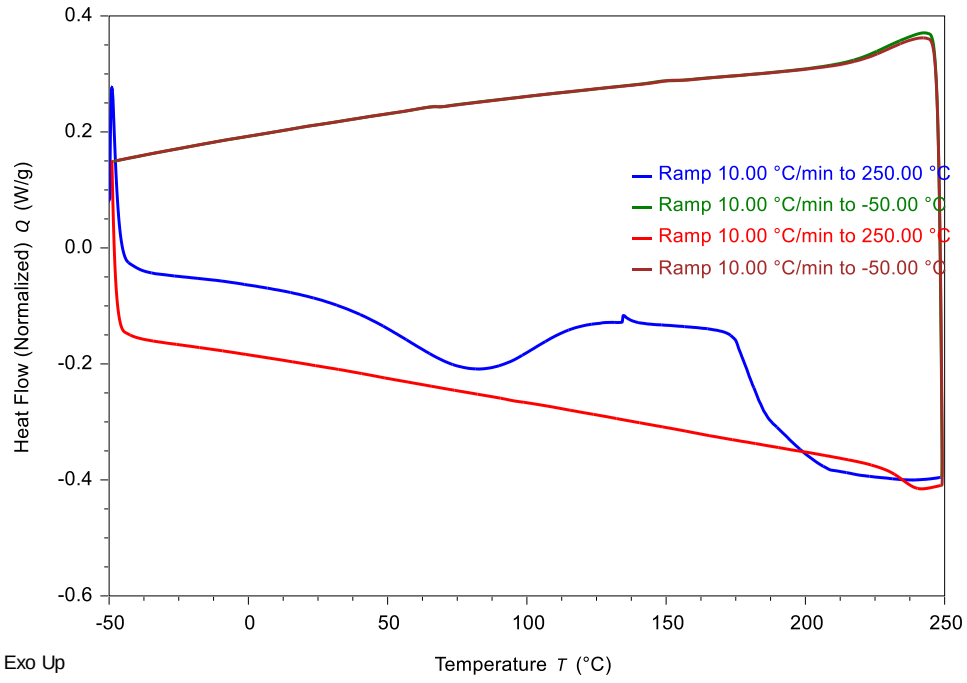

Figure A35. Representative DSC traces for poly-*endo*-dicyclopentadienone (oxaPDCPD) /w 2.33 mol% GC3.

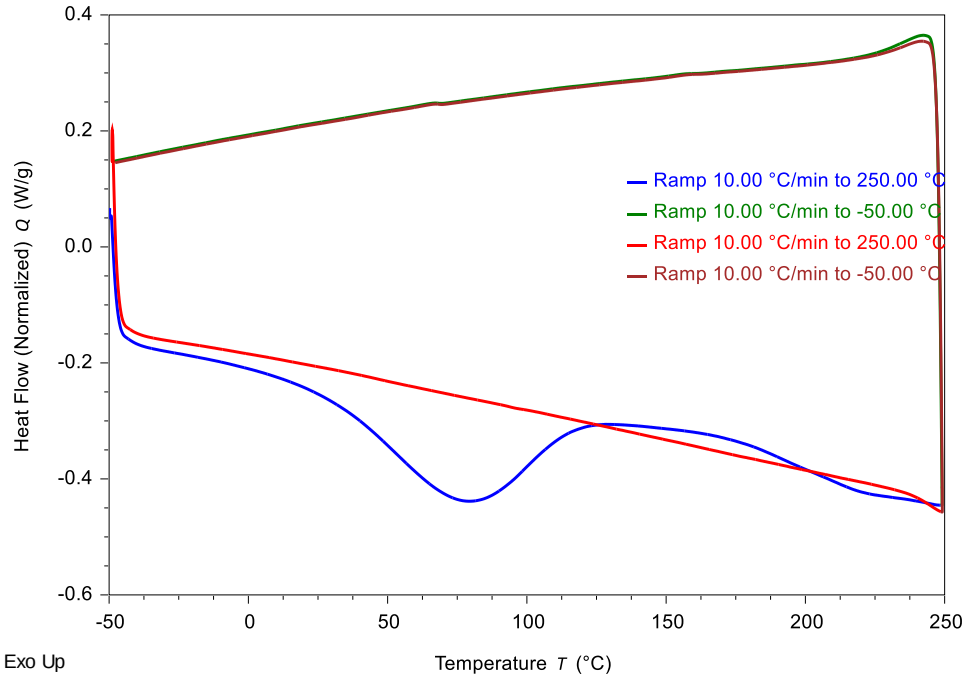

Figure A36. Representative DSC traces for poly-*endo*-dicyclopentadienone (oxaPDCPD) /w 1.17 mol% GC3.

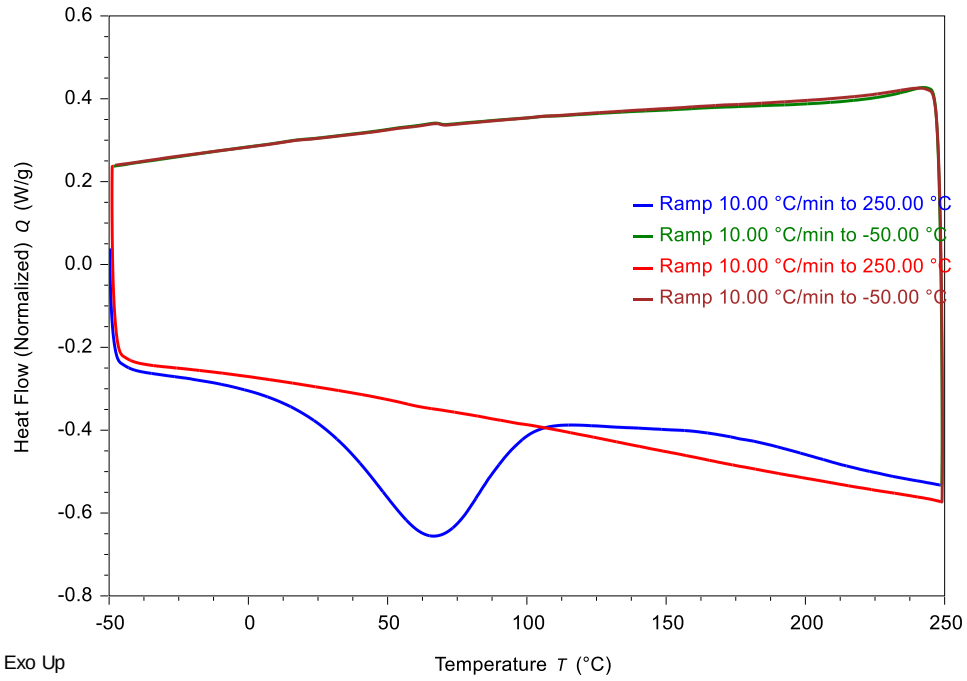

Figure A37. Representative DSC traces for poly-*endo*-dicyclopentadienone (oxaPDCPD) /w 0.58 mol% GC3.

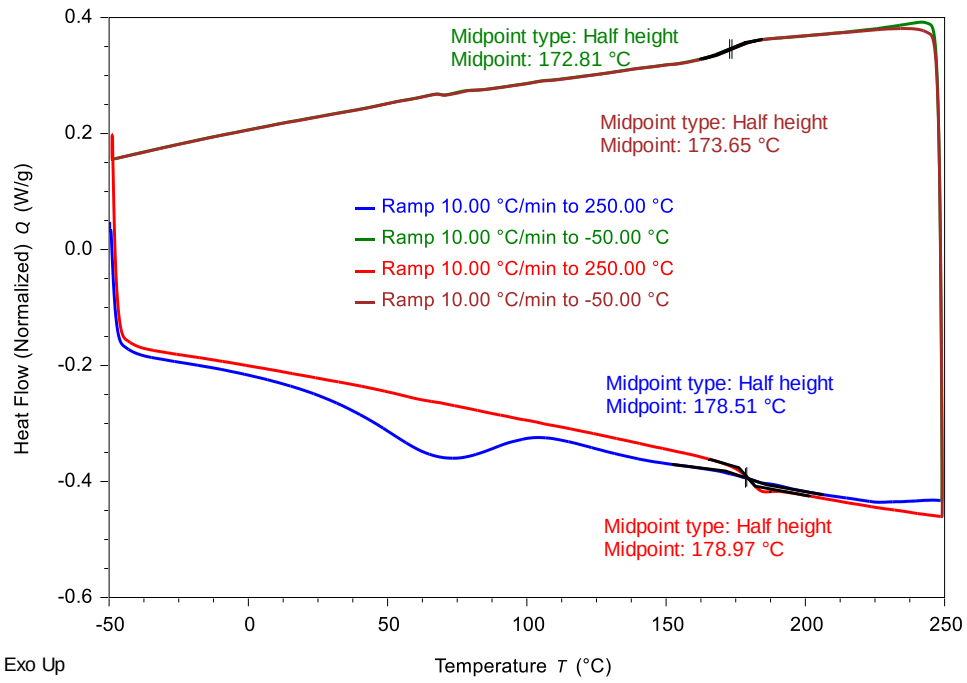

Figure A38. Representative DSC traces for poly-*endo*-dicyclopentaenone (oxaPDCPD$_{RD}$) /w 2.33 mol% GC3.

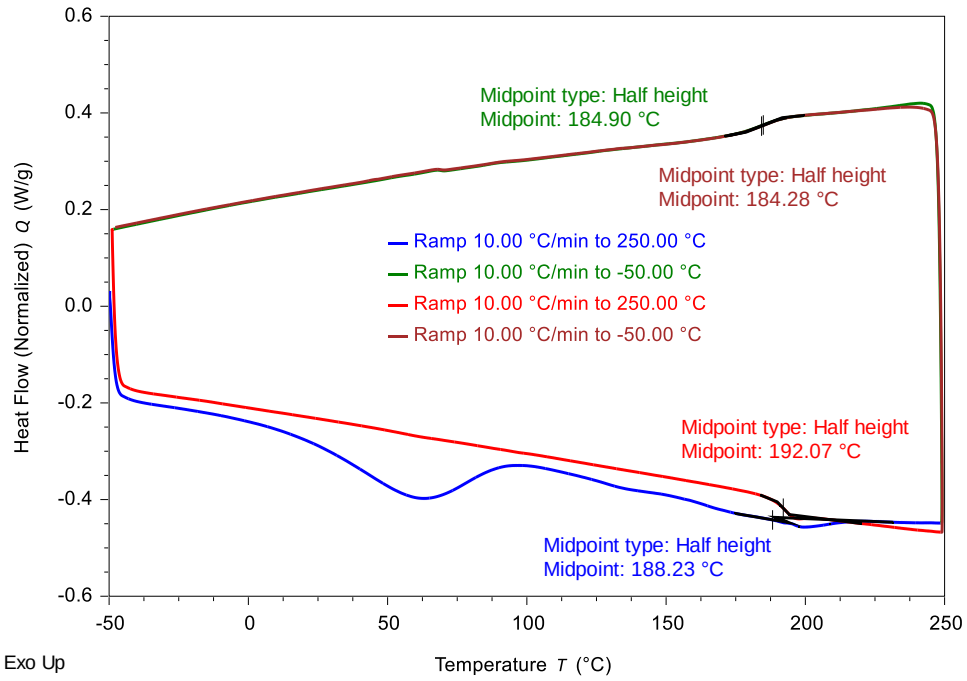

Figure A39. Representative DSC traces for poly-*endo*-dicyclopentaenone (oxaPDCPD$_{RD}$) /w 1.13 mol% GC3.

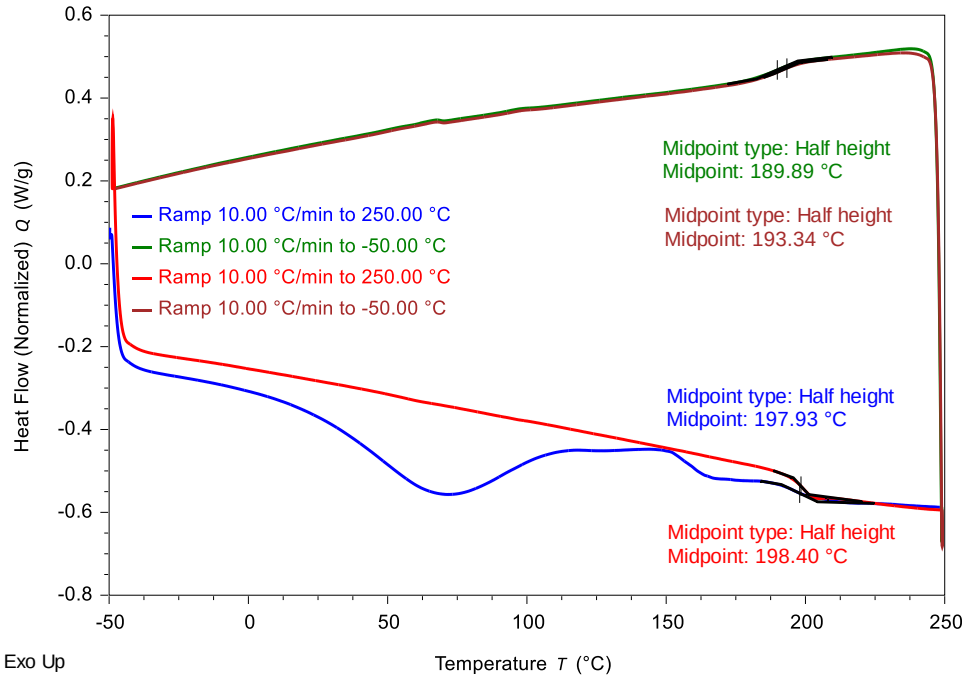

Figure A40. Representative DSC traces for poly-*endo*-dicyclopentaenone (oxaPDCPD$_{RD}$) /w 0.60 mol% GC3.

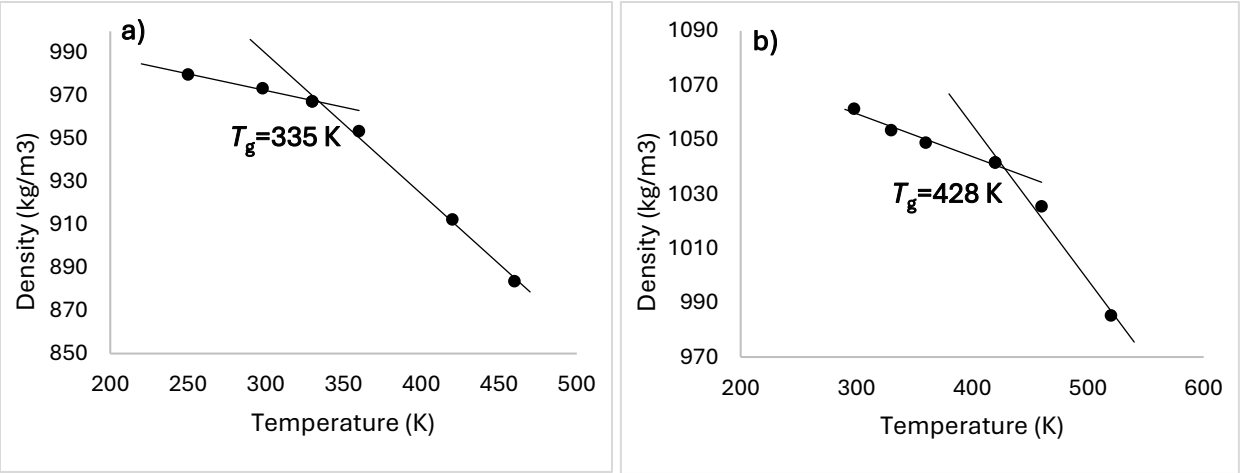

Figure A41. Calculated profile of the density versus temperature for a) linear 20-mer of PDCPD and b) linear oxaPDCPD (i.e. non-crosslinked PDCPD and oxaPDCPD).

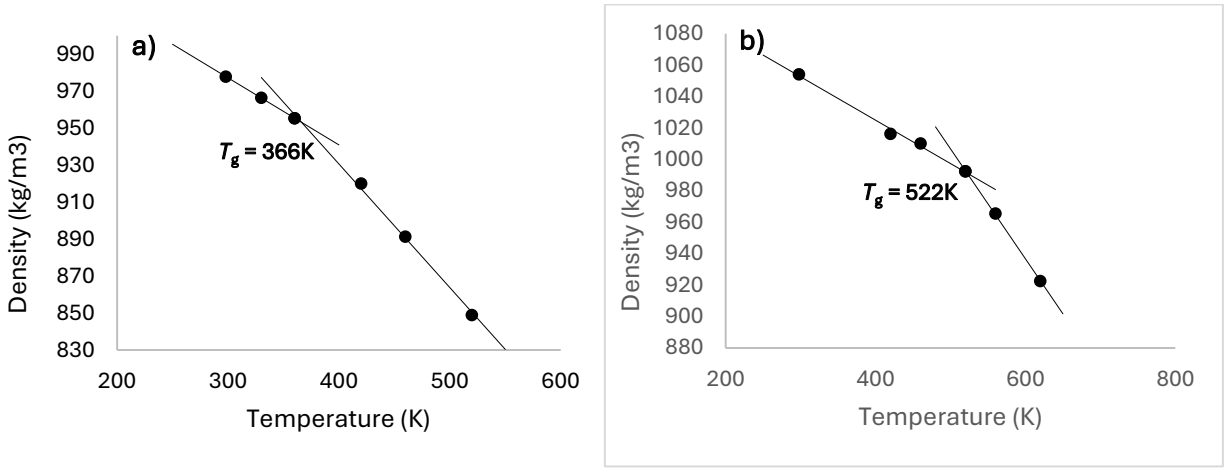

Figure A42. Calculated profile of density and T_g of the system composed of crosslinked 40-mer a) non-functionalized and b) oxa-type chains. (crosslinked PDCPD and oxaPDCPD).

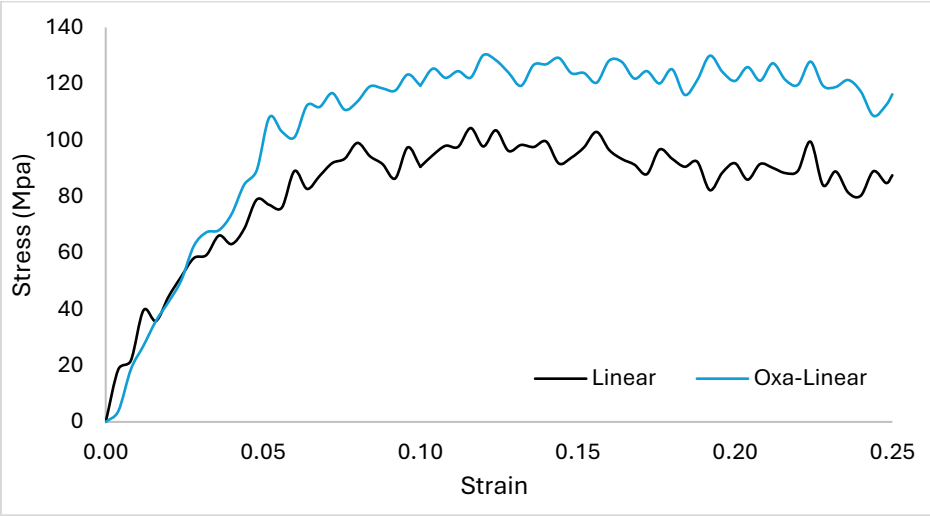

Figure A43. Calculated stress response of non-functionalized linear and oxa-linear PDCPD structures at the strain rate of $8x10^{9}s^{-1}$ (at 298K).

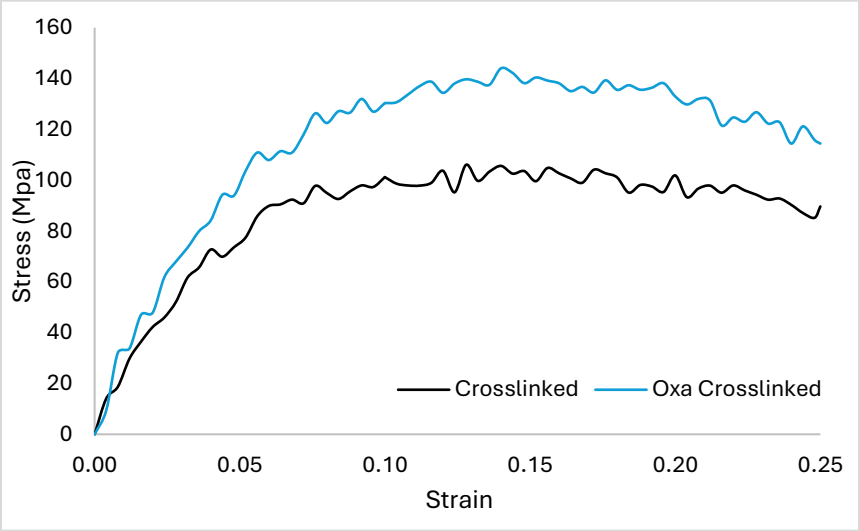

Figure A44. Calculated stress response of the crosslinked structures of PDCPD and oxaPDCPD at the strain rate of $8x10^{9}s^{-1}$ (at 298K).

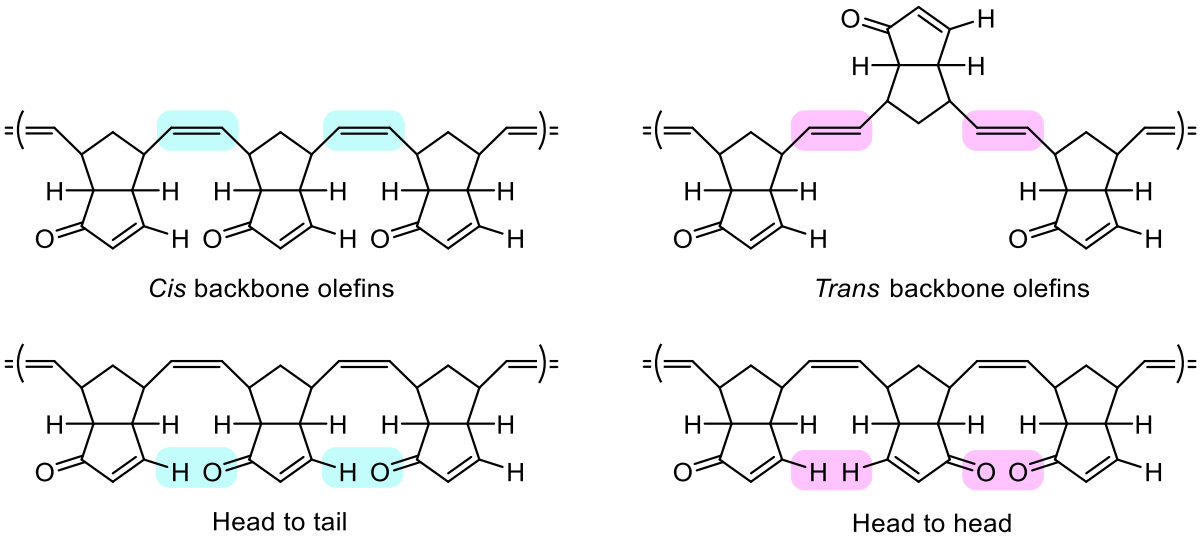

Figure A45. The four types of structure arising from different primary polymerization outcomes studied in this work.

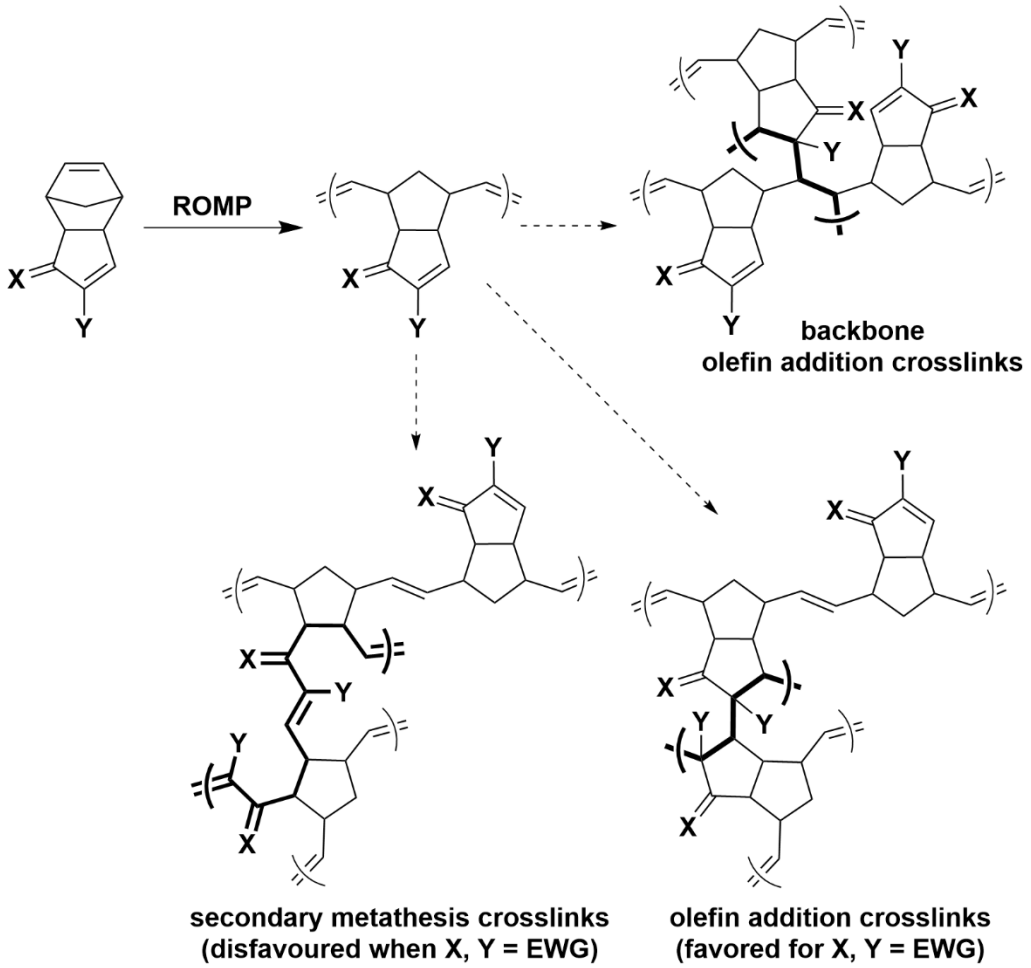

Figure A46. Potential crosslink motifs in polydicyclopentadiene based materials. Unfunctionalized polydicyclopentadiene (**1**$_{p,c}$) is known to contain at least some secondary metathesis crosslinks when ruthenium catalysts are used for ROMP, but to contain mostly olefin addition crosslinks when tungsten or molybdenum catalysts are employed. The metathesis crosslinking pathway is disfavoured when electron-withdrawing groups are added to the unstrained olefin of the monomer, such that covalent crosslinking in **3**$_{p,c}$ and **4**$_{p,c}$ is believed to occur exclusively through an olefin addition pathway.

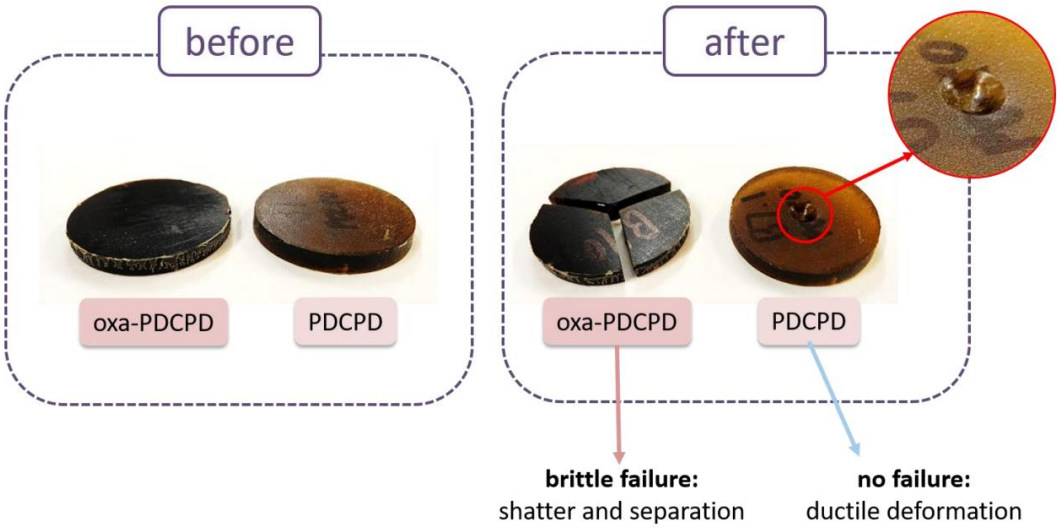

Figure A47. rim-oxaPDCPD and rim-PDCPD disks before and after a 2 kg weight with a 20° semiconical punch was dropped upon them from a height of 1 m in a Gardner impact tester.

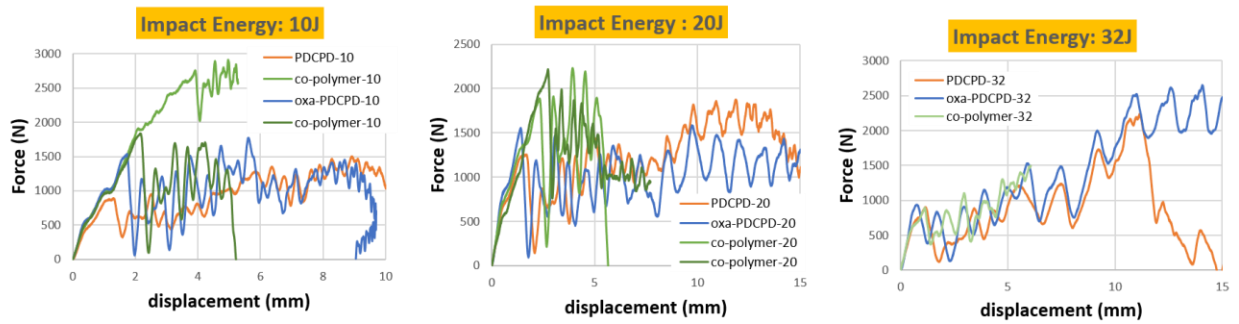

Figure A48. rim-PDCPD (orange curves), rim-oxaPDCPD (blue curves), and rim-poly(**1**$_{m}$-*co*-**4**$_{m}$) (green curves), tested for impact strength according to ASTM D7136. The samples were tested using an Instron CEAST 9340 instrument equipped with a semi-spherical tip insert with a diameter of 12.7 mm. Testing was carried out using three different impact energies (10, 20 and 32 J), established by varying the drop weight between 3.3 and 10.3 kg, and varying the drop height between 197 and 317 mm. The data indicate that at low and moderate impact energies, the copolymer is capable of absorbing more energy than either of the two homopolymers. At the highest impact energy, all three polymers behaved similarly.

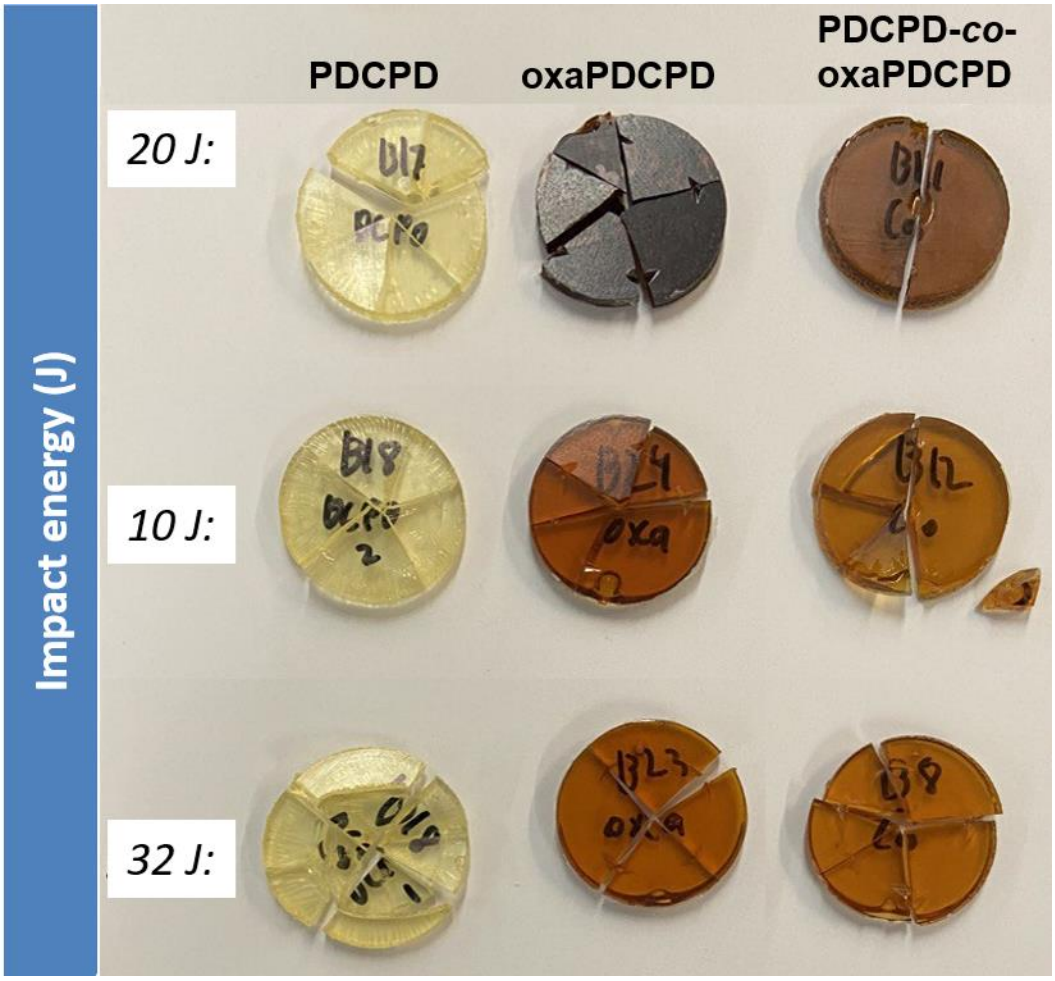

Figure A49. Physical appearance of the samples after impact testing according to ASTM 7136.

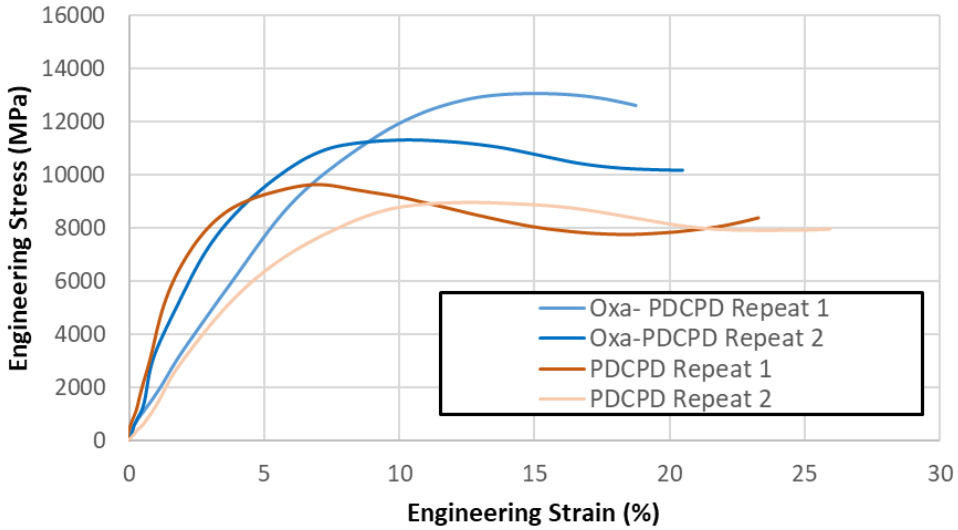

Figure A50. High strain rate compression testing using a split-Hopkinson pressure bar system. oxaPDCPD (blue curves) was found to absorb more energy than PDCPD (red curves). A striker diameter of 1.5” was used, together with a testing pressure of 59 Pa.

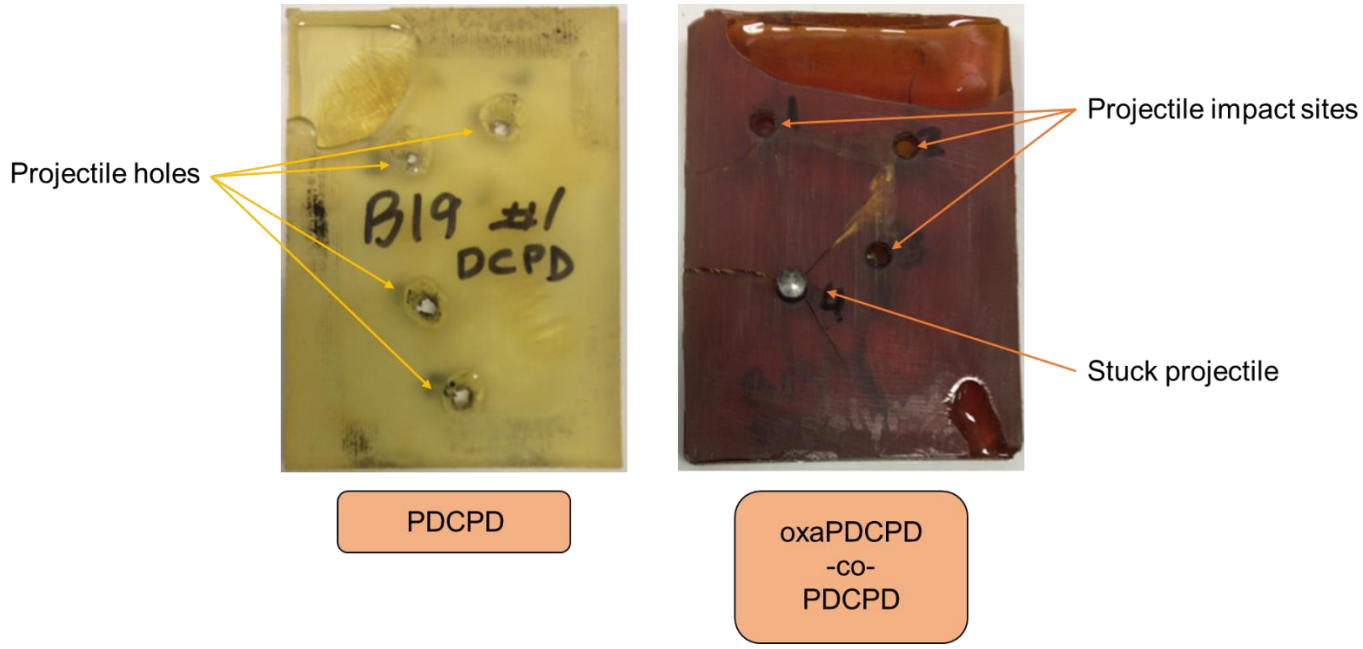

Figure A51. rim-PDCPD and rim-PDCPD-*co*-oxaPDCPD 10 mm thick plaques after ballistic testing using 17-grain projectiles loaded with 1.5 grains of Trailboss powder. The average incoming velocity for all projectiles was 301 m/s. The average calibrated velocity reduction was 74% for PDCPD samples, and 93% for copolymer samples formulated with 1:1 oxaDPCD:DCPD. Qualitatively, PDCPD plaques tended to show clean holes where projectiles had passed through, while copolymer plaques were able to stop projectiles completely.

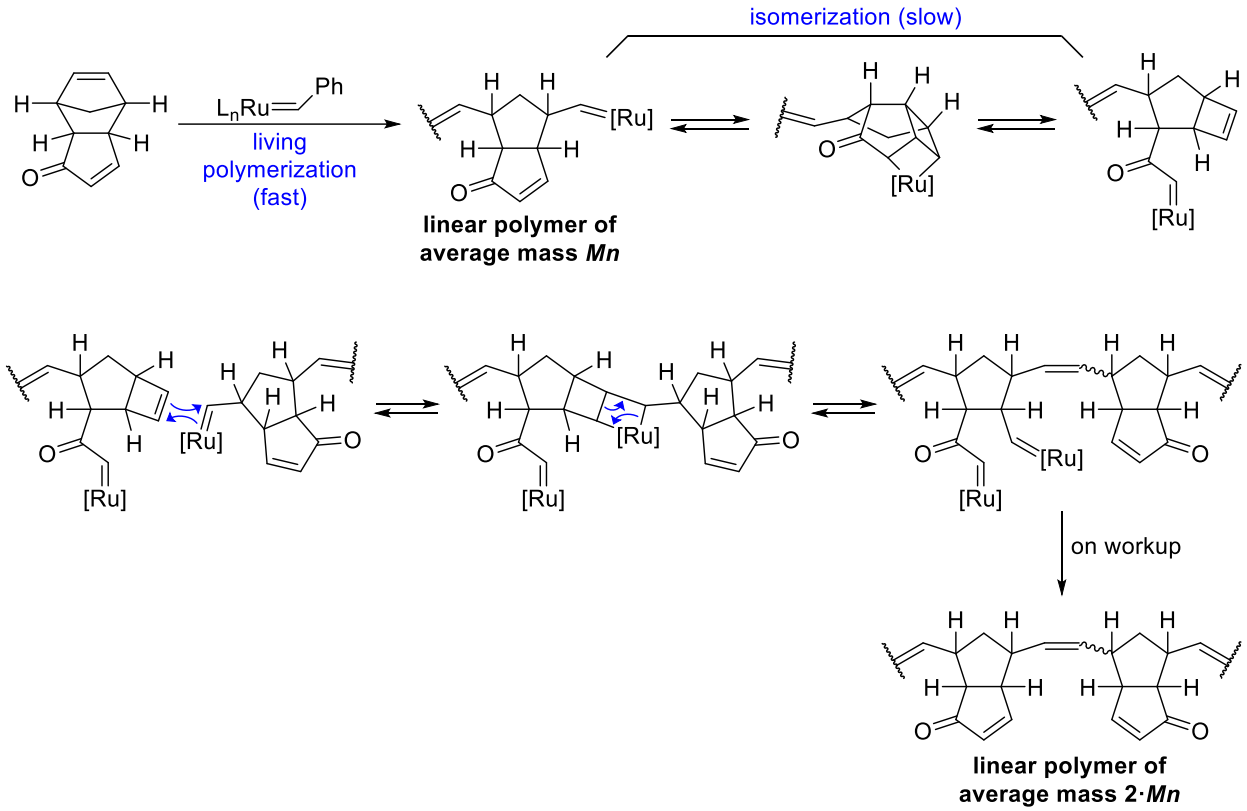

Figure A52. Proposed dimerization mechanism of linear oxaPDCPD chains produced in a living polymerization reaction with Grubbs 3rd generation catalyst.

Table A1. GPC data for formation of linear polymers with Grubbs 3rd and 2nd generation catalyst.[a]

Reaction	M_n (kDa)	M_w (kDa)	M_w/M_n	Predicted M_n (kDa)
Oxa 2.33 mol% GC3	14.6	26.6	1.82	6.3
Oxa 1.17 mol% GC3	38.7	64.2	1.66	12.6
Oxa 0.58 mol% GC3	65.0	119.5	1.84	25.1
OxaRD 2.33 mol% GC3	7.6	9.3	1.23	6.4
OxaRD 1.13 mol% GC3	17.8	23.8	1.33	13.2
OxaRD 0.60 mol% GC3	32.7	49.8	1.52	24.6
Oxa 1.98 mol% GC2	87.1	149.1	1.71	7.5
Oxa 1.02 mol% GC2	84.3	210.1	2.49	14.5
Oxa 0.46 mol% GC2	100.1	229.1	2.29	31.5

[a]M_n and M_w values were measured using a GPC instrument calibrated with polystyrene standards

Table A2. Mechanical data comparison of molded poly-endo-dicyclopentadiene and poly-endo-dicyclopentadienone and poly-endo-dicyclopentadiene-*co*-dicyclopentadienone (rim-PDCPD, rim-oxaPDCPD and rim- PDCPD-*co*-oxaPDCPD).

Property	PDCPD	oxaPDCPD	PDCPD-*co*-oxaPDCPD
Young's Modulus (GPa)	1.22 ± 0.02	1.47 ± 0.14	3.62 ± 0.27
Ultimate Tensile Strength (MPa)	39.8 ± 1.8	53.5 ± 2.3	49.1 ± 7.9
Compression Strength (MPa)	56 ± 7	70 ± 3	64 ± 7
Storage Modulus (MPa)	1005 ± 81	1601 ± 152	1247 ± 33
Glass Transition Temperature (°C)	175.5 ± 4.7	208.9 ± 8.7	180.0 ± 11.2
Strain at Break (%)	7.2 ± 1.7	4.6 ± 1.2	1.9 ± 0.2

Table A3. Estimated distance between crosslinks of reaction injection molded polymers.

	rim-oxaPDCPD	aged rim-oxaPDCPD[a]	rim-PDCPD w/ 5% ENB	rim-PDCPD-*co*-oxaPDCPD	rim-oxaPDCPD$_{RD}$ w/ 20% ENB	rim-oxaPDCPD (20% ENB)
M_c (g/mol)	1270 ± 111	110	1914 ± 159	1302 ± 47	3187 ± 823	1975 ± 122

[a]Sample aged 104 days @120°C.

Table A4. Hardness comparison between reaction injection molded poly-*endo*-dicyclopentadiene and poly-*endo*-dicyclopentadienone (rim-PDCPD and rim-oxaPDCPD).

Material	**Hardness (Vickers)**
PDCPD	13.9 ± 0.6
oxaPDCPD	16.6 ± 1.1

Table A5. Masses of reaction injection molded polydicyclopentadiene and polydicyclopetnadienone (rim-PDCPD and rim-oxaPDCPD) cylinders (4.73 x 9.96 mm) swollen in methanol and toluene.

Time (days)	rim-oxaPDCPD Mass (g)	rim-oxaPDCPD Mass (g)	rim-oxaPDCPD Mass (g)	rim-oxaPDCPD Mass (g)	rim-oxaPDCPD Mass (g)	rim-oxaPDCPD Mass (g)
	MeOH 1	MeOH 2	MeOH 3	Toluene 1	Toluene 2	Toluene 3
0	0.4262	0.4237	0.4276	0.4233	0.426	0.4303
1	0.6385	0.641	0.7215	0.5133	0.5186	0.5485
2	0.7569	0.7604	0.8813	0.5368	0.544	0.5969
3	0.8392	0.8365	0.9783	0.547	0.5539	0.6175
5	0.9324	0.9231	1.08	0.5538	0.5596	0.6331
7	0.9633	0.95	1.1132	0.552	0.5574	0.6359
9	0.9811	0.9669	1.1238	0.5493	0.5532	0.6354
12	0.9825	0.9752	1.1322	0.5464	0.5495	0.6349
Time (days)	**rim-PDCPD Mass (g)**	**rim-PDCPD Mass (g)**	**rim-PDCPD Mass (g)**	**rim-PDCPD Mass (g)**	**rim-PDCPD Mass (g)**	**rim-PDCPD Mass (g)**
	MeOH 1	MeOH 2	MeOH 3	Toluene 1	Toluene 2	Toluene 3
0	0.3706	0.3674	0.3661	0.3679	0.3712	0.3722
1	0.3708	0.3677	0.3673	1.058	1.0348	1.0505
2	0.371	0.3681	0.367	1.1248	1.1221	1.0915
4	0.3717	0.3678	0.3698	1.1041	1.0786	1.0364
6	0.3723	0.3691	0.3687	1.0808	1.0333	1.0112
8	0.3735	0.3706	0.3698	1.0443	0.9973	0.9833
11	0.3751	0.3723	0.3745	1.01	0.9803	0.9657
13	0.3759	0.3731	0.3745	0.9929	0.9683	0.9544

Table A6. Contact angles measured on reaction injection molded polymer samples.

H_2O	rim-PDCPD	$_{PR}$PDCPD	rim-oxaPDCPD	rim-PDCPD-*co*-oxaPDCPD
average (°)	108.16	120.45	94.14	94.12
standard deviation	6.53	12.20	11.25	6.51
n	15	19	19	15
standard error	1.7	2.8	2.6	1.7
CH_2I_2	PDCPD vs. CH_2I_2	$_{PR}$PDCPD vs. CH_2I_2	oxaPDCPD vs. CH_2I_2	rim-PDCPD-*co*-oxaPDCPD
average (°)	48.13	47.87	47.35	35.48
standard deviation	6.00	6.95	12.15	8.09
n	7	17	18	13
standard error	2.3	1.7	2.9	2.2

Table A7. Components of the systems under study (non-equilibrated structures)

		# of residues	MW	Fragment of the PDCPD structure (pre-equilibration schematic)
Linear	Non-functionalized	20	2,672	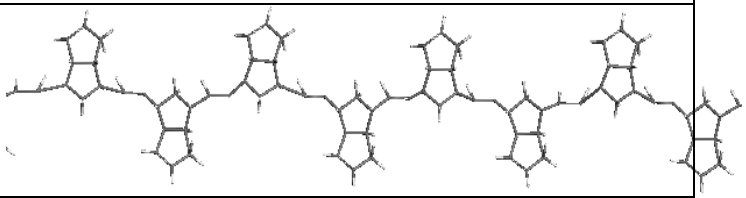
	Oxa		2,952	
Crosslinked	Non-functionalized	40	5,346	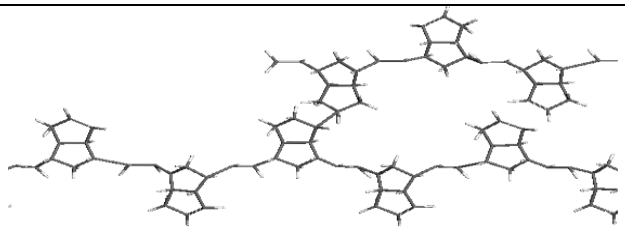

Table A8. Calculated Young's modulus as the initial slope of the stress-strain curve.

	PDCPD	oxaPDCPD
Linear	1.46 ± 0.16	1.75 ± 0.17
Crosslinked	1.48 ± 0.16	1.88 ± 0.19

Table A9. Comparison of the overall intermolecular interactions in non-functionalized PDCPC and oxaPDCPD linear and crosslinked structures.

		Average Dipole (q·Å)	Electrostatic Interactions (10^5 kcal/mol)	van der Waals Interactions (10^5 kcal/mol)
Linear	PDCPD	0.29	0.52	0.75
	oxaPDCPD	2.59	1.81	0.84
Crosslinked	PDCPD	0.44	1.08	1.49
	oxaPDCPD	3.77	3.54	1.68

Table A10. Comparison of the overall intermolecular interactions in non-functionalized PDCPC and oxaPDCPD linear and crosslinked structures.

		Average Dipole (q·Å)	Electrostatic Interactions (10^5 kcal/mol)	van der Waals Interactions (10^5 kcal/mol)
Linear	PDCPD	0.29	0.52	0.75
	oxaPDCPD	2.59	1.81	0.84
Crosslinked	PDCPD	0.44	1.08	1.49
	oxaPDCPD	3.77	3.54	1.68

Table A11. Average interaction energies between ring ethylene hydrogen atoms and ketone oxygen atoms (kcal/mol).

	Intra-chain	Inter-chain
Linear	-1.23	0.0
Crosslinked	-1.05	0.0

Table A12. Relative electronic energies (in kcal/mol) for different primary structures of hexamers of oxaPDCPD.

Structure		Relative Energy
All *cis*, head-to-head	**(D)**	13.1
All *cis*, head-to-tail	**(C)**	11.0
All *trans*, head-to-head	**(B)**	1.6
All *trans*, head-to-tail	**(A)**	0

Table A13. Tabulated thermal and mechanical data for reaction injection molded polymers.

Material	Density (g/cm^3)	Tensile Strength (MPa)	Strain at Break (%)	Young's Modulus (GPa)	Storage Modulus (MPa)	Compression Strength (MPa)	Glass Transition Temperature DMTA (°C)
PDCPD	1.04	39.8 ± 1.8	7.2 ± 1.7	1.22 ± 0.02	1005 ± 81	56 ± 7	175.5 ± 4.7
oxaPDCPD	1.16	53.5 ± 2.3	4.6 ± 1.2	1.47 ± 0.14	1601 ± 152	70 ± 3	208.9 ± 8.7
Poly(1_m-*co*-4_m)	1.04	49.1 ± 7.9	1.9 ± 0.2	3.62 ± 0.27	1247.2 ± 32.9	64 ± 7	180.0 ± 11.2
oxaPDCD-*co*-ENB (20%)	1.09	N/A	N/A	N/A	1197 ± 80	N/A	173.2 ± 1.7
oxaPDCPD$_{RD}$-*co*-ENB (20%)	1.07	N/A	N/A	N/A	1277 ± 20	N/A	177.9 ± 13.6

Appendix B: Supplemental Spectra, Plots, Figures and Tables for Chapter 3

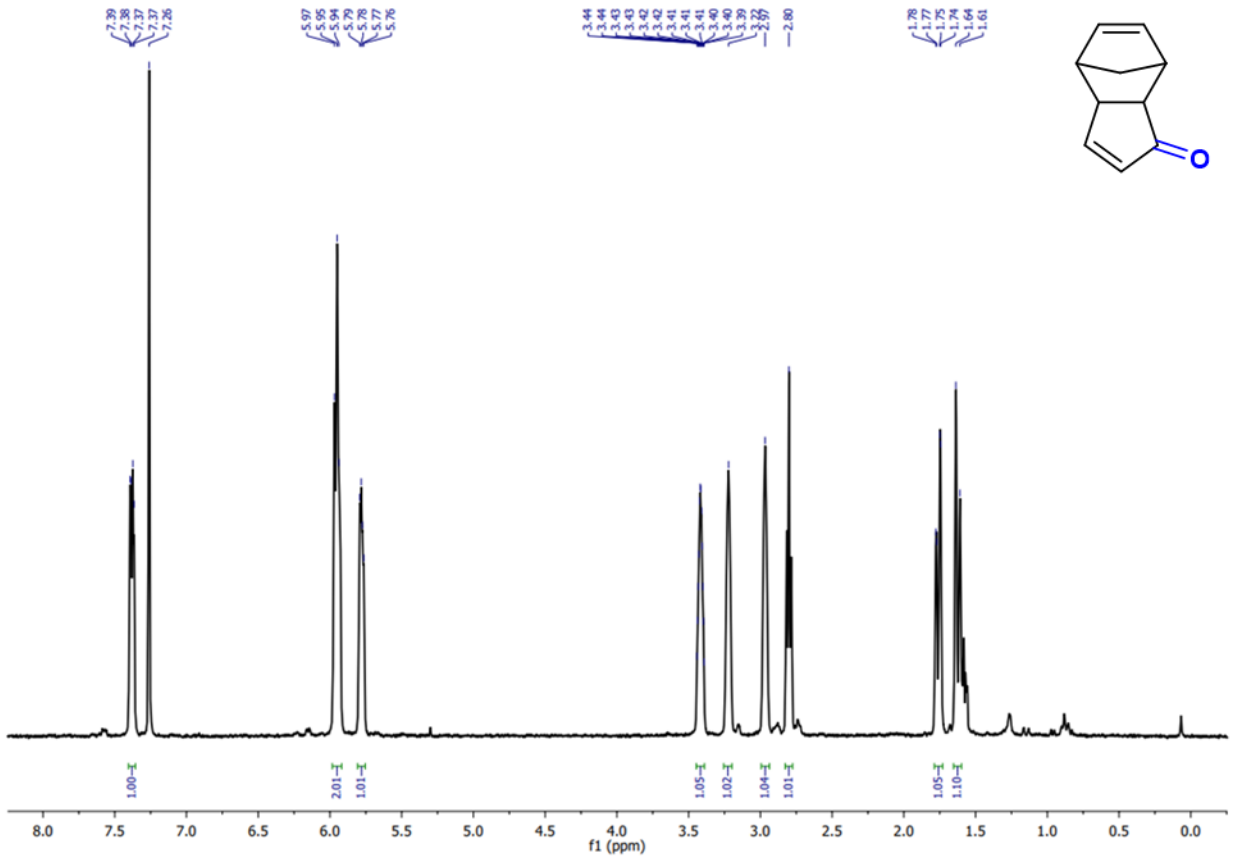

Figure B1. ^{1}H NMR spectrum for *endo*-dicyclopentadienone at 300.27 MHz in $CDCl_3$. Contains trace *exo*-dicyclopentadienone.

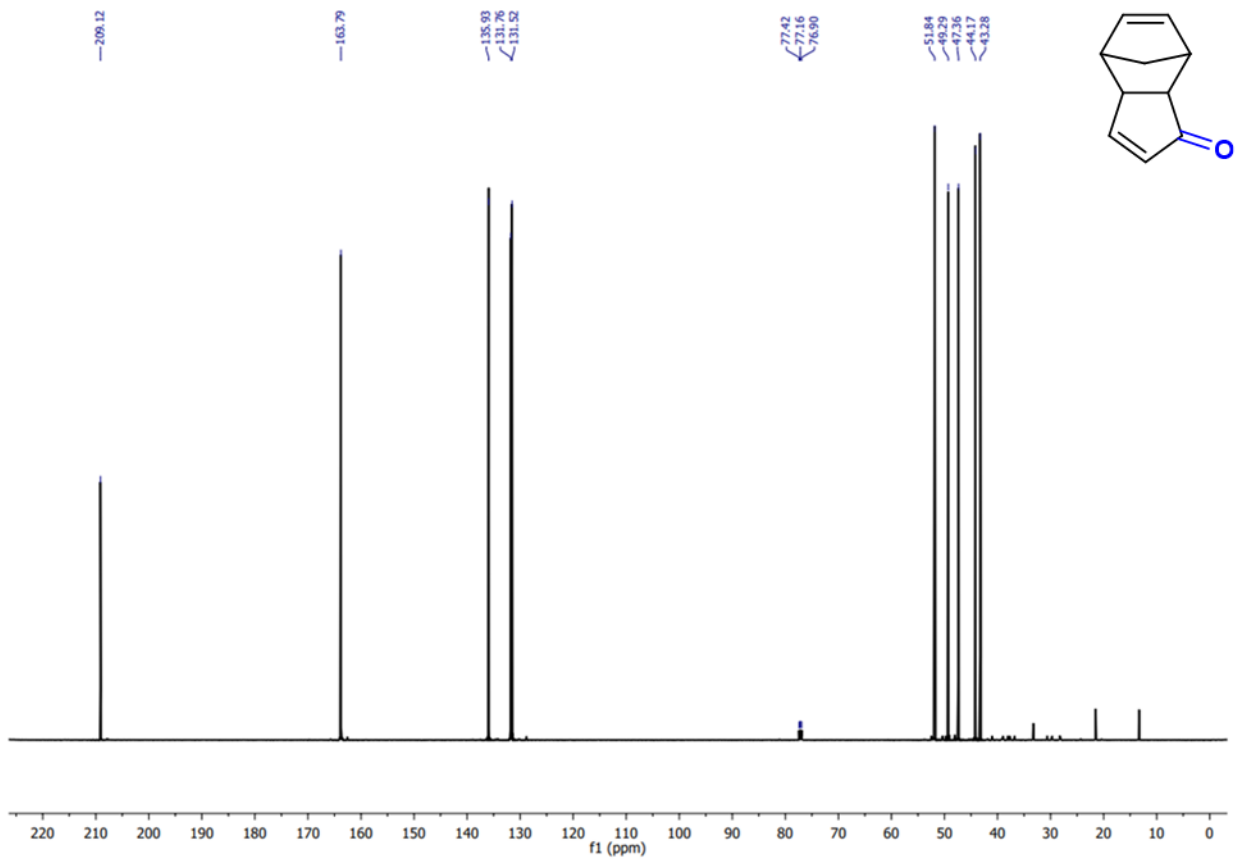

Figure B2. ^{13}C NMR spectrum for *endo*-dicyclopentadienone at 125.81 MHz in $CDCl_3$.

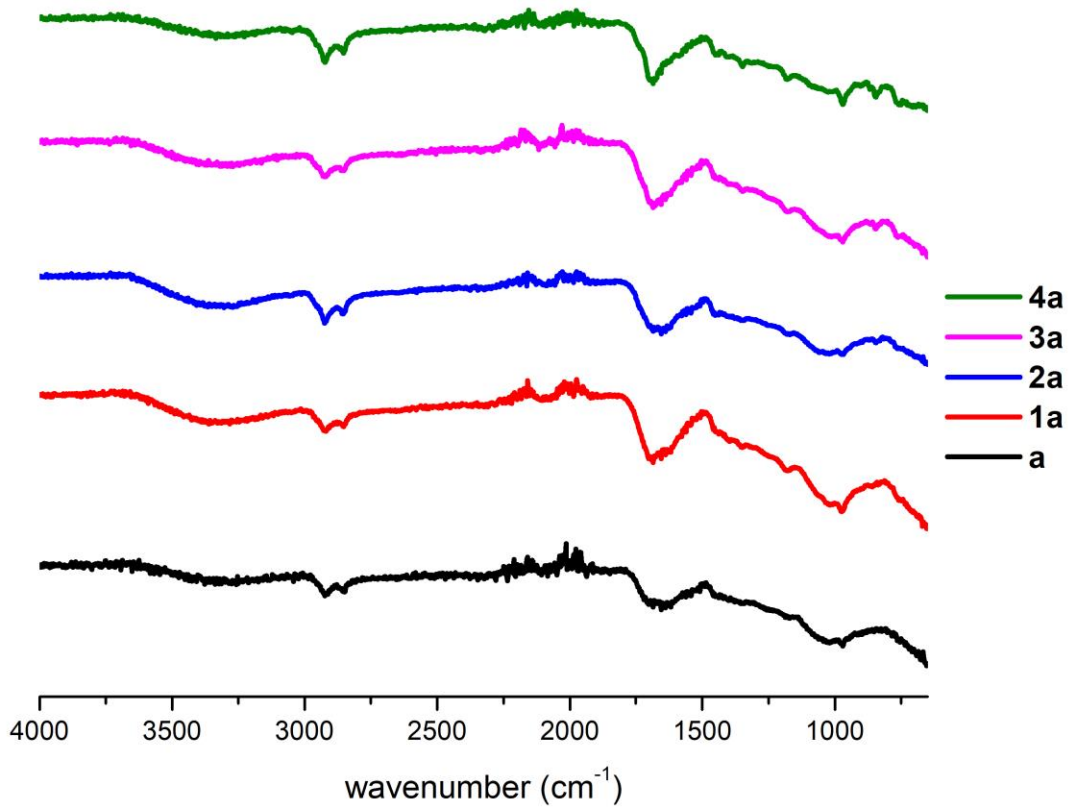

Figure B3. AT-IR spectrum of **a-type** polymer and copolymers after exposure to air for greater than 24 hours.

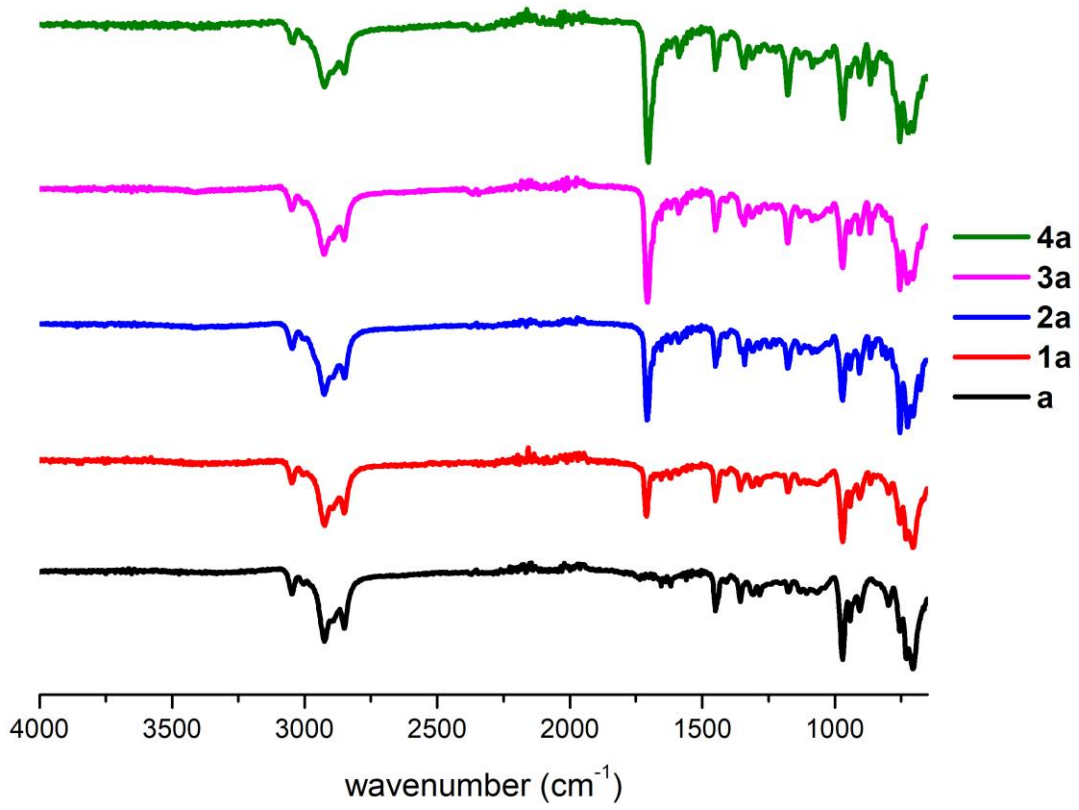

Figure B4. AT-IR spectrum of freshly exposed surface of **a-type** polymer and copolymers.

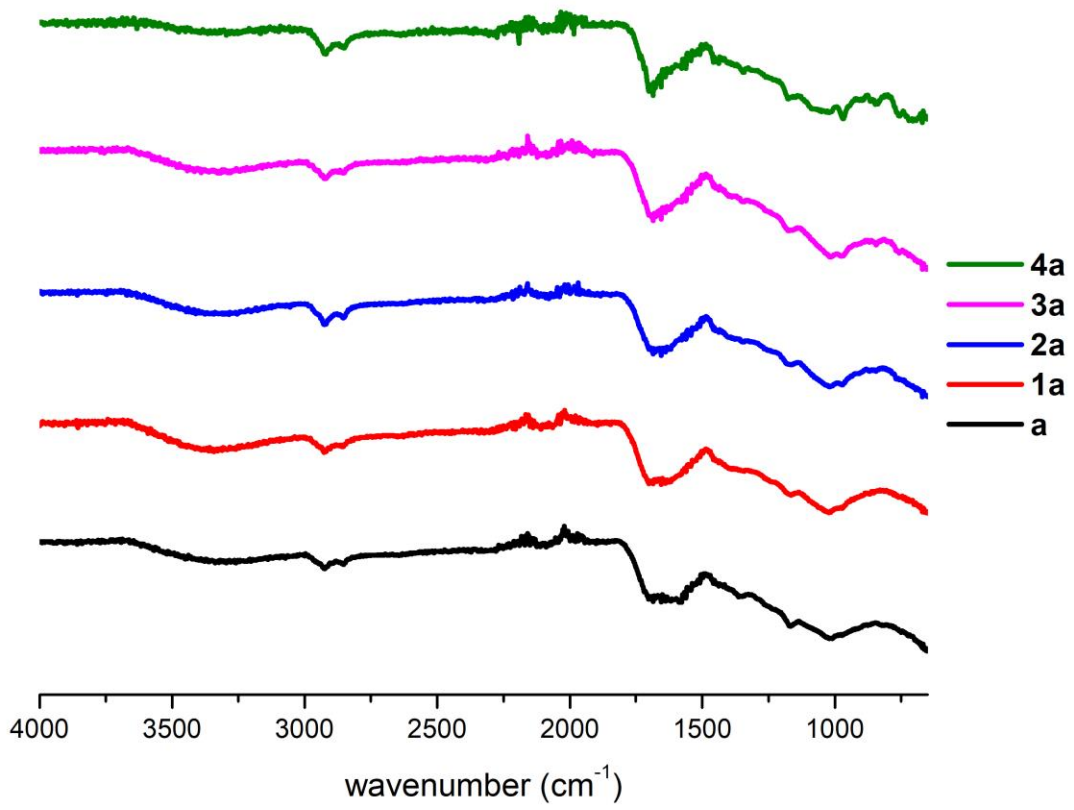

Figure B5. AT-IR spectrum of **a-type** polymer and copolymers after heating during DMTA.

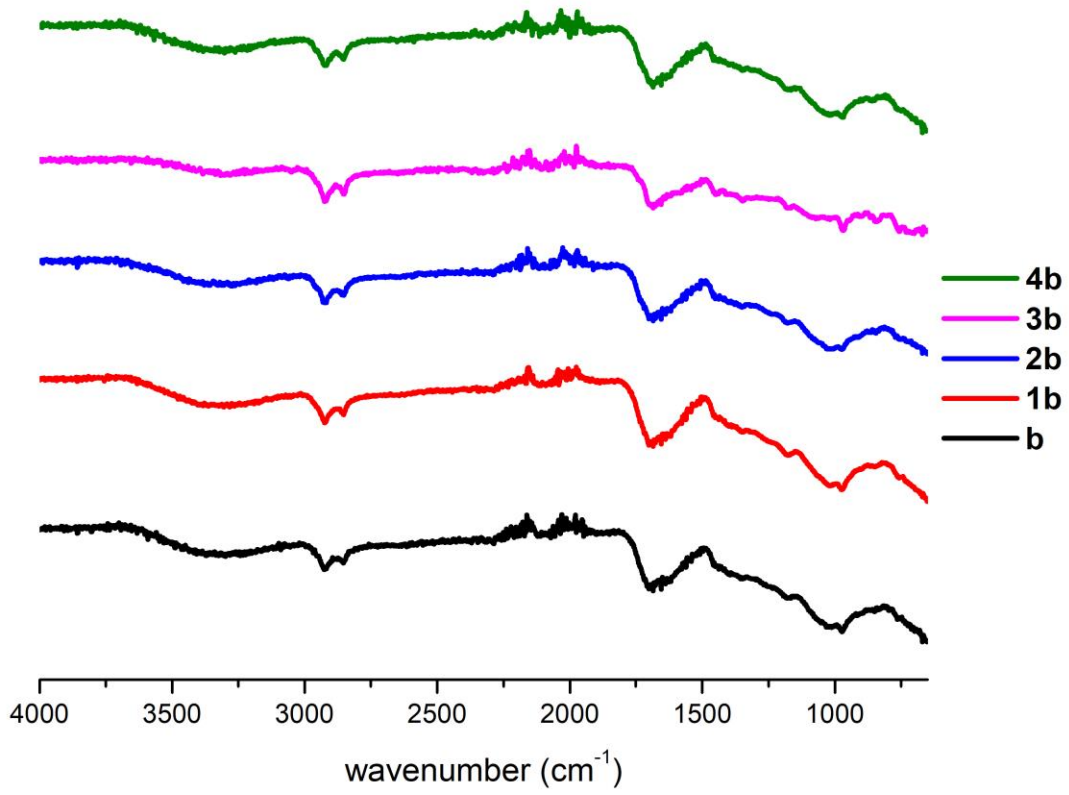

Figure B6. AT-IR spectrum of **b-type** copolymers after exposure to air for greater than 24 hours.

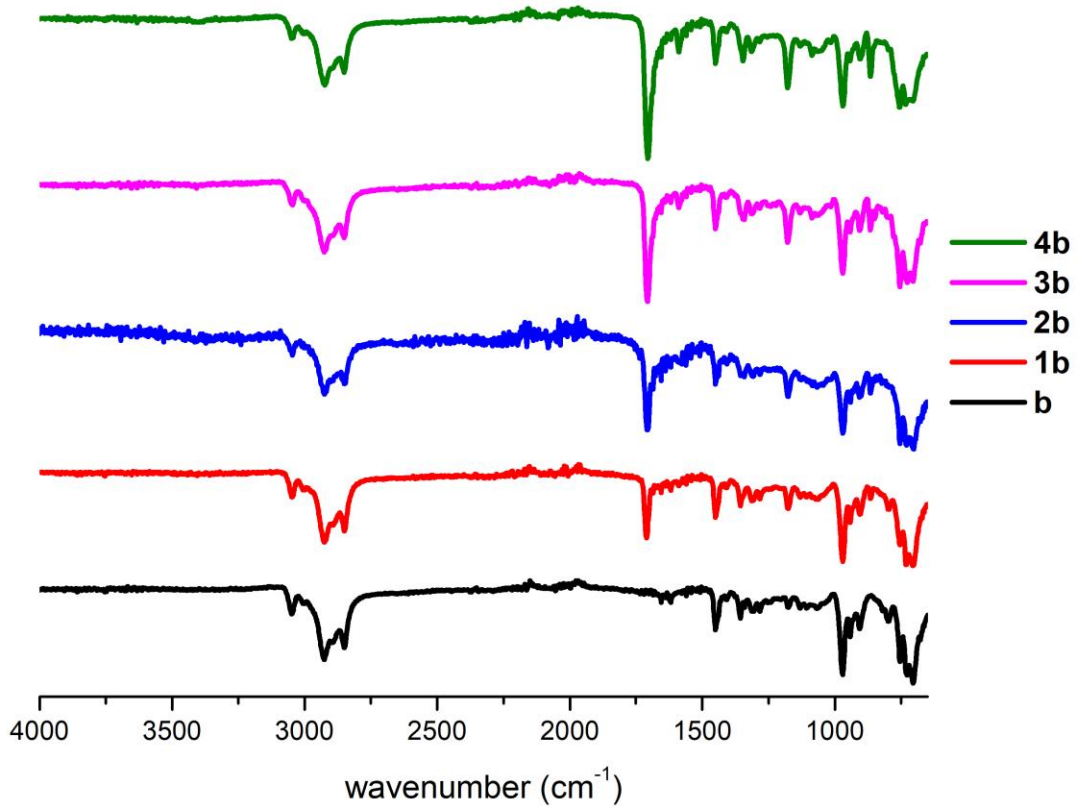

Figure B7. AT-IR spectrum of freshly exposed surface of **b-type** copolymers.

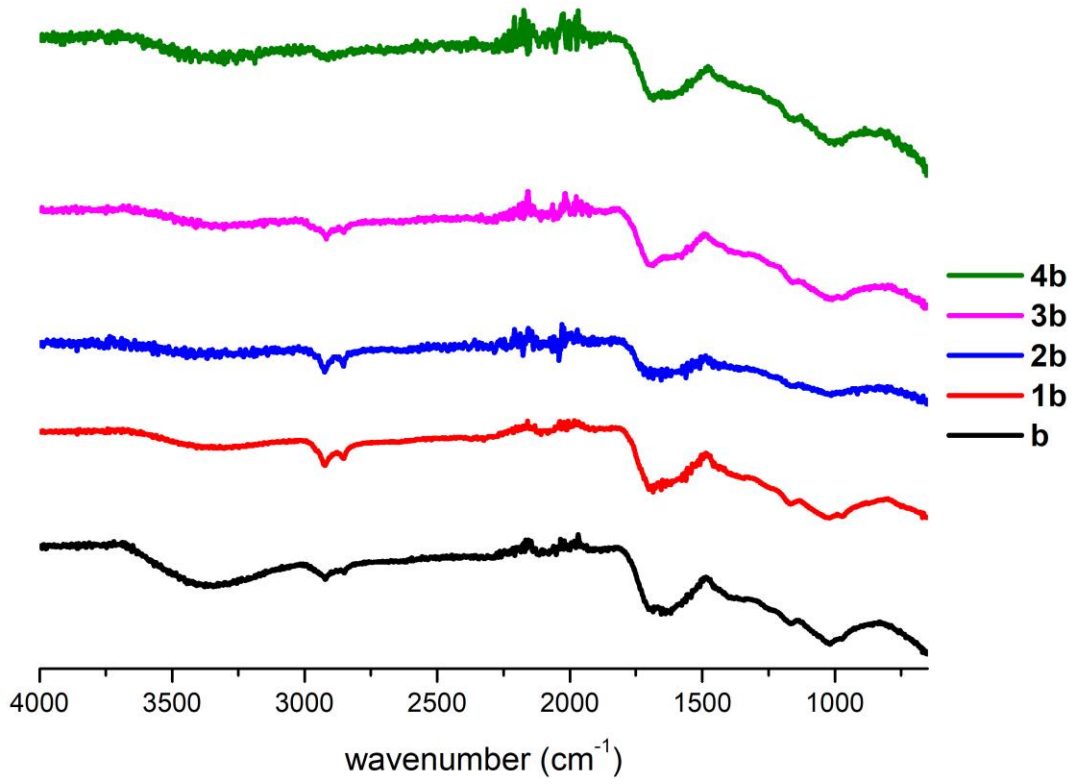

Figure B8. AT-IR spectrum of **b-type** copolymers after heating during DMTA.

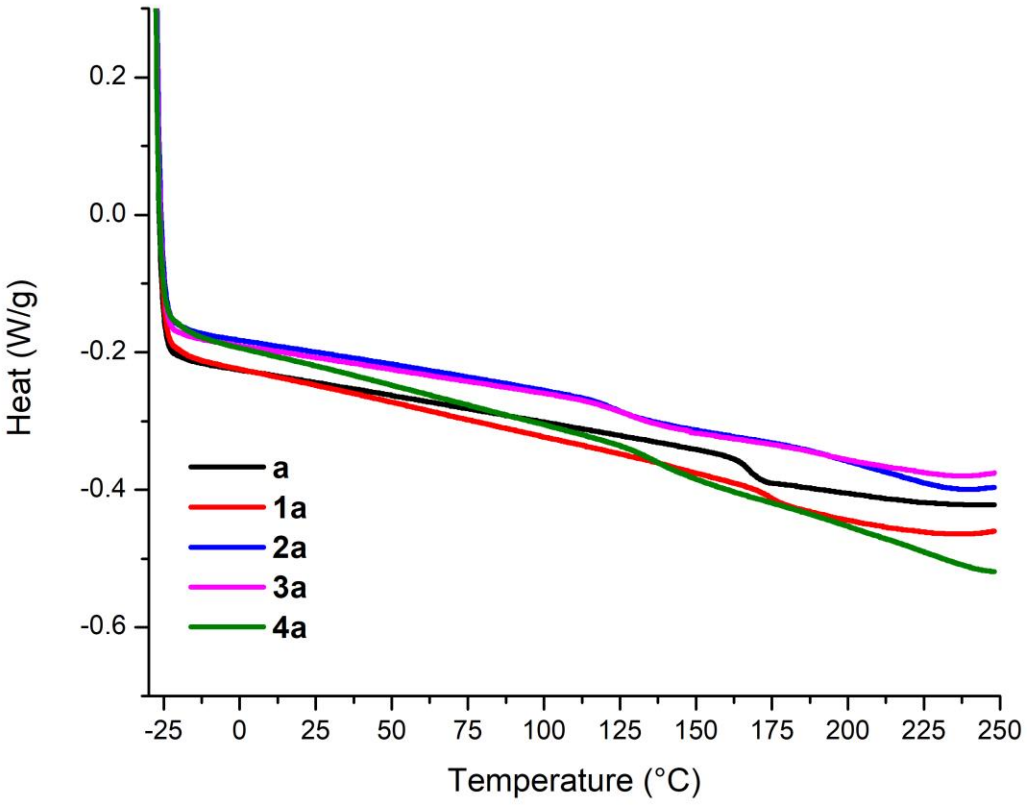

Figure B9. Differential scanning calorimetry heating traces of **a-type** polymer and copolymers from which glass transition temperatures were extracted.

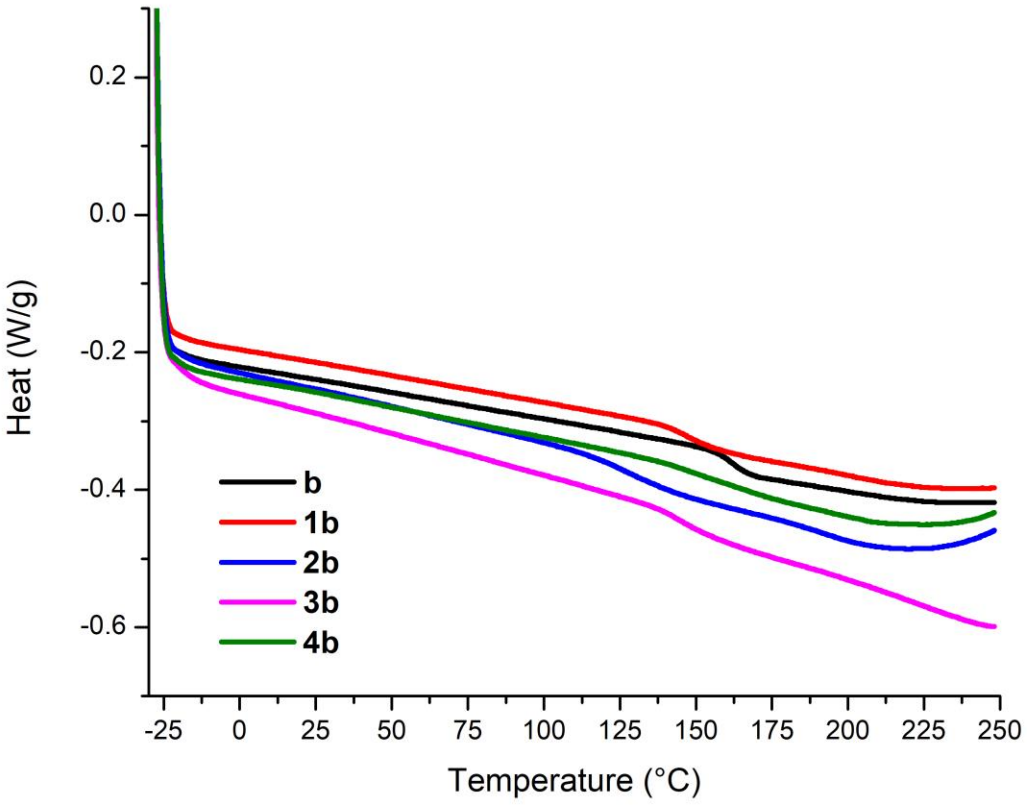

Figure B10. Differential scanning calorimetry heating traces of **b-type** copolymers from which glass transition temperatures were extracted.

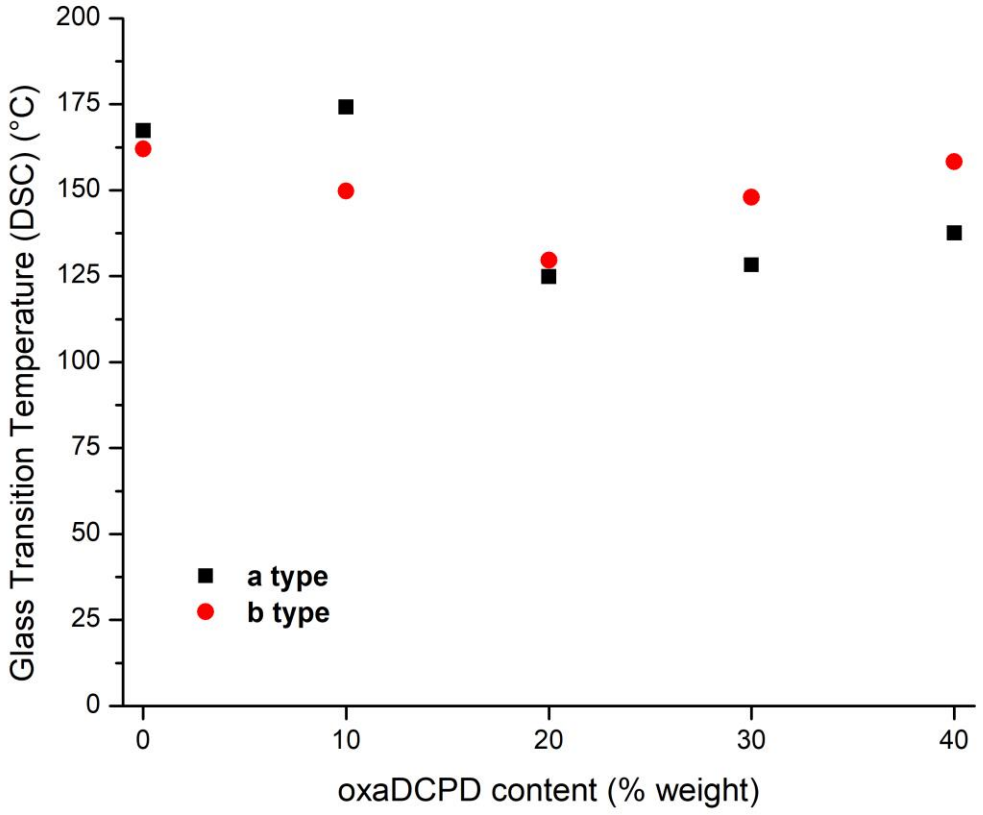

Figure B11. Glass transition temperatures as determined by differential scanning calorimetry of homopolymers and copolymers.

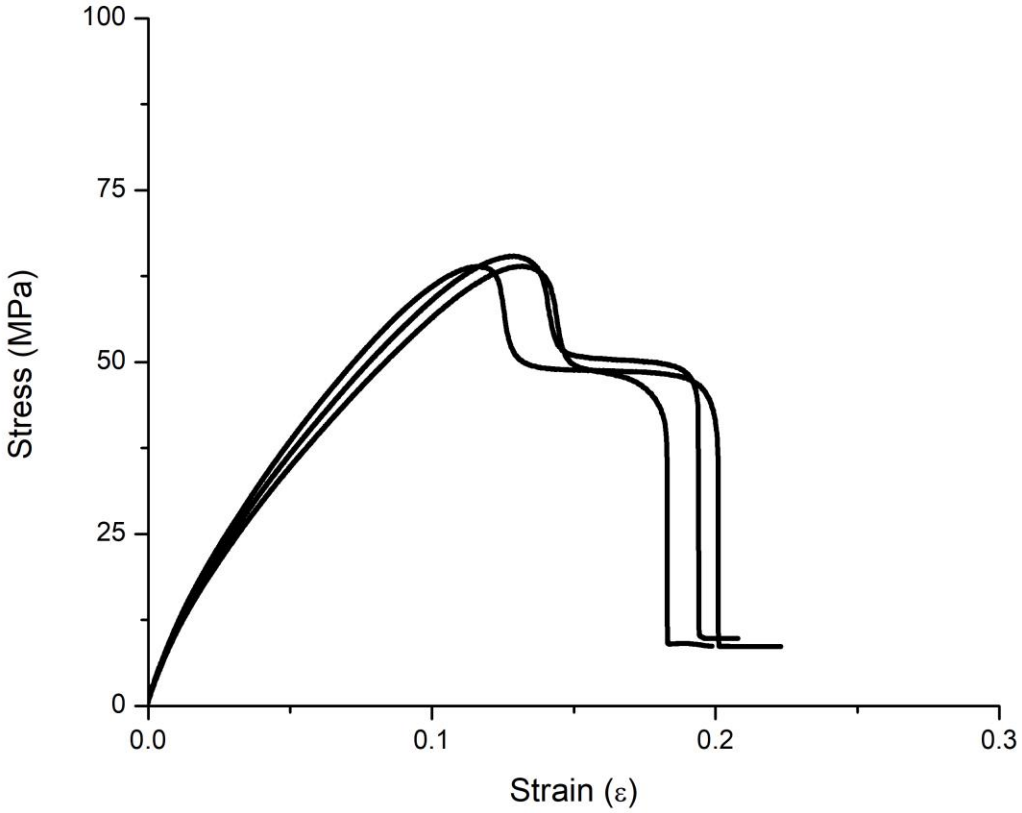

Figure B12. Stress-strain curves of **a-type** polymer.

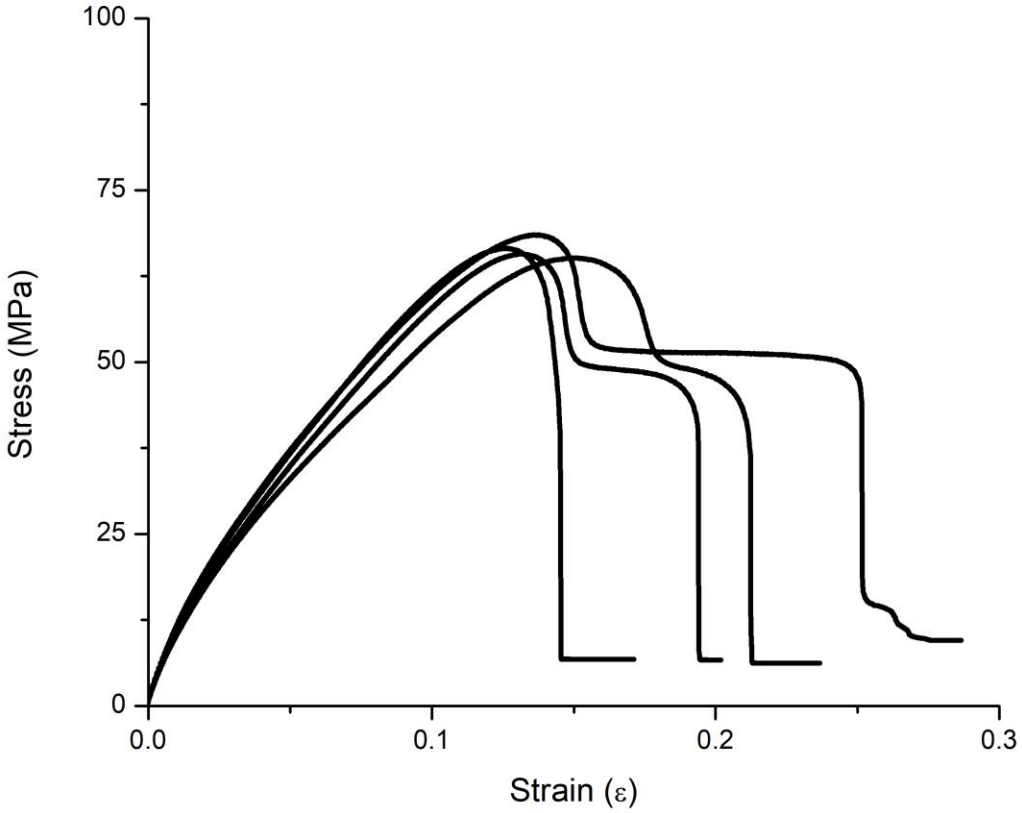

Figure B13. Stress-strain curves of **1a-type** copolymer.

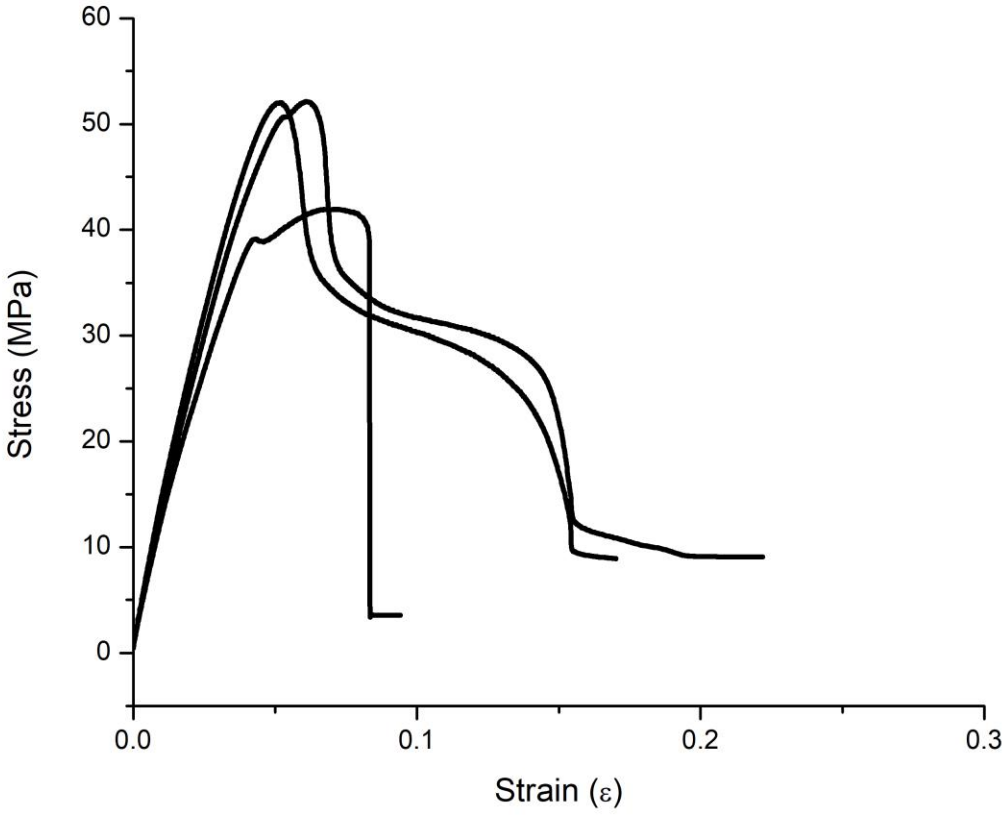

Figure B14. Stress-strain curves of **2a-type** copolymer.

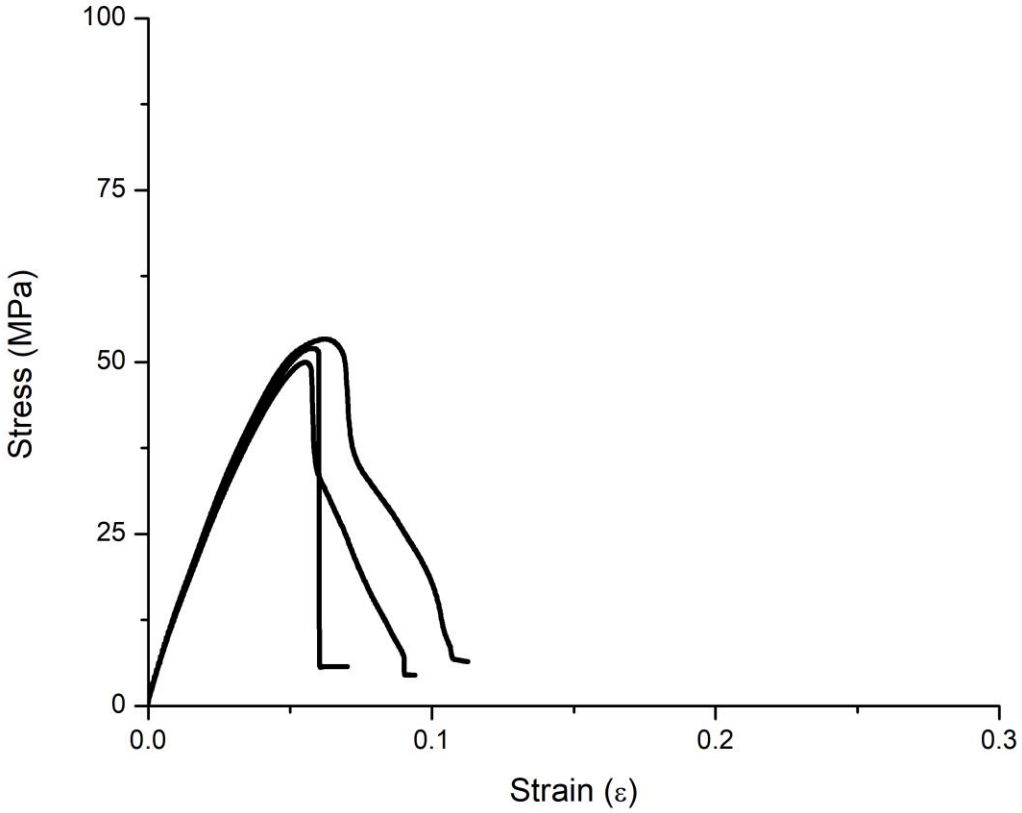

Figure B15. Stress-strain curves of **3a-type** copolymer.

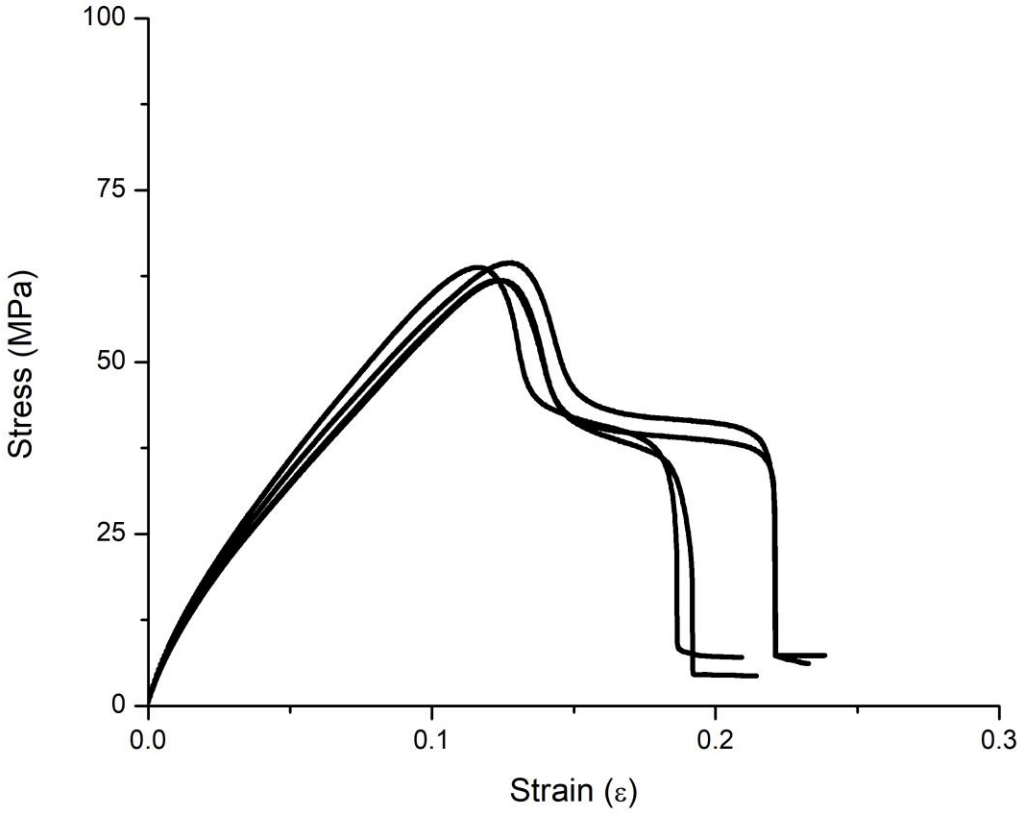

Figure B16. Stress-strain curves of **4a-type** copolymer.

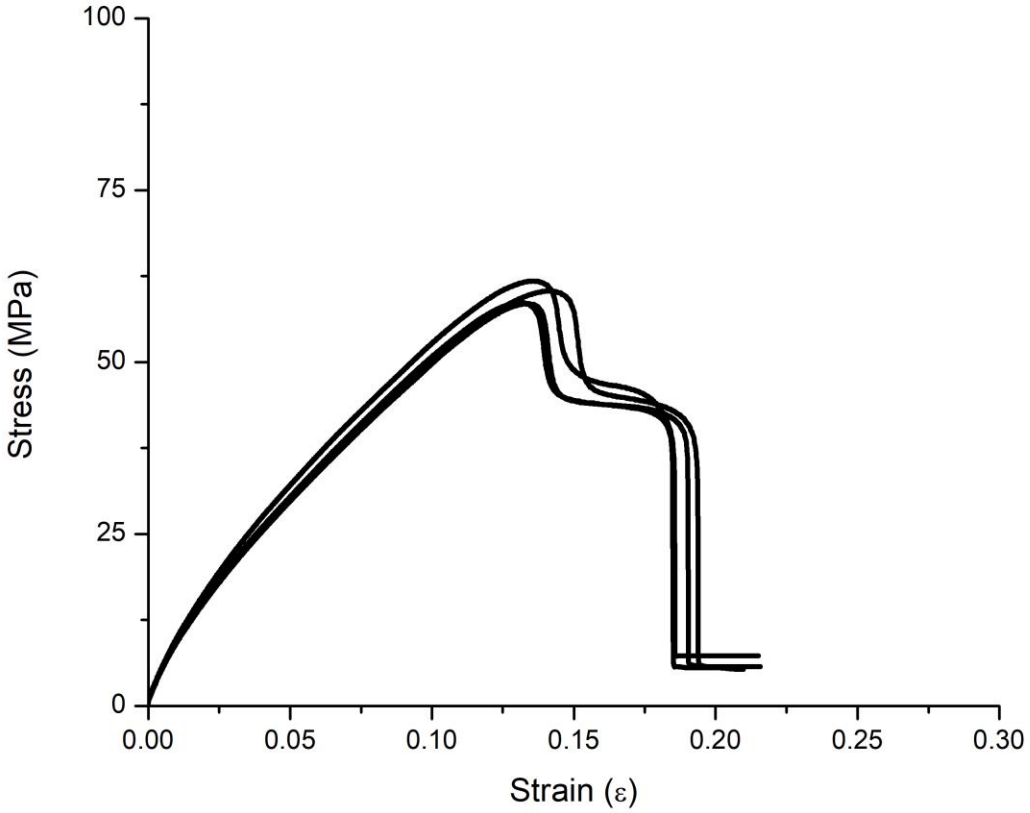

Figure B17. Stress-strain curves of **b-type** copolymer.

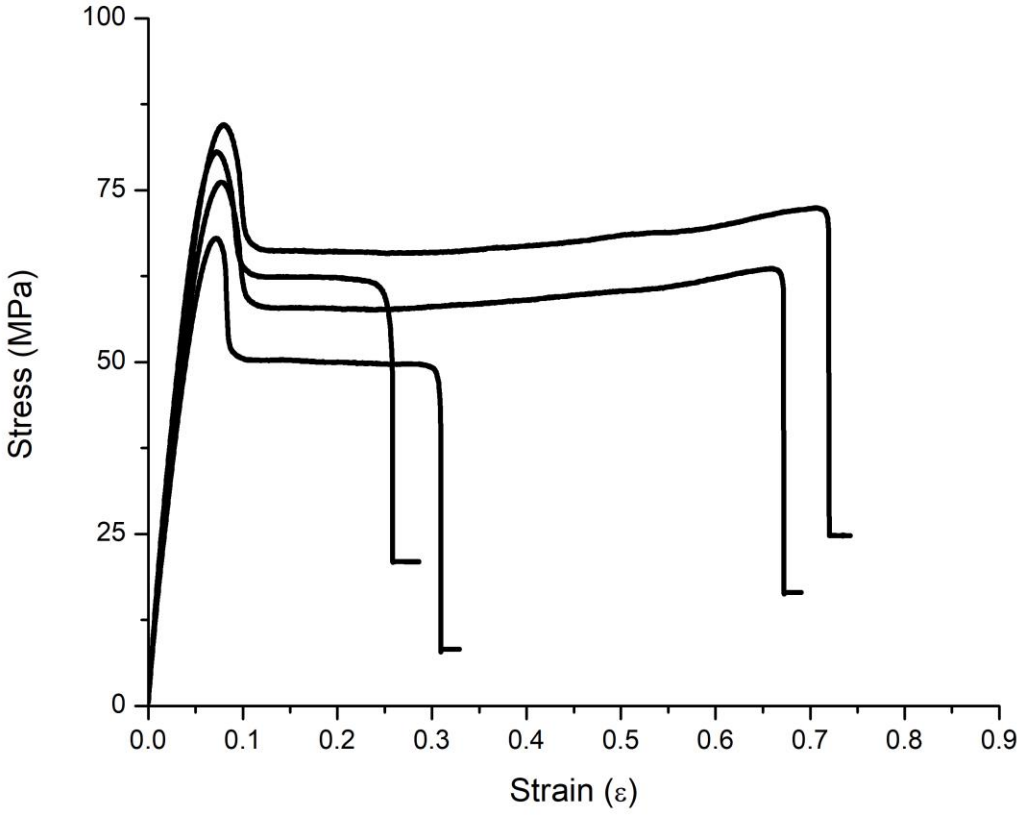

Figure B18. Stress-strain curves of **1b-type** copolymer.

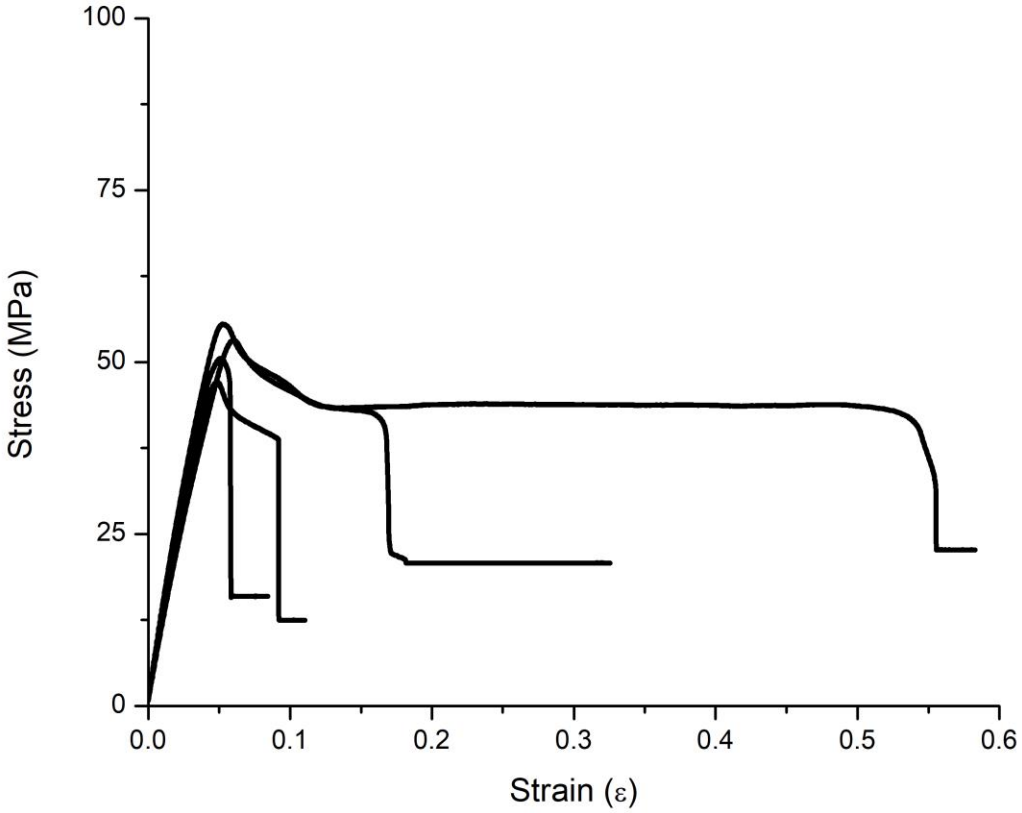

Figure B19. Stress-strain curves of **2b-type** copolymer.

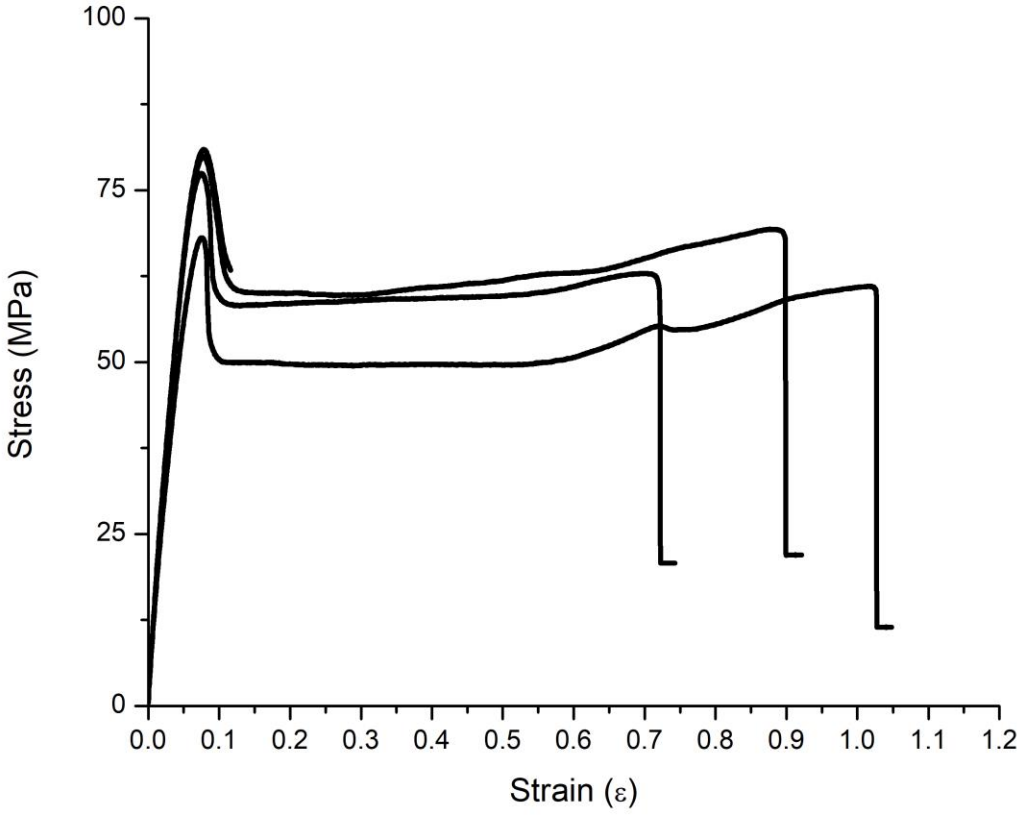

Figure B20. Stress-strain curves of **3b-type** copolymer.

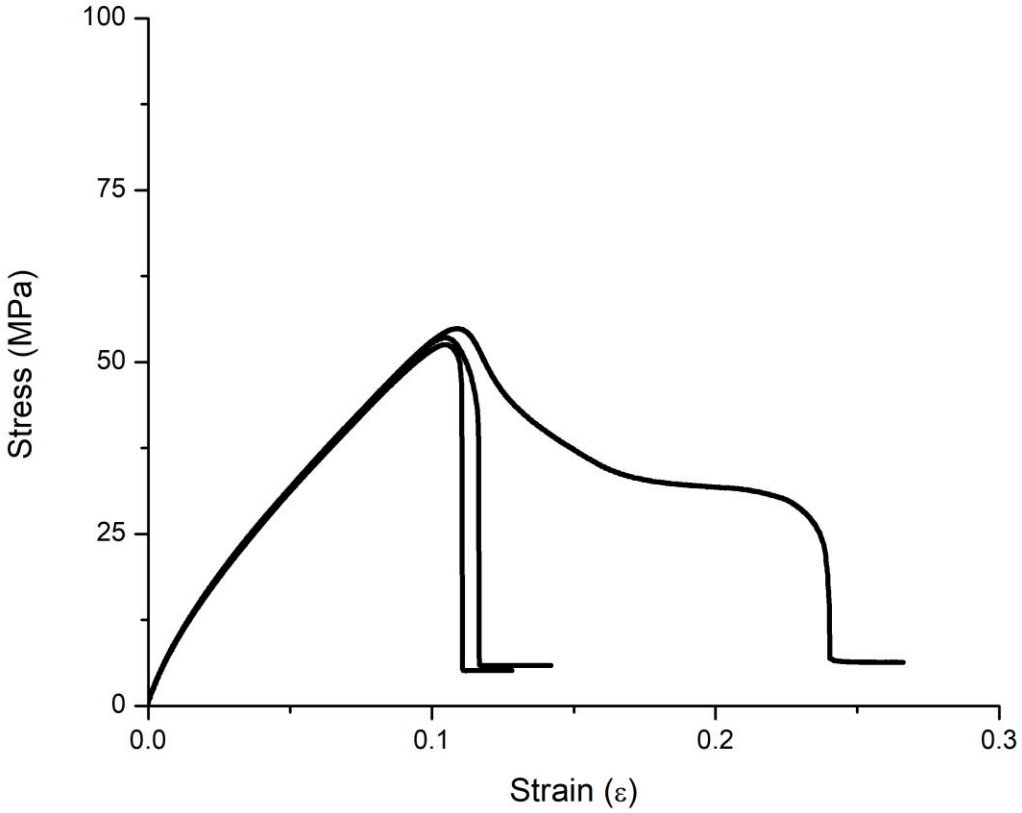

Figure B21. Stress-strain curves of **4b-type** copolymer.

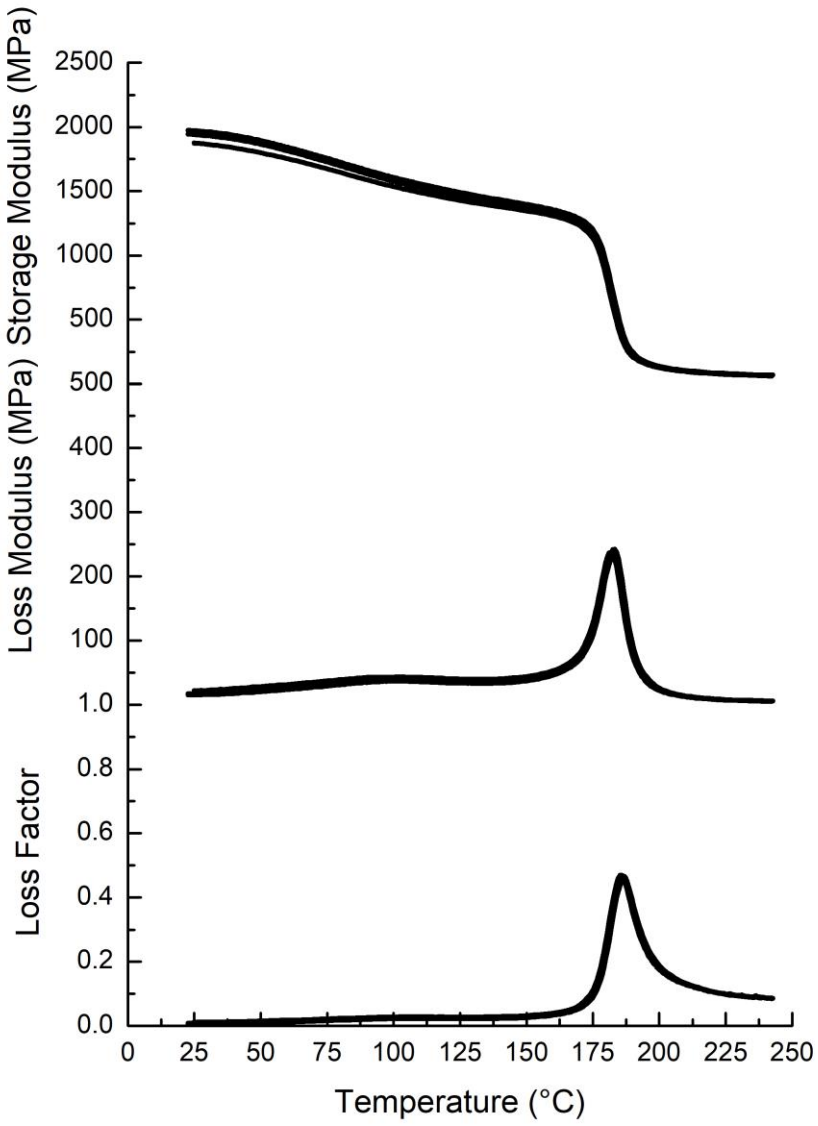

Figure B22. DMTA traces of reaction injection molded **a-type** polymer.

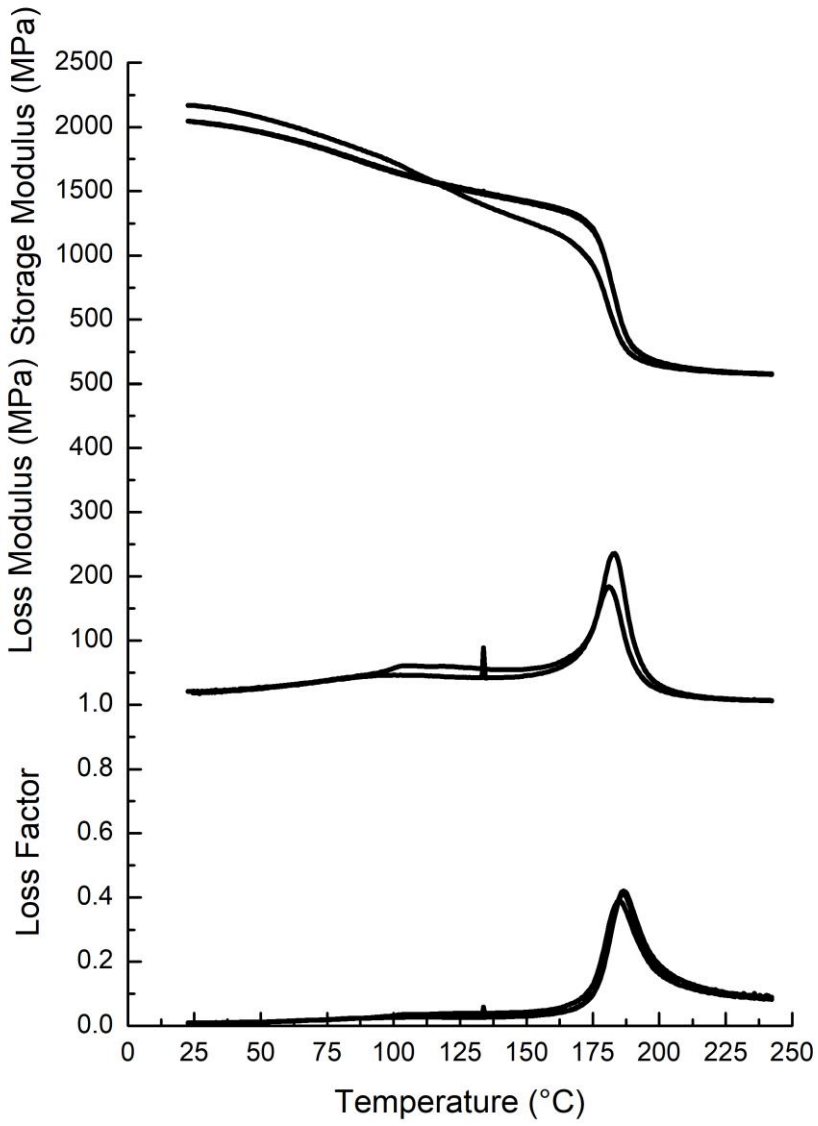

Figure B23. DMTA traces of reaction injection molded **1a-type** copolymer.

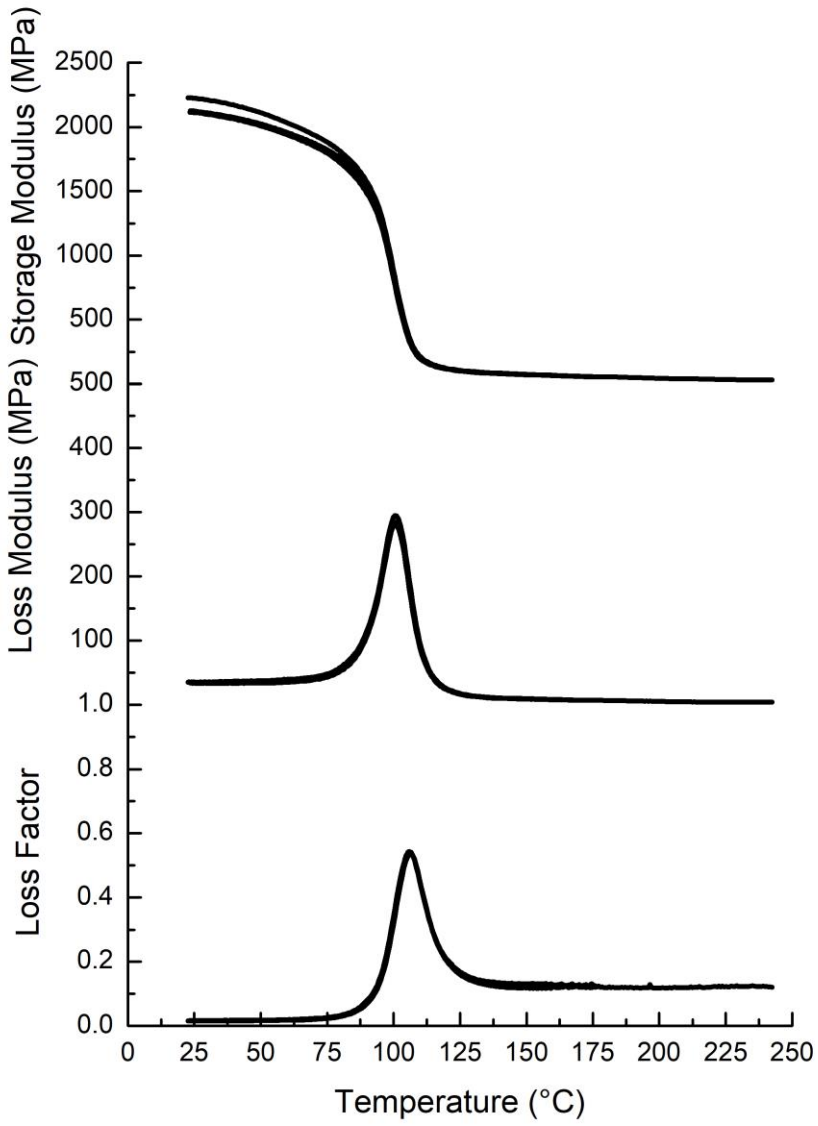

Figure B24. DMTA traces of reaction injection molded **2a-type** copolymer.

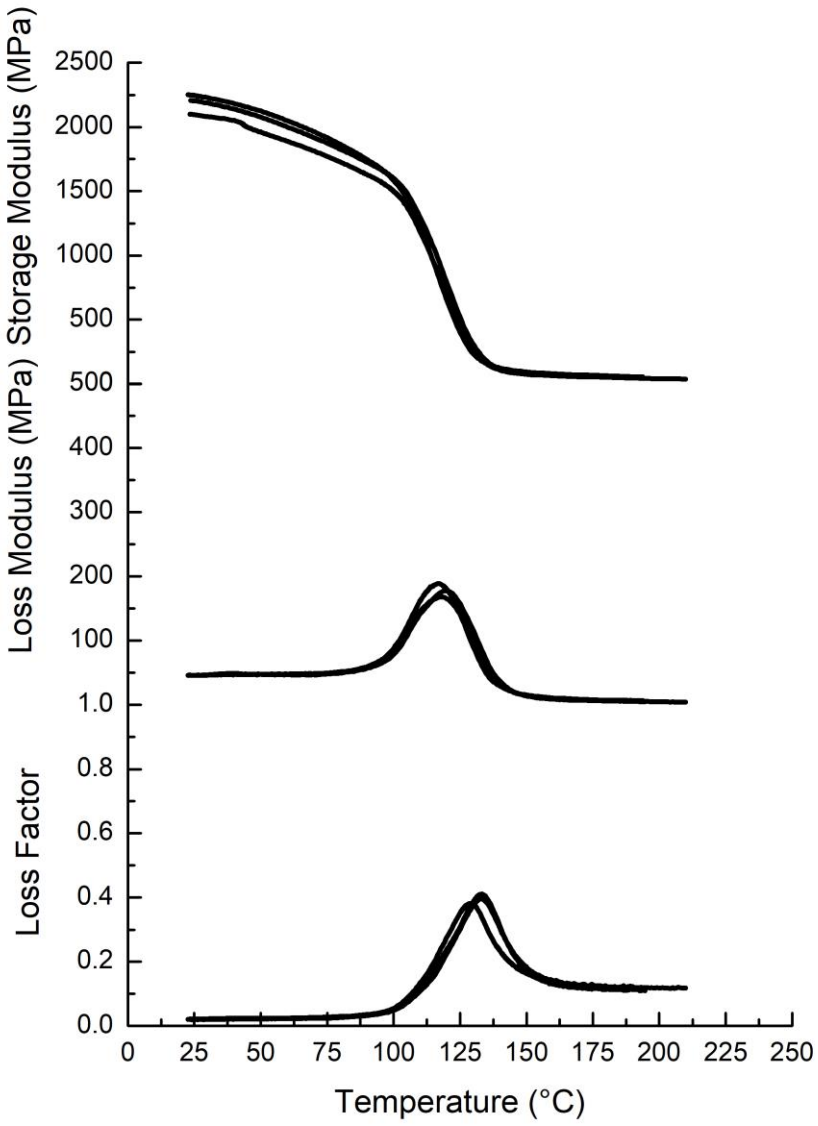

Figure B25. DMTA traces of reaction injection molded **3a-type** copolymer.

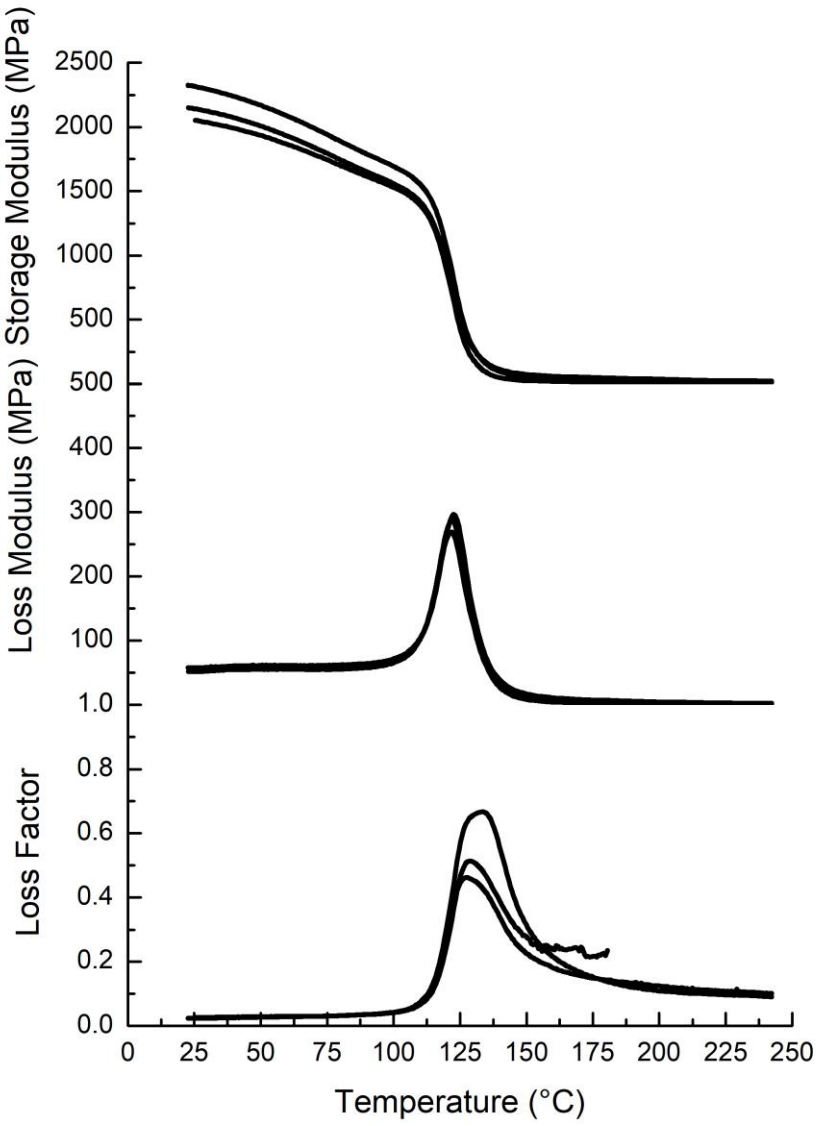

Figure B26. DMTA traces of reaction injection molded **4a-type** copolymer.

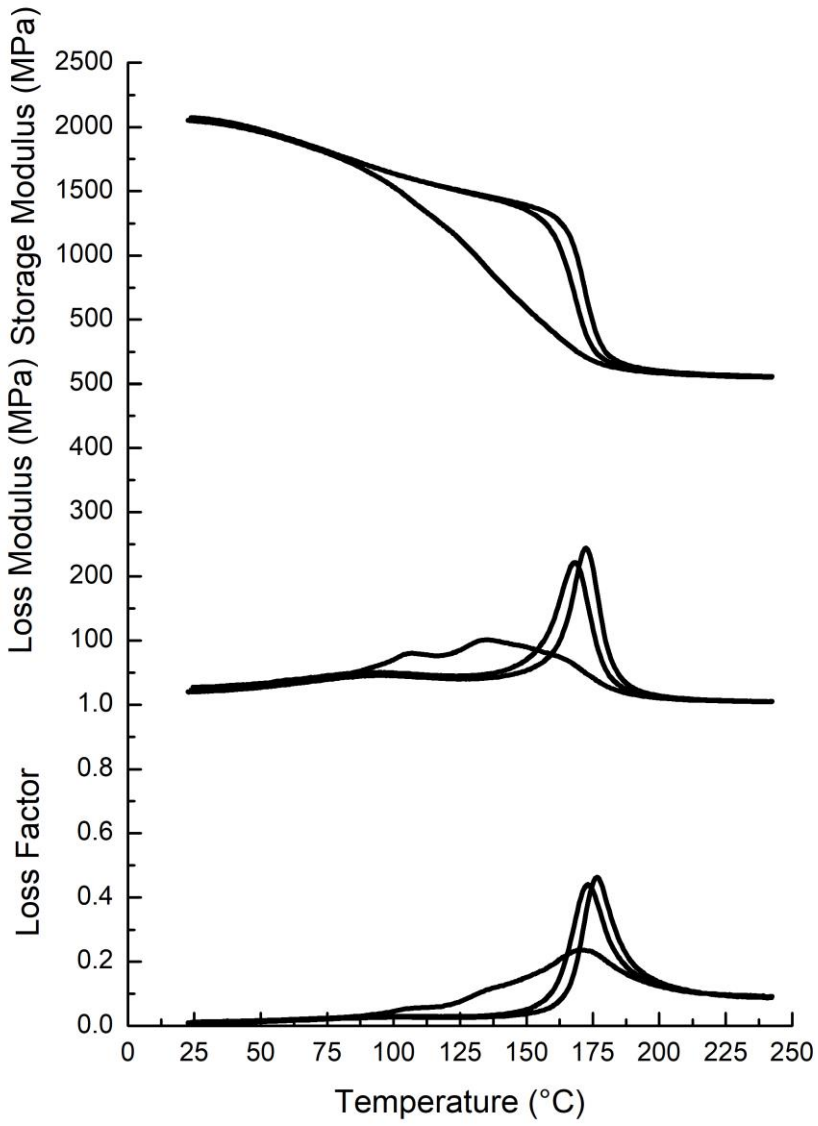

Figure B27. DMTA traces of reaction injection molded **b-type** copolymer.

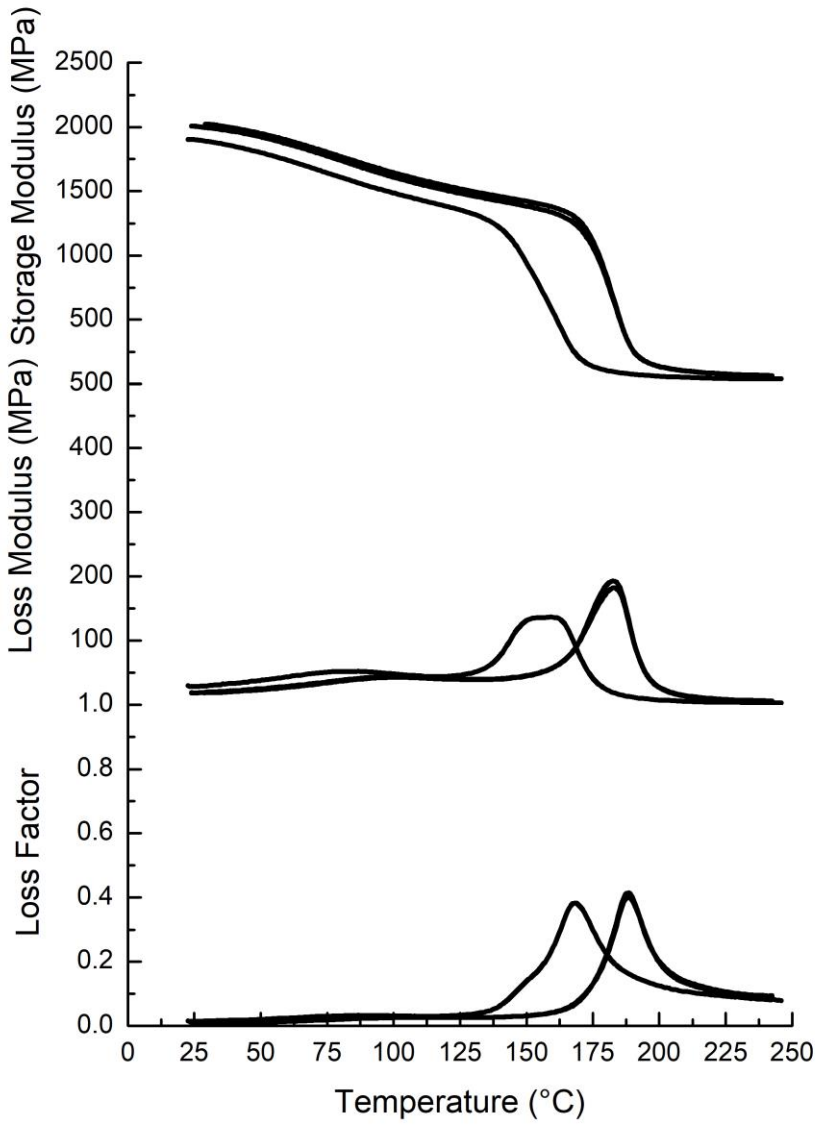

Figure B28. DMTA traces of reaction injection molded **1b-type** copolymer.

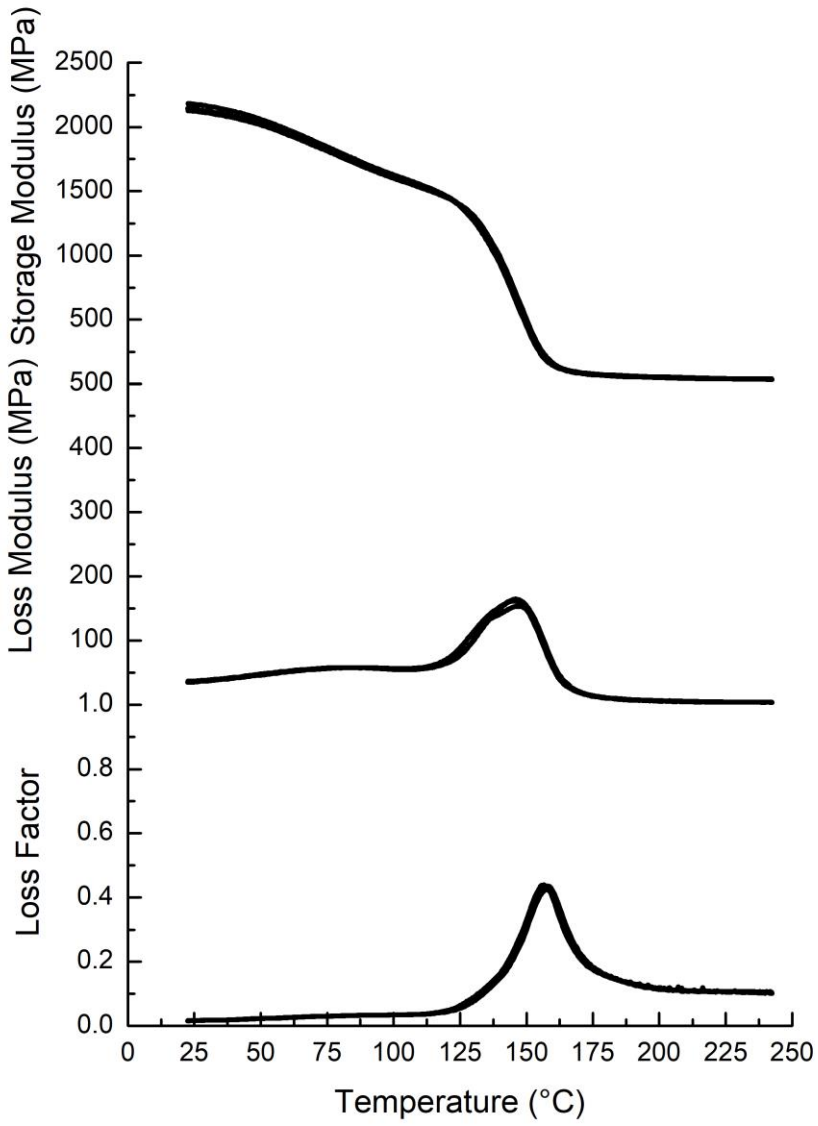

Figure B29. DMTA traces of reaction injection molded **2b-type** copolymer.

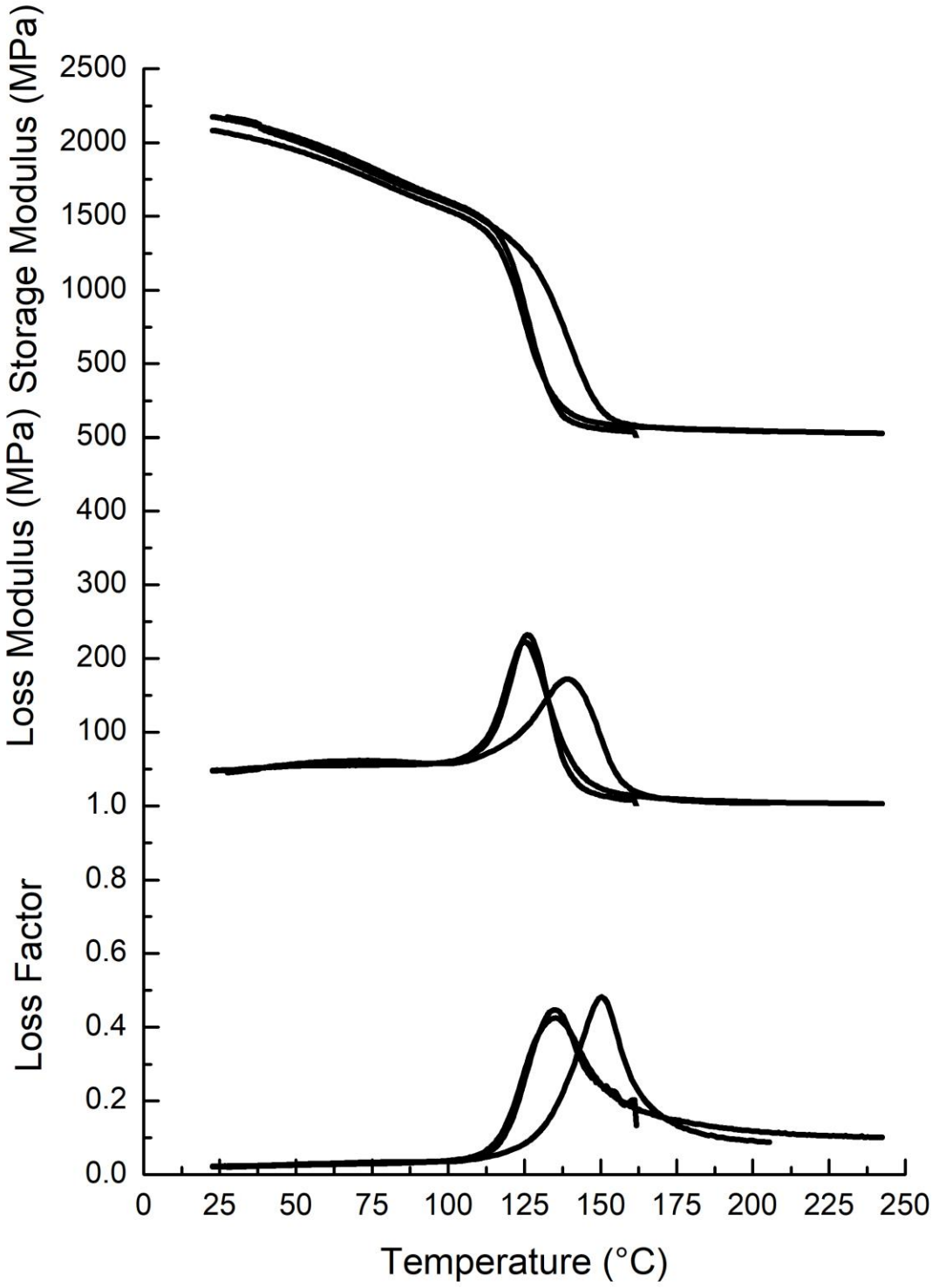

Figure B30. DMTA traces of reaction injection molded **3b-type** copolymer.

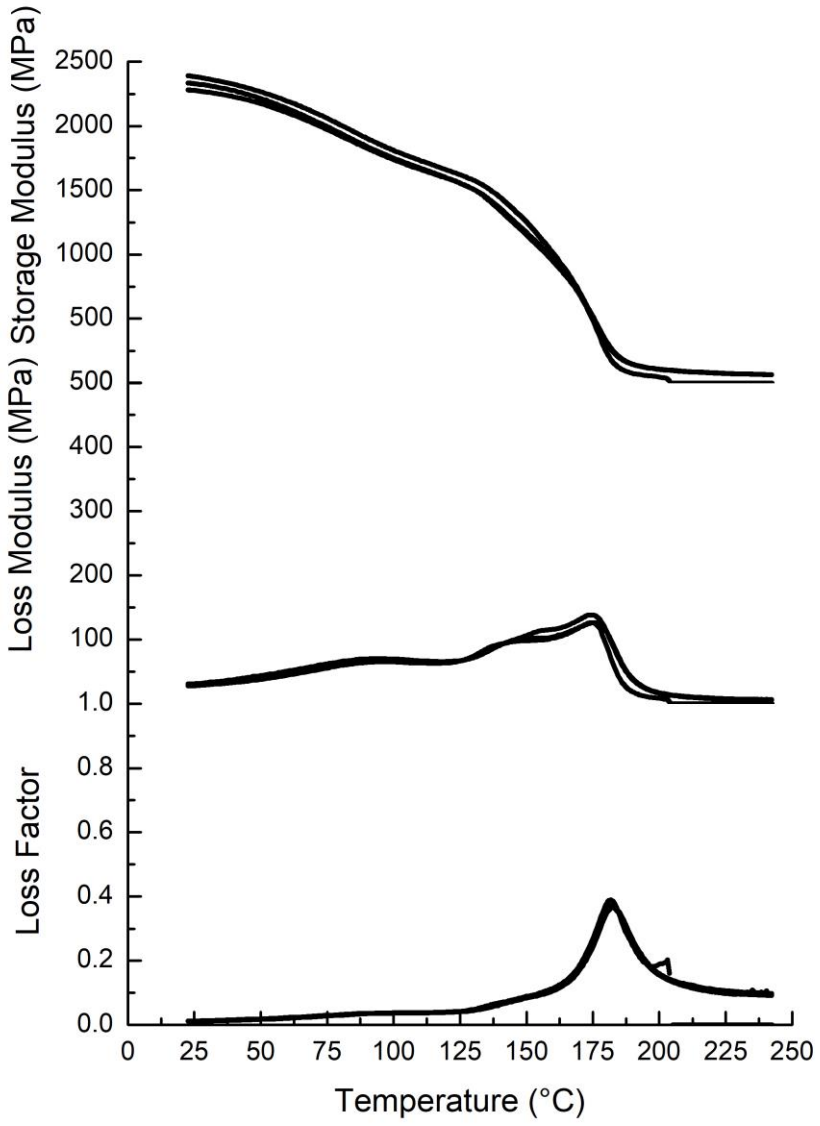

Figure B31. DMTA traces of reaction injection molded **4b-type** copolymer.

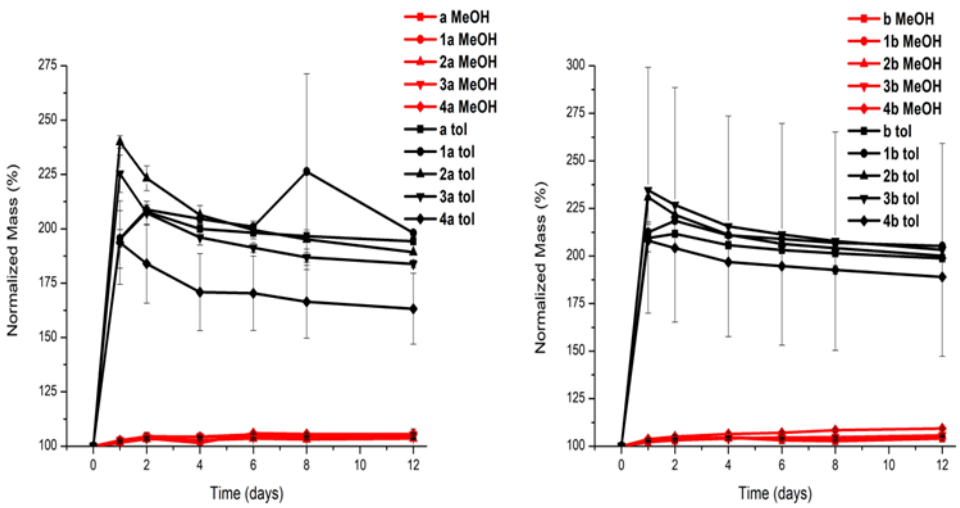

Figure B32. Swelling of **a** and **b** type polymers and copolymers in polar (methanol, black) and nonpolar (toluene, red) solvents.

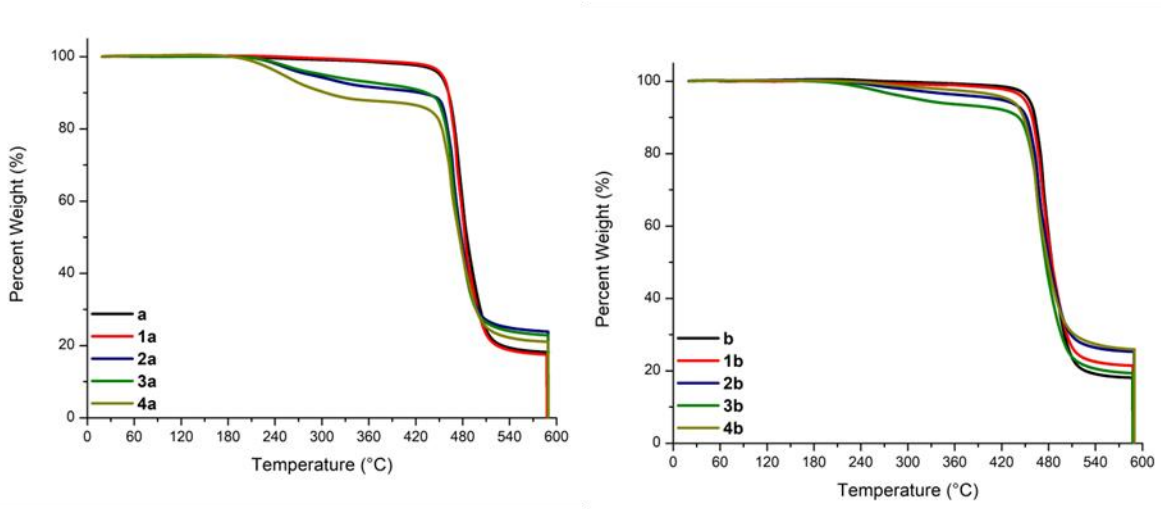

Figure B33. Thermogravimetric analysis of copolymers. Complete mass loss starts at approximately 450 °C.

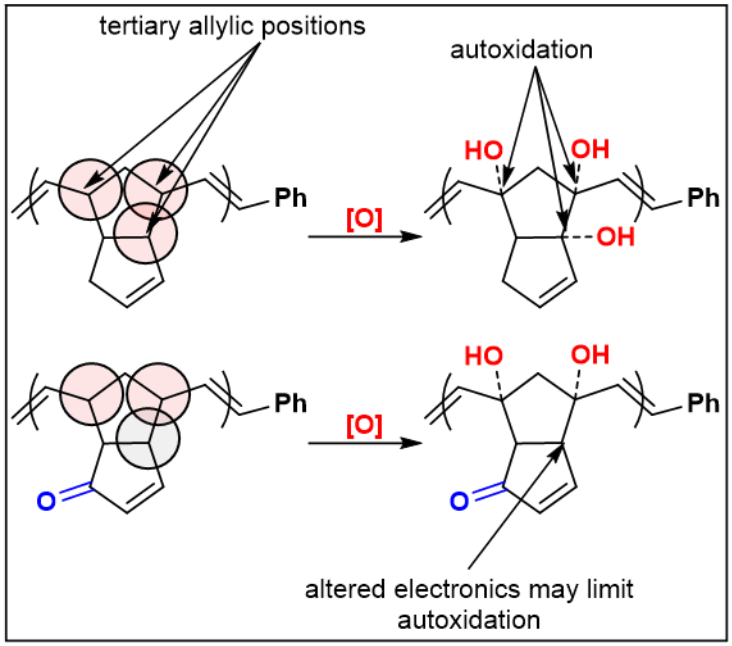

Figure B34. Proposed mechanism of autoxidative resistance.

Table B1. Summary of thermal properties, and densities of polymers and copolymers.

Material	Glass Transition Temperature (DMTA, °C)	Glass Transition Temperature (DSC, °C)	Density
a	186.1 ± 0.8	167.28	1.07 ± 0.005
1a	186.0 ± 0.8	174.12	1.08 ± 0.003
2a	106.1 ± 0.4	124.84	1.10 ± 0.001
3a	131.4 ± 2.5	128.26	1.12 ± 0.016
4a	129.7 ± 3.1	137.59	1.12 ± 0.012
b	173.4 ± 3.0	161.96	1.06 ± 0.007
1b	181.8 ± 11.7	149.76	1.09 ± 0.015
2b	157.4 ± 0.7	129.56	1.11 ± 0.003
3b	140.0 ± 8.9	147.91	1.11 ± 0.008
4b	182.1 ± 0.4	158.27	1.11 ± 0.001

Table B2. Summary of mechanical properties of polymers and copolymers.

Material	Tensile Strength (Mpa)	Strain at Break (%)	Toughness (MPa)	Young's Modulus (GPa)	Storage Modulus (MPa)	Loss Modulus
a	64.4 ± 0.8	0.19 ± 0.01	8.5 ± 0.5	0.99 ± 0.05	1929.8 ± 49.3	18.4 ± 3.2
1a	66.5 ± 1.5	0.20 ± 0.04	9.1 ± 2.4	0.97 ± 0.05	2082.6 ± 72.9	19.5 ± 1.3
2a	48.7 ± 5.8	0.13 ± 0.04	4.1 ± 1.3	1.27 ± 0.1	2153.8 ± 78.5	34.6 ± 0.8
3a	51.8 ± 1.7	0.08 ± 0.02	2.6 ± 0.8	1.29 ± 0.03	2180.7 ± 78.5	46.1 ± 0.2
4a	63.0 ± 1.3	0.21 ± 0.02	8.2 ± 0.8	0.91 ± 0.04	2170.8 ± 132.8	54.7 ± 2.9
b	59.8 ± 1.6	0.19 ± 0	7.3 ± 0.3	0.83 ± 0.03	2058.7 ± 13.1	23.6 ± 3.5
1b	77.3 ± 7.0	0.49 ± 0.2	29.3 ± 16.7	1.62 ± 0.1	1975.9 ± 65.9	22.4 ± 5.6
2b	51.6 ± 3.6	0.22 0.2	8.9 ± 9.9	1.29 ± 0.1	2146.8 ± 27.8	36.3 ± 1.0
3b	76.6 ± 5.9	0.69 ± 0.4	39.6 ± 22.7	1.54 ± 0.08	2137.9 ± 54.2	47.1 ± 1.8
4b	53.7 ± 1.2	0.16 ± 0.07	5.2 ± 2.6	0.84 ± 0.01	2330.4 ± 76.9	30.2 ± 1.5

Appendix C: Supplemental Spectra, Plots, Figures and Tables for Chapter 4

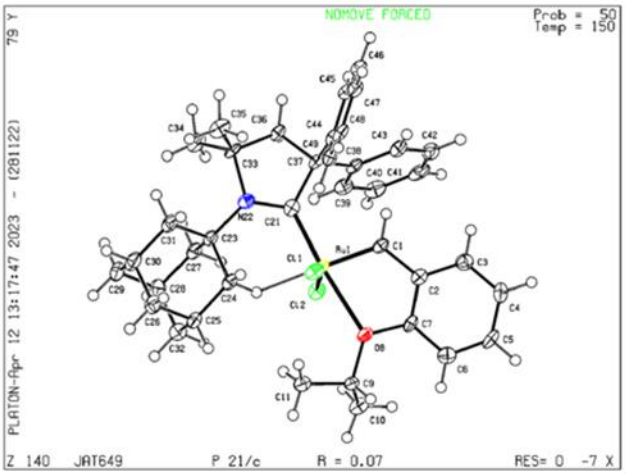

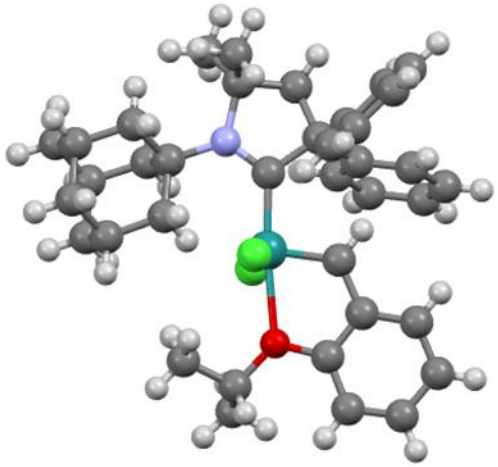

Bond precision:	C-C = 0.0106 A	Wavelength=0.71073	
Cell:	a=10.0164(10)	b=16.4772(17)	c=19.363(2)
	alpha=90	beta=98.413(4)	gamma=90
Temperature:	150 K		

	Calculated	Reported
Volume	3161.3(6)	3161.4(6)
Space group	P 21/c	P 21/c
Hall group	-P 2ybc	-P 2ybc
Moiety formula	C38 H45 Cl2 N O Ru	C38 H45 Cl2 N O Ru
Sum formula	C38 H45 Cl2 N O Ru	C38 H45 Cl2 N O Ru
Mr	703.72	703.72
Dx,g cm-3	1.479	1.479
Z	4	4
Mu (mm-1)	0.698	0.698
F000	1464.0	1464.0
F000'	1460.56	
h,k,lmax	13,21,25	12,21,25
Nref	7255	7260
Tmin,Tmax	0.897,0.959	0.740,0.959
Tmin'	0.840	

Correction method= # Reported T Limits: Tmin=0.740 Tmax=0.959
AbsCorr = MULTI-SCAN

Data completeness= 1.001 Theta(max)= 27.499

R(reflections)= 0.0723(6064) wR2(reflections)= 0.2167(7260)

S = 1.094 Npar= 393

Figure C1. X-ray crystal structure of complex **4**.

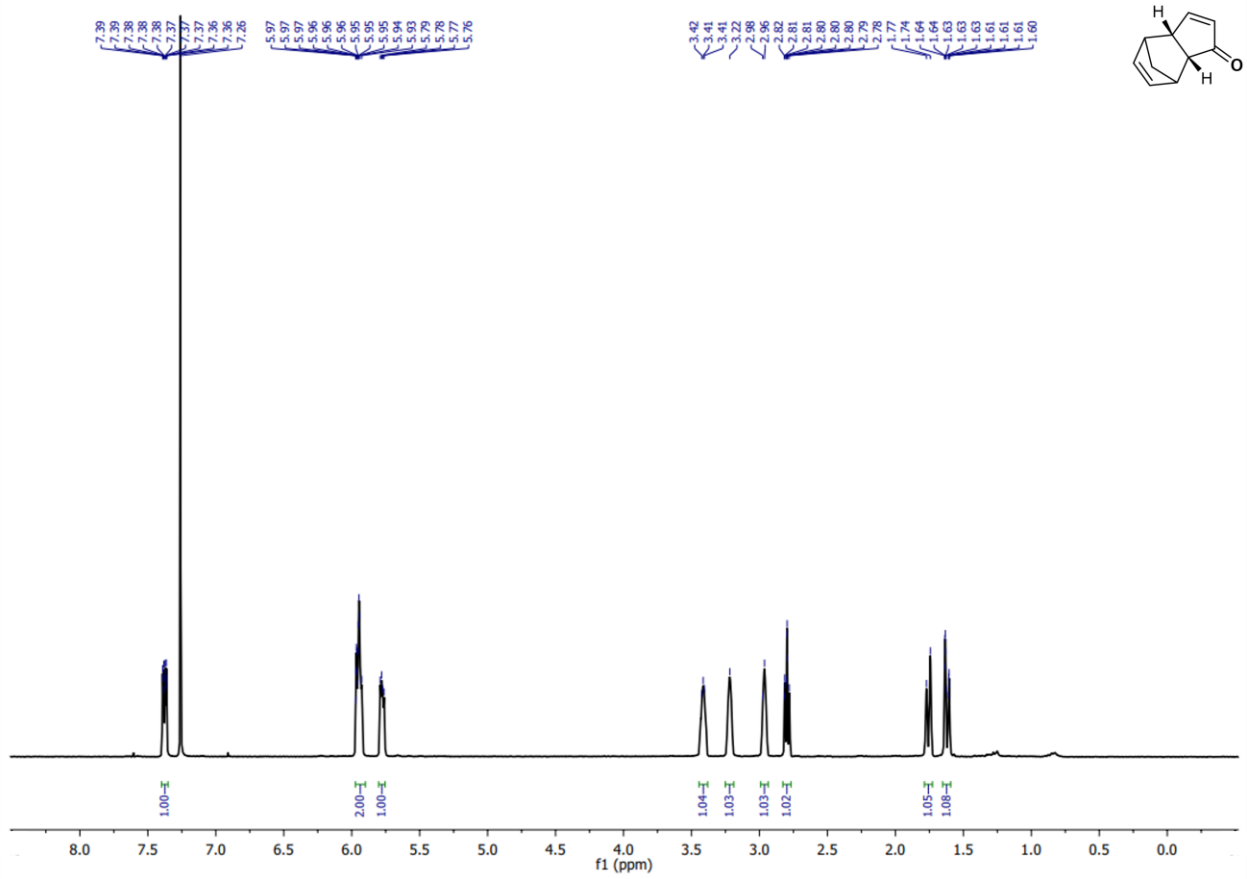

Figure C2. ^{1}H NMR spectrum of *endo*-dicyclopentadienone at 300.27 MHz in $CDCl_3$.

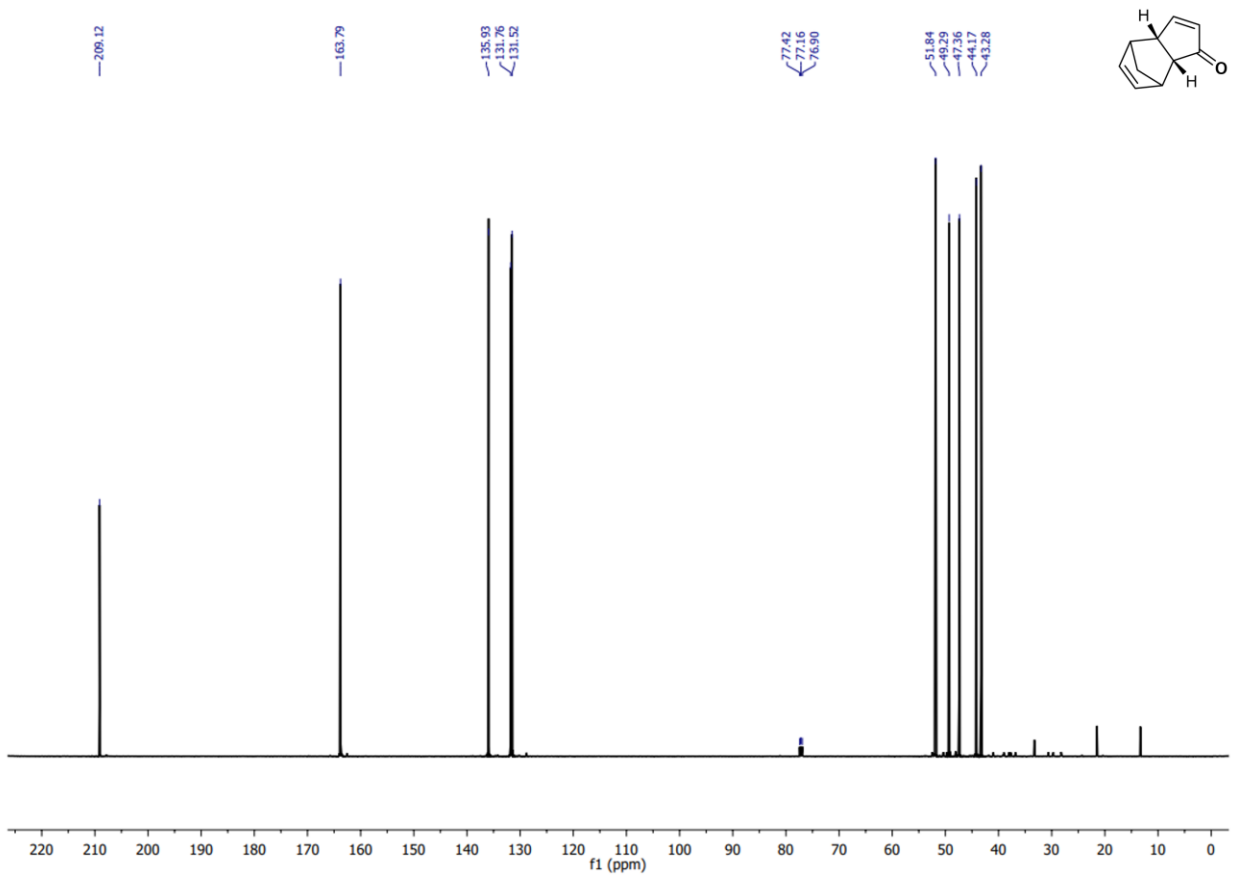

Figure C3. ^{13}C NMR spectrum of *endo*-dicyclopentadienone at 125.81 MHz in $CDCl_3$.

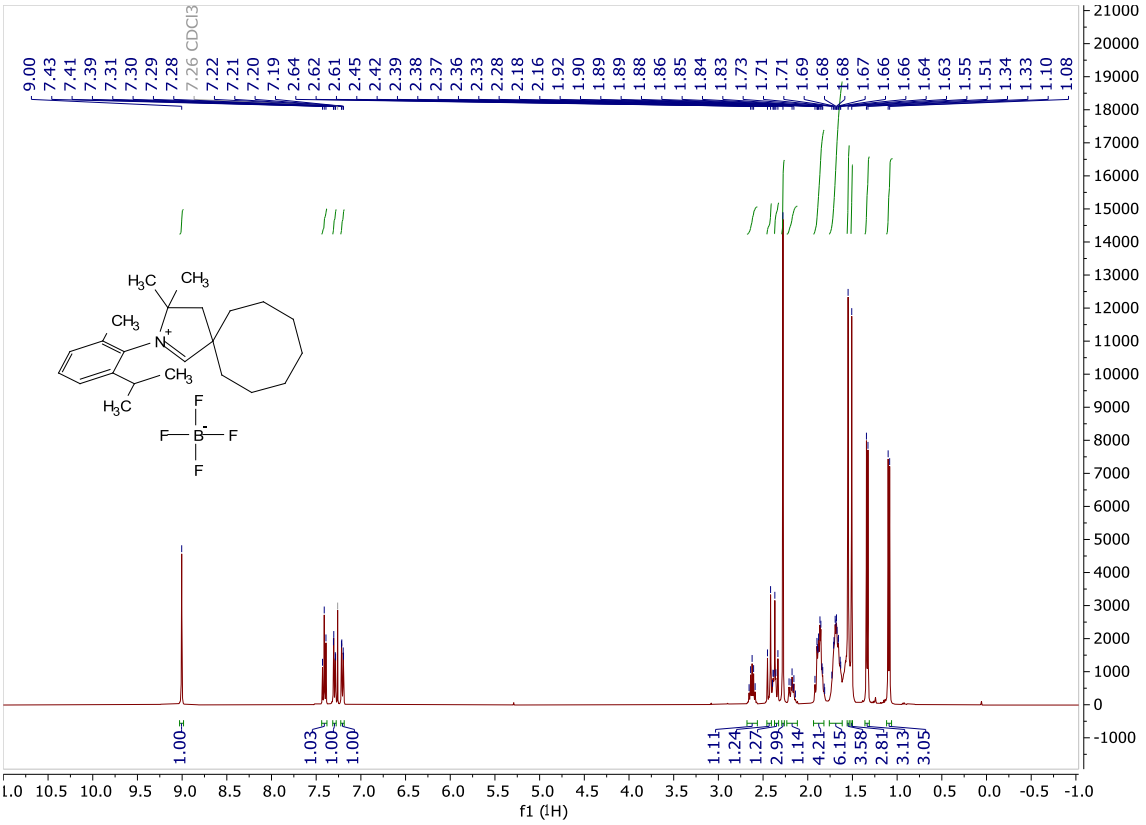

Figure C4. ^{1}H NMR of **CAAC-e** at 400 MHz in $CDCl_3$.

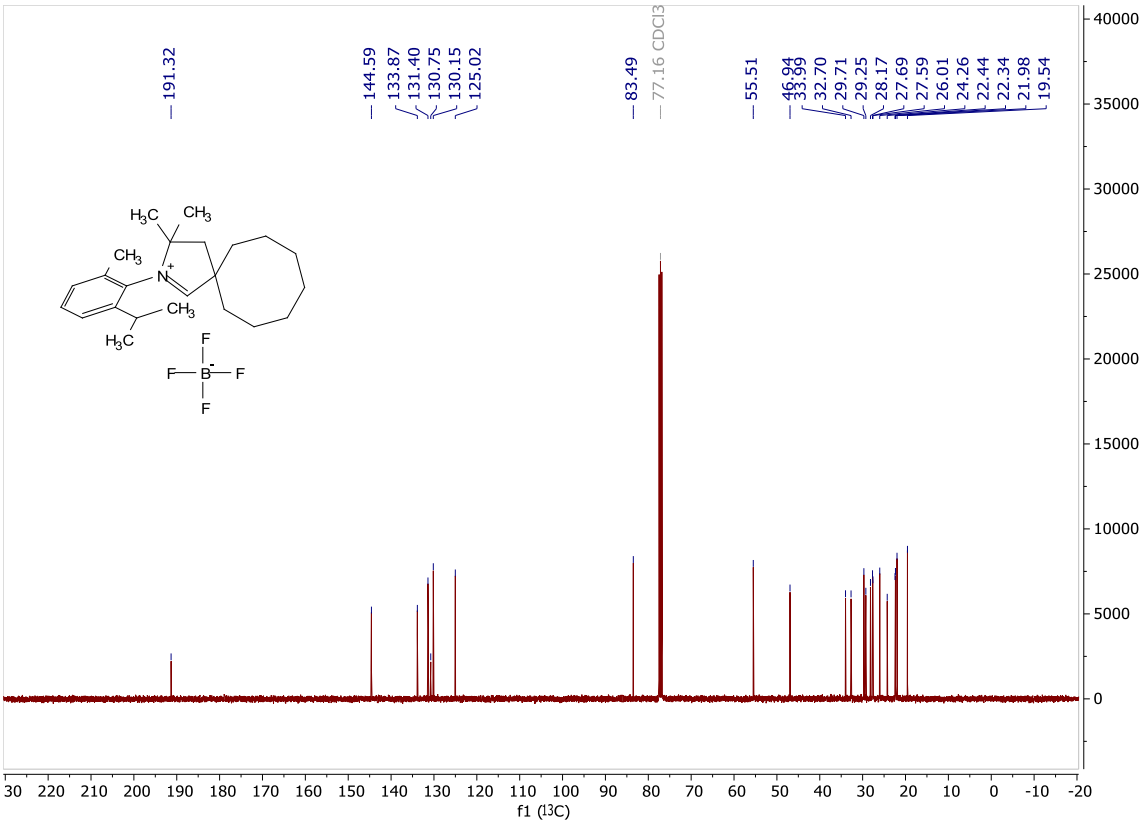

Figure C5. ^{13}C NMR of **CAAC-e** at 101 MHz in $CDCl_3$.

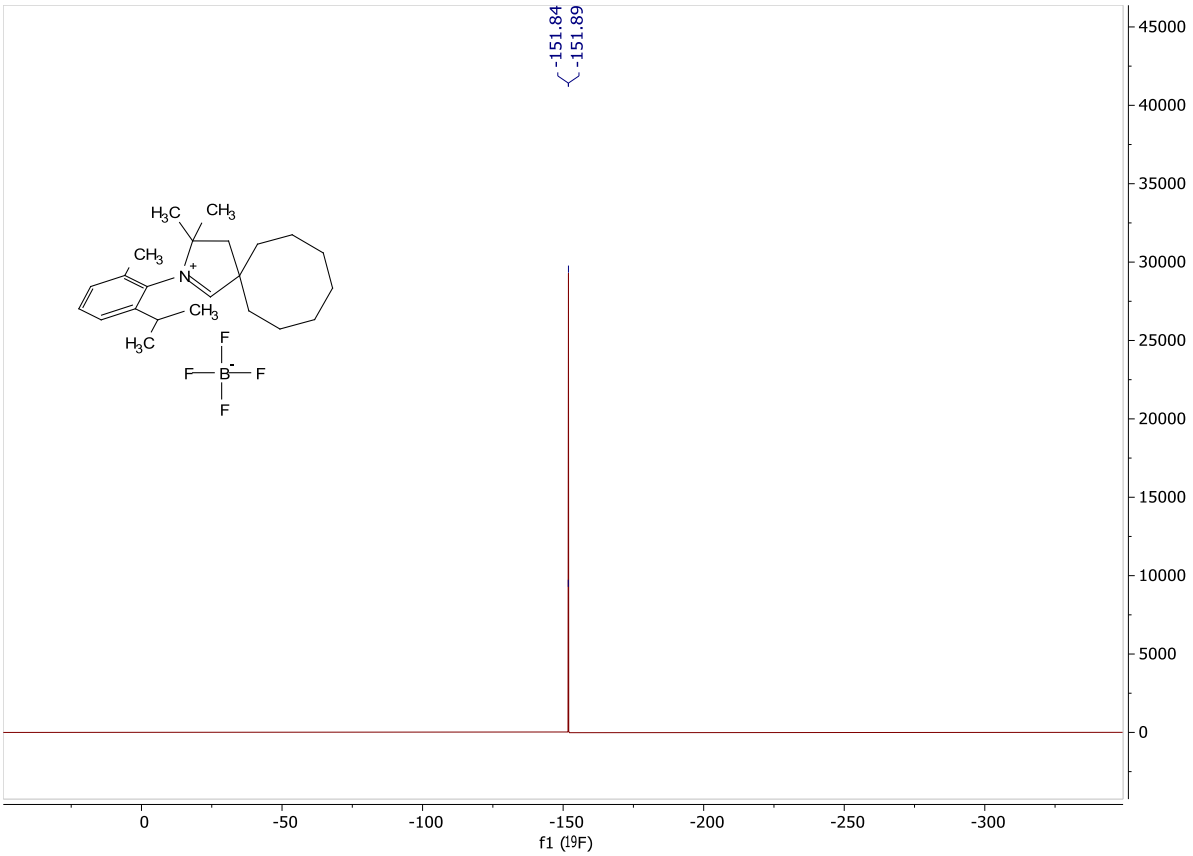

Figure C6. ^{19}F NMR of **CAAC-e** at 376 MHx in $CDCl_3$.

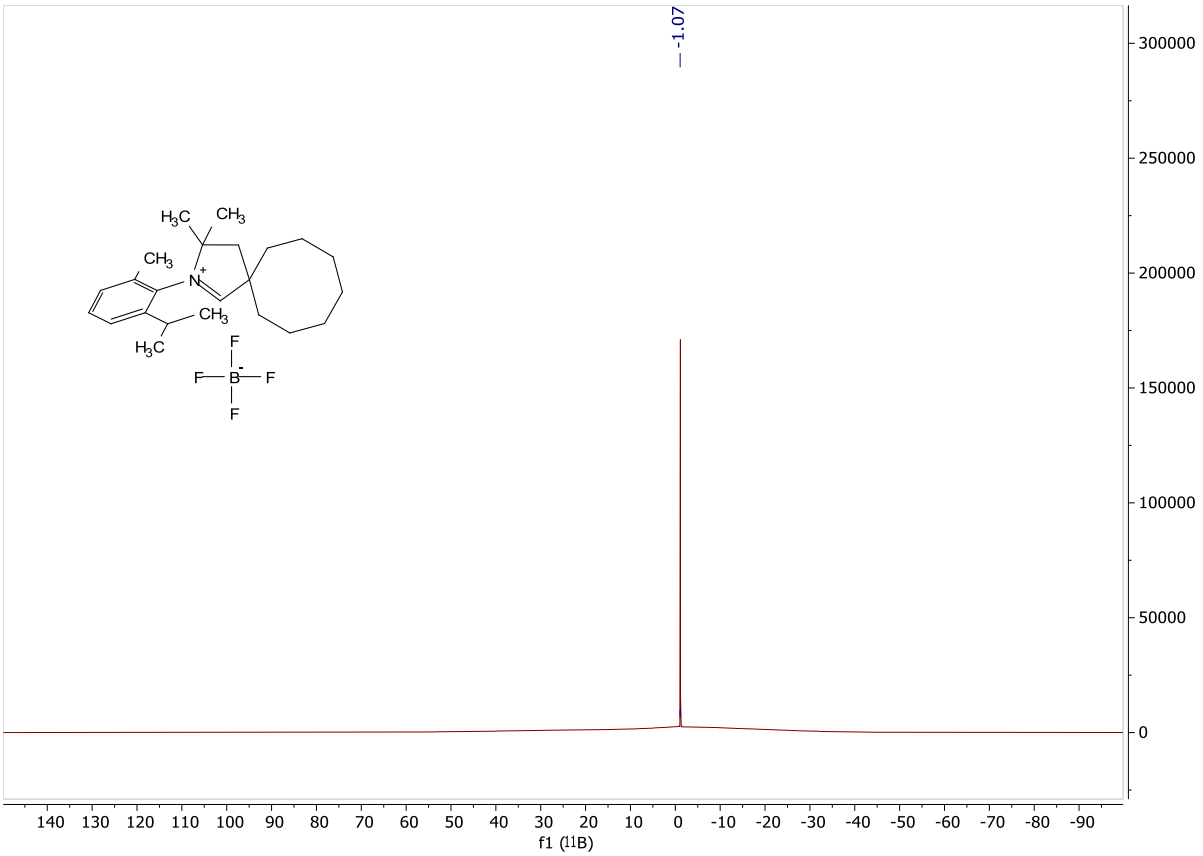

Figure C7. ^{11}B NMR of **CAAC-e** at 128 MHz in $CDCl_3$.

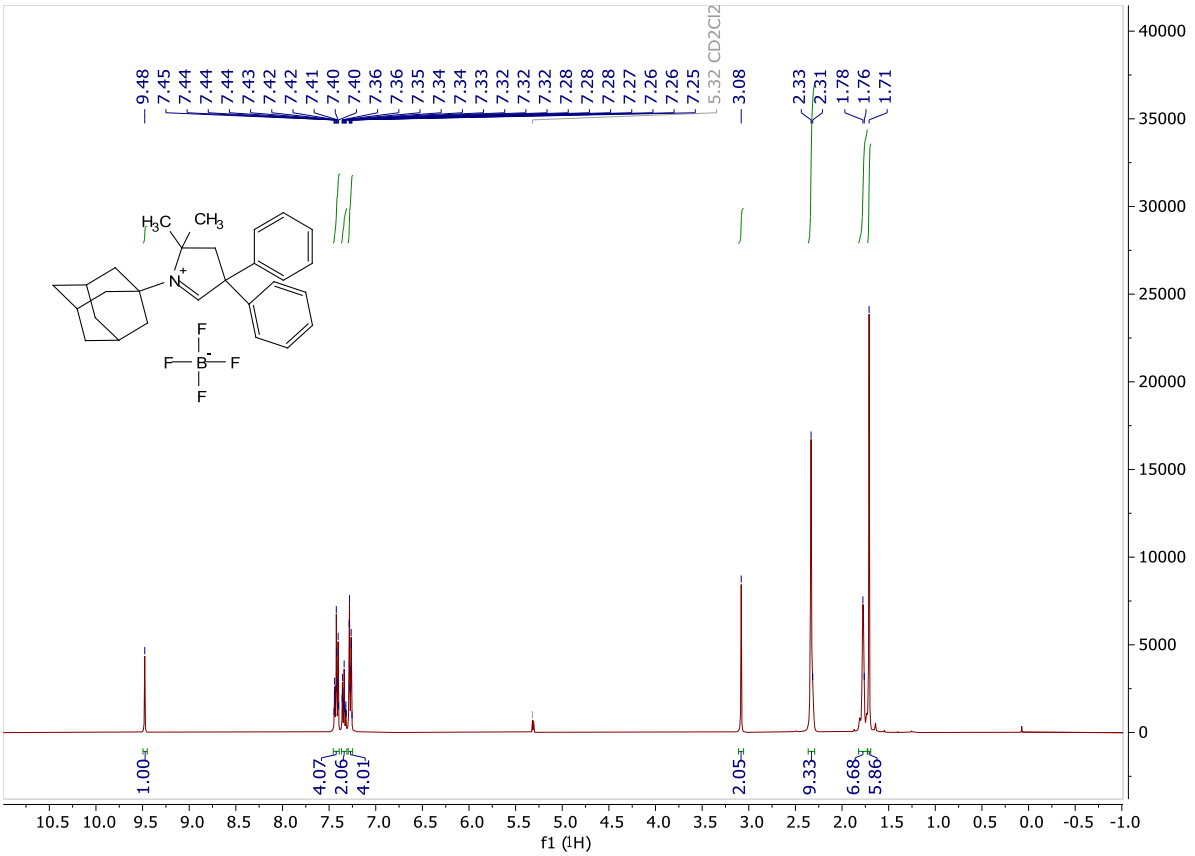

Figure C8. ^{1}H NMR of **CAAC-f** at 400 MHz in CD_2Cl_2.

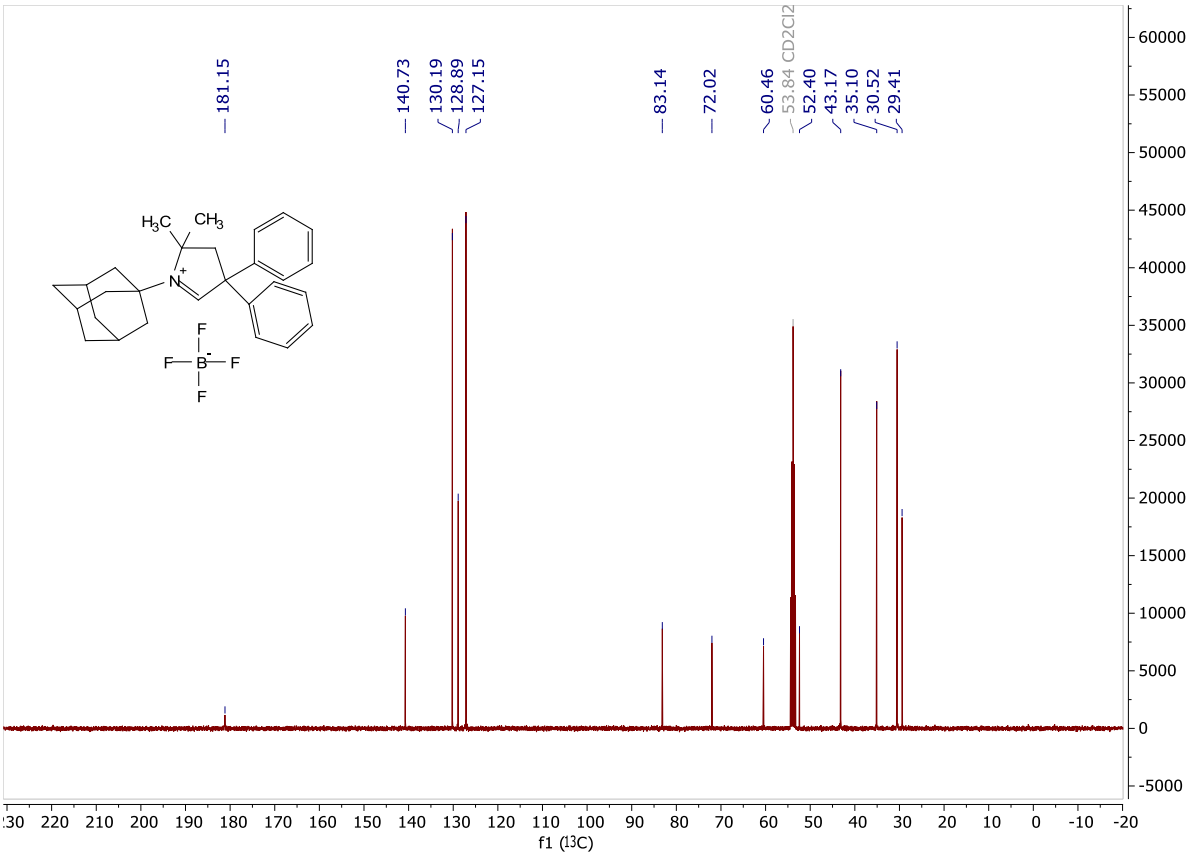

Figure C9. ^{13}C NMR of **CAAC-f** at 101 MHz in CD_2Cl_2.

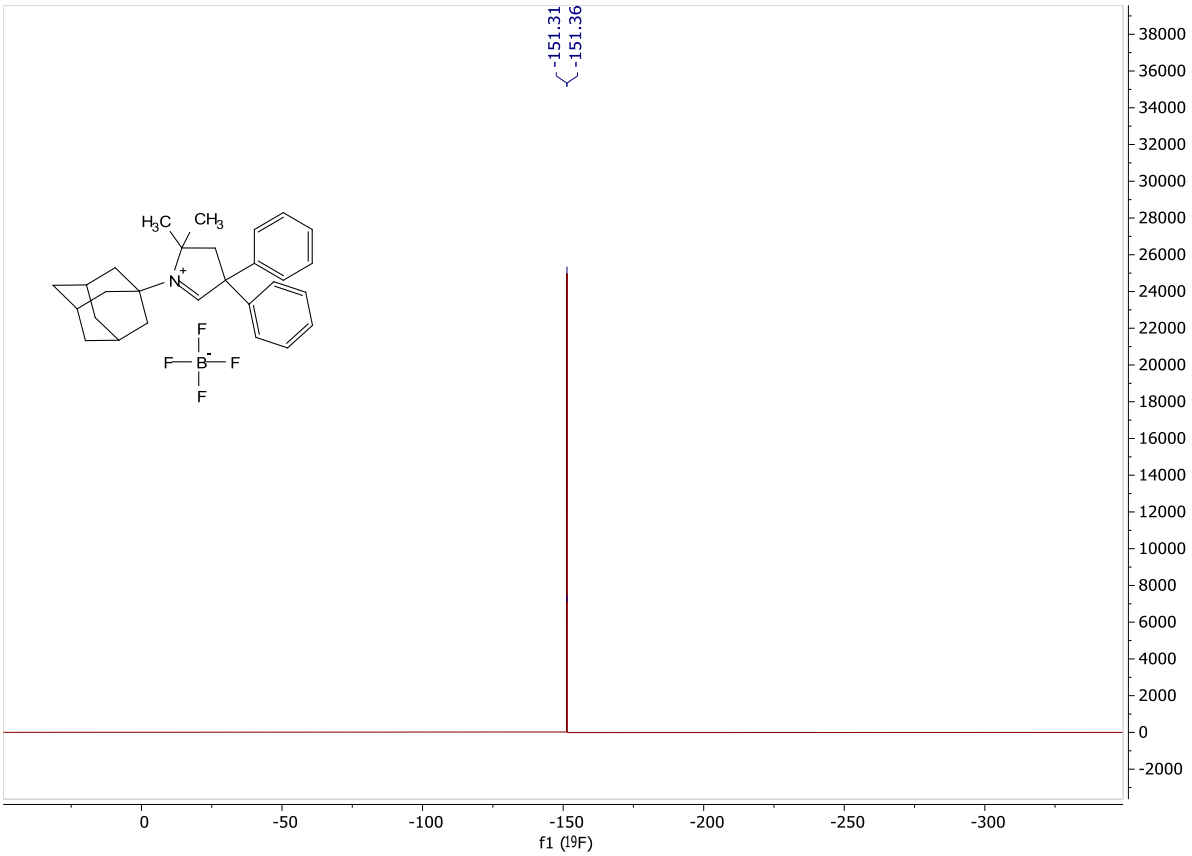

Figure C10. ^{19}F NMR of **CAAC-f** at 376 MHz in CD_2Cl_2.

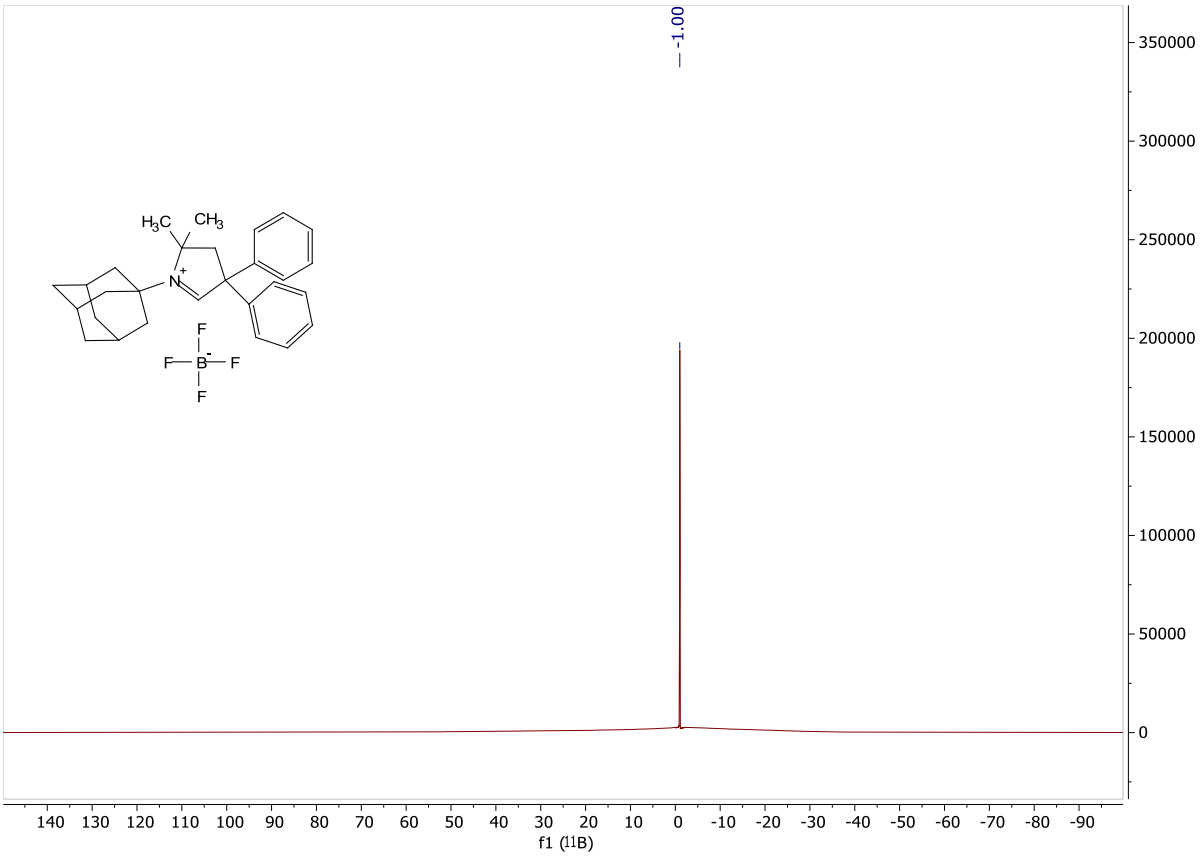

Figure C11.. ^{11}B NMR of **CAAC-f** at 128 MHz in CD_2Cl_2.

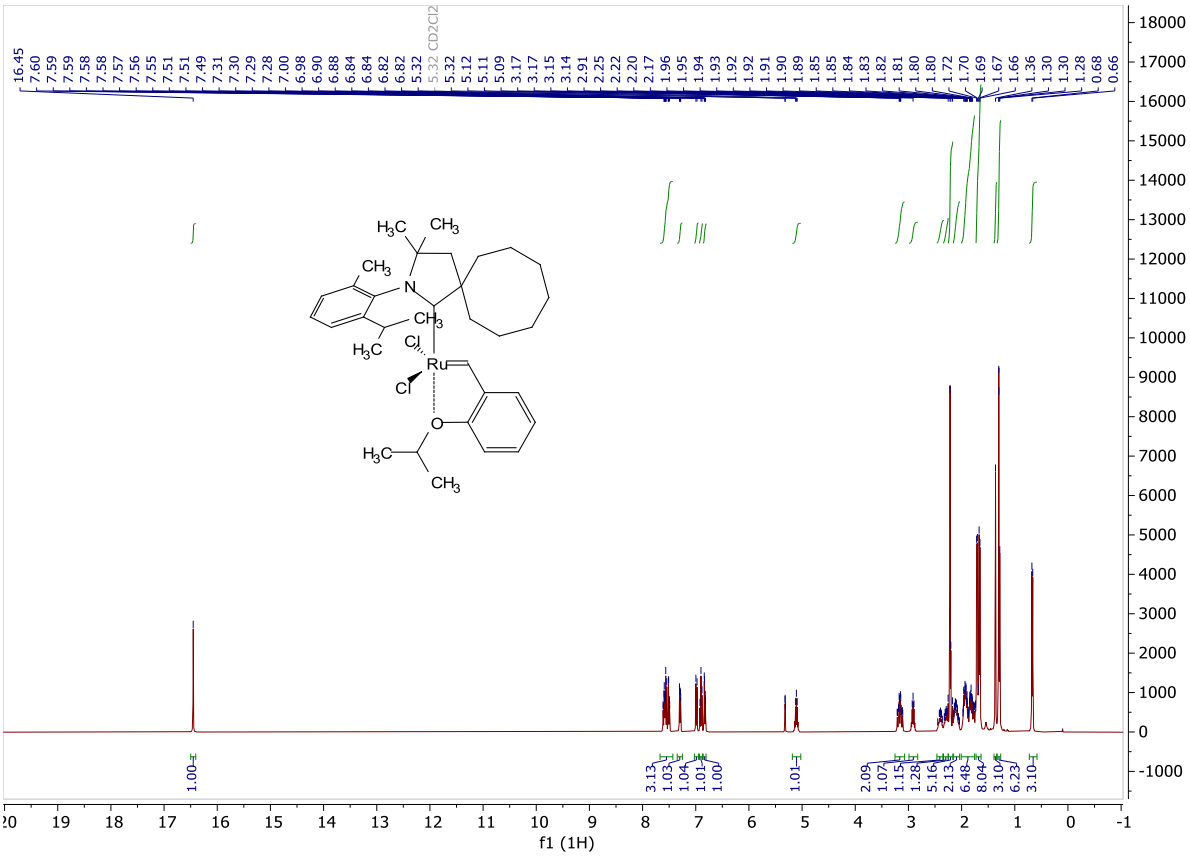

Figure C12. ^{1}H NMR of initiator **10** at 400 MHz in CD_2Cl_2.

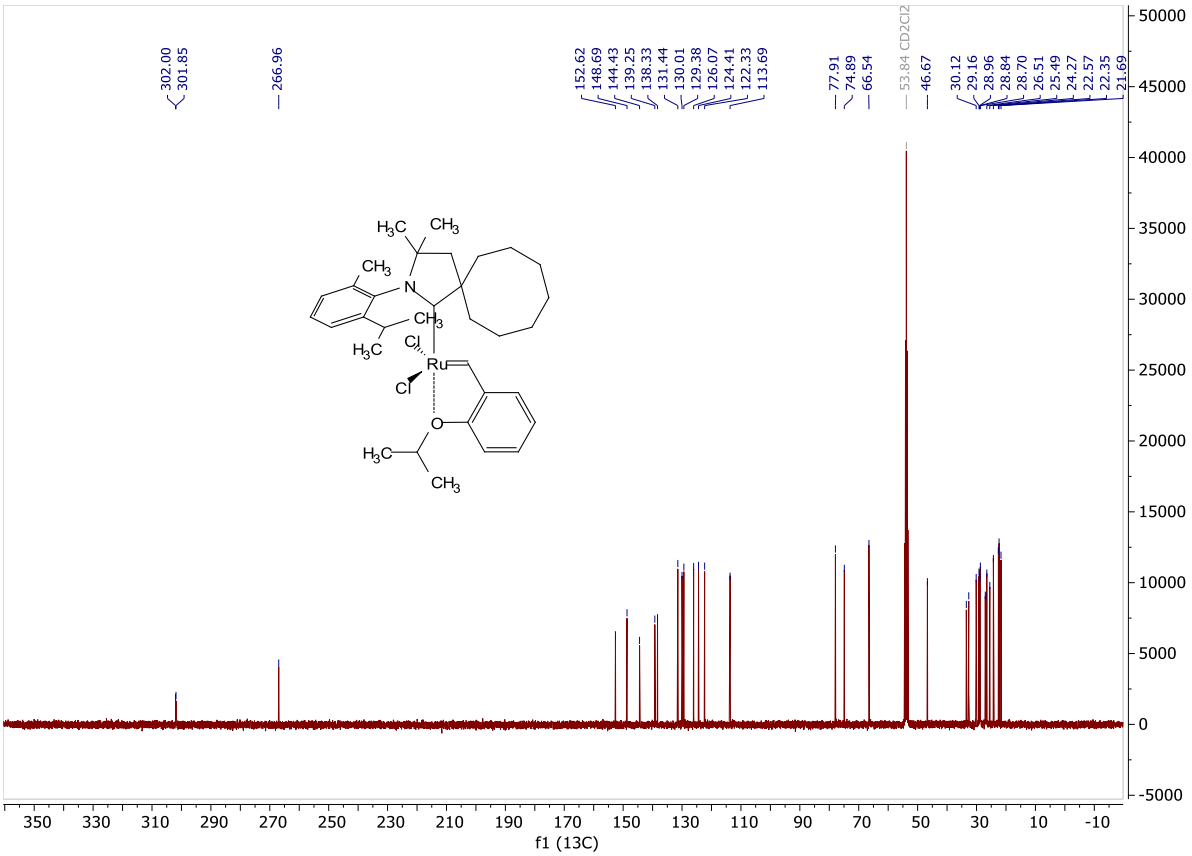

Figure C13. ^{13}C NMR of initiator **10** at 101 MHz in CD_2Cl_2.

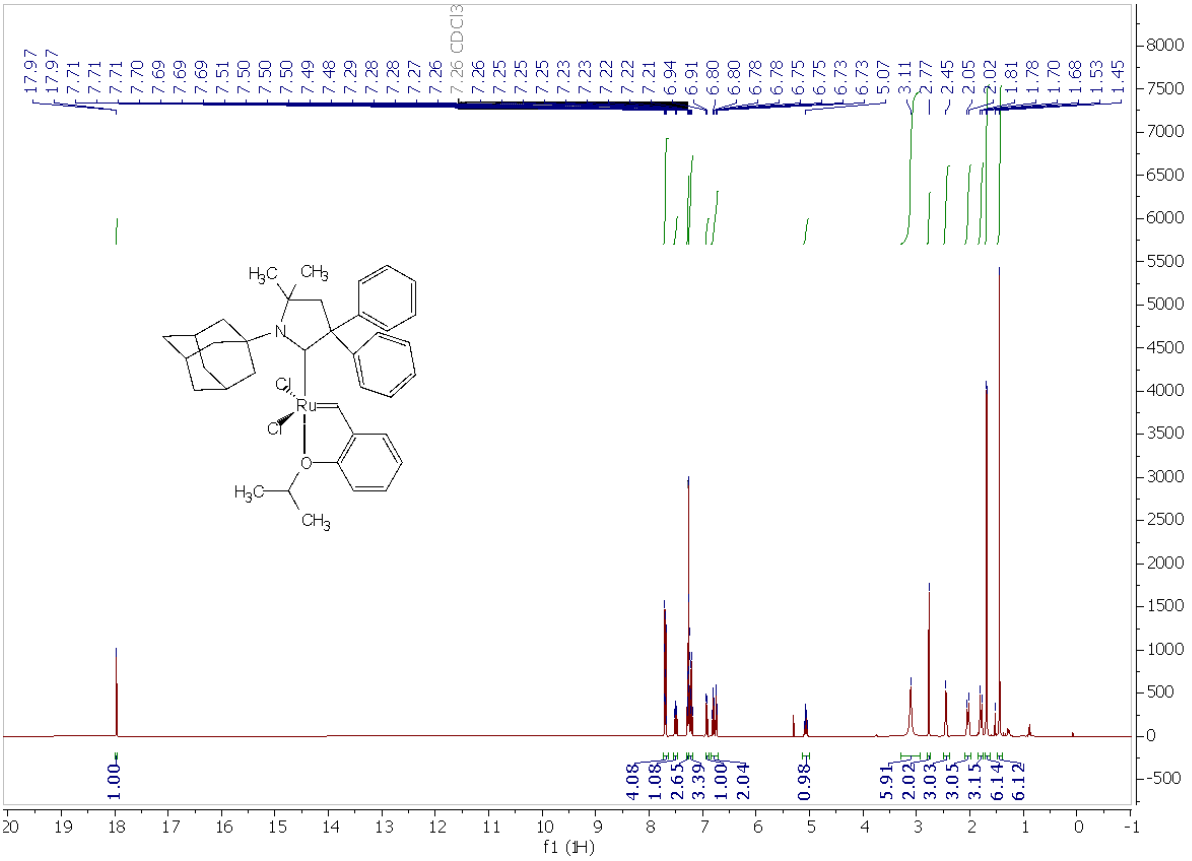

Figure C14. ^{1}H NMR of initiator **4** at 400 MHz in $CDCl_3$.

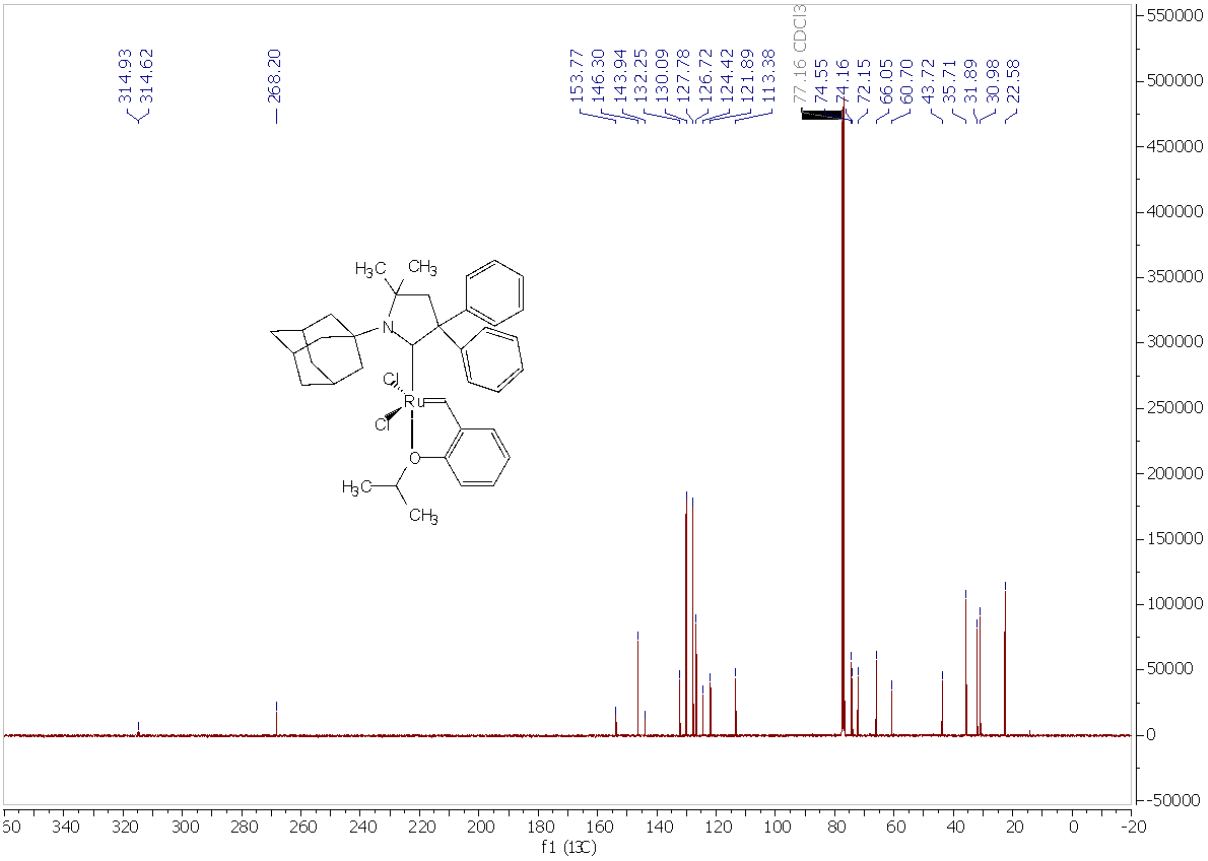

Figure C15. ^{13}C NMR of initiator **4** at 101 MHz in $CDCl_3$.

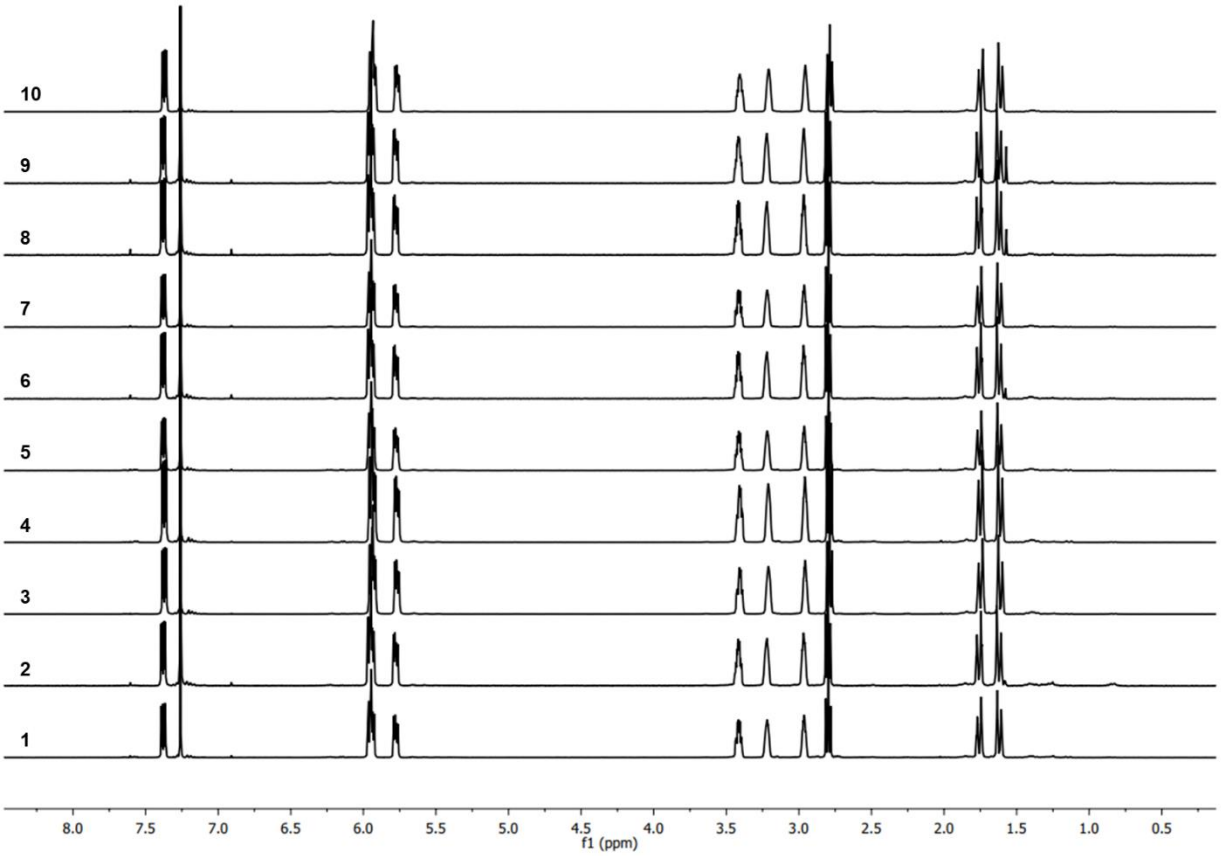

Figure C16. ^{1}H NMR spectra for **type-c** resin treated with various initiators at 0.005 mol% catalyst loading that failed to generate glassy polymer at 300.27 MHz in $CDCl_3$. # corresponds to initiator used.

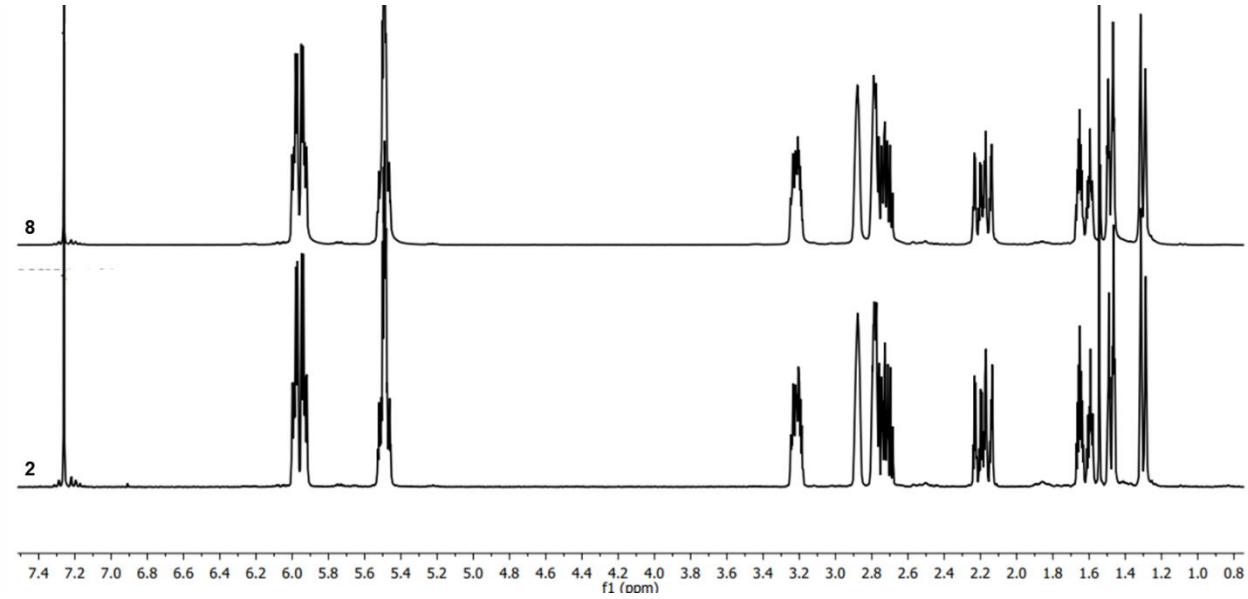

Figure C17. ^{1}H NMR spectra for **type-a** resin treated with various initiators at 0.005 mol% catalyst loading that failed to generate glassy polymer at 300.27 MHz in $CDCl_3$. # corresponds to initiator used.

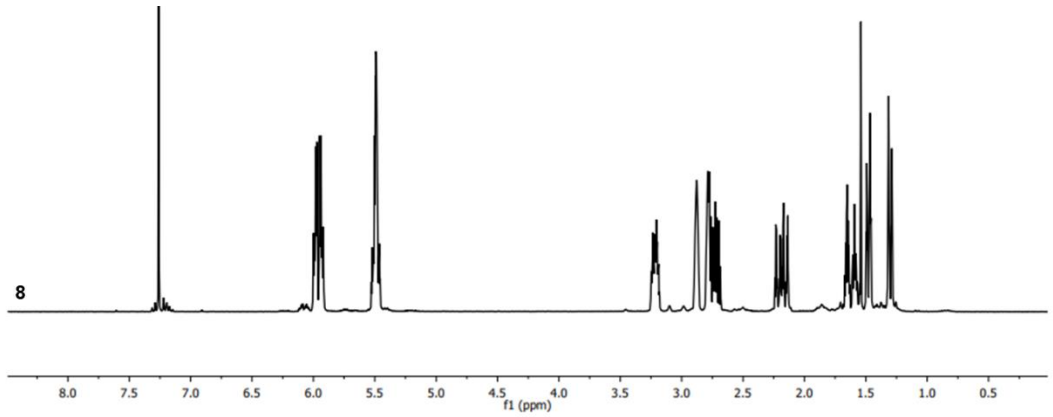

Figure C18. ^{1}H NMR spectra for **type-b** resin treated with various initiators at 0.005 mol% catalyst loading that failed to generate glassy polymer at 300.27 MHz in $CDCl_3$. # corresponds to initiator used.

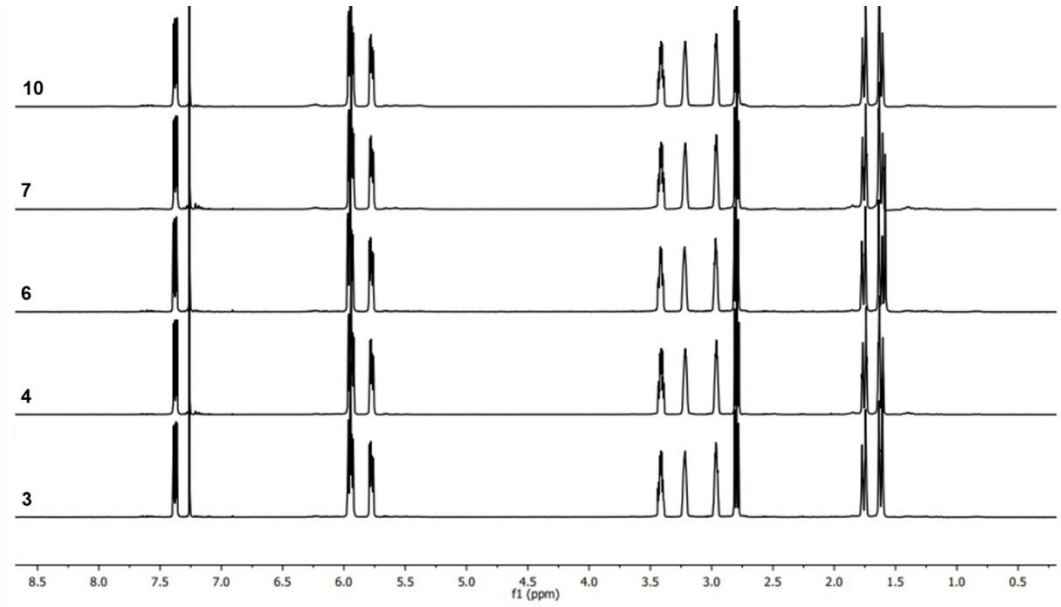

Figure C19. ^{1}H NMR spectra for **type-c** resin treated with various initiators at 0.02 mol% catalyst loading that failed to generate glassy polymer at 300.27 MHz in $CDCl_3$. # corresponds to initiator used.

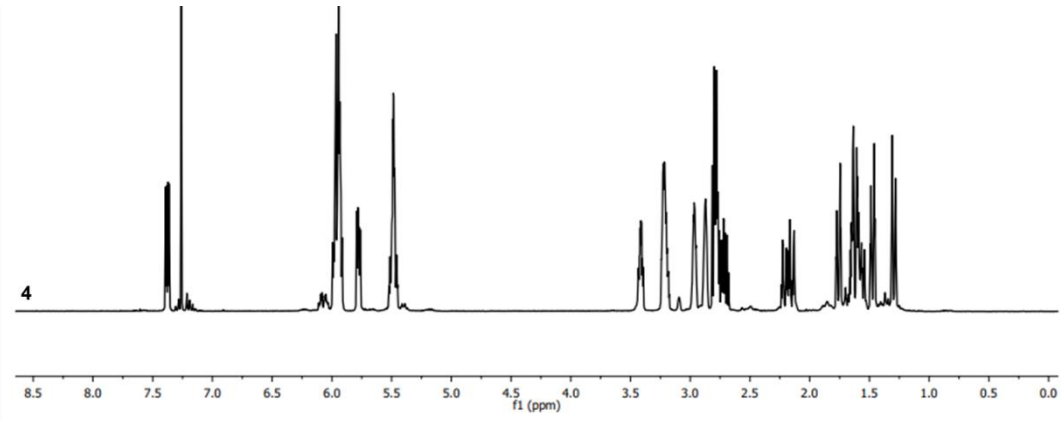

Figure C20. ^{1}H NMR spectra for **type-d** resin treated with various initiators at 0.02 mol% catalyst loading that failed to generate glassy polymer at 300.27 MHz in $CDCl_3$. # corresponds to initiator used.

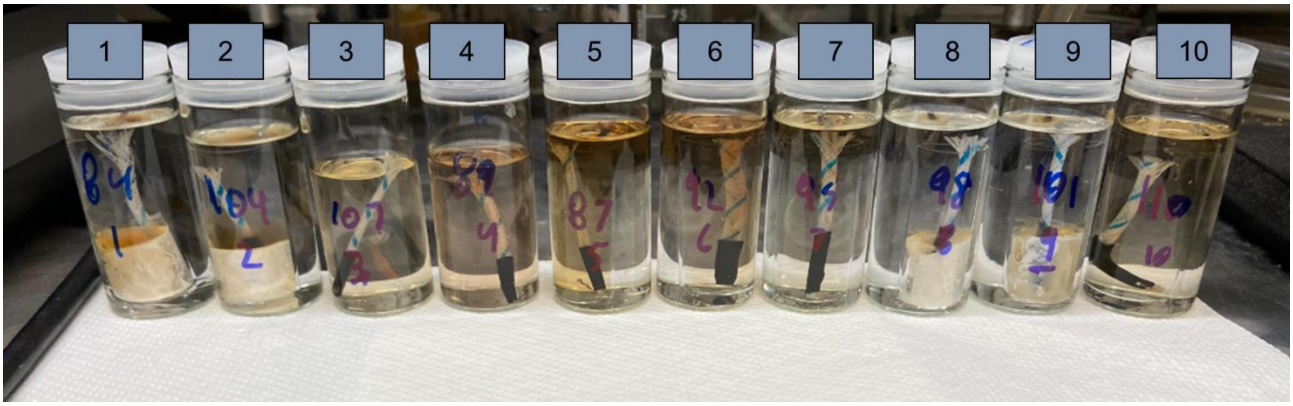

Figure C21. Swelling of **type-c** resins treated with various initiators at 0.005 mol% loading in dichloromethane (DCM). Ethyl vinyl ether (EVE) was added to the DCM in a 1:60 EVE:DCM to prevent further solution state polymerization. # corresponds to initiator used.

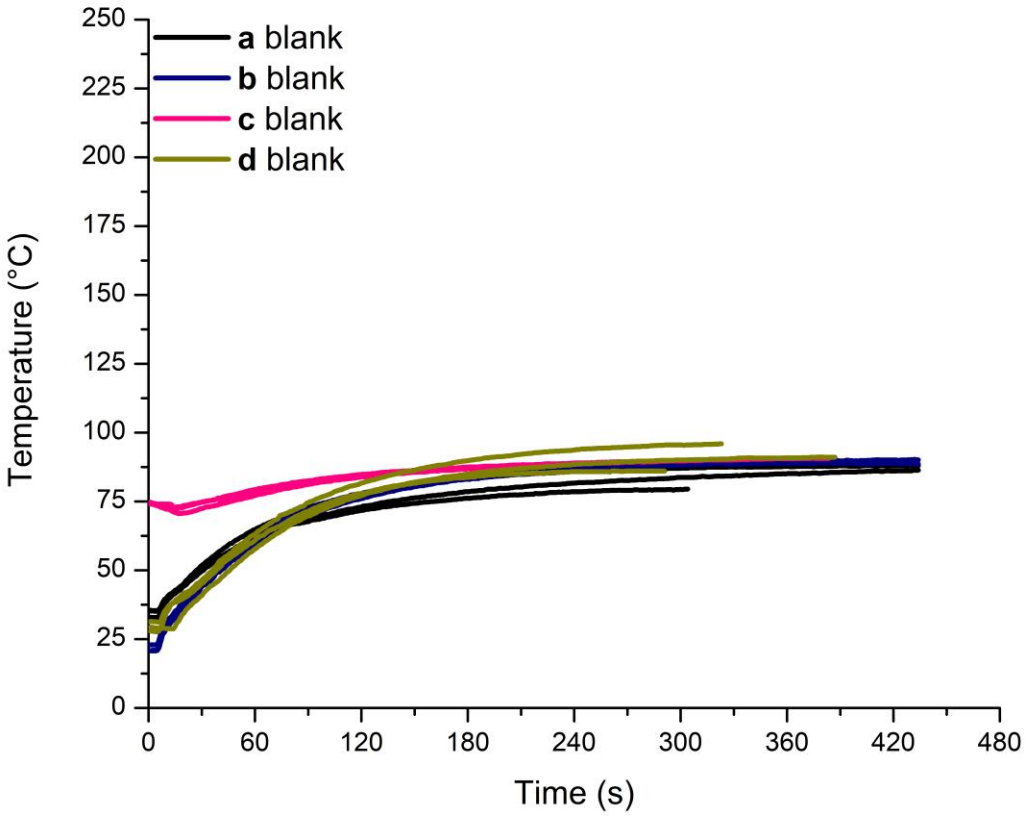

Figure C22. Thermograms of **type-a**, **b**, **c**, and **d** resins with no initiator addition.

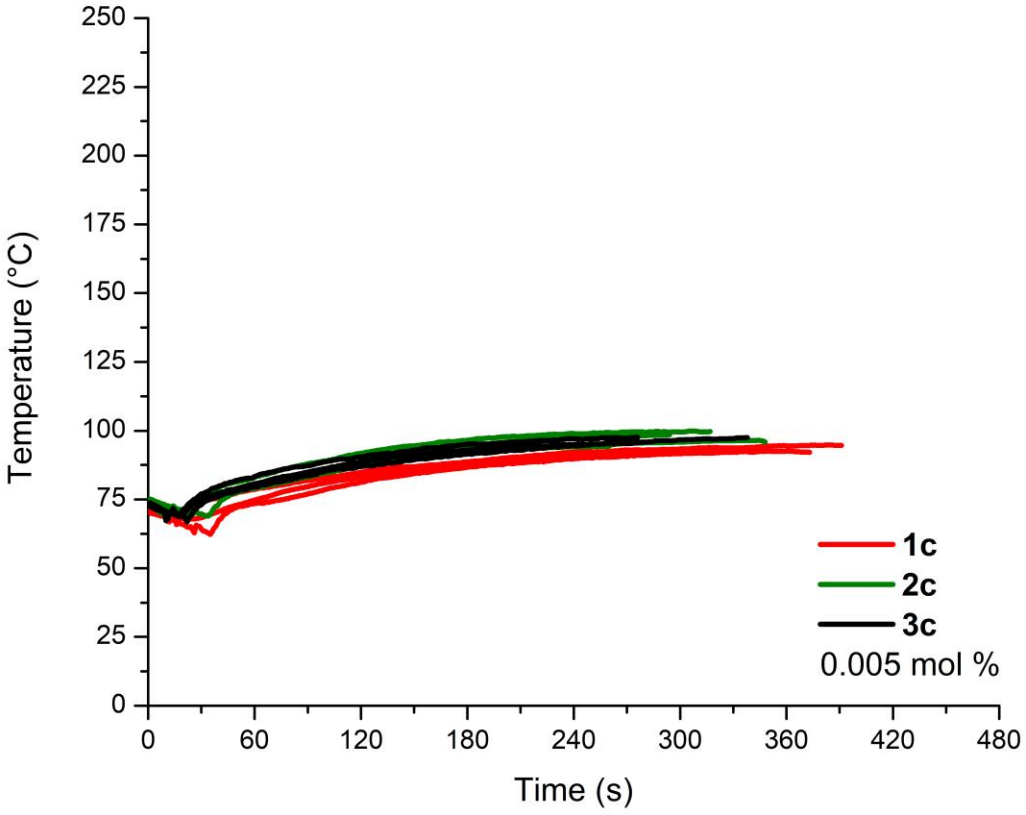

Figure C23. Thermograms of **type-c** resin treated with commercially available initiators at 0.005 mol% loading. All reactions failed to generate glassy polymer.

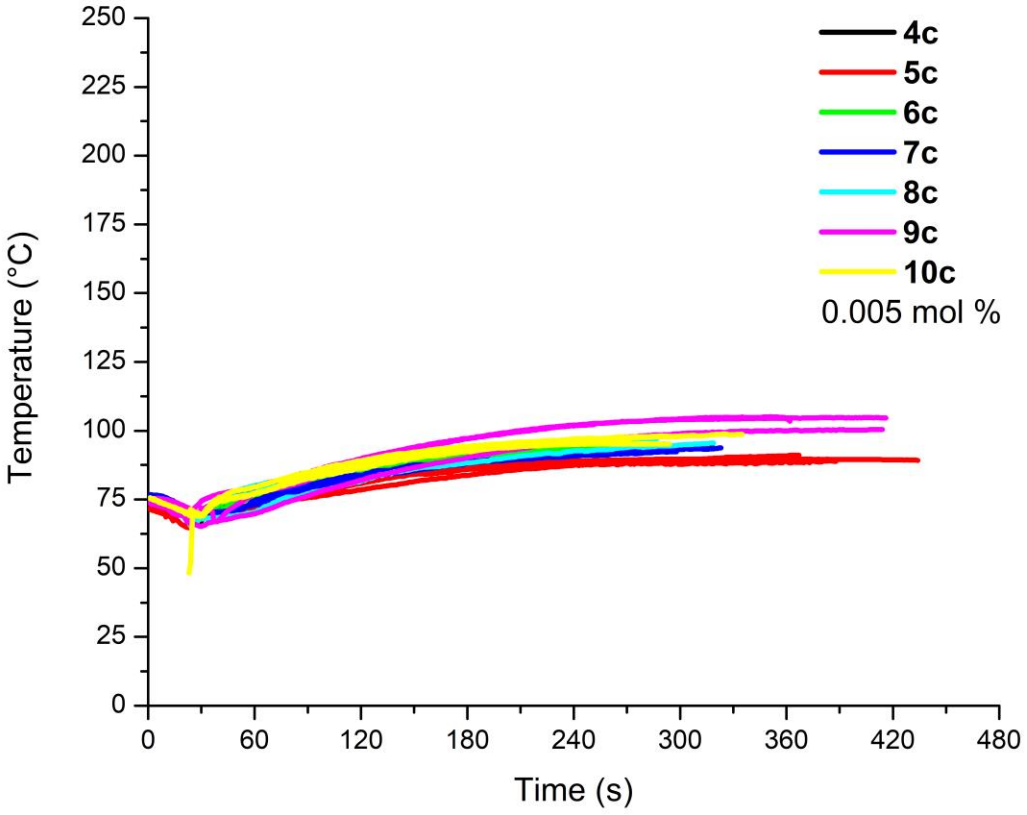

Figure C24. Thermograms of **type-c** resin treated with prepared initiators at 0.005 mol% loading. All reactions failed to generate glassy polymer.

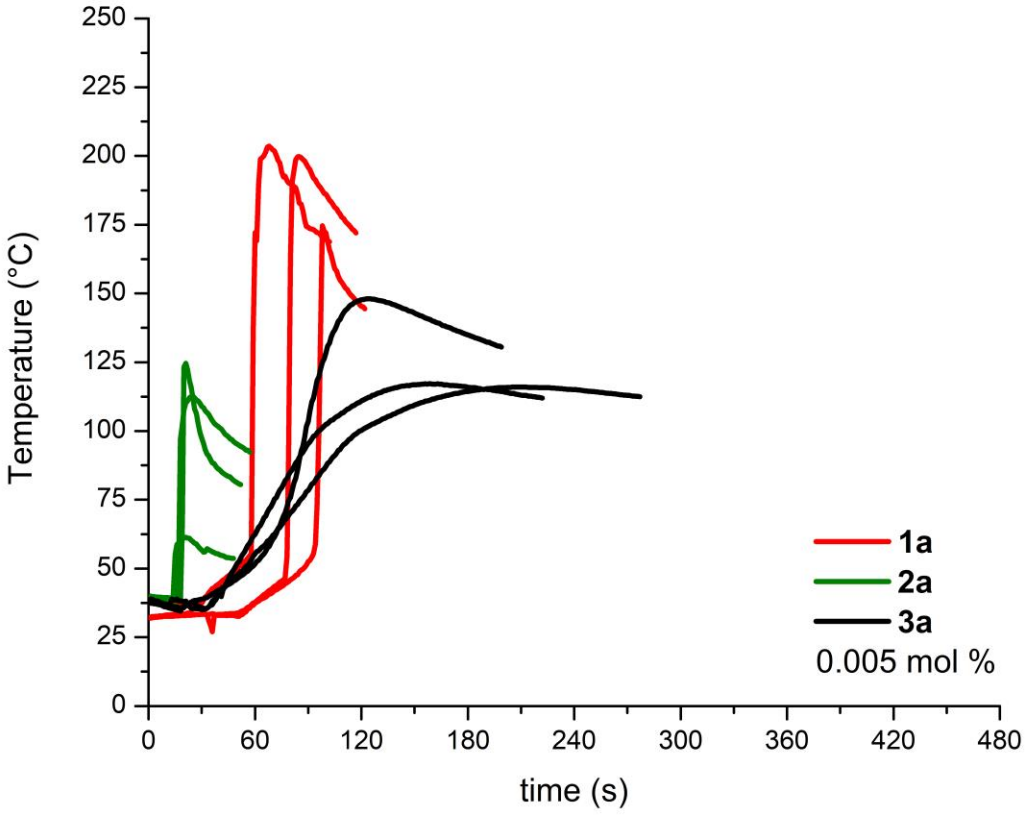

Figure C25. Thermograms of **type-a** resin treated with commercially available initiators at 0.005 mol% loading.

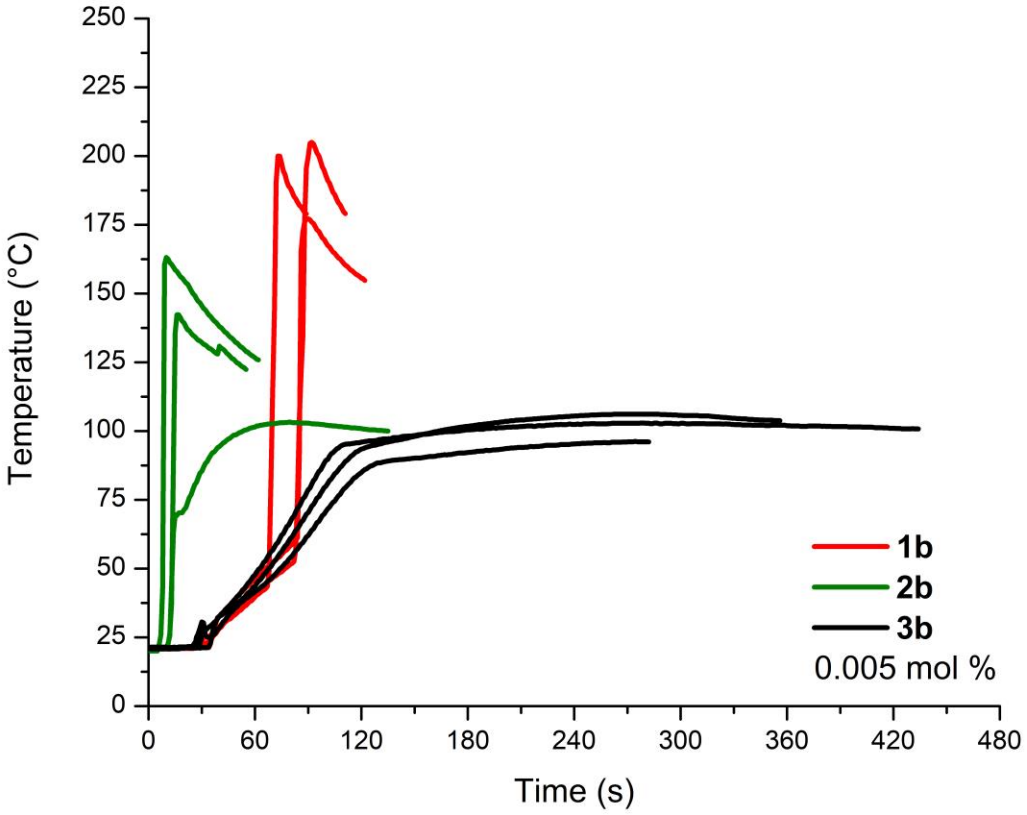

Figure C26. Thermograms of **type-b** resin treated with commercially available initiators at 0.005 mol% loading.

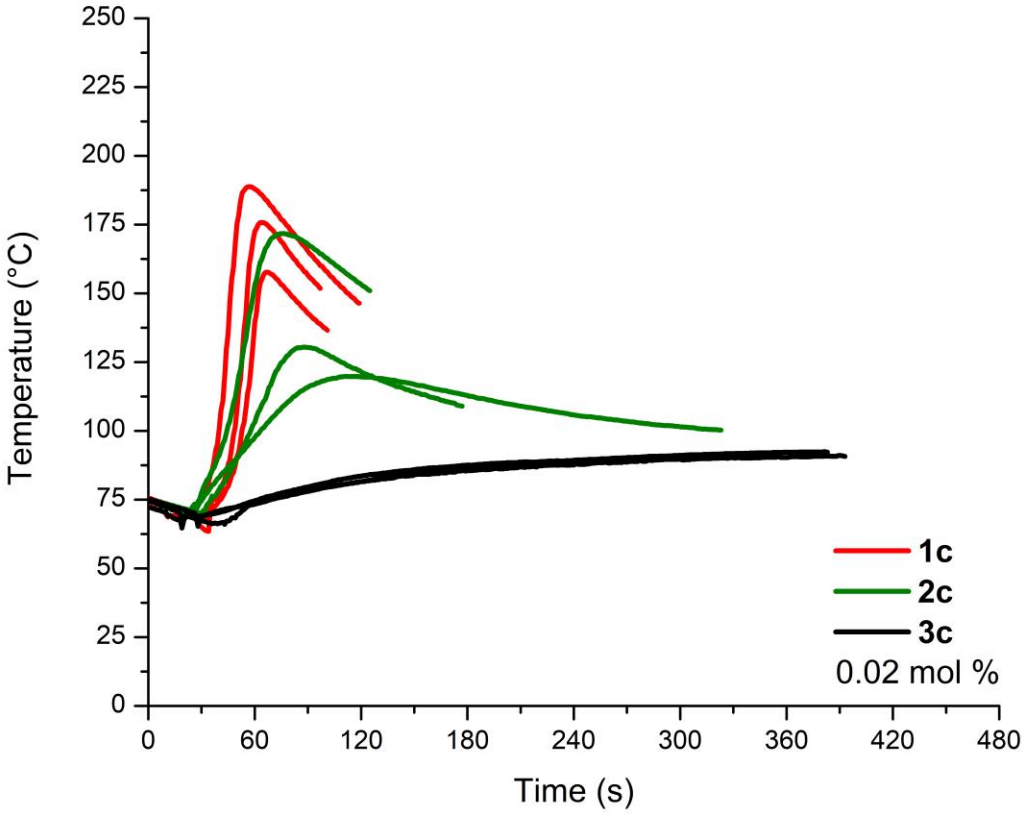

Figure C27. Thermograms of **type-c** resin treated with commercially available initiators at 0.02 mol% loading.

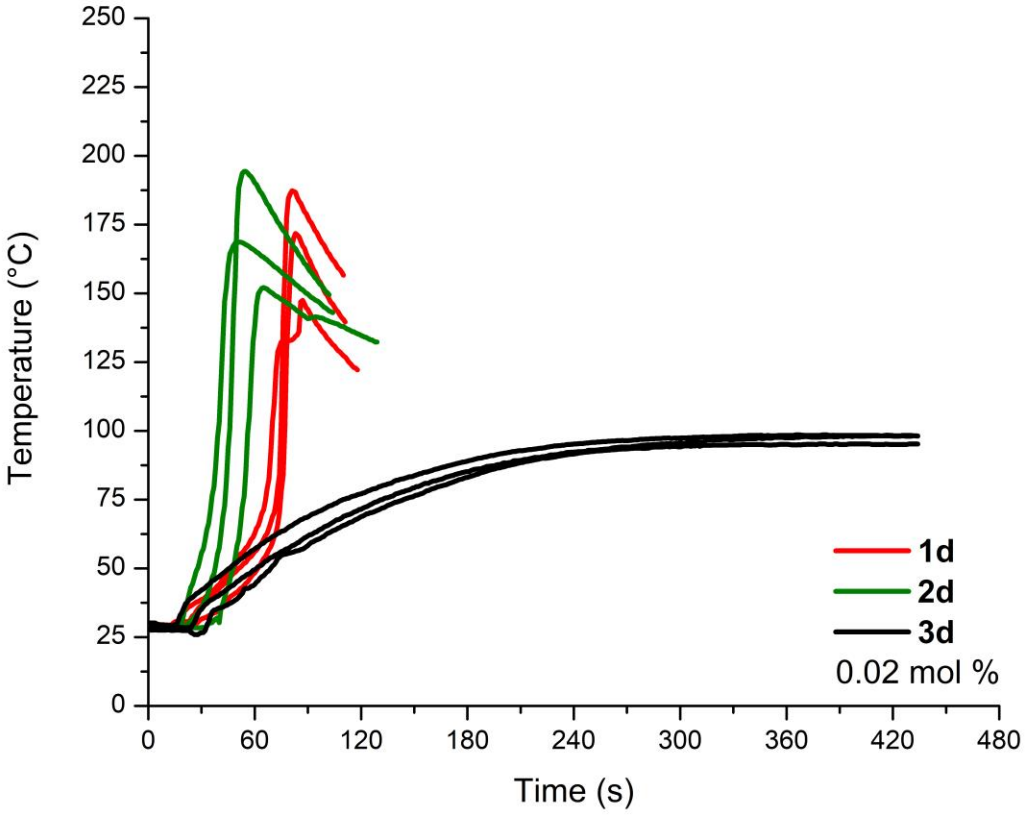

Figure C28. Thermograms of **type-d** resin treated with commercially available initiators at 0.02 mol% loading.

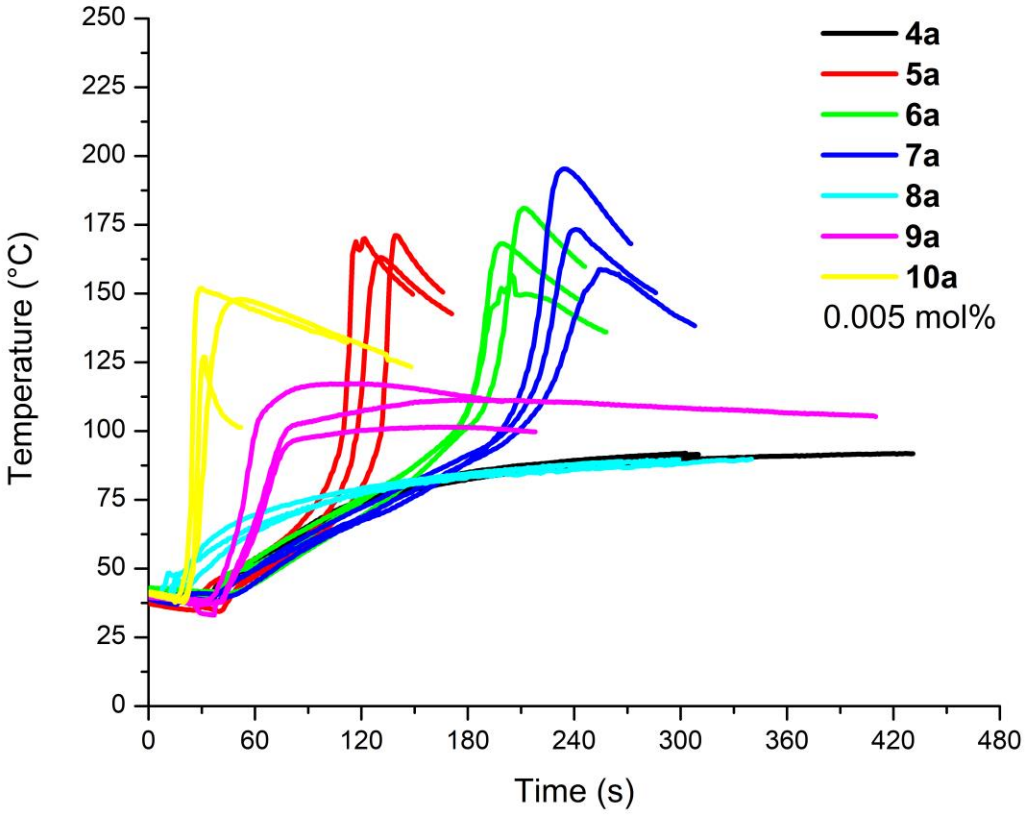

Figure C29. Thermograms of **type-a** resin treated with prepared initiators at 0.005 mol% loading.

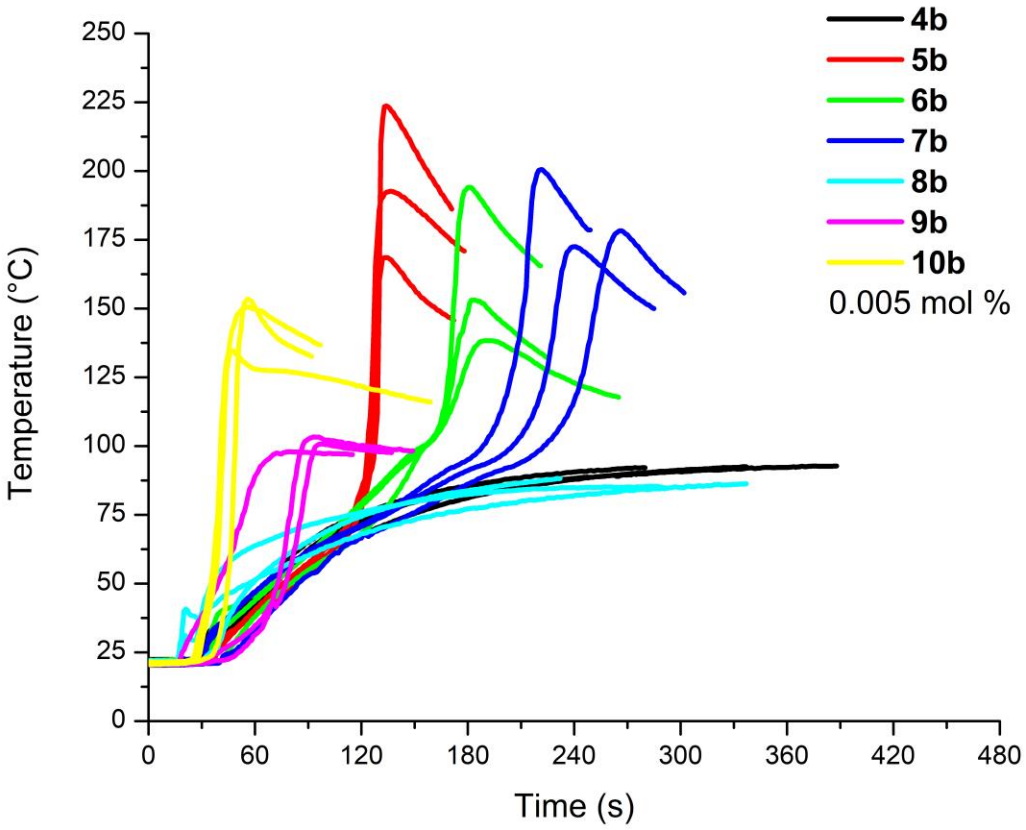

Figure C30. Thermograms of **type-b** resin treated with prepared initiators at 0.005 mol% loading.

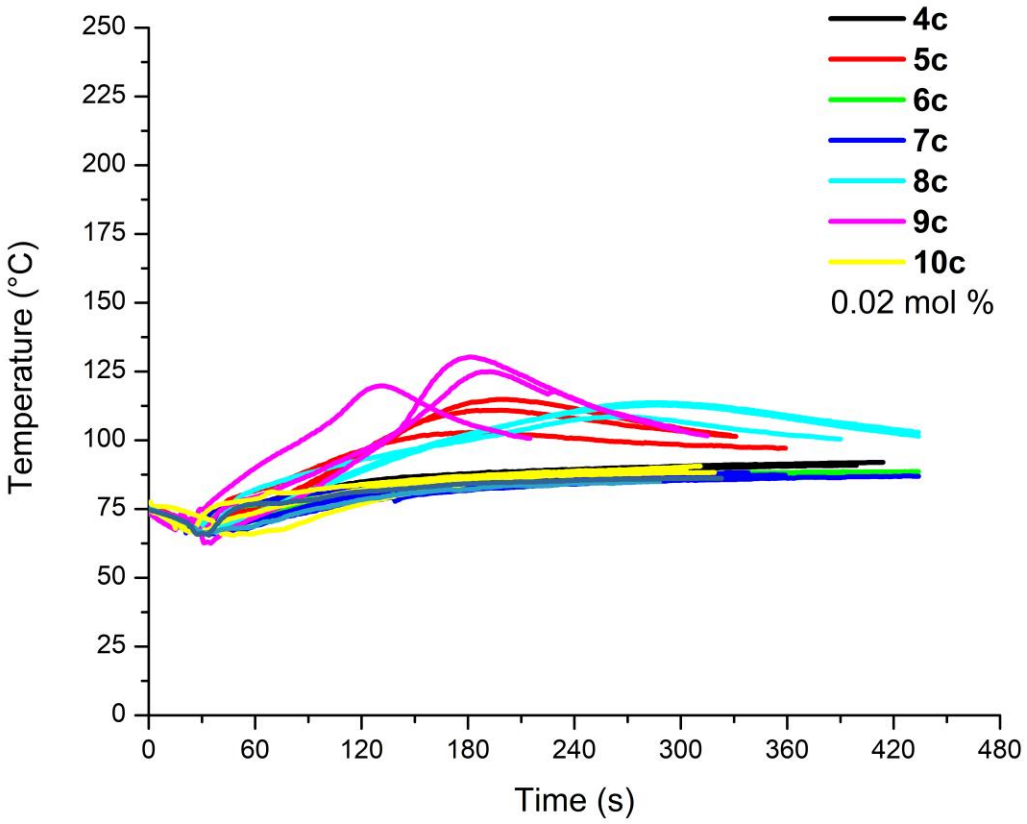

Figure C31. Thermograms of **type-c** resin treated with prepared initiators at 0.02 mol% loading.

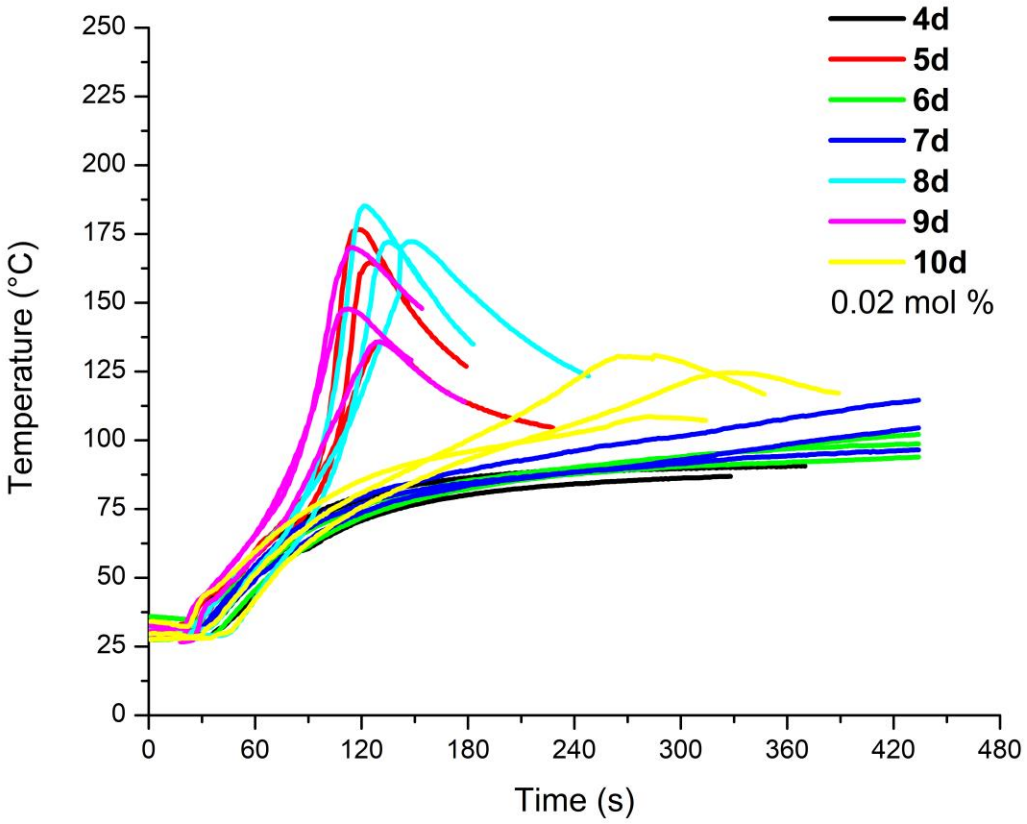

Figure C32. Thermograms of **type-d** resin treated with prepared initiators at 0.02 mol% loading.

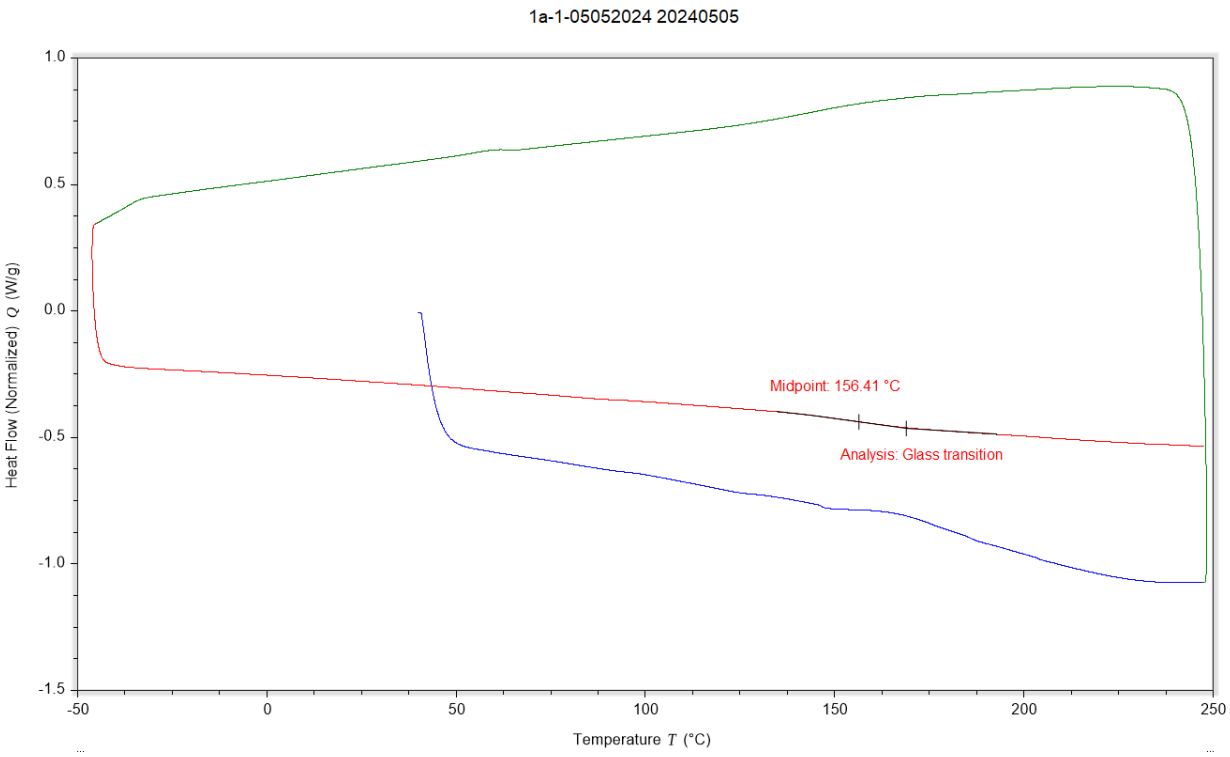

Figure C33. DSC trace for material **1a**.

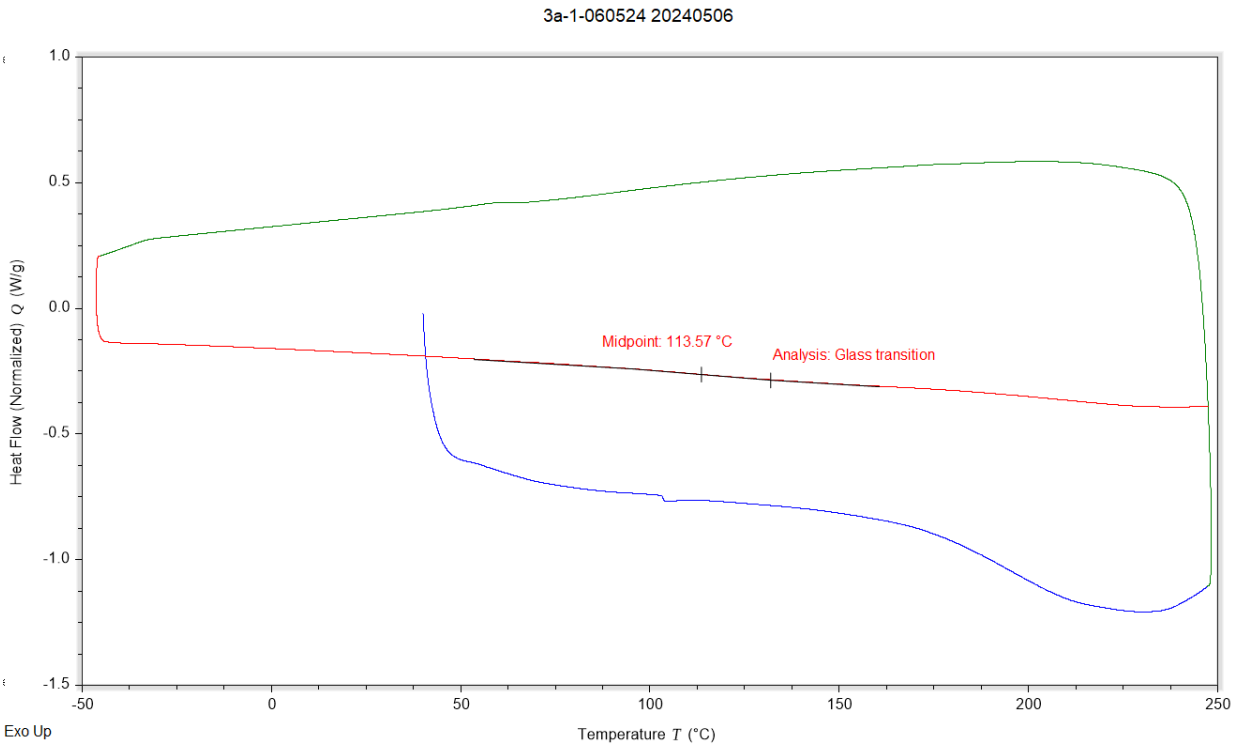

Figure C34. DSC trace for material **3a**.

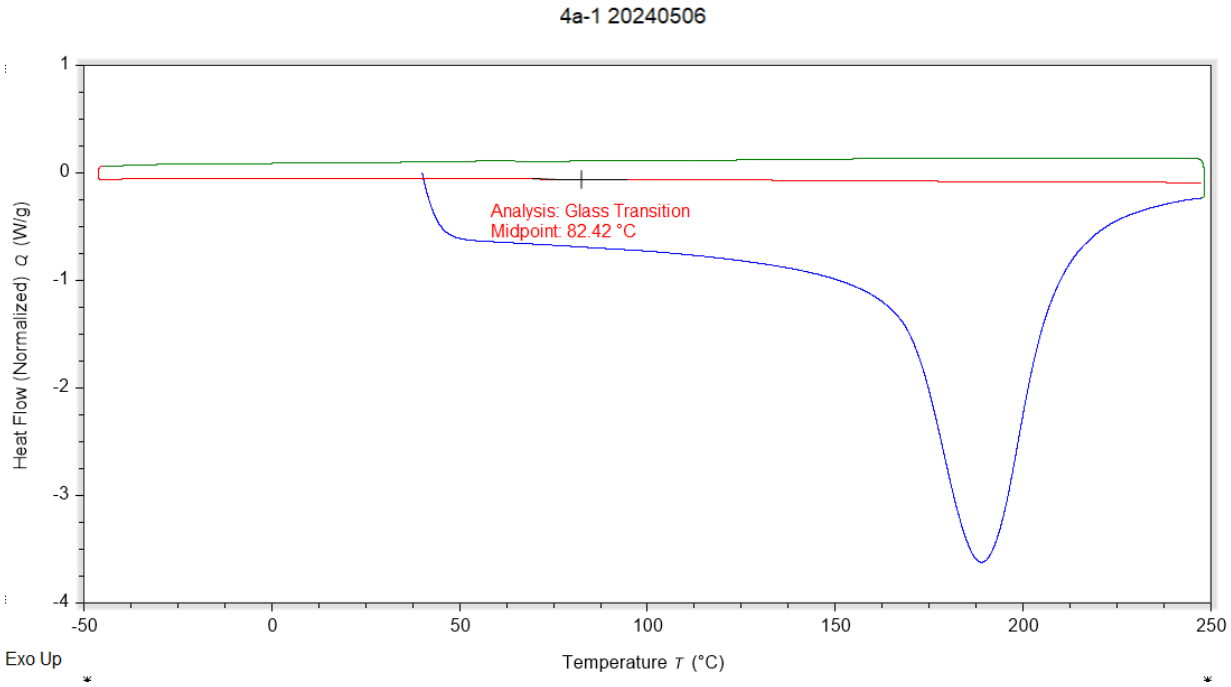

Figure C35. DSC trace for material **4a**.

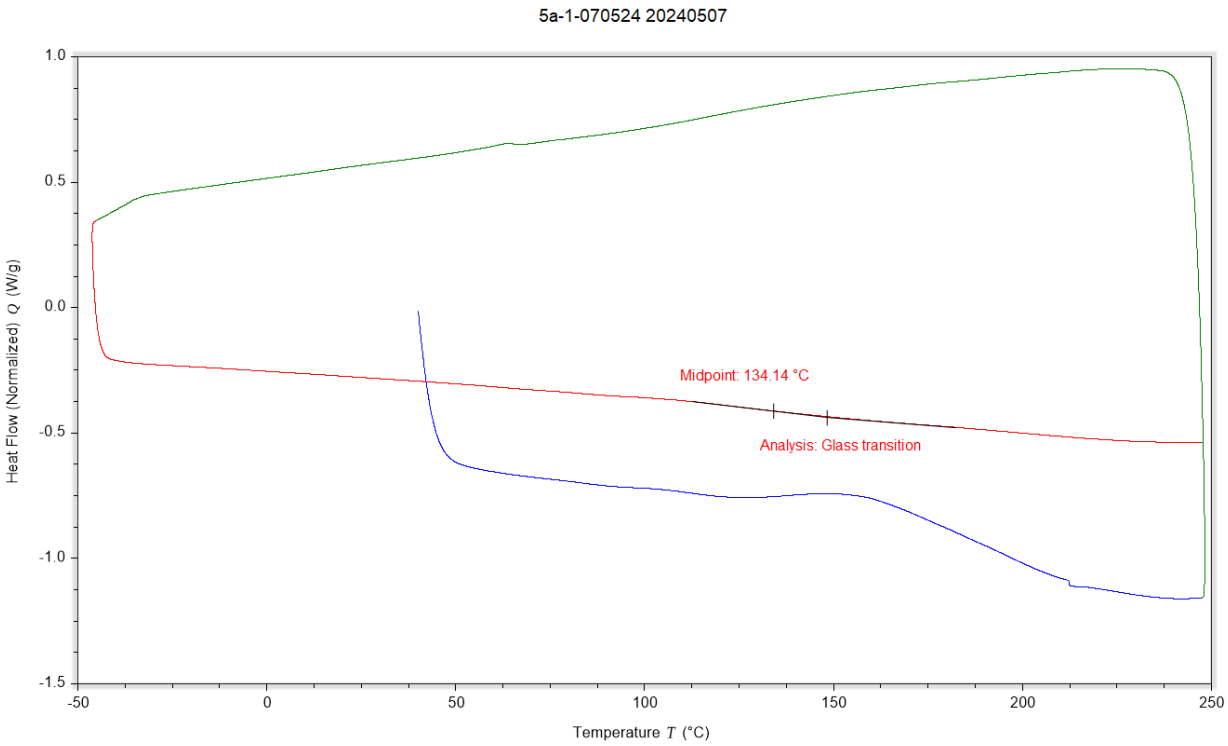

Figure C36. DSC trace for material **5a**.

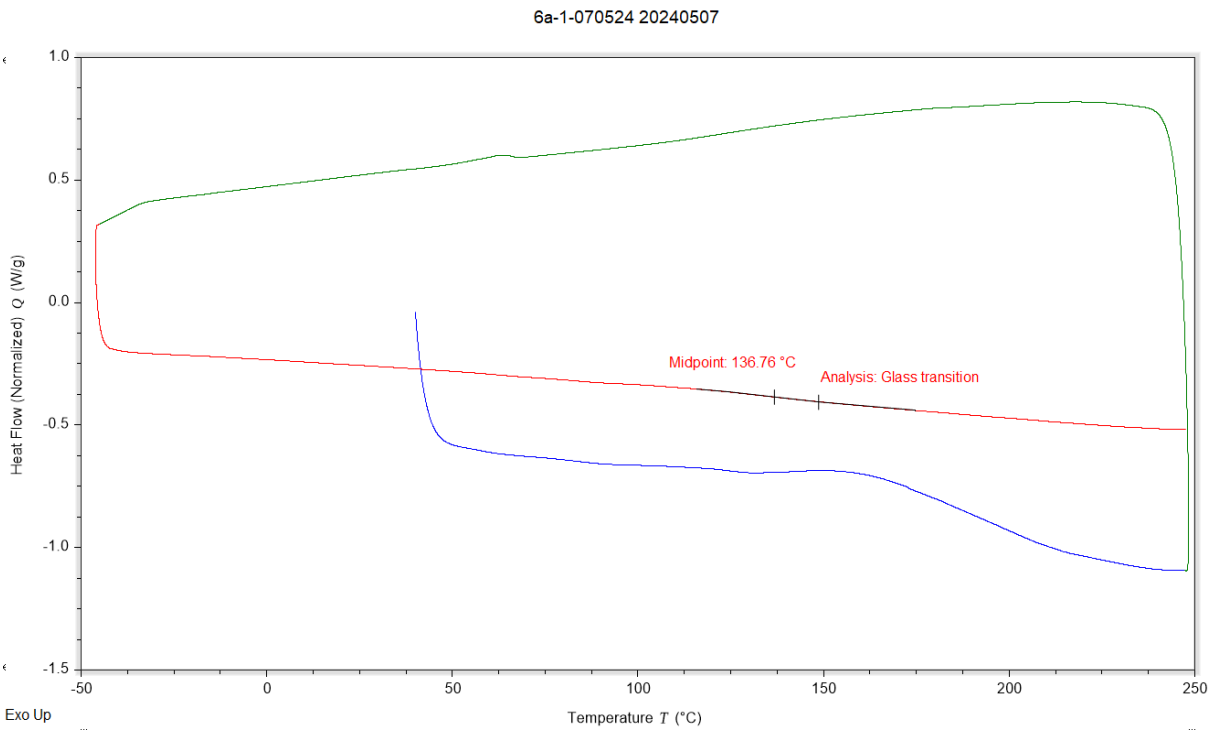

Figure C37. DSC trace for material **6a**.

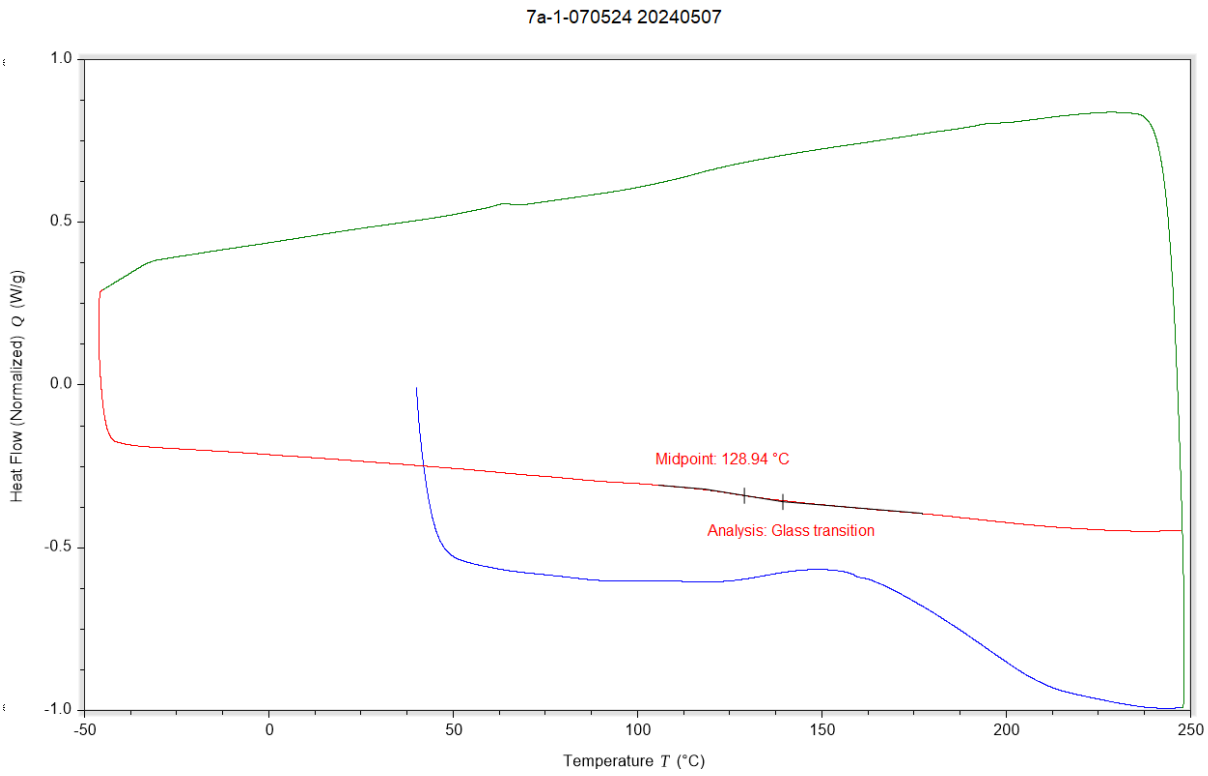

Figure C38. DSC trace for material **7a**.

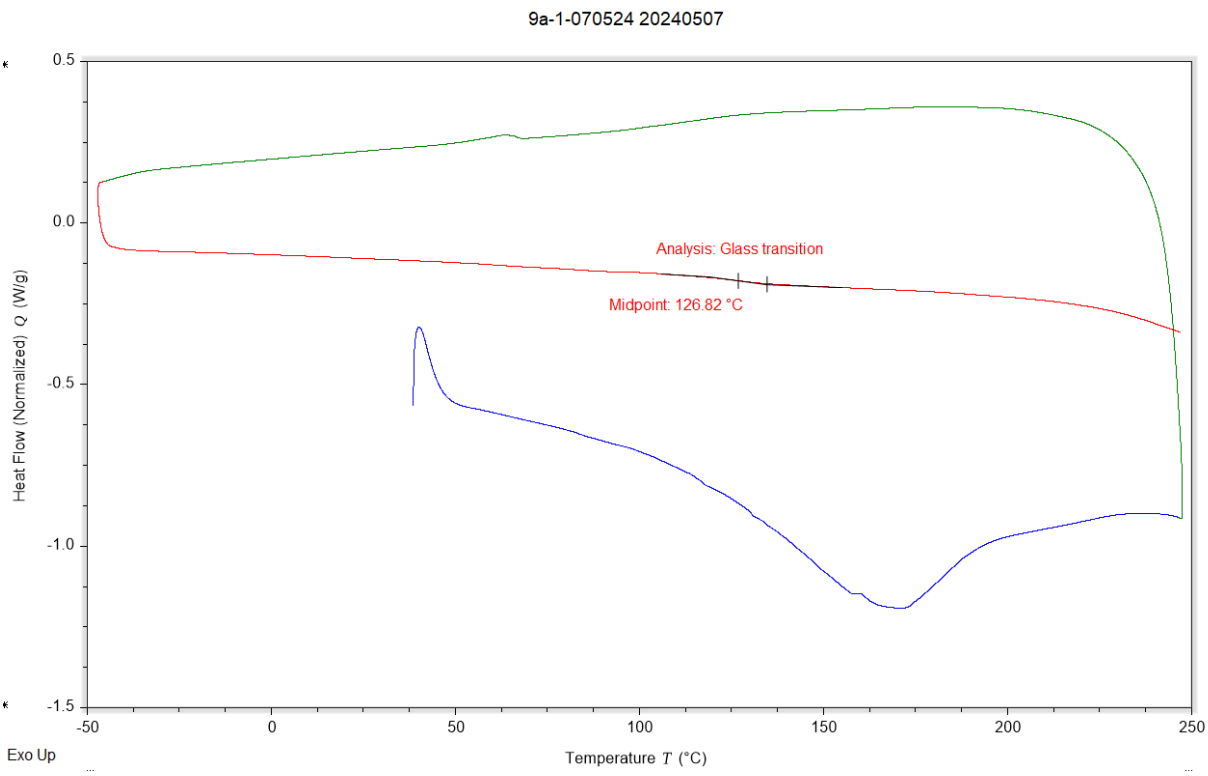

Figure C39. DSC trace for material **9a**.

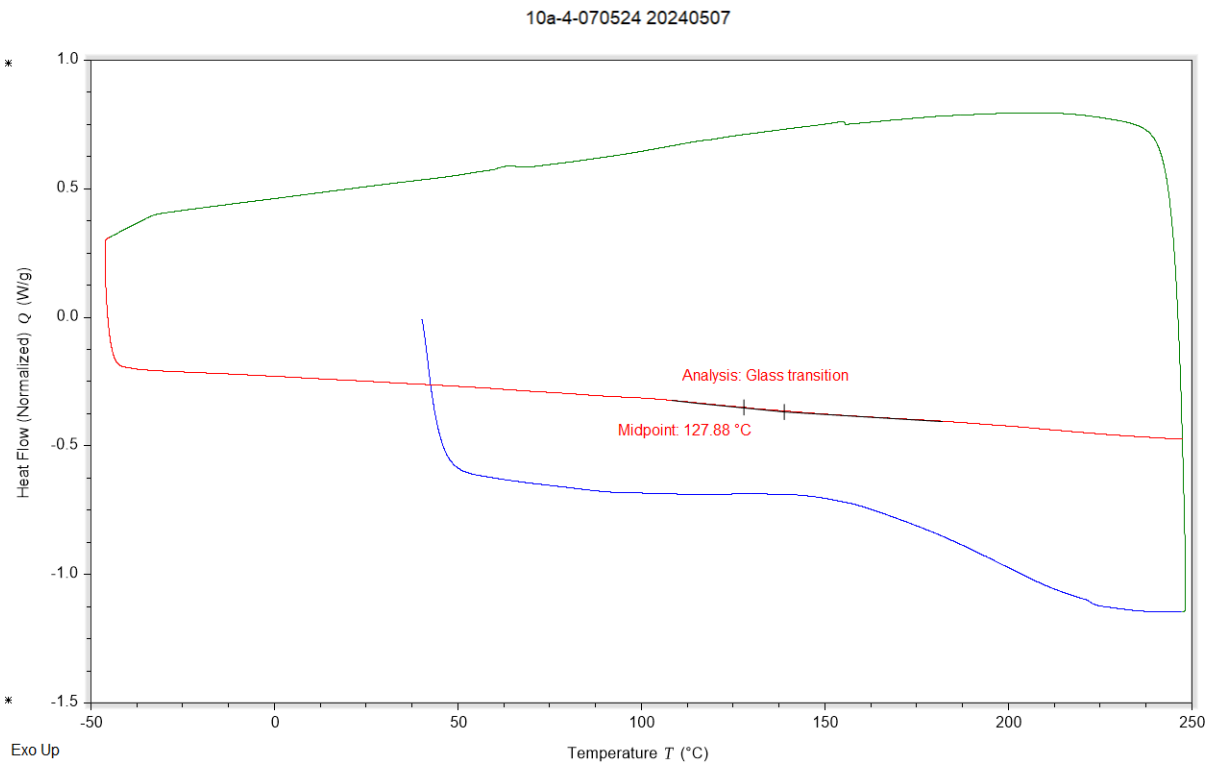

Figure C40. DSC trace for material **10a**.

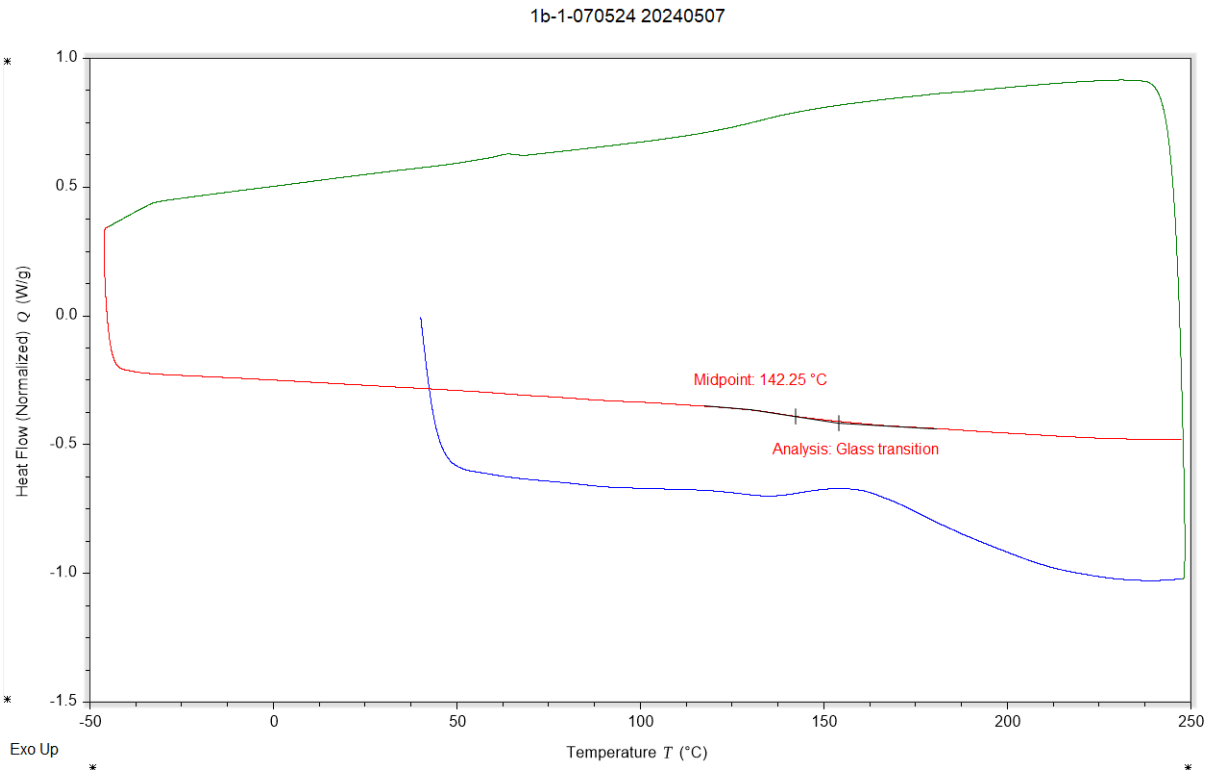

Figure C41. DSC trace for material **1b**.

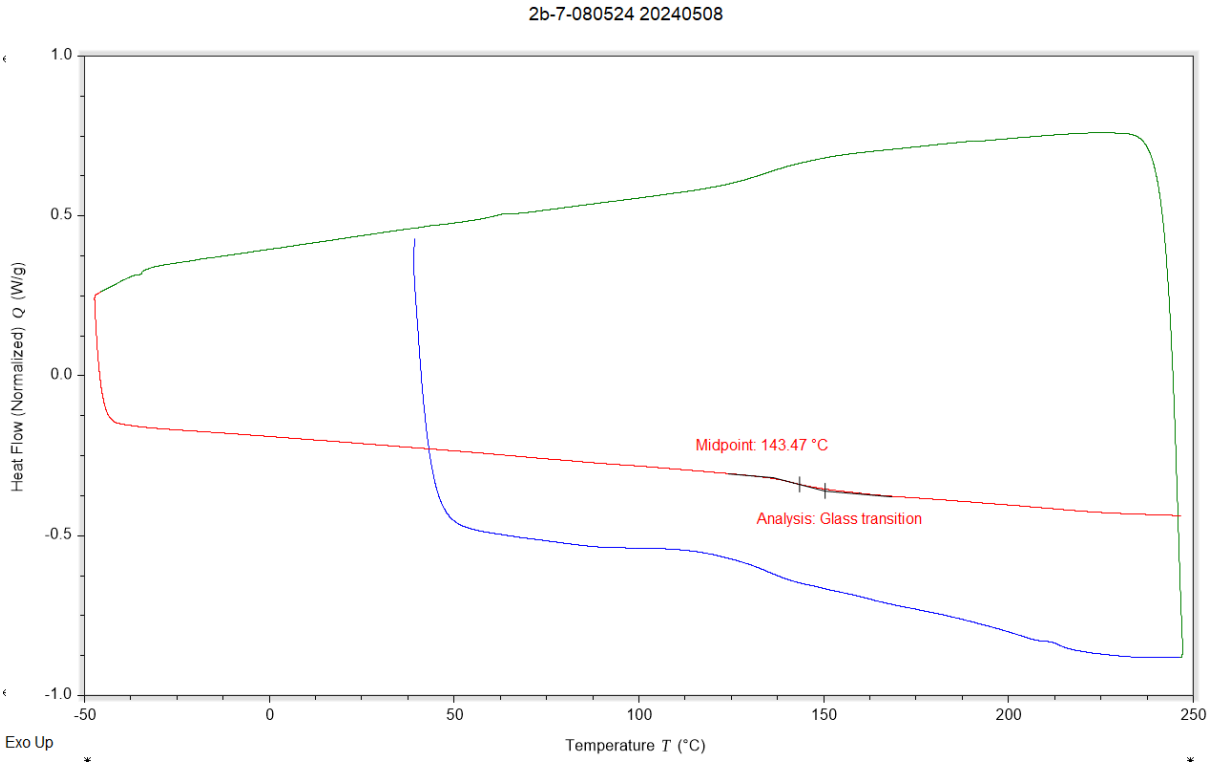

Figure C42. DSC trace for material **2b**.

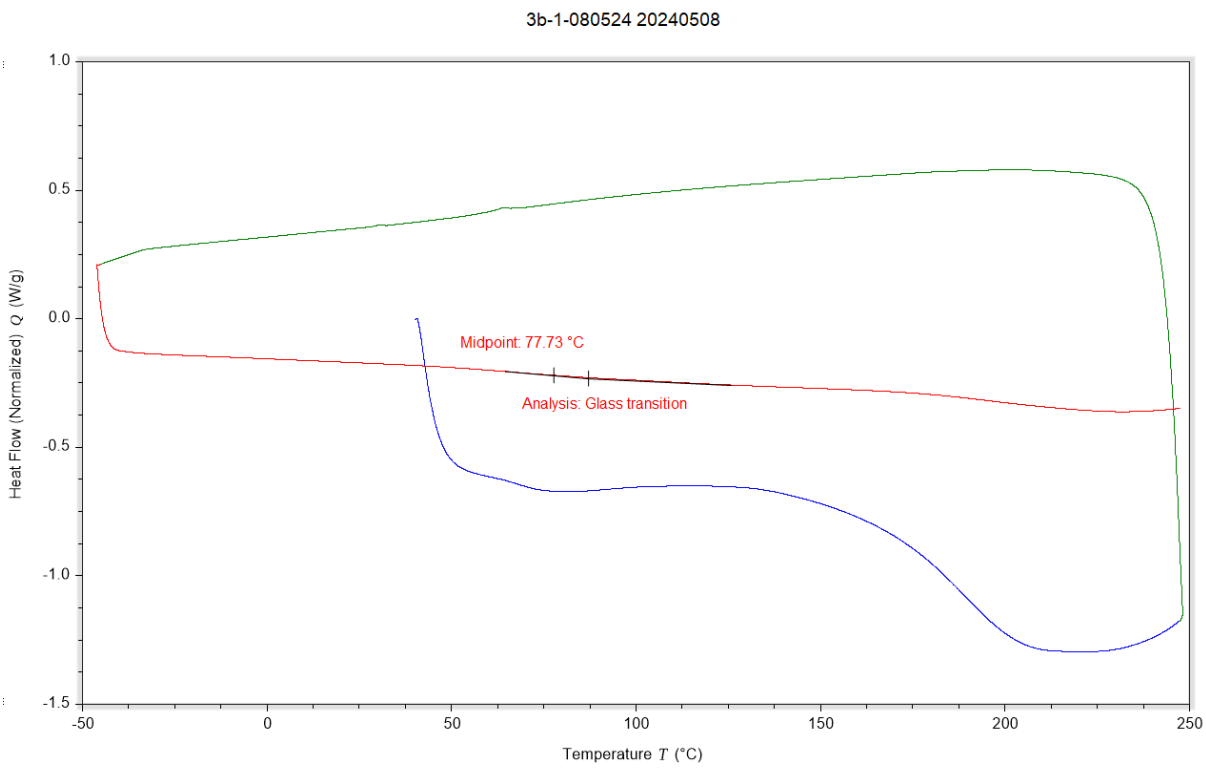

Figure C43. DSC trace for material **3b**.

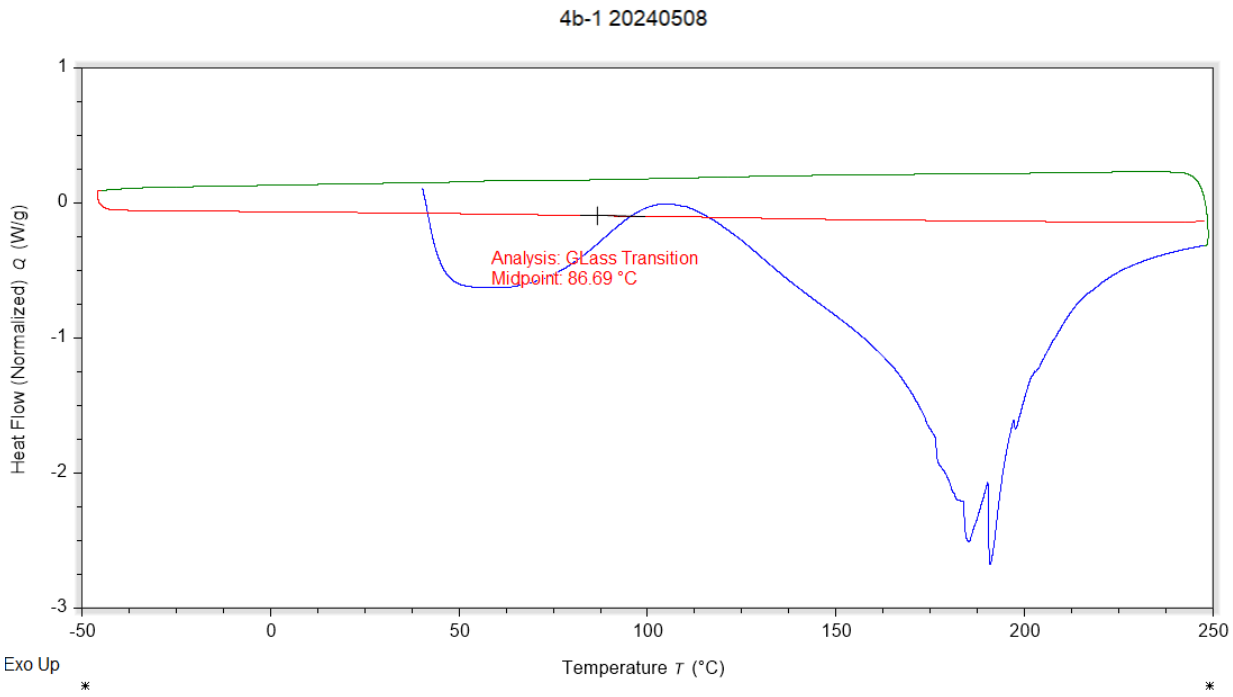

Figure C44. DSC trace for material **4b**.

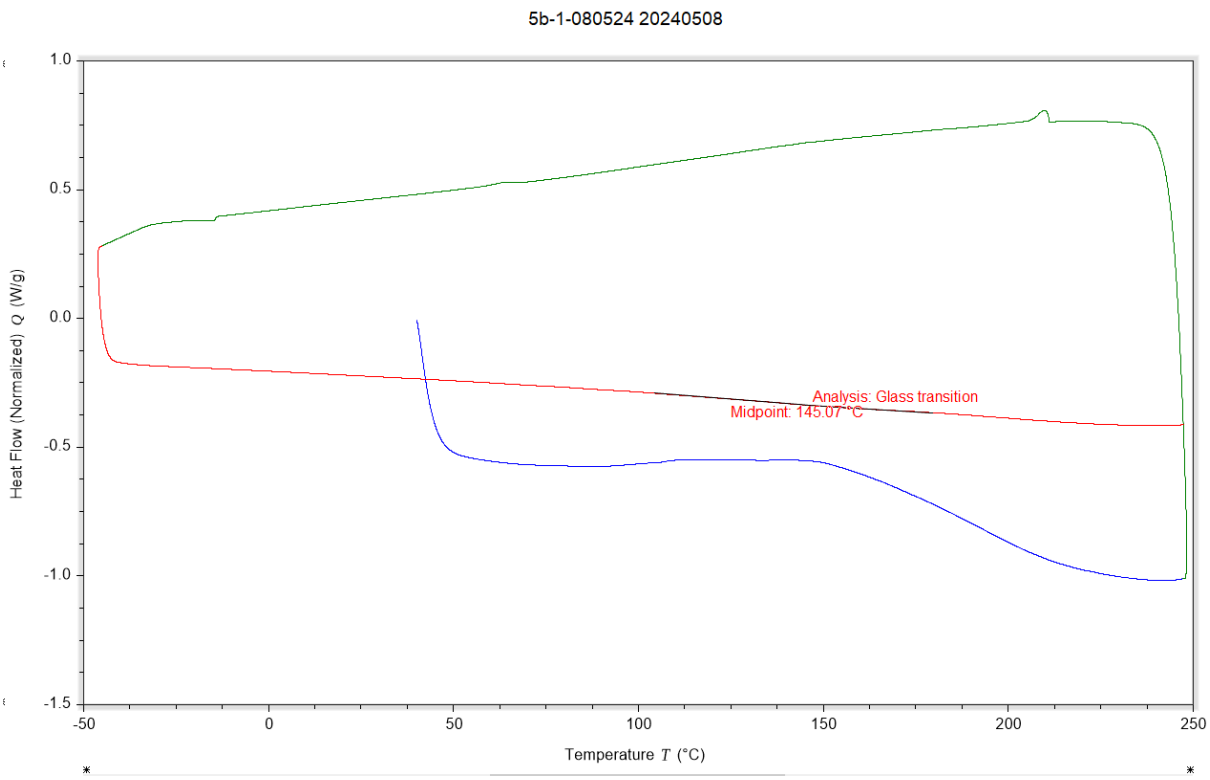

Figure C45. DSC trace for material **5b**.

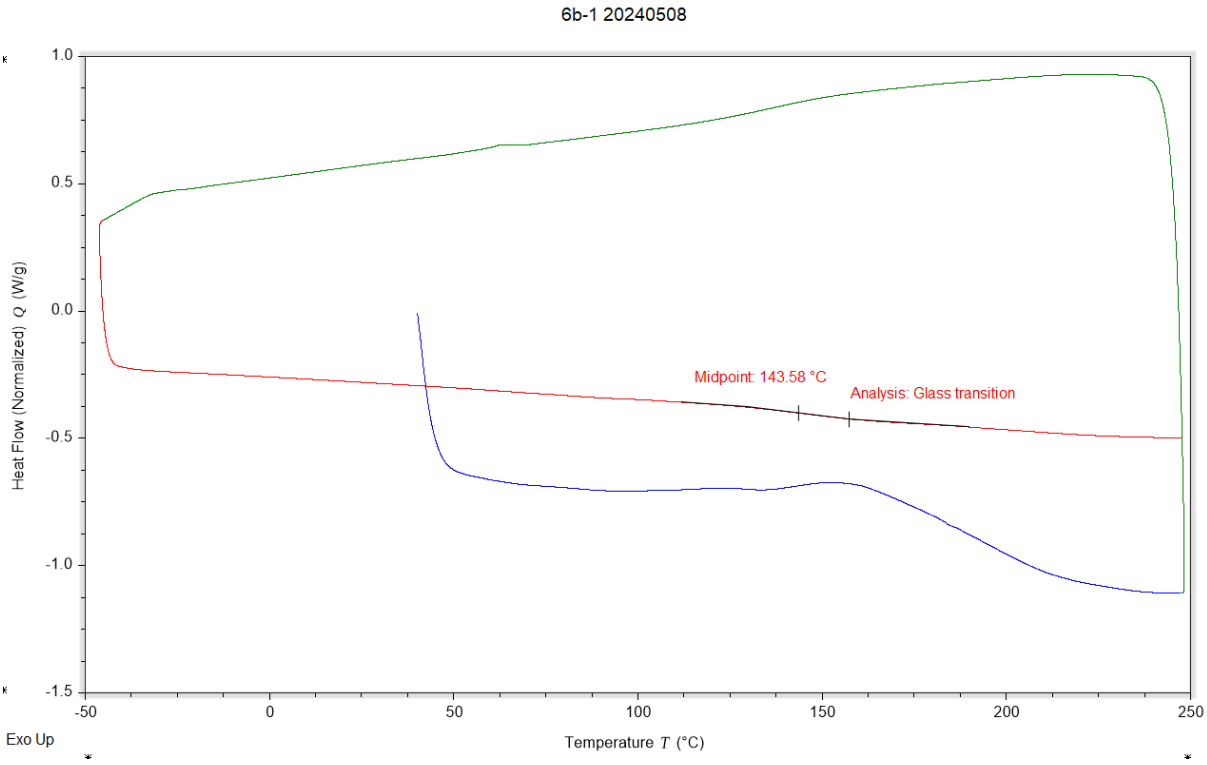

Figure C46. DSC trace for material **6b**.

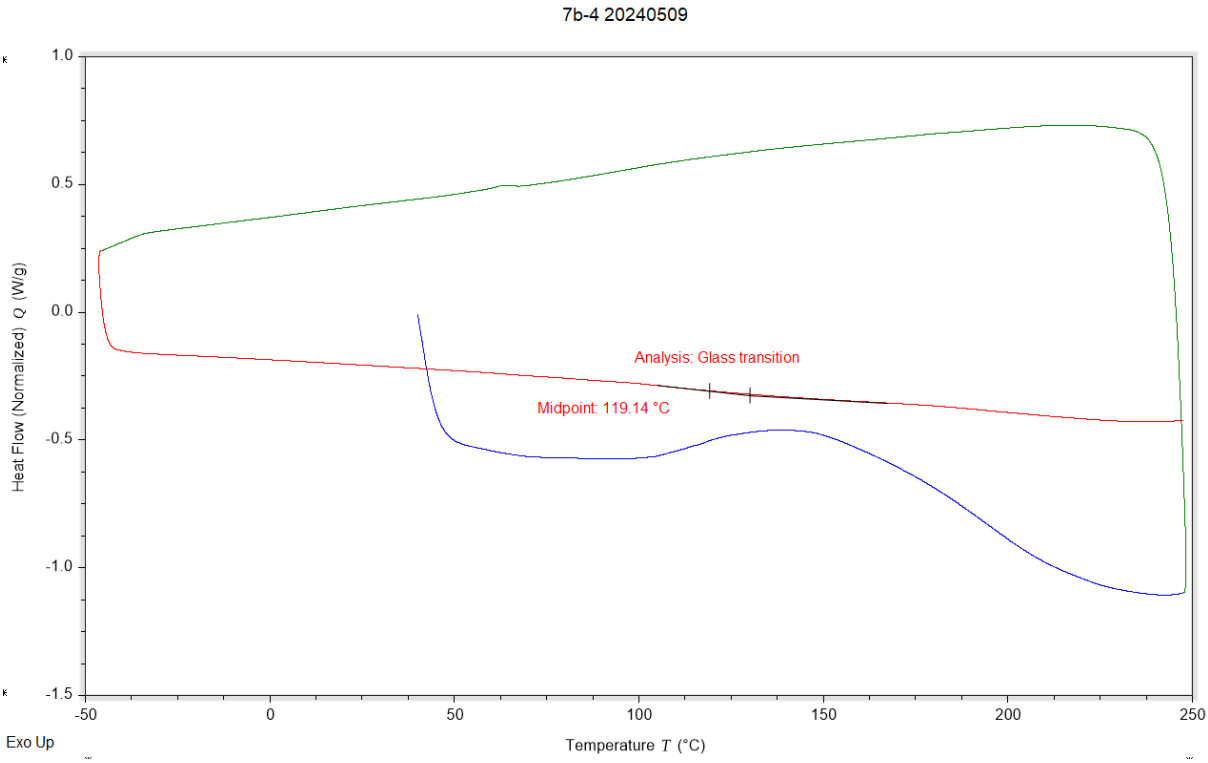

Figure C47. DSC trace for material **7b**.

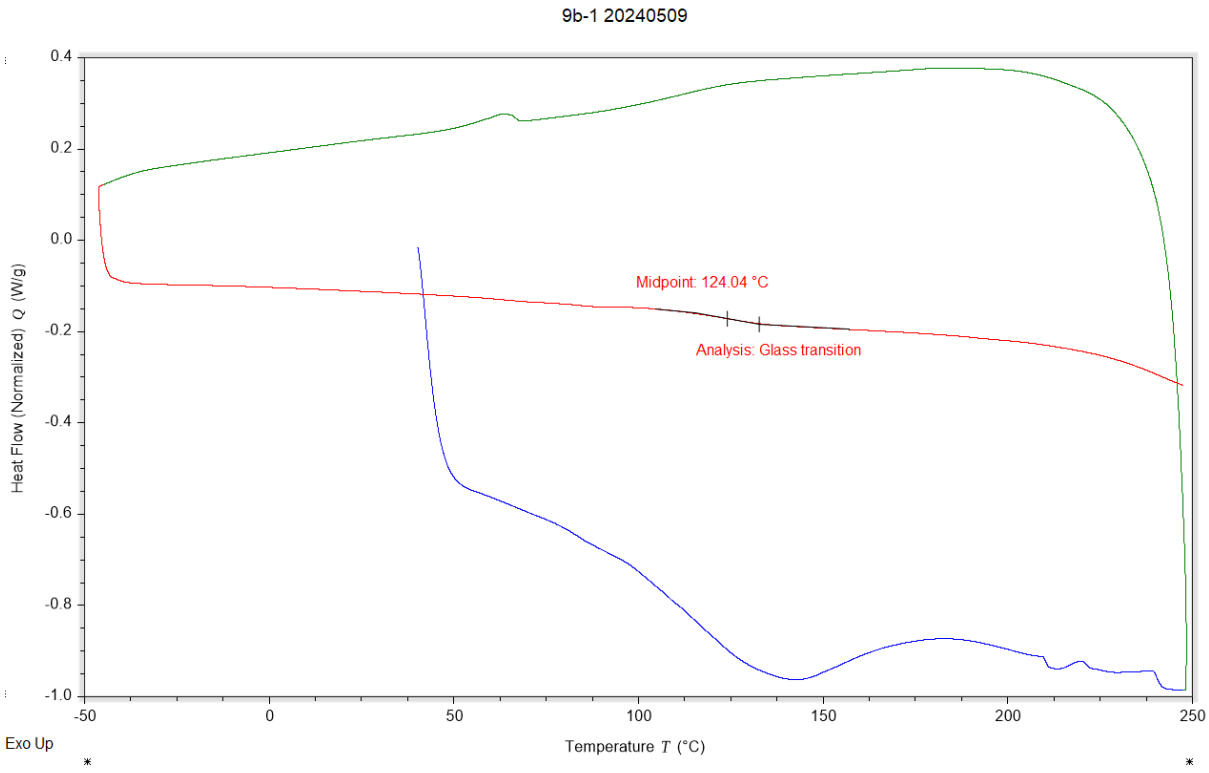

Figure C48. DSC trace for material **9b**.

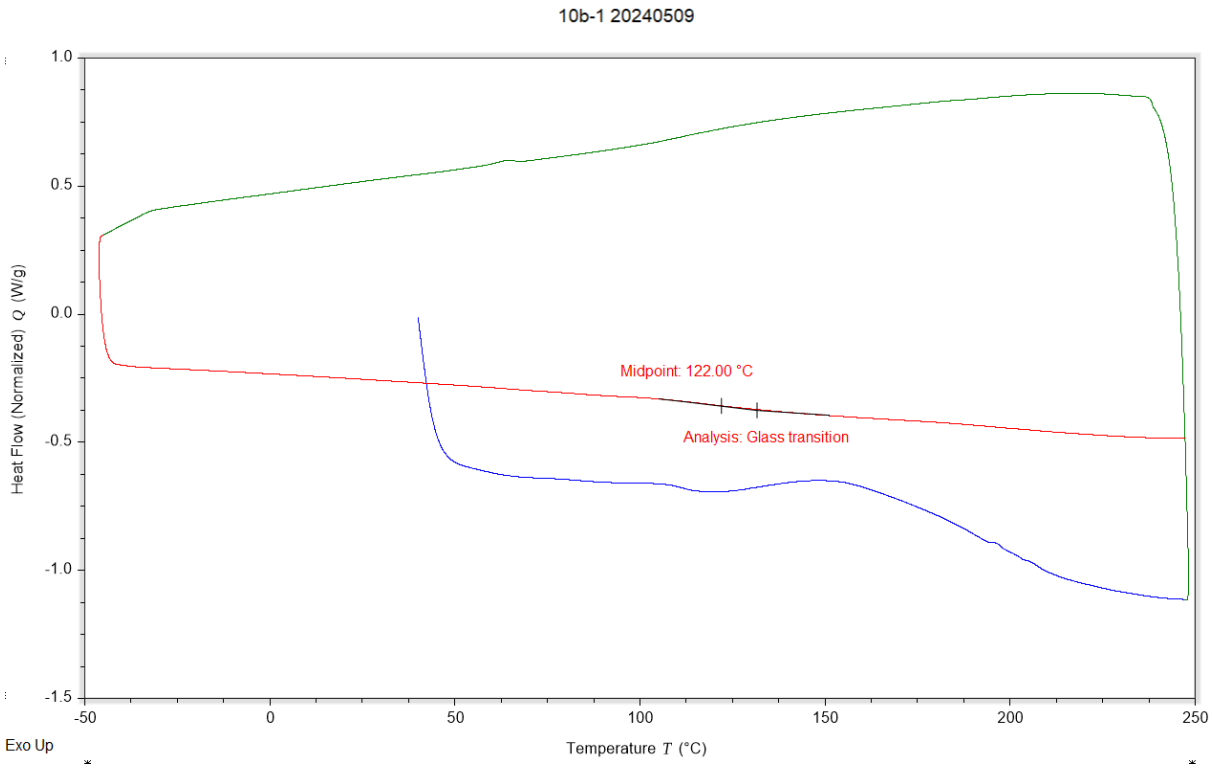

Figure C49. DSC trace for material **10b**.

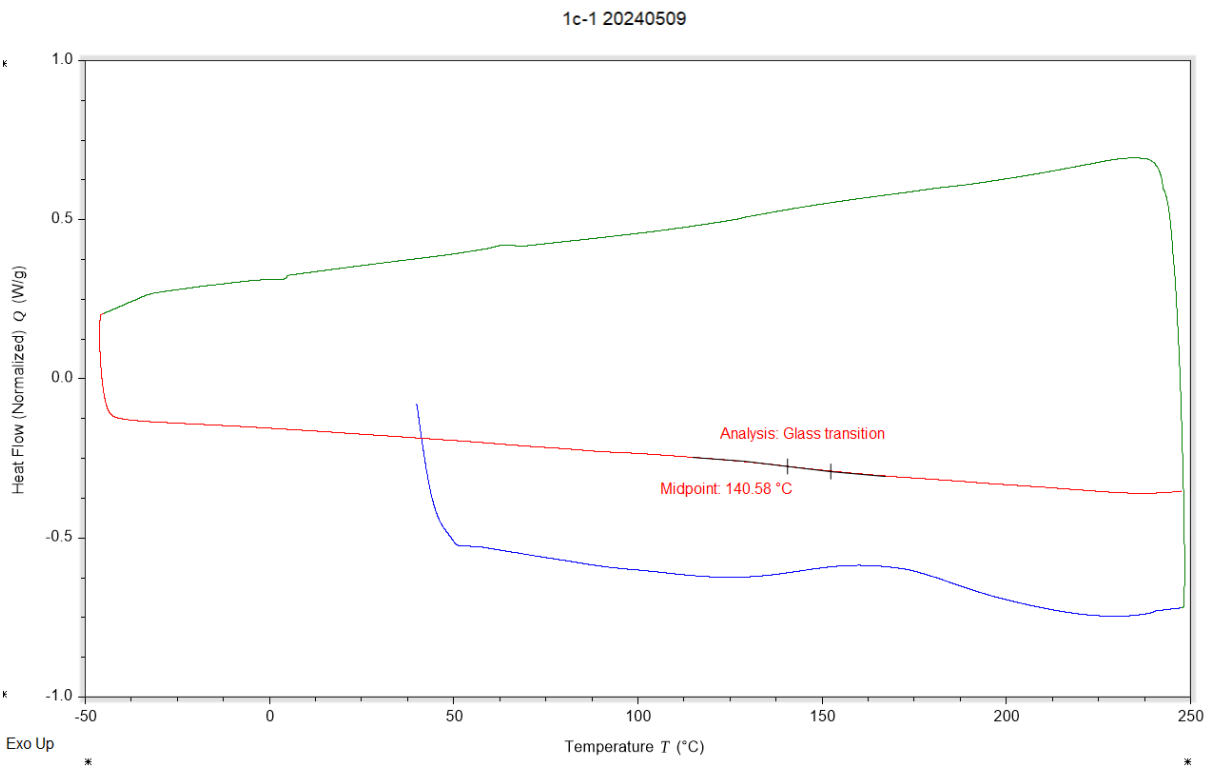

Figure C50. DSC trace for material **1c**.

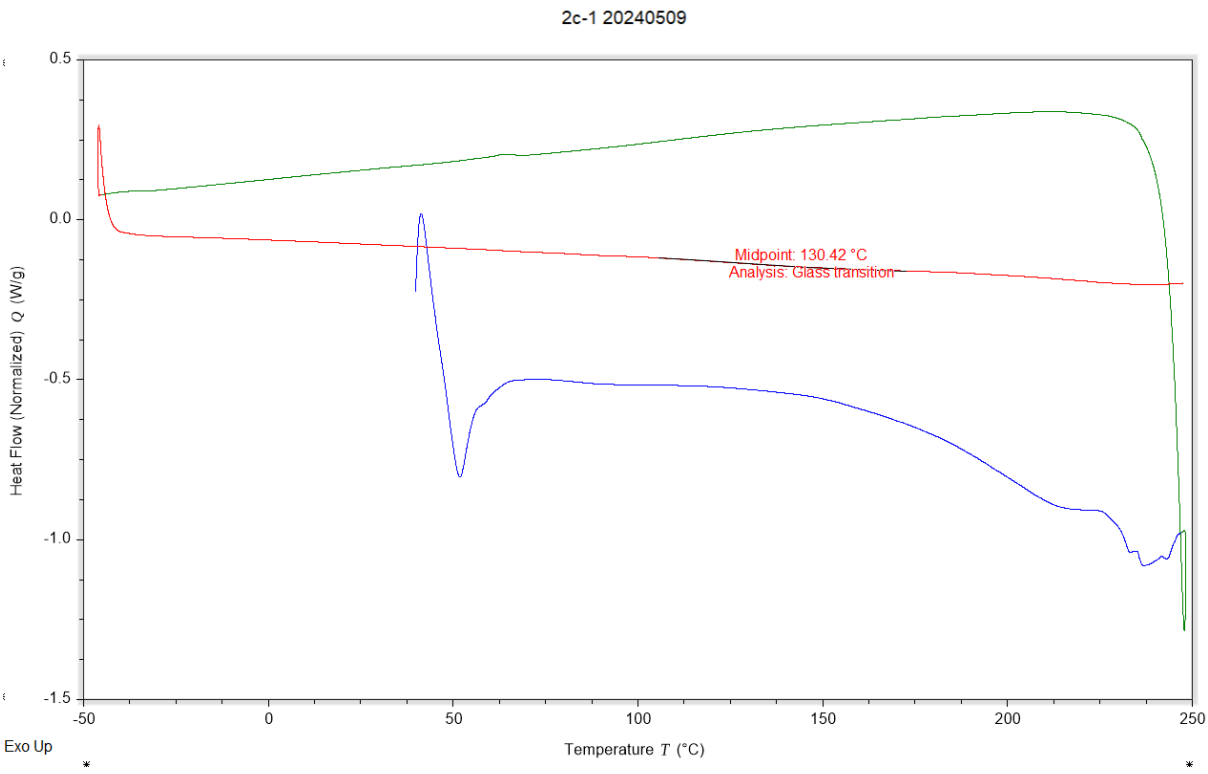

Figure C51. DSC trace for material **2c**.

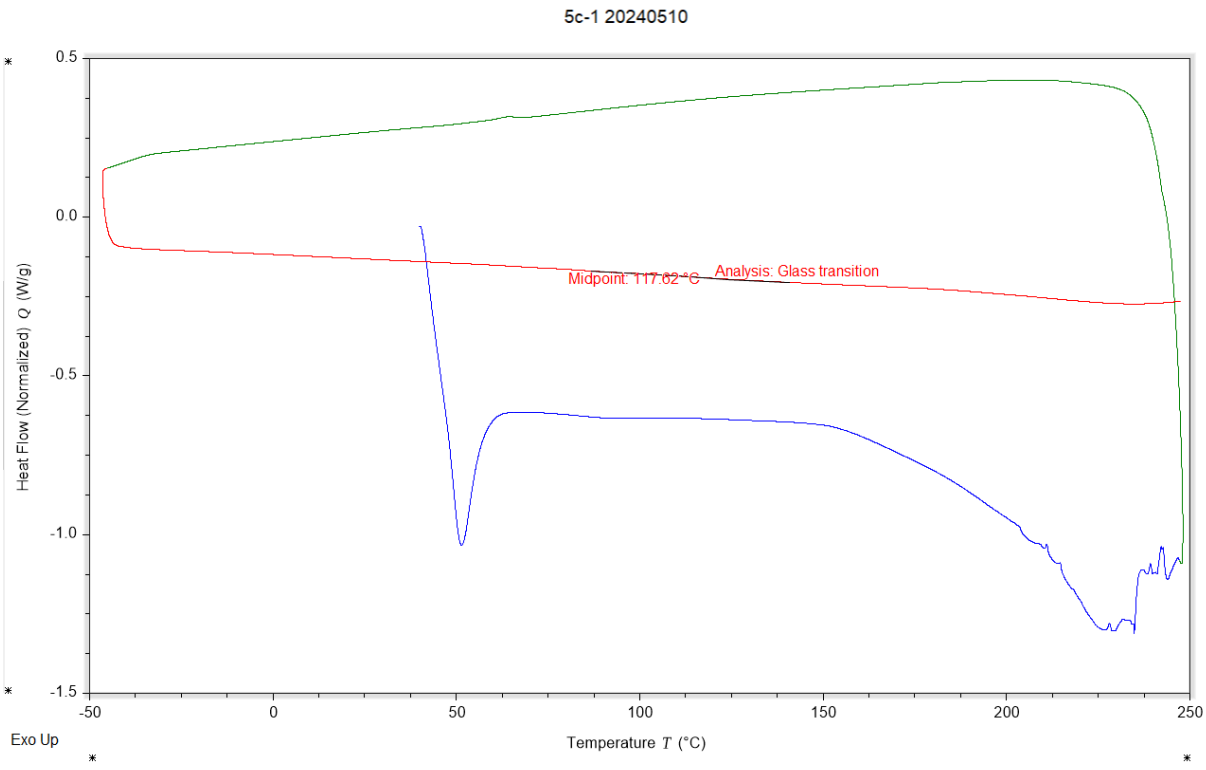

Figure C52. DSC trace for material **5c**.

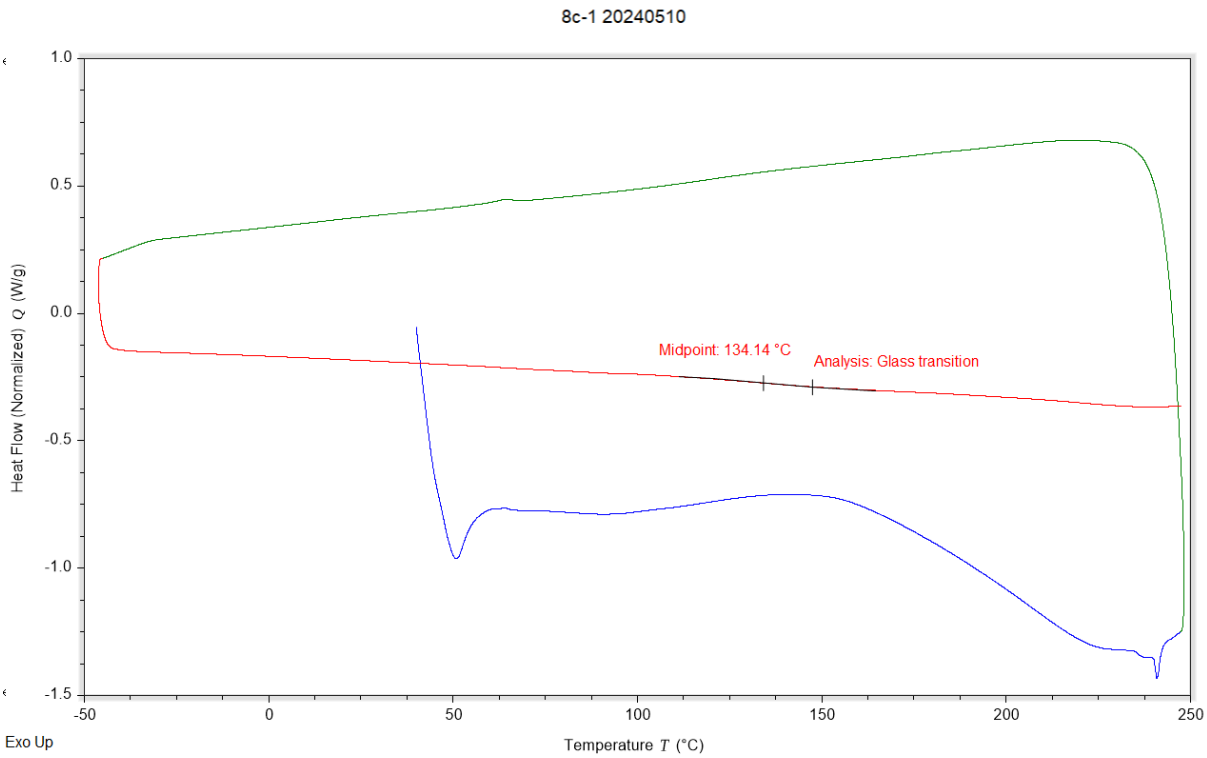

Figure C53. DSC trace for material **8c**.

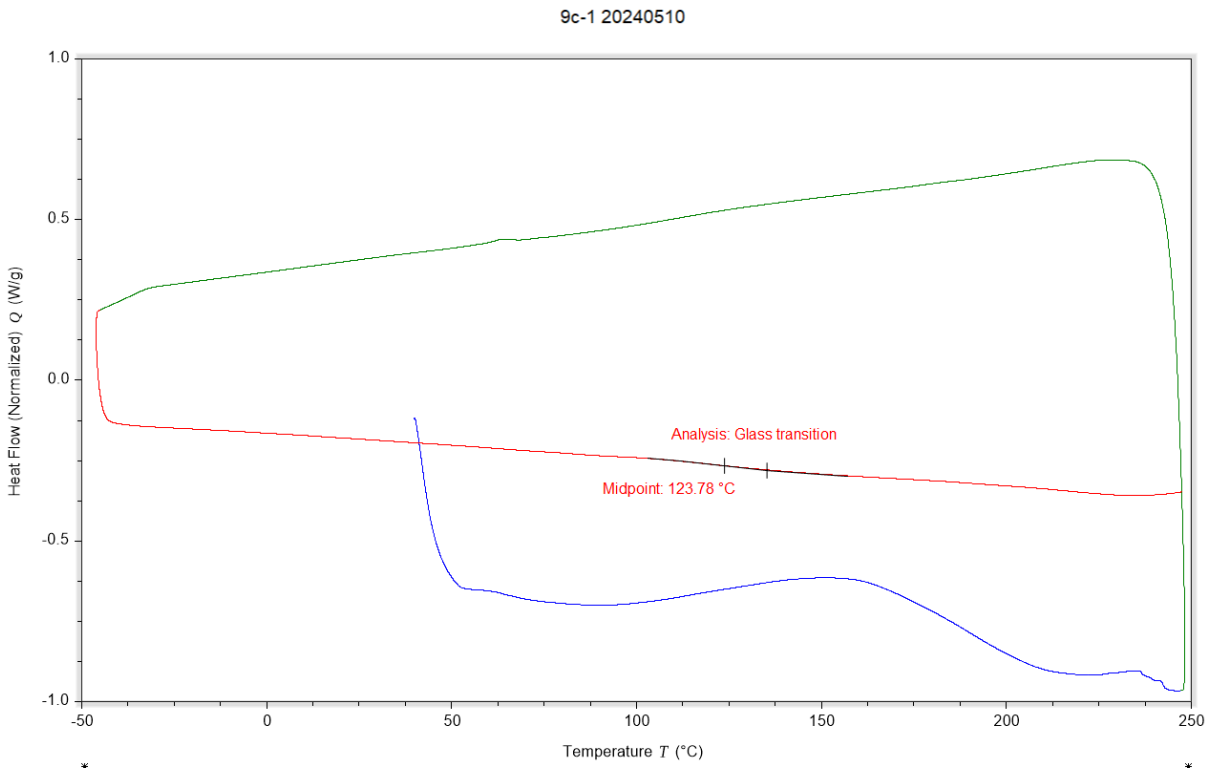

Figure C54. DSC trace for material **9c**.

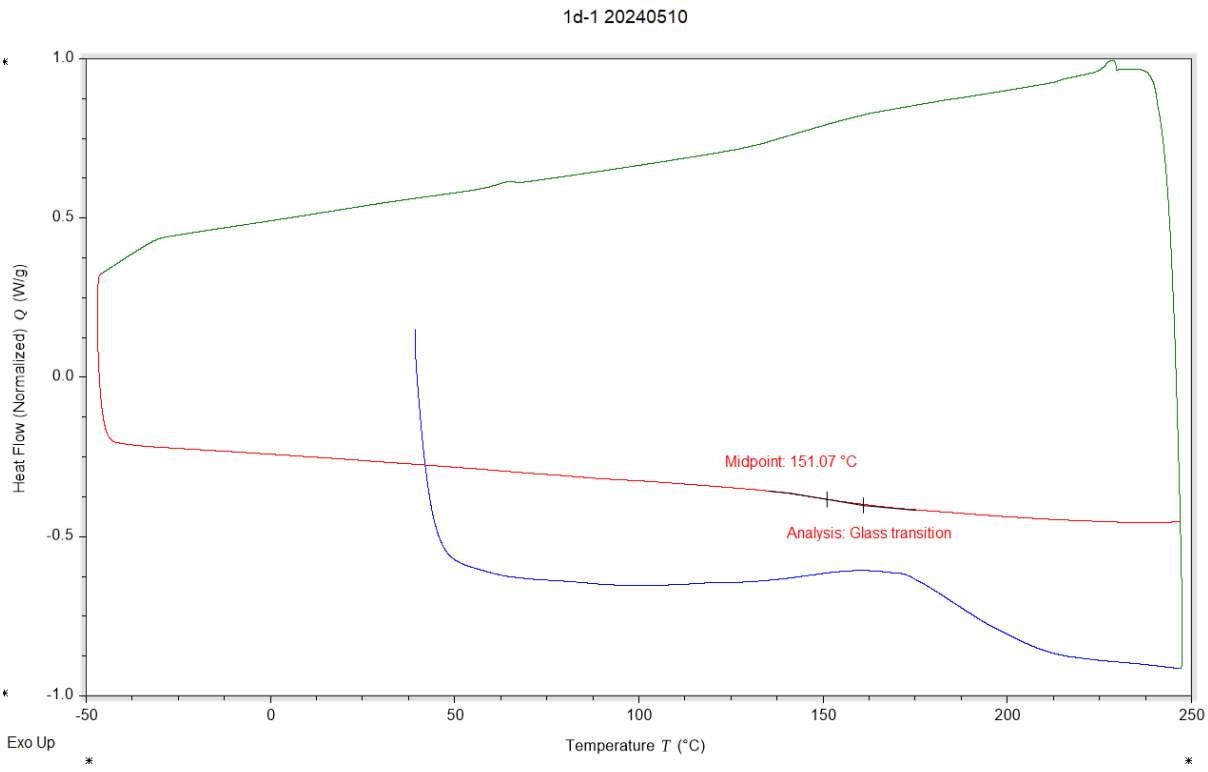

Figure C55. DSC trace for material **1d**.

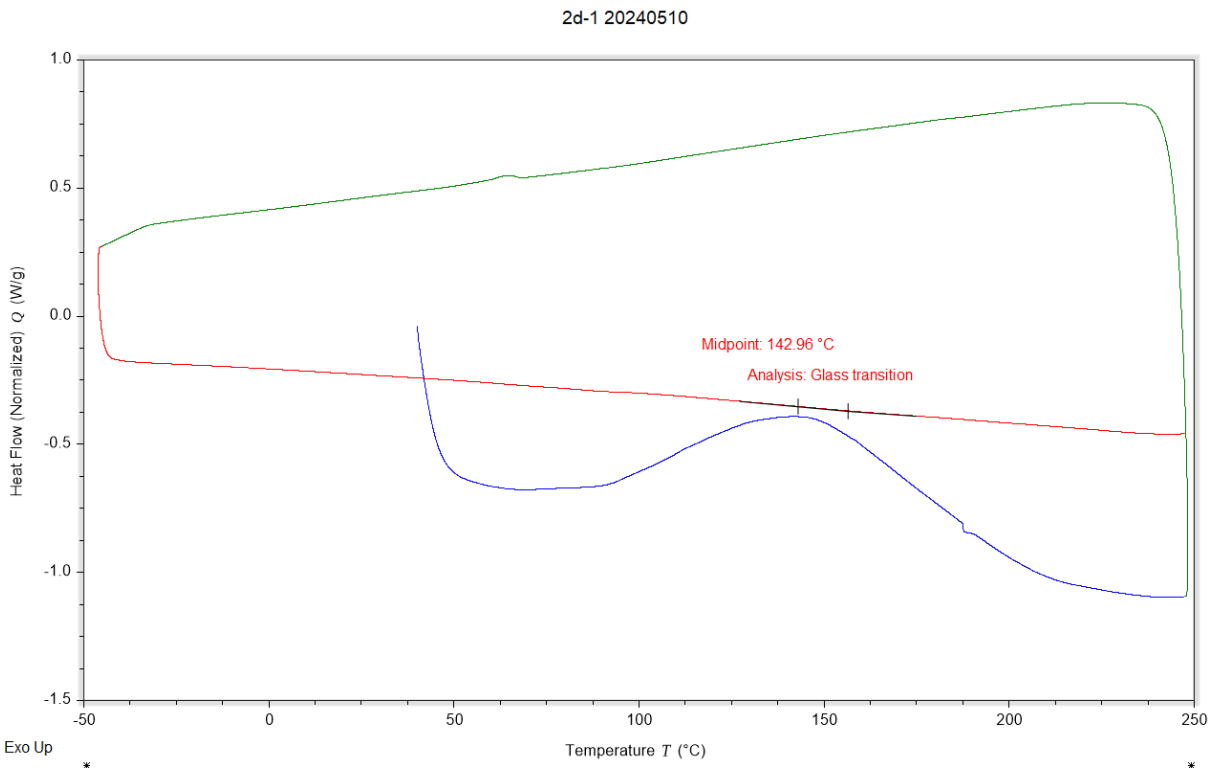

Figure C56. DSC trace for material **2d**.

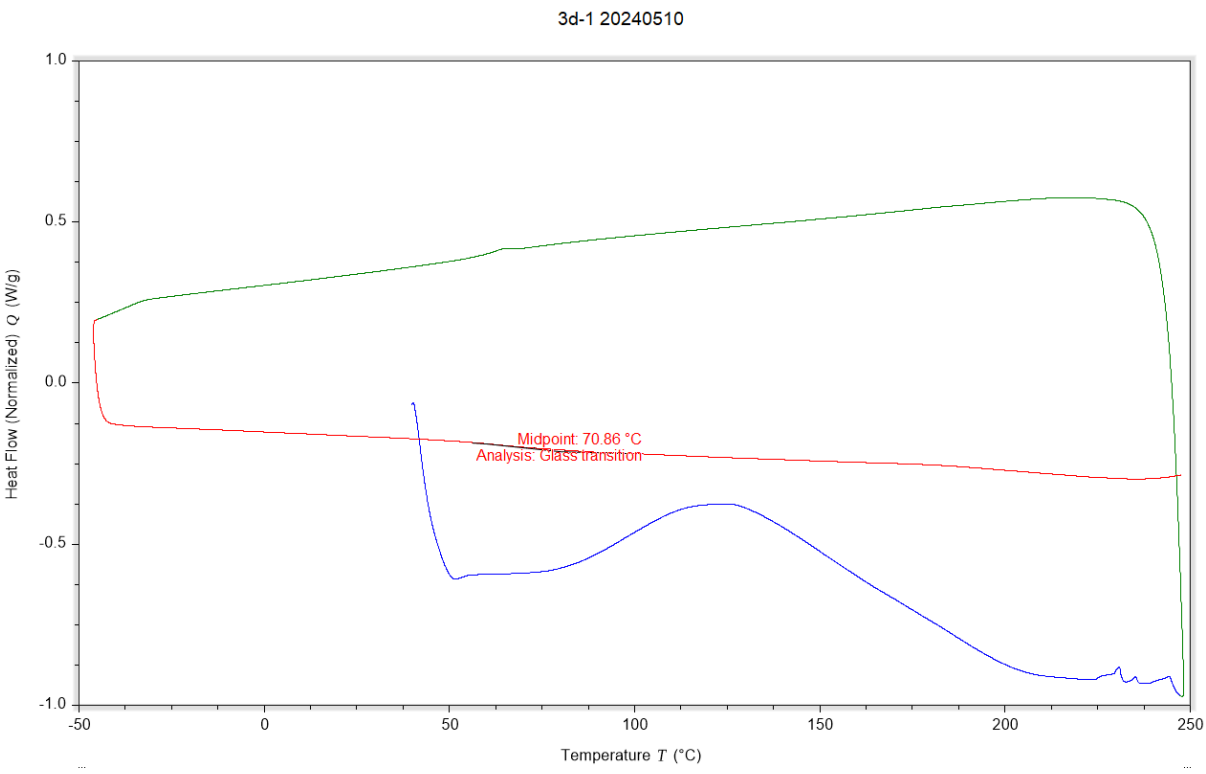

Figure C57. DSC trace for material **3d**.

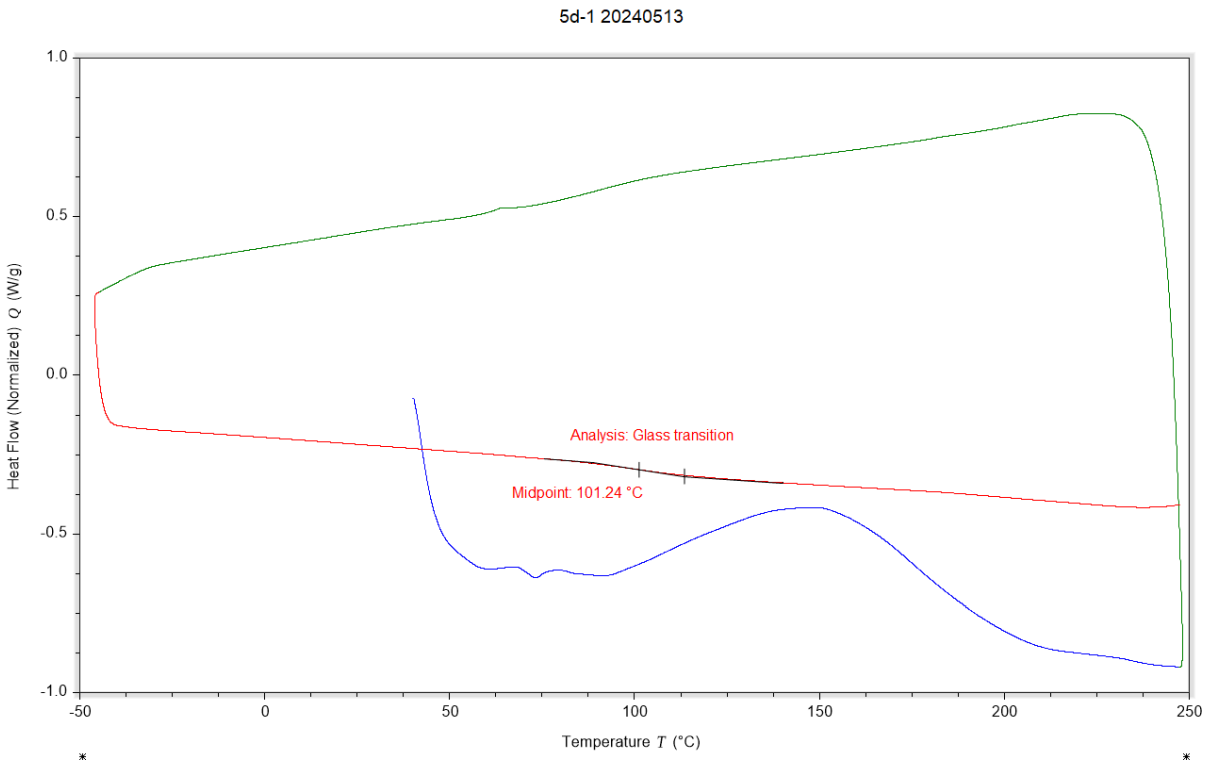

Figure C58. DSC trace for material **5d**.

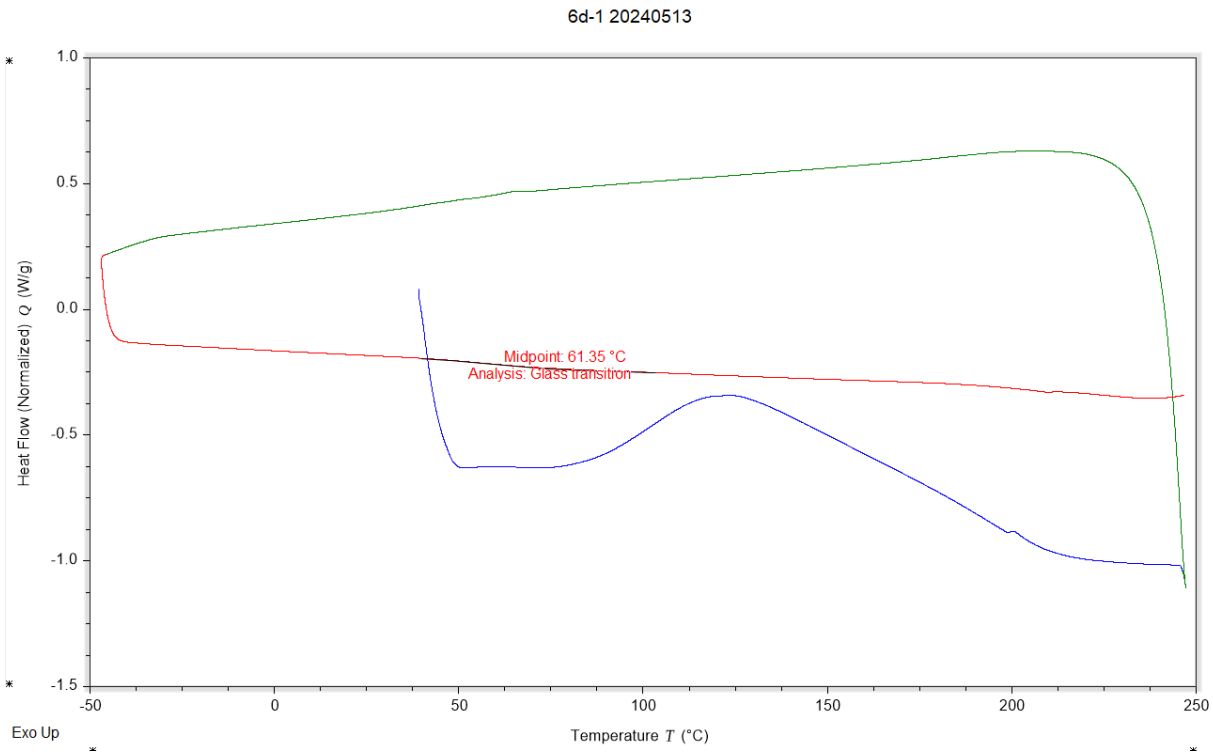

Figure C59. DSC trace for material **6d**.

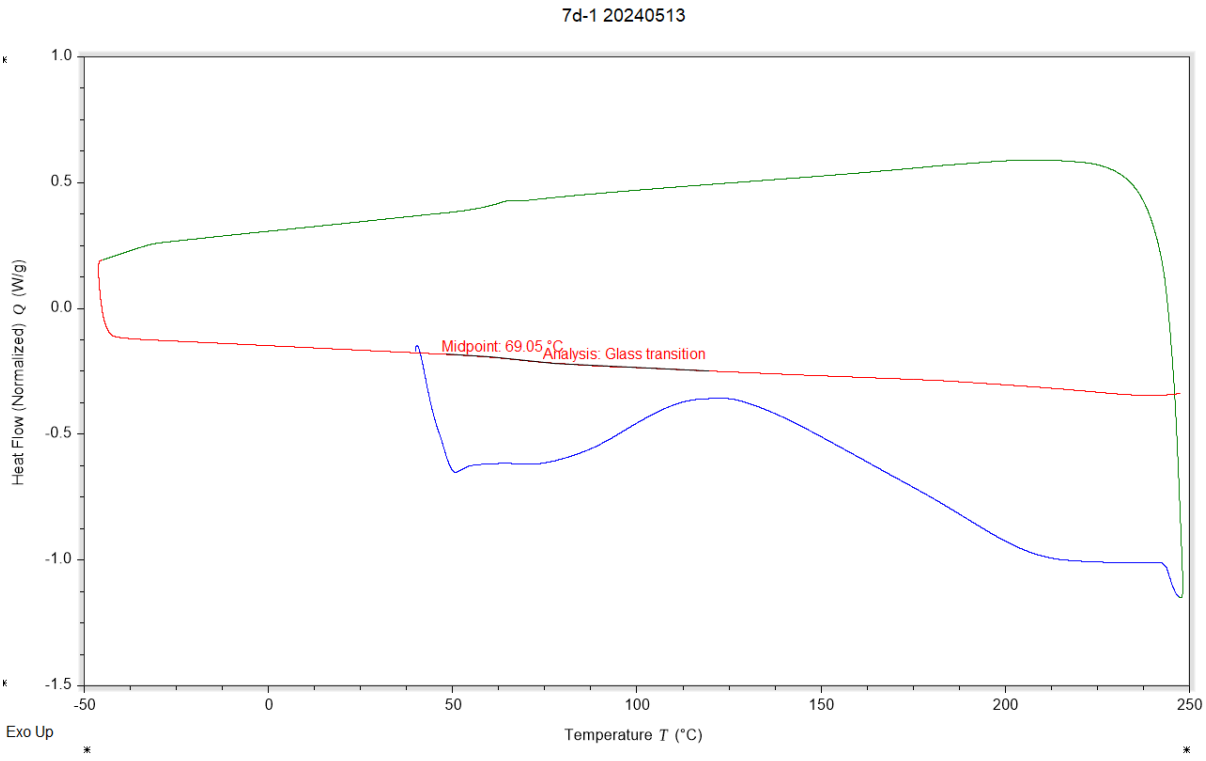

Figure C60. DSC trace for material **7d**.

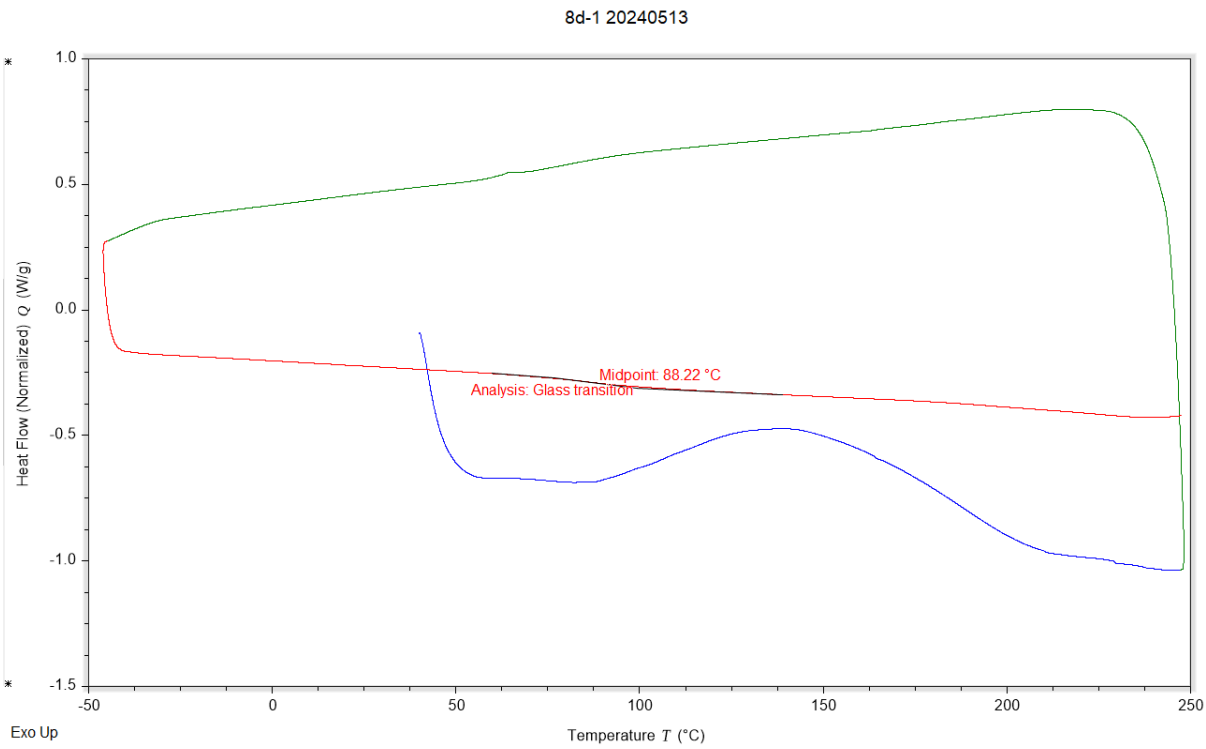

Figure C61. DSC trace for material **8d**.

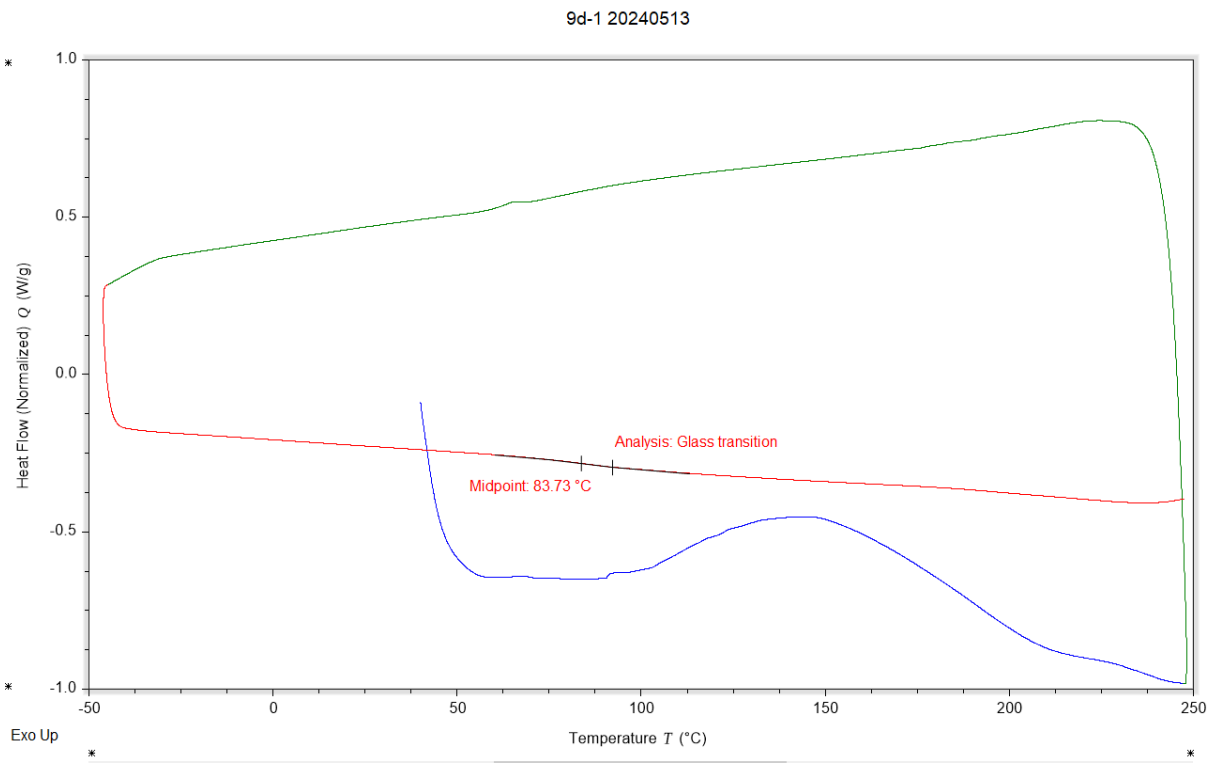

Figure C62. DSC trace for material **9d**.

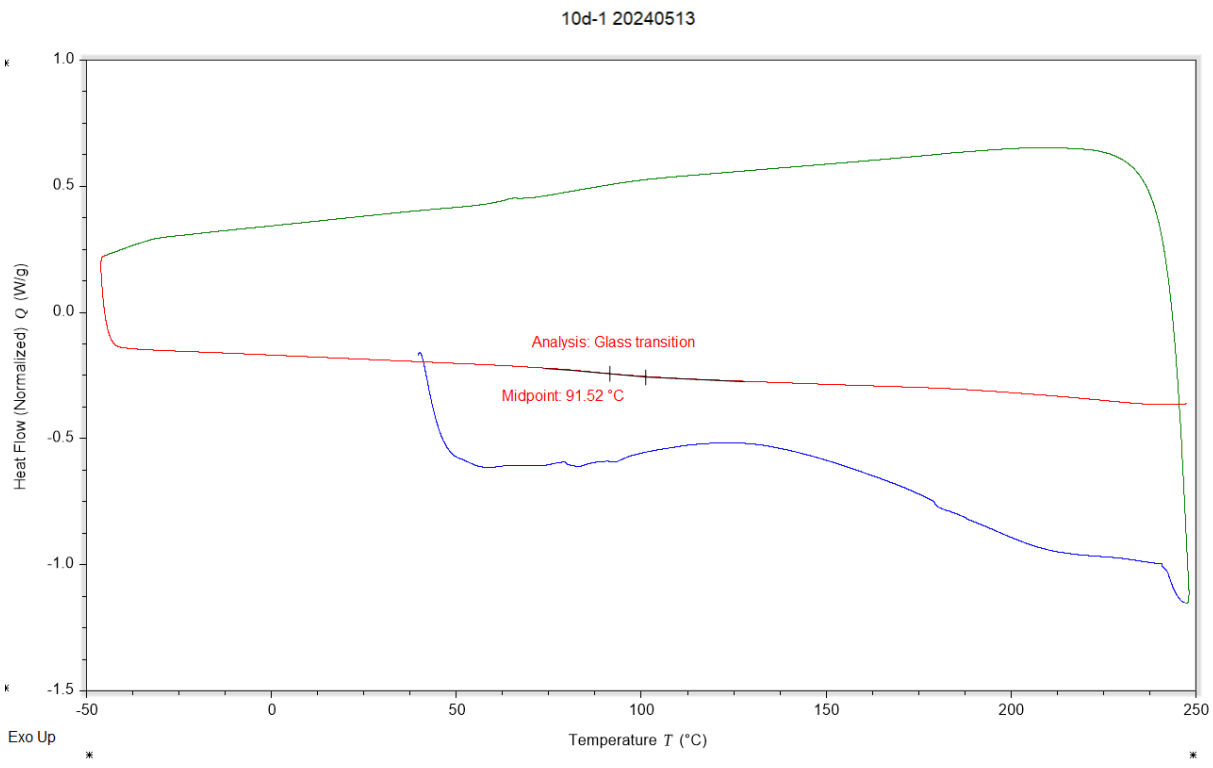

Figure C63. DSC trace for material **10d**.

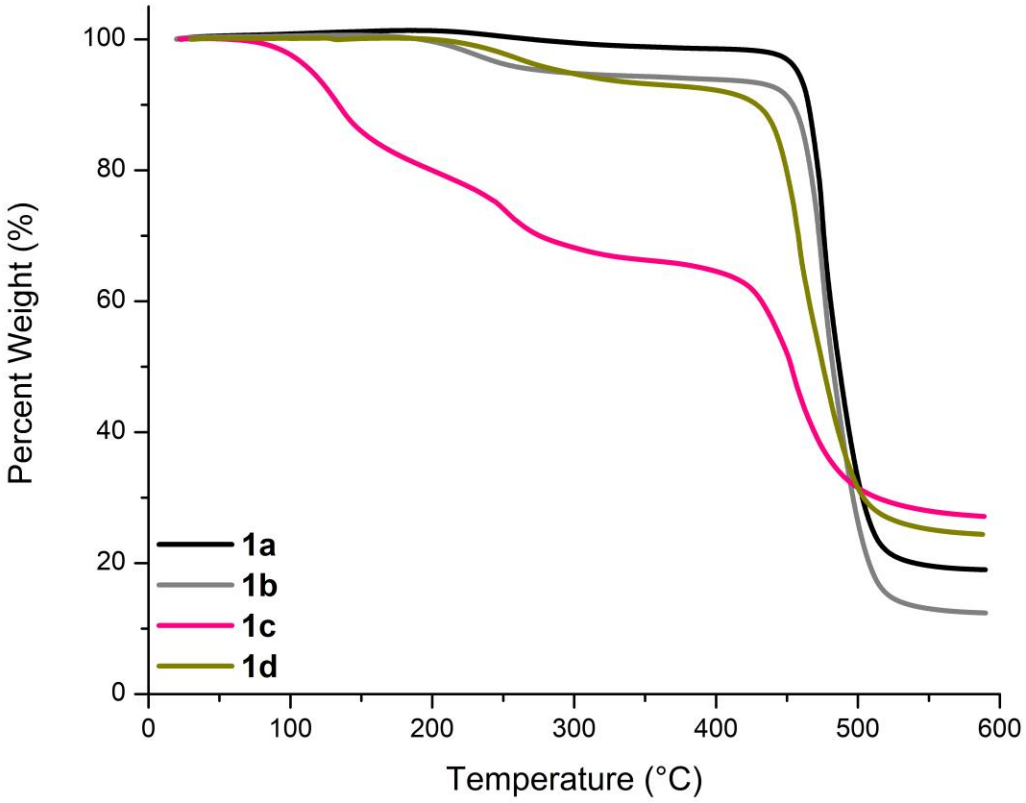

Figure C64. Thermogravimetric analysis of **type-a**, **b**, **c**, and **d** resins.

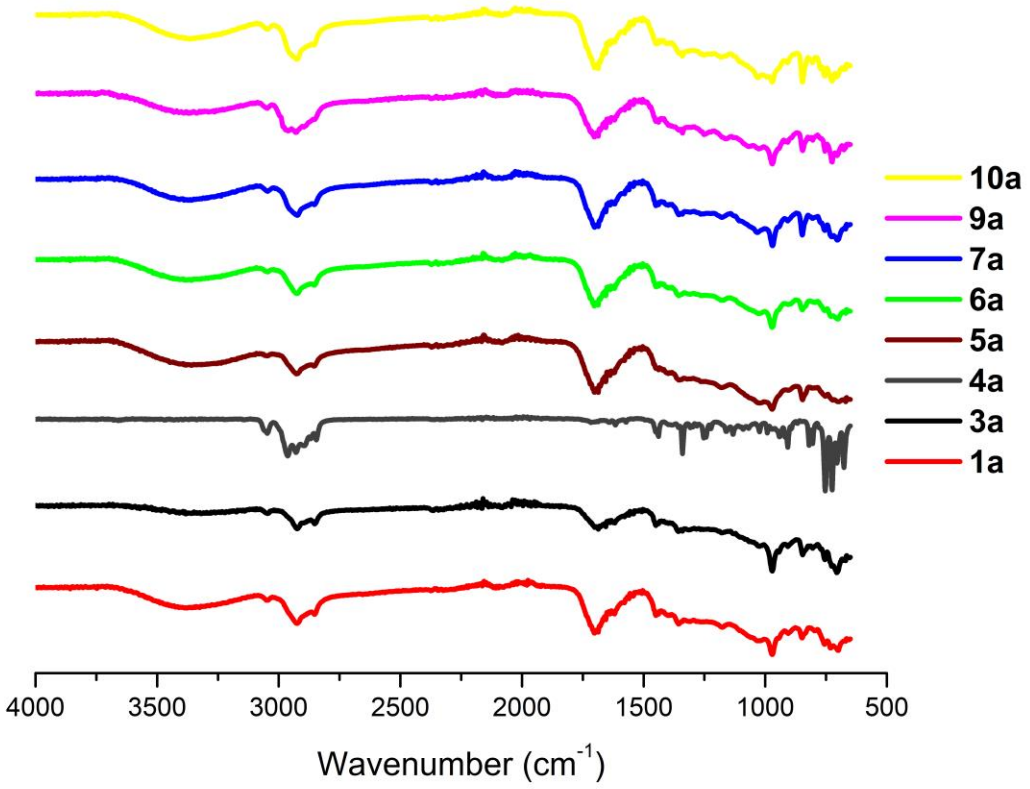

Figure C65. Normalized ATR spectra of materials made with **type-a** resin.

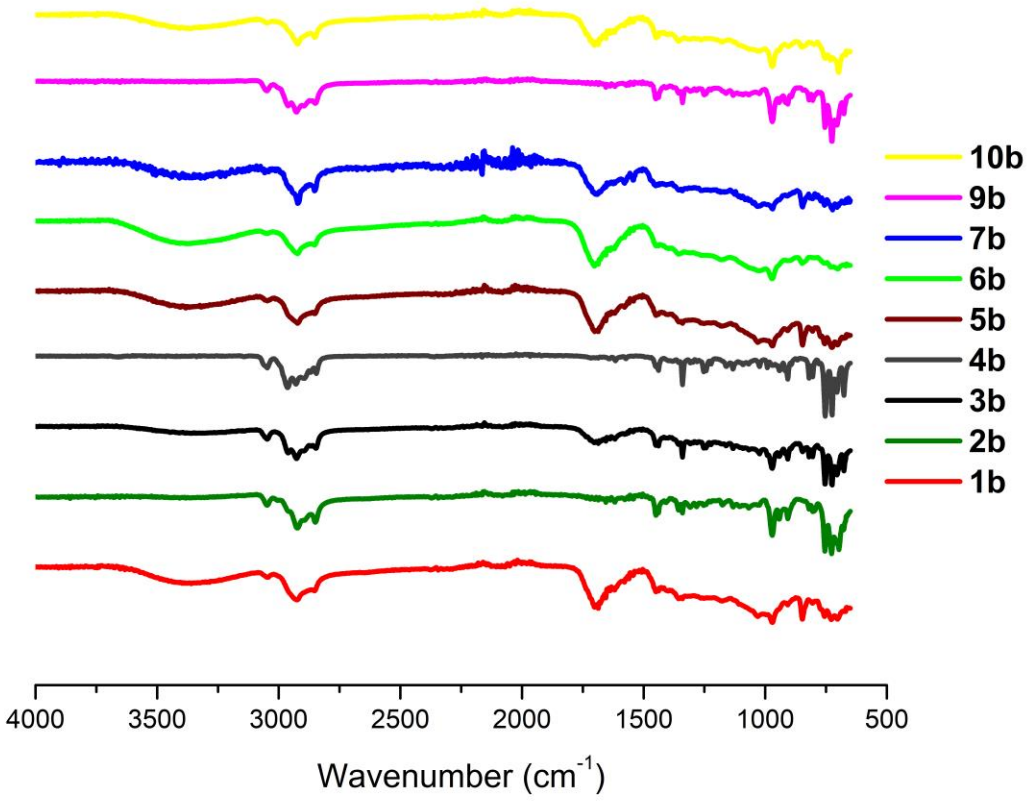

Figure C66. Normalized ATR spectra of materials made with **type-b** resin.

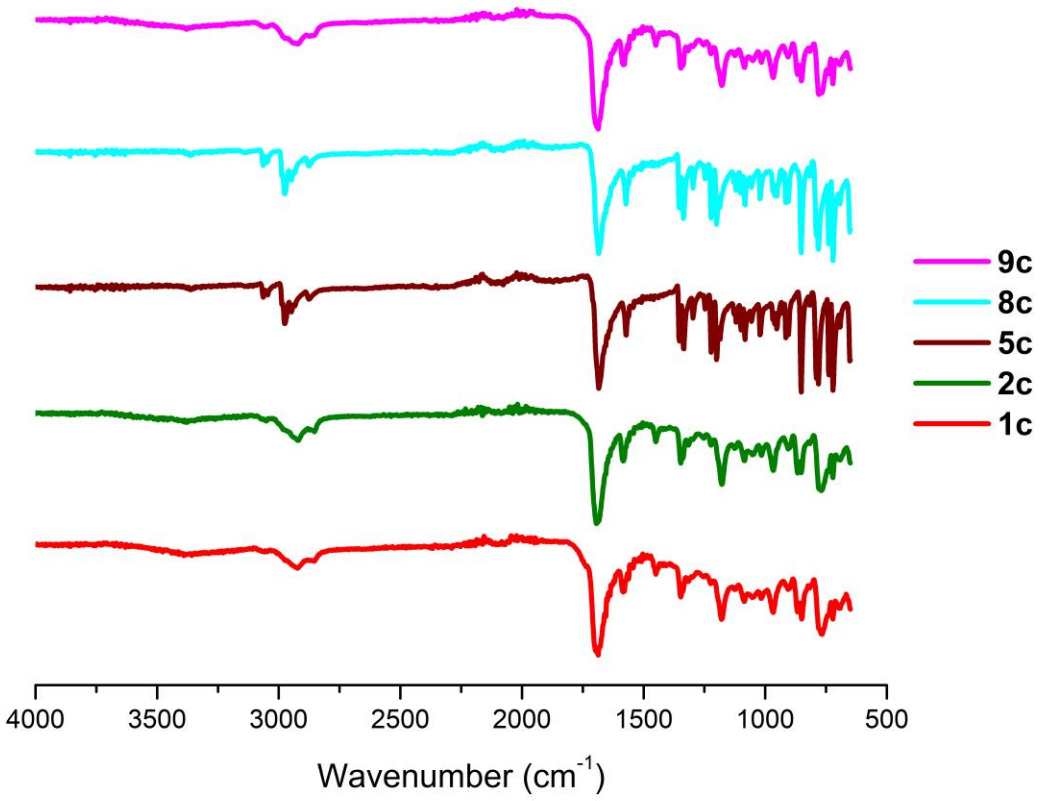

Figure C67. Normalized ATR spectra of materials made with **type-c** resin.

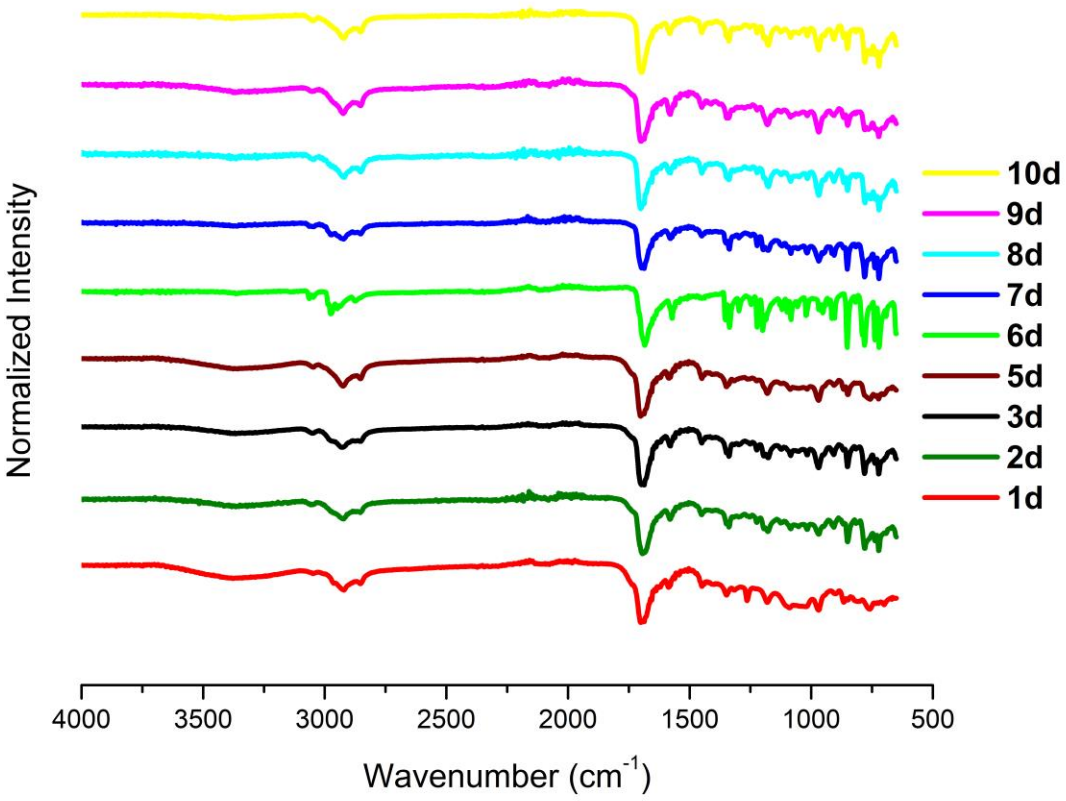

Figure C68. Normalized ATR spectra of materials made with **type-d** resin.

Table C1. Observations of polymerizations after heating and cooling.

Catalyst	Type-a (0.005 mol%) Observation	Type-b (0.005 mol% Observation	Type-c (0.005 mol%) Observation	Type-c (0.02 mol%) Observation	Type-d (0.02 mol%) Observation
1	Glassy polymer	Glassy polymer	Flaky white polymer and solid crystalline monomer	Glassy polymer, trace monomer on edges	Glassy polymer
2	Bits of polymer floating in monomer/resin	Glassy polymer	Flaky white polymer and solid crystalline monomer	Glassy polymer, trace monomer on edges	Glassy polymer
3	Nearly glassy rubber	Hard gel/rubber	Solid crystalline monomer	Solid crystalline monomer	Nearly glassy rubber
4	Very soft and odorous gel	Very soft and odorous gel	Solid crystalline monomer	Solid crystalline monomer	Liquid Monomer
5	Glassy polymer	Glassy polymer	Solid crystalline monomer	Hard gel/rubber	Glassy polymer
6	Glassy polymer	Glassy polymer	Solid crystalline monomer	Solid crystalline monomer	Glassy polymer
7	Glassy polymer	Glassy polymer	Solid crystalline monomer	Solid crystalline monomer	Glassy polymer
8	Bits of polymer floating in solidified resin	Bits of polymer floating in liquid resin	Solid crystalline monomer	Glassy polymer	Glassy polymer
9	Glassy polymer	Hard gel/rubber, odorous	Flaky white polymer and solid crystalline monomer	Glassy polymer	Glassy polymer
10	Glassy polymer	Glassy polymer	Solid crystalline monomer	Solid crystalline monomer	Glassy polymer

Table C2. Table of peak temperatures achieved.

Catalyst	Peak temperature of type-a resin (°C) at 0.005 mol%	Peak temperature of type-b resin (°C) at 0.005 mol%	Peak temperature of type-c resin (°C) at 0.005 mol%	Peak temperature of type-c resin (°C) at 0.02 mol%	Peak temperature of type-d resin (°C) at 0.02 mol%
1	192.6 ± 15.7	194.1 ± 14.8	93.6 ± 1.1	174.1 ± 15.6	168.9 ± 20.1
2	99.5 ± 33.7	136.2 ± 30.4	98.3 ± 1.6	140.6 ± 27.4	171.7 ± 21.3
3	127.0 ± 18.2	101.7 ± 5.0	96.9 ± 1.0	91.2 ± 1.2	97.3 ± 1.82
4	91.8 ± 0.2	92.5 ± 0.4	93.4 ± 1.4	91.2 ± 0.7	89.5 ± 2.2
5	168.1 ± 4.3	194.9 ± 27.7	89.9 ± 1.0	109.5 ± 6.1	159.1 ± 20.9
6	168.6 ± 12.2	161.8 ± 28.9	94.7 ± 0.5	88.6 ± 1.0	99.7 ± 4.4
7	175.8 ± 18.4	183.8 ± 14.8	93.3 ± 0.8	87.6 ± 0.5	110.2 ± 8.6
8	89.5 ± 0.5	86.6 ± 1.4	96.8 ± 1.1	111.7 ± 2.7	176.5 ± 7.5
9	113.3 ± 12.9	100.7 ± 2.8	103.4 ± 2.6	124.9 ± 5.3	151.2 ± 17.4
10	149.9 ± 2.9	146.2 ± 10.1	97.4 ± 1.9	89.5 ± 1.2	121.4 ± 11.4

Table C3. Table of smoke times achieved at 90°C

Catalyst	Smoke time of type-a resin (s) at 0.005 mol%	Smoke time of type-b resin (s) at 0.005 mol%	Smoke time of type-c resin (s) at 0.02 mol%	Smoke time of type-d resin (s) at 0.02 mol%
1	84 ± 15	85 ± 10	63 ± 5	84 ± 3
2	22 ± 2	36 ± 39	93 ± 18	57 ± 7
3	167 ± 44	283 ± 7	N/A	N/A
4	N/A	N/A	N/A	N/A
5	131 ± 9	135 ± 2	196 ± 10	125 ± 7
6	205 ± 7	186 ± 7	N/A	N/A
7	243 ± 10	243 ± 22	N/A	N/A
8	14 ± 3	31 ± 19	282 ± 1	135 ± 2
9	77 ± 14	87 ± 13	169 ± 32	120 ± 10
10	38 ± 13	53 ± 6	310 ± 9	300 ± 28

Table C4. Table of glass transitions (T_g) values.

Catalyst	T_g of type-a (°C)	T_g of type-b (°C)	T_g of type-c (°C)	T_g of type-d (°C)
1	156.41	142.25	140.58	151.07
2	N/A	143.47	130.42	142.97
3	113.57	77.73	N/A	70.86
4	82.42	86.69	N/A	N/A
5	134.14	145.07	117.62	101.24
6	136.76	143.58	N/A	61.35
7	128.94	119.14	N/A	69.05
8	N/A	N/A	134.14	88.22
9	126.82	124.04	123.78	83.73
10	127.88	122	N/A	91.52
11	N/A	N/A	N/A	N/A

Table C5. Vickers microhardness values.

Catalyst	Vickers microhardness of type-a (HV1)	Vickers microhardness of type-b (HV1)	Vickers microhardness of type-c (HV1)	Vickers microhardness of type-d (HV1)
1	14.8 ± 0.4	13.4 ± 1.1	11.3 ± 0.7	15.7 ± 0.5
2	N/A	11.6 ± 3	4.4 ± 1.3	14.9 ± 0.4
3	N/A	N/A	N/A	N/A
4	N/A	N/A	N/A	N/A
5	14.4 ± 0.5	13.1 ± 1.6	N/A	11.6 ± 0.5
6	15.9 ± 0.2	15.5 ± 0.5	N/A	N/A
7	15.8 ± 0.6	14.3 ± 0.6	N/A	N/A
8	N/A	N/A	8.9 ± 1.2	11.4 ± 1.4
9	N/A	N/A	10.1 ± 1.5	14.3 ± 0.5
10	8.6 ± 2.8	13.1 ± 2.5	N/A	4.9 ± 3

Table C6. Vickers hardness expressed as modulus.

Catalyst	Vickers microhardness of type-a (MPa)	Vickers microhardness of type-b (MPa)	Vickers microhardness of type-c (MPa)	Vickers microhardness of type-d (MPa)
1	145.2 ± 3.9	131.5 ± 10.8	110.9 ± 6.9	154.0 ± 4.9
2	N/A	113.8 ± 29.4	43.2 ± 12.8	146.2 ± 3.9
3	N/A	N/A	N/A	N/A
4	N/A	N/A	N/A	N/A
5	141.3 ± 4.9	128.5 ± 15.7	N/A	113.8 ± 4.9
6	156.0 ± 2.0	152.1 ± 4.9	N/A	N/A
7	155.0 ± 5.9	140.3 ± 5.9	N/A	N/A
8	N/A	N/A	87.3 ± 11.8	111.8 ± 13.7
9	N/A	N/A	99.1 ± 14.7	140.3 ± 4.9
10	84.4 ± 27.5	128.5 ± 24.5	N/A	48.1 ± 29.4

Table C7. Approximated tensile strength.

Catalyst	Tensile strength of type-a (MPa)	Tensile strength of type-b (MPa)	Tensile strength of type-c (MPa)	Tensile strength of type-d (MPa)
1	48.4 ± 1.3	43.8 ± 105.9	37.0 ± 2.3	51.339 ± 1.6
2	N/A	37.9 ± 288.7	14.4 ± 4.3	48.723 ± 1.3
3	N/A	N/A	N/A	N/A
4	N/A	N/A	N/A	N/A
5	47.1 ± 1.6	42.8 ± 154.0	N/A	37.932 ± 1.6
6	51.993 ± 0.7	50.7 ± 48.1	N/A	N/A
7	51.7 ± 2.0	46.8 ± 57.7	N/A	N/A
8	N/A	N/A	29.1 ± 3.9	37.278 ± 4.6
9	N/A	N/A	33.0 ± 4.9	46.761 ± 1.6
10	28.1 ± 9.2	42.8 ± 240.6	N/A	16.0 ± 9.8

Appendix D: Interview Scripts for Chapter 5

Sample Interview Script 1:

1. Tell me about yourself and your company:
    a. How long have you operated, size, location, how many centers, where are your customers.
    b. What is your role and what responsibilities do you have?
2. Have you worked with polydicyclopentadiene?
    a. If yes how long,
    b. If not what thermosetting materials do you work with?
3. What is your process for preparing to make a part?
    a. How do you prepare your resin?
4. Why are you interested in crosslinking materials?
5. Is control over the crosslinking process advantageous
6. What about surface energy/ability to paint?
7. Material strength?
8. Do you use glass fibers in your manufacturing?
9. Do you paint or bond anything you make? What about your customers?
10. Is sustainability important for you and/or your customers?
11. What regulations and policies have recently affected your industry?
12. Are their market sectors you would like to break into but cannot?
13. What have you tried to do to improve your material?
    a. strength/modulus?
    b. fiber adhesion?
    c. painting/bonding?
14. What is your experience with fire regulations in the automotive sector?
15. How much do you pay for:
    a. DCPD
    b. Catalyst
16. In a typical part, how much of the cost is catalyst compared to DCPD?
17. What are your tooling costs?
18. What was the last major change you made to your systems?
19. What do you consider when making a change to your resin system?
20. Where do you see the future of PDCPD?
21. What would you desire most to improve the workflow of making PDCPD parts?
22. Thank you so much for your time.
23. Is there anything else I should have asked you about?
24. Is there anyone else in your company that I should speak to?
25. If I have additional questions, would it be okay to follow up?
26. Who else should I be talking to!

Sample interview script 2:

1. Tell me about yourself and your organization:
    a. How long have you operated, size, location, how many centers, where are your customers.
2. What is your role and what responsibilities do you have?
3. Have you worked with polydicyclopentadiene? If yes how long, if not what thermosetting materials do you work with?
4. What sort of armour are the armed forces looking to develop?
    a. personal armour vs vehicle armour
5. What is this armour made of?
    a. steel vs ceramic
6. Are you concerned with multi hit capabilities?
7. What do the (Canadian) forces look for in a helmet?
8. What are the cost concerns with implementing a new armour or helmet system?
9. What lifetime expectations does the army have of its armours?
10. Are the armed forces concerned with the sustainability of its armour sourcing? lifecycle?
11. Do you foresee any specific challenges with integrating a new armour system onto personal, vehicles, helmets etc.
12. Besides ballistic performance is their other characteristics that are desired in armour systems?
    a. Soldier systems?
    b. Vehicle armour
13. Material strength?
14. Do you use glass fibers in your manufacturing?
15. Do you paint or bond anything you make? what about your customers?
16. Is sustainability important for you and/or your customers?
17. What regulations and policies have recently affected your industry?
18. Are their market sectors you would like to break into but cannot?
19. How would a new armour system like a PDCPD integrate with existing systems and allies?
20. What sort of liability concerns does DND have for various armours?
21. How do you suggest I approach other DND associated manufactures like helmet makers and body armour makers, can you put me in touch with anyone?
22. Is there anything else I should have asked you about?
23. How do you suggest I approach other DND associated manufactures like helmet makers and body armour makers, can you put me in touch with anyone?
24. If I have additional questions, would it be okay to follow up?
25. Who else should I be talking to?